

DTIC FILE COPY

2

AGARD-R-740

AGARD-R-740

AGARD

ADVISORY GROUP FOR AEROSPACE RESEARCH & DEVELOPMENT

7 RUE ANCELLE · 92200 · NEUILLY SUR SEINE · FRANCE

AD-A192 214

AGARD REPORT No.740

Special Course on Fundamentals of Fighter Aircraft Design

DISTRIBUTION STATEMENT A
Approved for public release
Distribution Unlimited

DTIC
ELECTE
JAN 21 1988
S D

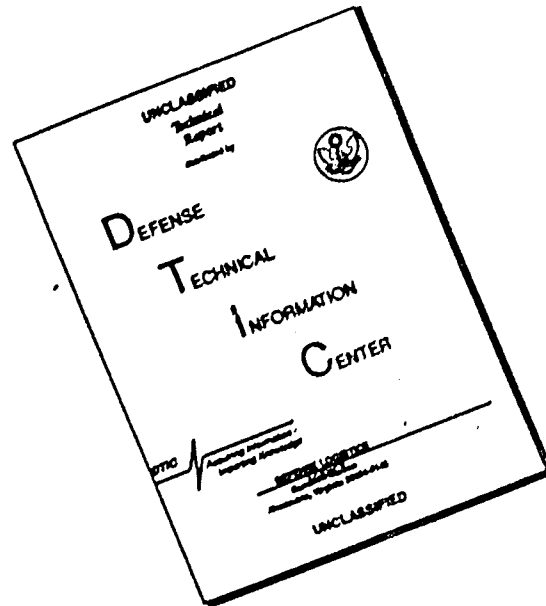
NORTH ATLANTIC TREATY ORGANIZATION



DISTRIBUTION AND AVAILABILITY
ON BACK COVER

88 1 15 021

DISCLAIMER NOTICE



THIS DOCUMENT IS BEST QUALITY AVAILABLE. THE COPY FURNISHED TO DTIC CONTAINED A SIGNIFICANT NUMBER OF PAGES WHICH DO NOT REPRODUCE LEGIBLY.

NORTH ATLANTIC TREATY ORGANIZATION
 ADVISORY GROUP FOR AEROSPACE RESEARCH AND DEVELOPMENT
 (ORGANISATION DU TRAITE DE L'ATLANTIQUE NORD)

AGARD Report No. 740
 SPECIAL COURSE ON FUNDAMENTALS OF
 FIGHTER AIRCRAFT DESIGN



Accession For	
NTIS CRA&I	<input checked="" type="checkbox"/>
DTIC TAB	<input type="checkbox"/>
Unannounced	<input type="checkbox"/>
Justification	
By	
Distribution /	
Availability Codes	
Dist	Avail and/or Special
A-1	

The material assembled in this book was prepared under the combined sponsorship of the Fluid Dynamics Panel, the von Kármán Institute and the Consultant and Exchange Programme of AGARD and was presented as an AGARD Special Course at the von Kármán Institute, Rhode-St-Genèse, Belgium on 17–21 February 1986, and as Short Courses at Athens, Greece on 24–25 February 1986 and at Ankara, Turkey on 27–28 February 1986.

THE MISSION OF AGARD

The mission of AGARD is to bring together the leading personalities of the NATO nations in the fields of science and technology relating to aerospace for the following purposes:

- Exchanging of scientific and technical information;
- Continuously stimulating advances in the aerospace sciences relevant to strengthening the common defence posture;
- Improving the co-operation among member nations in aerospace research and development;
- Providing scientific and technical advice and assistance to the Military Committee in the field of aerospace research and development (with particular regard to its military application);
- Rendering scientific and technical assistance, as requested, to other NATO bodies and to member nations in connection with research and development problems in the aerospace field;
- Providing assistance to member nations for the purpose of increasing their scientific and technical potential;
- Recommending effective ways for the member nations to use their research and development capabilities for the common benefit of the NATO community.

The highest authority within AGARD is the National Delegates Board consisting of officially appointed senior representatives from each member nation. The mission of AGARD is carried out through the Panels which are composed of experts appointed by the National Delegates, the Consultant and Exchange Programme and the Aerospace Applications Studies Programme. The results of AGARD work are reported to the member nations and the NATO Authorities through the AGARD series of publications of which this is one.

Participation in AGARD activities is by invitation only and is normally limited to citizens of the NATO nations.

The content of this publication has been reproduced directly from material supplied by AGARD or the authors.

Published October 1987

Copyright © AGARD 1987
All Rights Reserved

ISBN 92-835-1560-9



Printed by Specialised Printing Services Limited
40 Chigwell Lane, Loughton, Essex IG10 3TZ

PREFACE

The various aspects of fighter aircraft design have not been the subject of many publications during the short history of aircraft construction. Since the requirements for transport and fighter-type aircraft diverged significantly 50 years ago, the design of military airplanes of any type has been at least "Company confidential" and performance data have been "Top secret" in each country.

On the other hand, the so-called "primary task" in aerodynamics, namely the problem: "What shape would an airplane have to give certain desirable properties" has proved in the past to be much harder to solve than the analysis of a given geometry. Nevertheless some books have been published, most of them dealing with the design of aircraft having wings of large aspect ratio flying at subsonic speed. The typical "design-point" for optimum cruise has overruled other conflicting problems. The requirements for modern fighter airplanes have led however to a much different position. Many "design-points" have to be matched and many disciplines such as aerodynamics, propulsion, structures, materials, avionics, performance and weights have to be compromised by a team of highly qualified and experienced engineers. Concerning aerodynamics, even classical principles such as design for attached flow conditions everywhere are not applied in the case of highly non-linear vortex-controlled wings. Concerning the impact of materials, classical experience concerning aeroelasticity of a swept wing has been revised.

To avoid a priori any conflict with current development of fighter aircraft in different countries, this special course has been restricted to "Fundamentals". But in order to provide at least an overview to all the above-mentioned major disciplines in aircraft design, we have brought together experts to give an example of "interdisciplinary cooperation" — a special course for students, young engineers in industry and research institutes and people having technical interests outside of their professional routine.

The course will start with basic mission requirements and their impact on aircraft sizing. The aerodynamic design of the wing-body configuration, the use of non-linear lift control, stability and control, and the question of performance optimization will be treated separately but not independently. The impact of materials and aeroelasticity will be outlined and special attention will be given to major aircraft components such as the engine-intake, afterbody, and airframe-store compatibility. Experimental and theoretical work will be demonstrated as playing complementary roles, and some recommendations for the future development of engineering tools will be derived in conclusion.

SPECIAL COURSE STAFF

Special Course Director: Dipl. Ing. P.W.Sacher
Messerschmitt-Bölkow-Blohm-GmbH
LK122
Postfach 80 11 60
D-8000 München 80
Federal Republic of Germany

LECTURERS

Dr K.J.Orlik-Rückemann
National Aeronautical Establishment
National Research Council
Montreal Road
Ottawa, Ontario K1A0R6

Mr C.L.Bore
British Aerospace plc (Kingston)
Richmond Road
Kingston-upon-Thames
Surrey KT2 5QS
United Kingdom

Dr H.Gödel
Messerschmitt-Bölkow-Blohm-GmbH
UL-LKE 291
Postfach 80 11 60
D-800 München 80
Federal Republic of Germany

Mr R.C.Sellars
British Aerospace plc
Aircraft Division
Preston, Lancashire PR 4 1AX
United Kingdom

Mr B.Costes
B.P. 72
ONERA
92322 Châtillon
France

Dr J.E.Lamar
Mail Stop 394
NASA Langley Research Center
Hampton, Virginia 23665
USA

Mr J.Leynaert
B.P. 72
ONERA
92322 Châtillon
France

Mr J.L.Parker
Air Force Wright Aeronautical Laboratories
Mail Stop FIA
Wright-Patterson AFB
Ohio 45433
USA

Mr P.Perrier
AMDBA
B.P. 300
78 Quai Carnot
92214 St. Cloud
France

Dr H.Yoshihara
Boeing Military Airplane Company
Mail Stop 33-18
P.O. Box 3707
Seattle, WA 98124
USA

LOCAL COORDINATOR

Professor J.Wendt
Von Kármán Institute for Fluid Dynamics
Chaussée de Waterloo 72
B-1640 Rhode St. Genèse
Belgium

AGARD REPRESENTATIVE

Mr R.H.Rollins, II
Fluid Dynamics Panel Executive
AGARD
7 rue Ancelle
92200 Neuilly-sur-Seine
France

CONTENTS

	Page
PREFACE	iii
SPECIAL COURSE STAFF	iv
	Reference
FUNDAMENTALS OF FIGHTER AIRCRAFT DESIGN by P.W.Sacher	1
MISSION REQUIREMENTS AND AIRCRAFT SIZING by J.L.Parker	2
DESIGN OF WINGS AND WING/BODY CONFIGURATIONS FOR TRANSONIC AND SUPERSONIC SPEEDS by H.Yoshihara	3
NONLINEAR LIFT CONTROL AT HIGH SPEED AND HIGH ANGLE OF ATTACK USING VORTEX FLOW TECHNOLOGY by J.E.Lamar	4
AIRCRAFT DYNAMICS – AERODYNAMIC ASPECTS AND WIND TUNNEL TECHNIQUES by K.Orlik-Rückemann	5
TECHNIQUES FOR PERFORMANCE OPTIMISATION IN CRUISE AND MANOEUVRABILITY by P.Perrier	6
FUNDAMENTALS OF FIGHTER AIRCRAFT DESIGN: ENGINE INTAKE AND AFTERBODY by J.Leynaert	7
COMMENTS ON PROPULSION/AIRFRAME INTEGRATION FOR IMPROVING COMBAT AIRCRAFT OPERATIONAL CAPABILITIES by Ph.Poisson-Quinton	7A
AIRFRAME/STORE COMPATIBILITY by C.L.Bore	8
AEROELASTICITY AND OPTIMIZATION IN FIGHTER AIRCRAFT DESIGN by H.Gödel and H.Hörnlein	9
MATERIALS FOR FIGHTER AIRCRAFT by R.J.Sellers	10
THE ROLE OF EXPERIMENTAL INVESTIGATION AND COMPUTATIONAL FLUID DYNAMICS DURING FIGHTER AIRCRAFT DESIGN by P.W.Sacher	11
REQUIREMENTS AND RECOMMENDATIONS FOR THE DEVELOPMENT OF THEORETICAL CODES AND EXPERIMENTAL FACILITIES IN THE NEAR FUTURE by B.Costes	12

"FUNDAMENTALS OF FIGHTER AIRCRAFT DESIGN"

by
 P.W. Sacher, LKE122
 Messerschmitt-Bölkow-Blohm GmbH
 Helicopter and Military Aircraft Division
 P.O. Box 80 11 60, D-8000 München 80, FRG

There have been several reasons for the Fluid Dynamics Panel of AGARD to decide for a special course on Fundamentals of Fighter Aircraft Design. Following the technical programme of the FDP during the past years, the aeronautical engineer has found many subjects related to a special technical discipline and directed to industrial applications. But in nearly all cases the analysis of given geometry by experimental or theoretical techniques has overruled the more important engineering task - the design of a new shape which has desired properties. But in all cases concerning successful flying aircraft the result of engineering work has been a design compromise achieved by the fruitful cooperation of all technical relevant disciplines.

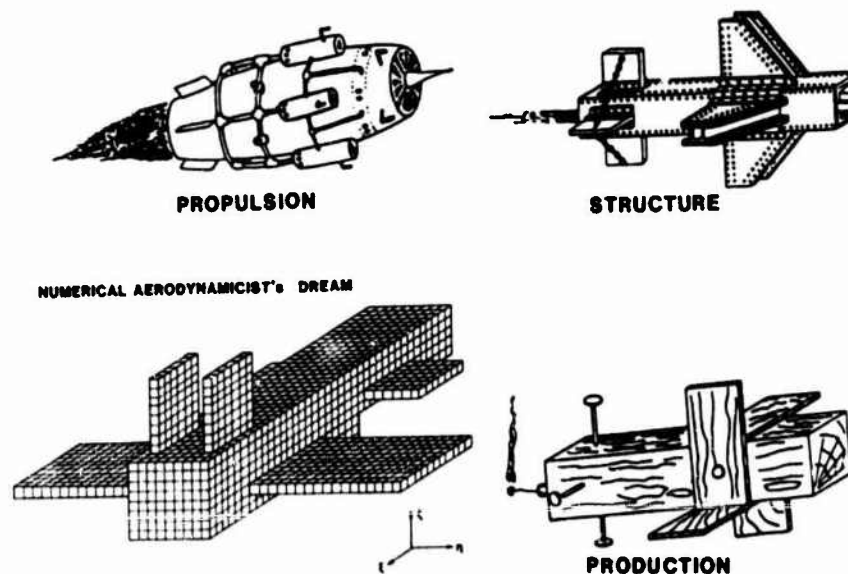


Fig. 1 The aeronautical engineer's "Dream Configuration"

So one of the most important intentions of the present course has been to attract people from different aeronautical disciplines, working at industry and research institutes and to look for links within the different branches of aerodynamics like Wind Tunnel Test Technique, Computational Fluid Dynamics, Vortex Dynamics, Unsteady Aerodynamics, Viscous Flow Drag Prediction and their impact on designing aircraft components.

In the specific case of a fighter aircraft, the design compromise must cover more than one design requirement:

- Classical Design - Compromise
 - Short T.O./Landing - High Supersonic Speed (Tornado)
 - Transonic Maneuverability - Supersonic SEP (Advanced Combat A/C, ACA)
 - Clean Design - Store Compatibility (F4)
 - Aerodynamic Performance - Detectability/RCS (Medium Range Mission Fighter, MRM)
- Design-Optimization - Techniques (Strategies)
 - Wing/Body/Tail-Arrangement (Area-Rules/Wave Drag)
 - Design for Supersonic Flow (Panel Methods)
(min. Ind. Drag, min. Wave Drag, min. Trim-Drag)
 - Design for Sub- and Transonic Flow (Panel Methods/SPE)
 - Trade-off and Analysis using FPE/Euler-Solutions
("SPE" stands for Small Perturbation Potential Flow Equation,
"FPE" for Full Potential Flow Equation)

So as a result of different design requirements the resulting A/C shape reaches from Variable Sweep Wing Concept (performance low speed/high speed) to Strake-Trapezoidal-Wings (transonic Maneuverability) and to Canard-Delta-Configurations (supersonic performance). In more recent time detectability (Radar-Cross-Section) plays an important role. Typical examples for existing A/C are shown in Fig. 2

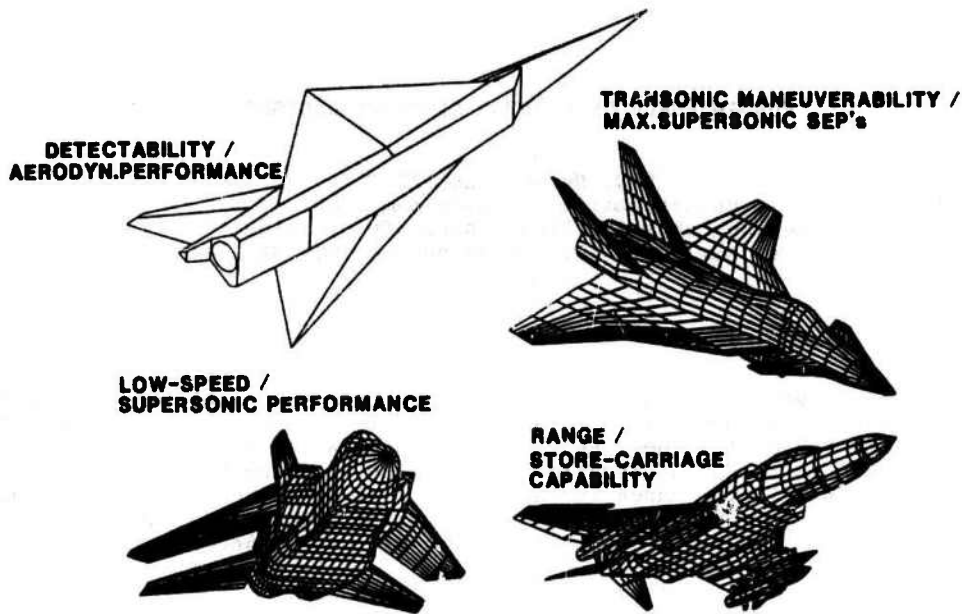


Fig. 2 The "Classical Design Compromise" leads to different A/C geometries.

In all cases of designing a new fighter A/C the intention is to extend the capabilities of the new A/C beyond the existing limits for the flight envelopes. Fig. 3 shows how this envelope defines the usable region of altitude versus speed for a specific A/C.

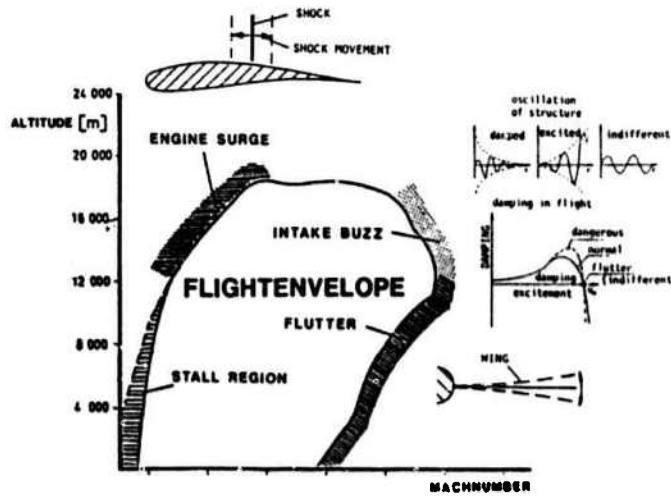


Fig. 3 Typical Flight Envelope for Fighter A/C

Before dealing with the more specific Key Problem Areas of Fighter A/C design at least two of the most important general aerodynamic flight limitations have to be discussed.

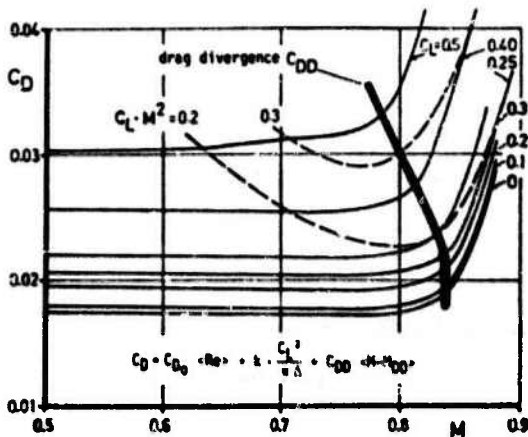


Fig. 4 Breguet's Range Formula

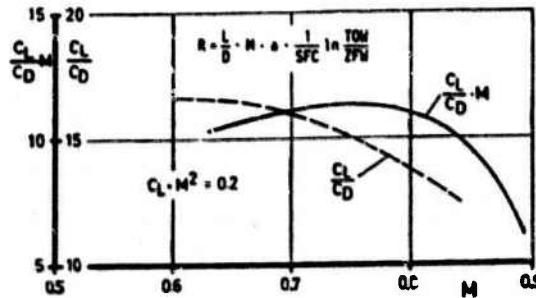


Fig. 5 Transonic Drag Rise

Breguet's range formula according to Fig. 4 shows the aerodynamic impact on the max. flight range, the relation lift over drag (L/D). Together with Specific Fuel Consumption (SFC) and Take-Off-Weight/Zero Fuel Weight (TOW/ZFW) is the "aerodynamic efficiency" (L/D) the most important design parameter for maximum range. Fig. 5 demonstrates the impact of compressibility (speed) on drag. The transonic drag rise defines in most practical applications the limit of efficient flight, $C_L \cdot M^2$ as an optimum. So far limitations according to Fig. 4 and 5 lead to single "Design Points".

The design of fighter type A/C is significantly different from the design of civil projects. This is of course due to the fact that the requirements for fighter A/C do not allow any optimization for a single design condition. While minimum DOC overrules any other requirements in civil transport airplane design, various conflicting design requirements have to be fulfilled in a fighter project. (Fig. 2 has already shown how different fighter A/C looks like).

Key Problem Areas for fighter A/C design could be identified as:


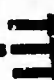
- (1) Performance in trans- and supersonic regime.
(= Design for attached Flow)
- (2) High Angle-of-Attack (HAOA)
 - Vortex (-separated) Flow Control
 - Post Stall capability
 - high Maneuverability
 - lateral, directional stability
(= Non-linear Design)
- (3) A/C Components
 - Intake/Airframe Compatibility
 - Engine/Afterbody integration
 - Aerodynamics of Controls
- (4) Detectability
 - RCS (Radar-Cross-Section)
 - IRS (Infrared-Signature)

Only Key Problem No. 1 and 2 may be outlined more in detail:

As an example to achieve a good compromise between conflicting transonic maneuver- and supersonic speed requirements (Key Problem No. 1) the Delta-Wing may be considered as a practical solution:

Delta concept: Supersonic	low wave drag (area ruling, thin profiles) 30% improvement to existing A/C
Subsonic	as good as existing A/C if: <ul style="list-style-type: none"> • Unstable config. (low trim drag, tailored lift/drag) use of canard, to get c.g. as aft as necessary • Cranked delta, (increase AR) • Regain suction force by wing (leading-edge) design • Optimum canard/wing interference

Aerodynamic efficiency L/D is just one (important) factor which contributes to A/C performance. Stress analysis leads to structural optimization and so far to minimum weight for a given load. The chosen "Design Philosophy" in combination with a suitable "Design Procedure" requires a series of "Design Tools" which are described later on in the main lectures:

DESIGN- -PHILOSOPHY	<ul style="list-style-type: none"> • min. ind. drag • min. wave drag • min. trim drag • min. wing root bend.mom. • min. shock-extension 	<div style="text-align: center;">  </div>	performance stress/structure/weight efficiency (drag rise/buffet)
HOW TO PROCEED	<ul style="list-style-type: none"> • DEFINITION OF <ul style="list-style-type: none"> - pressure (u/l), - pressure (u)+thickness - Δc_p + thickness • MINIMUM PROCEDURE FOR DRAG (or/and pitching moment) <ul style="list-style-type: none"> - C_L + spline (x,y) (+ thickness) (+ C_M) 	<div style="text-align: center;">  </div>	RESULT: camber/thickness/twist camber/twist/pressure(l) camber/twist camber/twist/pressure (u/l)
	$F = D + \lambda_1 (L - \bar{L}) + \lambda_2 (M - \bar{M})$		"LAGRANGE operator"

The design for partially separated flow conditions ("Non-linear Design") has been identified as "Key Problem Area" No. 2.

Fig. 6 shows typical "Key Problem Area No. 2" for a first generation supersonic fighter A/C and the more recent developments which are characterized by the use of controlled "Vortex-Type-Separated" Flow. Also the arrangement of aerodynamic control-devices (Flaps, Slats, Canards) is significantly different.

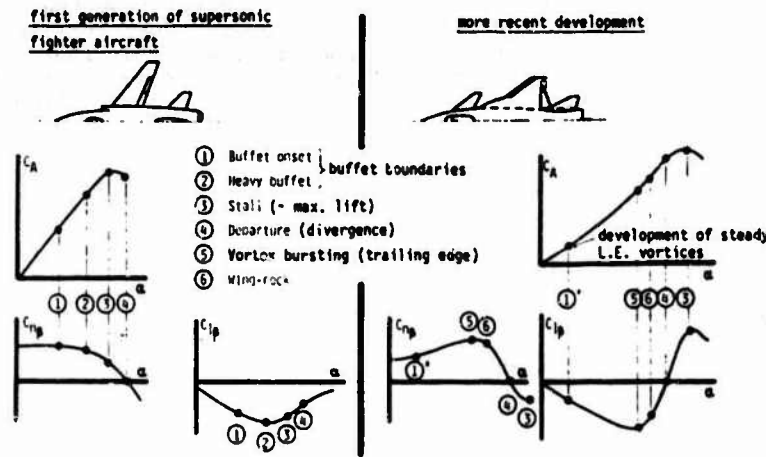


Fig. 6 Aerodynamic Key Problem Area No. 2 (schematically) in Fighter A/C Design.

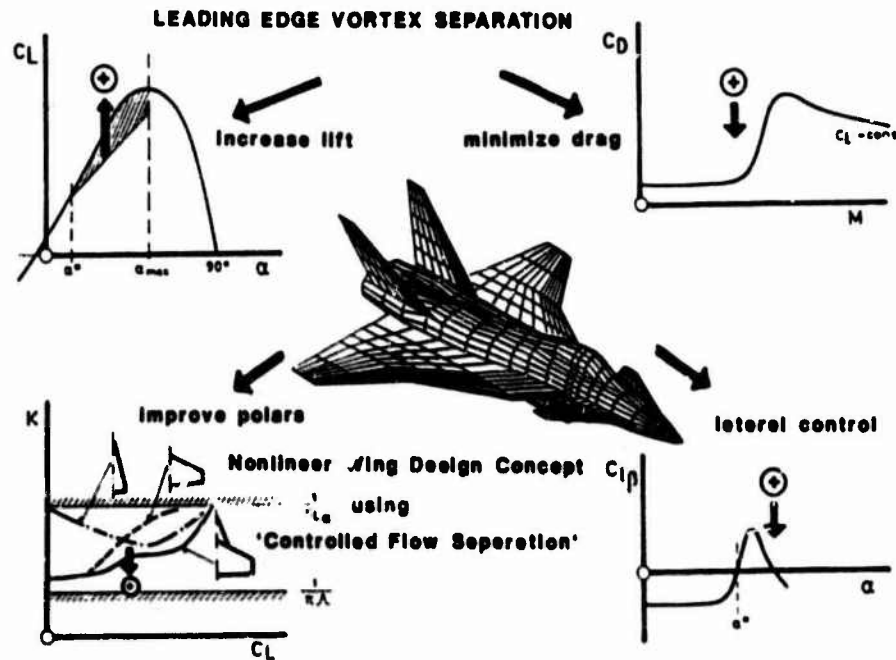


Fig. 7 Controlled Vortex Flow Separation to increase A/C Performance

Conventional technology and advanced technology has to be combined in order to extend the flight envelope of already existing A/C.

To conclude the introductory remarks, Aerodynamic Design Tools for Phase I of any new project, the "Conceptual Design-Phase", will be shown in Fig. 8

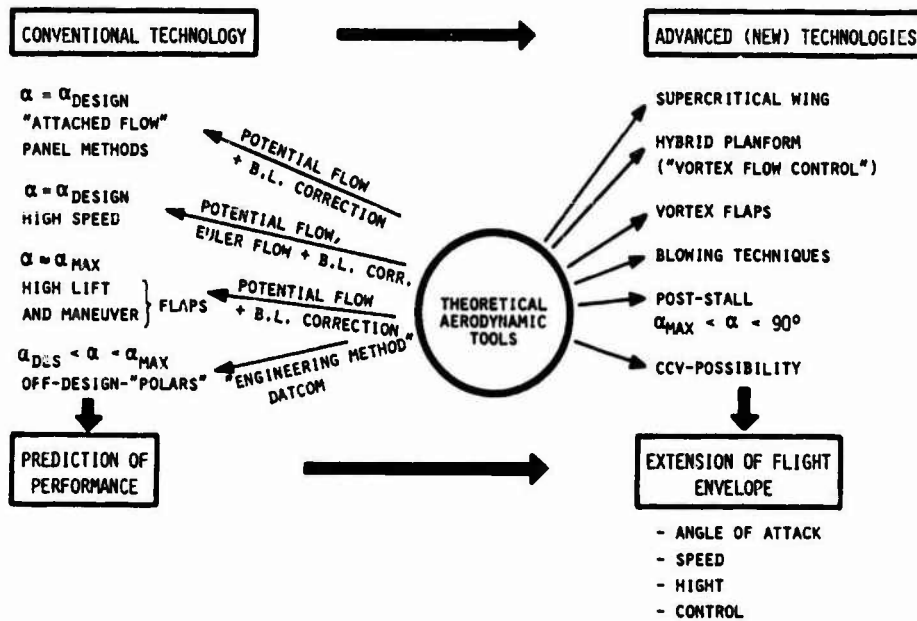


Fig. 8 Summary of Design Tools for the Conceptual Design Phase (B. L. = Boundary Layer, CCV = Controlled Configured Vehicle)

Three main reasons exist for restricting the present special course to Phase I according to Fig. 9

- It is commonly well known that the development of military airplane of any type underlies many restrictions concerning publication. Not only "Company confidential" is a severe handicap because of competition as in civil projects, in the case of fighter A/C many additional restrictions are due to national classification requirements. So we tried to avoid any conflict with current developments in different countries.
- Within the time limit of a one week special course only a small number of topics could have been selected and only a limited number of experts could have been made available to give the presentations.
- Further special courses or lecture series may follow this first approach (see e.g. FMP "Integrated Design of Advanced Fighters", AGARD LS 153, 1987)

	PHASE I CONCEPTUAL DESIGN	PHASE II PRELIMINARY DESIGN	PHASE III DETAIL DESIGN
KNOWN	<ul style="list-style-type: none"> • BASIC MISSION REQMTS • RANGE • ALTITUDE • SPEED • BASIC MATERIAL PROPERTIES σ/p E/p ρ/LB 	<ul style="list-style-type: none"> • AEROELASTIC REQMTS • FATIGUE REQUIREMENTS • FLUTTER REQUIREMENTS • OVERALL STRENGTH REQMTS 	<ul style="list-style-type: none"> • LOCAL STRENGTH REQUIREMENTS • PRODUCEBILITY • FUNCTIONAL REQMTS
RESULTS	<ul style="list-style-type: none"> • GEOMETRY • AIRFOIL TYPE • α_R • $\alpha_{1/C}$ • λ • Δ 	<ul style="list-style-type: none"> • DESIGN OBJECTIVES • DRAG LEVEL • WEIGHT GOALS • COST GOALS 	<ul style="list-style-type: none"> • BASIC INTERNAL ARRNGMT • COMPLETE EXTERNAL CONFIG • CAMBER, TWIST DISTRIBUTIONS • LOCAL FLOW PROBLEMS SOLVED • MAJOR LOADS, STRESSES, DEFLECTIONS
			<ul style="list-style-type: none"> • DETAIL DESIGN • MECHANISMS • JOINTS, FITTINGS, & ATTACHMENTS • DESIGN REFINEMENTS AS RESULTS OF TEST & OPER.

Fig. 9 Design Phases of Aircraft after L.M. Nicolai

MISSION REQUIREMENTS AND AIRCRAFT SIZING

by
 James L. Parker
 Chief, Design Branch
 Technology Assessment Office
 Flight Dynamics Laboratory
 AFWAL/FIAD
 Wright-Patterson AFB, OH 45433
 USA

SUMMARY

The development of requirements for new fighter aircraft involves defining threats, targets and scenarios for the future. Current fighter requirements emphasize the need for close-in-combat and beyond visual range combat capability to achieve superiority in the air-to-air role. High sortie rates and the ability to perform air-to-surface missions are also primary requirements. Conceptual design and aircraft sizing are used to help define requirements. With conceptual design tools, different fighter designs can be sized for different missions. These configurations allow life cycle cost and effectiveness analysis to be performed which provides the basis for the definition of the requirement. The process allows the requirement to be constrained to a technologically feasible and economically affordable solution.

2.1 Introduction

The process of developing mission requirements is one of matching beliefs about the future with the financial and human resources available for the development and operation of new aircraft. This is as it has always been. The decisions about the kind and number of ships in the Spanish Armada had to have involved the same elements as the decision to develop the latest fighter aircraft. The mistakes with respect to those decisions are more obvious in retrospect than they can be to the requirements developer looking 20 to 30 years into the future.

The major activities in the development of a requirement are shown in Figure 1. The development of requirements begins with a definition of a scenario which reflects a potential military conflict for some specific time in the future. The scenario includes targets, threats and military goals, including timelines. Based on the scenario preliminary mission requirements are defined. A number of different sets of preliminary requirements may be defined from the same scenario and military goals, reflecting different ways of doing the job. These will be the basis for the conceptual design of a spectrum of different aircraft, each of which will be sized for the range and payload specified in its preliminary mission requirement. The cost of each aircraft will be estimated as will its energy maneuverability, signatures, vulnerable areas and all other characteristics required to estimate the survivability, combat effectiveness and sortie rate. The results of such analyses will be used to compare the different conceptual designs with existing aircraft. This process is repeated until a concept emerges which offers sufficient increased military capability to warrant development and is low enough in cost to permit engineering development within funding constraints. When such a concept has been defined, a requirement can be published.

It is implicit that a requirement is not simply a statement of a military need, but a specification for a specific system concept. A specification for a fighter that is impossible to build or so expensive that it is impractical to develop and produce does not, in my view, constitute a requirement. The desire for a leak proof ballistic missile defense system does not constitute a requirement by this definition. The requirement will emerge when, and if, a system can be defined which is affordable and effective.

This is not to say that all of the design features of the aircraft have been defined at the time the requirement is published. The YF-16 and YF-17 were both proposed to satisfy the same light weight fighter requirement. From the designers perspective these two aircraft are quite different. However, when one looks, not at the hardware itself, but rather at the performance characteristics and cost the systems were indeed similar. Figure 2 is a graphical illustration of the importance of the decisions made during the development of the requirement. The requirement is developed during the conceptual design phase. At the end of this phase nearly 70% of the total life cycle cost of the system will have been committed.

When the requirements specification has been agreed upon, the design teams in aircraft companies can proceed with the preliminary design phase. They will select specific designs and converge upon the details of subsystems and components. While there will be large differences in the details of these designs, the cost differences of the aircraft of different companies will not be large. The specifications of requirements limit the system concepts to narrow bounds and determine system costs for the life cycle of the aircraft. Most of the funds that will be expended for development, production and operation of the aircraft are committed once the requirement has been published.

2.2 Conceptual Design and Aircraft Sizing

Conceptual design is the process of developing aircraft configurations that satisfy a preliminary set of mission requirements. Although these will be paper designs, they must be configurations that could be converted into real hardware given the resources to do so. During the conceptual design phase many

different configurations must be examined. There will be several sets of requirements, several configurations which satisfy each of the requirements, and many variations of each of the specific configuration examined using tradeoff analysis. This analysis is necessary to insure that each configuration is near the minimum cost for a specific set of requirements. Unless a configuration is nearly optimum, conclusions relative to the viability of a particular mission will not be valid. Comparisons between alternative configurations will also be invalid if one configuration is near optimum and another is far from optimum.

The relationship of conceptual design to the more detailed design phases is shown in Figure 3. Even within the domain of conceptual design, there are different levels of methods depending on how much time is available for a particular study and the required level of fidelity. Figure 3 illustrates three levels of design prior to entering the preliminary design phase. At the lowest level are those methods used prior to the initial layout. These are often referred to as "back of the envelope" methods. The intermediate level is the level used in sizing codes to perform tradeoff analysis. The upper level overlaps to the preliminary design methods. This level is used for more detailed analysis of the baseline design and for analysis of the final sized configuration.

Conceptual design may be divided into the three phases shown in Figure 4. The conceptual design process is a highly interactive trial and error process. Each succeeding phase feeds back information to its predecessor. The design is continually altered until a configuration emerges whose geometry and mass properties are compatible with some set of requirements. This necessitates that the design procedures and methods allow rapid turnaround so as to be compatible with the environment of many and frequent changes.

During the initiation phase the designer starts with only a set of preliminary requirements and must define enough design parameters to produce a layout of a baseline configuration. The designer must select an avionics suite, a propulsion system, weapons and the major airframe parameters. He must have an understanding of the scenario, the technology and of how design parameters relate to design requirements. Much of what goes on in this phase depends on the experience and acumen of the designer. It also depends on his data base and the bag of tricks that he has developed.

Avionics, propulsion and weapons will depend, to a large degree, upon manufacturers who specialize in these areas. The avionics must be selected for the wide variety of functions required for the particular mission and scenario. A typical avionics suite for a fighter will consist of some, or all, of the functions shown in Figure 5. In a modern fighter avionics can weigh 2000 to 3000 lbs. Its real estate takes highest priority and the optical and infrared apertures and microwave antenna can have considerable impact on the design, signatures and performance of the aircraft. The life cycle cost of the avionics is now typically 1/3 of the total life cycle cost. The reliability and maintainability have a major influence on the operational readiness of the aircraft.

Technology advances in avionics tends to increase rather than decrease the avionics cost and weight because the number of functions that can be performed and the capability offered by these advances more than offsets with the cost and other penalties. There is a tendency to add more avionics because of the promise of increased effectiveness. Although there is a certain amount of resistance against this trend, increasing sophistication in defensive threats and offensive systems seems to demand it.

During the initiation phase the designer will want to consider a wide variety of engines. The ability to do this has been greatly enhanced by the availability of the Pratt and Whitney parametric engine deck. During the initiation phase this deck can be run to produce thrust and SFC for all of the critical flight conditions for a variety of engine cycles. The designer can do some "back-of-the-envelope" performance calculations for each of these cycles and select the one which gives the minimum fuel. This is very approximate because the data is all uninstalled and the engine thrust-to-weight ratio declines with decreasing specific fuel consumption (SFC). The tradeoff between these two opposing effects cannot be properly conducted during the initiation phase. Nevertheless, this procedure does give some basis for selecting an engine cycle. Where there are a wide variety of subsonic and supersonic flight conditions in the mission, one often finds that the sensitivity of aircraft weight to engine cycle selection is not great; consequently, the penalty for selecting a non optimum cycle is acceptable for design initiation.

Weapons are one of the major influences on the design of the aircraft. Usually, the choice of weapons is a combination of existing weapons and conceptual weapons. If conceptual weapons are used, the conceptual design of the weapons has to be developed in the same way as is being described for the aircraft. The designer has to assure that the fire control avionics are matched to the weapons. He also has to provide for carrying all of the existing weapons. In many fighter studies, conceptual weapons are integrated with the airframe. These weapons are designed for the primary mission and carried either internally, submerged, tangential or pelletized to minimize drag and observables (Figure 6). The existing weapons are either carried externally on conventional racks and pylons or pelletized in a conceptual pallet.

At the end of the initiation phase it is necessary for the designer to select a size and weight for the initial layout. It is possible to do a fair job of weighing and sizing an aircraft at this stage even before there is any drawing actually on the board. Simplified versions of weights and aerodynamic methods are used in conjunction with simple performance equations and the uninstalled thrust and SFC data. Computer programs have been written to assist in this process. Requirements are input into these programs and the geometry of the aircraft and the gross weight are output. During the initiation stage computer programs are not of great benefit. Experience is the biggest factor. The designs and requirements are unique so that preprogrammed codes are usually not as useful at this stage as in other phases of the design process.

During the concept development phase a layout must be produced. This rough layout is essential for several reasons. It provides the basis for mass properties and aerodynamic analysis. The internal arrangement helps to resolve the weight and balance. The adequacy of the volume which has been allocated

for systems is checked. Landing gear is located to provide adequate balance and tail strike layout is also used to develop the area progression which is very critical for supersonic. Once a satisfactory layout has been completed an analysis of the configuration can be conducted. The geometry of the configuration could be transferred directly to a sizing program and sizing conducted if the methods contained in the sizing program are capable of analysis of the particular design. This is rarely the case since configurations which respond to new requirements must employ very advanced technologies and are frequently different from anything that has previously been built. For this reason, an analysis of the configuration is usually done in the areas shown in Figure 7. The mass properties and aerodynamic analysis will be performed before sizing. These analyses permit the sizing code to be calibrated to reflect the peculiarities of the baseline configuration. The remainder of the areas will be analyzed after the configuration is sized.

A method for sizing of aircraft is an important design tool for the reasons shown in Figure 8. Sizing methods are used to determine the weight and cost of an aircraft that is needed to satisfy a particular set of mission requirements. By repeating the sizing process for various missions, different sets of requirements can be assessed. This sizing process is also used to evaluate the impact of certain advanced technologies. Any technology that has an impact on the gross weight, aerodynamics or engine performance can be evaluated through the methods used in the sizing process. Sizing is done during the conceptual design phase of a project. The conceptual design aircraft will provide inputs for effectiveness analysis. The selected configuration will also be used as the starting point for more detailed design phases.

The state-of-the-art in aircraft sizing is to layout a baseline design and match the fuel available with the fuel required for a specified mission for this baseline as shown in Figure 9. The baseline design is usually developed on the drawing board or with a computer aided design system. An analysis of the aerodynamics, stability and control, mass properties and propulsion performance is performed on the baseline. The analysis results are used to calibrate a computerized sizing code which allows the baseline to be sized to a mission. The aircraft is scaled holding a constant thrust-to-weight ratio (T/W) and wing loading (W/S) to keep the point performance approximately constant.

These sizing codes are valuable tools and very refined in some cases. Most sizing codes allow one, not only to resize to different mission, but to conduct tradeoff analysis on at least the wing loading and the thrust to weight ratio. The specific excess power, turn rates, landing and takeoff distances, acceleration times and other point performance requirements can be overlaid on the plots of W/S and T/W to show the design space for which all of the requirements are satisfied. In cases where several different performance points are being simultaneously considered, it is an excellent approach to evaluating the combined effects of all performance requirements. This process will be discussed in detail later.

In concept fuel match sizing is a rather simple process. Given a fuel sizing mission and a baseline design the fuel required for that design to perform the mission can be calculated by summing the fuel required for each mission leg, with appropriate fuel allowances and reserves. If the fuel calculated for the mission does not equal the fuel available in the baseline design, the aircraft is scaled up or down depending upon whether there was excess or insufficient fuel for the mission. This process converges on a sized aircraft where the fuel available equals the fuel required. Figure 10 illustrates the reason for this convergence. Since there are many items in the aircraft such as the payload, avionics, crew, crew station, and so forth, which do not scale with the size of the aircraft, the fuel fraction of the baseline will increase as it is scaled up and decreased as it is scaled down. Because the fuel fraction required for the mission is much less sensitive to size than the fuel available, the two curves usually intersect. Convergence is by no means guaranteed, however. In some cases, the two curves are so nearly parallel that they do not converge within the region of scalability of the baseline. In some cases the curves may actually diverge.

While this seems to be a rather simple process it is, in reality, quite complex. The problem stems from scaling the aircraft. When the size of the baseline is altered practically everything in the aircraft changes; balance, stability margin, landing gear size and placement, drag and lift, control surface sizing to mention just a few. Each point on the curve in Figure 10 is a different design. No computer code can adequately account for all of these effects. Consequently, the range of scalability must be carefully considered. After sizing the aircraft, the geometry of the sized vehicle is laid out again and the process repeated.

Mission sensitivities can be conducted using the same basic sizing method previously described, as shown in Figure 11. For mission sensitivities, the fuel required curve is constructed for each of the mission variations of interest. The intersection of these curves with the fuel available curve can be plotted versus the mission parameter of interest. Radius, combat fuel, cruise and dash speed, altitude and alternative combinations of mission legs can be varied in this same way. For these mission sensitivities the W/S and aircraft T/W are held constant so that the energy maneuverability is changed as little as possible.

Fuel match sizing only satisfies the mission fuel requirements. It is still necessary to insure that all of the point performance requirements are met. These point performance requirements include specific excess power, sustained and available turn rates, landing and takeoff distances and acceleration capability. There may be dozens of these points since energy maneuverability at many different Mach number and altitude combinations are usually specified. In order to simultaneously satisfy all of the point performance requirements, tradeoff analyses are conducted. The fuel match sizing has to be conducted for several different W/S and T/W values. The results of these fuel match calculations for each W/S and T/W can be plotted on a single graph as shown in Figure 12.

Figure 13 shows how the point performance constraints can be displayed on a map of W/S, T/W, and gross weight. The hash marks on the constraint lines indicate the portion of the solution space which will not simultaneously satisfy both the P and sustained turn constraints. Any combination of W/S and T/W above the constraint lines (opposite the hash marks) will satisfy both constraints. The intersection

of the two constraint lines define the minimum gross weight aircraft which satisfies both performance requirements.

Figure 13 can be used to illustrate the value of the graphical display of this information as opposed to a computer optimization. The P constraint line is very nearly the same as a T/W line whereas the sustained turn rate constraint is nearly horizontal. This means that if both the engine size and the wing loading are increased the sustained turn rate will be maintained whereas the P will increase substantially. Thus, added P can be achieved with little increase in the gross weight of the aircraft. This is apparent on the graph but would not be known if the computer were allowed to optimize the solution.

The foregoing discussion of aircraft sizing and tradeoff analysis has been concerned with only two design parameters, W/S and T/W. Even at the conceptual level there are many more design parameters that must be considered in the design and sizing of the aircraft. Figure 14 gives examples of parameters that have a first order effect on the size of the aircraft. Values had to be assumed for all of these parameters for the baseline design and it is necessary to conduct tradeoff analysis to select the values yielding the lowest gross weight. Figure 15 is an example of a wing sweep versus aspect ratio tradeoff. Such tradeoffs must be performed for all first order parameters. The W/S versus T/W tradeoff shown in Figure 13 represents a local optimum for the specific value of each of the parameters shown in Figure 14 that were selected for the baseline design. The large number of design parameters involved greatly increased the complexity of the tradeoff analysis.

No discussion of conceptual design would be complete without a discussion of conceptual design methods. Conceptual design relies heavily on empirical methods. In the early phases of the design process analytical methods are inappropriate for several reasons. First, the methods should predict what the weight or drag of a configuration would be given the normal time to refine the design in the preliminary and detailed design phase. Every bump will not be removed from the area progression curve during conceptual design. This prediction must account for technology advances. Second, the method must be comprehensive, that is, all weight, drag, lift, thrust loss, and signature contribution, from every source, must be predicted. Few analytical methods do this. For example, the most sophisticated structural analysis codes predict less than 50% of the weight of any structural component. Since structure accounts for only 30% of a fighter's weight, a complex finite element analysis code will predict less than 15% of the total weight. This is inadequate for conceptual design. Third, the time to input and run analytical codes is inconsistent with the number of people on a conceptual design team and the turn around time required during the conceptual design phase. All of these factors tend to make the conceptual design methods a rather specialized field.

Conceptual design is encompassing more areas than it has in the past, as shown in Figure 7. This is because all of these areas are included in the requirements and it is necessary to be able to evaluate them at that level. Much more attention is currently being focused on logistics factors and cost than has been the case in the past. Signatures and vulnerable areas are important for effectiveness analysis. Methods have been developed for analysis of these factors and it is now expected that such analysis data will be produced in the conceptual design phase.

Conceptual design involves the use of computers in many aspects of the design process. Codes for sizing, performance, and analysis have been in existence for many years. More recently the development of graphic software and high resolution terminals permit the configuration layout to be done at the terminal. Layout of a configuration is a high skill level function whether it is done with the aid of a computer or on the board. A design created on the board may be digitized into the computer for analysis purposes as shown in Figure 16.

One of the more important advantages of the use of computer aided design systems to develop configuration geometry may be the ability to generate the input to analysis programs that require a large amount of geometry data, such as aerodynamic paneling codes or finite element structural analysis. Figures 17, 18, & 19 show output taken directly from the terminal screen of a computer aided design (CAD) system. Figure 17 is a graph of the area progression and the volume of the components. Figure 18 shows a perimeter plot with wetted area. Figure 19 is a far field wave drag analysis. All of this output is available once the geometry is in the computer.

Another example of the use of geometry files is to fabricate models. Figure 20 shows a configuration file being displayed on a color terminal. Figure 21 is a photograph of the face of the terminal displaying this same configuration. Finally, Figure 22 shows a model that was fabricated from this same geometry file. The configuration geometry file was transferred to a commercially available CAD system and then to a numerically controlled milling machine to fabricate the model. It is well within the state-of-the-art to create geometry input for different analysis tools and to interface files for model fabrication.

2.3 Fighter Requirements

This section will present a summary of some of the key issues that are addressed during the process of defining a fighter requirement. The publication of a requirement for a new fighter is a commitment of tens of billions of dollars in total life cycle cost, not including weapons. Such a commitment of funds assures that the decisions as to when a new fighter development will begin go far beyond the technical considerations alone. The enormous political and economic implications of a new aircraft development have a major influence on what is developed and when it is developed. These aspects of the gestation of a requirement are not addressed in this paper.

Before attempting to discuss the principal issues that must be addressed in defining a fighter requirement, there must be some agreement as to what is meant by a fighter aircraft. A fighter may be defined as any aircraft whose primary mission is to maintain air superiority by engaging in air-to-air combat. This definition includes the mission roles of air superiority fighter, fighter escort and fighter interceptor. It does not preclude, as a secondary role, air-to-surface attack, reconnaissance or other

roles. Because of the expense of developing and maintaining different aircraft in the same general weight and performance class, ground attack may be included as a secondary role for fighter aircraft. A discussion of fighter aircraft would be incomplete without some consideration of the air-to-surface role.

Among the contents of a typical fighter requirement are those illustrated in Figure 23. All of the requirements listed contribute to the ability of the fighter to perform its mission. The cause and effect between these requirements and the general capabilities that are sought in a fighter must be established in order to provide the rationale for each of the requirements. Each of the requirements contribute to the cost of the fighter, consequently it must be shown that it is needed. A rationale that has been used to justify performance is that a margin is needed of over the threat to assure success in combat. This rationale usually contributes to at least a part of any fighter requirement. Even this simple rationale has its problems however. Many important questions remain unanswered such as; how much of a performance margin is needed, is it needed over the entire flight envelope, is performance really important since technology A, B or C substitute for the need for performance, can weapon performance substitute for aircraft performance and can quality of aircraft replace quantity. These are difficult questions but answers are needed to formulate a requirement. Analysis, simulation and test all are used to attempt to provide answers to these questions.

The following discussion of fighter requirements focuses on the major categories of capability listed in Figure 24. All of the requirements contribute to one of these general capabilities. A quantitative assessment of this contribution is beyond the scope of this lecture. The purpose of this discussion is to highlight the major concerns which currently influence fighter design.

Close-in-Combat

Close-in-combat has traditionally been the very essence of fighter aircraft design. Close-in-combat is sometimes referred to as a dogfight because of the twisting, turning maneuvers of the combatants. Figure 25 is a graphical output from a close-in-combat simulation which supports the analogy. For early air superiority fighters, the only armament was a gun which was most effective at 300 to 800 ft. Close-in-combat literally meant within gun range. The pilot was the target acquisition and fire control system. The addition of the IR missile did little to fundamentally alter what was important in fighter design. The IR missile still required the pilot to maneuver to the 6 o'clock position before the missile was effective. In recent years there have been a number of advances that are altering all of this. The improvements in the all aspect missile is one of the principal new technologies that may change forever the nature of the fighter design. Early evidence from simulations and actual combat indicates that there is some reason to believe that this is so. On the other hand, we have heralded the end to the dogfight before, only to have it reappear due to the failure of the missile systems to deliver as promised. There is still reason to believe that even in this advanced age of avionics, the missile will not be the total solution. In any event, the user has not seen fit to dispense with the classical maneuverability of the fighter. Since the user has the final prerogative when it comes to requirements, it is still important to understand what effect they have on the aircraft.

The characteristic that is generally thought of as defining a fighter aircraft is its ability to maneuver to a position of advantage in aerial combat and succeed in shooting down the opponent. Enough has been said and written on this subject to fill many books. Still, when it comes to making a definitive statement of the maneuverability requirements for advanced fighters, the task is not easy. This is partly due to the many diverse technologies that open up new possibilities for air combat. It is also due to the fact that the design of an aircraft involves many compromises and must be constrained to the funds available. Requirements cannot ask for all of everything, so one is faced with the problem of deciding what is most important.

In the mind's eye one can envision close-in-combat as two opposing aircraft approaching each other, engaging in a dogfight with one aircraft eventually shooting down the other. This, in fact, is the scenario that has flavored much thinking with respect to fighter requirements and analyses. Models have been developed which can simulate such engagements and it is straight forward to translate the analysis results into design requirements. The outcome of the analysis of many such engagements has been correlated against maneuverability parameters. These correlations result in the conclusion that the important maneuverability parameters are specific excess power, sustained turn rate, instantaneous (available) turn rate and acceleration.

Specific excess power is defined by the following equation:

$$P_s = \frac{(T - D)V}{W} \quad \text{Eq (1)}$$

Where P_s = Specific Excess Power

T = Thrust
D = Drag
W = Aircraft Weight
V = Velocity

Specific excess power varies with the flight condition and it is common to display P_s as a function of Mach number and altitude as shown in Figure 26. P_s is assessed both for level flight and turning flight where the drag is higher. As the turn rate is increased the point is reached where the thrust equals the drag. At this point, the aircraft has reached its maximum sustained turn rate. Thus, the line on the 5g plot in Figure 26 where $P_s = 0$ determines the boundary of the 5g sustained normal load factor capability for this particular aircraft. The turn rate can be further increased at a sacrifice in energy level. When the aircraft turn rate is increased to the point where $C_{L_{max}}$ is reached, it can be increased no further. This is the available turn rate (ATR) or instantaneous turn rate.

For an aircraft that is well designed aerodynamically P_g in one g level flight is primarily determined by the aircraft thrust-to-weight ratio (T/W). Very high thrust engines are desired for high P_g . The high thrust-to-weight ratio of modern fighter engines, $(T/W)_E$, allows the achievement of very high P_g values for future fighters. Even given modern high $(T/W)_E$ engines, the increments in P_g can cost dearly in increased gross weight of the aircraft. Consider a hypothetical aircraft, for example a well designed supercruiser fighter, with a combat wing loading of 56 lbs/ft² and a combat T/W of 0.52. This equates to an unstalled sea level static thrust-to-weight ratio of about 1.0. The P_g of such a hypothetical aircraft at M=0.9 and altitude of 30,000 ft would be about 370 ft/sec. If 100 fps more of P_g were required, a combat T/W of 0.636 would be needed. Figure 27 shows the results of resizing this aircraft to the new P_g requirement to be over 10,000 lbs in weight. This is a rather extreme case because of mission fuel requirements, but it illustrates the point that P_g requirements are to be carefully considered in developing a requirement for a new aircraft. This sizing was done with a $(T/W)_E$ of 9.0. If a higher $(T/W)_E$ were achieved through technology advances in fighter engines, the results would be less dramatic.

Maximum sustained turn rate ($\dot{\theta}$) is a second important design requirement which contributes to close-in-combat capability. $\dot{\theta}$ is the angular velocity measured in degrees per second. Sustained turn rate is also commonly expressed in "g's" which is the normal load factor. Sustained turn rate and normal load factor are related by the following formula.

$$\dot{\theta} = \frac{K}{V} \sqrt{n^2 - 1} \quad \text{Eq (2)}$$

Where: $\dot{\theta}$ = turn rate
n = normal load factor

The g's for a maximum sustained turn are related to the wing loading and thrust to weight ratio by the following approximation:

$$n_s = \frac{q}{W/S} \sqrt{\frac{1}{K} \left(\frac{T}{qS} - C_{D0} \right)} \quad \text{Eq (3)}$$

Where: n_s = maximum steady state normal load factor
q = dynamic pressure
W/S = combat wing loading
T = thrust
K = wing drag-due-to-lift factor for uncambered wing
S = wing reference area
 C_{D0} = zero lift drag coefficient

It is apparent from Eq (3) that the maximum sustained turn capability of a fighter is a function of both the combat thrust and combat wing loading. A tradeoff analysis is required to determine the correct combination of wing loading and thrust-to-weight ratio. Figure 28 shows the results of such a tradeoff analysis. There is a unique combination of W/S and T/W for lowest gross weight for any required sustained n_s , as shown by the minimum point on the curve.

Figure 29 is another presentation of the results of a tradeoff analysis of W/S and T/W. This plot maps constant gross weight lines on a T/W versus W/S plot. The point of tangency of these gross weight lines with the lines of constant sustained g's defines the minimum gross weight. The locus of combinations of T/W and W/S which minimize the gross weight for each g level is dramatized by this plot. Gross weight is quite sensitive to the requirement for additional maximum sustained turn rate capability. The requirement for an additional 0.5 sustained load factor can increase the gross weight by 10%.

The third requirement which effects the outcome of dogfight engagements is the maximum instantaneous turn rate also called available turn rate (ATR). This parameter is effected only by the maximum lift coefficient of the wing and the wing loading. ATR is not affected by engine thrust and relates to load factor by Eq (1). Maximum instantaneous load factor is given by the following equation.

$$n_z = \frac{C_{Lmax} q}{W/S} \quad \text{Eq (4)}$$

Where: n_z = maximum instantaneous load factor
 C_{Lmax} = maximum lift coefficient
q = dynamic pressure
W/S is the wing loading

Although there is a loss of energy when the aircraft is turning at a rate greater than the maximum sustained turn rate, the instantaneous turn rate is nevertheless an important parameter. In the one-on-one engagement modeled in Figure 25 nearly all of the engagement is conducted at conditions where the $P_g < 0$.

Over a large part of the flight envelope the maximum instantaneous load factor will be limited by the structural design limits of the aircraft rather than the C_{Lmax} of the wing. This is graphically illustrated in Figure 30.

The tradeoffs illustrated here are very complex if done correctly. The problem is multidimensional since the aerodynamic efficiency of the total aircraft is involved. This implies that the planform of the aircraft should be optimized at each point in the W/S versus T/W plane. The engine cycle is also involved as well as the structural efficiency. A further complicating factor is that there are many constraints other than turn rate and P_g . The global optimization problem resulting from the many parameters and many

constraints is large. In general, however, the type of tradeoffs illustrated here are used for making decisions relative to fighter requirements.

As mentioned earlier the result of combat simulations have been correlated against the P_s sustained turn rate and available turn rate. These parameters produce a good statistical correlation with exchange ratio in one-on-one combat. If an engagement is other than one-on-one the outcome is different than one would predict by one-on-one analysis. Whereas in a one-on-one engagement, the exchange ratio (number of aircraft killed/number of aircraft lost) can reach almost any value depending on the difference in the level of energy maneuverability between opponents, in one-versus-two or two versus two engagements the results do not correlate as well. Multiple aircraft engagements are much more difficult to analyze and much more dependent on the tactics used by the opponents. Analysis, simulation and operational evaluation have all been used to evaluate the multiple engagement problem. The results of many simulations are shown in Figure 31. One general conclusion is that requirements cannot be based exclusively on energy maneuverability but that maneuverability is still significant, although it is most important in 1 versus 1 combat. The results of analysis of engagements of multiple aircraft, do not alter the desire to have an energy maneuverability margin over any projected threat. As a consequence a section on turn rates and specific excess power will be included in any requirements document.

There are several new technologies that also have a bearing on the reliance on energy maneuverability for success in air-to-air combat. These technologies increase the volume of the envelope for which the armament may be used effectively. Included in this category are trainable guns, unconventional flight modes, off bore-sight missiles, and all aspect missiles. The effect of these technologies is to increase the time of the target in the lethal envelope of the armament during an air-to-air engagement as shown in Figure 32. In the past, guns and missiles have been limited primarily to engagements from the rear quadrant for high probability to kill. The rear aspect missiles are IR missiles which depend on viewing engine hot parts in order to home on the target. In terms of combat tactics they do not change the emphasis or aircraft performance since it is still necessary to position near "6 o'clock" for an effective target kill. The all aspect missile, trainable gun, unconventional flight modes and off bore-sight missiles on the other hand, permit engagement from any position relative to the target. With an all aspect missile it is only necessary that the target be acquired and within range. In theory these technologies could be substituted for some of the energy maneuverability requirements with no loss in effectiveness. Analysis and flight demonstrations have been performed which indicate that fighters employing these technologies can succeed against fighters which have superior energy maneuverability but lack these technologies. In the future, these technologies may have an influence on the level of energy maneuverability required. At present, however, there is inadequate demonstrated capability from these technologies to alter the thinking about fighter requirements significantly.

Beyond Visual Range (BVR) Combat

The more serious problem associated with the focus on aircraft performance for close-in-combat, however, is that the nature of air combat may be changing. The factors contributing to the change are illustrated in Figure 33. There are still some who maintain the view that long range missiles, avionics and reduced signatures do not alter the fundamental nature of air combat. At one time the failure of missiles to live up to expectations seemed to support their case. Recent combat experience, however, seems to indicate otherwise. While there have been fatal flaws in some missile systems in the past, progress has been made toward correcting these deficiencies. The acceptance of long-range missiles as the primary armament for aircraft has a fundamental impact on fighter requirements. Long range missiles shift the emphasis from the close-in-combat arena to the other types of combat shown in Figure 34. BVR combat includes the N versus N combat in which the friendly aircraft can easily be distinguished from the opposition by position and the 1 versus 1 versus 1 combat where there is general chaos among combatants. In this latter case, knowledge of the target position does not identify the aircraft and any aircraft may be simultaneously both being attacked and attacking. Of course, BVR may also be a one versus one situation and close-in-combat may involve multiple aircraft.

An engagement may begin at beyond visual range and end in a dogfight as illustrated in Figure 35. This simulation begins at a separation distance of 40 nm where the first missiles are fired. The combatants begin maneuvers at this point but are constrained to keep each other in their field of view. After the BVR missiles fail to effect a kill, the engagement eventually turns into a dogfight. The relative magnitude of the scale between BVR and CIC is shown in Figure 35. Typical BVR simulations begin at 40 to 50 nm whereas CIC simulations start at 3 nm. This figure also serves to illustrate that the maneuvers in BVR simulation are not nearly as violent as CIC maneuvers.

The fundamental capabilities that contribute to success in CIC are the same in BVR combat i.e. to see without being seen, to shoot without being shot at, and to kill without being killed. The aircraft characteristics which contribute to these capabilities are greatly different, however. The relative maneuverability between the opposing aircraft has very little to do with the outcome of the engagement. Low speed missileer aircraft such as the one shown in Figure 36, which have very little energy maneuverability, have been shown in analysis to have very favorable exchange ratios in certain air combat situations, if they have effective long and medium range missiles. A missileer is like a porcupine; very dangerous if it is attacked but not very effective in an offensive role.

BVR combat is not new. Long range radar guided missiles have been operational for many years on F-14s, F-15s, F-4s and many other aircraft. Even so, it is not really clear what will make a good BVR fighter in a tactical situation. At present, the issues shown in Figure 37 dominate the discussions. Speed with maneuverability is one of the key issues. A fighter with a sustained high speed cruise capability has the ability to provide defensive capability as shown Figures 38, 39, and 40. The higher speed capability allows the interceptor to be farther away from its base than a lower speed aircraft in any given period of time, (Figure 39). The average speed from base to intercept point defines the capture envelope. Fewer aircraft are able to penetrate the defense simply because the interceptor cannot get to the intercept point before the threat has flown by. This larger radius of action makes it possible to defend a larger area from a given base, thus reducing the number of interceptors and interceptor bases

required. Speed also allows an interceptor to catch up to floating targets from the rear as shown in Figure 40. The delay time and target speed have a dramatic effect on the interceptor speed required to capture the target.

A second advantage of a high speed capability for a fighter is the expansion of the missile launch envelope due to the higher launch speed. The launch speed of the aircraft is added to the missile's energy permitting the missile to be launched at a greater range than the opponent's missile. Figure 41 shows the relative launch envelope area difference due to speed differential.

In the chaotic situation there is another advantage to speed. Where the position and velocity vector of the targets are random and plentiful the aircraft that is fast and maneuverable has more firing opportunities. This is due, not only to the expanded launch envelope, but to the fact that a faster aircraft will overtake more of the slow movers in the same way that the fastest car on the autobahn will encounter more cars than the automobile moving at the average traffic speed. Figures 42 and 43 show two cases; one with the blue aircraft at twice the speed of the red and the other with the blue aircraft at half the speed of the red aircraft. In the first case the blue aircraft has three firing opportunities and is not fired upon. In the latter case the blue aircraft is fired on twice and does not fire on any opponent. In the scenario of chaotic combat, the speed advantage yields more firing opportunities.

In head-on engagements, speed can also have a detrimental effect. Figure 44 illustrates this point. Two head-on intercept situations are shown here; one is equal speeds for opposing aircraft (upper left) the other is with blue at a higher speed than red. In both cases the aircraft continue their head-on attack until missile impact. In the former case, the impact is simultaneous. In the latter case the red missile impacted before the blue missile. The blue aircraft literally flew into the red missile. Most long range missile guidance systems require that the aircraft continue to close on its target after the missile has been launched.

The disadvantage of the engagement kinematics with a high speed aircraft can be mitigated to some extent by supersonic maneuverability. The analysis of the use of maneuverability at supersonic speed and the design implications are shown in Figure 45. The basic tactic is to maneuver away from the attacking aircraft as much as possible without losing the ability to track and retain speed for a reattack. What one tries to achieve is the maximum F-Pole which is the separation distance between the aircraft at the time of blue missile impact. Figure 46 illustrates the effect that maneuver has on increasing the F-Pole. Maximizing the F-Pole increases the probability of killing the target before the guidance in the threat missile "goes active." When the missile guidance goes active, it no longer depends on the launch aircraft for any kind of assistance and it will kill the target irrespective of the existence of the launch aircraft. F-Pole is plotted in Figure 47 for increasing speed and increasing normal load factor. Note that F-Pole always increases with increasing load factor but some threshold must be passed before the F-Pole begins to increase with speed. All of this must be tempered with the ability to keep the target in the sensor field of view so that blue does not lose its own kill capability. It should be obvious that F-Pole can also be increased by slowing down. Although reattack capability and the ability to disengage may be lost by slowing down, it is better than getting killed.

A hypothetical supersonic maneuvering engagement is illustrated in Figure 48. In this case both red and blue initiate a maneuver after firing their missiles, both initial shots miss. Blue, however, with its speed advantage, can initiate a successful reattack. The result of this situation is that blue survives and red is killed as a result of the reattack.

With regard to the requirement for speed, analysis results are still inconclusive. When combined with supersonic maneuverability, speed offers the advantage of an increased number of favorable encounters, increased missile launch envelopes, the ability to disengage and a larger defended area. On the negative side is the earlier intercept of the threat aircraft in head-on engagements where the launch aircraft are restricted by the need to illuminate the target. Overall, sustained supersonic speed capability is likely to be a requirement for future fighter aircraft.

In addition to supersonic speed and maneuverability, there is a requirement for control of radar, infrared and visual signatures. This obviously contributes to the ability to see without being seen. Figure 49 illustrates this point. Signature reduction reduces the BVR launch envelope because BVR missiles are dependant on return from the threat aircraft for launch, guidance and fusing. The most favorable situation is illustrated in Figure 50. If the blue missile can impact the target before the red aircraft detects the blue aircraft, red has no probability of killing blue. This, of course, means that the RCS of the blue aircraft must be low enough that the threat radar cannot detect it with its acquisition/track radar at the time of impact and that blue must have a missile of sufficient range so that this can be achieved.

Figure 51 shows the results of many 4 versus 4 engagement simulations. These tend to confirm what one would expect, that is, increasing speed, maneuverability and reduced signature, when combined, result in higher exchange ratios in BVR combat than do any one of the three by themselves. It also shows the advantage of reduced signature and maneuverability can be lost if the speed advantage is not maintained.

Air-to-Surface Requirements

The role of attacking ground targets may seem to be a contradiction of terms when addressing the subject of fighter requirements. There are sound reasons for including the ground attack role as part of a discussion of fighter requirement, however. The main reason is that aircraft that are designed as air superiority fighters may end up having, as either their primary or secondary role, that of ground attack. A fighter that has no capability to perform air-to-surface missions is of less value than an aircraft that can perform both. The flexibility that the "swing" capability offers is that the fighter force can be allocated to ground attack roles as the nature of the battle changes. Analysis indicates that this has an important effect on the outcome when one looks at the total campaign. It is necessary to look at the

whole campaign to see this effect. Models that simulate only the air combat capability cannot adequately account for the value of a fighter with multiple role capability.

The issues which dominate the specification of air-to-surface requirements are shown in Figure 52. These issues do not really change with time, technology or class of aircraft. The problem does get worse with time, however. At the top of the list is survivability. Survivability dominates all of the other issues because it has such a large impact on the others. The target acquisition and target kill functions are complicated enormously by having to fly either low and fast or high and fast to enhance the survivability. Range and payload are also both compromised in the interest of survivability. Higher speed, lower signature and increases in countermeasures all eat away at range and payload. Nevertheless, without the capability to find and hit targets, or without sufficient weapons to inflict relevant damage, the most survivable aircraft is of no value.

Figure 53 shows the lethal radius of surface-to-air missiles (SAM) defenses against a subsonic aircraft penetrating a highly defended area in Europe. It is clear from this figure that there are no sanctuaries for an aircraft penetrating this zone regardless of the penetration altitude. As the altitude is increased, however, the defenses are less dense. The two regions of primary interest for penetration of defenses are shown in Figure 54. The supersonic high altitude region has the advantage of fewer SAM defenses but has the inherent problem of hitting targets. There are currently no air-to-surface weapons that are effective from the high and fast flight regime. A number of research and development efforts have been undertaken to remedy this situation, but, even for advanced weapons, there are significant problems in killing many targets of interest. Figure 54 also shows a thermal cost discontinuity at approximately Mach 2.5. At this point, material and fabrication costs for both the airframe and engine increase markedly.

Analysis indicates that supersonic high altitude penetration does have its benefits in terms of reducing effective SAM envelope. The percentage of SAMs that are effective at high altitude is substantially reduced and the area in which the aircraft is vulnerable to attack by SAMs is reduced by the speed because the exposure time is shorter. The combined effects of speed and altitude are graphically displayed in Figure 55. When combined, these two effects make the high altitude region the flight corridor that is least vulnerable to successful attack by SAMs.

Figure 56 compares the targets killed from high and low altitude penetrating corridors over a 30 day campaign. Two curves are shown for the low altitude corridor; one with terrain masking and penetration aids and the other without. It is clear from this analysis that, without terrain masking and penetration aids, low altitude penetration is not effective. Terrain masking is available only in areas that are hilly or mountainous. Over flat terrain the survivability of aircraft penetrating at low altitude is going to be reduced over what can be achieved with terrain following flight in rough terrain.

Terrain masking is a two edge sword, however. What protects an aircraft from the threat prevents targets from being seen from the aircraft. The probability of target acquisition over moderately rough terrain from an aircraft of traveling at Mach 0.9 is illustrated in Figure 57. Note that at an altitude of 200 ft the probability of acquisition of the target is 0.05, that is, only one of twenty targets will even be acquired. Even fewer targets will actually be attacked and killed. It is apparent that this is an unacceptable mode of operation. Even if the defenses never killed a single aircraft, they would have been completely effective because they forced the aircraft to fly where it cannot fight.

The target acquisition problem is also complicated by the environment. Figure 58 makes this point. Even without battlefield smoke, visual detection can only be relied upon for target detection about 12% of the time in winter. Infrared, because of its capability to detect targets at night and through light haze, allows one to detect targets 43% of the time. Radar, being nearly insensitive to both weather and darkness, increases the acquisition time to nearly 100%. There is keen interest in IR and radar acquisition systems for this reason.

All of this paints a rather bleak picture of the air-to-surface mission for fighter aircraft. Even when the effects of signature control, speed, countermeasures and vulnerability reduction are combined the air-to-surface role probability cannot be effectively accomplished without the support of other systems for defense suppression, standoff jamming, target acquisition, navigation and target identification. All of this overhead detracts from the overall cost effectiveness of airpower and adds many more elements for potential enemy attack.

Sortie Generation

The topic of sortie generation relates to the number of sorties which can be produced daily by an aircraft, squadron or wing. Most of what has been said in the previous discussion has been concerned with the ability of aircraft to kill targets. The ability of the aircraft to get off the ground in a condition that permits it to perform its mission is also a primary factor in the overall effectiveness of the fighter. A fine and sophisticated machine that can kill anything within miles but spends all of its time in the hanger with master mechanics repairing its fine sophisticated equipment is of no value. Neither is an aircraft which functions wonderfully until the first bomb hits its runway. These are some of the many concerns which currently have much influence on fighter requirements. There are many proponents of the view that we have been only concerned with the performance of our fighters and too little concerned with the logistics, maintainability and other design factors that contribute to sortie generation.

By itself the number of sorties produced per day by an aircraft does not mean much. One can read accounts of World War II Stuka pilots in very adverse conditions producing over 10 sorties per day. These were obviously very short missions with very little armament. A modern aircraft that is going to be on a mission two or more hours with several tons of payload is not going to produce ten missions per day. On short missions, AV-8's and A-10's can still produce sorties at this rate during a surge period. Sustained rates are much lower for longer range fighter aircraft, however.

The sortie generation issues of current interest are listed in Figure 59. Sortie generation spans a broad spectrum of concerns. At the top of the list is the desire to minimize the time spent in maintenance. Maintenance not only affects sortie generation but all of the logistics associated with the aircraft. If the statistics can be believed, steady progress has been made in recent years in increasing the mean time between failures in spite of the increase in sophistication of fighters. Figure 60 shows one plot of statistical data of several fighters. Current fighters show MTBFs exceeding the time of a single mission. Part of this increase can be attributed to the increase in mean time between failure (MTBF) of the radar system as shown in Figure 61. This curve shows the MTBF prior to 1960 to be zero. Whether this is fact or not is questionable, however, it does confirm the stories that the MTBF for early radars was shorter than the time between the beginning of the taxi and the time that the wheels were off the runway. Current avionics has a sufficiently high MTBF, that improvements in avionics will no longer have a major effect on the MTBF of the aircraft.

Statistics on MTBF and mean time to repair (MTTR) tell only part of the story. Missions can be flown, and will be flown, in wartime situations without all systems in perfect operating condition. Surge sortie rates will be much higher than the sortie generation potential shown in Figure 62. However, for sustained sortie generation the data indicates that current fighter can produce between two (2) and three (3) sorties per day. The requirements for future fighters are likely to be much higher than this. How these are to be achieved is currently a topic of study.

Another important factor in the ability to generate sorties is the turn around time, that is, the time to rearm and service the aircraft when no repairs are required. Many approaches have been proposed to speed the process of arming an aircraft. Conformal pellets, with all of the weapons on a single pallet, is an example of a technique of speeding up the process. The problem is more complicated where the base has been contaminated with chemical or biological agents. A large reduction in time to perform all operations occurs when such contamination is present. Obviously, this has an adverse effect on the sortie generation. Future fighters will be required to operate in such environments. The aircraft must include the necessary provisions to protect the pilot and internal equipment. Provisions for servicing and rearming must be such that they can be performed with crews in protective gear.

The landing and takeoff distance will determine whether fighter aircraft can continue to operate after an air base attack. Figure 63 shows the results of an Israeli attack on an Egyptian air base during the Yom Kippur war. All of the runways are severely cratered. To continue operation the aircraft must be able to operate between the craters. The shorter segment of runway for landing and takeoff required, the more insensitive the fighters will be to runway cratering. This effect is illustrated in Figure 64.

A final issue with regard to sortie generation is the ability to operate from rough and soft fields. For modern fighters this capability has been completely lost. Nor is there any thought of returning to the days when a fighter could operate from a muddy farm field. There will be a requirement for fighters to operate from cratered runways that have been repaired and to taxi from shelters across unpaved surfaces to the portion of the runway that has been repaired or survived the attack. This may not seem on the surface to be much of a compromise in the design but it does have a considerable influence on the design of the landing gear and the basic size of the aircraft itself.

Summary of Requirements

Emphasis in air combat capability is divided between focus on CIC and BVR combat. For close-in-combat the focus is on the classic maneuverability parameters; P , sustained and instantaneous turn rate and acceleration. For BVR combat the technology focus is on the weapon and fire control system. The vehicle characteristics which are likely to be of most interest for BVR are sustained supersonic cruise with maneuverability, and control of the signatures. Future fighter will probably have, as a secondary role, the attack of ground targets. Survivability dominates the ground attack mission. High speed, high altitude and low altitude terrain following attack are the penetration profiles of interest in high threat areas but acceptable survivability and target attack will not be achieved without supporting systems. Sortie generation from a damaged and contaminated airfield is needed to achieve productivity in a wartime situation. High reliability and the ability to turn aircraft around rapidly in a chemical/biological environment is necessary. In addition, STOL or VTOL with soft field capability is needed to operate from damaged airfields.

2.4 Effectiveness Analysis

No discussion of requirements would be complete without mention of effectiveness analysis. The amount of data that is available for modern fighters from an actual warfare is very sparse. Furthermore, the next generation of fighter aircraft will not be operational for ten or more years. The actual threats will change during the 30 or more years of development and operation. It is necessary, therefore, to devise methods for assessing the combat effectiveness of conceptual fighter aircraft designs.

There are many methods of assessing the effectiveness of advanced aircraft. These range from digital simulation models to operational evaluation tests. In the early phases of a program, before requirements are defined, the models must be at the same level as the conceptual design methods. The characteristics of the conceptual designs must feed these analysis tools and the turn around time on the data must be on the order of days or weeks.

The majority of analysis models that are used to assess conceptual fighter aircraft designs fall into the general categories shown in Figure 65. The digital close-in-combat models were originally developed for one-on-one combat. They have been expanded in recent years to 4 versus 4 models. The flight path of the aircraft are based on equations of motion. Aircraft characteristics are predicted from the conceptual designs. The tactics of the engagement are input and fixed at the beginning of program execution and no feedback from a pilot is available as the simulation progresses, as would be the case for manned simulations.

The BVR combat simulators are similar to the CIC simulators except that the BVR usually include a more detailed missile flyout trajectory as part of the simulation. ECM, IFF and sensors are emphasized heavily. For the BVR case the missile flyout trajectory is modeled with more fidelity because the BVR maneuvers are constrained by the ability to keep the target in the field of view until the BVR missile locks on the target. The constraints on the aircraft maneuvers due to the inability to lock on before launch at long range is a major factor in BVR effectiveness. Group strategies and tactics are included. The digital combat evaluation model illustrated in Figure 66 is an example of a BVR model that evolved from an earlier CIC model.

SAM flyout models such as the one illustrated in Figure 67 are sophisticated models that simulate the flight characteristics of the missile, the missile guidance system and the capabilities of the site acquisition and tracking system. Aircraft can be flown through these sites and their probability of survivability calculated. The AAA models are similar to the SAM models except that the projectiles are not guided. None of these models include the human factors in the operation of the defense sites.

Sortie generation models such as the one illustrated in Figure 68 simulate the operations performed at the base from the time the aircraft lands until the time it takes off. Allowances are made for servicing and rearming cues. Air base damage effects include the cratering of runways, repair times associated with craters, slow downs due to chemical or biological attacks and all other operations that determine how long it takes to turn an aircraft around in a wartime situation.

Finally, there are campaign models. Figure 69 shows the air operations that are included in a campaign evaluation. A campaign evaluation, to be complete, should also include the ground forces. Even conceptual level campaign models are very complex and time consuming to run. There are certain fundamental questions that are not answered unless one goes to this level, however. The priorities of the roles of air power is an example of the type of questions that are only examined at this level. For a fighter aircraft the emphasis on the air-to-air role versus the air-to-surface role is a campaign level evaluation.

No one seriously expects effectiveness models to fully simulate the actual combat situation. Still, they are essential in developing requirements and prioritizing technologies. There must be some assessment of how well future fighters do in their assigned roles. The models help in this process, not by replacing judgement and common sense, but by providing an accounting mechanism for the essential ingredients in the combat environment and identifying the purpose of each requirement. It also provides insight into the fundamental problems by simulating each of the essential mission roles. It is this insight that provides the rationale for requirements and technology needs.

All of this may appear to be quite unscientific when compared with the refined design and analysis tools that have been developed by engineers and scientists. It is a fact of life, however, that judgements about what requirements are, in fact, desirable and how desirable these requirements actually are, is being evaluated with these models. Regardless of how much our design methods are perfected, if we select the wrong "desirable properties" then we will have fighter aircraft that are not doing what needs to be done to win wars. This is where the emphasis must be. We do not place the palace guards on the front lines of the battle and we do not wish to place elegant aircraft designs that do not provide the needed combat capability into the battle.



REQUIREMENTS DEVELOPMENT PROCESS

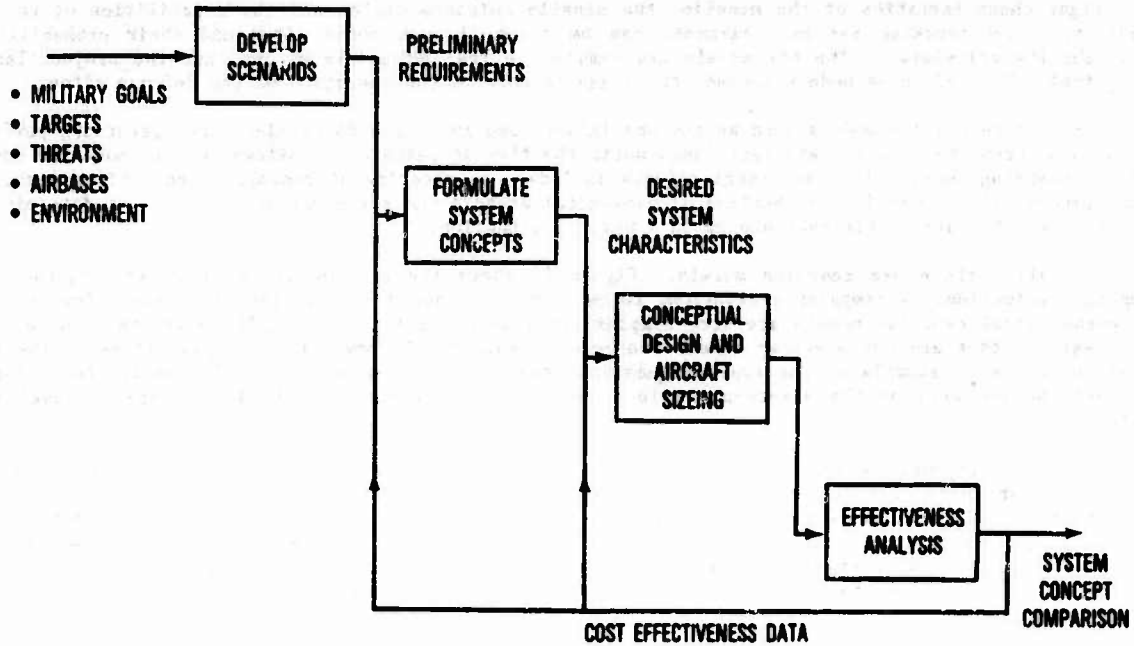
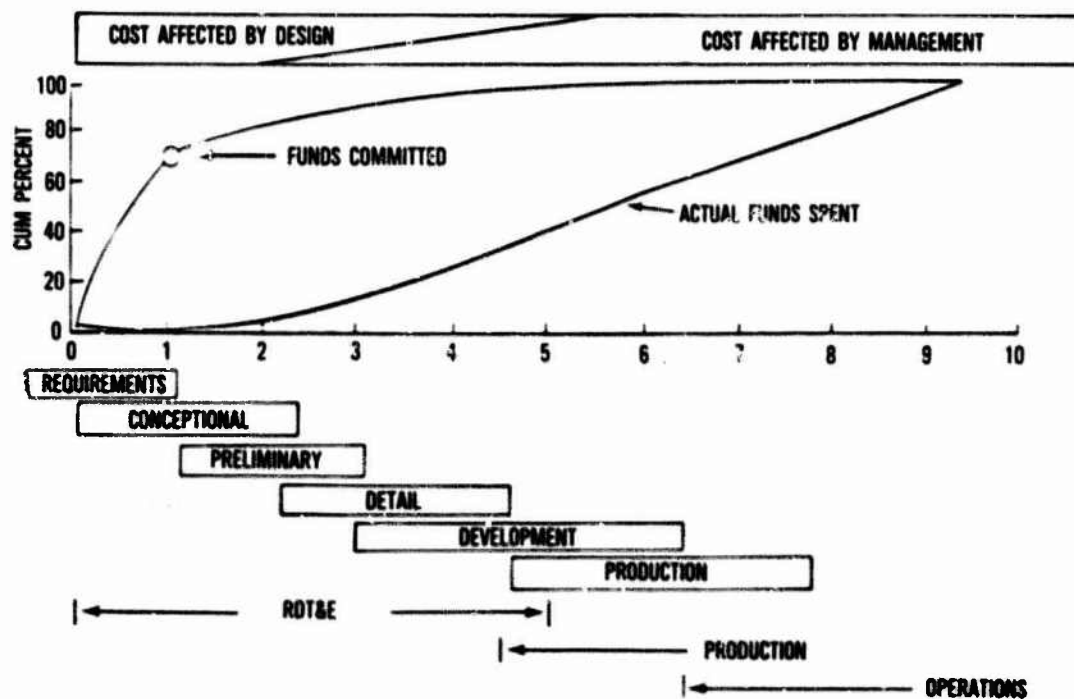


FIGURE 1



FUNDS ARE COMMITTED EARLY IN THE AIRCRAFT LIFE CYCLE



REF: LECTURE BY DR. L. NICOLA, JULY 14, 1930.

FIGURE 2

EXAMPLES OF AERONAUTICS FUNCTIONS
IN MODERN FIGHTER AIRCRAFT

**RELATIONSHIP OF CONCEPTUAL DESIGN
TO THE OVERALL DESIGN PROCESS**

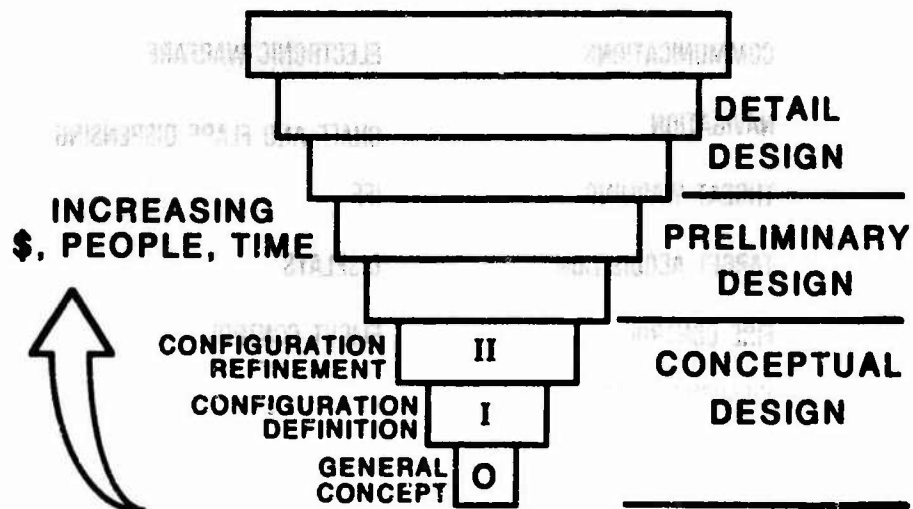


FIGURE 3



OVERALL CONCEPTUAL DESIGN PROCESS

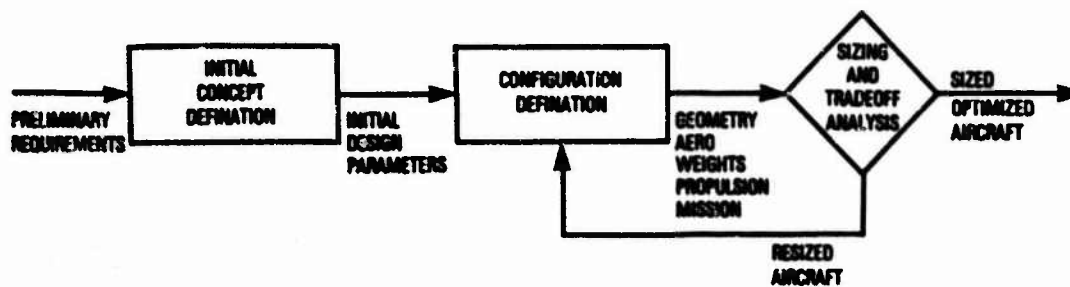


FIGURE 4



EXAMPLES OF AVIONICS FUNCTIONS IN MODERN FIGHTER AIRCRAFT

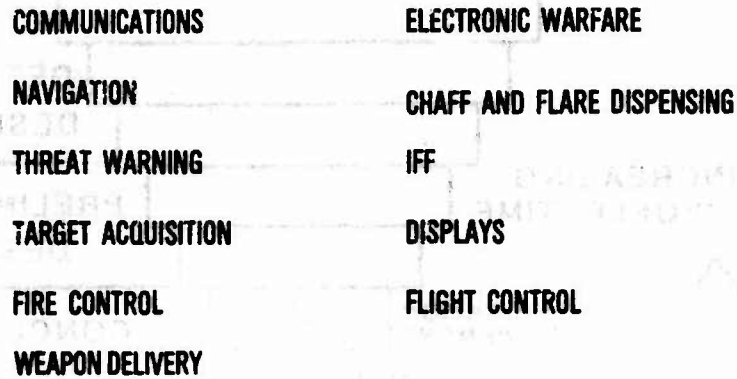


FIGURE 5



EXAMPLES OF INTEGRATION OF CONCEPTUAL WEAPONS

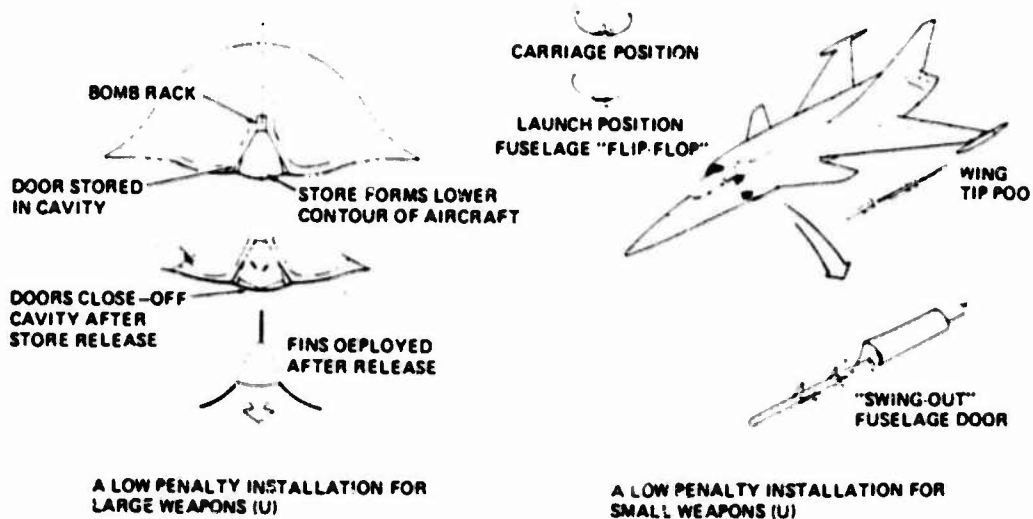


FIGURE 6



DESIGN ANALYSIS PERFORMED ON NEW CONFIGURATIONS



FIGURE 7



USES FOR AIRCRAFT SIZING

HELPS DEFINE REQUIREMENTS

PROVIDES A TOOL FOR ASSESSING TECHNOLOGIES

**PROVIDES AIRCRAFT CHARACTERISTICS FOR EFFECTIVENESS
ANALYSIS**

**DEFINES A STARTING CONFIGURATION FOR PRELIMINARY
DESIGN**

FIGURE 8



FUEL MATCH SIZING

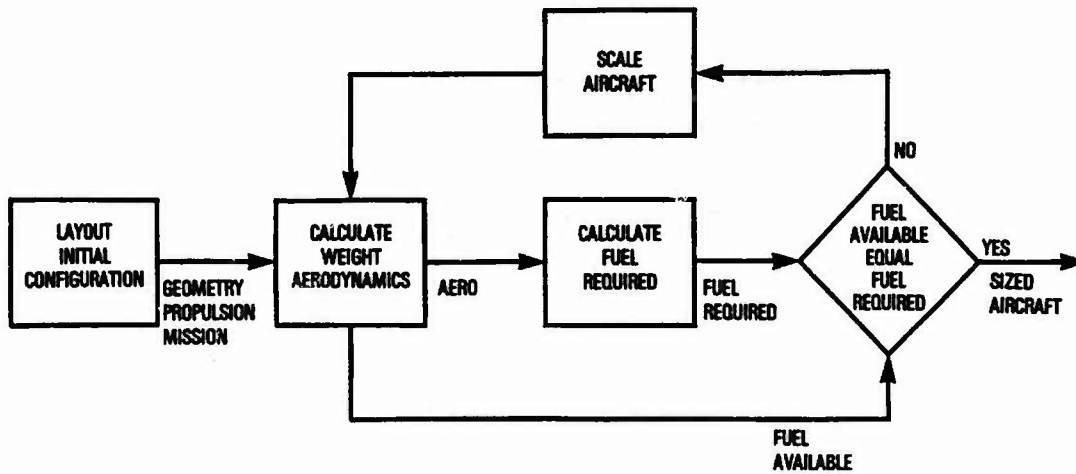


FIGURE 9



FUEL MATCH SIZING

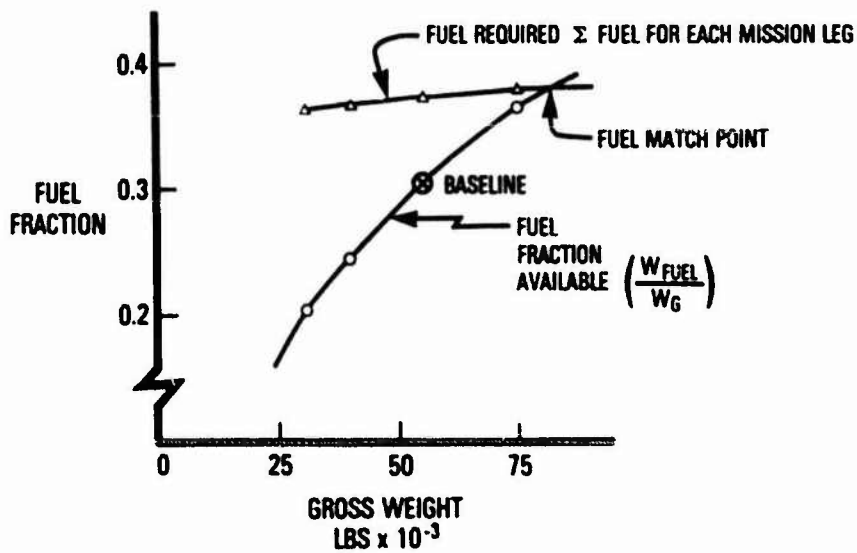


FIGURE 10



MISSION SENSITIVITIES

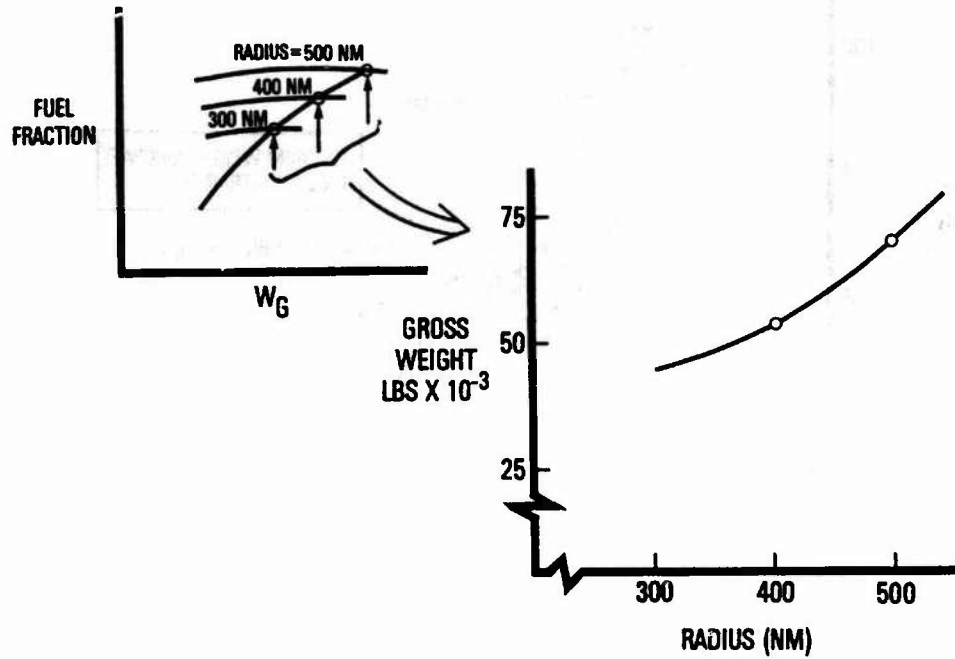


FIGURE 11



TRADEOFF ANALYSIS

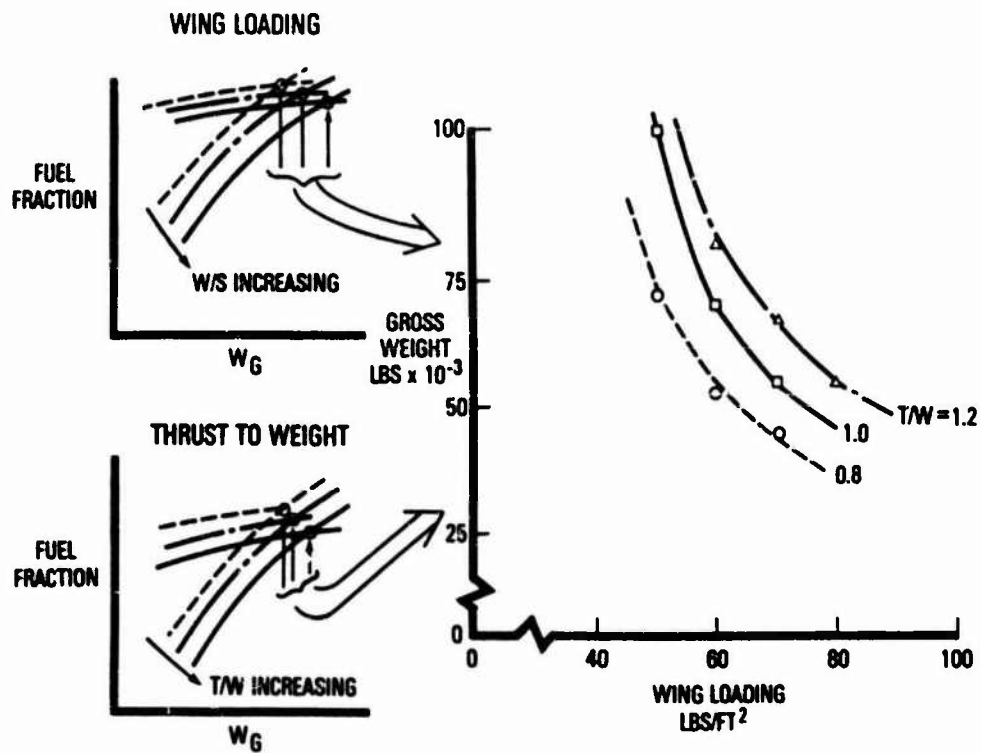
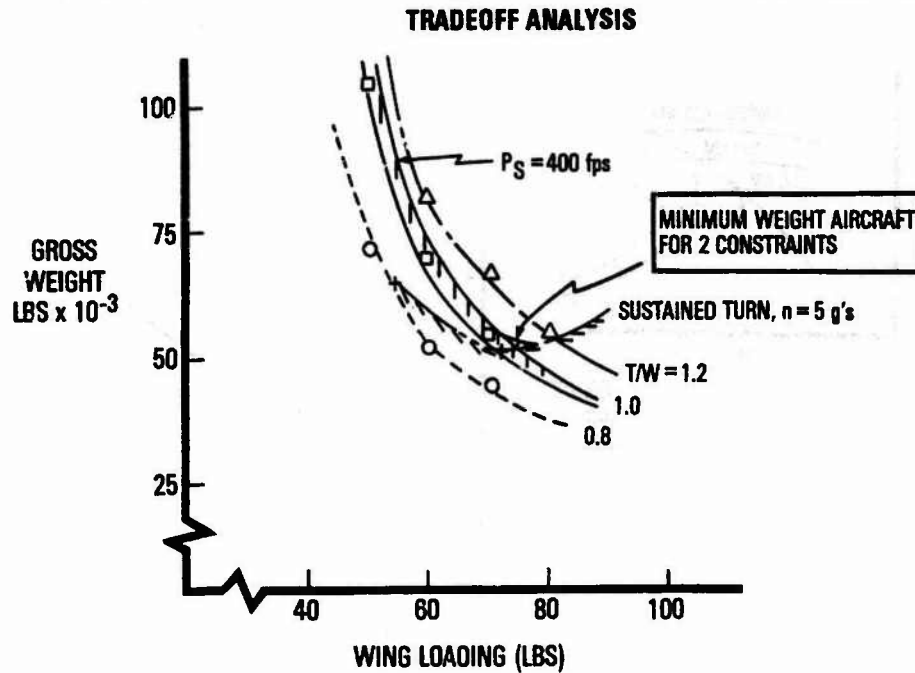


FIGURE 12



EFFECTS OF POINT PERFORMANCE CONSTRAINTS ON AIRCRAFT SIZE



EXAMPLES OF FIRST ORDER DESIGN PARAMETERS AFFECTING AIRCRAFT SIZING

ENGINE PARAMETERS

BYPASS RATIO
OVERALL PRESSURE RATIO
TURBINE INLET TEMPERATURE

BODY PARAMETERS

CROSS SECTION vs STATION
FINENESS RATIO

WING PARAMETER

AREA
SWEEP
THICKNESS
ASPECT RATIO

EMPANNAGE PARAMETERS

TAIL SIZE
TAIL ARM

OTHER

PAYLOAD PROVISIONS
AVIONICS WEIGHT/VOLUME
LANDING GEAR LOCATION/SIZE
STABILITY MARGIN

FIGURE 14



ASPECT RATIO-WING SWEEP TRADEOFF

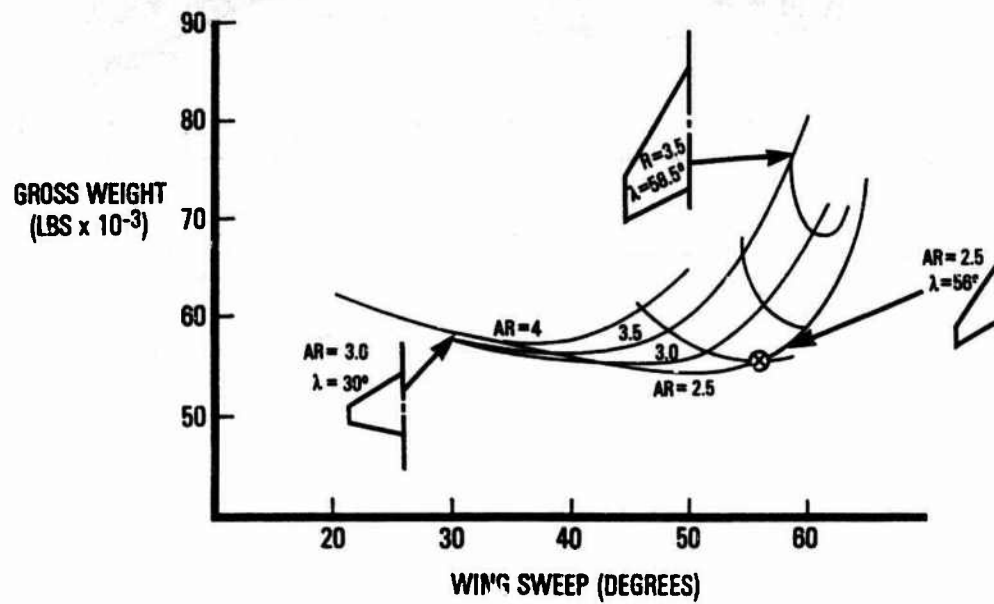


FIGURE 15

PREPARATION OF GRAPHICAL DATA BASE FOR ANALYSIS PURPOSES

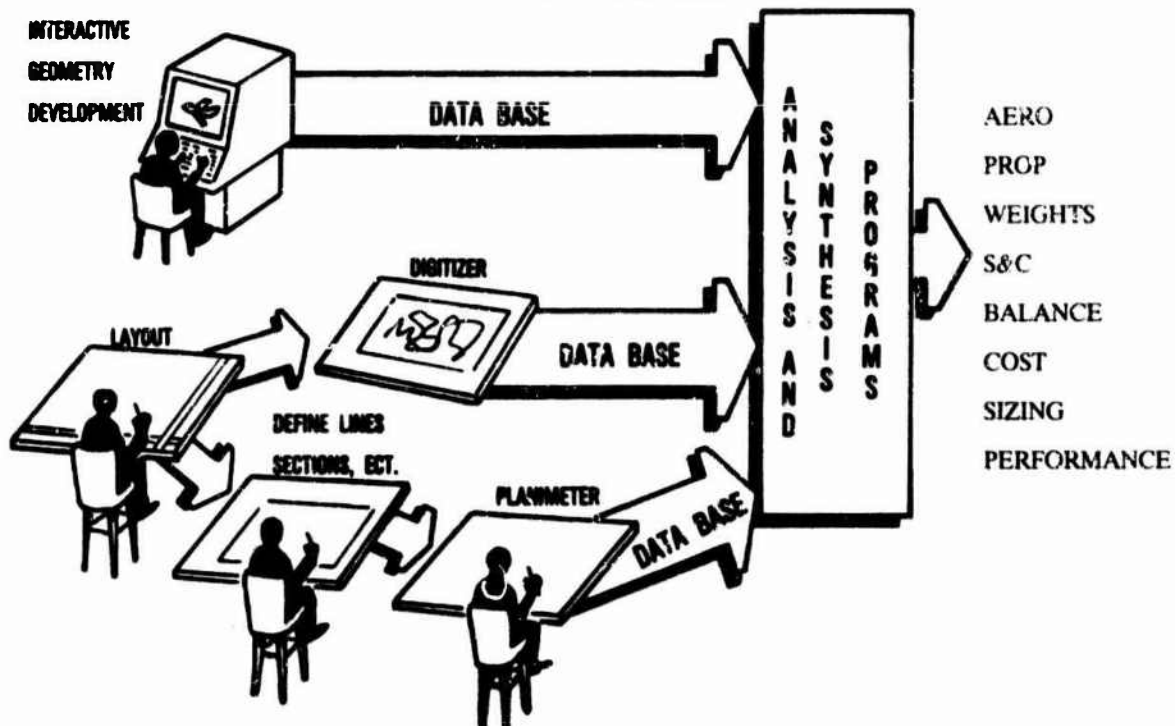


FIGURE 16

COMPUTER GENERATED AREA DISTRIBUTION

ASPECT RATIO-WING SWEEP TRADEOFF

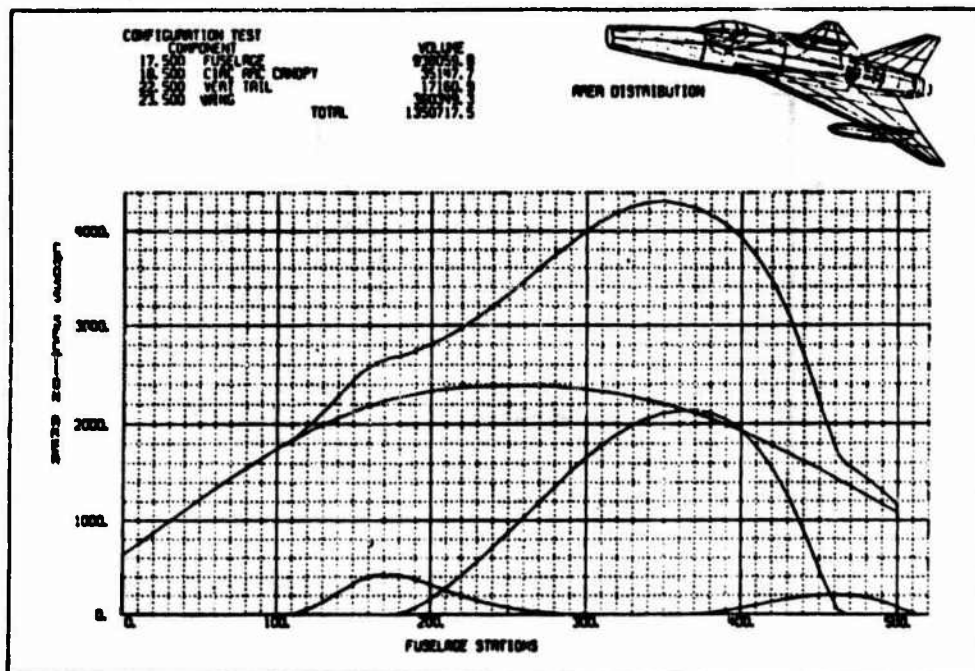


FIGURE 17

COMPUTER GENERATED WETTED SURFACE

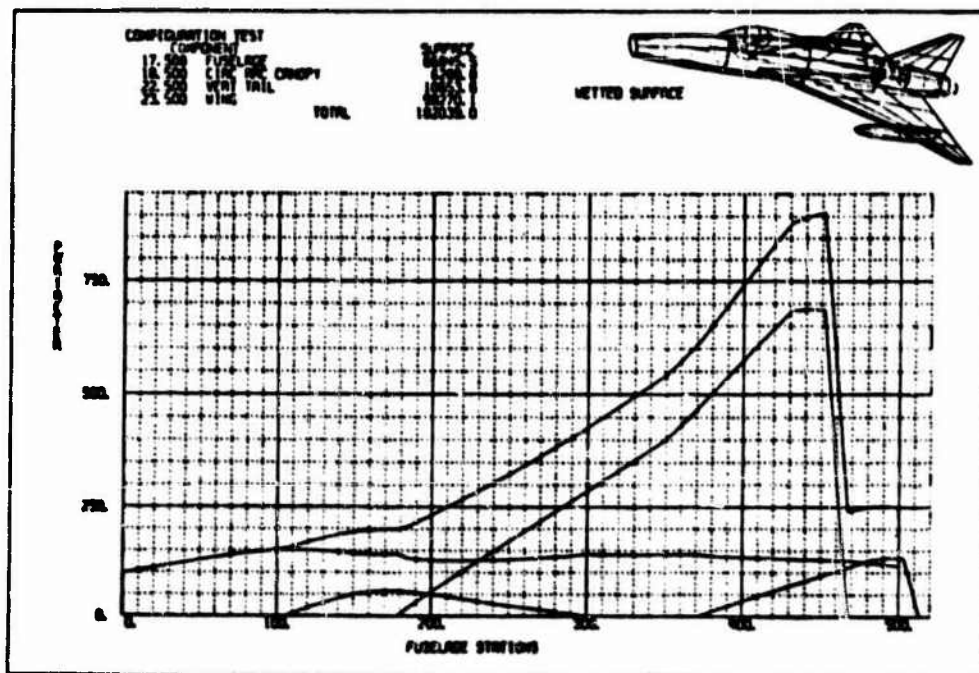


FIGURE 18

COMPUTER GENERATED WAVE DRAG ANALYSIS

SUPERSONIC MACH NUMBER (0 TO EXIT)

1.0

COMPUTATION TEST

17.000 FUSELAGE

10.000 CONE AND CANOPY

20.000 VERT TAIL

20.000 WING

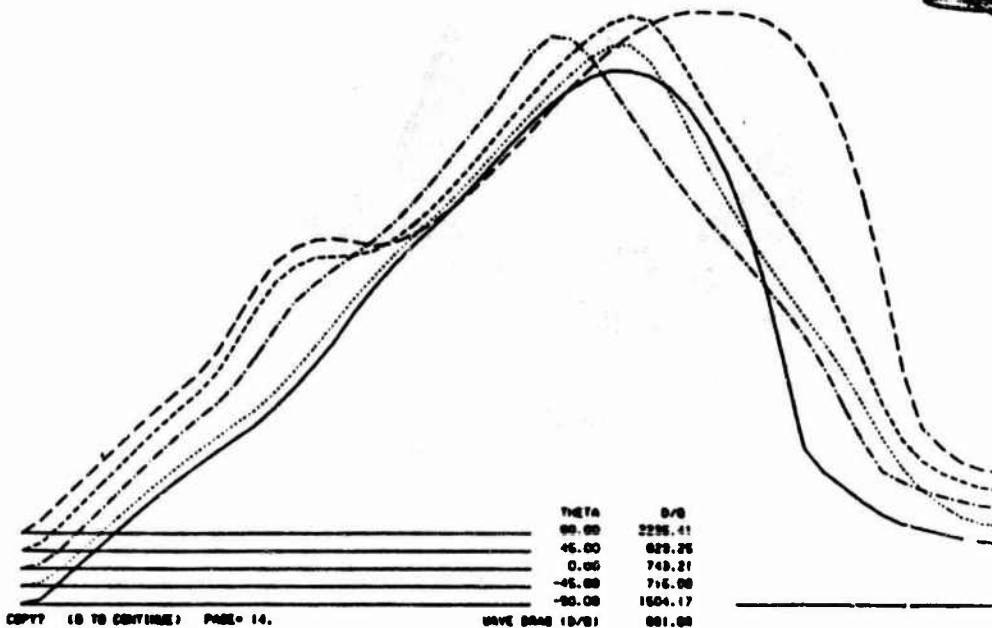


FIGURE 19



PHOTOGRAPH OF THE DISPLAY SCREEN



FIGURE 20



COMPUTER GENERATED WAVE DRAG ANALYSIS
PHOTOGRAPH OF THE DISPLAY SCREEN

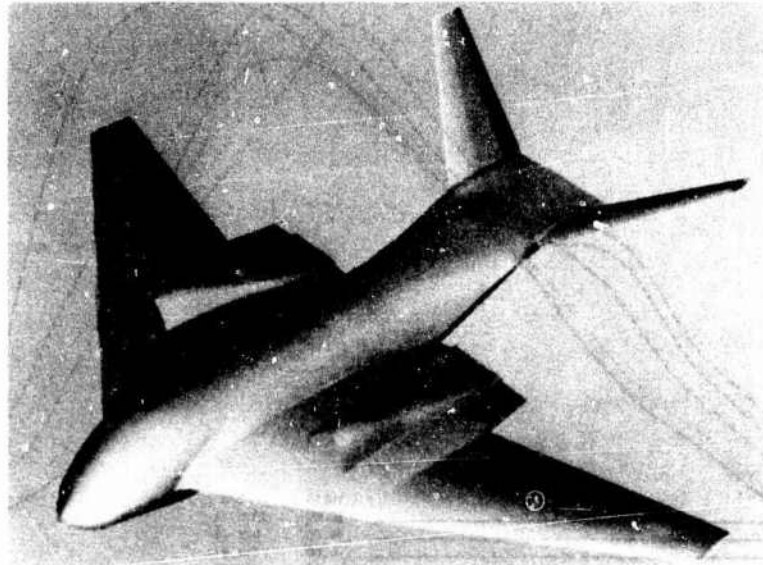


FIGURE 21



DISPLAY MODEL MADE FROM CAD FILE



FIGURE 22



EXAMPLE CONTENTS OF TYPICAL FIGHTER REQUIREMENTS

PERFORMANCE REQUIREMENTS

MISSION PROFILES (RANGE/SPEED/ALTITUDE/PAYLOAD)

MANEUVERABILITY (PS, TURN RATES, ACCELERATION)

LANDING AND TAKEOFF DISTANCES

OBSERVABLES (RADAR/IR SIGNATURES)

AVIONICS FUNCTIONS AND CAPABILITIES

SUSTAINABILITY

MEAN TIME BETWEEN FAILURES

MEAN TIME TO REPAIR

COST LIMITATION

ACQUISITION COSTS

LIFE CYCLE COSTS

FIGURE 23



PRINCIPLE ISSUES IN DEFINING FIGHTER REQUIREMENTS

CLOSE IN COMBAT

BEYOND VISUAL RANGE COMBAT

SORTIE GENERATION (SUSTAINABILITY)

AIR-TO-SURFACE

FIGURE 24



ONE-VRS-ONE CLOSE-IN-COMBAT SIMULATION

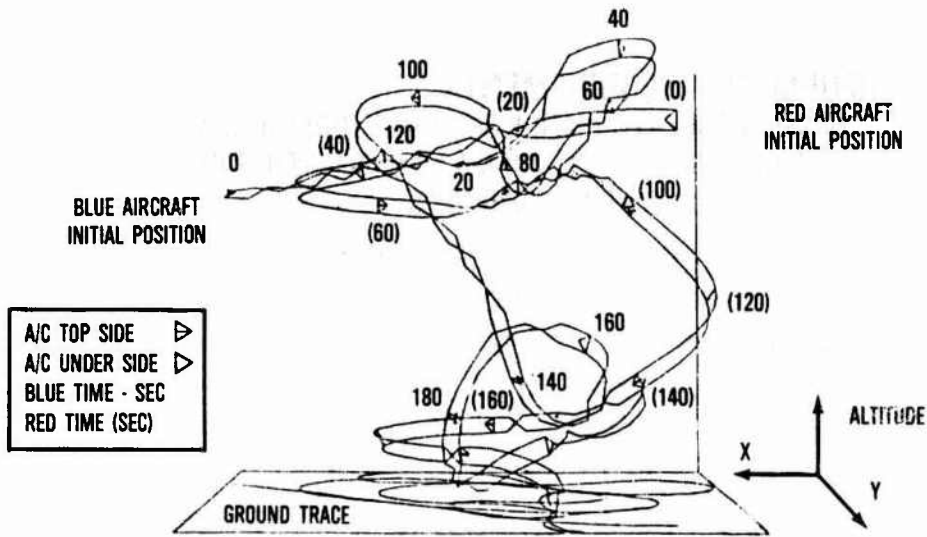


FIGURE 25



TYPICAL SPECIFIC EXCESS POWER PLOTS FOR FIGHTER AIRCRAFT

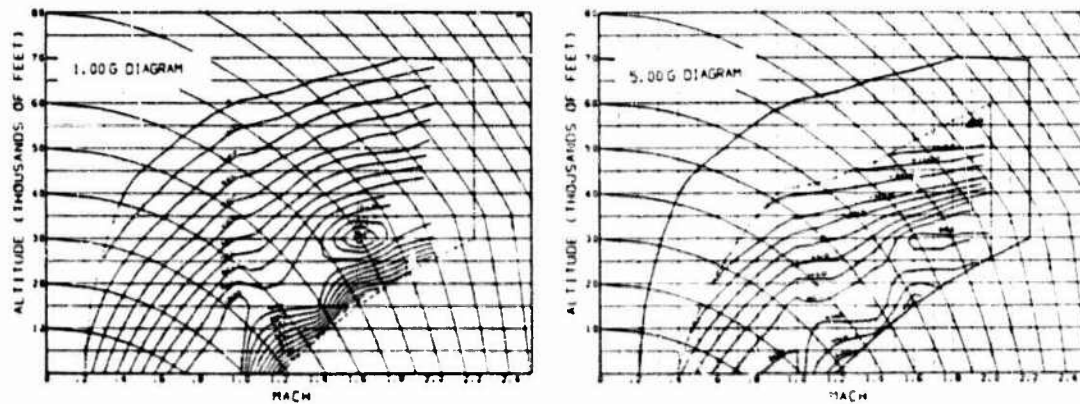


FIGURE 26



EFFECT OF INCREASING P_S REQUIREMENT

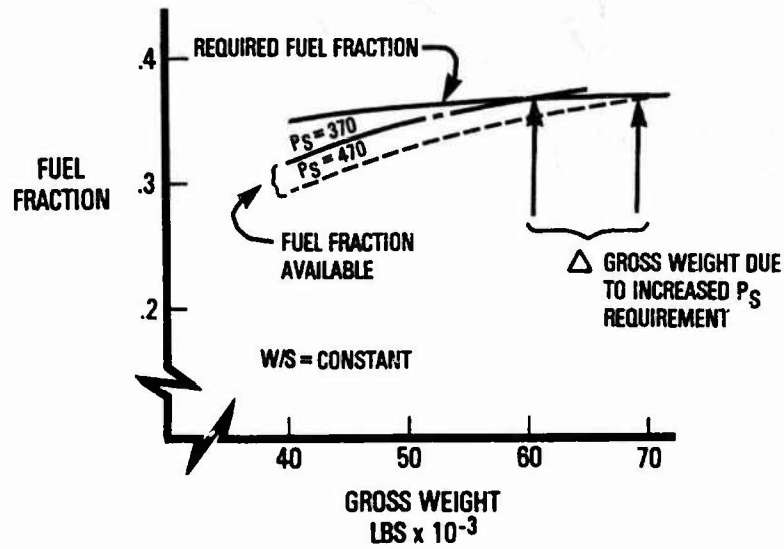


FIGURE 27



GROSS WEIGHT TRADEOFF ANALYSIS FOR CONSTANT MAXIMUM SUSTAINED RATE REQUIREMENT

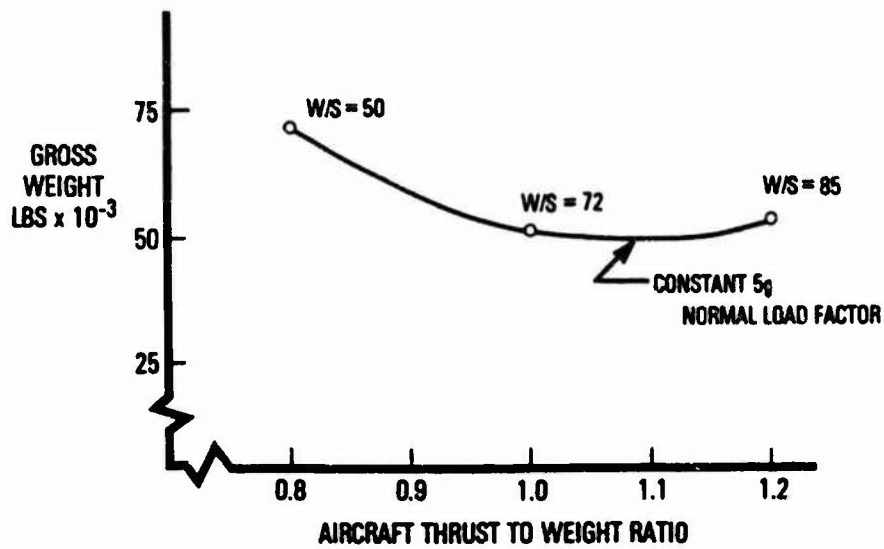


FIGURE 28



OPTIMUM W/S AND T/W FOR VARYING MAXIMUM SUSTAINED LOAD FACTOR REQUIREMENT

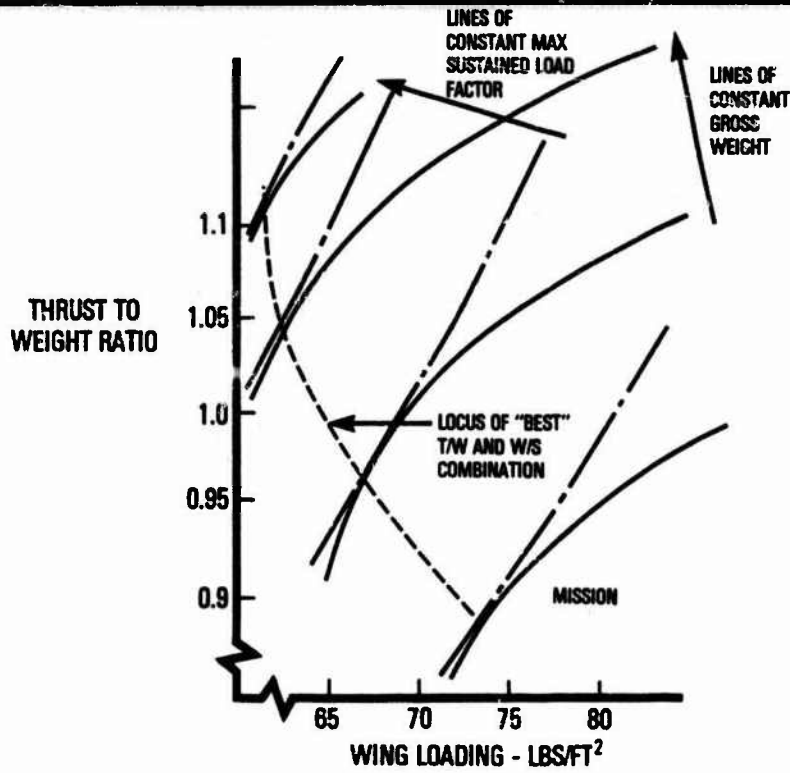


FIGURE 29



TYPICAL FIGHTER AVAILABLE NORMAL LOAD FACTOR

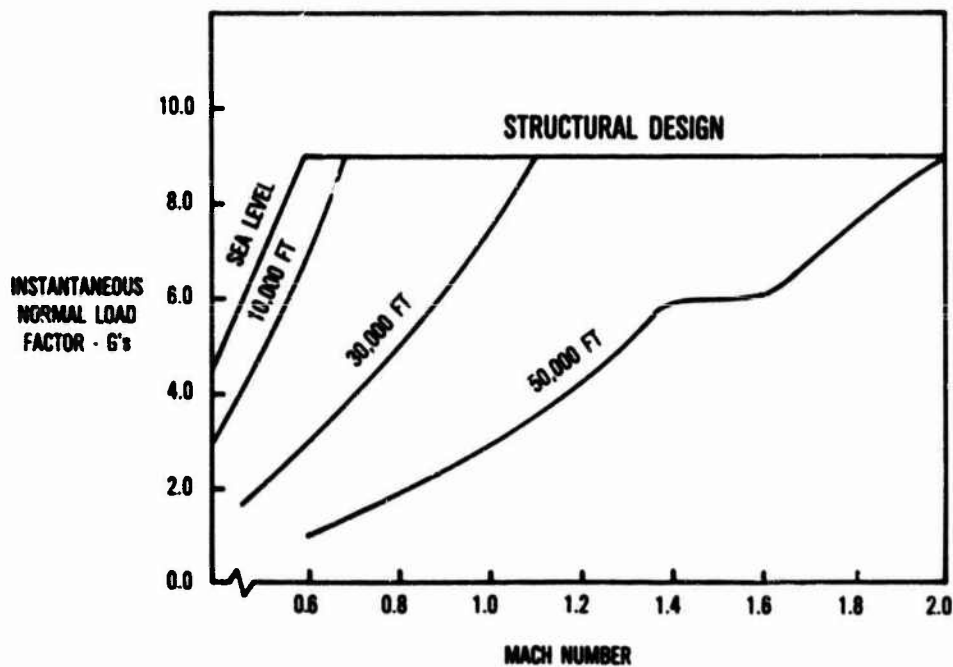


FIGURE 30



MANEUVERABILITY IS USEFUL IN OTHER THAN 1V1 COMBAT BUT LESS SO THAN FOR 1V1

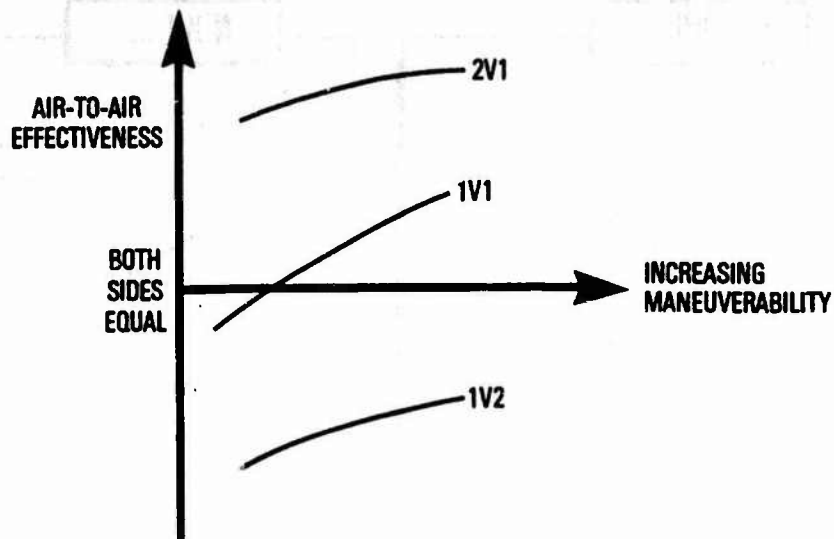


FIGURE 31



ALL ASPECT AND OFF BORESIGHT WEAPONS INCREASE FIRING OPPORTUNITIES

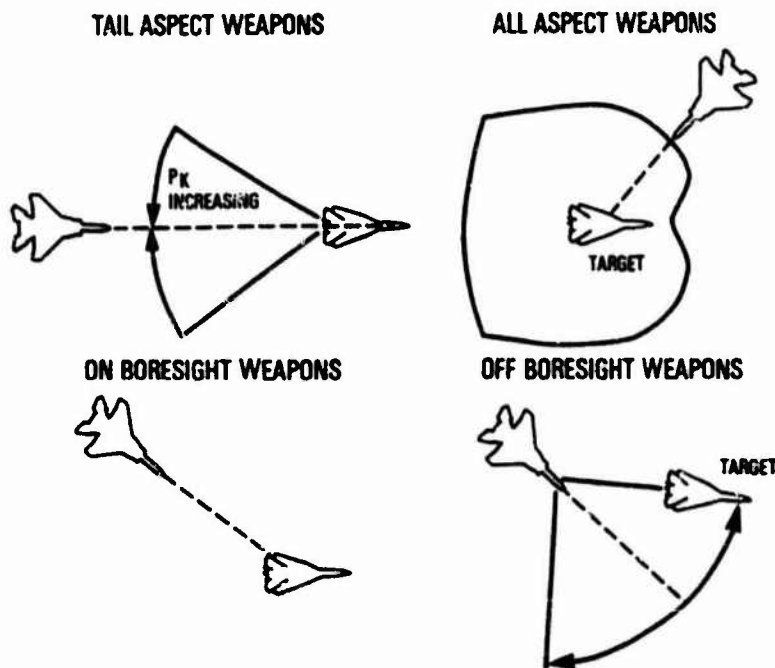


FIGURE 32



THE NATURE OF AIR COMBAT IS CHANGING

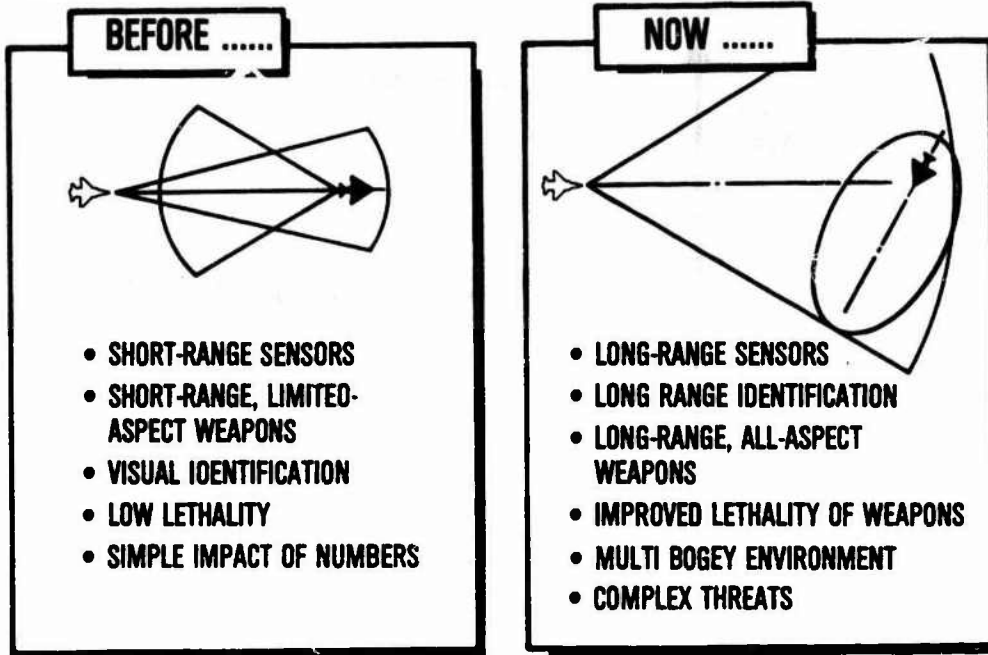
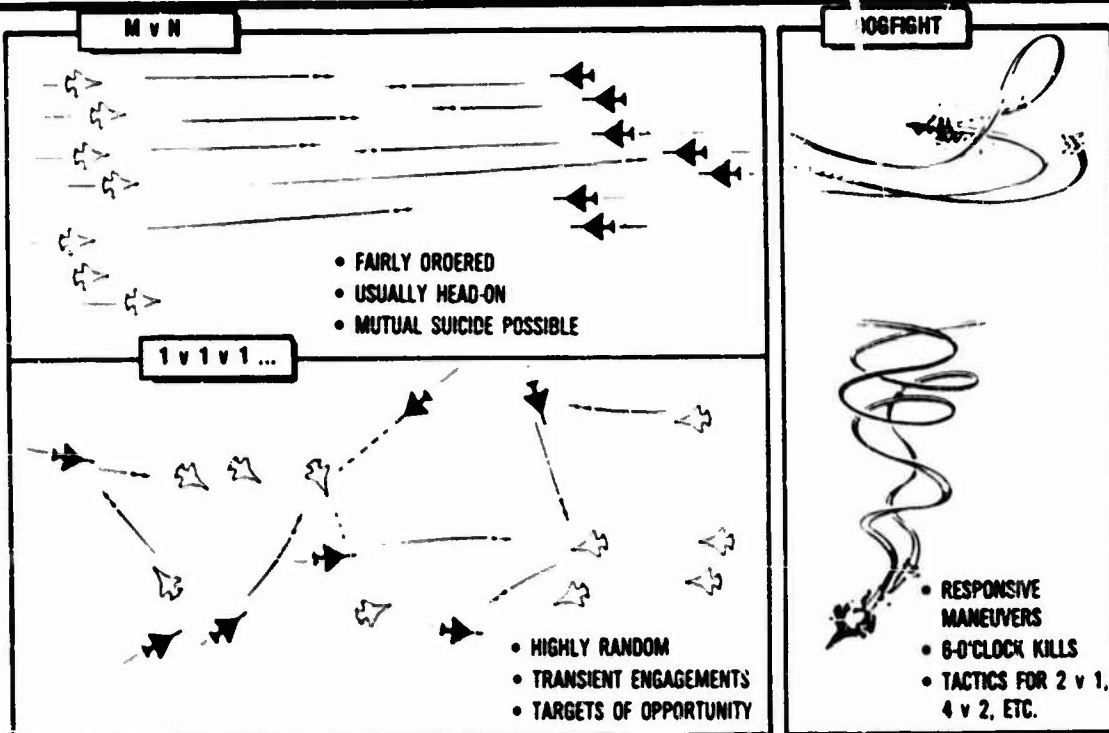


FIGURE 33



THERE ARE THREE KINDS OF AIR COMBAT ...



... EACH MAKES DIFFERENT DEMANDS ON THE AIRCRAFT / WEAPON SYSTEM

FIGURE 34



SIMULATION OF BVR COMBAT ENDING IN A DOGFIGHT

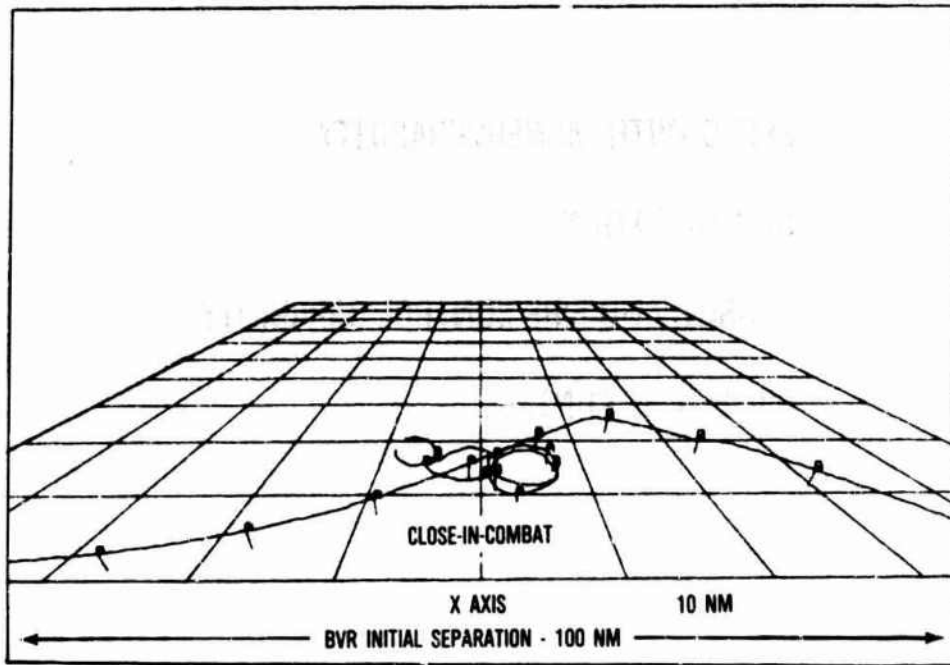


FIGURE 35

MISSILEER SYSTEM CONCEPT



FIGURE 36



PRIMARY BVR REQUIREMENTS ISSUES

SPEED WITH MANEUVERABILITY

IDENTIFICATION

MISSILE AND FIRE CONTROL CAPABILITY

SIGNATURE CONTROL

FIGURE 37



DEFENSIVE INTERCEPTS

A SPEED ADVANTAGE OVER ATTACK FORCE

- AREA DEFENDED INCREASES DRAMATICALLY
 - FEWER DEFENSIVE BASES NEEDED
- INTERCEPT BEFORE ATTACKER LAUNCHES AIR TO GROUND WEAPON

INCREASES THE PROBABILITY OF INTERCEPT BEFORE THE THREAT REACHES THE TARGET

- MISSILE LAUNCH ENVELOPE ENHANCED

FIGURE 38



SUPERSONIC PERSISTENCE OPENS THE AIR DEFENSE ENVELOPE

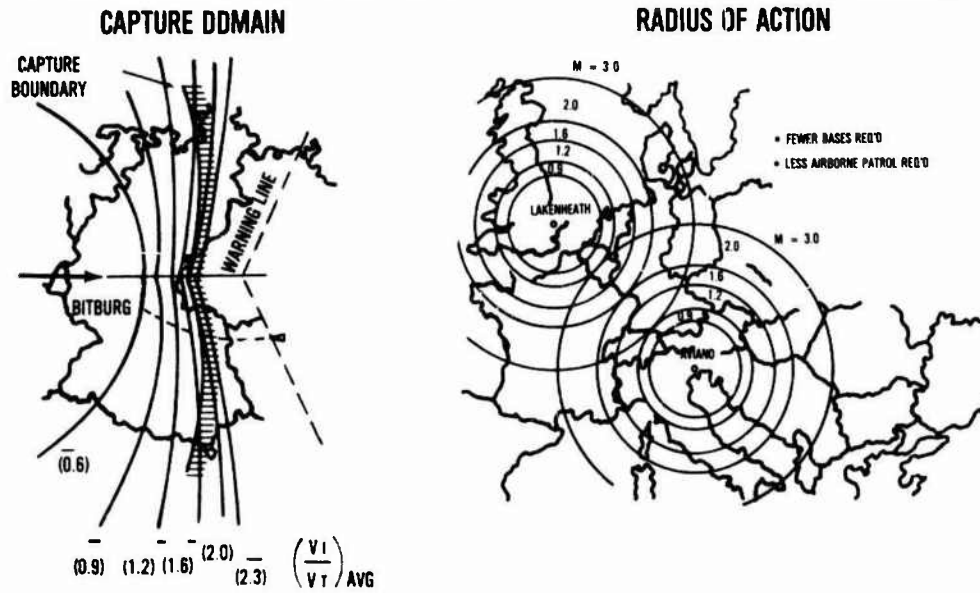


FIGURE 39



EFFECT OF SPEED ON TAIL CHASE ENGAGEMENT

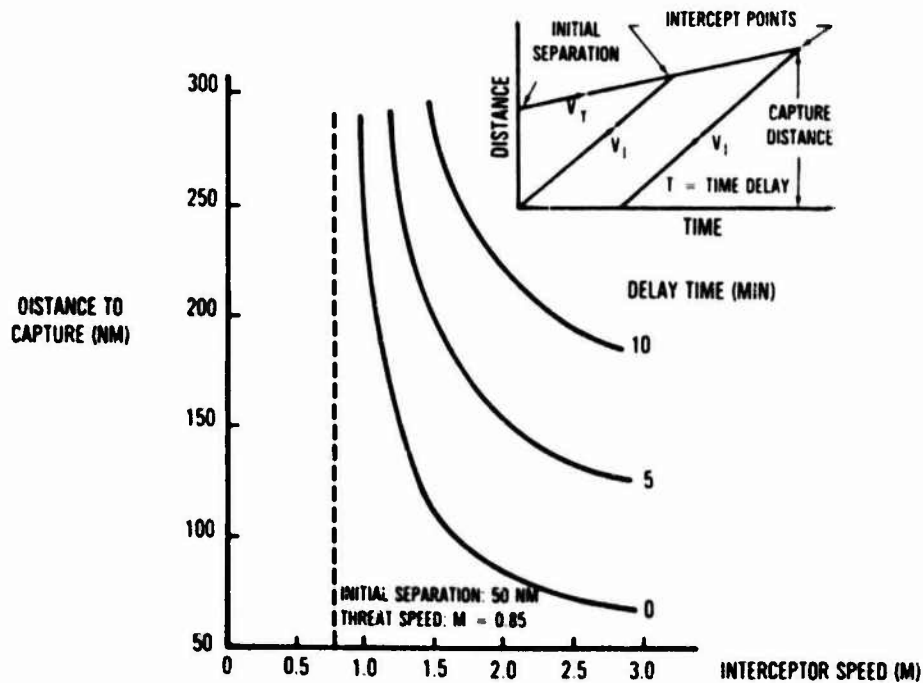
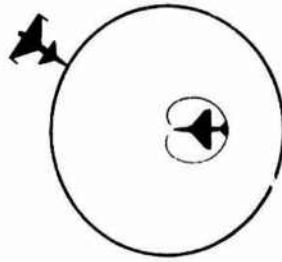


FIGURE 40



ADVANTAGE IN MISSILE LAUNCH ENVELOPE

BLUE ON RED



RELATIVE
LAUNCH
ENVELOPE
AREA

RED ON BLUE



BLUE ON RED
RED ON BLUE

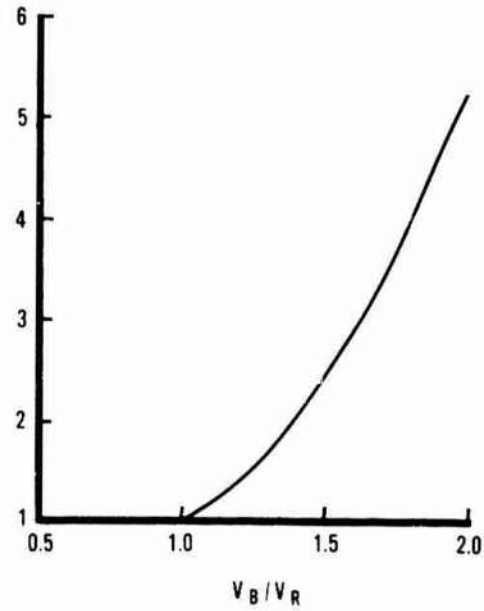


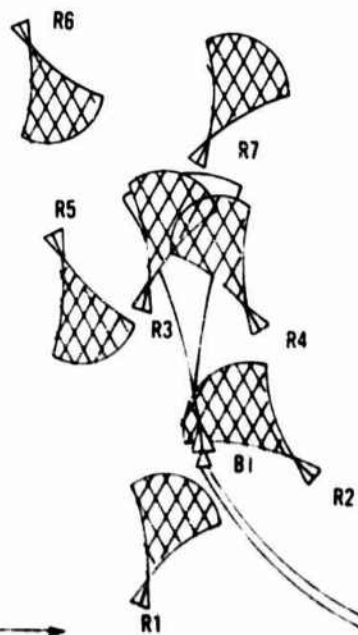
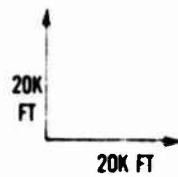
FIGURE 41



SLASHING BLOW-THRU ATTACK

40,000 FT
CO-ALTITUDE

BLUE
M = 2.2g
RED
M = 1.2g



TWENTY SECOND
CAPTURE
BOUNDARIES

FIGURE 42



SUBSONIC ATTACK ON SUPERSONIC THREATS

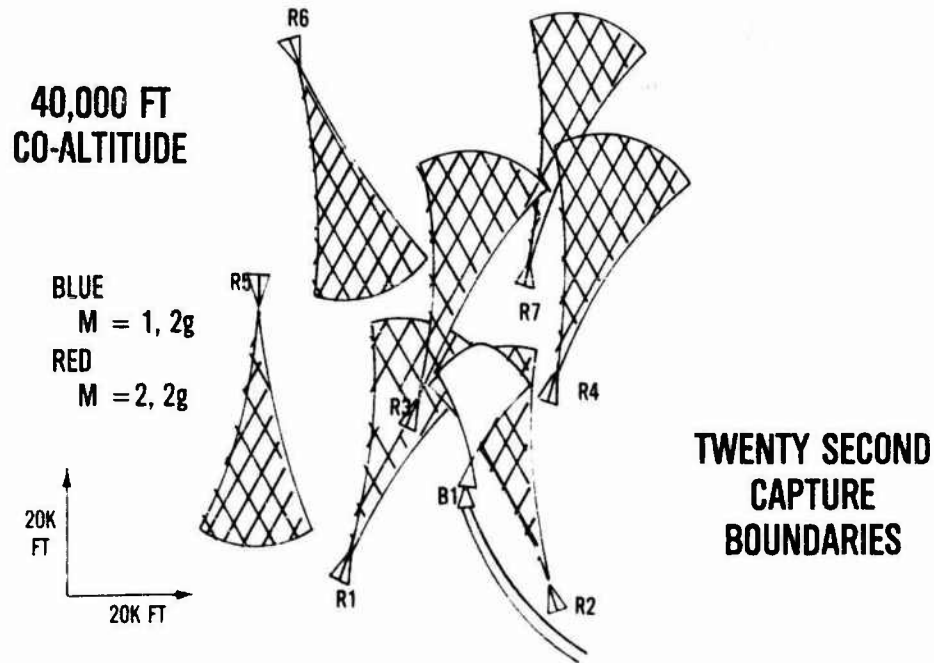
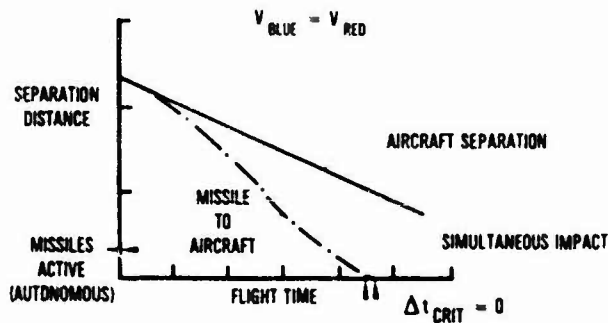


FIGURE 43



BVR MISSILE EXCHANGE TIMELINES

CO-ALTITUDE HEAD-ON NON-MANEUVERING ATTACK



- SIMULTANEOUS MISSILE LAUNCH
- EQUAL MISSILES
- NO EVASIVE TACTICS OR COUNTERMEASURES

RED MISSILE IMPACTS FIRST IF BLUE HAS A SPEED ADVANTAGE

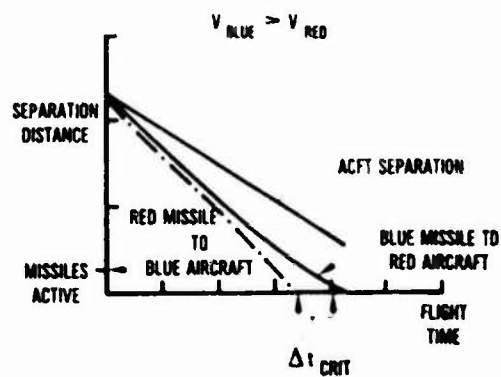


FIGURE 44



SUPERSONIC MANEUVER REQUIREMENTS

ANALYSIS

- EFFECTIVE USE OF SPEED REQUIRES AN ABILITY TO MANEUVER IN A MISSILE EXCHANGE ENGAGEMENT
 - THREAT MISSILE ENVELOPE REDUCED WITH MANEUVERING
 - COMBINATION OF SPEED AND MANEUVER CAN MAXIMIZE AIRCRAFT / MISSILE SEPARATION
 - TARGET RE-ATTACK OPTION AVAILABLE WITH MANEUVERING
- VERTICAL MANEUVERS ALSO HAVE A PAYOFF IN MISSILE EXCHANGE
 - ALTITUDE ADVANTAGE INCREASES MISSILE LAUNCH RANGE

IMPLICATIONS

- WIDE ANGLE TARGET ILLUMINATION TO STAY WITH MANEUVERING AIRCRAFT
- EFFICIENT SUSTAINED AND INSTANTANEOUS MANEUVERS REQUIRED
- TIME AT SUPERSONIC MANEUVER (PERSISTENCE) IS IMPORTANT

FIGURE 45



TIMELINE ANALYSIS

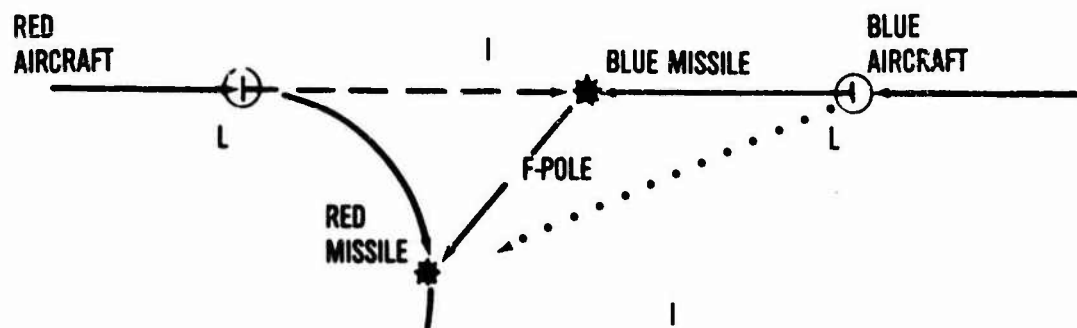


FIGURE 46



F-POLE VS SPEED AND MANEUVER

- LAUNCH AIRCRAFT AND TARGET AIRCRAFT NOSE-ON AT MISSILE LAUNCH
- MISSILE LAUNCH AT MAXIMUM EFFECTIVE RANGE
- LAUNCH AIRCRAFT MAKES LEVEL TURN AFTER LAUNCH
 - CONSTANT MACH
 - CONSTANT G
- TARGET AIRCRAFT FLIES STRAIGHT AND LEVEL AT CONSTANT SPEED

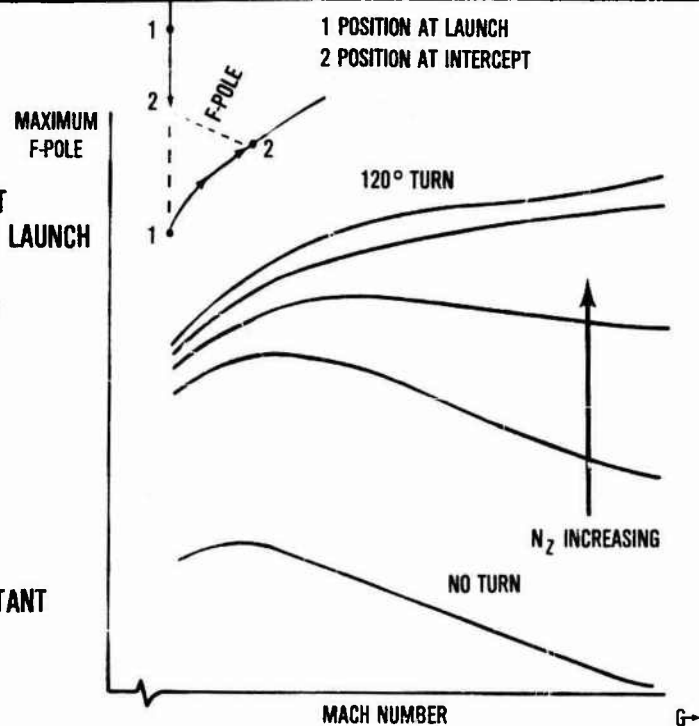


FIGURE 47



HEAD-ON ENGAGEMENT TYPICAL MANEUVERS PLANFORM VIEW

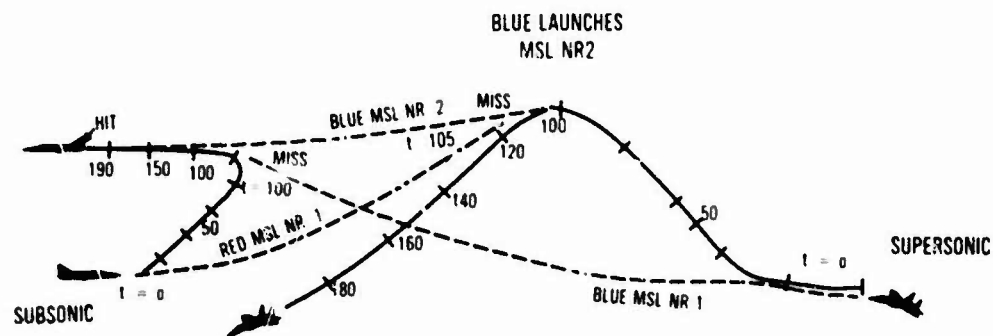


FIGURE 48



SPEED AND SIGNATURE

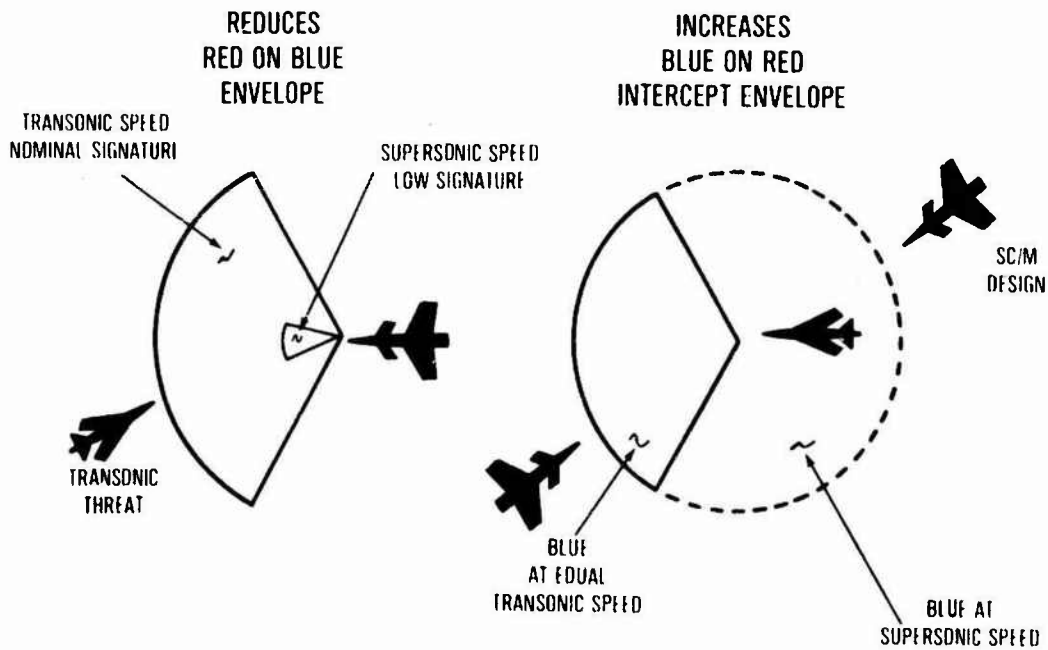


FIGURE 49



AVIONICS / WEAPON INTEGRATION

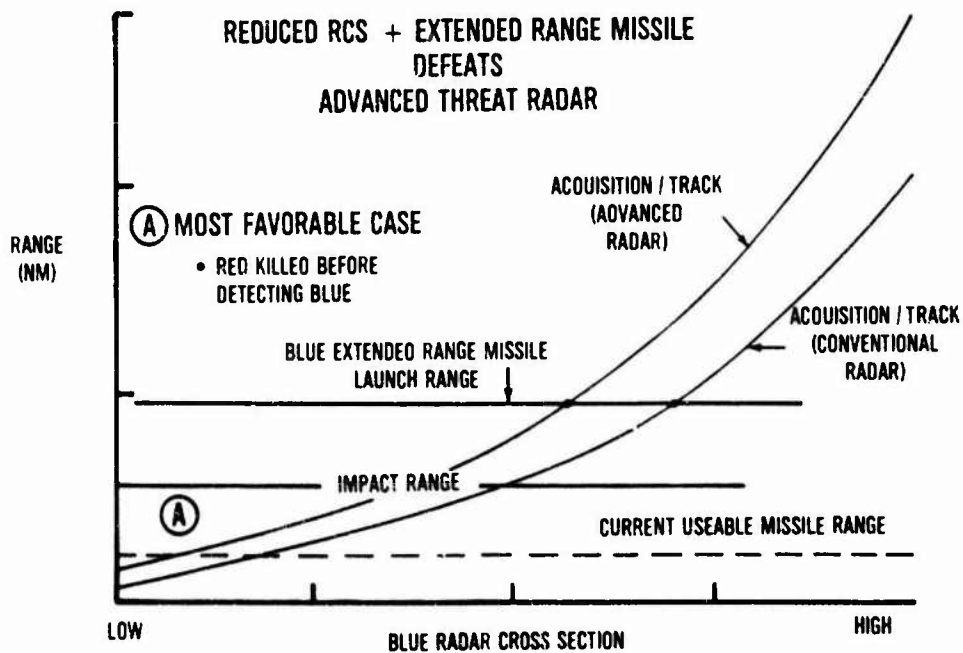


FIGURE 50



BVR ENGAGEMENT TRADES

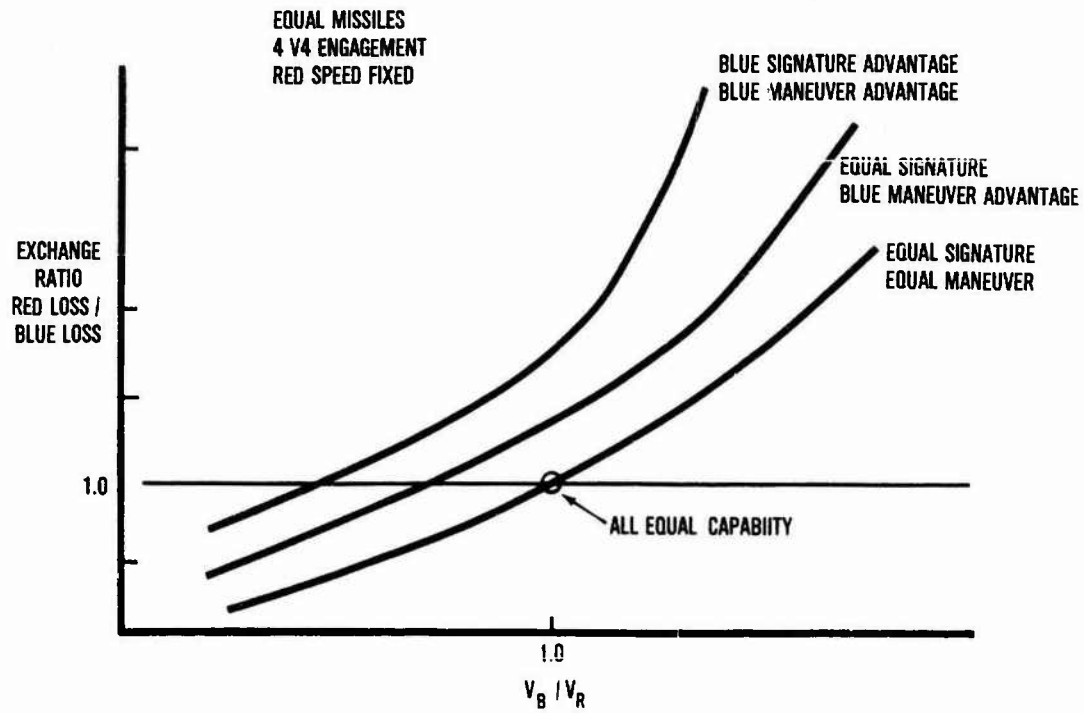


FIGURE 51



PRIMARY AIR-TO-SURFACE ISSUES

- SURVIVABILITY
- TARGET ACQUISITION
- TARGET KILL
- RANGE / PAYLOAD

FIGURE 52

Typical SAM Defense Coverage

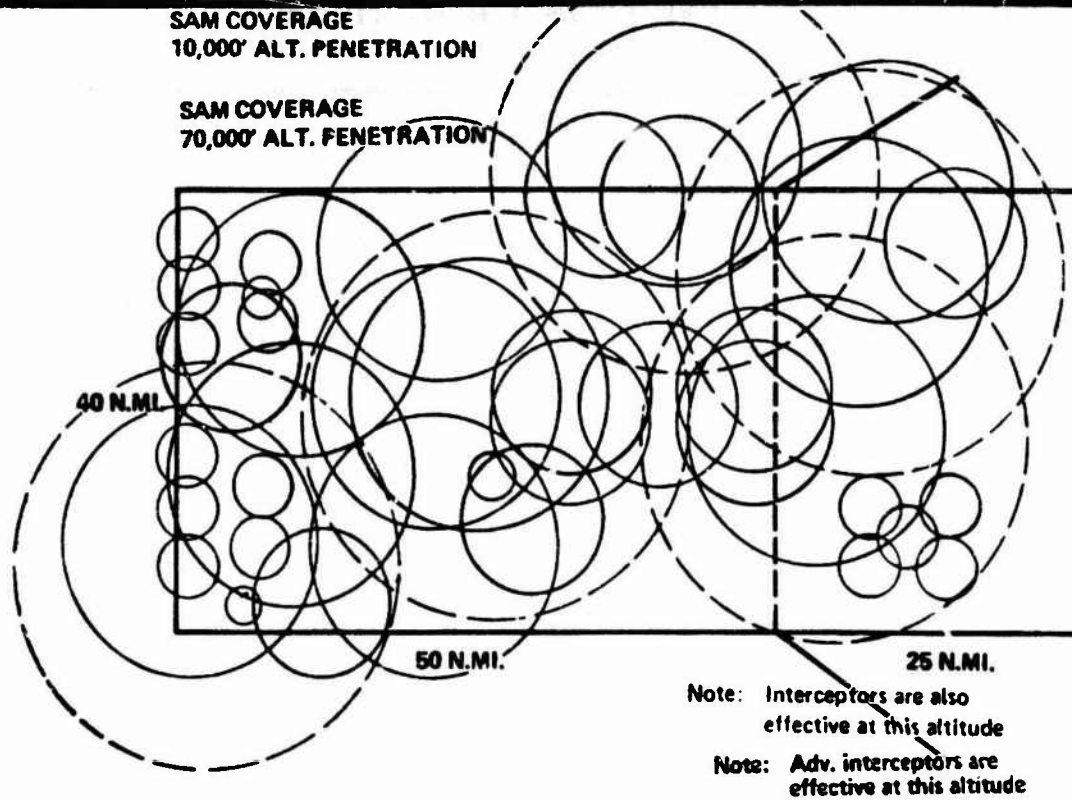


FIGURE 53



DESIRABLE PENETRATION CORRIDORS

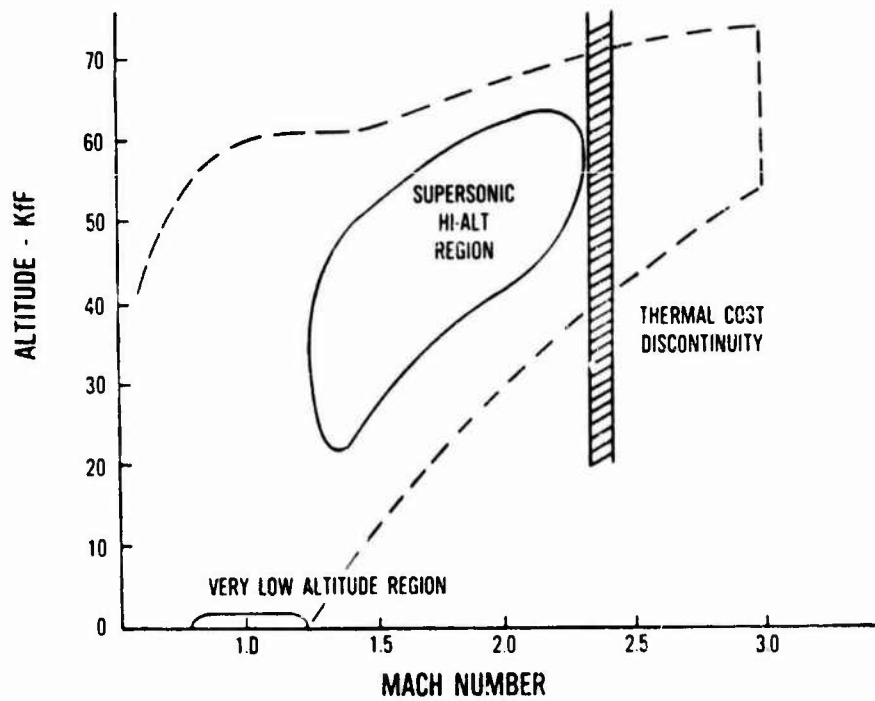


FIGURE 54



TYPICAL SAM THREAT DISTRIBUTION

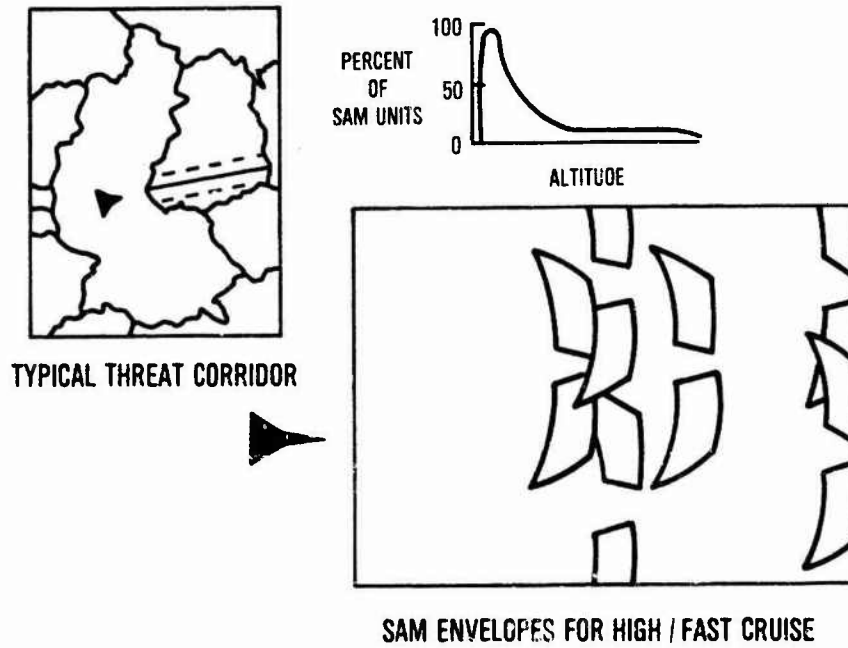


FIGURE 55



AIR-TO-SURFACE TARGET KILLS

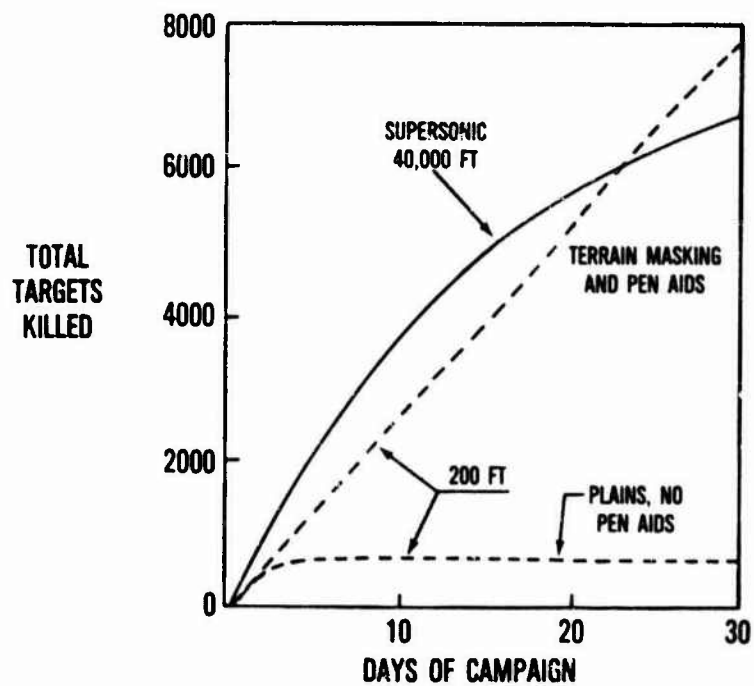


FIGURE 56

PHYSICAL CHALLENGES FACING LOW ALTITUDE TARGET ACQUISITION

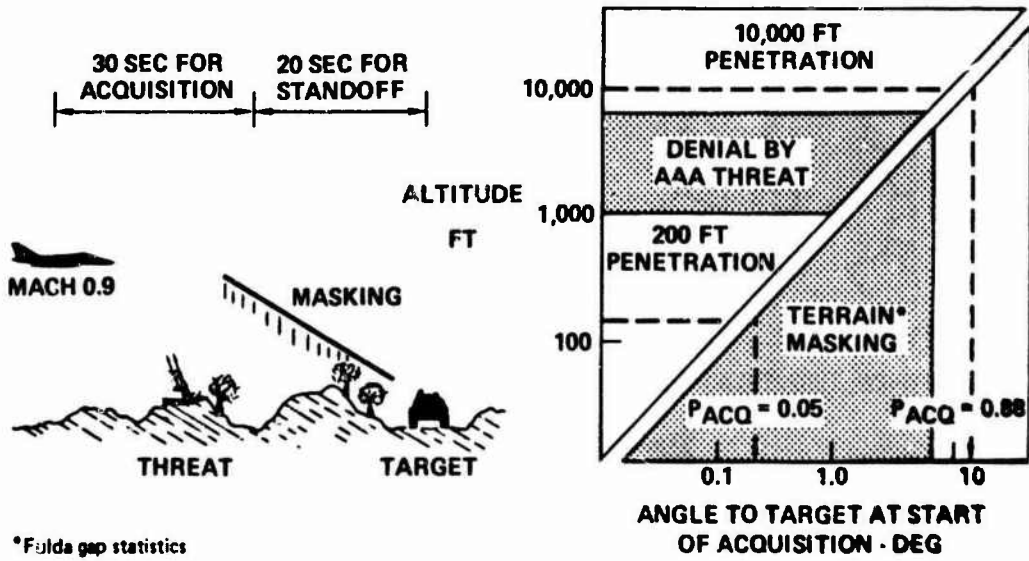


FIGURE 57



EFFECTS OF EUROPEAN ENVIRONMENT ON TARGET ACQUISITION

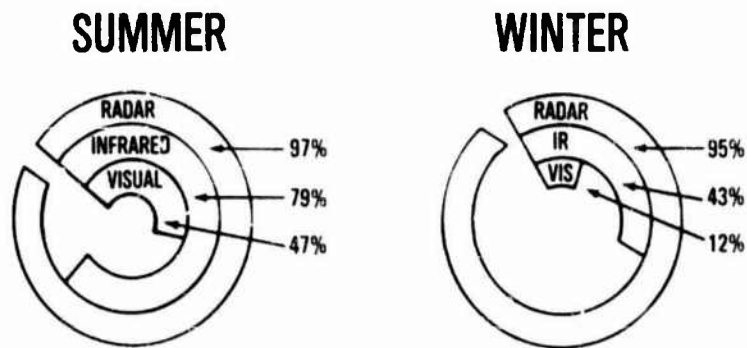


FIGURE 58



PRIMARY SORTIE GENERATION ISSUES

- MEANTIME BETWEEN FAILURES
- MEANTIME TO REPAIR (INCLUDING BATTLE DAMAGE)
- TURNAROUND TIME (IN CHEMICAL, BIOLOGICAL OR RADIOLOGICAL ENVIRONMENT)
- LANDING AND TAKEOFF DISTANCE
- SOFT FIELD AND ROUGH FIELD CAPABILITY

FIGURE 59



MEANTIME BETWEEN FAILURES FOR ALL AIRCRAFT SYSTEMS

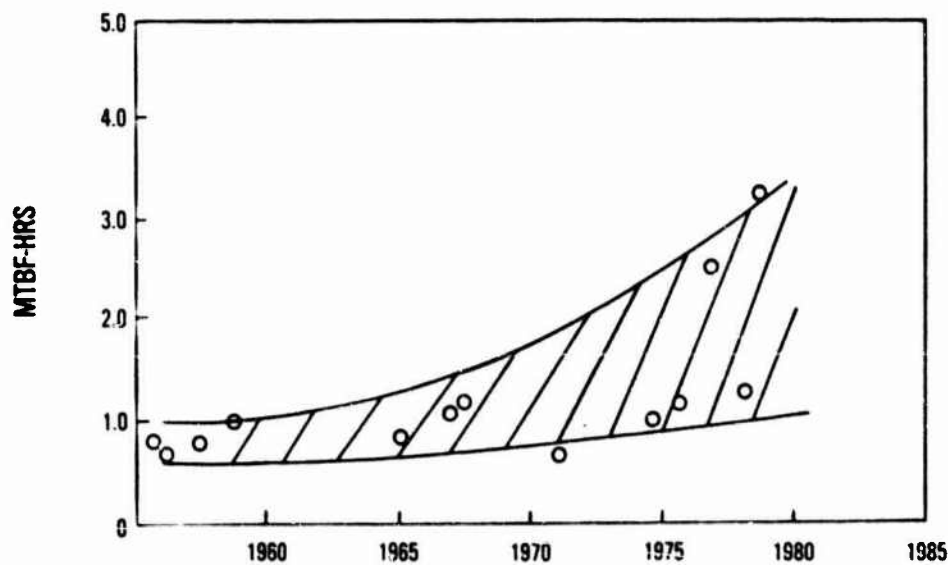


FIGURE 60



RADAR SYSTEM RELIABILITY

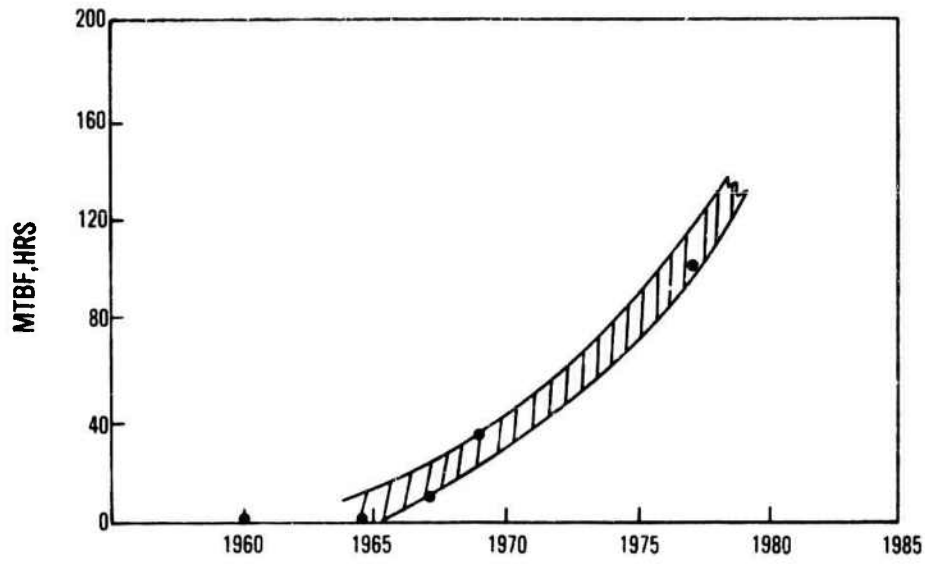


FIGURE 61



SUSTAINED SORTIE GENERATION CAPABILITY

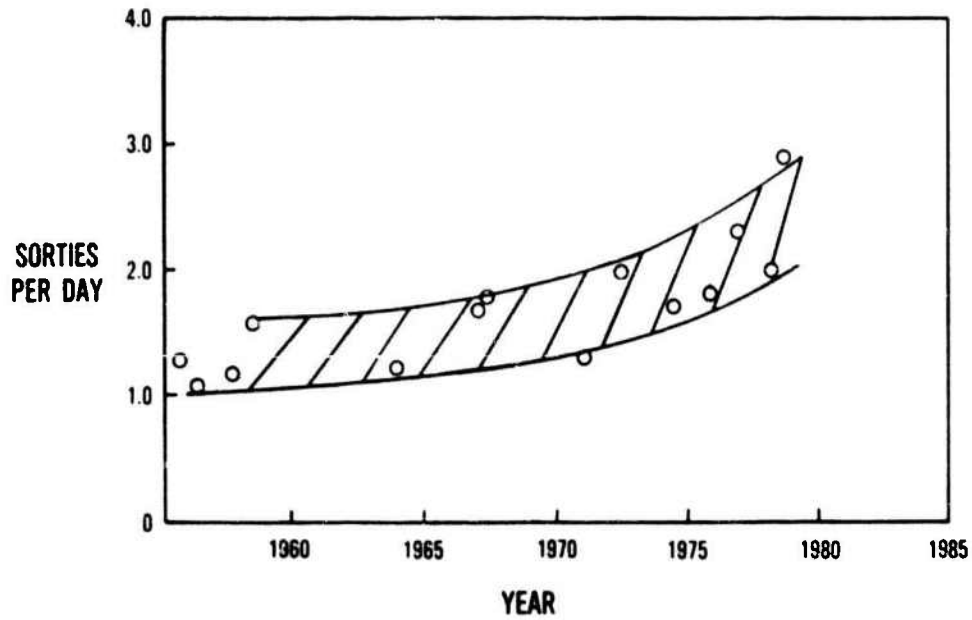


FIGURE 62



RUNWAY CRATERING AS A RESULT OF AN AIRBASE ATTACK

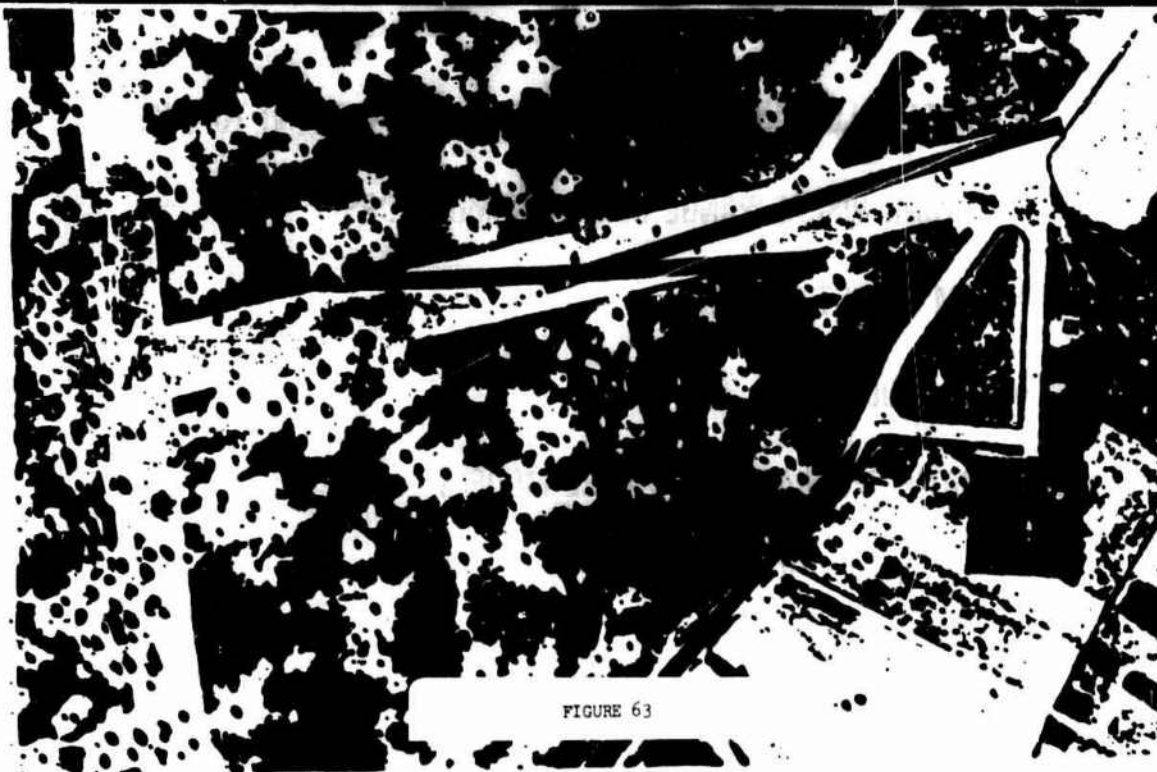


FIGURE 63



EFFECT OF TAKEOFF PERFORMANCE ON SORITE GENERATION AFTER RUNWAY ATTACK

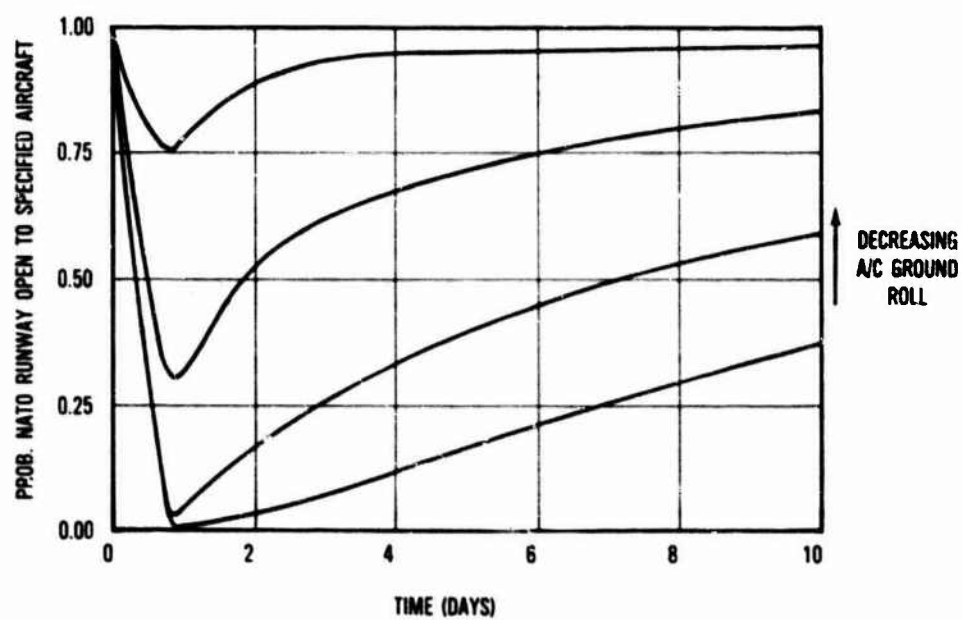


FIGURE 64



CONCEPTUAL LEVEL EFFECTIVENESS MODELS

- DIGITAL CLOSE-IN-COMBAT ENGAGEMENT MODEL (IVI TO 4V4)
- BEYOND VISUAL RANGE COMBAT SIMULATORS
- SAM FLYOUT MODELS
- AAA MODELS
- SORTIE GENERATION AIR BASE MODELS
- CAMPAIGN MODELS

FIGURE 65

Advanced Air-to-Air System Performance Evaluation Model - AASPEM

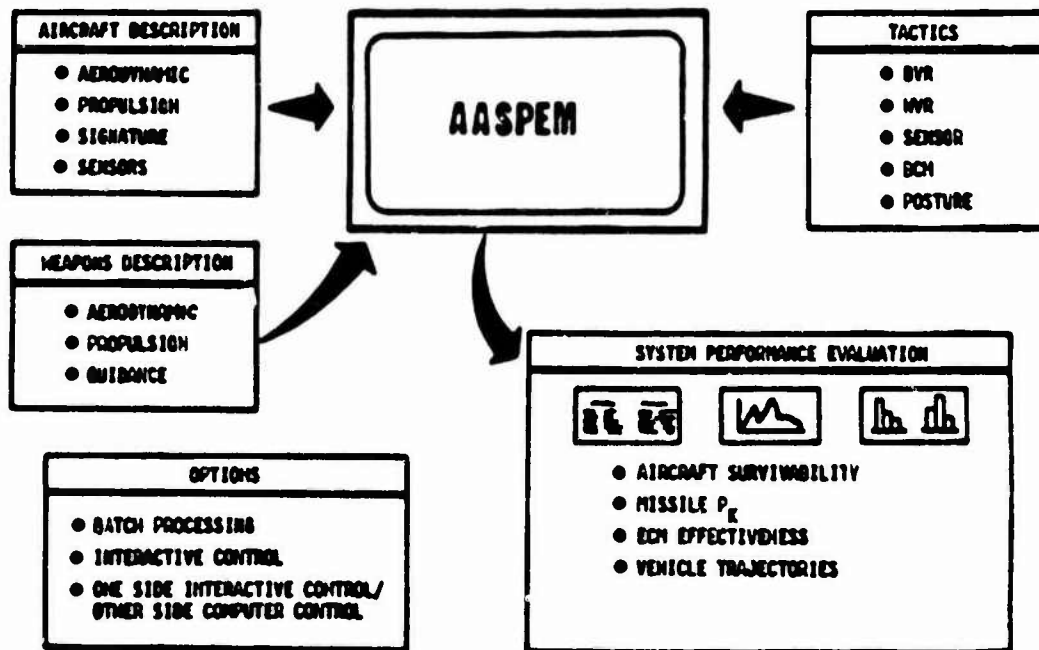
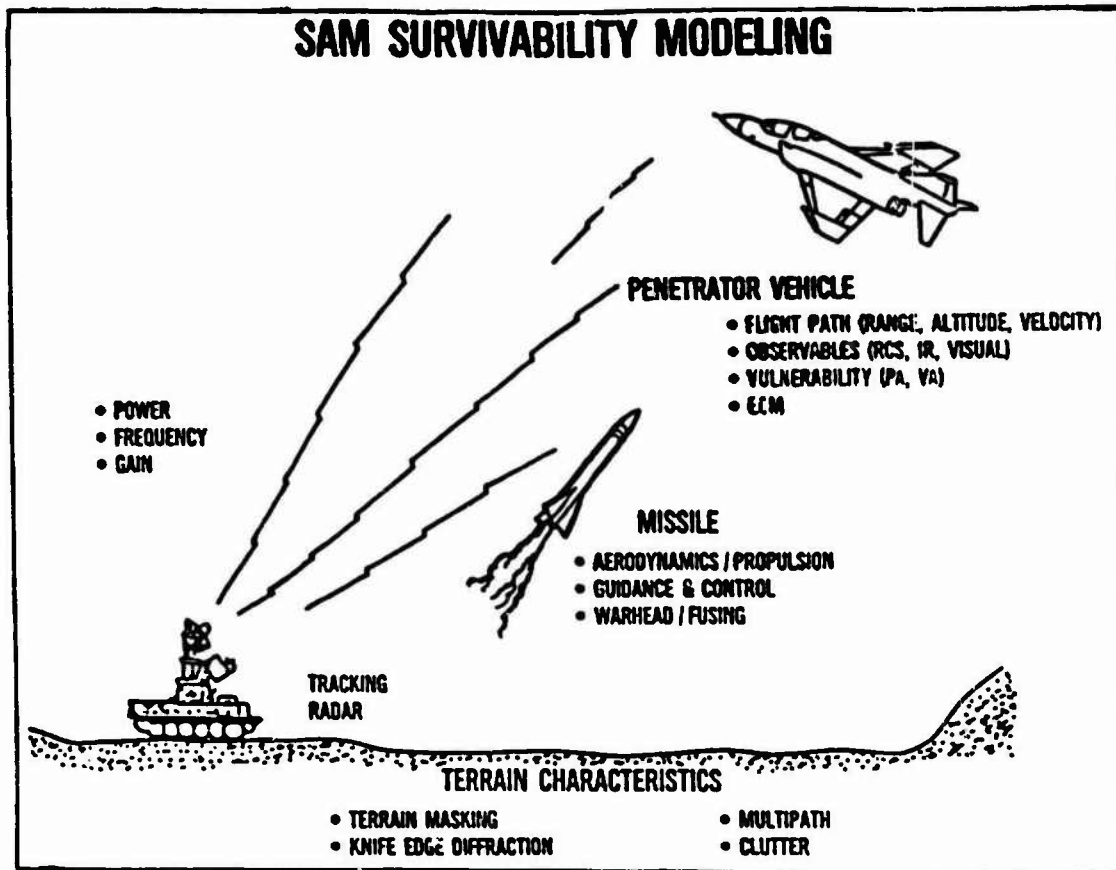


FIGURE 66



SINGLE BASE SORTIE GENERATION MODEL

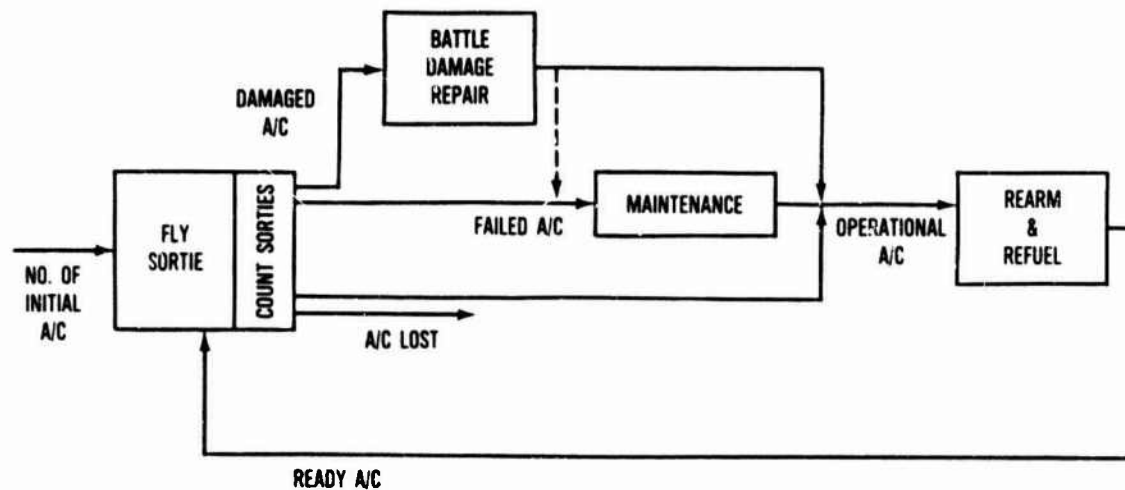


FIGURE 68

CAMPAIGN EVALUATION

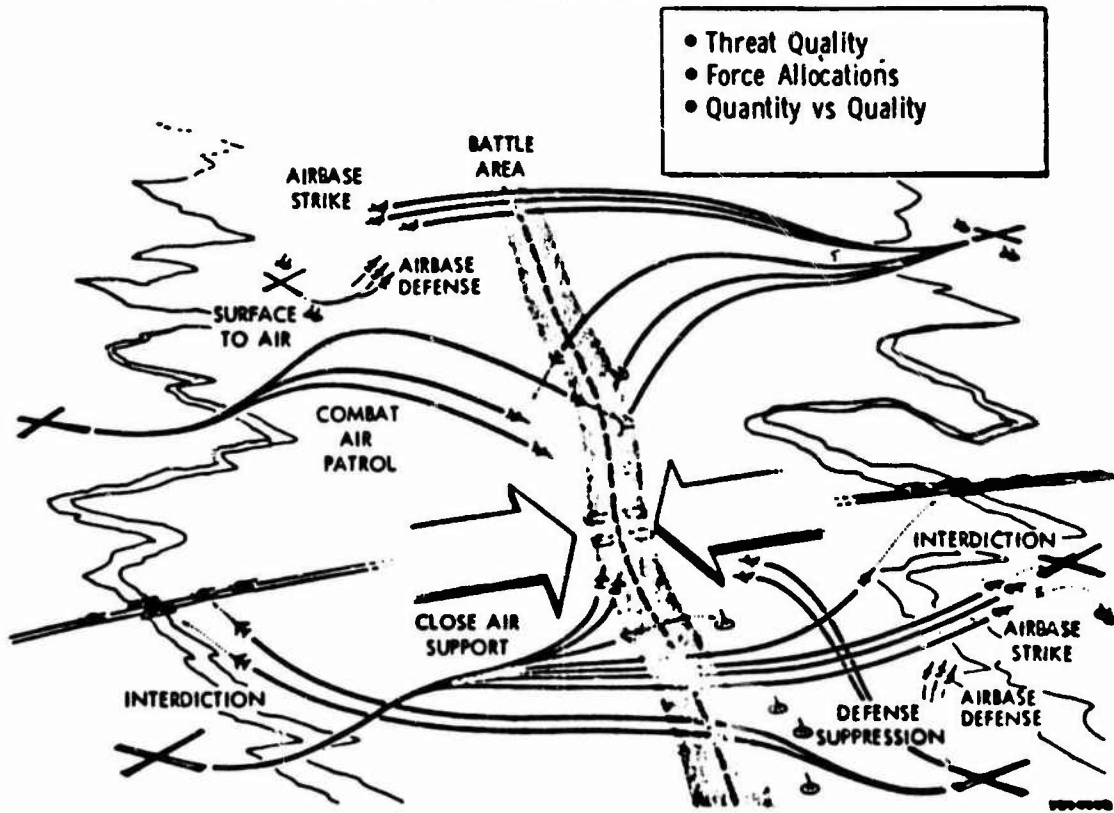


FIGURE 69

DESIGN OF WINGS AND WING/BODY CONFIGURATIONS FOR
TRANSONIC AND SUPERSONIC SPEEDS

H. Yoshihara
Boeing Military Airplane Company
Seattle, WA, 98124, USA

SUMMARY

Procedures to design wing/fuselage configurations at transonic and supersonic conditions are described. This is preceded by an introductory section sketching the significant flow features as the shock wave and separation patterns for typical fighter wings which affect the performance, followed by a description of the interference effects due to the fuselage.

1. INTRODUCTION

In the present chapter we consider primarily the transonic and supersonic design of the wing/fuselage for a supercruiser fighter at cruise conditions. Variable geometry concepts are then used on the cruise design to meet other mission requirements as the supersonic and transonic maneuverability for survivability and weapons delivery. Constraints on the aerodynamic design may be further required to alleviate non-aerodynamic consequences as excessive wing root bending moments. The expected flows at cruise lifts are relatively well-behaved and well-understood compared to the flows at the higher angle of attack maneuver conditions.

The starting point for the optimization is the baseline wing/fuselage configurations evolved from a pre-design study which yields candidate configurations that meet approximately the mission requirements. When the design is biased to the supersonic cruise condition, typical wings evolved are highly swept with a subsonic leading edge (65° - 70° for a Mach number 2 cruise) with small thickness ratio and aspect ratio. If, however, some weighting is given to the transonic maneuver condition, wings with less sweep result which have sharp supersonic leading edges (40° - 50° sweep at Mach 2). Here for example a supersonic leading edge is defined as that for which the Mach number normal to the leading edge is supersonic.

In the introductory sections we describe the flows for the above wings at cruise and maneuver lifts for a sequence of Mach numbers in the transonic and supersonic range. Salient features as the shock configuration and viscous effects are sketched. The interference effects of adding a fuselage are then described.

Current wing/fuselage optimization procedures are next outlined for the cruise optimization, first for the simpler supersonic case where the linear inviscid theory provides a viable first approximation; and then for the considerably more difficult transonic case which is essentially nonlinear and viscous. In the latter case a linear optimization procedure is still used to provide a starting configuration. Nonlinear analysis methods are then used to search for a more optimal configuration. Such search procedures are either ad hoc guided by prior experience incorporating for example uniform upper surface isobars, or more formal using procedures as the method of steepest descent.

The flows at maneuver lifts are essentially nonlinear and viscous for both the supersonic and transonic cases with free shear layer separations and shock-induced separations present. Because of the complexity of these flows, only isolated design examples using nonlinear analysis methods have appeared in the literature. Description of some of these cases will conclude the chapter.

2. FLOW STRUCTURE FOR SWEEP AND DELTA WINGS

We now describe the significant flow features as the shock wave pattern for the two sample wings described in the Introduction. In Fig. 1 we consider first the sequence of shock patterns for the swept wing of moderate sweep at cruise lifts for various free stream Mach number. In the high subsonic case a rear shock typically first appears as shown in Figure 1a. It is usually attributed to a coalescence of compression waves generated along the symmetry plane (3D effect), but clearly streamwise flow constraints that necessitated the terminating shock in planar airfoils must also play a role (2D effect).

With an increase in the free stream Mach number towards one, the rear shock is strengthened, displacing downstream and extending laterally primarily in the inboard direction. Additionally a forward shock now appears (Fig. 1b) which originates from the neighborhood of the wing apex. This shock wave is weak and hence swept approximately at the Mach angle corresponding to the "plateau" pressure. It closely forms the upstream influence limit of the leading edge kink and the symmetry plane in much the same manner as the shock wave for a wing at supersonic speeds with a supersonic leading edge. In Figure 1b the forward shock is shown intersecting the rear shock. The rear shock outboard of the intersection point is relabeled the outboard shock because of its significance as the strongest shock segment. Shock-induced separation will usually first arise aft of the outboard shock. As the Mach number is increased, the separation suddenly worsens, and the outboard shock reverses its downstream displacement and moves upstream. This occurs when the reattachment is abruptly displaced downstream of the trailing edge by a Type B interaction which we shall shortly describe. This upstream movement will decrease the shock sweep, still further strengthening the shock wave and worsening the shock-induced separation. This severely separated flow is highly unsteady, and if it occurs over a

sufficient stretch of the trailing edge, a significant wing buffet will arise.

The sequence of flows in the transonic range for the above wing at a given moderate transonic Mach number and for increasing angle of attack is physically similar to the sequence described above. Deteriorations of the flow that arise for the increasing lifts are the direct consequence of the strengthening of the outboard shock leading first to drag divergence and then to the onset of buffet and to its worsening. For sufficiently large angles of attack, leading edge separation appears greatly complicating the flow. We shall defer description of these flows to a later paragraph in this section.

Let us now return to the sequence of flows at the cruise lift and consider the flows in the supersonic range. With the increase of the Mach number to supersonic values the rear shock eventually displaces downstream to the trailing edge in the usual case of a supersonic trailing edge, thereby eliminating the rear separation responsible for the buffet. A detached bow shock will now appear, and the forward shock adjusts its sweep approximately to the new "plateau" pressure. As the supersonic cruise Mach number is approached, the wing leading edge becomes exposed to the free stream as the bow shock sweeps across the leading edge onto the wing assuming its cruise location. The forward shock will disappear when the bow shock sweeps onto the planform.

The shock configuration for the case of the highly swept delta wing with a subsonic leading edge is generally similar to that described above, but a given flow pattern sketched above is displaced to a higher Mach number due to the unloading effect of the higher leading edge sweep and lower aspect ratio. The effects due to the higher leading edge sweep is illustrated in Figure 2 for the case of a flat swept wing of 53.5° leading edge sweep, aspect ratio of 2.8, and with a 6% RAE 102 airfoil. This sequence of flow features for varying Mach number and angle of attack was obtained by Rodgers and Hall (Ref. 1) from surface oil flow pictures. Here the angles of attack are extended well into the maneuver range. The shock patterns to be expected for the above delta wing at the cruise condition would then follow those at 3° in Fig. 2.

The shock and separation patterns for a given wing at a specific Mach number and angle of attack are directly dependent upon the planform shape and the twist and camber distributions and may accordingly differ in detail to those described above. Thus for example the wing leading edge radius and camber will affect the upper surface plateau pressures which in turn will affect the sweep of the forward shock and hence the location of the outboard shock.

Consider finally the viscous effects and in particular the separation patterns. In the upper part of Fig. 3 we first show the viscous interactions arising over the upper surface of an airfoil to illustrate a Type B interaction (Ref. 2) which plays an important role in the separation phenomena for swept wings. Type B interactions arise when the boundary layer encounters two successive adverse pressure gradients as for example the shock wave and the trailing edge pressure recovery. Here the boundary layer thickness and the displacement thickness (measure of the loss of velocity profile fullness) both increase abruptly after passage through the shock wave making the boundary layer more susceptible to separation as it encounters the second adverse pressure gradient. In Ref. 3 a 3D version of the Type B interaction was described where additionally the influence of the degraded state of the boundary layer at an inboard span station propagated tipward along the limiting (surface) streamlines and worsened the separation further outboard as shown in the lower part of Fig. 3. This 3D Type B viscous effect plays a direct role in the promotion of severe separation aft of the outboard shock of Figure 1b. These Type B interactions are reflected in both the 2D and 3D integral boundary layer equations by the greatly enhanced growth rate of the form factor H (which governs separation) as the H increases and exceeds a value of the order of 2. (Here the form factor H is increased when the boundary layer encounters an adverse pressure gradient.)

The above separation aft of the outboard shock wave, labeled the bubble-type, must be contrasted to the free-shear layer separation arising along a swept leading edge or along the forward shock as shown for example in Figure 2 at a Mach number of 0.6 and angle of attack of 9° and at a Mach number of 1.15 and angle of attack of 9° respectively.

Of major importance in maneuver flows is the free shear layer separation vortices which arise both on the fuselage and on the forward portion of the wing. The properties of such vortices are well understood, so that we shall briefly summarize those features that affect the performance. In Fig. 4 we first show the principal effects of the separation vortices on the spanwise pressure distribution for a thin delta wing at subcritical Mach numbers (Ref. 4). Here the primary vortex, formed by the vorticity shed from the leading edge, eliminates the large theoretical nose suction that arise in attached flow (see Fig. 4) and induces a suction peak further inboard beneath the vortex. At a larger angle of attack, the adverse pressure gradient formed on the outboard side of the suction peak becomes sufficiently strong to cause a secondary separation. The secondary separation then alters the pressure distribution as shown in Fig. 4 by lowering the suction peak and increasing the suction outboard of the lowered peak.

The presence of the leading edge separation vortices in the case of a sharp leading edge stabilizes the flow relative to the highly unsteady separated flow for a more-conventional blunted leading edge, producing steady enhanced lift. Kuchemann advocated this use of vortices in designs in his concept of controlled separations. The severe drawback of using vortex flows for maneuver enhancement is the large accompanying drag. Dr. Lamar later will describe the use of leading edge flaps to take advantage of the increased lift with the vortices without incurring the severe drag penalty.

With regard to the calculation of these vortex flows, when the leading edge is sharp, inviscid Euler methods can be used to predict the effects of the primary vortex since the location of the separation line is fixed at the leading edge. If secondary separations are present, inviscid Euler methods are no longer adequate (see Fig. 4); and viscous flow methods must be used. For wings with rounded leading edges or for the case of the fuselage, the separation line is not known a priori, so that a viscous flow method as the Navier/Stokes code must be used.

The property of vortex flows that decisively limits the maneuver performance is the appearance of vortex bursting where the well-ordered spiraling vortex is suddenly changed to a chaotic flow. Bursting occurs in two forms, the spiral type and the bubble type. These types are shown occurring simultaneously on the same delta wing in the classical photograph from Ref. 5, which is reproduced in Fig. 5. Much is known about vortex bursting (see Ref. 6), but also there is much that is not fully understood; most importantly for applications, methods to predict its occurrence do not exist. In many respects bursting has similarities with boundary layer separation, both being triggered by adverse pressure gradients. Evidence however indicates bursting to be independent of Reynolds number.

For a delta wing of given sweep, vortex bursting will first arise downstream of the trailing edge. With increase of the angle of attack, the burst point will move upstream and will eventually move onto the wing at which point wing stall occurs. There is a strong influence of the leading edge sweep on the movement of the burst point with angle of attack. With increasing sweep, the burst point for a given angle of attack is pushed further downstream, delaying the burst stall to a higher angle of attack. This behavior results from the stronger more burst-resistant vortex formed with the greater sweep. The arrival of the burst point at the trailing edge and hence the onset of the burst stall is shown as a function of the angle of attack and the leading edge sweep in Fig. 6 from Ref. 7.

The burst stall dependence on the leading edge sweep can have a disastrous effect on lateral stability just below the burst stall boundary. Here a wing yaw can push the upwind wing with reduced sweep into the stall region, while the downwind wing will move further into the unstalled region. A catastrophic roll moment will result. Finally, the possible interference of the separation vortices from the nose and strakes on the rear stabilizing surfaces, under high-lift yaw conditions, poses a challenging design problem for the proper placement of the rear surfaces.

With the increase of the Mach number to supersonic values, leading edge separation will still occur so long as the leading edge is subsonic. Relative to the subcritical case, the primary vortex, though closer to the wing, is weaker inducing significantly smaller suction on the wing. Cross-flow shocks can arise with increase of the angle of attack resulting in a variety of flow configurations as shown in Fig. 7 from Ref. 8. Also shown here is a sketch of the sequence of flows arising at $M = 3.5$ for increasing angles of attack.

3.0 WING/FUSELAGE INTERFERENCE

We shall now describe the significant interference effects due to the fuselage restricting the discussion to the transonic case where the effects are more profound. These effects are well known, and they will be illustrated by several examples taken from a recent review by A. B. Haines (Ref. 9). We consider first the case of an untwisted swept wing of 30° sweep mounted centrally on a fuselage with a circular cross-section. In Fig. 8 we show the pressure distributions with and without the fuselage at two Mach numbers, $M = 0.4$ and 0.8 . In this figure we shall consider only the experimental results given by the symbols. (The solid and dashed lines are computed results which are described in Ref. 9.) If we compare the pressure distribution for the wing alone (curve A) with the wing/fuselage distribution (curve B) along the juncture where the largest interference arises, we see the typical effect of the fuselage of depressing the wing-alone suction. This effect is larger at the higher Mach number. Such an unloading will deteriorate the span load distribution, leading not only to a reduced lift, but to an increase of the induced drag. This inboard unloading is usually eliminated by locally increasing both the angle of attack and the wing chord. In Fig. 8 we cannot show the spanwise extent of the fuselage interference since the wing-alone pressure distribution was not given at the outboard station. It is however well known that at low speeds the fuselage interference rapidly attenuates in the spanwise direction being confined to the inboard stations. With increase of the Mach number into the transonic range, there is some spanwise spread of the interference, but at some point a forward shock will appear confining the fuselage interference to the region downstream of the shock. This will next be shown in the second example.

In Fig. 9 we consider the case of a "flat" untapered wing mounted centrally on a cylindrical fuselage of circular cross-section. Here the fuselage interference is shown by a calculation with an exact potential method. For this transonic case the fuselage interference has generated a significant forward shock. As described in the previous section for the wing, this shock forms the upstream limit of the fuselage interference which limits the spanwise extent of the interference. Experimental wing/fuselage pressure distributions are also given in Fig. 9 to support the calculations.

In the final example given in Fig. 10 another aspect of the fuselage interference is illustrated by comparing the interference due to two different fuselages with an elliptic or square cross-section. Here the significant differences of the two fuselages are not only the cross-section shapes below the wing but the streamwise rate of change of the cross-sectional area upstream of the wing. Thus if we compare the two cases at the same angle of attack (curves A and B), we see the greater suction plateaus and a stronger shock system on the wing for the elliptic fuselage. This is primarily due to the greater Mach numbers generated upstream of the inboard portion of the wing by the elliptic forebody. (Here for example slender body theory would suggest the lift to be dependent on the streamwise rate of change of the fuselage cross-sectional area.) The effect of the increased oncoming Mach number for the elliptic fuselage is seen to have a dramatic effect at the innermost span station at 0.24 semi-span. The large difference of the suction at the inboard station for the two fuselages now propagates spanwise along the characteristics producing the difference in the pressures seen at the outermost span station. Here also changes in the forward shock have contributed to the outboard interference by altering the outboard shock.

In summary the addition of the fuselage in the transonic case produces significantly reduced suction in the inboard region of the wing which will be confined downstream of the forward shock when such a shock is present. The fuselage may additionally produce changes in the inboard wing flow by altering the oncoming Mach numbers upstream of the wing. The resulting inboard wing flow change is then propagated spanwise along the characteristics.

With such significant interference effects due to the fuselage, it is not difficult to anticipate the importance of the interference effects that will arise by the addition of strakes and canards in the transonic case.

The interference effects of the fuselage at supersonic conditions, though not unimportant, are less profound being confined laterally by the characteristic zone of influence. We shall thus omit this subject in the present review.

4. SUPERSONIC CRUISE DESIGN

The specific problem on hand is to evolve changes to the baseline configuration at the cruise Mach number which minimize the drag for a prescribed lift and pitching moment. Geometric constraints on the fuselage and wing may be additionally required for structural and internal volume requirements and for the avoidance of flow separations when an inviscid method is used for the optimization. In the following we shall describe how this problem is typically addressed for the simpler supersonic case.

In the supersonic case linear small disturbance inviscid theory serves as a good first approximation for supercruiser fighter configurations at cruise lifts. Here viscous interactions are weak. With planar boundary conditions valid for the wing, the optimization problem can be divided into the thickness problem and the lifting problem.

Consider first the thickness problem. For the determination of the wave drag, the farfield perspective is used in the form of the well-known supersonic area rule. In brief the drag of a given configuration is obtained by evolving its equivalent axial symmetry body as follows. The area of the equivalent body at a given point along the fuselage axis is obtained by introducing the aft free stream Mach cone with the cone apex at the given point. A sequence of tangent planes around the cone are constructed, and the area of the configuration intersected by each of these tangent planes is determined. The average of these areas then yields the local area of the equivalent axial symmetric body. Configuration changes respecting the geometry constraints are made to drive the equivalent body towards an optimal shape as the Sears-Haack body. In general the thickness distribution of the wing is kept unchanged, it being selected initially by structural considerations. Addition of inboard strakes and permissible fuselage variations are frequently considered to obtain the smoothest equivalent shape approaching the optimal shape. Practical guidance in the use of the area rule is given by Harris (Ref. 10).

In the lifting problem, the correct procedure would be to mount the zero thickness wing onto the optimized fuselage. Frequently to simplify the problem, the wing alone is considered. A variational problem is then posed seeking the camber distribution for the given planform which minimizes the wave drag for a prescribed Mach number, lift, pitching moment, and possibly with geometric constraints.

A representative optimization procedure is due to Carlson and Miller (Ref. 11). Here a sequence of significant loadings l_i ($i = 1, 2, \dots, N$) is defined, and the corresponding cambers c_i yielding these loadings are then determined by quadrature distributing lifting doublets or elemental horseshoe vortices on the planform. For non-simple planforms the integrations must be carried out numerically.

For the optimization the sequence of loadings is now superimposed with coefficients a_i , and the functional

$$F = D + k_1(L - L_0) + k_2(M - M_0)$$

is formed where k_1 and k_2 are the constant Lagrangian multipliers, L_0 and M_0 are the constrained values of the lift and moment, and the total lift L , the drag D , and the pitching moment M are given by

$$L = \int \sum a_i l_i ds \quad D = \int (\sum a_i l_i) (\sum a_i c_i) ds$$

$$M = \int x (\sum a_i l_i) ds.$$

The functional F is therefore a function of the coefficients a_i and k_1 and k_2 . The minimum of F will yield the minimum of D when the lift and moment constraints are fulfilled, and it is obtained by setting the partial derivatives of F with respect to each a_i and k_j to zero; that is,

$$\partial F / \partial a_i = 0 \quad (i = 1, 2, \dots, N);$$

$$\partial F / \partial k_1 = L - L_0 = 0$$

$$\partial F / \partial k_2 = M - M_0 = 0.$$

Note that the second set of equations will insure the lift and moment constraints. The solution to the above system of equations then yields the a_i 's; and the optimum camber is then given by $C = \sum a_i c_i$.

The above procedure is illustrated by an example from Ref. 12 for the planform shown in the lower part of Fig. 11 at the Mach number of 3.5, for a lift coefficient of 0.1, and with a pitching moment of zero about the center of gravity shown in Fig. 11. Eight elemental loadings shown in Fig. 11 were used. These are arbitrary, but if they are skillfully chosen such that each is physically significant in an unique manner, fewer elemental loadings will be required. In Fig. 12 the resulting optimal camber is shown. Here it is seen that a large negative displacement of the root chord trailing edge has resulted making it difficult to mount the wing on the fuselage. The optimization was repeated adding an additional constraint on the vertical coordinate at the root chord trailing edge using the Lagrangian multiplier k_3 . The resulting constrained camber shape is compared to the original unconstrained camber in Fig. 12. A comparison of the resulting drag-due-to-lift factors is shown in Fig. 13. The penalty of adding the moment and trailing edge constraints is seen to be small in this case. The performance penalty due to constraints in general will depend strongly on the case on hand.

In the above example the leading edge was supersonic, so that a leading edge suction force did not arise nor were large upper surface suction forces generated.

In the case of a subsonic leading edge, upwash upstream of the leading edge arises generating large upper surface suction forces. More importantly, a leading edge suction force is generated. Theoretically the latter force is due to the linear solution singularity at the leading edge of the zero thickness wing. The significance of the leading edge suction force is shown in Fig. 14 where the drag-due-to-lift factor $C_D/\beta C_L^2$ determined by linear theory is plotted versus $\beta \cot \Lambda_{1e}$. Here C_D and C_L are the drag and lift coefficients, Λ_{1e} the leading edge sweep angle, and $\beta^2 = M^2 - 1$ where M is the free stream Mach number. Here also the significant effect of the trailing edge sweep Λ_{te} on the drag factor is shown due primarily to the influence of the aspect ratio on the induced drag.

The theoretical leading edge suction force used above in Fig. 14 is not fully realized in a real flow due to flow separation. For design purposes an attainable leading edge suction force was defined in Ref. 13 using local sweep theory and incorporating empirical inputs to account for flow separation. It was expressed in terms of a thrust factor k_t , the fraction of the theoretical suction force attained in a real flow; and it was given as a function of the local sweep and leading edge radius, the inviscid flow loading about the leading edge, and the free stream Mach number and Reynolds number.

In Fig. 14 we show an example from Ref. 15 for a wing/fuselage with a 70°-sweep wing showing the appreciable leading edge suction force that can arise. Here the chordwise force coefficient C_A , which reflects directly the leading edge suction force, is plotted versus the angle of attack at four values of the free stream Mach number in the range 1.6-2.95. Here, aside from the experimental values, three calculated values are shown, with and without the full theoretical suction force, and with the attainable thrust from Ref. 13. The relative amount of the suction force generated can be gauged by comparison with the calculated values with and without the theoretical suction. The results here show that the measured suction force is of the order of one-half of the theoretical value up to an angle of attack of 4°. The calculated values of the C_A using the attainable suction are seen to agree closely with the measurements.

Another interesting test/theory comparison is from Ref. 15 for a series of 70°-sweep arrow wings at $M = 2$ optimized at several design C_L 's using the linear optimization code omitting the leading edge suction force. In Fig. 16 the resulting maximum lift-to-drag ratio $(L/D)_{max}$ and the zero-lift pitching moment C_{mo} are plotted against the design lift coefficient $C_{L,d}$. Here the measured values are compared with two calculated results, with the attainable suction and without it. Though the pitching moment is closely predicted by both calculations, the linear theory calculations without the leading edge suction have greatly over-predicted the $(L/D)_{max}$. The results using the attainable suction closely match the measurements.

The cause for the poor test/theory match in Fig. 16 in the case of the linear theory without the suction was due to the large nose-down leading edge camber generated by the optimization which invalidated the linear theory. In the absence of the leading edge suction force, the optimization drove the leading edge camber to large negative values to create forward-facing surface elements on which the large upper surface suction pressures could act to create a thrust. With leading edge suction included, this drive towards large negative cambers is halted by the decrease in the leading edge suction force, thereby preventing an invalidation of the linear theory. The above results point to the need of a twist/camber optimization method which incorporates the attainable leading edge suction. Such a procedure was developed in Refs. 16 and 17. We shall conclude this section by an example from the latter reference.

The objective of Ref. 17 was the redesign of an existing Mach 2 supersonic fighter with a 40°-sweep wing biased in part for a transonic maneuver requirement, to a new configuration biased solely for supersonic cruise. The use of the existing fuselage was required, though a more slender fuselage nose was permitted in the new design. The pre-design analysis for a cruise lift coefficient of 0.08 resulted in the planform shown in Fig. 17 where also the baseline fighter model is shown. Here the leading edge sweep Λ_{1e} was selected such that $\beta \cot \Lambda_{1e} = 0.75$ where $\beta^2 = M^2 - 1$; that is, a leading edge sweep of 55.5° at $M = 2$. The trailing edge sweep was selected at 20°, a compromise of the aerodynamic preference of a large sweep for reduced drag-due-to-lift and the structural preference for reduced structural sweep. A break in the leading edge sweep was additionally incorporated, increasing the inboard sweep to obtain an increased inboard structural depth without an increase of the local thickness ratio.

The wing camber was optimized in the presence of a simplified fuselage using a total of 14 elemental loadings, constraining the lift, pitching moment, and the root chord geometry to enable the resulting wing to be mounted on the existing fuselage. In the optimization the attainable leading edge suction force was used. The resulting design was further modified by trial and error to limit the leading edge suction to 0.7 of the vacuum pressure coefficient and the maximum adverse pressure gradient to a specified empirical value to prevent flow separations.

In addition to the wing change, the fuselage nose was made more slender. The resulting improved (smoother) normal area distribution is contrasted to the original distribution in Fig. 18. A significant decrease of the zero-lift drag should result from the smoother area distribution. The expected estimate of the drag improvements is summarized in Fig. 19 where also the effect of the redesigned inlet is shown which was tailored to the supersonic cruise condition.

The resulting research model was tested, and in Fig. 20 the measured untrimmed $(L/D)_{max}$ and the $M(L/D)_{max}$ are compared to those for the baseline fighter model. At the $M = 2$ cruise point, an improved value of $(L/D)_{max} = 5.5$ was achieved in the redesign compared to the original value of 4.1. The improvement here must be largely attributed to the planform improvement permitted by the removal of the transonic maneuver bias.

Also shown in Fig. 20 are the results for three designs from an earlier NASA/Langley interceptor/fighter study. Ref. 17 attributes the higher performance of the SCIF 4 and 5 models to the absence of the geometric constraints on the wing root chord required in the research model by the mounting considerations on the existing fuselage.

Finally some results are given showing the viability of the computational method used in Ref. 17. In Fig. 21 the measured drag polars for the research model with and without the camber are compared to the three calculated values with no suction force, with the theoretical suction force, and with the attainable suction force. Remarkable test/theory match is seen here for both models when the attainable suction is used.

5. TRANSONIC CRUISE DESIGN

The problem on hand is again one of starting from a baseline wing/fuselage configuration evolved from a predesign study and incorporating changes to the wing and fuselage such that the drag is minimized for a given lift and pitching moment. Permissible configuration changes are usually constrained by non-aerodynamic considerations as described earlier. The fundamental aspects of the cruise design of the wing/fuselage can be illustrated by considering the configuration typified by that given earlier in Fig. 10 with a wing sweep of 40° . We shall in the following confine the discussions to such configurations.

The transonic problem is non-linear, and viscous effects are significant. Direct optimization procedures as used in the supersonic case are no longer possible, and one must turn to a laborious search process using both the wind tunnel and the computer. Here the search is greatly expedited by prior experience.

The cause of the flow degradation that limits the transonic cruise performance is well known and is due to shocks and their interaction with the boundary layer. Drag divergence, the abrupt increase of the drag with Mach number at a constant lift, is the direct consequence of the entropy generation by the shock and the concomitant displacement pressure drag arising from the shock/boundary layer interaction. To avoid a strong shock wave, wing sweepback and twist are employed together with fuselage contouring to maintain adequately swept shock waves. Additionally high performance airfoil sections, as the supercritical airfoils, are incorporated into the fighter wing as a starting point despite the absence of a locally planar environment.

A typical design procedure starts by using the subcritical theory in the form of the Mach one area rule to contour the fuselage and to modify the inboard portion of the wing, perhaps adding a wing glove. The panel method is then used to determine the wing incidence and twist as well as additional thickness modifications of the wing to obtain uniformly swept upper surface isobars as well as an elliptic spanwise load distribution for minimum induced drag. In some cases the elliptic loading is relaxed to a less fuller distribution to moderate the root bending moment. This linear subcritical analysis surprisingly yields a useful first approximation, particularly the wing twist which has been found to be satisfactory for the supercritical design point. The next step is the refinement of the subcritical design using for example an exact potential code together with a boundary layer code. This is followed by a final tailoring of the design in the wind tunnel assisted by computations.

To illustrate one aspect of the transonic cruise design problem, an example from Ref. 18 is considered where fuselage fairings at the wing juncture region were added to improve the wing/fuselage interference. Two fairings A and B shown in Fig. 22, were added to the wing/fuselage (elliptic cross-section) of Fig. 10. Fairing A was shaped to fit the wing-alone streamline at the fuselage juncture location, whereas fairing B was shaped to fit the wing-alone streamline at the 40% semi-span. In Fig. 23a the chordwise pressure distributions obtained in a wind tunnel test are compared with and without the fairings at the 24% semi-span station. The Mach number was 0.82, and the angle of attack was 4.12° . As might be expected, fairing A showed the best performance largely eliminating the forward shock and greatly weakening the rear shock. The addition of the fairings however reduced the lift coefficient from the original value of 0.42 to 0.288. A more meaningful comparison is given in Fig. 23b where the lift coefficients were more closely matched. Relative to the baseline case the forward shock was displaced upstream and the rear shock significantly weakened by the fairing A. In Fig. 23 the spanwise variations of the difference of the sectional drags between the two fairings are compared for several Mach numbers. Here the fairing interference is seen to spread rapidly spanwise with increase of the Mach number. The difference of the total drags plotted versus the Mach number is also given in Fig. 24, again showing the superiority of the fairing A. In summary the fairings have clearly decreased the drag, but this gain was moderated by an accompanying decrease of the lift.

The second example is from Ref. 19 which demonstrates a nonlinear optimization procedure using the exact potential code in a steepest descent search. The starting point is the selection of a series of relevant elemental shape changes each characterized by a parameter. The configuration with various combinations of the elemental shape changes are calculated with the nonlinear flow code, and the resulting drag and lift are determined. Only those cases with the prescribed lift are retained. For these cases the drag is plotted as a function of the shape parameters, and the direction of the greatest drag decrease in the parameter space is ascertained. A suitable point along this path of steepest descent is then used to define an improved configuration. The above procedure is repeated starting from this improved configuration. With many nonlinear calculations necessary, essential ingredients in the above procedure are a computer code that is fast and easy to use, a geometry code with an accurate interpolation scheme, and finally an effective mesh generator.

The example from Ref. 19 is the C-141 swept wing shown in Fig. 25 at the Mach number of 0.77 and a design lift coefficient of 0.60. The shape changes considered were the variations of the coordinates at four points along the upper surface chord at three span stations. The location of the four points were selected to cover the expected location of the supersonic region (see Fig. 25). That is, a combination of 12 parameters defined the optimal shape change. In Fig. 26 the optimized shape and corresponding

pressure distributions are shown compared to the baseline shape and pressure distribution. It is seen that the shock wave has been essentially eliminated. The airfoil thicknesses, except for the root chord, have been slightly decreased by the optimization. Finally Fig. 27 shows the drag divergence Mach number to be increased by approximately 0.02. The above optimization required 12 iterations and 1.43 hours on the Cray XMP computer with a single CPU. Nonlinear optimization procedures such as the above method using the steepest descent search will become an important design tool in the not too distant future.

Finally some comments are appropriate on the role of shockless airfoils and wings which can be generated with available techniques. To be sure a shockless airfoil will have zero pressure drag, but the general experience has been that a greater lift-to-drag ratio (L/D) can be achieved by permitting a weak shock. In the case of the shockless airfoil the recompression on the upper surface must be initiated sufficiently far upstream to generate the smooth gradual pressure recovery required to avoid the shock wave. By permitting a benign shock the recompression can be delayed to a point further downstream thereby generating greater lift without significantly adding an entropy increase and hence a drag increase. With the benign shock the (L/D) is increased relative to the shockless airfoil.

6. SUPERSONIC MANEUVER DESIGN

As the angle of attack is increased into the maneuver lift range, the flow becomes highly nonlinear, and the linear inviscid optimization methods are no longer valid. As described earlier, separation vortices on the fuselage and wing leading edge region arise as well as cross-flow shocks on the wing with accompanying shock-induced separations. The flow becomes, not only nonlinear, but rotational and viscous as well. When the flow is nonlinear, there are no convenient optimization methods as in the linear cruise case.

The basic features of the wing/fuselage are usually established by the supersonic cruise requirements. High lift performance is then addressed by incorporating variable geometry devices as leading and trailing edge flaps. The detailed performance of high-lift devices, both at supersonic and transonic speeds, will be covered in a later lecture by Dr. John Lamar. In the present section we shall confine our attention to two specific high-lift wing design examples using exact potential methods. Wind tunnel tests are available for these cases.

The first example is from Ref. 20 where the problem of moderating the cross-flow shock is addressed using the exact potential method. Potential methods can be used when the viscous effects are weak and the shocks are sufficiently weak that the entropy generation is negligible. The configuration considered is shown in the upper part of Fig. 28 which was conical except in the aft portion. The surface of a conical configuration can be generated by straight lines passing through the wing apex. Such a configuration was selected, since in a supersonic flow the velocities are invariant along rays passing through the wing apex, and the 3 dimensional (3D) potential equation can be simplified to a 2D equation in the cross-flow plane.

The leading edge sweep $\Delta\lambda_e$ was 57° . The design Mach number M was chosen such that the leading edge was subsonic with $\beta \cot \Delta\lambda_e = 0.83$ where $\beta^2 = M^2 - 1$. The value 0.83 was found to be more appropriate for the nonlinear high-lift conditions than the value of 0.75 evolved from linear experience. For $\Delta\lambda_e = 57^\circ$, the resulting Mach number was 1.62. The design lift coefficient was 0.4.

The starting baseline configuration is the flat wing. The calculated spanwise pressure distribution for this wing is given in the left part of Fig. 28 which shows the presence of a strong cross-flow shock. Experiments further indicated the presence of a shock-induced separation. Also shown in the left part of Fig. 28 are the measured pressures which are seen to agree closely with the calculations. Such an agreement is surprising in view of the strong shock/boundary layer interaction present.

The objective was to modify the above baseline wing to eliminate or greatly weaken the cross-flow shock keeping the lift coefficient invariant. To accomplish this, the leading edge portion of the upper surface was modified to reduce the large nose suction and the large Mach numbers upstream of the shock. This was accomplished by tailoring the nose radius, incorporating a nose-down leading edge camber, and reducing the convex curvature upstream of the shock. For the present highly nonlinear flow a trial and error search was required to evolve the proper combination of the above changes. The resulting configuration and pressure distribution are shown in the right part of Fig. 28. The design is seen to be highly successful with the cross-flow shock essentially eliminated. Comparison of the calculated results with the experiments here again shows excellent agreement. Finally in Fig. 29 the drag-due-to-lift for the two wings is plotted versus the lift coefficient. Notable here was the drag reduction of 65% of the theoretically possible reduction determined by linear theory. Here the theoretical "worst and best" values predicted by the linear theory are only approximate, but they are the only available estimates.

The second example is from Ref. 21 where the above design approach was applied to a fighter wing shown in the right part of Fig. 30. The optimization search was carried out with the 3D exact potential code. The design Mach number and lift were respectively 1.62 and 0.4. The resulting pressure distribution is given in the left part of Fig. 30 showing a relatively weak cross-flow shock. Here again excellent test/theory agreement was obtained. The success of the design is more clearly seen in Fig. 31 where a drag reduction of 52% of the theoretically possible reduction as estimated by linear theory was achieved. The resulting drag coefficient at the design lift, not surprisingly, was very large.

7. TRANSONIC MANEUVER DESIGN

The use of leading edge vortices to improve the transonic maneuverability of a fighter (a Harrier model) from Ref. 22 is next described. The resulting flow problem is much too complex for analysis by existing methods. Ref. 22 is an outstanding example where prior experience and the skillful use of the wind tunnel have evolved a successful design.

An inboard strake was added to the existing model as shown in the upper part of Fig. 32. The purpose of the strake is to generate a leading edge vortex that trails downstream over the inner part of the wing inducing a tipward surface flow. This then thins the boundary layer, essentially eliminating the severe separation that was present in the inboard region. The strake vortex further promotes earlier leading edge separation outboard of the strake/wing juncture creating a second (wing panel) separation vortex starting at the juncture. This vortex, trailing diagonally downstream over the inner half of the outboard wing panel, sweeps out the separation in this region. Sketches of the oil flow pictures with and without the strake from Ref. 22 are given in the left part of Fig. 32 showing the elimination of the separation in the inboard half of the wing. Note also that the forward shock with the strake now originates at the further outboard strake/wing juncture leading to a considerably shortened outboard shock.

The resulting performance improvements due to the strake can be seen in the right part of Fig. 32 where the lift, rolling moment, and the rms value of the root bending moment are plotted versus the angle of attack. Here the root bending moment indicates the onset of buffet and gives a measure of the buffet intensity for the model. In summary one finds

1. significant delay of stall (lift plot);
2. removal of wing-drop tendency (rolling moment plot); and
3. greatly reduced buffet intensity (root bending moment plot).

Not shown above is the drag. Skillful tailoring of the strake was required in Ref. 22 to achieve the above performance without the large drag increases associated with the vortex flows. Having to fit the strake on the existing structure was a further design constraint.

Obtaining meaningful results at large angles of attack in the wind tunnel is at best a difficult task due to the severe unsteadiness of the flow. The above wind tunnel results obtained in the ARA (Bedford) Wind Tunnel were subsequently confirmed by a flight test.

8. SUMMARIZING REMARKS

The fluid dynamics of the flow over fighter configurations at transonic and supersonic cruise conditions is reasonably well understood. Optimization procedures for the supersonic case, based on linear inviscid theory, yield a good first approximation. For wings with subsonic leading edges, inclusion of the attainable leading edge suction force leads to improved results. Improved more-global modeling of the attainable suction is required, but it may be more expedient in the future to turn instead to Navier/Stokes analyses.

Transonic flows at cruise conditions are essentially nonlinear and viscous. Optimal designs must then be evolved by a search process using prior experience with the wind tunnel and the computer as complementary tools.

The above search can be guided for example by the method of steepest descent. In such a nonlinear design approach an essential ingredient is an applicable computer code which is fast and relatively easy to use. The speed of the computer code is essential to enable an economic calculation of the many cases required in the search process.

Present theoretical design tools are also inadequate to treat the maneuver problem at all Mach numbers. Here a skillful use of the wind tunnel is the only recourse at the present.

The examples used in the present review are not fully representative of the material existing within NATO. Examples were used that were readily available to the author which illustrated the design problem.

9. REFERENCES

1. Rodgers, E., and Hall, I., An Application to the Flow about Plane Swept-back Wings at Transonic Speeds, *J. of Royal Aero. Soc.*, Vol. 64, No. 596, 1960.
2. Pearcey, H., Osborn, J., and Haines, B., The Interaction Between Local Effects at the Shock and Rear Separations, AGARD CP 35, 1968.
3. Wai, J., and Yoshihara, H., Computation of Turbulent Separated Flows over Wings, Proceedings 3rd Symposium on Numerical and Physical Aspects of Aerodynamic Flows, Cal. State U.-Long Beach, 1985. (To be published by Springer Verlag).
4. Hummel, D., On the Vortex Formation over a Slender Wing at Large Angles of Incidence, AGARD CP 247, 1979.
5. Lambourne, N., and Bryer, D., The Bursting of Leading Edge Vortices-Some Observations and Discussions of the Phenomenon, British ARC R&M 3282, 1962.
6. Wedemeyer, E., Vortex Breakdown, AGARD Lecture Series 121, 1982.
7. Werle, H., Sur l'ecatement des Tourbillons, ONERA N.T. 175, 1971.
8. Szodruch, J., and Ganzer, U., On the Lee Side Flow over Delta Wings at High Angle of Attack, AGARD CP 247, 1978.
9. Haines, B., Aerodynamic Interference-A General Overview, AGARD Lecture Series Report 712, 1983.
10. Harris, R., An Analysis and Correlation of Aircraft Wave Drag, NASA TN X-947, 1964.
11. Carlson, H., and Miller, D., Numerical Methods for the Design and Analysis of Wings at Supersonic Speeds, NASA TN D-7713, 1974.
12. Sorrells, R., and Miller, D., Numerical Method for Design of Minimum Drag Supersonic Wing Camber with Constraints on Pitching Moment and Surface Deformations, NASA TN D-7097, 1972.
13. Carlson, H., Mack, R., and Barger, R., Estimation of Attainable Leading Edge Thrust for Wings at Subsonic and Supersonic Speeds, NASA TP-1500, 1979.
14. Miller, D., Supersonic Wing Design Concepts Employing Nonlinear Flows, 14th ICAS Proceedings, 1984.

15. Carlson, H., and Miller, D., The Influence of Leading Edge Thrust on Twisted and Cambered Wing Design for Supersonic Cruise, AIAA Paper 81-1656, 1981.
16. Carlson, H., and Mack, R., Estimation of Wing Nonlinear Aerodynamic Characteristics at Supersonic Speeds, NASA TP-1718, 1980.
17. Miller, D., and Schemensky, R., Design Study Results of a Supersonic Cruise Fighter Wing, AIAA Paper 79-0062, 1979.
18. Treadgold, D., and Wilson, K., Some Aerodynamic Interference Effects that Influence the Transonic Performance of Combat Aircraft, AGARD CP 285, 1980.
19. Cosentino, G., and Holst, T., Numerical Optimization Design of Advance Transonic Wing Configurations, AIAA Paper 85-0424, 1985.
20. Mason, W., and Miller, D., Controlled Supercritical Cross-Flow on Supersonic Wings-An Experimental Validation, AIAA Paper 80-1421, 1980.
21. Mason, W., A Wing Concept for Supersonic Maneuvering, NASA CR 3763, 1983. (Results reviewed in Ref. 13).
22. Moss, G., Some UK Research Studies of the Use of Wing-Body Strakes on Combat Aircraft Configurations at High Angles of Attack, AGARD CP 247, 1978.

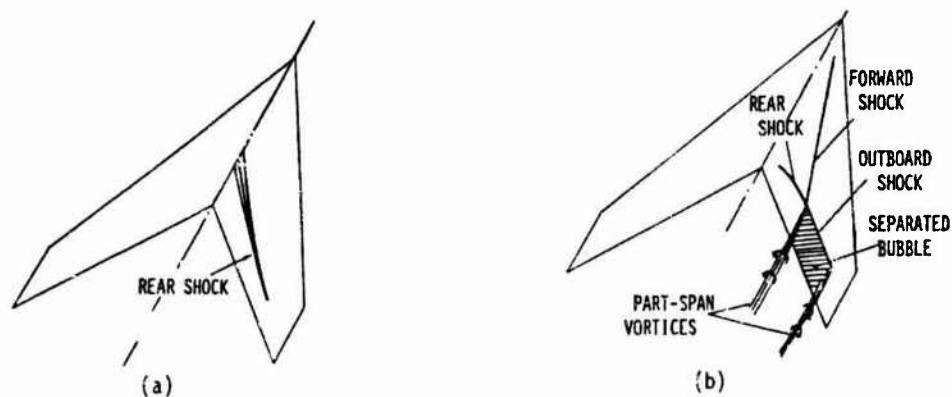


Figure 1. Sketch of Transonic Flow Features over Swept Wings.

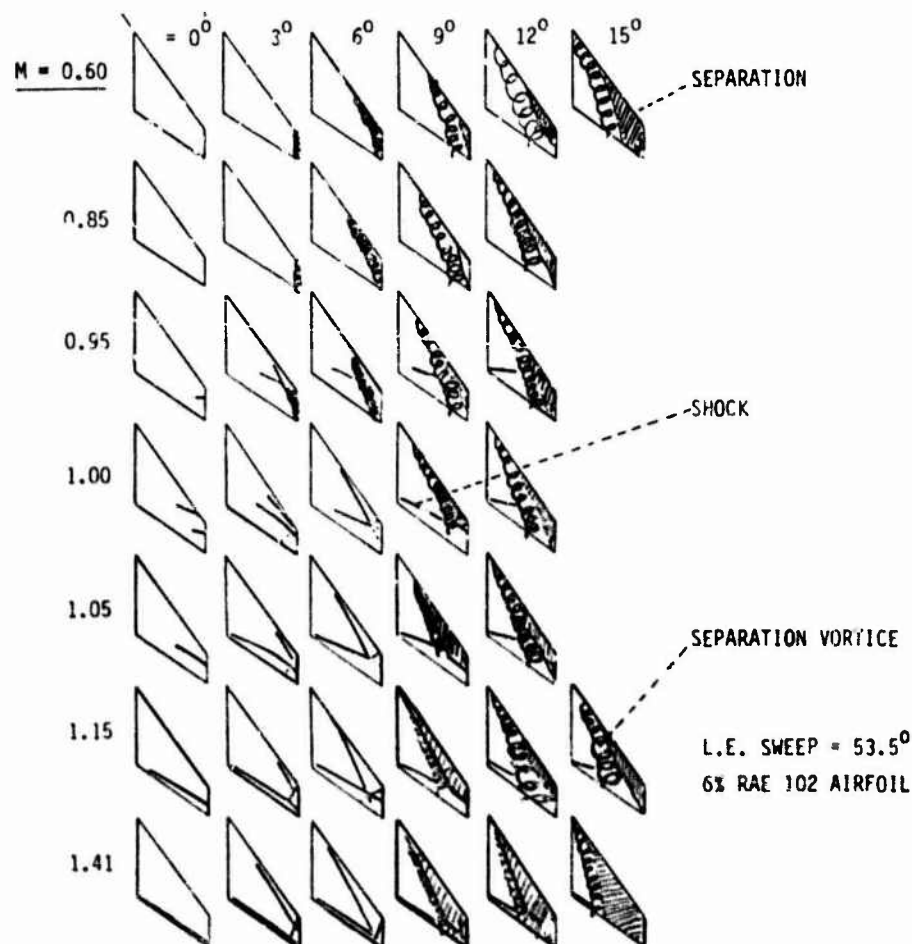


Figure 2. Upper Surface Flow Features for a Highly Swept Wing. (Ref. 1)

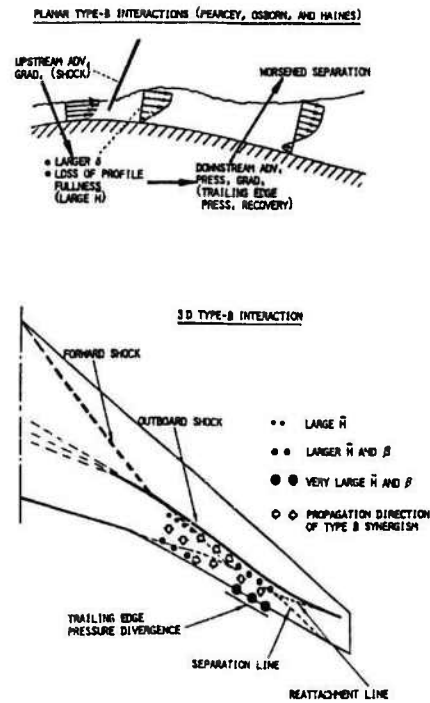


Figure 3. 2D and 3D Type B Viscous Interactions.

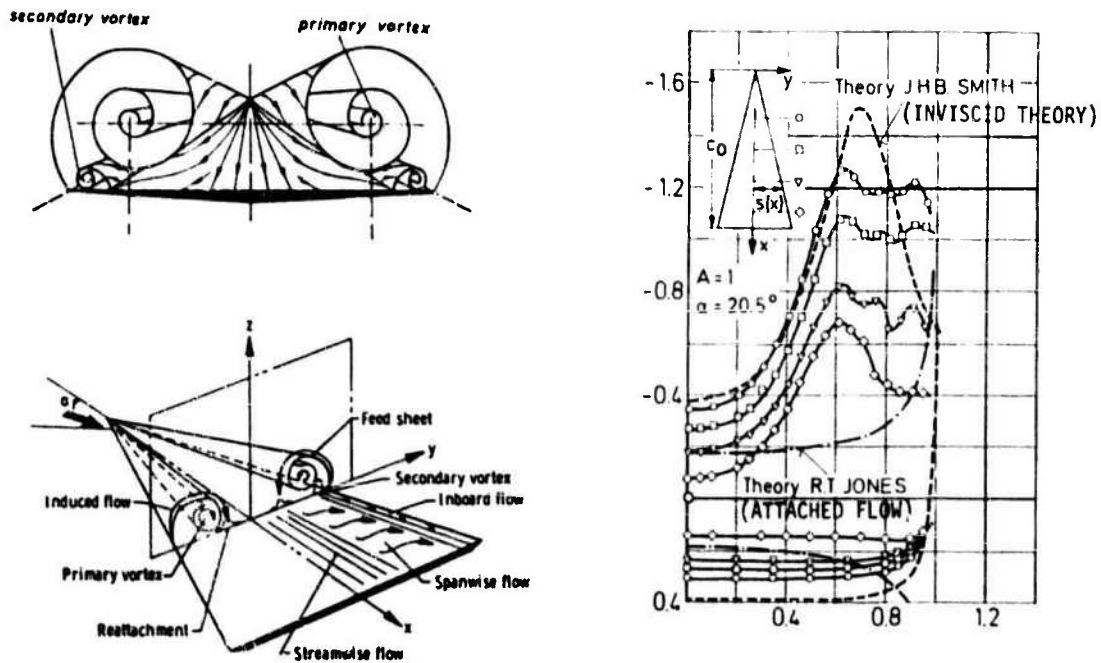


Figure 4. Primary and Secondary Separation Vortex Flows.
(From Ref. 4)

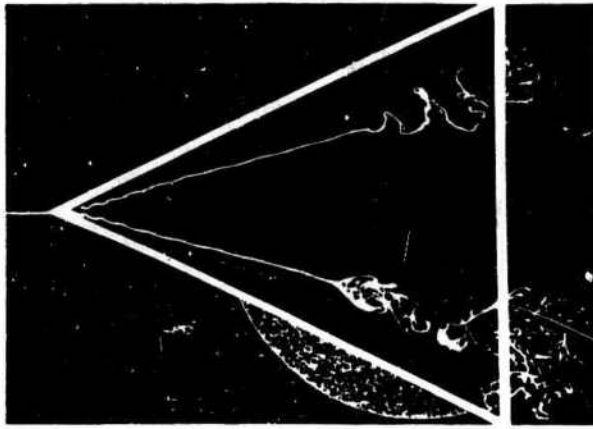


Figure 5. Spiral and Bubble Type Vortex Bursting. (From Ref. 5)

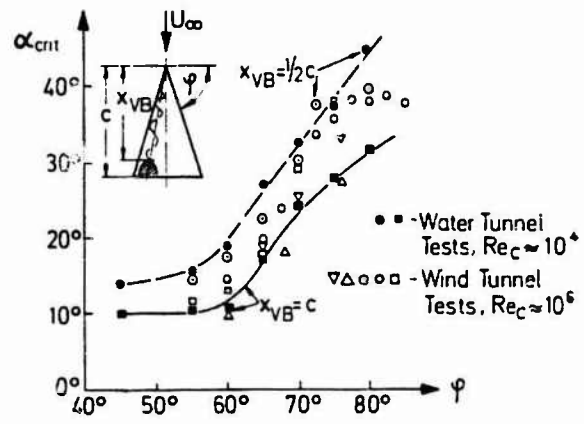


Figure 6. Vortex Burst Point Location. (From Ref. 7)

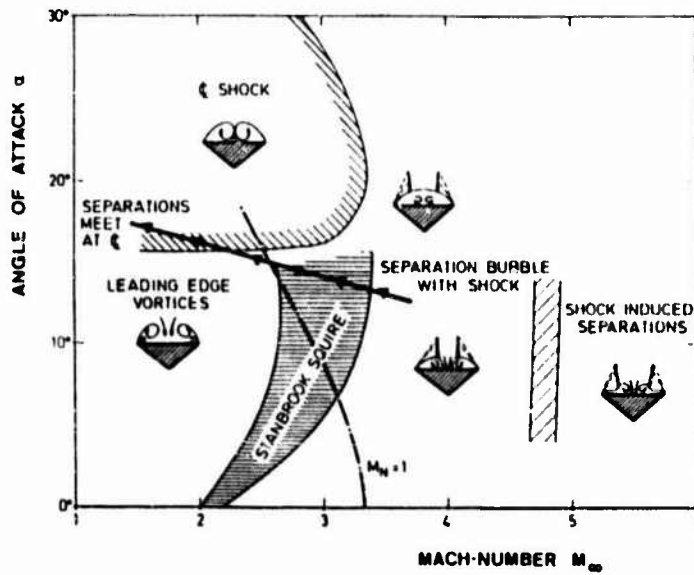
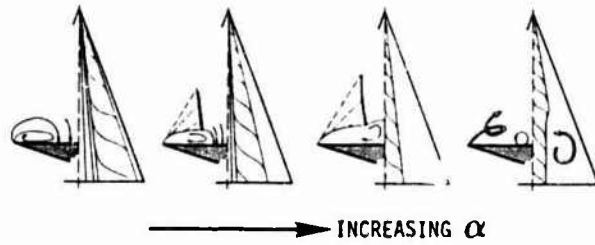


Figure 7. Classes of Lee-Side Separated Flows. (From Ref. 8)

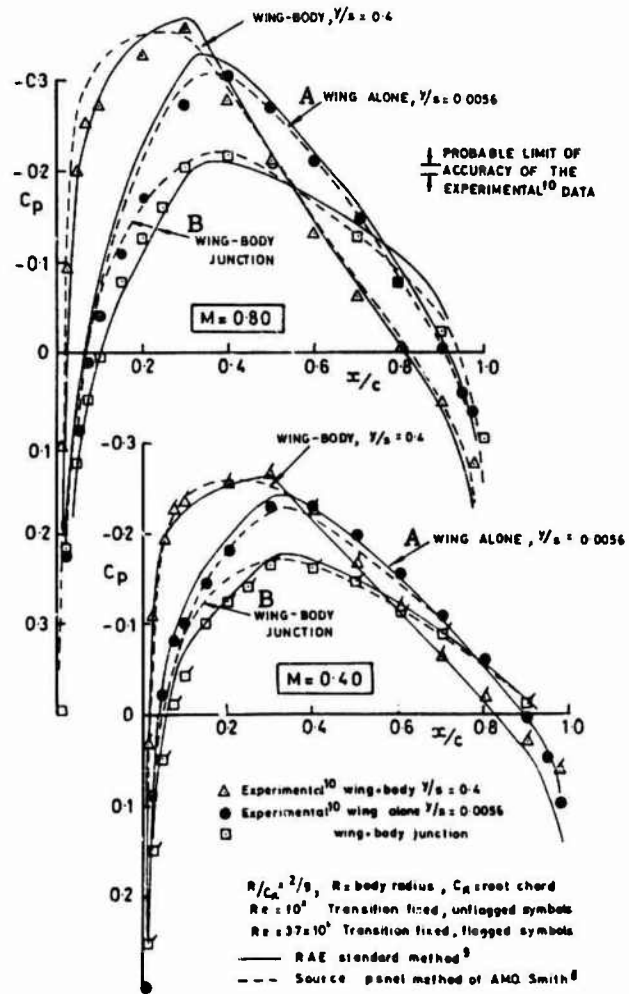


Figure 8. Wing/Fuselage Interference, Case 1.
(From Ref. 9)

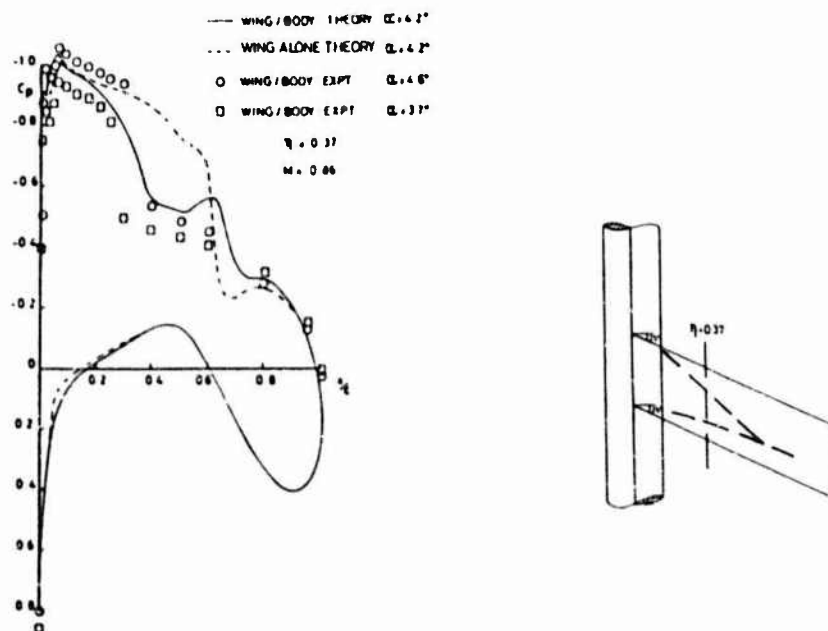
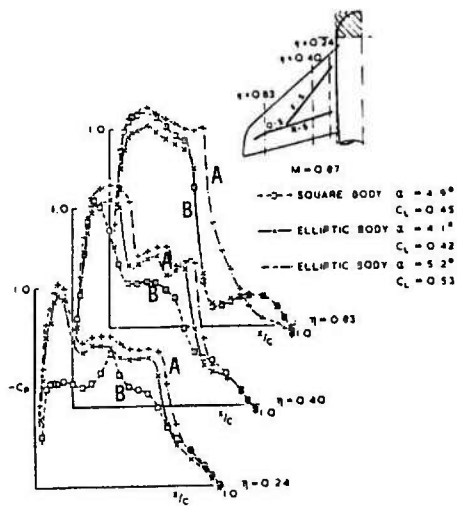
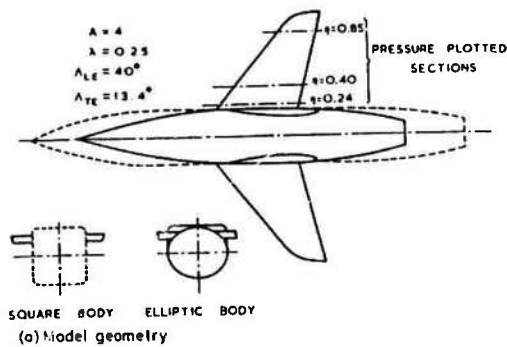


Figure 9. Wing/Fuselage Interference, Case 2.
(From Ref. 9)



(b) Pressures of design Mach number, $M = 0.87$



(a) Model geometry

Figure 10. Wing/Fuselage interference: Effect of Fuselage Shape. (From Ref. 9)

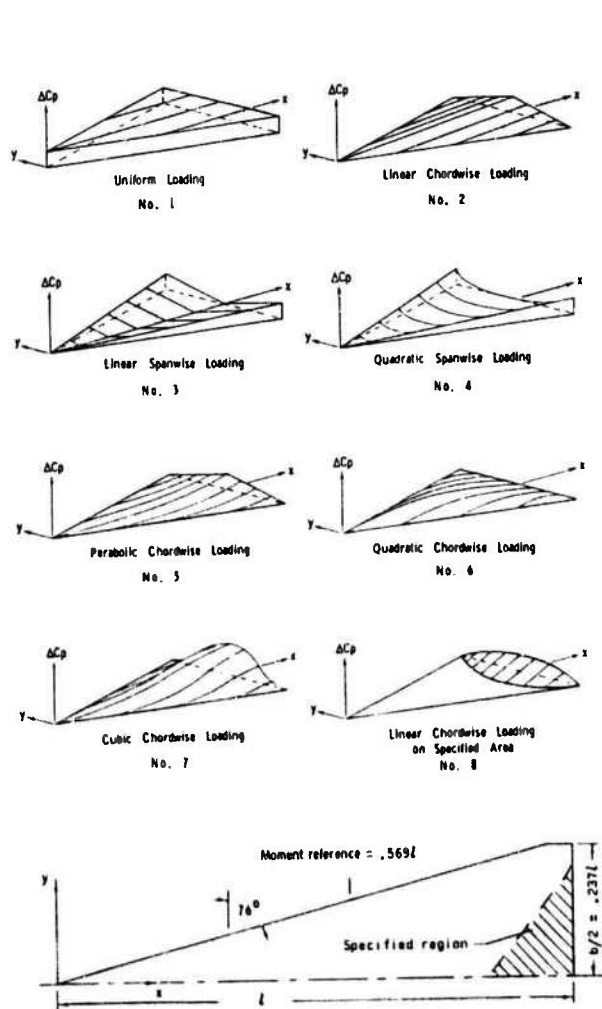


Figure 11. Supersonic Camber Optimization, Basic Loadings. (From Ref. 12)

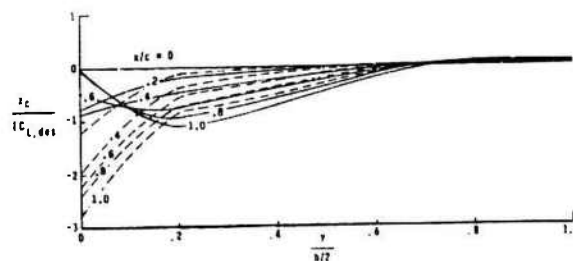


Figure 12. Resultant Camber Shapes for 76° Sweep Delta Wing. (From Ref. 12)

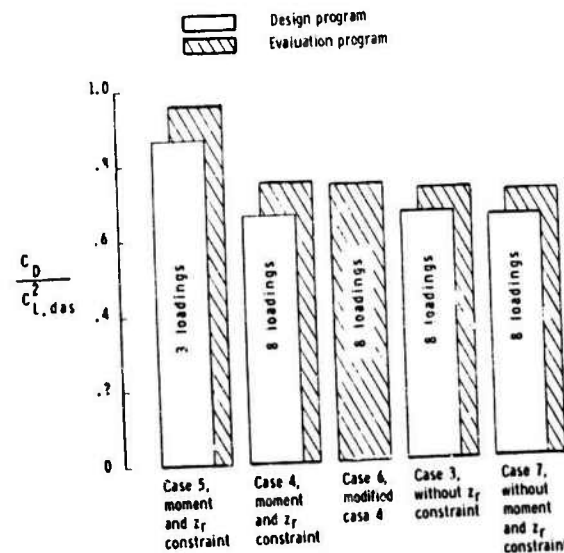


Figure 13. Effect of Constraints on Drag-due-to-Lift. (From Ref. 12)

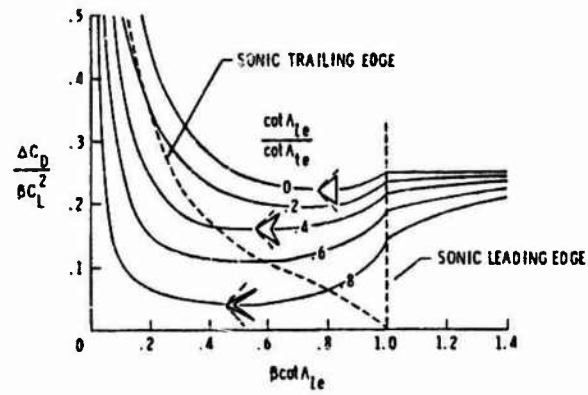


Figure 14. Linear Theory Drag-due-to Lift with Full Leading Edge Suction. (From Ref. 15)

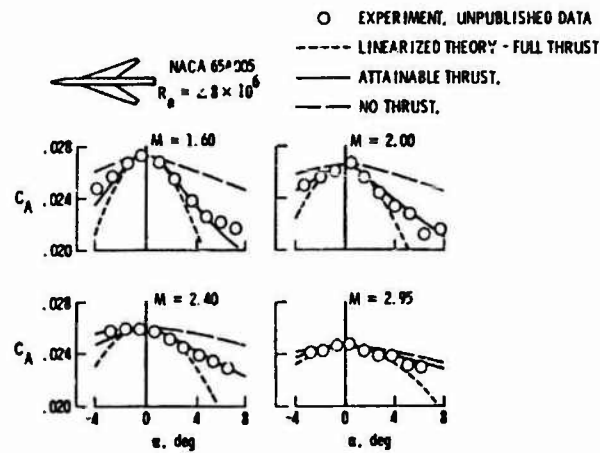


Figure 15. Axial Force Coefficient, Measure of Leading Edge Suction Force. (From Ref. 15)

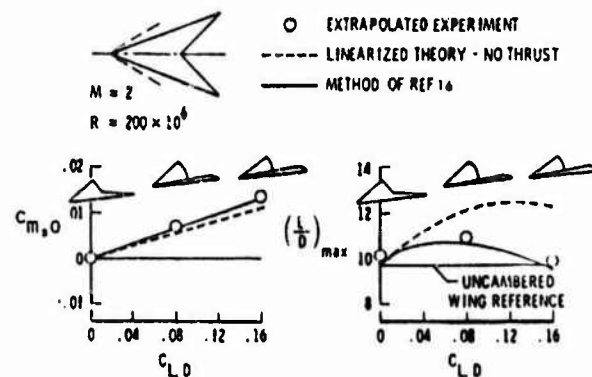


Figure 16. Test/Theory Comparison Using Attainable Leading Edge Suction Force. (From Ref. 15)

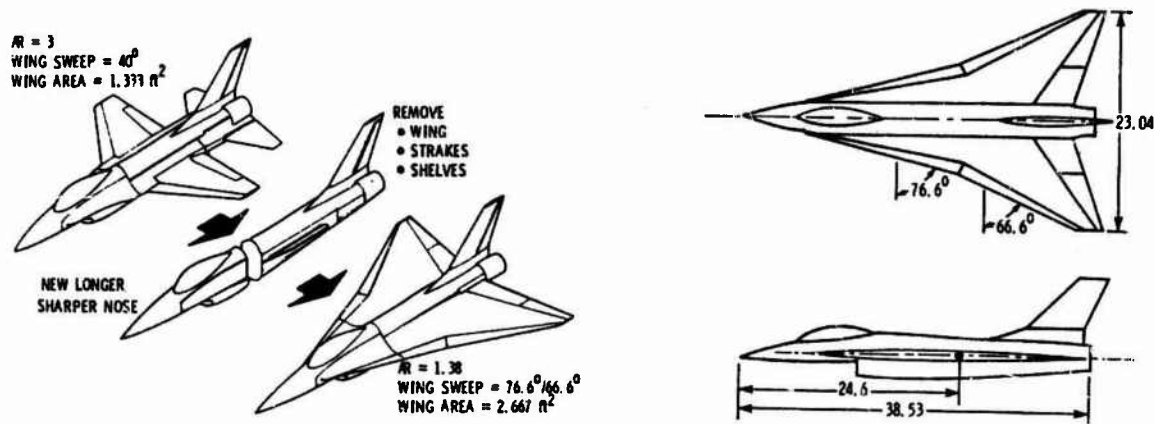


Figure 17. Fighter (Before) and Research (After) Models
(From Ref. 17)

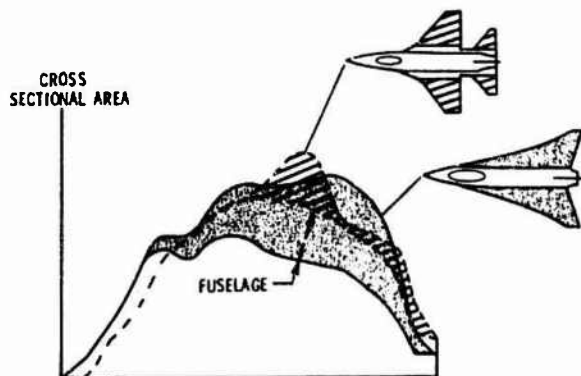


Figure 18. Comparison of the Mach-One Area Distributions. (From Ref.17)

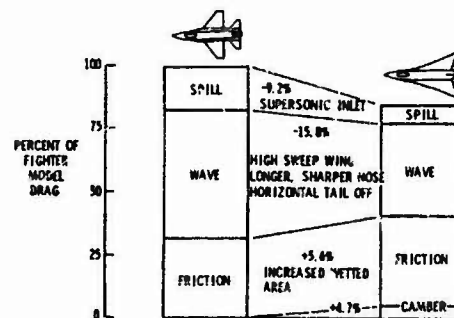


Figure 19. Pre-Design Drag Improvement Estimates. (From Ref. 17)

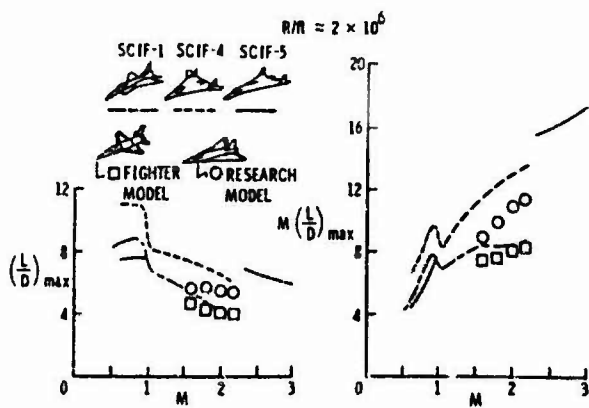


Figure 20. Comparison of the (L/D) and M(L/D).
(From Ref. 17)

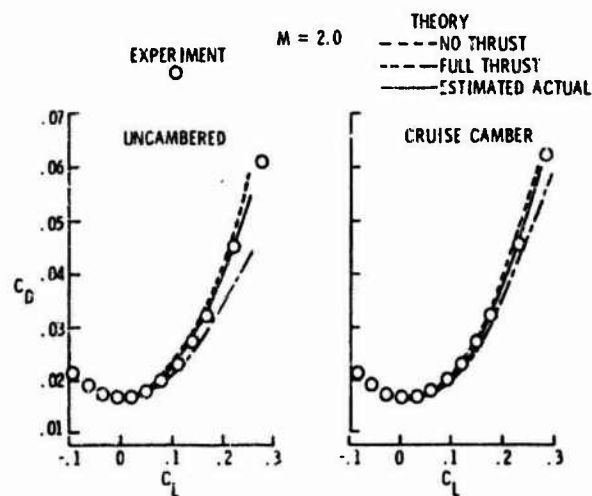


Figure 21. Test/Theory Comparison of the Drag Polars Using Attainable Suction. (Ref. 18)

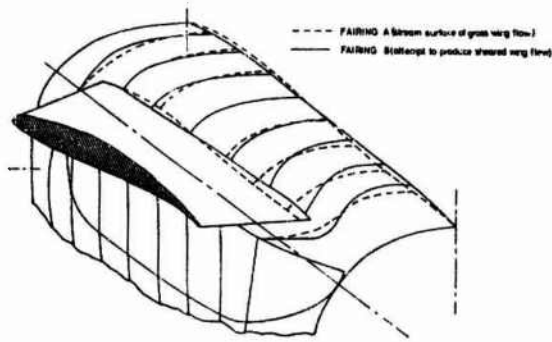


Figure 22. Comparison of Fairings A and B.
(From Ref. 18)

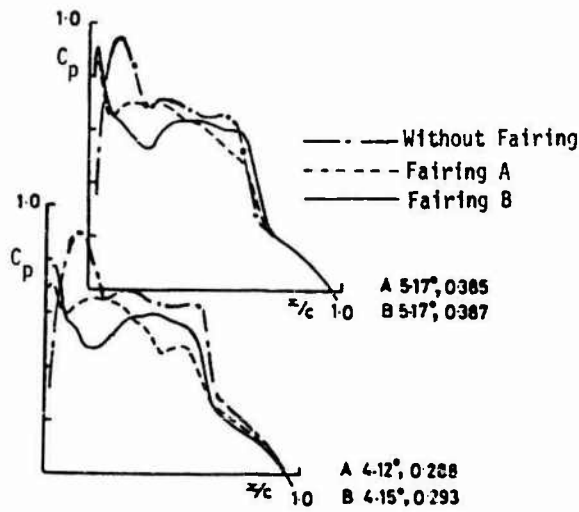


Figure 23. Resultant Pressure Distributions.
(From Ref. 18)

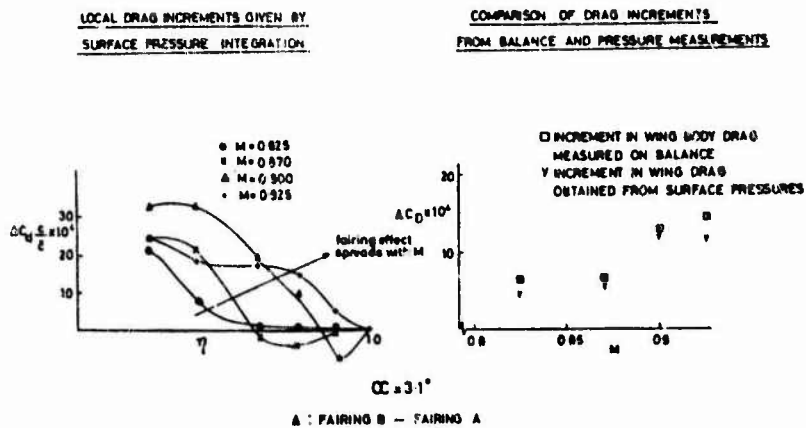


Figure 24. Spanwise Variation of Local Drag Differences Between Fairings A and B, and Total Drag Differences versus Mach Number. (From Ref. 18)

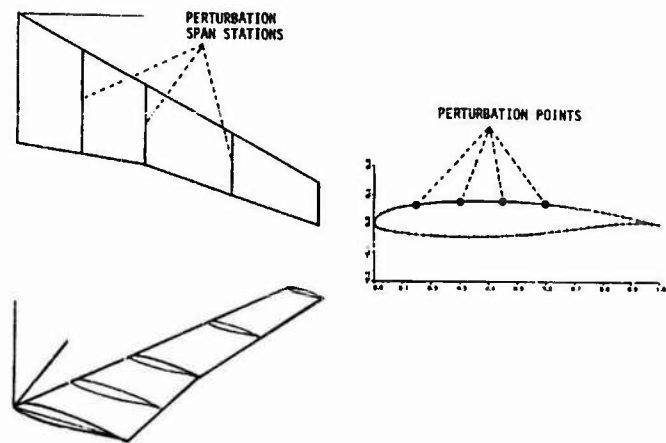


Figure 25. C-141 Wing Planform and Design Control Points.
(From Ref. 19)

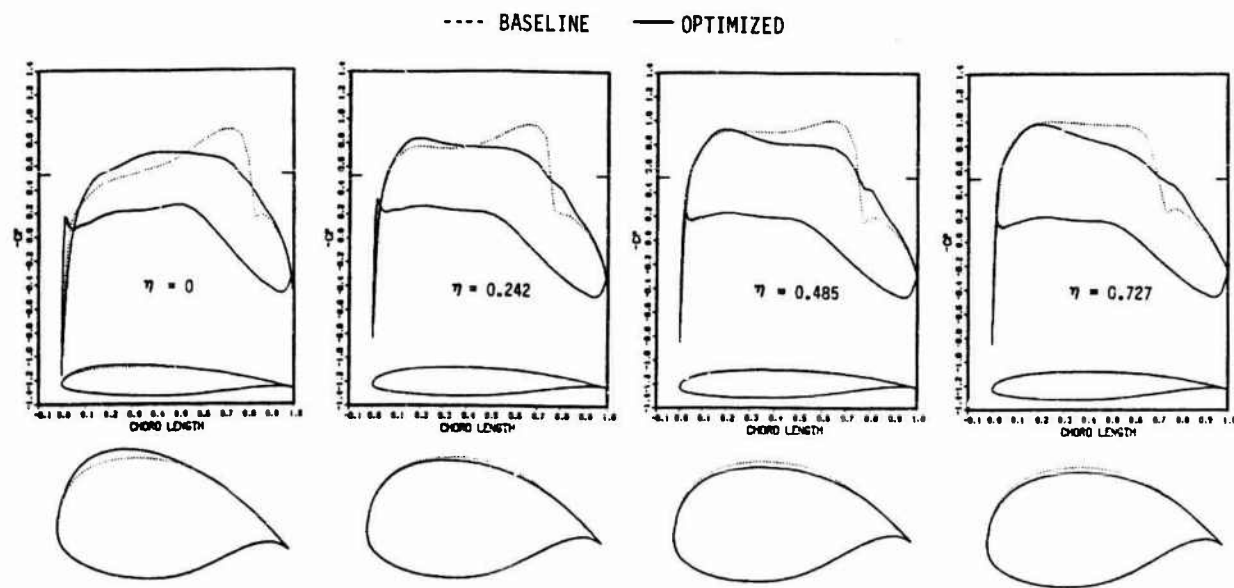


Figure 26. Optimized Configuration and Pressure Distribution.
(From Ref. 19)

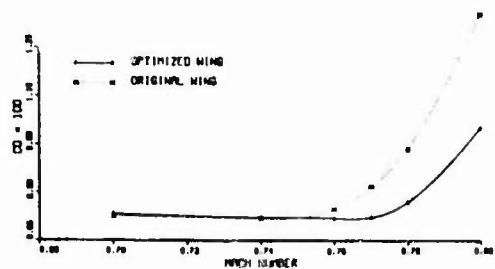


Figure 27. Comparison of the Drag-Rise. (From Ref. 19)

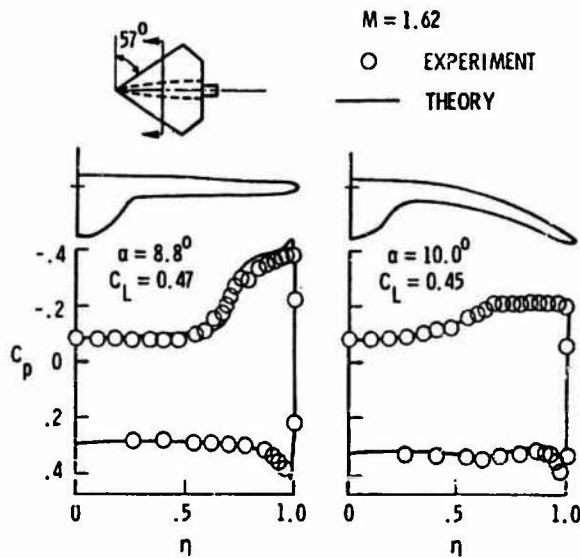


Figure 28. Supersonic Maneuver Improvement, Conical Case. (From Ref. 20)

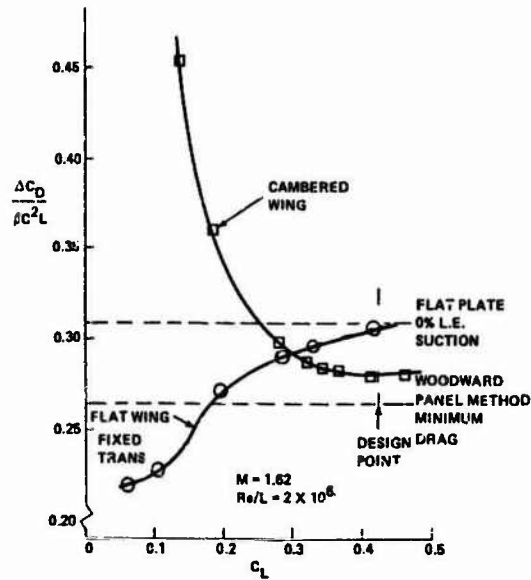


Figure 29. Resultant Drag-due-to-Lift Improvement, Conical Case. (From Ref. 20)

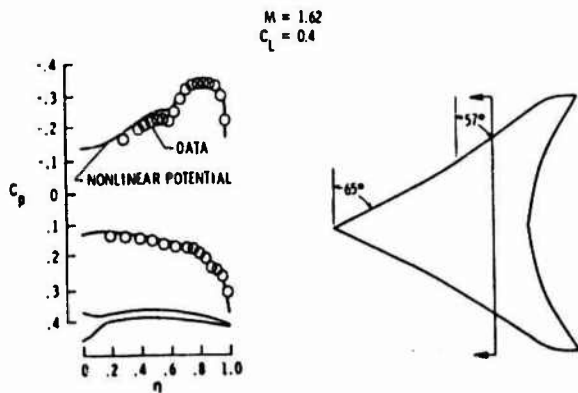


Figure 30. Supersonic Maneuver Improvement, Fighter Wing. (From Ref. 21)

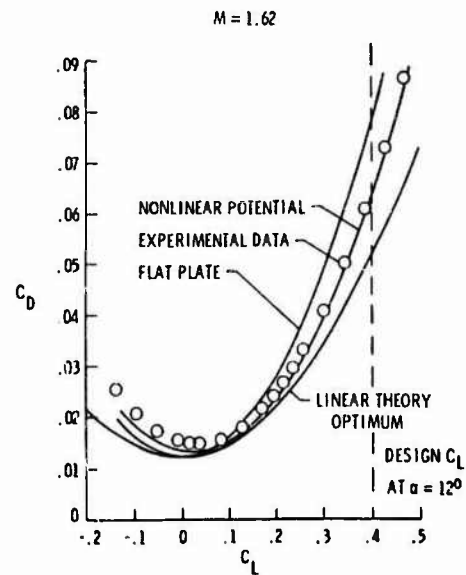


Figure 31. Drag-due-to-Lift Improvement, Fighter Wing. (From Ref. 21)

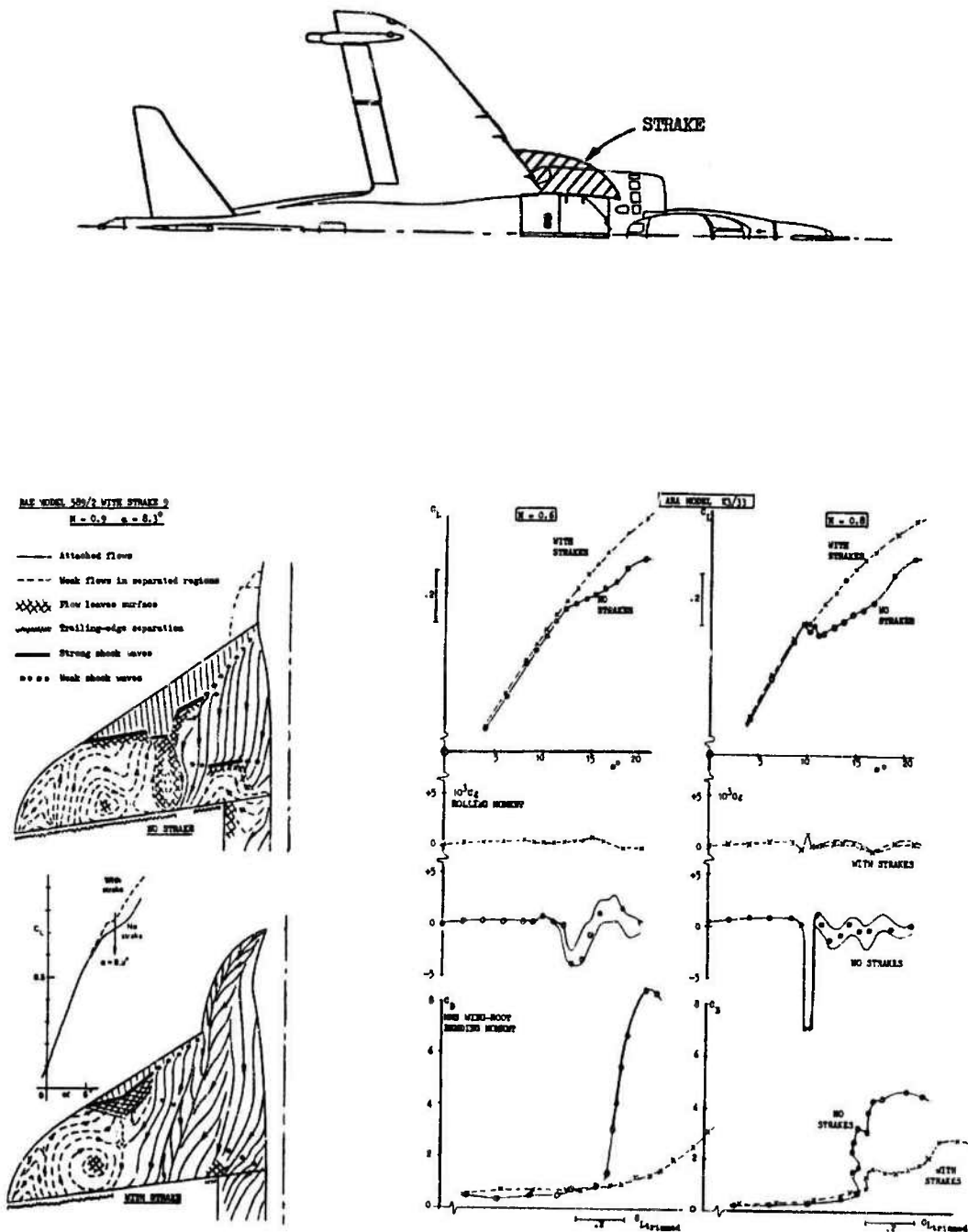


Figure 32. Use of a Wing Strake to Improve the Transonic Maneuverability. (From Ref. 22)

NONLINEAR LIFT CONTROL AT HIGH SPEED AND HIGH ANGLE OF ATTACK
USING VORTEX FLOW TECHNOLOGY

John E. Lamar
Senior Research Scientist
NASA Langley Research Center
Mail Stop 294
Hampton, Virginia 23665-5225
U.S.A.

SUMMARY

Nonlinear lift control at subsonic, transonic and low supersonic speeds owes its origin to the separated but organized vortical flows interacting with the wing upper surface. Since most of this flow originates near the wing or control-surface leading-edge, a variety of devices have been studied experimentally which interact with and/or control this flow in order to gain a beneficial effect. The benefits (effects) originally studied were only associated with lift enhancement. Whereas, now the studied benefits encompass performance increase, attention to changes in trimmed conditions and longitudinal stability, improvements in lateral stability, and the attendant variation with changing Mach number.

For those devices that can be theoretically modeled, state-of-the-art computer codes have been used for device design and/or analysis. Comparisons at design and off-design conditions are presented for validation purposes.

LIST OF SYMBOLS

A	aspect ratio of wing
b	span
C_D	drag coefficient, $\frac{\text{drag}}{q_\infty S}$
C_L	lift coefficient, $\frac{\text{lift}}{q_\infty S}$
C_{L0}	lift coefficient at $\alpha = 0^\circ$
$C_{L\alpha}$	lift coefficient curve slope, $\frac{\delta C_L}{\delta \alpha}$
C_l	rolling moment coefficient, $\frac{\text{rolling moment}}{q_\infty S_{\text{ref}} b}$
$C_{l\beta}$	lateral stability derivative, $\frac{\delta C_l}{\delta \beta}$
C_m	pitching moment coefficient, $\frac{\text{pitching moment}}{q_\infty S_{\text{ref}} \bar{c}}$
$C_{m\alpha}$	pitching moment coefficient curve slope, $\frac{\delta C_m}{\delta \alpha}$
C_n	yawing moment coefficient, $\frac{\text{yawing moment}}{q_\infty S_{\text{ref}} b}$
$C_{n\beta}$	directional stability derivative, $\frac{\delta C_n}{\delta \beta}$
C_p	pressure coefficient, $\frac{p - p_\infty}{q_\infty}$
ΔC_p	lifting pressure coefficient, $C_{p,u} - C_{p,l}$
C_μ	inlet momentum coefficient, $\frac{\dot{m} V_I}{\rho q_\infty S_{\text{ref}}}$
c	chord
\bar{c}	reference chord, mean aerodynamic chord primarily used
D	diameter of the pumped vortex suction apparatus
F(X)	objective function in optimization process

g	acceleration due to gravity; also, inequality constraint in optimization process
h	vertical distance between inlet centerline of the pumped vortex suction apparatus and wing chord plane; also, equality constraint in optimization process
L/D	lift-to-drag ratio, C_L/C_D
M	Mach number
\dot{m}	mass flow rate
p	static pressure
q	dynamic pressure
R_a	ratio of exposed strake area to wing reference area, S_s/S_{ref}
S, S_{ref}	wing reference area
V	velocity
V_x	X-component of the total velocity vector
V_y	Y-component of the total velocity vector
V_z	Z-component of the total velocity vector
X, Y, Z	coordinate axes centered at wing leading edge apex for LEE study
X_f, Y_f, Z_f	vortex flap coordinate axes centered at the apex of the flap, see figure 34
\mathbf{x}	vector of design variables
Δx_i	incremental step of i^{th} design variable
\bar{x}/c	fractional distance along the local chord of the called out surface

Subscripts/Superscripts:

BD	breakdown
b	body
d	design
I	inlet of pumped vortex suction apparatus
i	design variable index
LE	leading edge
LEE	leading-edge extension
l, \bar{l}	lower surface; also, lower
max	maximum
opt.	optimum
r	root
s	strake
swb	strake-wing-body
T	theory
TE	trailing edge
t	tip
tot	total
u	upper surface; also, upper
w	wing
wb	wing-body
o	value at $C_L = 0.0$
∞	freestream

Greek Symbols:

α	angle of attack, degrees
β	angle of sideslip, degrees
δ	flap deflection angle in plane normal to hingeline, positive downward, degrees
δ_A	aileron deflection angle, positive downward, degrees
δ_T	strake anhedral angle, positive downward, degrees
η	fraction of wing theoretical semispan, ($b_T/2 = 16.771$ in.), see figure 30
η_{LEE}	b_{LEE}/b_w , $b_w/2 = 16.15$ in. for wing in LEE study, see figure 30
θ	angular distance along local chord; 0 at leading edge; π at trailing edge
Λ	leading-edge sweep angle, degrees
Λ_h	hingeline sweep angle, degree
λ	wing taper ratio, c_t/c_r

Abbreviations:

AD	analytically designed
CLDESL	lower bound of design lift coefficient
CLDESU	upper bound of design lift coefficient
FVS	Free Vortex Sheet
LEE	leading-edge extension
LEVF	leading-edge vortex flap
PAN AIR	Panel Aerodynamics
PSS	Pseudo-Stagnation Streamline
PSSS	Pseudo-Stagnation Stream Surface
R.F.	Related Flow
STOL	Short Takeoff and Landing
3-D	three dimensional
TCDI(X)	calculated total induced drag coefficient
TCL(X)	calculated total lift coefficient
TEF	trailing-edge flap
VLM-SA	Vortex Lattice Method coupled with Suction Analogy
VORCAM	VORtex lift of CAMbered wings

INTRODUCTION

Historically, up to and including the 1960's, fighter aircraft were designed to perform their primary functions best with attached flow, and to handle the occurrence of separated flow in such a way that resulting control problems, such as loss of aileron effectiveness, were avoided or delayed. Experimental experience and theoretical tools available for configurations made it clear (then and now) that attached flow would be best for obtaining the lowest drag and/or highest lift/drag. For configurations that must satisfy an extensive set of multimission requirements, references 1 and 2 point out that the variable-sweep wing was found to be an appropriate geometrical and aerodynamical solution. This wing promotes attached flow during each phase of the mission. Examples of implementations of this concept are the United States Air Force (USAF) F-111, Navy (USN) F-14 (see fig. 1), the European Tornado, and the large variety of planes developed by the Soviet Union.

However, there exists a need for design concepts which provide some degree of multimission capability without resorting to variable sweep. One particularly important combination of mission capabilities is that of very high transonic maneuverability coupled with supersonic capability in a relatively lightweight fighter. To perform these tasks the design flow field will encompass both attached and vortical flows (ref. 1). Both the European Fighter Aircraft and the USAF's Advanced Tactical Fighter are examples of vehicles which will likely have this particular mission combination.

Organized vortical flow was successfully employed in the 1960's by SAA3 of Sweden in their closely-coupled canard-wing Viggen aircraft. This arrangement used a canard with trailing-edge flaps to control the aircraft and to delay gross upper surface separation on the wing. The latter occurred through a favorable interaction with the stable canard tip vortex and led to a more maneuverable aircraft at higher angles of attack. In the 1970's and into the 1980's the concept of using a trailing vortex system to control the flow on the main wing upper surface downstream was extended to include the direct lift benefits from the forward surface, e.g., strake, and has been incorporated into the F-16, F-18 and F-16XL aircraft (see fig. 2). This type of flow may be generated along the leading and/or side edge of a strake or the inner portion of a highly-swept cranked wing. The latter can be thought of as an extension of the off-design (and perhaps even on-design) vortex flow present on the Concorde (ref. 3).

Strakes and highly swept portions of cranked wings are only two means of generating stable vortex systems for main wing flow control. There are other fixed geometries or passive devices which have also been shown to perform similar functions. In addition, a variety of variable geometry devices have also been experimentally and analytically investigated which successfully manage the wing flow field through vortex flow creation or suppression as required. Also, the validated tools for the analysis and design of configurations generating significant amounts of vortical flow, which were lacking during the 1960's, began to become available during the 1970's. Furthermore, continued progress has been made in the development of these computational methods to the extent that now they are useful for both analysis and design (ref. 4). In particular, for some devices, among them the vortex flap (ref. 5), both the estimation of the aerodynamic characteristics and the design may be done effectively using analytical tools.

This paper deals with the control of the nonlinear lift associated with vortical type flow at high angle of attack in various speed regimes. Since control is associated with the impact of a deployed device, there is considerable emphasis in this paper on devices, be they fixed or variable. The devices highlighted are either relatively new, or older ones which have been the subject of new research. In addition, published theoretical solutions in either the analysis or design mode are presented with respect to pertinent data and the comparisons discussed. Where no computational solutions exist, selected data sets are given to illustrate the aerodynamic impact of representative devices.

VORTICAL FLOW CONTROL DEVICES

TYPES AND WIND TUNNEL CHARACTERISTICS

Fixed

Three fixed vortex flow control devices are covered in this section; including strakes, leading-edge extensions, and vortex generators.

Strakes

The general longitudinal aerodynamic effects of adding a strake to a wing-body are well known, but are repeated in summary form on figure 3 for completeness. In particular, strakes organize the wing flow field to a higher value of α , i. e., increase wing α_{BD} , which leads to a larger nose-up pitching moment when this vortex system breaks down. Also, on this figure, two experimental studies are highlighted. The first is to determine the effect of strake shape on the strake vortex system with emphasis on its α_{BD} characteristics; and the second is the effect of strakes on lifting surfaces which interact.

Planform Effects.- The photograph on the left of figure 3 shows a typical strake-wing-body in the strake effectiveness study. Reference 6 reported that, for a range of analytically and empirically designed strakes, those which developed a higher value of the section leading-edge suction force at their spanwise extremities generally had the higher values of α_{BD} at the wing trailing edge. Related low-speed wind-tunnel studies, reported in references 7 and 8, show the magnitude of the effect of planform shaping to be significant on C_L , both in terms of $C_{L,max}$ (fig. 4) and the post $C_{L,max}$ behavior (fig. 5), as well as on C_m (fig. 6). Figure 4 shows the gothic-like strakes to be more area efficient in terms of overall $C_{L,max}$ production than the reflexive type for R_a , ratio of exposed strake area to wing reference area, less than 0.25. This figure also shows that both types generate $C_{L,max}$ values significantly above what one could expect to occur from a wing area enlargement by the same amount. Figure 5 shows the post $C_{L,max}$ variation to be at a higher, almost constant, level for the gothic strake in comparison with the others in that R_a range. For nearly the same slenderness ratio (total length over exposed semispan) as the gothic strake, the middle-sized reflexive strake configuration on the right has similar post $C_{L,max}$ characteristics to those of the gothic configuration, but at an overall reduced C_L level. So, whereas increasing R_a does lead to an increase in $C_{L,max}$, making the strake less slender does not necessarily improve the post $C_{L,max}$ behavior.

Regarding C_m , the addition of any strake to the wing-body produces a configuration which is often less stable, as seen in figure 6, and has pitchup near $C_{L,max}$. The general reduction in stability before pitchup is due to vortex system enlargement, which puts the highest induced velocities farther from the lifting surface, and strake vortex burst or breakdown ahead of the wing trailing edge. At higher values of α , the burst

position moves forward across the wing upper surface and causes the aerodynamic load center to have a similar shift, hence pitchup results.

Figure 7 presents a summary (from ref. 8) of strake-wing-body-vertical tail lateral-directional characteristics reported by Luckring, from which it is apparent that all combinations were generally stable up to approximately 20° . For larger values of α the data become highly nonlinear and adverse, with this occurrence being delayed to a higher α for the largest reflexive strake arrangement.

Even for strakes which have good characteristics in combination with one planform, may not produce a net benefit when a configuration embraces several strake-wing planforms. An example of such an arrangement is a "Space-Jet" concept (configuration of ref. 9) shown on the right of figure 3. It is conceived of as being a candidate for a follow-on to the Space Shuttle, in which the inventors, Jackson et al. (ref. 10) envisioned using vortex lift to help this turbo-jet-powered vehicle takeoff horizontally. However, the resulting closely spaced interacting vortical flow systems were determined not to interact favorably.

Mach Number Effects.- Figures 8 and 9 (from ref.7) show the effects of Mach number on the wing-afterbody and strake-forebody C_L and C_m components, respectively, for a strake-wing-body model having a metric break and two balances. There, the C_m is plotted with $C_{L,tot}$ so that the contributions to the total model, shown in figure 10, can be isolated and presented in a similar format. Figure 10 shows that for the total configuration the C_L increases with Mach number at a fixed α . From figure 8 the wing-afterbody is seen to behave in the same manner as the total configuration; whereas, from figure 9 the strake-forebody shows a reduction in lift with increasing Mach number. It is somewhat surprising that the strake-forebody lift coefficient should fall off with increasing Mach number since it is basically a low-aspect-ratio lifting surface and hence should exhibit very little sensitivity to changes in Mach number. Evidently the cause for the reduction in C_L is the decrease in wing upwash associated with the increasing subsonic Mach number, as reported in reference 8.

However, it is not surprising that the increase in $C_{L,max}$, which occurs at $M = 0.5$, shows up on the wing-afterbody graph since the wing is a moderate-aspect-ratio lifting surface and, therefore, Mach number sensitive. Due to model and/or balance limitations, $C_{L,max}$ was not reached at $M = 0.7$. Lastly, the overall pitchup tendency previously mentioned results from the pitchdown tendency of the wing-afterbody at higher values of α or $C_{L,tot}$ being exceeded by the pitchup of the strake-forebody. Configurations of this type with vortex breakdown on the lee side would need to employ a low tail for stability and control.

Leading Edge Extensions - LEE

Enhancing the aerodynamic characteristics of moderate aspect ratio wings in the low-to-moderate α range can be accomplished by employing a leading-edge extension or LEE. Two examples are given. The first is for a LEE applied to a thick round-edged, 60° diamond shape, low-speed glider called the DM-1. The problem to be solved with this device, shown in figure 11, was to energize the flow on the leeward side of the wing so as to generate a $C_{L,max}$ value closer to that measured on thin sharp-edged wings. (Note that this device was successful as seen by the organized flow in the photograph on this figure at $\alpha = 18.9^\circ$.) This figure, developed from reference 11, shows the final placement of the LEE to be inboard. The lower drag is associated with low surface pressures acting between the LEE and the maximum thickness line of the wing section, thereby producing an aerodynamic thrust.

An ideal arrangement would be for the LEE to be mounted to a thick round-edge wing along the stream surface associated with smooth onflow at the attached flow design condition. For flight attitudes above that for smooth onflow, which would occur for takeoff, landing, and maneuver, a vortex would be generated in the region between it and the upper surface. This would energize the leeward surface flow and produce the lower pressures needed for drag reduction and lift enhancement. A methodology for accomplishing this is given later.

The second application is more recent and is to the outer wing panel of a transonic fighter model where improvements were sought in the drag polar by using vortices to energize the wing flow in the tip region at the higher values of α . This investigation, illustrated in figure 12, is intriguing because it involves the interaction of a vortical flow over the outboard portion of a fighter wing designed for attached supercritical flow. The early and advanced designs depicted in the figure are maneuver configurations developed by Mann et al. (ref. 12) using transonic methodology. In this effort to alleviate the shock-induced flow separation that eventually occurs in the wingtip region as lift increases, the attached flow design was supplemented with a sharp LEE (intended to be deployable for this application) on the outer part of the wing. Pressure measurements reported in reference 12 indicated that there was less flow separation on the outer panel with the LEE, which corresponds to the drag reduction obtained at high C_L . Further research of this vortex control concept is necessary in order to fully understand the implications of combining vortical flows with supercritical attached flows for maneuver wing designs.

The aerodynamic changes brought about by the introduction of vortex generators are highlighted in figure 13. There it is pointed out that the alteration in flow field results in a drag reduction due to improved leading-edge suction, and a slight lift loss due to the suppression of the leading-edge vortex. Another significant feature of the vortex generators is their ability to improve longitudinal stability. The devices delay the inboard movement of the tip vortex, which increases tip vortex lift and delays pitchup, compared to a wing without these devices.

Typical devices, and the ones reported on herein, are the pylon, fence, and slot. These fixed devices are generally placed at the leading edge (refs. 13-16) of round-edged wings. Each device produces a vortex that flows streamwise over the upper surface of the wing and splits the primary leading-edge vortex into segments. The outer vortex helps to keep the flow in that region from developing into a large scale "stall flow" until higher angles of attack are reached, thus alleviating pitchup.

Movable

Roll Control Device

An in-plane extension or retraction of the side-edge of a cropped delta wing (see fig. 14), caused by pivoting a portion of the wing about the tip leading edge, has led to a roll control (raked-tip) device for enhancing the high- α lateral characteristics. This patented device (ref. 17) was first discussed in reference 18. Its purpose is to modulate the strength of the vortex system and the associated reattachment area so that significant amounts of rolling moment can be generated at attitudes where other devices, such as ailerons, are known to be ineffective. The concept works best when the raked tips of a wing move laterally in the same direction during deployment. The device has been found to generate essentially a linear growth rate of rolling moment with either increasing α or tip rake angle, as opposed to a nearly constant value with aileron deflection, as shown by figure 14. Furthermore, the deployment of this device produced either no- or a proverse-yawing moment.

Articulating Strakes

An alternate approach for improving usable lift at high α is to utilize variable strake geometry as a lifting and control device. Moss (ref. 19) evaluated variable incidence and camber, while Rao and Huffman (ref. 20) studied the effects of anhedral on a hinged-strake concept. The hinged strakes are articulated to suppress the strake vortices, and thus eliminate or reduce the vortex breakdown effect. The hinged strakes, which are structurally separate from the wing, are attached to the fuselage through longitudinal hinges. The effect of hinged strakes on high- α aerodynamic characteristics is shown in figure 15 for a wing-body-vertical tail configuration. With respect to the strake-off configuration, the addition of the planar-strake ($\delta_r = 0^\circ$) leads to

the characteristic vortex breakdown condition evidenced by a peak in C_L accompanied by pitchup. Note also the opposite lateral-directional behavior as α approaches 30° due to the asymmetric breakdown of the strake vortices being different from that of the basic configuration. Deflecting the strakes to 30° anhedral greatly alleviates these vortex breakdown effects. Rao presents (ref. 21) additional data analysis to show that horizontal-tail effectiveness is increased by symmetric deflections of the strakes, and that large rolling moments occur due to asymmetric deflections that become larger than conventional ailerons at high α .

Vortex Flaps - Various Kinds

Concept and History.- Since the vortex flap concept has been well documented by various authors (e.g., refs. 5 and 22-24) only a brief review of the NASA Langley contribution will be presented. A depiction of its history is presented by figure 16. In 1978, an attempt to utilize leading-edge vortex flow for a transonic maneuver configuration was jointly pursued by NASA and General Dynamics for a cranked arrow wing called "Pre-Scamp". The resulting transonic, point-design, highly-warped, surface produced an impressive L/D and close to 76-percent effective leading-edge suction at a design $C_L = 0.5$ at $M = 0.85$ (ref. 25). Naturally, the camber was off-design under other conditions, especially at low C_L , so ways were sought to achieve the same benefit of vortex flow utilization, but without fixed camber. During the same wind-tunnel entry, a flat wing of the same planform with simple leading- and trailing-edge devices was also tested. The drag polar for this flapped configuration (fig. 17) indicated that effective suction levels approaching those of the designed camber shape could be achieved at the design conditions. The middle sketch on figure 16 shows that within a short time the general plan for implementing the vortex flap concept, by a combination of appropriately deflected leading- and trailing-edge flaps, was well understood. Experimental studies by Rao (ref. 26), among others, in which only the leading-edge flap was deployed, continued to provide additional evidence of the validity of using a device of this type in order to reap improvements in L/D or effective suction.

In order to have a proper implementation of the leading-edge vortex flap (LEVf) concept for drag reduction, it is important that two fluid mechanics phenomena occur. The first is that the shed leading-edge vortex system be entirely confined to the flap upper surface, which allows for the high suction pressures, associated with the nearby vortex, to generate significant amounts of aerodynamic thrust. This is accomplished by

having a proper combination of design variables, discussed later. The second is the avoidance of hingeline separation by having flow reattachment occur there.

To explore the LEVF concept, many analytical and experimental studies were conducted by employing various combinations of design variables; as typified by the sketches at the lower-left and upper-right of figure 16, respectively. The Free Vortex Sheet (FVS) method (ref. 27) was demonstrated by Frink (ref. 28) to be a useful tool in this process. The experimental studies were performed by many researchers and typical results reported in references 21 and 29. An examination of the results from these and other studies led Frink, in 1982 (ref. 30), to the development of a LEVF design procedure. A typical result is shown on the lower right of figure 16.

Types.- The typical vortex flap used for drag reduction is a lower surface device (or a simple hinged device deflected downward) and has been found to be effective at transonic speeds in the angle of attack range generally between 10° and 15° . Figure 18, taken from reference 5, shows typical lower surface devices which could be of the folding (Krueger), hinged, or tabbed types along with accompanying flow sketches. There are other uses for vortex flaps, as indicated on the left and top right parts of figure 18. These devices and flow sketches show how large amounts of lift can be generated at low wing angles of attack by deflecting an upper surface (ref. 31) or apex vortex flap (refs. 21 and 32) upward.

Apex Fence.- A variation of the last two devices is the apex fence (see fig. 19 and ref. 33). The fence is a variation of the upper surface flap in that it is deployed from there, is only part span, and works best when its hingeline is near the leading edge. Its relationship to the apex flap is twofold: both devices are located on the forward portion of the wing; and the fence provides a practical way of generating an apex flap type of vortex flow. The latter is mentioned because in an actual application the apex region of the wing would be covered by the fuselage. The apex flap and fence are both pitch controllers in that they provide a nose-up C_m ahead of the center of gravity at low α which requires a nose-down C_m aft for trim. This leads to a downward deflection of the trailing-edge flap and an overall increase in C_L . At high α , the apex fence generates a nose-down C_m which aids in pitch recovery.

Lower Surface LEVF.- Since transonic maneuver is one of the key items for future fighters, only the lower surface type will be considered for the remainder of this discussion; although it is interesting to note how, with appropriate articulation, the vortex flap may play a multimission role and even promote STOL-like performance. Conceptual sketches are shown in figure 20 for a simple hinged leading-edge device to work in conjunction with trailing-edge flaps so as to yield benefits over the entire flight envelope. The best sustained maneuver capability is obtained with the vortex flap deflected down causing a forward rotation of the vortex force vector. Takeoff and instantaneous maneuver lifts are maximized with the flap undeflected, while increases in lift and drag for landing are achieved with the flap deflected up. Deflecting the flap down at large angles on touchdown orients the vortex on the back side of the flap, increases drag, and provides negative lift on the wheels for shorter stopping distance. At subsonic and supersonic cruise, the flow may be attached and the flap functions like a cambering surface. Research is underway to quantify these benefits and a summary of recent experimental and theoretical work can be found in reference 34. Furthermore, from research reported in this reference, the LEVF has been determined, in general, not to be harmful to the lateral characteristics of the model to which it is applied.

The characteristics associated with many of the lower surface flap geometry changes are depicted in figure 21. Rao (refs. 21, 23, and 26) demonstrated that reducing the length of the vortex flap inboard improved efficiency. In addition, shaping the flap inboard improves the vortex formation while shaping outboard promotes vortex flow attachment at the hingeline, both of which reduce drag and delay pitch-up. Increasing flap size was shown by Rao (ref. 26) and Schoonover (ref. 35) to delay the inboard movement of the vortex, which combines with the increased flap frontal area to reduce drag.

In recent studies on an arrow wing configuration (ref. 36) and a cropped delta wing model (ref. 37), Rao demonstrated that flap segmentation is an effective technique to reduce the flap area while still achieving the same L/D as without segmentation. The flap segments generate multiple vortices that remain closer to the leading edge, improving the efficiency of the vortex flow in the tip region, which delays tip stall and improves the longitudinal stability characteristics.

Another variation of the folding flap (fig. 18) has been devised by Rao (ref. 38) in which the hingeline is moved away from the leading edge so that upon deflection the device resembles a forward facing split flap, much like one of the upper surface devices. It is called the 'cavity' flap and is shown in figure 22. When applied to a 60° delta wing in a preliminary test, improvements in the subsonic L/D, relative to a LEVF hinged at the leading edge, were found to exist over a wide C_L range for a 20° deflection, but not at 40° . This device is one which still needs to be optimized.

Staudacher in reference 39 summarizes data from a number of sources on wings with single- and double-hinged leading-edge and trailing-edge flaps. One conclusion reached is that only lower surface LEVFs applied to wings with leading-edge sweeps greater than 65° will show higher aerodynamic efficiencies, L/D, relative to the flap systems developed for attached flow. This is a rational conclusion from his paper and it is acknowledged that an attached flow solution will, in general, be the better one. The difficulty occurs in the transonic maneuver when attached flow cannot be maintained all over the

flap system and thin wing even for some moderate sweep wings. The flow will first separate in the tip region or along a hingeline without reorganizing. (This led Mann et al., reference 12, to incorporate a LEE-type device on their moderately swept wing to organize the tip flow and hence produced a higher L/D.) The utilization of the available shed vortex system is one of the major reasons for using a LEVF. Flap systems designed for attached flow may work as well in this environment as a poorly designed LEVF system (i.e., one which violates the two fluid mechanics phenomena stipulated previously), in that they do not promote vortex system capture on the flap surface. However, should vortex capture occur on the attached flow flap system, the ability to maintain it there is inferior to that of a properly designed LEVF system.

Trailing Edge Flap

In general, the trailing-edge flap (TEF) performs the same whether the flow type be vortical or attached; in that its downward deflection causes a significant increase in C_L and L/D to occur. Furthermore, when the TEF operates in combination with the LEVF, the aerodynamic benefit of deflecting the TEF may be larger than that associated with the leading-edge device alone. A negative synergism may occur upon the deployment of both devices, as reported by Staudacher in reference 39 and illustrated on figure 23. Just as in attached flow, TEF hingeline separation will occur on the upper surface for this device at too large deflection angles. The most effective range of downward deflection angles is from 0° to 20° .

Jet Augmented

Another approach for favorably effecting high- α aerodynamic performance is to use jet flows to augment and control the wing vortex. Many jet-augmented vortex concepts have been studied and three promising ones are shown in figure 24. These concepts are the fluid strake, spanwise blowing, and pumped vortex. Their function is to delay vortex breakdown and organize the wing upper-surface flow field to yield the desired aerodynamic benefits by the addition of energy to the system.

Fluid Strake.- The fluid strake concept (refs. 40 and 41) uses a jet sheet formed by blowing through a series of small in-line orifices located symmetrically on the sides of the fuselage ahead of the wing. The intent is to create the effect of a "fluid" strake that can be activated to obtain the high- α benefits of a solid strake, such as those discussed in figures 3 and 15. (Note this may be done either symmetrically or asymmetrically, depending upon the individual blowing rates.) The jet sheet generates a stable vortex flow over the wing, which increases $C_{L,max}$ and improves the drag polar and vertical tail effectiveness at high α . The lift augmentation of the fluid strake is comparable to that obtained with spanwise blowing.

Spanwise Blowing.- This concept energizes the leading-edge vortex by blowing a jet spanwise over the upper surface of a wing in a direction approximately parallel to the leading edge. Pressure data obtained by Campbell (ref. 42) demonstrated that full vortex lift could be achieved at inboard wing stations with relatively small blowing rates, but progressively higher values are required to obtain full vortex-lift levels at the more outboard span stations. Research by Erickson and Campbell (ref. 43) and Staudacher et al. (ref. 44) on fighter models showed that spanwise blowing increases lift, improves the drag polar, and linearizes pitching moment at moderate to high α . Spanwise blowing has significant effects on lateral-directional aerodynamics, which appear to be configuration dependent. Both rudder and aileron effectiveness are improved by spanwise blowing (ref. 44). Furthermore, it results in more stable roll damping and, as demonstrated in a free-flight experiment (ref. 45), helps eliminate wing rock.

Pumped Vortex.- Building on the work of Hummel (ref. 46), Taylor, et al. (ref. 47) investigated a pumped-vortex concept and showed the criticality of the location of the suction device used to pump the vortex downstream. Using an injector drive system, they were able to significantly increase the axial flow in the vortex which stabilizes the system to a higher value of α . The effects of the suction device on the lift characteristics for a blended delta model are shown in figure 25, which indicates that increasing C_μ increases C_L at moderate α and increases $C_{L,max}$. The augmented lift levels obtained here are higher than those obtained in Hummel's suction experiment because of the much higher C_μ values used for this test. These larger values induce higher velocities over the wing upper surface which even increases the potential flow lift contributions.

PROGRESS IN ANALYTICAL DESIGN

Much of the design work on devices for vortex flow management continues to be done empirically by creative engineers who are guided by a thorough understanding of the principles of fluid mechanics and aeronautical engineering. However, for some devices, including the strake, leading-edge-extension and vortex flap, sufficient progress has been made with available analytical tools to produce useful geometrical shapes. These are the topic of this section. In particular, details from two recently published design methods, one each for the LEE and LEVF, are presented for the convenience of the reader.

Strake

Reference 48 describes a correlation that was found to exist between the stability of the leading-edge vortex system and the leading-edge suction distribution. Those distributions which were roughly triangular and had high peaks near the tip developed stable vortex systems. This may be interpreted in a physical sense for separated flows, with the aid of the leading-edge suction analogy, in that they are more stable for shapes which have higher levels of separation induced vorticity near the tip.

However, to take advantage of this correlation for planform design, a simplification of the flow field was necessary in order to be able to solve the problem efficiently for the planform variables in terms of the leading-edge suction distribution. The assumptions employed in going from 3-D potential flow to the simplified flow field, called "Related Flow", are given in figure 26. Note the other assumptions which specifically impact the resulting planform. It is intended that these shapes would be used for strakes which would carry their isolated-planform performance characteristics from "Related Flow" over to the 3-D integration with a wing-body configuration. A typical resulting shape is gothic, as indicated in this figure. Strake shapes developed using this approach have been tested on a wing-body in both the water and wind tunnel, and selected wind-tunnel results have been reported previously in this paper.

Leading Edge Extension - LEE

This section presents a summary of a methodology for LEE design, which is detailed in reference 49. It has as its goal the enhancement of the off-design aerodynamic characteristics of thick, swept, cambered and twisted wings at high-subsonic and low-supersonic speeds without altering the on-design flow. (The particular configuration that prompted this work is a 58° delta for which a wing alone data base exists.) In order to do this, the LEE is to be mounted to the wing along the dividing stream surface, called herein, the "pseudo"-stagnation stream surface (PSSS), associated with the attached flow design lift coefficient ($C_{L,d} > 0$). The surface - to be determined - is called "pseudo" stagnation because, at its intersection with the wing, the velocity components are not all zero. The PSSS is a dividing stream surface which separates the incoming flow into two regimes, in general, over the upper and under the lower wing surface. Two streamwise cuts through the PSSS are shown schematically on the upper right of figure 27 and illustrate the surface curvature.

A summary of the assumptions employed in determining the PSSS (fig. 27) is as follows:

There exists a PSSS associated with a swept-wing aircraft at the attached flow design condition.

The intersection of the PSSS with a number of parallel XZ planes spanning the wing produces curves which are representative of the Pseudo-Stagnation Streamline (PSS) leading to the pseudo-stagnation point (i.e., $|V_x| \rightarrow \text{minimum}$, $|V_z| = 0$. (Note that $|V_y|$ is not assumed to be small nor zero, it is just not initially considered.)

The PSS shapes are derived from the local slopes of the resultant velocities

$\sqrt{v_x^2 + v_z^2}$ at appropriate points in the XZ plane.

A spanwise surface fitted linearly through the resulting intersections is an approximation of the PSSS described in the first assumption.

Constraints associated with an acceptable, and hopefully optimum, solution for the LEE are summarized in figure 27 as:

Its presence on the wing does not change the pressures and therefore the aerodynamic performance of the wing alone at the design lift coefficient.

The net lifting pressure across it approaches zero (targetted value) at the design lift coefficient.

It maintains a minimum planform area and chord length especially in the tip region where the wing local chord becomes shorter.

Its intersection with the wing remains on the wing lower surface.

At the bottom of figure 27 are sketches that indicate how the flow is envisioned to behave both at and above α_d .

A variety of analytical tools were examined for potential application in developing this methodology, as discussed in reference 49, but the ones chosen were PAN AIR (ref. 50) for determining the PSSS, and the VLM-SA (ref. 51) for establishing an appropriate extent for the LEE. (Note: Skin-friction drag is ignored throughout.)

PSSS Determination.- To find the PSSS with PAN AIR, its survey network mode (non-load bearing and not touching the surface) was invoked at some 16 spanwise locations for the desired Mach and α associated with $C_{L,d}$. In each of these parallel XZ planes the

resultant of each set of V_x and V_z velocities is drawn at its corresponding panel center and superimposed with the adjacent leading edge. A typical result is given in figure 28. From these velocity vectors a PSS curve was graphically determined by connecting a tangent to the vectors which terminated on the surface near where $V_z = 0$ and V_x was minimum. After all these streamwise curves were determined they were joined in a piecewise linear manner to produce the PSSS.

It is essential to examine the degree of accuracy of the determined PSSS solution for the thick delta of figure 29. For this purpose, the PAN AIR code was employed once again to model the wing+PSSS combination at the design condition (i.e., $\alpha_d = 6.0^\circ$, $M = 0.8$) by specifying the PSSS to be a lifting surface. Figure 29a shows the effect of the PSSS presence on the wing pressure distribution at a typical wing section to be insignificant. Also, as shown in figure 29b, the net lifting pressure across the PSSS appears small except at the local leading edge for the same typical section. From these results, it is evident that the addition of the PSSS surface does not cause much change in the performance of the wing model at the design condition. Therefore, it is concluded that the determined PSSS solution is close to the actual dividing stream surface (i.e., PSSS) and, hence, now that portion which is to be occupied by the LEE must be determined.

LEE Planform Optimization.- The VLM-SA code is employed in an attempt to optimize the PSSS planform shape. This optimum shape would then be designated as the shape of the LEE device. The aerodynamic effectiveness of 36 different LEE planform shapes were examined for the given wing by considering the influence of geometrical parameters such as constant chord (c_{LEE}), constant sweep (λ_{LEE}), and span extent (η_{LEE}). The planform view of these parameters relative to the basic wing geometry is illustrated schematically in figure 30. Although the twist and camber of the basic wing is represented by its mean camber surface, the thickness effect is ignored by the VLM-SA code. As discussed later, the analytical solution for the basic wing model which was first intended to provide a base line for comparative assessments of the LEE device appears to be inadequate. As a result, throughout this study the aerodynamic effectiveness of different wing+LEE combinations were therefore emphasized relative to one another rather than to the basic wing.

Figure 31 was prepared for the purpose of comparing the relative aerodynamic effectiveness of the different LEEs as a function of their geometrical parameters. In general, this investigation revealed that, with the same planform area, constant chord is relatively more effective than LEEs having sweep angles less than that of the wing. Therefore, two LEE planforms, each with 89-percent span extent relative to the wing span, one with 1.2" and the other with 0.8" constant chord, were selected as being the best candidates for the final LEE design planform.

Towards the Design Objective.- Several detailed modifications, described in reference 49, were made to both the wing and LEE in order to have the lifting pressure on the LEE be nearly zero. One of the biggest changes was rotating the LEE downward about 7 degrees to account for the three-dimensionality of the flow, i.e. no longer neglecting V_y . The final result, using the 1.2" LEE, is shown in figure 32 where the configuration is called Mod-wing and Mod2-LEE to reflect all the geometrical changes made.

Movable Device - LEVF

Analytical design procedures for the vortex flap, a particular movable device, will be discussed herein. The items to be determined for its design are flap planform shape, deflection angle and wing angle of attack for specified C_L and Mach number. There are some four different schemes which have been developed that will be considered in this section. All are summarized and one is described in detail.

VORCAM - Lan and Chang

Lan and Chang in references 52 and 53 developed VORCAM (VORtex lift of CAMbered wings), which has as one option that of designing a portion of a contiguous wing surface to represent an integral vortex flap inset into the wing. VORCAM is an improved version of Woodward's chord plane aerodynamic panel method (ref. 54) which uses the suction analogy (ref. 55) to calculate the vortex induced aerodynamic effects on cambered wings, including those with vortex flaps, and is valid in the linear range at subsonic and supersonic speeds. The design process employed is that of determining the corner points of the inset flap, its deflection angle and wing angle of attack by repetitive analysis using the optimizer CONMIN (ref. 56) in order to maximize the L/D at the $C_{L,d}$. Figure 33 shows an example of a initial guess and final planform for a VORCAM designed vortex flap. The initial α and δ_{LE} are 5° and 0° , respectively, with the final values being 17.5° and 54.9° .

Free Vortex Sheet - Boeing

The Boeing Company designed LEVFs for the USAF AFTI/F-111 program using the subsonic FVS method. Reference 57 reports solutions were obtained at high values of C_L and Mach by using a design by analysis mode. The FVS is a panel method which models both the wing-plus-flap combination and free sheet, and solves for the singularity strength on both, and position of the latter, by an iterative process for each set of angle of attack and Mach number. Hence, this is a two level convergence process: first to obtain a converged answer for all specified parameters, and second to change the flap and angle of attack incrementally until an acceptable planform, etc. result.

Carlson's method (ref. 58) has similarities to the previous two, in that it uses linear theory which has been modified for attainable thrust concepts and a modeling of the distributed pressures associated with a vortex system over the wing. It uses flap segmentation to seek a deflection set which yields the highest effective leading-edge suction. The flap planform and segmentation are based on representing the camber required for attached flow on the wing. The inclusion of trailing-edge flap segmentation and deflection is an integral part of this method.

VORCAM - Huebner

This method is also VORCAM analysis based, but differs in that the flap geometry can extend beyond the wing leading edge, i.e. a "bolt-on" flap implementation, and a different type (more efficient) optimizing procedure is employed. The work reported is based on reference 59 in which the primary goal is to develop the vortex flap planform, deflection angle, and wing angle of attack to maximize L/D and satisfy $C_{L,d}$ at $M = 1.5$ for the F-106B aircraft. This speed was chosen as typical of a supersonic maneuver for an advanced tactical fighter. The F-106B was chosen as the application aircraft since its 60° swept leading edge is capable of generating measurable amounts of vortex flow.

Optimization Background.- This new design procedure uses the Automated Design Synthesis (ADS) code of Vanderplaats (ref. 60). ADS is a general purpose numerical optimization program containing a wide variety of algorithms to solve the generalized constrained optimization problem. It minimizes an objective function, F , which is a function of the design variables, X , and the subject to inequality constraints (g), equality constraints (h), and limiting values on each design variable:

$$\begin{aligned} g_j(X) &< 0 & j &= 1, m \\ h_k(X) &= 0 & k &= 1, l \\ X_i^l &< X_i < X_i^u & i &= 1, n \end{aligned} \quad (1)$$

For the specific task of designing vortex flaps for the F-106B, the optimization goal is to minimize the objective function, $F(X)$, given by

$$F(X) = \frac{TCDI(X) + C_{D_0}}{TCL(X)} \quad (2)$$

where $TCDI(X)$ is the calculated total induced drag coefficient, C_{D_0} is the value of drag coefficient at zero lift, defined by

$$C_{D_0} = C_{D_0, \text{experiment}} - C_{D_0, \text{VORCAM}} \quad (3)$$

and $TCL(X)$ is the calculated total lift coefficient. Minimizing this objective function is identical to maximizing its multiplicative inverse, which is the lift-to-drag ratio. This is accomplished under the inequality constraints

$$\begin{aligned} g_1(X) &= TCL(X)/CLDESU - 1. \\ g_2(X) &= . - TCL(X)/CLDESL \\ g_3(X) &= X(1)/X(2) - 1. \end{aligned} \quad (4)$$

where g_1 and g_2 are upper and lower $C_{L,d}$ constraints, respectively, and g_3 is a geometry constraint discussed in the next section. No equality constraints were used in this procedure since they are the most difficult type to satisfy without relaxing convergence tolerances. Finally, the manner in which the flap model was generated from the design variables required bounds on their values that can be expressed by

$$0.01 < X_i < 1., i = 1, 7 \quad (5)$$

Analytical Flap Modeling.- Figure 34 shows a typical flap, its design variables, and its important features in flap coordinates. The X_f axis corresponds to the wing leading edge (hingeline) in global axes, and the dimensions of the flap have been normalized to have a range of zero to one. The Y_f variable determines the flap planform shape. Using the VF-D4 flap (developed by Frink) as an initial guess, this procedure models the planform shape in three regions. Regions one and three are parabolas which are uniquely defined by their two end-points and a slope condition at the points where they meet with region two, which is a straight line. The specific design variables needed to define this flap are shown in the figure. $X(1)$ and $X(2)$ determine the extent of the three regions in the X direction; $X(3)$ through $X(5)$ provide actual planform chord length and ultimately planform shape, $X(6)$ specifies the flap deflection angle and $X(7)$ is the model angle of attack.

It is worthy to note a few things about this method. The apex of the flap is shown to be at the origin of the flap axes. In reality, the chord length at this point need not be zero, but it is not a design variable and remains constant throughout the design process. The value of $X(1)$ can go to zero while the value of $X(2)$ can go to one. Thus, the possibility exists that a flap design solution could yield a constant chord, taper,

or inverse taper flap. Furthermore, the value of X(6) was chosen in such a way that it represents the arctangent of the flap deflection angle.

Certain geometrical constraints arise based on this method. In order to restrict the flap to a reasonable size, X(3) through X(5) are constrained such that their maximum values are no more than 10 percent of the leading-edge hingeline length. Also, to avoid meaningless flap shapes, the value of X(2) must be greater than or equal to X(1).

Optimization Algorithm Development.- The development of the optimization procedure is based on a programming synthesis system described in reference 61. VORCAM, ADS, and all supporting programs and subroutines used in this design procedure are linked by a series of nested procedure files, shown schematically in figure 35. Note how the analysis module is not called directly by the optimizer. Moreover, it only functions when the analysis module provides the necessary values and gradients of the objective function and constraints. It uses this information in design space to determine improved values for the design variables, which are then used to calculate an approximate value of the objective function (constraints also) by linear extrapolation using the following first order Taylor's series:

$$F_{\text{new}} = F_{\text{old}} + \sum_{i=1}^7 \frac{\partial F}{\partial X_i} \Delta X_i \quad (6)$$

Once the objective function calculated by the optimizer and linear-extrapolation-analysis loop converges, the updated design variables are returned to the analysis preprocessor and the cycle is repeated until the objective function does not vary by more than 0.10 percent for three successive cycles. At this point, the final design variable values are input into VORCAM to produce final design aerodynamic values, and the process terminates.

Applications.- Two specific applications for the F-106B (60° delta) are given. The design conditions are $M = 1.5$ at $C_L = 0.223$, and $M = 0.3$ at $C_L = 0.5$.

The initial geometric design variable values X(1) - X(5), associated with the supersonic application, were taken from the design solution of vortex flap VF-D4 at $M = 0.3$, along with X(6) which specifies flap deflection angle. The design variable X(7), which determines α was started at an arbitrary value corresponding to $\alpha = 4^\circ$. Convergence was achieved in 11 cycles.

Figure 36 shows the initial and final planform shapes and other pertinent results from this design study. The flap chord has decreased for most of the flap, designated VF-D01, except near the flap tip where it increased slightly. Flap planform area decreased by 6.5 percent. The flap deflection angle converged at 18.47° , which is quite close to the slope value at and perpendicular to the leading edge of the cambered wing. Finally, the angle of attack converged at 5.06° .

A comparison of the aerodynamic performance of VF-D01 and VF-D4 on the F-106B is shown in figure 37. The VF-D01 design shows an improvement in L/D of 0.6 at $C_{L,d}$ or 9 percent over the L/D value for the VF-D4 at 10° deflection. Further, the improved L/D values extend throughout the entire C_L range. The initial design solution is also included to show the total performance improvement from the beginning to the end of the design process.

Figure 38 shows the aerodynamic characteristics of these two flap designs at $\delta_{LE} = 30^\circ$ and $M = 0.3$. The purpose of this is to determine the aerodynamic characteristics of flap VF-D01 at an off-design Mach number. Minor variations occur for C_L and C_m versus α ; however, a measurable improvement in L/D_{max} is noted. Thus, the flap optimized for $M_d = 1.5$ would be quite satisfactory at $M = 0.3$.

The subsonic design conditions are the same as used for the VF-D4 and the initial planform design variables were taken from that shape. Only eight cycles were required to reach a converged solution for a new flap, designated the VF-D02, and it is compared in figure 39 with the initial design. The inboard 20 percent of the VF-D02 is nearly identical to the initial design, followed by a slightly smaller flap chord over the next 20 percent, and an increased chord on the outer 60 percent of the flap. The table on this figure allows for a comparison of the alpha and deflection angles required by each to meet the design C_L . The values for these parameters are seen to be close.

A comparison of the theoretical aerodynamic characteristics for the initial and final VORCAM vortex flap design solutions are shown in figure 40. The changes in C_L and C_m vs. α are minimal; however, there is again a measurable improvement in L/D, approximately 0.4 or 4 percent, at $C_{L,d}$.

CORRELATIONS WITH THEORY

Fixed

Strake-Wing-Body Combination

Figures 41 and 42 (from ref. 7) present comparisons between measured and theoretical data for a complete strake-wing-body and for its components, strake-forebody and wing-afterbody, respectively. The theoretical results, called high- and low- α , are based on

extensions to the suction analogy, outlined on figure 43, and described in reference 7. For the complete configuration (fig. 41) at $M = 0.2$ it is seen that up to $C_{L,max}$ the data are better predicted by the high- α method. Above the corresponding α , neither theory appropriately models the flow, hence the agreement is poorer. It is also seen that the two theories generally bracket the C_m data, again up to $C_{L,max}$ or vortex breakdown. The ability of these two simple theories to do this is encouraging, in that they are able to estimate collectively the nonlinear C_m versus $C_{L,tot}$ characteristics for this class of configurations. It can be noted that the low- α theory estimates better the C_m results than those obtained with the high- α theory. This occurs because the low- α theory produces a load center farther aft at a particular value of $C_{L,tot}$ even though this value is larger than the data at the same angle of attack. The potential-flow curve is added to the $C_{L,tot}$ versus α plots for reference.

The wing-afterbody and strake-forebody longitudinal aerodynamic data and the high- α and low- α theories are given in figure 42 for $M = 0.2$. Just as for the complete configuration, the individual data components are generally well estimated by the high- α theory or a collective combination of theories up to $C_{L,max}$ or large-scale vortex breakdown. What is particularly useful is that the individual C_m components are tightly bracketed by the high- α and low- α theories. The C_L data for the strake-forebody and wing-afterbody are well estimated by the high- α theory until the strake vortex begins to breakdown on the strake or ahead of the wing trailing edge, respectively. Lastly, note that at the higher angles of attack the wing-afterbody lift variations follow the potential curve even though the flow is closer to a Helmholtz type.

LEE Related

PAN AIR Evaluation.- In order to evaluate the PAN AIR code for thick delta wings at high subsonic speeds, the surface pressures for the basic 58° wing, used in the computational studies with the LEE, were computed at $\alpha = 6.0^\circ$ and $M = 0.8$. The result at $\eta = 0.30$ is presented in figure 44 with data from reference 62, taken in the NASA Langley 7- by 10-Foot High-Speed Tunnel. The comparison shows good agreement between the theoretical and experimental data except in the peak pressure region on the upper surface. The difference may be due to either differences in geometry (sting shroud omitted in PAN AIR) or flow types between the experimental configuration and theoretical modeling.

VLM-SA Evaluation.- As part of the utilization of VLM-SA code for unusual configurations, i.e. wing+LEE combinations, it is important to examine the analytical results relative to existing data. Two data sets are compared; one by Wilson and Lovell (ref. 11), on the thick DM-1 with and without the LEE, and the wing used in the wing+LEE design study, already presented in figure 31.

The DM-1 is a symmetrical wing configuration with an airfoil section like the NACA 0015-64 and no twist, so the LEE design lift coefficient ($C_{L,d}$) was zero. Although the effect of leading edge radii is included in the resulting VLM-SA solutions, the thick DM-1 is approximated by its projected planform (flat DM-1) in this study.

Experimental values for the lift and drag polars obtained by Wilson and Lovell are compared in figure 45 with the VLM-SA solutions. Obviously, the code over estimated the lift for both the DM-1 and DM-1+LEE combination throughout the angle-of-attack range. However, the drag polar comparison shows that, for the basic DM-1, the VLM-SA solutions have the same variation as the experimental data up to $C_L = 0.6$. Beyond this lift coefficient, the curves differ due to the disorganized flow over the basic DM-1, which causes both a drag increase and lift decrease (ref. 11). As a result, the theoretical drag polar is lower than the experimental data. For the DM-1+LEE combination, the VLM-SA over estimates the drag in the lift coefficient range of about 0.05 to 0.80. This difference was rather expected, because the resulting VLM-SA solutions do not include the effect of the low pressures acting between the LEE and upper surface maximum thickness line of the wing section to produce a thrust. Hence the computed C_p values are higher than the experimental data. Therefore, by analogy, it is expected that the VLM-SA solution for the drag would be higher than measured for the configurations considered in the LEE design section. This is the reason why only relative comparisons are offered there.

Figure 31 shows a sample of the available L/D experimental data (ref. 63) for the basic wing (zero LEE area) at four different angles of attack (6° , 8° , 10° , and 12°) and $M = 0.8$. These data appear as asymptotic values of the VLM-SA solutions for the wing+LEE.

Movable - Vortex Flap

VORCAM Subsonic Modeling Studies

Reference 59 presents paneling studies for modeling the F-106B cambered wing and vortex flap, and a study to determine the best method of modeling its cambered fuselage from the various options available in VORCAM. The paneling arrangement which agreed best with the longitudinal subsonic data was 4 spanwise strips within the fuselage contour, 14 spanwise strips on the wing-flap combination, and 10 chordwise panels on both. Figure 46 shows the paneling layout. The best fuselage modeling that could be accommodated in VORCAM was the one which included fuselage cambering and no accounting for body thickness effects. The supersonic solutions were obtained using the same modeling as determined best for the subsonic ones.

Figure 47 provides a comparison of longitudinal results for the F-106B with the VF-D4 vortex flap at $M = 1.5$ from VORCAM and measured data (ref. 64). In general, the theory and experiment are in good agreement, although C_{m_0} is slightly underpredicted. Concentrating on L/D , we see that both theoretical solutions overpredict the experimental results. Further, the experiment predicts that an L/D advantage for flap-added solution is not obtained until $C_L = 0.45$. This is due to the flap being greatly overdeflected for this speed.

As a result of the experimental data, a study was performed to determine the theoretical effect of flap deflection on L/D versus C_L . Results for the baseline and F-106B with vortex flap VF-D4 at three deflection angles are shown in figure 48. As can be seen, theoretical predictions for flap deflections at 10° and 20° show a slight increase in L/D from the baseline solution. Furthermore, the solution for the 10° flap deflection maintains slightly higher L/D values than the baseline throughout the C_L range.

CONCLUDING REMARKS

A variety of devices have been discussed for providing lift control by use of vortex flow technology. Some are fixed, like the strake and leading edge extension, while others are movable, like the leading-edge vortex flap. Some have already been widely used while others are just now being developed. The diversity of implementing a particular concept has also been highlighted, which reflects the variety of possible solutions to a single problem. For some devices there are theoretical techniques which can be used in their design, while for others wind tunnel testing will have to suffice for now in an empirical design process employing sound engineering principles from fluid mechanics. Furthermore, for those devices which can be modeled theoretically, the agreement with data is generally good. For others, the application of available theories needs to be done or wind tunnel testing performed in order to develop the needed data correlations.

REFERENCES

1. Polhamus, E. C.: Applying Slender Wing Benefits to Military Aircraft. J. Aircraft, Vol. 21, No. 8, pp. 545-559, Aug. 1984.
2. Loftin, L. K.: Quest for Performance - The Evolution of Modern Aircraft. NASA SP-468, pp. 255-259, 1985.
3. Morgan, M., Sir: A New Shape in the Sky. Aeronautical Journal, pp. 1-18, Jan. 1972.
4. Lamar, J. E.; and Campbell, J. F.: Recent Studies at NASA-Langley of Vortical Flows Interacting with Neighboring Surfaces. AGARD CP 342, Paper No. 10, 1983.
5. Lamar, J. E.; and Campbell, J. F.: Vortex Flaps - Advanced Control Devices for Supercruise Fighters. Aerospace America, pp. 95-99, Jan. 1984.
6. Frink, N. T.; and Lamar, J. E.: Water Tunnel Investigation of the Effect of Strake Design Variables on Strake Vortex-Breakdown Characteristics. NASA TP 1676, Aug. 1980.
7. Lamar, J. E.; and Frink, N. T.: Experimental and Analytical Study of the Longitudinal Aerodynamic Characteristics of Analytically and Empirically Designed Strake-Wing Configurations at Subcritical Speeds. NASA TP 1803, June 1981.
8. Lamar, J. E.; and Luckring, J. M.: Recent Theoretical Developments and Experimental Studies Pertinent to Vortex Flow Aerodynamics-With a View Towards Design. AGARD CP 247, Paper No. 24, Jan. 1979.
9. Small, W. J.; Riebe, G. D.; and Taylor, A. H.: Aerodynamics of a Turbojet-Boosted Launch Vehicle Concept. Journal of Spacecraft and Rockets, Vol. 18, No. 1, pp. 36-43, Jan.-Feb. 1981.
10. Jackson, L. R.; Weidner, J. P.; Small, W. J.; and Martin, J. A.: Orbiter/Launch System. U.S. Patent 4,265,416, May 1981.
11. Wilson, H. A.; and Lovell, J. C.: Full-Scale Investigation of the Maximum Lift Flow Characteristics of an Airplane Having Approximately Triangular Plan Form. NACA RM L6K20, Nov. 1946.
12. Mann, M. J.; Mercer, C. E.; and Campbell, R. L.: Supercritical Maneuvering Fighter Configuration Wind-Tunnel Investigation at Mach Numbers of 0.60 to 0.95. NASA TM-84513, Sept. 1982.
13. Johnson, T. D., Jr.; and Rao, D. M.: Experimental Study of Delta Wing Leading-Edge Devices for Drag Reduction at High Lift. NASA CR-165846, Feb. 1982.

14. Tingas, S. A.; and Rao, D. M.: Subsonic Balance and Pressure of a 60-Degree Delta Wing with Leading-Edge Devices. NASA CR-165923, May 1982.
15. Rao, D. M.; and Johnson, T. D., Jr.: Investigation of Delta Wing Leading-Edge Devices. J. Aircraft, Vol. 18, No. 3, pp. 161-167, March 1981.
16. Rao, D. M.; and Johnson, T. D., Jr.: Alleviation of the Subsonic Pitch-Up of Delta Wings. J. Aircraft, Vol. 20, No. 6, pp. 530-535, June 1983.
17. Lamar, J. E.: Vortex-Lift Roll-Control Device. U.S. Patent 4,132,375, Jan. 1979.
13. Lamar, J. E.: Prediction of Vortex Flow Characteristics of Wings at Subsonic and Supersonic Speeds. J. Aircraft, Vol. 13, No. 7, pp. 490-494, July 1976.
19. Moss, G. F.: Some UK Research Studies of the Use of Wing-Body Strakes on Combat Aircraft Configurations at High Angles of Attack. AGARD CP No. 247, Paper No. 4, Oct. 1978.
20. Rao, D. M.; and Huffman, J. K.: Hinged Strakes for Enhanced Maneuverability at High Angles of Attack. J. Aircraft, Vol. 19, No. 4, April 1982.
21. Rao, D. M.: Vortical Flow Management for Improved Configuration Aerodynamics-Recent Experiences. AGARD CP 342, Paper No. 30, 1983.
22. Runyan, L. J.; Middleton, W. D.; and Paulson, J. A.: Wind Tunnel Test Results of a New Leading Edge Flap Design for Highly Swept Wings - A Vortex Flap. Supersonic Cruise Research '79 - Part 1, NASA CP-2108, pp. 131-147, Nov. 1980.
23. Rao, D. M.: Leading-Edge 'Vortex Flaps' for Enhanced Subsonic Aerodynamics of Slender Wings. ICAS 80-13.5, Oct. 1980.
24. Lamar, J. E.; and Campbell, J. F.: Design Related Study of Transonic Maneuvering Slender Wings Having Vortex Flaps. Tactical Aircraft Research and Technology, Vol. 1, NASA CP-2162 Part 2, pp. 543-562, Oct. 1980.
25. Lamar, J. E.; Schemensky, K. T.; and Reddy, C. S.: Development of a Vortex-Lift Design Procedure and Application to a Slender Maneuver-Wing Configuration. J. Aircraft, Vol. 18, No. 12, pp. 259-266, April 1981.
26. Rao, D. M.: Leading-Edge Vortex Flap Experiments on a 74-Deg. Delta Wing. NASA CR-159161, Nov. 1979.
27. Johnson, F. T.; Lu, P.; Tinoco, E. N.; and Epton, M. A.: An Improved Panel Method for the Solution of Three-Dimensional Leading Edge-Vortex Flows. Volume I - Theory Document. NASA CR-3278, July 1980.
28. Frink, N. T.: Analytical Study of Vortex Flaps on Highly Swept Delta Wings. ICAS 82-6.7.2, 1982.
29. Frink, N. T.; Huffman, J. K.; and Johnson, T. D., Jr.: Vortex Flow Reattachment Line and Subsonic Aerodynamic Data for Vortex Flaps on 50° to 74° Delta Wings on Common Fuselage. NASA TM-84618, Dec. 1983.
30. Frink, N. T.: Concept for Designing Vortex Flap Geometries (U). NASA TP 2233, Dec. 1983.
31. Rao, D. M.: Upper Vortex Flap - A Versatile Surface for Highly Swept Wings. ICAS 82-6.7.1., 1982.
32. Buter, T. A.; and Rao, D. M.: Experimental and Computational Investigation of an Apex Flap Concept on a Delta Wing. NASA CR-166080, April 1983.
33. Wahls, R. A.; Vess, R. J.; and Moskovitz, C. A.: An Experimental Investigation of Apex Fence Flaps on Delta Wings. AIAA Paper No. 85-4055, Oct. 1985.
34. Compilation of Papers in: Vortex Flow Aerodynamics Conference. Jointly Sponsored by NASA Langley and USAF Wright Aeronautical Laboratories, at Hampton, Va., Oct. 1985.
35. Schoonover, W. E., Jr.; and Ohlson, W. E.: Wind-Tunnel Investigation of Vortex Flaps on a Highly Swept Interceptor Configuration. ICAS 82-6.7.3, 1982.
36. Rao, D. M.: Exploratory Subsonic Investigation of Vortex-Flap Concept on Arrow Wing Configuration. Supersonic Cruise Research '79 - Part 1, NASA CP-2108, pp. 117-129, Nov. 1980.
37. Rao, D. M.: Segmented Vortex Flaps. AIAA Paper No. 83-0424, 1983.
38. Rao, D. M.: Towards an Advanced Vortex Flap System - The 'Cavity' Flap. Presented in: Vortex Flow Aerodynamics Conference; Jointly Sponsored by NASA Langley and USAF Wright Aeronautical Laboratories, at Hampton, Va., Oct. 1985.

39. Staudacher, W.: Leading-Edge Flap Systems for Slender Wings - "Vortex Flaps"?. ICAS 84-2.8.3, 1984.
40. Huffman, J. K.; Fox, C. H., Jr.; and Ziegler, H.: Subsonic Longitudinal and Lateral-Directional Static Aerodynamic Characteristics of a General Research Fighter Configuration Employing a Jet Sheet Vortex Generator. NASA TM-74049, Jan. 1978.
41. Ziegler, H.; and Wooler, P. T.: Aerodynamic Characteristics of a Jet Sheet Vortex Generator. NASA CR-158904, June 1978.
42. Campbell, J. F.: Augmentation of Vortex Lift by Spanwise Blowing. J. Aircraft Vol. 13, No. 9, pp. 727-732, Sept. 1980.
43. Erickson, G. E.; and Campbell, J. F.: Improvement of Maneuver Aerodynamics by Spanwise Blowing. NASA TP 1065, Dec. 1977.
44. Staudacher, W.; et al.: Aerodynamic Characteristics of a Fighter-Type Configuration During and Beyond Stall. AGARD CP 247, Paper No. 8, Oct. 1978.
45. Anglin, E. L.; and Satran D.: Effects of Spanwise Blowing on Two Fighter Airplane Configurations. J. Aircraft, Vol. 17, No. 12, pp. 883-889, Dec. 1980.
46. Hummel, D.: Study of the Flow Around Sharp-Edged Slender Delta Wings with Large Angles of Attack. NASA TT F-15, 107, Sept. 1973.
47. Taylor, A. H.; Jackson, L. R.; and Huffman, J. K.: Vortex Lift Augmentation by Suction on a 60° Swept Gothic Wing. AIAA Paper No. 82-0231, 1982.
48. Lamar, J. E.: Analysis and Design of Strake-Wing Configurations. J. Aircraft, Vol. 17, No. 1, pp. 20-27, Jan. 1980.
49. Ghaffari, F.; and Lamar, J. E.: An Attached Flow Design of a Noninterfering Leading Edge Extension to a Thick Delta Wing. AIAA Paper No. 85-0350, Jan. 1985.
50. Sidwell, K. W.; Baruah, P. K.; and Bussoletti, J. E.: PAN-AIR A Computer Program for Predicting Subsonic or Supersonic Linear Potential Flows about Arbitrary Configurations Using a Higher Order Panel Method. NASA CR-3252, May 1980.
51. Lamar, J. E.; and Herbert, H. E.: Production Version of the Extended NASA-Langley Vortex Lattice FORTRAN Computer Program - Volume I. User's Guide. NASA TM-83303, April 1982.
52. Lan, C. E.; and Chang, J.-F.: Calculation of Vortex Lift Effect for Cambered Wings by the Suction Analogy. NASA CR-3449, July 1981.
53. Lan, C. E.; and Chang, J.-F.: VORCAM - A Computer Program for Calculating Vortex Lift of Cambered Wings by the Suction Analogy. NASA CR-165800, Nov. 1981.
54. Woodward, F. A.; Tinoco, E. N.; and Larsen, J. W.: Analysis and Design of Supersonic Wing-Body Combinations, Including Flow Properties in the Near Field. Part I - Theory and Application. NASA CR-73106, Aug. 1967.
55. Polhamus, E. C.: A Concept of the Vortex Lift of Sharp-Edge Delta Wings Based on a Leading-Edge-Suction Analogy. NASA TN D-3767, Dec. 1966.
56. Vanderplaats, G. N.: CONMIN - A FORTRAN Program for Constrained Function Minimization - User's Manual. NASA TM X-62282, 1973.
57. Schoonover, W. E., Jr.; and Smith, F. R.: Design and Wing-Tunnel Evaluation of Vortex Flaps for the USAF AFTI/F-111. Presented in: Vortex Flow Aerodynamics Conference; Jointly Sponsored by NASA Langley and USAF Wright Aeronautical Laboratories, at Hampton, VA, Oct. 1985.
58. Carlson, H. W.: The Design and Analysis of Simple Low Speed Flap Systems with the Aid of Linearized Theory Computer Programs. NASA CR 3913, Aug. 1985.
59. Huebner, L. D.: Performance Analysis and Supersonic Design of Wing Leading-Edge Vortex Flaps for the Convair F-106B. Masters Thesis, The George Washington University School of Engineering and Applied Science, Sept. 1985.
60. Vanderplaats, G. N.: ADS - A FORTRAN Program for Automated Design Synthesis - Version 1.00. NASA CR-172460, Oct. 1984.
61. Rogers, J. L., Jr.; Sobieszczanski-Sobieski, J.; and Bhat, R. B.: An Implementation of the Programming Structural Synthesis System (PROSSS). NASA TM-83180, Dec. 1981.
62. Chu, J.; and Lamar, J. E.: Summary of a High Subsonic Force/Pressure Experiment for 58 Degree Cambered/Twisted Delta Wings. AIAA Paper No. 86-0169, Jan. 1986.

- 63. Chu, J.; Lamar, J. E.; and Luckring, J. M.: Longitudinal Test and Evaluation of Six 58 Deg. Cambered and Twisted Thick Delta Wings at High Subsonic Speeds. (U) NASA TM-85786, March 1985.
- 64. Hallissy, J. B.; Frink, N. T.; and Huffman, J. K.: Aerodynamic Design and Testing of Vortex Flap Configurations for the F-106B Aircraft. Presented in: Vortex Flow Aerodynamics Conference; Jointly Sponsored by NASA Langley and USAF Wright Aeronautical Laboratories, at Hampton, VA, Oct. 1985.

ACKNOWLEDGEMENTS

The author wishes to thank Mr. N. T. Frink and Dr. D. M. Rao for providing original figures; Mr. T. D. Johnson, Jr., for his many helpful suggestions regarding the manuscript; and my wife, Joyce, and Mrs. Bernice Barrack for manuscript preparation.



GENERAL DYNAMICS F-111

GRUMMAN F-14

Ref. 1

- 1.- U.S. variable sweep fighter aircraft--slender wing mode.

NORTHROP-MCDONNELL DOUGLAS F-18



GENERAL DYNAMICS F-16

Ref. 1

- 2.- Vortex-lift strake-wing fighters.

- Organizes wing flow field to higher α
- Increases C_L and nose-up moment at higher α

Strake-wing-body (Typical)



Ref. 7

- Investigate $\alpha > \alpha_{BD}$ characteristics

Space jet

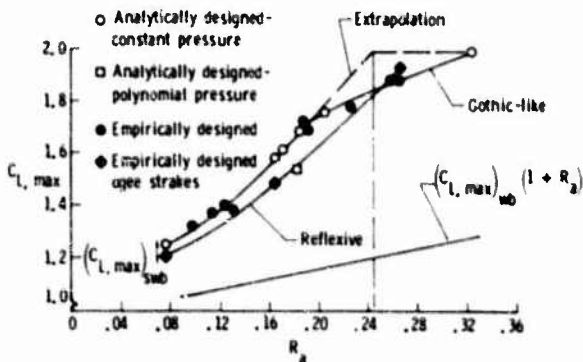


Configuration of ref. 9

- Investigate interacting vortex flows

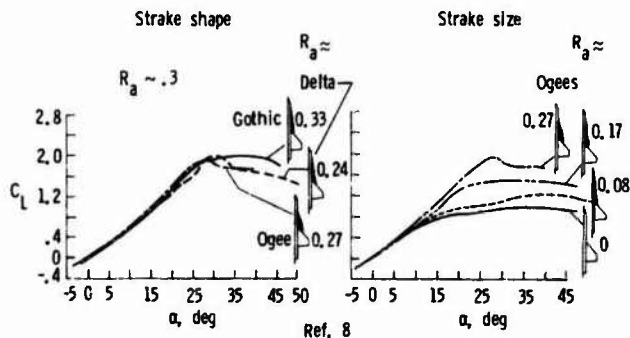
- Investigate shape effects

- 3.- Use of strakes.



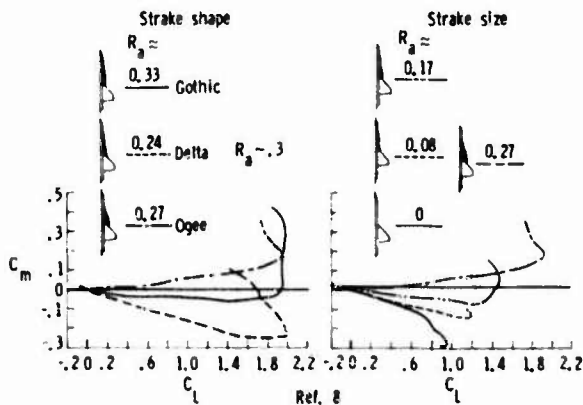
Ref. 7

- 4.- Effect of strake shape on $(C_{L,max})_{swb}$; $M = 0$.



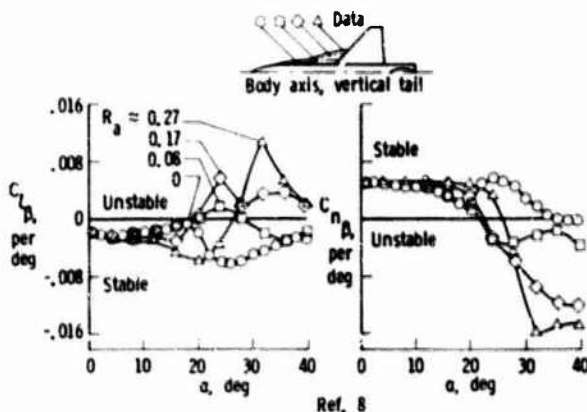
Ref. 8

- 5.- Effect of strake shape and size on C_L characteristics; $\Lambda = 44^\circ$, $M = 0.2, 0.3$.



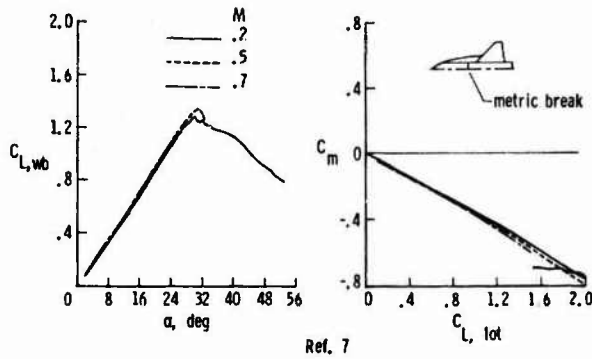
Ref. 8

- 6.- Effect of strake shape and size on C_m characteristics; $\Lambda = 44^\circ$, $M = 0.3$.

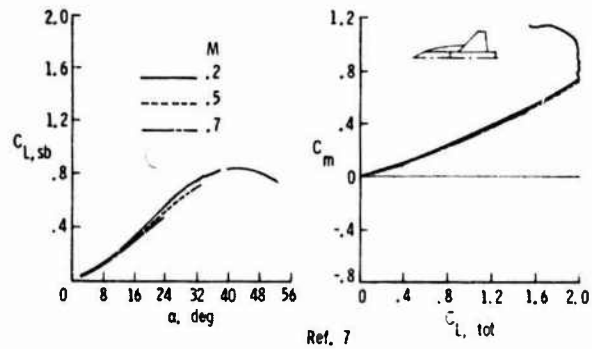


Ref. 8

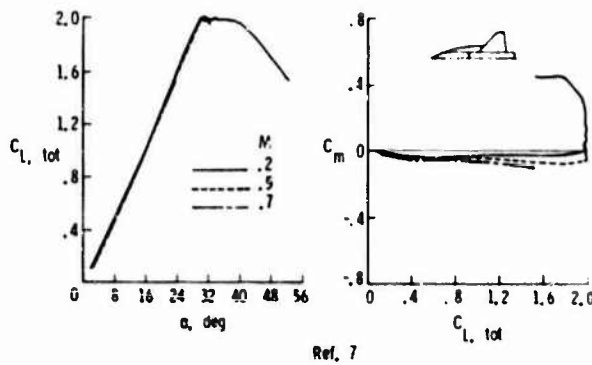
- 7.- Strake span effect on lateral-directional characteristics; $\Lambda = 44^\circ$, $M = 0.3$.



8.- Effect of M on longitudinal aerodynamics for wing-afterbody; Strake AD 24, $\Lambda = 44^\circ$.

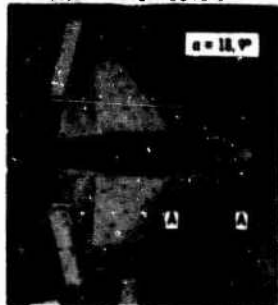


9.- Effect of M on longitudinal aerodynamics for strake-forebody; Strake AD 24, $\Lambda = 44^\circ$.

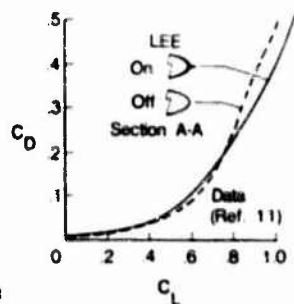


10.- Effect of M on longitudinal aerodynamics for strake-wing-body; Strake AD 24, $\Lambda = 44^\circ$.

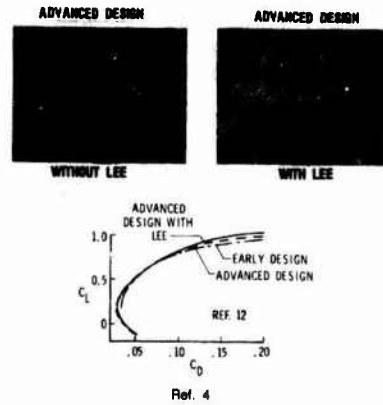
Artic. - NACA 0015-64



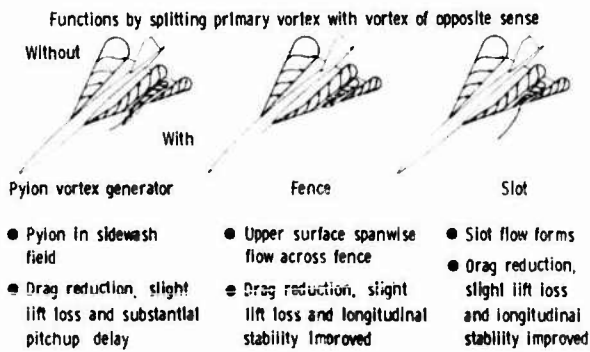
- Organizes wing LE flow at higher α
- Improves drag polar at higher C_L



11.- Effect of LEE on drag polar for thick low-speed glider (DM-1); $\Lambda = 1.8$, $\Lambda = 60^\circ$, $M = 0$.



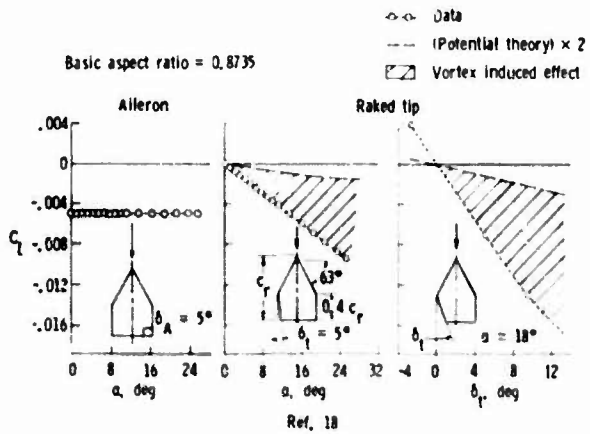
12.- Effect of leading-edge extension (LEE) on drag polar for thin transonic fighter; $A = 3.28$, $\Lambda = 45^\circ$, $\lambda = 0.21$, $M = 0.85$.



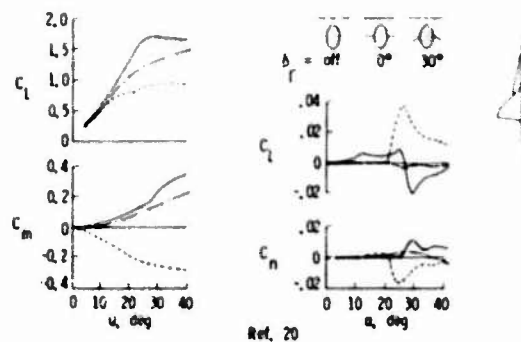
Ref. 13-16

Ref. 13-15

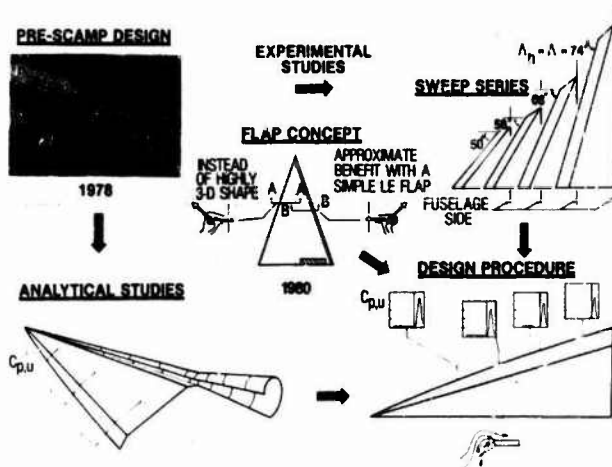
13.- Vortex generators.



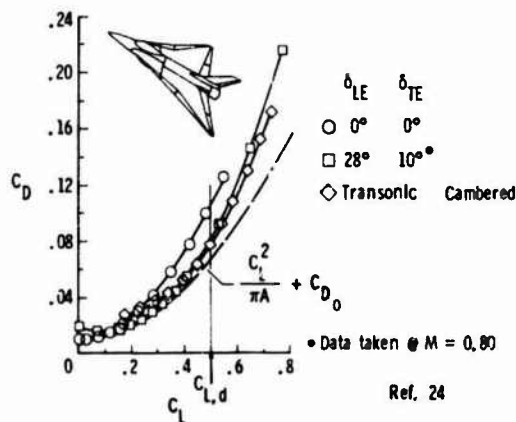
14.- Roll-control device effectiveness on cropped delta wing; $M = 0.2$.



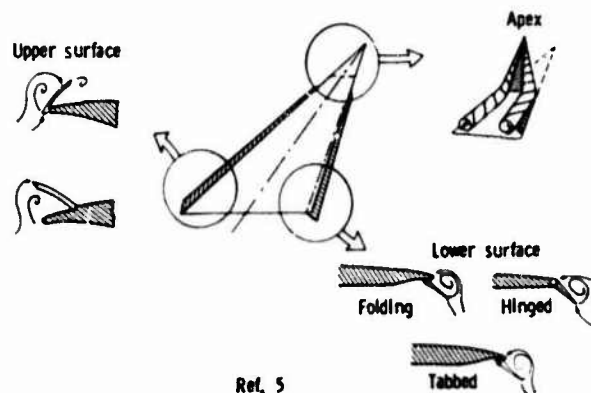
15.- Effect of hinged strake on high-alpha aerodynamic characteristics; $\Lambda = 2.50$, $\Lambda = 44^\circ$, $\beta = 0^\circ$, $M = 0.30$.



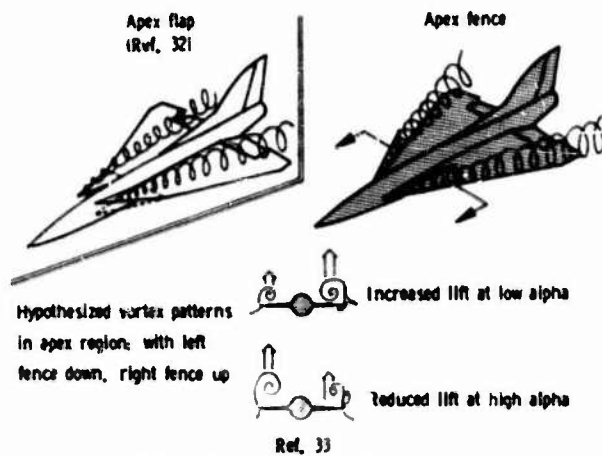
16.- Vortex flap history; transonic aerodynamics.



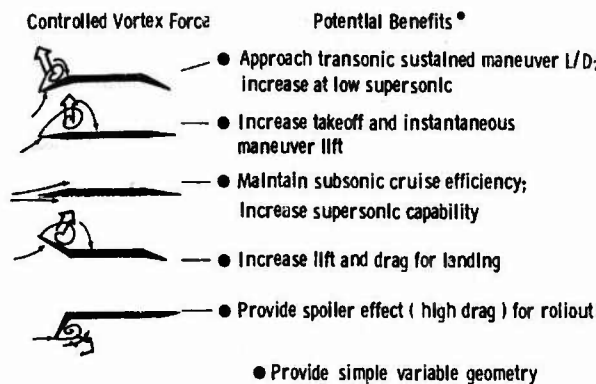
17.- Drag polar for vortex flap applied to joint NASA/General Dynamics wing; $A = 1.383$, $M = 0.85$.



18.- Types of vortex flaps; flow patterns.



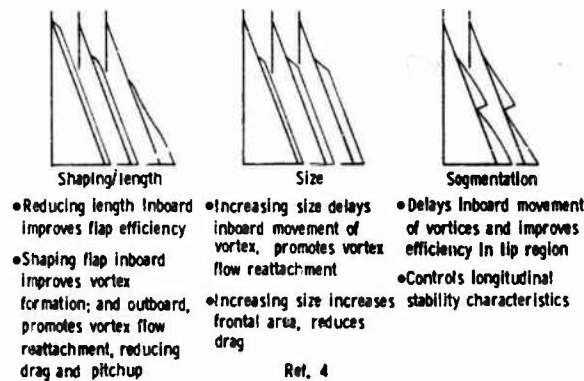
19.- Apex fence concept.



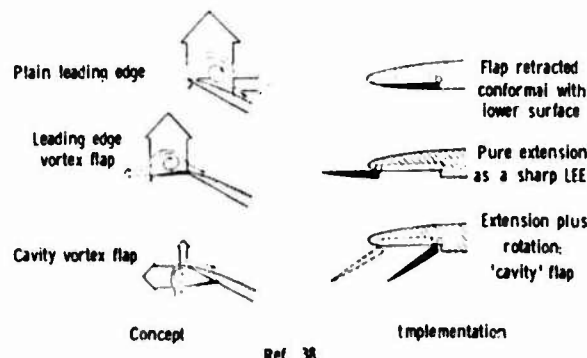
* Compared to current production fighters

Ref. 5

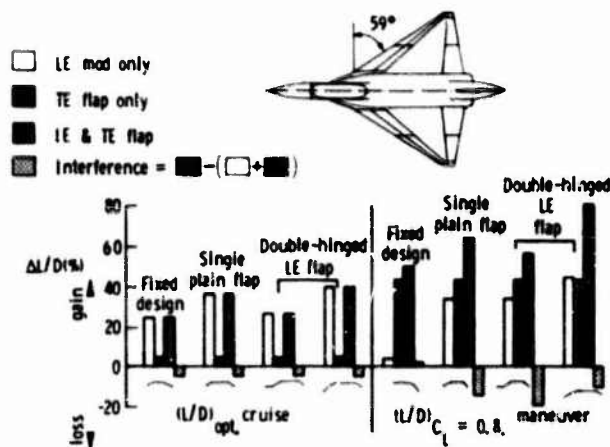
20.- Uses of a vortex flap.



21.- Characteristics of various lower surface vortex flap geometries.

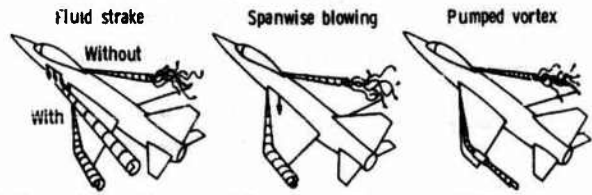


22.- The 'cavity' vortex flap.



23.- Changes in L/D due to camber devices from planar wing values.

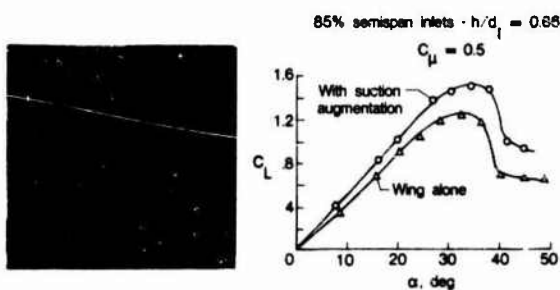
- Delay vortex breakdown
- Organize wing upper surface flow



- Forms stable vortex flow over wing
- Increases $C_{L,max}$ and improves drag polar at high α
- Energizes vortex
- Improves high α longitudinal stability and performance
- Increases axial flow in vortex
- Increases C_L at moderate α
- Increases $C_{L,max}$

Ref. 4

24.- Jet-augmented vortex concepts.



Ref. 47

25.- Effect of pumped vortex on blended-delta lift characteristics; $A = 1.75$, $M = 0.15$.

"Related flow" (R.F.) assumptions

- Only concerned with flow near LE
- Only cot ($\theta/2$) chord load used
- ΔC_p specified spanwise
- Sharp leading edge simulation
- No physical or induced camber allowed

Other assumptions

- Triangular suction distribution-prescribed
- Performance: Isolated strake (R.F.)—strake-wing-body (3-D flow)

Ref. 6

26.- Features of isolated strake design process.

Assumptions

- Existence of a PSSS
- PSS is representative of PSSS streamwise cut
- PSS can be found from a tangent to velocities near LEE
- PSSS approximation can be constructed from the PSS

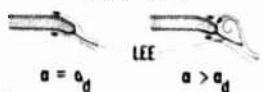
Constraints

- Unaltered wing pressures at α_d
- Zero lifting pressures at α_d
- Minimum planform area
- Intersects wing on the lower surface

Schematic representation of pseudo-stagnation stream surface (PSSS)

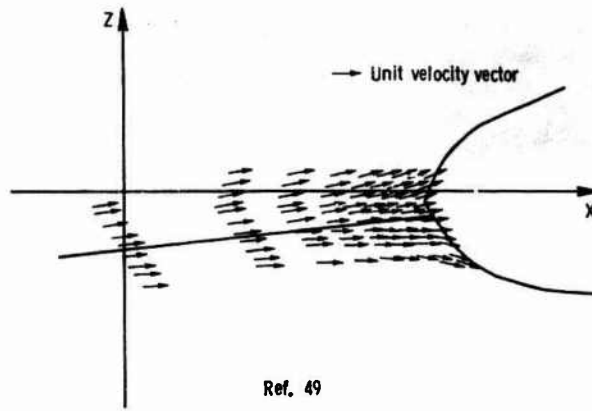


Desired LEE flow field (streamwise cut)



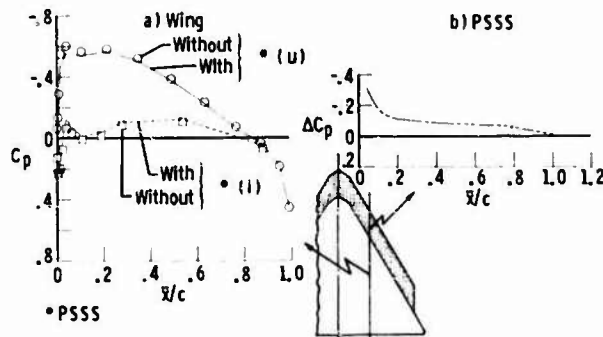
Ref. 49

27.- Leading-edge extension (LEE) design methodology.



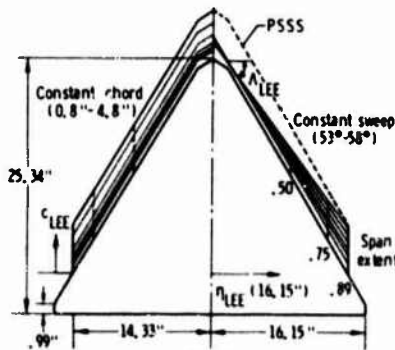
Ref. 49

28.- Graphically determined PSS from typical section velocity field.



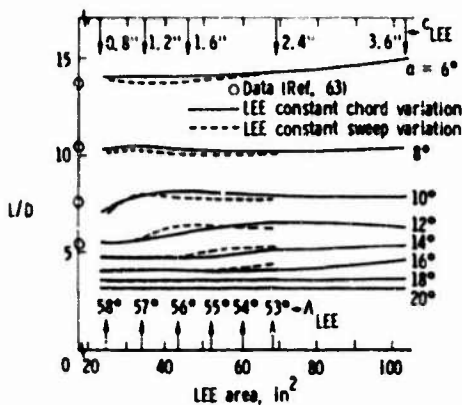
Ref. 49

29.- Effect of wing and PSSS pressures from combination; $\eta = 0.34$, $\alpha_d = 6.0^\circ$, $M = 0.8$.



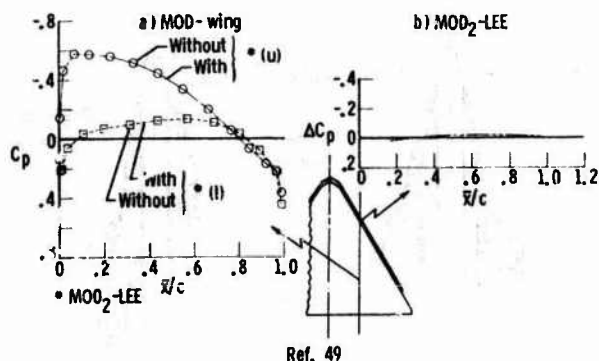
Ref. 49

30.- LEE design parameters and ranges.

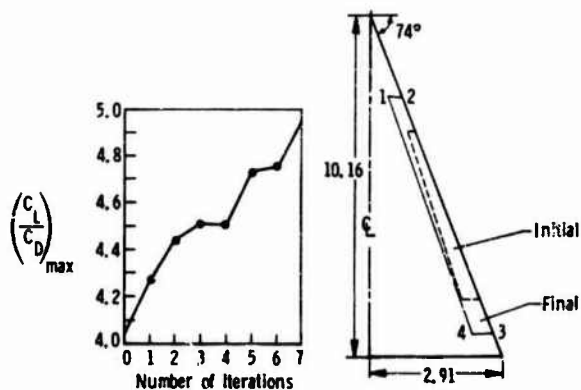


Ref. 49

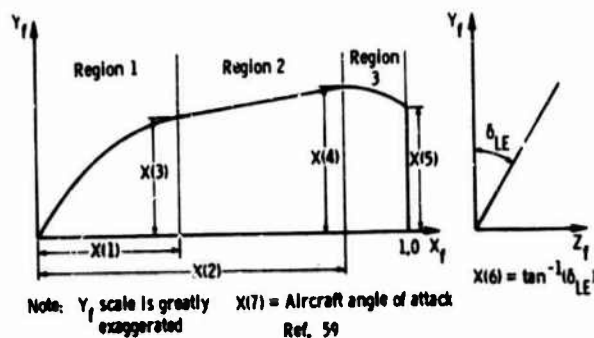
31.- Effect of LEE planform geometrical parameters on lift-to-drag ratio; $\eta_{LEE} = 0.89$, $M = 0.8$.



32.- Effect of mod-wing and mod₂-LEE pressures from combination; $\eta = 0.34$, $\alpha_d = 6.0^\circ$, $M = 0.8$.

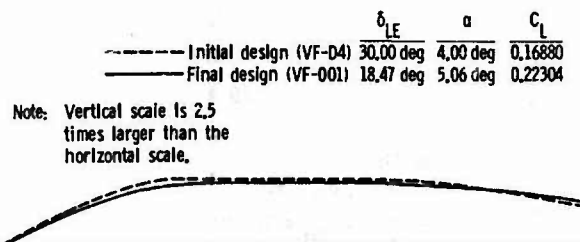


33.- Lan/Chang integral LEVF design using VORCAM; 74° delta, $M = 0.2$, $C_{L,d} = 0.6$, $C_{D_0} = 0.0088$.

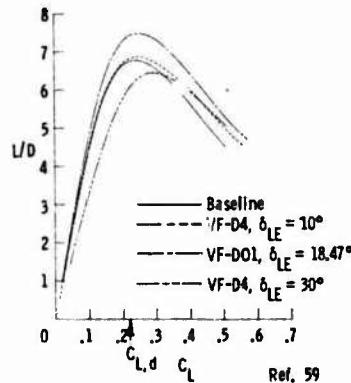


Note: Y_f scale is greatly exaggerated. $X(7)$ = Aircraft angle of attack. Ref. 59

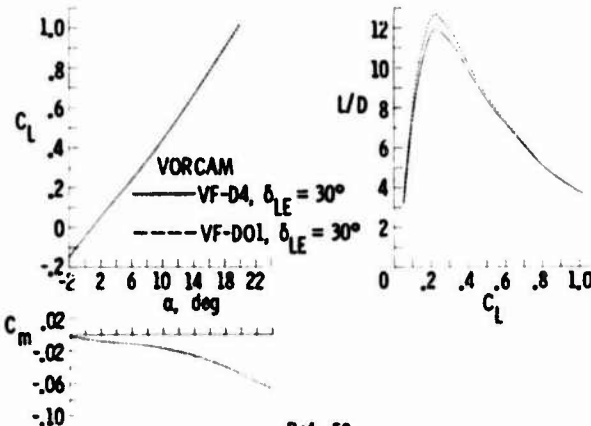
34.- Analytical vortex flap model with design variables.



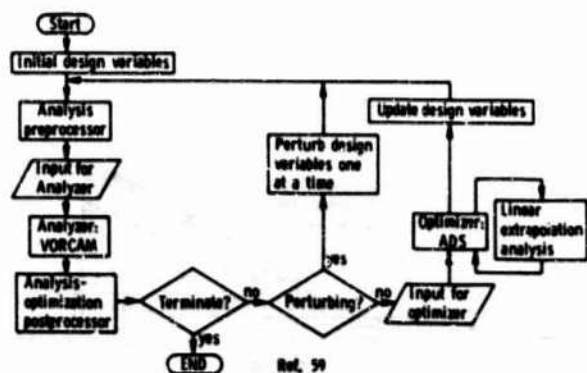
36.- Initial and final vortex flap design results for the F-106B; $M_d = 1.5$, $C_{L,d} = 0.223$.



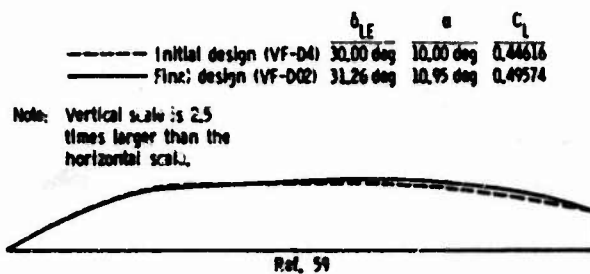
37.- Performance of VF-D01 with VF-D4 on F-106B at $M = 1.5$.



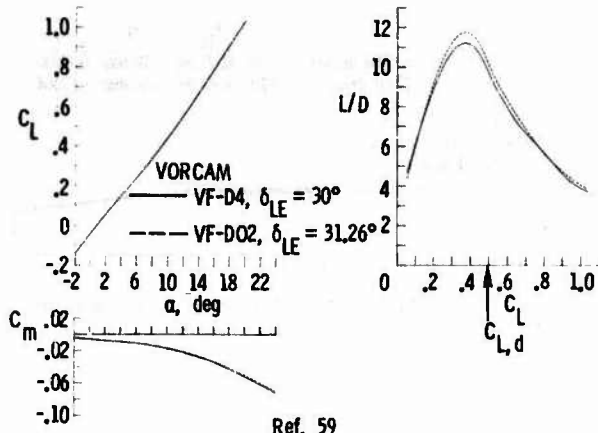
38.- Assessment of longitudinal aerodynamics for two vortex flaps on F-106B at $M = 0.3$.



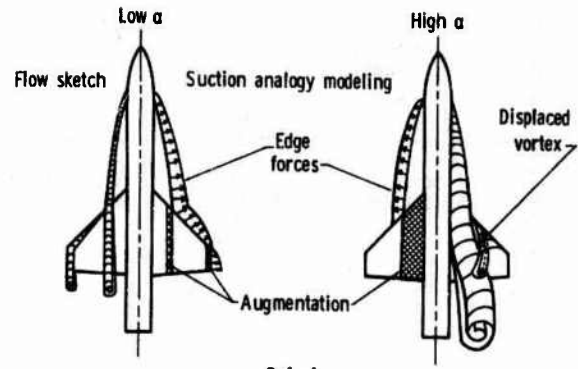
35.- Supersonic design method flow chart using analysis-optimization process.



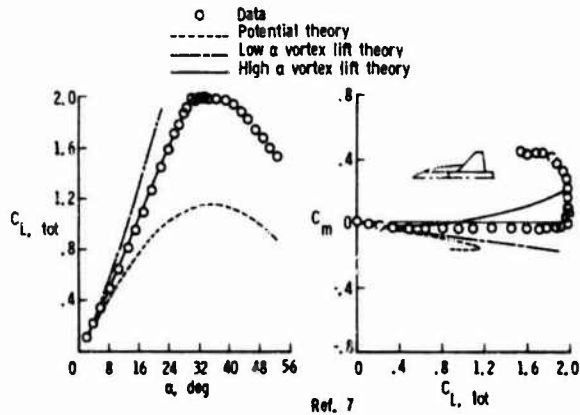
39.- Initial and final vortex flap design results for the F-106B; $M_d = 0.3$, $C_{L,d} = 0.5$.



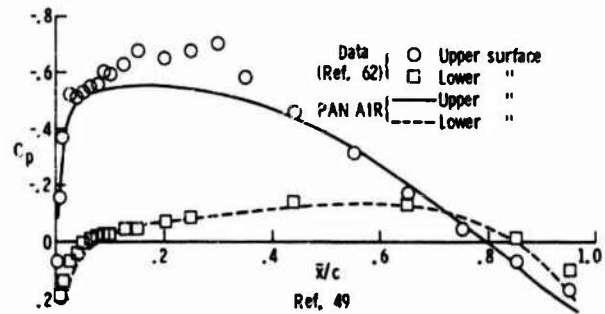
Ref. 59
40.- Assessment of longitudinal aerodynamics for two designed vortex flaps on F-106B; $M_d = 0.3$.



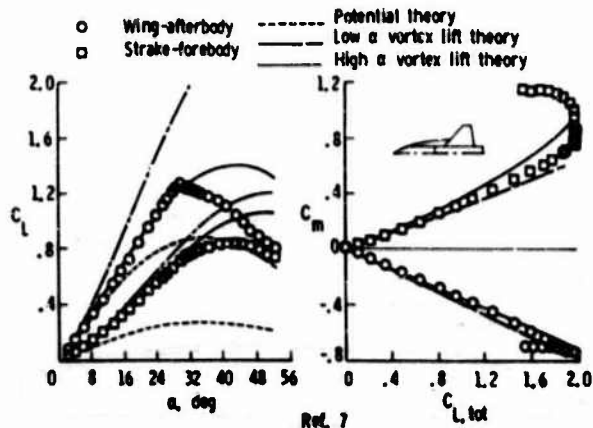
Ref. 4
43.- Effect of α on vortex flow models for complex configurations; VLM-SA/Lamar, Luckring.



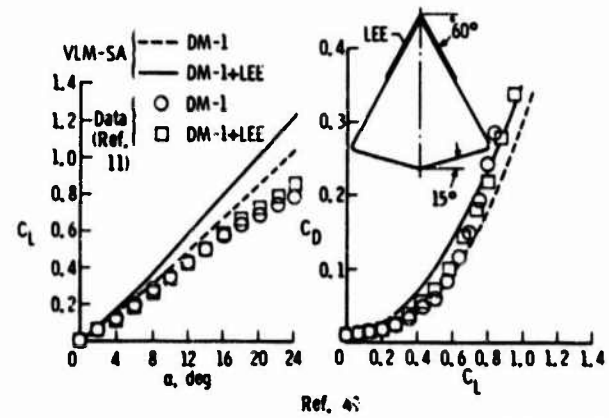
Ref. 7
41.- Complete longitudinal aerodynamic characteristics for strake-wing-body; Strake AD 24, $A = 44^\circ$, $M = 0.2$.



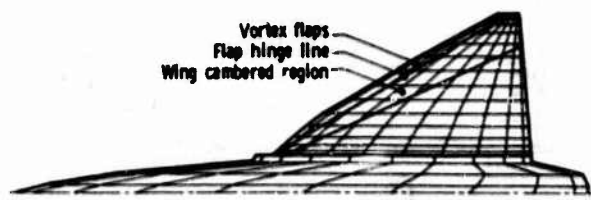
Ref. 49
44.- Experimental and theoretical pressures for the mod-wing; $\eta = 0.30$, $\alpha_d = 6.0^\circ$, and $M = 0.8$.



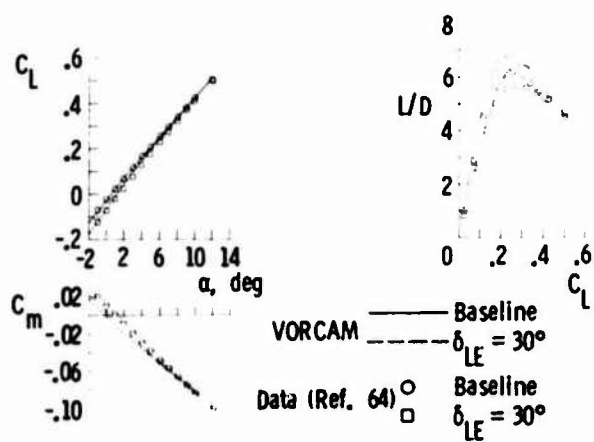
Ref. 7
42.- Component longitudinal aerodynamic characteristics for strake-wing-body; Strake AD 24, $A = 44^\circ$, $M = 0.2$.



Ref. 45
45.- Experimental and theoretical lift and drag polar; $A = 1.8$, $M = 0$.

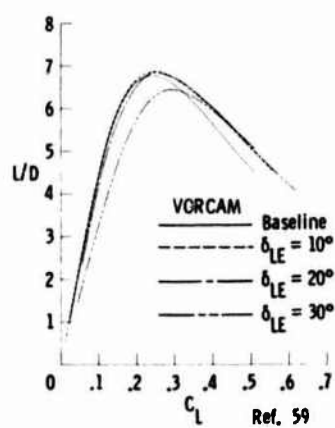


Ref. 59
46.- Typical scheme for F-106B with vortex flap; VF-D4, $\delta_{LE} = 30^\circ$.



Ref. 59

47.- Effect of vortex flap addition on longitudinal aerodynamics for F-106B; VF-D4, M = 1.5.



48.- Effect of flap deflection on L/D for F-106B; VF-D4, M = 1.5.

AIRCRAFT DYNAMICS - AERODYNAMIC ASPECTS AND WIND TUNNEL TECHNIQUES

by
K.J. Orlik-Rückemann
Unsteady Aerodynamics Laboratory
National Research Council of Canada
Ottawa, Ontario, KIA 0R6, CANADA

1. INTRODUCTION

The dynamic behaviour of modern fighter aircraft depends much more on the unsteady aerodynamics considerations than in the past. Until quite recently an aircraft designer would display only a passing interest in that subject, concentrating probably on classical problems such as aeroelasticity and flutter. Dynamic stability parameters were most often determined by low angle-of-attack calculation methods, without much recourse to experiments; indeed suitable facilities were rather scarce and the priority habitually assigned to dynamic stability testing very low indeed. The results obtained from those few dynamic experiments that were performed were most often used to confirm that there were no particular problems present rather than to be applied as one of the design parameters or inputs. And yet, for most of the aircraft of the past, such a modest level of investment in unsteady aerodynamics and dynamic characteristics of aircraft was, in fact, quite adequate, and many excellent aircraft were successfully designed in this fashion.

It was only with the advent of modern advanced requirements for a fighter aircraft performance that this time-honoured methodology had become clearly inadequate. The new requirements include the ability to fly at high angles of attack in the presence of extensive regions of separated or vortical flows, relaxed static stability, greatly increased agility and the interest in unorthodox geometries such as closely-coupled-canard or tail-first configurations. There is also considerable interest in the ability to perform very rapid maneuvers and in the aerodynamic characteristics of large amplitude motions. The time lags and the unsteady phenomena associated with the resulting flow fields may significantly affect the dynamic behaviour of modern fighter aircraft and may become as important for aircraft design as the classical static performance criteria.

The unsteady aerodynamics involved is mostly very complex and, although considerable effort is now applied to the development of various analytical and numerical methods of calculations, the most important source of data - at the present time - consists of experimental techniques. Consequently, in this lecture, a review will first be made of the various aerodynamic aspects affecting aircraft dynamic behaviour, to be followed by a survey of the most pertinent experimental techniques. In both cases the presentation will emphasize applications to high performance fighters, such as are exemplified, for instance, by flight at high angles of attacks.

2. AERODYNAMIC ASPECTS

The aerodynamic aspects of aircraft dynamics were reviewed by the present author in an 1983 survey paper in the Journal of Aircraft (Ref. 1). For completeness, this reference is reproduced in full at the end of notes for this lecture. It therefore only remains to add a few remarks about some of the most recent developments in this field.

2.1 Rapid, Large-Amplitude, Pitch-up Motions

High-angular-rate, large-amplitude pitch-up motions may result in maximum lift coefficients far beyond the steady maximum values. In low speed experiments involving two-dimensional airfoils that perform pitch-up motions at constant pitch rate, $\dot{\alpha}$, up to a maximum angle of attack, α_{max} , and then remain at that angle, dynamic lift levels of three times the corresponding steady lift values have been observed (Ref. 2). This is illustrated in Fig. 1, where the maximum lift coefficient, $C_{L,max}$, is plotted versus a dimensionless pitch rate, $k = \dot{\alpha}c/2V$, for different values of α_{max} , where c is the airfoil chord and V the free stream velocity. As deduced from measurements of the unsteady pressure distributions during such motions, this lift augmentation is caused by an energetic separation vortex which originates at the leading edge and convects downstream as the angle of attack increases. This mechanism is similar to the well-known phenomenon of deep dynamic stall (Fig. 2), as described e.g. by McCroskey in his 1982 review of Unsteady Airfoils (Ref. 3). Although dynamic stall has previously been of interest mostly in connection with the helicopter blade oscillations and wind turbines, it may now prove to be very important also for the attainment of sustained dynamic maneuvering in the post-stall flight regime such as e.g. described by Herbst (Ref. 4) as "supermaneuverability" (Fig. 3). Of course, for such a purpose, the characteristics of complete configurations, rather than merely two-dimensional data, will be needed. Experiments are now being planned to obtain such information.

For performance evaluation it may be useful to present the effect of the aircraft motion-time history in some integrated fashion, rather than as the maximum lift coefficient that can be achieved only momentarily. One such possibility, proposed in Ref. 2, is to consider the area bounded by the lift-time curve from above and the static maximum lift from below, which may be said to define an effective impulse function, I_C , over a cycle. Such a representation allows for comparison of airfoil (or aircraft) performance between cases where the motion-time history is fundamentally different and this approach therefore lends itself well for lift optimization analysis. The variation of I_C with k for two airfoils is shown in Fig. 4. Results are depicted for several values of α_{max} and V . A rapid increase in I_C at low k is followed by a more gradual increase or even a gradual decrease at higher values of k . Furthermore, the maximum performance does not necessarily increase monotonously with α_{max} , but is achieved by terminating the unsteady motion and maintaining an α_{max} at or near the value for which, for a given k , the maximum C_L can be obtained. It is believed that such conditions correspond to the occurrence of the strongest and most persistent vortex.

2.2 Wing Rock

Wing rock is an undamped oscillation, primarily around the roll axis, that is exhibited by many modern fighter aircraft when flying at higher angles of attack. Several possible scenarios for the occurrence of wing rock have already been discussed in Ref. 1. Since wing rock is a very debilitating phenomenon, causing maneuver limitations ranging in severity from degradation in tracking effectiveness to loss of control, a considerable amount of work is currently being done to alleviate this problem by increasing our understanding of the underlying basic

aerodynamic phenomena. This work ranges all the way from efforts to postulate mathematical models for the prediction of wing rock characteristics, such as reported in Refs 5-7, to systematic low speed investigations, such as performed at NASA Langley Research Center and described by Nguyen et al in Ref. 8.

The NASA Langley studies comprise (a) wing rock encountered on highly-swept configurations, such as slender delta wings, and (b) wing rock induced by slender forebodies. The former type, already discussed in Ref. 1, seems to be associated with the alternating lifting-off and reattachment of leading edge vortices during each oscillation cycle. This results in the occurrence of incremental rolling moments which promote and oppose the oscillation in an alternating fashion. The latter type of wing rock is associated with the motion of forebody vortices and their interaction with the wing and empennage. In both cases strong vortex flows are present and it is the motion of these vortices, the mutual interaction of the two main forebody vortices or the two leading edge vortices (because of the slenderness of the wing), and possibly the phase lag between the motion of the vortices and the motion of the wing or aircraft, that provide the basic mechanism for the wing rock.

The importance of the forebody vortex flow for the occurrence of unstable damping in roll and, eventually, wing rock, is well illustrated in Figs 5 and 6. Damping in roll is shown for a range of angles of attack for an F-5 configuration with 3 alternative wings. The roll damping becomes highly unstable for all three wings in about the same range of angle of attack from 30° to 45° , indicating susceptibility to wing rock in that range of α . It is known that the full-scale F-5 aircraft is prone to large amplitude wing rock in the same angle-of-attack range. It is obvious that the planform of the wing is not responsible for the very unstable roll damping above $\alpha = 30^\circ$. Further corroboration was recently obtained during tests of a model of the X-29A Forward Swept Wing Airplane, which incorporates the exact fuselage forebody (which has a flat elliptical cross-section) of the F-5 but is completely different from the F-5 in almost every other aspect. Forced oscillation data for the X-29A showed the same lightly unstable roll damping in the 30° to 45° angle-of-attack range. It seems clear that the basic cause of the unstable roll damping in all these cases is the flow about the only common configuration feature, namely the forebody.

In order to generate sufficient rolling moments to cause wing rock, the basic forebody vortex flow must interact with some aircraft component further downstreams. This was illustrated during the Langley experiments during which the wing and vertical tail were alternatively removed from the model. It was shown that, with only the wing or only the vertical tail removed, the model still exhibited the wing rock, which only disappeared when both the wing and the vertical tail were removed at the same time.

With the forebody playing such a fundamental role in the generation of wing rock, it was only natural to investigate in some detail the effect of the forebody cross-section on the static lateral stability as well as on the wing rock occurrence and amplitude. This is now being done at NASA Langley (Ref. 8) on a generic fighter model, as part of a larger ongoing investigation, during which many forebodies and wings are systematically varied. Some preliminary results are shown in Figs 7 and 8 for the generic model configured with a trapezoidal wing with 26° leading-edge sweep and conventional tail. Four forebodies, all with the same 3.9:1 fineness ratio, but different cross-sectional shapes (circular, vertical ellipse, horizontal ellipse and triangular) were initially studied.

The preliminary results show that the forebody cross-section has a very strong influence on the static lateral stability, $C_{L\beta}$, with the horizontal-ellipse and triangular cross-sections providing the stiffest "restoring spring" effects in the angle-of-attack range in which wing rock was observed in the free-to-roll tests. Above that range, the forebody/wing/tail flow fields appear to be no longer strongly coupled. It is noteworthy that the same two cross-sections were also found to be highly susceptible to wing rock, causing the highest wing-rock amplitudes, reaching 30° . It is also interesting that the horizontal-ellipse forebody is similar to the F-5 forebody discussed earlier and that the wing-rock characteristics for those two configurations are quite similar.

Work is continuing at NASA Langley to further explore the forebody induced wing-rock phenomenon. Although most of the present effort is conducted at low Reynolds numbers and certainly will have to be complemented by experiments at higher Reynolds numbers, certain similarities between the results obtained so far and flight test data (such as those mentioned above) seem to indicate that at least the basic mechanism is being properly identified.

2.3 Tumbling

Recent design trends for future combat aircraft, such as the use of tail-first or tailless configurations and highly relaxed static stability, have rekindled interest in a dangerous flight phenomenon known as tumbling. Last investigated during and immediately after World War II (see Ref. 9), tumbling was identified as a potential danger for aircraft with design features that included one or more of those mentioned above; it was also pointed out that accelerations in a tumble may be exceptionally dangerous. Since the conventional aircraft will not tumble, no more work in this area was conducted for approximately 35 years.

Last year, however, studies were conducted in the NASA Langley 20 - Feet Vertical Spin Tunnel on a dynamically scaled model of the X-29A aircraft, which makes use of canards and highly relaxed static stability. After initially confirming the occurrence of tumbling (which was coupled with cyclic variations in linear as well as angular rates) in a series of free - tumbling tests, more controlled experiments were conducted in single-degree-of-freedom, free-to-pitch tests (Refs 8 and 10). Autorotation was obtained by either imparting an initial rotation to the model in the proper direction, or by releasing the model from a proper attitude with zero rate. Once initiated, the autorotation persisted indefinitely. It was found that the canard and wing flap positions had little effect on the motion, while the strake flaps had a very large effect. For instance, with strake flaps fully down, only nose-down autorotation could be induced, regardless of the initial release conditions. Reversing the strake flaps to full up permitted a nose-up autorotation.

Figures 9 and 10 show the static pitching-moment and pitch damping data obtained from static and forced-oscillation experiments, respectively. The highly unstable pitching moment characteristics for angles of attack lower than $+5^\circ$ and higher than $+145^\circ$, as well as pitch undamping in the regions of around $+130^\circ$ and -120° , are clearly visible. Using these data in a simulation programme, the time history of the motion for a full scale aircraft could be predicted (Fig. 11) and compared to scaled-up (in time) frame-by-frame readings of movies taken during the free-to-pitch tests (Fig. 12). Average pitch rate was about $-130^\circ/\text{sec}$, and maximum recycling values of axial and normal accelerations at the pilot station were 0 to $-3g$ and $+1.5g$, respectively. Although the

attitude data are predicted quite closely, the match of velocity and acceleration data is not nearly as good, indicating the need for further work in both obtaining the basic data and improving the mathematical model.

The above experiments were all performed with the controls fixed. Although it is unlikely that in a highly augmented modern aircraft the controls would remain fixed through a large amplitude motion such as tumbling, the susceptibility to tumbling remains as a possible threat in off-nominal situations involving failures in the aircraft control system. Unfortunately, one of the best means to increase resistance to tumbling is to limit an aircraft's agility in pitch. However, control laws are now being developed at NASA Langley for highly-relaxed-stability fighter aircraft, which - assuming that some controls are still operational - would ensure a combination of high agility and good resistance to pitch departure.

2.4 Flow Control

Any attempt to achieve high agility and true supermaneuverability must include the ability to manage and control the time dependent, separated flows that are characteristic of such flight conditions. In the past such attempts were primarily aimed at reducing or eliminating regions of separation and promoting flow attachment, as exemplified by the use of vortex generators on wings of many current aircraft. For a high agility fighter, however, the separated-flow areas can be expected to dominate the flow around the aircraft, and it is the manipulation and even enhancement of that separated flow rather than its reduction or elimination that becomes the primary goal of any flow control procedure. For instance, if the residence time of the leading edge separation vortex mentioned in Section 2.1 could be extended, beneficial effects on the dynamic lift enhancement and its duration would result.

As discussed by Lang and Francis (Ref. 11) we are, at the present time, only taking the first steps in any such control attempts of the unsteady separated flows. Most of these first efforts use the idea of an oscillating spoiler to force and manipulate the flow. One of the earliest such studies dealt with the unsteady loading induced by a harmonically oscillating fence on one surface of the airfoil and its effect on both a fixed and a moving trailing edge flap (Ref. 12). A related investigation of the spoiler-generated flow field (Ref. 13) revealed the developing vortical character of the separation zone and described the behaviour of the suction peak on the airfoil surface. In an extension of these experiments to higher angles of attack (Ref. 14), a spoiler located at the 20% chord location was found to induce small spanwise vortices which greatly affected flowfield curvature, possibly increasing lift. Subsequent measurements confirmed a 60 to 110% unsteady load enhancement over the maximum steady flow value. It was also shown that a pulsed air jet may be successfully employed in place of a spoiler.

The management of a 2 D separated flow region has been systematically investigated at IIT (Ref. 15). Separated flow field was generated by using a wedge of a height equal to the local thickness of the turbulent boundary layer and the unsteady vorticity field was controlled by an oscillating flap with a variable waveform. Results have shown local surface pressure coefficient increases of nearly one hundred percent (Fig. 13) and a reduction of flow attachment length to thirty percent of the natural steady flow separation case. It was observed that the most effective reattachment control occurred for reduced frequencies of 0.07 to 0.08 (Fig. 14), and that the use of a triangular waveform, with a 90% duty cycle, resulted in a better organized, energetic and persistent vortex than some other cases having the same amplitude and period. Similar results were subsequently obtained for a separated flow generated by a backward facing step (Ref. 16); in that work it was also suggested that the control imparted by an active flap oscillation is independent of whether the incoming boundary layer is transitional or turbulent.

Separation control can also be achieved by actively stimulating the separated shear layer by sound at selected frequencies, as recently shown in Ref. 17.

An example of manipulating the flow in a 3 D case is provided in Ref. 18 which deals with the wing rock induced by leading edge vortices, that was already discussed in Ref. 1 and Section 2.2. It was shown that by mounting a small delta canard in front of a main delta wing, self-induced roll oscillations of the entire configuration (in a free-to-roll experiment) were obtained in a much larger range of angle of attack and with larger roll amplitude than with the main wing alone (Fig. 15). This was ascribed to the increased time lag (because of the larger length of the canard-wing) between the wing response and the movement of leading-edge vortices. Up to 30° the vortices from the canard and the wing were combined, while at higher angles of attack the resulting vortex breakdown at the wing trailing edge was providing a damping which reduced the roll angle amplitude. In the range 44° α 46° an interesting unstable asymmetric oscillation was recorded (Fig. 16), which could easily flip from the positive to the negative roll angles and viceversa, and which was related to the capturing of one of the canard's vortices by the opposite semiwing while the other vortex was shed into the flow. Also at the lower semiwing, a major vortex breakdown was detected. These observations, although, in a sense, describing undesirable results of controlling the flow, provide a useful insight into the fluid dynamics of these rather complex phenomena.

2.5 Digital Datcom

Some of the static and dynamic stability derivatives may be obtained from a computerized version of the USAF Stability and Control Datcom, called Digital Datcom. This includes the direct and the cross derivatives, but not any cross-coupling derivatives. The configurations and speed regimes for which Digital Datcom methods for dynamic derivative prediction are available are listed in Fig. 17. More details, including a comparison with wind tunnel data for several configurations and Mach numbers (see examples in Fig. 18), can be found in Ref. 19. All Datcom methods for dynamic derivatives, however, assume attached flow and hence are restricted to the low angle of attack regime.

3. WIND TUNNEL TESTING TECHNIQUES

As mentioned in the Introduction, the most important source of dynamic stability data for the advanced flight conditions or unorthodox configurations which are of interest for the modern fighter design, lies in experimental investigations. Although, in principle, experiments can be performed both in wind tunnels and in free flight, the latter cannot be rigorously carried out until a prototype is built and even then it usually does not provide the well-defined experimental conditions which are available in a laboratory. On the other hand, of course, although wind-tunnel testing is usually conducted at too low a Reynolds number and may be subject to some form of wind-tunnel or support-interference effects, it does, by and large, provide valuable information, obtained under

well controlled test conditions. It is often only through a combination of both wind tunnel and flight data with some additional data sources such as dynamic model flight tests, analytical studies and piloted simulation that a complete data set required for a satisfactory design can be obtained (Fig. 19). However, as discussed by Chambers et al (Ref. 20), dynamic wind tunnel tests are also to some extent involved in each of these procedures. For example, conduct of piloted simulator studies cannot be accomplished without dynamic stability parameters, and the interpretation and analysis of dynamic model flight tests and airplane flight tests may be subject to considerable question without dynamic wind tunnel data. Dynamic wind-tunnel experiments appear, therefore, to constitute the most important experimental source for dynamic data and the remainder of this paper will be devoted to examining the various techniques that are presently available or under development for such testing.

Reviews of the wind-tunnel techniques for dynamic stability testing have been presented by the present author at several occasions in the past (Refs 21-24). Since Refs 23 and 24 are easily accessible to the AGARD community, the material presented therein will not be reproduced here but will only be included by a suitable reference, as appropriate. Of the multitude of techniques available (Fig. 20), only those that, in the author's opinion, are currently the most important or the most promising for the future, will be listed.

3.1 Single DOF Forced Oscillation - Measurement of Reactions

This is commonly referred to as the "forced oscillation" technique, and is, by far, the most often encountered and most versatile technique in use today. It can be used for angular oscillation, such as in pitch, yaw or roll, as well as for translational oscillation, such as in plunge or in lateral translation. In the former case, the dynamic derivatives around a fixed axis, i.e. composite derivatives (such as $C_{mq} + C_{m\dot{q}}$) (see Ref. 1), can be obtained while in the latter case derivatives due to linear acceleration (such as $C_{m\ddot{z}}$), - which in a linear situation are approximately equal to the derivatives due to the time rate of change of the angle in the same plane of motion (such as $C_{m\dot{z}}$) are measured. In most cases the drive is invariable (of the hydraulic or mechanical type), resulting in a constant amplitude sinusoidal oscillation. In some cases, an electromagnetic drive is used, resulting in a constant amplitude of the applied torque (or force), unless a motion-amplitude stabilizing circuitry is used. Although in all the cases the motion is in a single degree-of-freedom (DOF), all three aerodynamic moments and two aerodynamic forces (normal force and side force) can be measured, usually with a single-piece construction strain-gauge balance. The derivatives are obtained from the in-phase and quadrature components of the measured aerodynamic reactions with respect to the model motion, and the frequency and amplitude data. All direct, cross and cross-coupling derivatives can be obtained using this technique in various degrees of freedom. The direct derivatives can also be obtained from the measurement of the torque and its phase with relation to the induced motion. Examples of the instrumentation used at NAE and AEDC and of the required data acquisition and reduction systems are given in Ref. 25. Numerous applications of this technique, as used at NASA Langley, ONERA Chalais-Meudon, ONERA Modane, AEDC-VKF, AEDC-PWT, DFVLR and NAE, are described in Section 5 of Ref. 24. The technique is also used in Sweden (FFA, Ref. 26) and China (SARI, NAI and BIA). A recent sting-mounted Swedish pitch/yaw apparatus is shown in Fig. 21.

3.2 Multi DOF Forced Oscillation - Measurement of Motion

In this technique, the model is suspended elastically in such a way that it can oscillate in several degrees of freedom simultaneously, although one degree of freedom (choice depends on the oscillation frequency) is usually predominant. The amplitude and phase of the various motions (rather than of the various reactions, as in the preceding section), together with the information about the driving force or torque and frequency, are measured and fed into a system of equations of motion, which is then solved for the unknown stability derivatives. In the limiting case of a single DOF oscillation, the above technique reduces to the "constant-amplitude torque" subgroup of the preceding section, where the direct derivatives can be obtained from the amplitude and phase of the forced motion and the forcing torque and frequency (in the same DOF) by means of a direct calculation rather than indirectly by solving a system of equations. That type of technique is used at RAE - Bedford, DFVLR-AVA and NASA - Langley, as described in Section 6 of Ref. 24. In the latter case the model is elastically suspended for multi-DOF experiments by a system of cables, whereas at RAE and DFVLR the model is mounted on a spring unit (attached to the sting) which limits the number of DOFs to 2 or 3 (Ref. 27).

3.3 Single DOF Free Oscillation - Measurement of Motion

This technique is the oldest and the simplest of the various oscillatory techniques. It involves the evaluation of a decaying oscillatory motion performed by an elastically suspended model following some initial disturbance. No complicated drive or control system are usually required and the data reduction is relatively straightforward. Although the results are representative of an amplitude range rather than of a discrete value of amplitude, with modern instrumentation this amplitude range can be made sufficiently small so that any variations of the results with amplitude can be obtained as conveniently as with other methods. The technique, however, is limited to the measurement of the direct derivatives (damping and stiffness) only, and in its simplest form is not suitable for use under conditions of dynamic instability or in the presence of large static moments. For these reasons the free-oscillation technique is now gradually being replaced by the various forced-oscillation techniques. Some examples of its use in the past are given in Section 7 of Ref. 24.

3.4 Half-Model Testing

The use of half models (semi-span models) for testing of symmetrical configurations at symmetric flow conditions has been a recognized experimental procedure for a long time. The technique eliminates interference problems usually associated with the presence and with the motion of the sting, permits the use of models larger than otherwise possible and allows for a more convenient arrangement of the test equipment (utilizing the space outside of the wind tunnel). On the other hand, the use of half models has some problems of its own, such as the possible effect of the gap between the model and the wind tunnel wall and, at higher speeds, the effect of an interaction between the shock and the wall boundary layer. Since all applications are strictly limited to symmetrical flow conditions, the technique cannot be used at higher angles of attack, even for symmetrical configurations.

Half models can be used for experiments involving pitching or plunging oscillation using appropriate free- or forced- oscillation techniques described before. The technique is particularly recommended for cases

where static or dynamic sting interference effects may be significant or when the shape of the model afterbody is incompatible with a sting mounting. Other possible applications include the determination of the dynamic interference between two oscillating models and the measurement of the effect of the jet exhaust plume on the pitching or plunging oscillations of a model (Ref. 28). The technique is used for oscillatory testing in many countries, including Sweden (FFA), Canada (NAE), USA (AEDC), China (SARI, BIA) and Japan (NAL).

3.5 Rotary Motion

There are a number of wind tunnel techniques where the model is performing a continuous rotary rather than oscillatory motion, as discussed so far. The two most important varieties of such a rotary motion are as follows:

3.5.1 Rolling - a rotary motion of the model around the body axis or around the wind axis, at zero to moderate angles of attack, usually at zero sideslip and at low to moderate rotation rates. The main purpose of the rolling experiments is to determine stability derivatives due to rolling, such as encountered during a rolling maneuver. Although - strictly speaking - quite different, such derivatives are sometimes used interchangeably with those obtained from roll oscillation experiments. Rolling techniques can be further subdivided into techniques using steady roll and those using free decay of the roll rate. Apparatuses employing these techniques can be found at NASA - Langley, AEDC, FFA, BAC - Warton and DFVLR-Kön, and are described in Section 9.1 of Ref. 24.

3.5.2 Coning - a rotary motion of the model around the wind axis, at arbitrary angle of attack, usually non-zero angle of sideslip and low to moderate rotation rates. Such a motion is sometimes referred to as the lunar motion and the apparatuses employed for such experiments are usually called rotary balances. The main purpose of the coning experiments is to obtain the aerodynamic coefficients (rather than derivatives) as functions of the coning rate. These are required for a better simulation of the aerodynamic phenomena that are associated with the steady spin motion of aircraft and spin recovery. The coning motion is also one of the fundamental characteristic motions derived in the mathematical models of Tobak and Schiff (Ref. 29) and the aerodynamic moments measured during such a motion are required for prediction of even nonspinning maneuvers. It should be noted that many apparatuses used for steady roll about the wind axis can be used interchangeably as rotary balances, that is for the purpose of obtaining the various aerodynamic reactions as functions of the roll rate. The difference lies mainly in the instrumentation and in the data reduction. Several rotary balances are now in existence for both low-speed and high-speed wind tunnels, including those at NASA Langley, NASA-Ames, BAC-Warton, DFVLR-Kön, Aeronautica Macchi and IMF. These were described in Section 9.2 of Ref. 24 and in Ref. 30. A new rotary balance at RAE-Bedford (Ref. 31) is shown in Fig. 22.

All rotary balances, of course, can be used to obtain derivatives due to the rate of roll. In addition, by slightly tilting the axis of a rotary balance with respect to the wind axis, it is possible to superimpose an oscillatory motion in pitch and yaw on the main rotary motion. Such a motion, called "oscillatory coning", may permit the determination of additional derivatives, viz. those due to oscillatory pitch and yaw (Ref. 32).

3.6 Pure Rotation

Since the results of oscillatory experiments (such as in pitch) around a fixed axis are in the form of composite derivatives which contain derivatives due to pure rotation (such as q) and derivatives due to the time-rate-of-change of the angular deflection in the same plane of motion (such as $\dot{\alpha}$), there is a need to separate such component derivatives so that each can be inserted at its proper position in the equations of motion. To separate the two parts, additional experiments are required, in which either a pure angular motion (with the appropriate aerodynamic deflection angles remaining constant) or a pure translation (with the appropriate angular rates remaining zero) is simulated. As already discussed, under certain conditions the translational acceleration is aerodynamically equivalent to the time-rate-of-change of the aerodynamic angle in the same plane of motion. Effects of translational acceleration can be measured by single DOF forced oscillation experiments in vertical or lateral translation, as done at NAE, using methods described in Section 3.1. Simulation of pure angular motion (or pure rotation) in pitch or yaw can be achieved by snaking motion experiments or experiments in a suitably curved flow, while pure rolling can be simulated by experiments in a suitably arranged rolling flow. These latter techniques, which were all developed at NASA-Langley in the 1950's and have now been transferred, together with the 6 ft Stability Tunnel, to the Virginia Polytechnic Institute, will be briefly described in the following paragraphs. More details can be found in Ref. 33.

3.6.1 Snaking Motion - This combines yawing and lateral motions of a model in such a manner as to produce pure yawing. The apparatus (Fig. 23) generates an oscillatory motion in the xy plane so that the model always heads into the relative wind or, in other words, so that the instantaneous angle of yaw - which includes vector components generated by the two basic motions - remains constant at all times. This occurs when $\dot{y} = V \sin \psi$, at which condition the angle of yaw contributed by the yawing oscillation is exactly cancelled by the angle of yaw induced by the lateral oscillation. A comparison of data obtained by algebraic summation of snaking and translational oscillation tests with the data obtained from angular oscillation tests (around a fixed axis) is shown in Fig 24.

3.6.2 Curved Flow - This technique is based on the concept of simulating a steady curved-flight condition by using a fixed model and arranging the wind-tunnel flow in such a way that it is curved in a circular path in the vicinity of the model and that it has the velocity variation normal to the streamlines in direct proportion to the local radius of curvature. This is achieved by using flexible side walls for curving the flow and by employing special vertical-wire drag screens upstream of the test section for producing the desired velocity gradient in the flow across the tunnel (Fig. 25). These screens vary in size across the wind tunnel, with the most dense portion of the screens located at the inner radius of the curved test section. The technique allows measuring pure yawing (due to r only) or pure pitching (due to q only) derivatives with a fixed model mounted on a static balance. The simulation of the steady curved flight is not exact, however, and usually corrections have to be applied for the buoyancy effect caused by the static pressure gradient normal to the streamlines (which does not exist in curved flight). In addition, there are dissimilarities in the behaviour of the model boundary layer (which on the model in a curved flow tends to move towards the center of curvature, contrary to its normal tendency in curved flight), and possible problems due to a rather high degree of turbulence behind the wire screens. Hopefully, however, in many cases these phenomena may be considered to have only a minor effect on the measurements of the purely-rotary derivatives.

3.6.3 Rolling Flow - When a model at an angle of attack performs a rolling motion about a fixed body axis, the

resulting aerodynamic reactions are functions of both the roll rate and the simultaneously occurring time rate of change of the angle of sideslip. This is similar to the previously discussed composite effect resulting from pitching or yawing oscillation around a fixed axis. To obtain aerodynamic derivatives due to "pure" rolling, one can use a stationary model immersed in a rolling flow. The rolling flow must be generated in such a way that its velocity component normal to the tunnel axis increases proportionally to the radial distance. This can be achieved by using, upstream of the test section, a large rotor with several vanes that are specially shaped in order to impart a suitable solid core vortex motion to the flow. One fascinating future application of this technique would be to impart pitching or yawing oscillation to the model and obtain measurements of the various damping, cross and cross-coupling derivatives in the presence of the rolling flow, thereby providing valuable data for studies of the incipient spin and spin entry and, in particular, oscillatory spin (Ref. 33).

3.7 Control Surface Oscillation

So far we have dealt with dynamic stability testing of full or half models of complete configurations. A brief comment should also be included about the stability characteristics related to the oscillation or motion of the various control surfaces. These are normally of two kinds: (1) the hinge moment derivatives of an oscillating surface and (2) the derivatives of the aerodynamic reactions imparted to the model by the oscillation of a control surface. Although the main interest lies usually in the static control derivatives, the trend is increasing towards also obtaining some dynamic control derivatives, which may become important in connection with high-rate maneuvers and quick-acting controls. The necessary experiments are most conveniently performed using a half model of the aircraft configuration; the hinge moment measurements can be performed with any single DOF oscillation method mentioned before, whereas the aerodynamic reactions on the model itself can be obtained using methods similar to those employed for cross and cross-coupling derivative measurements. Some suitable experimental techniques are mentioned in Section 14 of Ref. 23.

3.8 Non-Linear Dynamic Loads

The various wind-tunnel techniques previously mentioned are characterized by the relatively small amplitude motion that they impart to the model. It has traditionally been assumed that under these conditions the resulting aerodynamic phenomena are linearly related to the model motion, implying that if a sinusoidal motion is used, as is typically the case, the aerodynamic reactions are also sinusoidal and of the same frequency as that of the model oscillation. In such a case the desired aerodynamic information can be represented in the form of stability derivatives that can be obtained using procedures like the ones discussed in Refs 25 and 28.

The applicability of the locally linearized aerodynamics model, implicit in the derivative formulation, to large amplitude and high rate maneuvers, has been increasingly questioned over the last few years. Consequently, a new wind-tunnel technique, specifically designed to investigate the aerodynamic loads acting on a model subjected to large amplitude and/or high rate motions has been recently developed at NAE.

3.8.1 Data Reduction - The goal is to measure the instantaneous value of the reactions in terms of the corresponding instantaneous value of the pertinent motion variables. Since no assumption of linearity is made, the components of the reactions at the oscillation frequency as well as at its harmonics need to be determined. Therefore the technique basically consists of measuring the Fourier coefficients of the balance outputs (deflections), which are converted into their causative loads by using the appropriate model-balance system mechanical transfer functions. The inverse Fourier Transform is then applied to the above coefficients in order to represent the reactions in the time domain. This apparently round-about approach is required in order to account for the dynamic response of the model-balance system, which can have a substantial impact on the observed balance outputs. Inertial effects are eliminated by means of tare measurements. Further details on the technique can be found in Ref. 34. The current implementation of the instrumentation system and data reduction procedures are described in Ref. 35.

3.8.2 Reaction Representation - Once the concept of stability derivatives can no longer be used, it becomes imperative to formulate an appropriate representation of the non-linear aerodynamic data in order to effectively utilize it in flight mechanics computations. One possible representation (Ref. 36) is based on the assumption that there is a well defined (although not necessarily single valued) relationship between the instantaneous value of any given aerodynamic reaction and the corresponding instantaneous value of the motion variables. In a topological sense, this representation implies the existence of a unique (again not necessarily single valued) "reaction hypersurface" that defines the reaction in terms of n motion variables.

If the hypersurface could be experimentally obtained in its entirety - e.g. by means of the technique summarized in the previous section - it could be used to carry out simulations without resorting to mathematical models. Practical considerations, however, limit the number of experiments that can be performed to obtain the very large data base required to suitably define the hypersurface, therefore necessitating some level of mathematical modelling to supplement the empirical data.

A detailed description of the hypersurface representation with its rather wide-ranging implications can be found in the above reference and is, therefore, not included here. However an example of how the representation can be applied to the simple case of a single DOF motion is briefly mentioned here for completeness. Let us consider a hypothetical case of a motion about the roll body axis where the reaction C_l is a function of ϕ and p only, in which case the reaction surface becomes three dimensional and can thus be readily visualized. A schematic hysteretical surface is arbitrarily postulated as an illustration (Fig. 26). The motion of the model is represented by a trajectory in the ϕ - p phase plane and the corresponding value of the reaction is defined by the reaction surface. The surface depicted in Fig. 26 is characterized by threshold values that are independent of the rate, corresponding to the case of "static hysteresis", as opposed to the situation shown in Fig. 27 where the thresholds are a linear function of rate, indicating a convective time lag effect on the threshold values. Both reaction surfaces are single valued everywhere except at the line defining the "step" indicating that "minor loops" are permissible under oscillation amplitudes below the threshold value. A double valued reaction surface where such minor loops do not occur is shown in Fig. 28, in which case the only way to transfer from one branch of the hysteresis curve to the other is by exceeding the threshold value.

The reaction surface for an 80 degree delta wing in subsonic flow has been approximately determined (Ref. 37), on the basis of experimental data obtained by Nguyen et al. (Ref. 38). Although sufficient information

was not available to precisely define the surface, the results indicate that the surface concept is applicable to this case.

4. CONCLUDING REMARKS

In this lecture a brief review was presented of some of the aerodynamic aspects of the dynamic behaviour of a modern, high performance fighter aircraft and of some of the more important experimental techniques that are available for measuring the dynamic stability parameters of an aircraft in a wind tunnel. Because of space limitations many topics had to be omitted and the reader is referred to the three volumes listed in "Bibliography", and in particular to Refs 1, 23 and 24 by the present author, for further details. More recent pertinent information can be found in Refs 39-46. It is hoped that the present review, together with the above additional material, may provide a useful insight into the aerodynamics of a maneuvering modern fighter and may serve as a guide to the large variety of wind tunnel methods that have to be used in order to obtain the dynamic data required for the design of such an aircraft.

5. REFERENCES

1. Orlik-Rückemann, K.J., "Aerodynamic Aspects of Aircraft Dynamics at High Angles of Attack", J. of Aircraft, Vol. 20, No. 9 Sept. 1983, pp 737-752.
2. Francis, M.S. and Keesee, J.E., "Airfoil Dynamic Stall Performance with Large-Amplitude Motions", AIAA Journal, Vol. 23, No. 11, Nov. 1985, pp 1653-1659.
3. McCroskey, W.J., "Unsteady Airfoils", Ann. Rev. Fluid Mech. 1982, 14, pp 285-311.
4. Herbst, W.B., "Supermaneuverability", Proc. of AFOSR-FJSRL - Univ. of Colorado Workshop on Unsteady Separated Flow, USAF Academy, Colorado Springs, August 1983, pp 1-9.
5. Ericsson, L.E., "The Fluid Mechanics of Slender Wing Rock", J. of Aircraft, Vol. 21, No. 5, May 1984, pp 322-328.
6. Lan, C.E., "Theoretical Prediction of Wing Rocking", AGARD CP-386, May 1985, Paper 32.
7. Hsu, C.H. and Lan, C.E., "Theory of Wing Rock", J. of Aircraft, Vol. 22, No. 10, October 1985, pp 920-924.
8. Nguyen, L.T., Whipple, R.D. and Brandon, J.M., "Recent Experiences of Unsteady Aerodynamic Effects on Aircraft Flight Dynamics at High Angles of Attack", AGARD CP-386, May 1985, Paper 28.
9. Stone, R.W., Jr. and Bryant, R.L., "Summary of Results of Tumbling Investigations Made in the Langley 20 - Feet Free Spinning Tunnel on 14 Dynamic Models", NACA RM L8 J 28, December 1948.
10. Whipple, R.D., Green, M.A. and Fears, S.P., "Preliminary Results of Experimental and Analytical Investigations of the Tumbling Phenomenon for an Advanced Configuration" AIAA 84-2108, August 1984.
11. Lang, J.D. and Francis, M.S., "Unsteady Aerodynamics and Dynamic Aircraft Maneuverability", AGARD CP-386, May 1985, Paper 29.
12. Lang, J.D., "The Interaction of an Oscillating Airfoil and/or Flap with a Separating Flow", Ph.D. Thesis, Cranfield Inst. of Tech. January 1975.
13. Francis, M.S., Keesee, J.E., Lang, J.D. Sparks, G.W. and Sisson, G.E., "Aerodynamic Characteristics of an Unsteady Separated Flow", AIAA Journal, Vol. 17, 1979, pp 1332-1339.
14. Luttgies, M.W. Robinson, M.C. and Kennedy, D.A., "Control of Unsteady Separated Flow Structures on Airfoils", AIAA-85-0531, AIAA Shear Flow Control Conference, March 1985.
15. Koga, D.J., Reisenhel, P.H. and Nagib, H.M., "Control of Separated Flowfields using Forced Unsteadiness", IIT Fluids Heat Transfer Report R 84-1, January 1984.
16. Reisenhel, P.H., "Reattachment Control behind a Rearward Facing Step Using Forced Unsteadiness", IIT M.Sc. Thesis, Dec. 84.
17. Ahuja, K.K., "Basic Experimental Study of the Coupling Between Flow Instabilities and Incident Sound", NASA CR 3789, March 1984.
18. Katz, J. and Levin, D., "Measurements of Canard-Induced Roll Oscillations", AIAA 85-1830, Snowmass, CO, August 1985.
19. Blake, W.B., "Prediction of Fighter Aircraft Dynamic Derivatives using Digital Datcom", AIAA-85-4070, Colorado Springs, October 1985.
20. Chambers, J.R., Dicarlio, D.J. and Johnson, J.L. Jr., "Applications of Dynamic Stability Parameters to Problems in Aircraft Dynamics", AGARD-LS-114, March 1981, Lecture 17.
21. Orlik-Rückemann, K.J., "Methods of Measurements of Aircraft Dynamic Stability Derivatives". NRC Canada LR-254, 1959.
22. Orlik-Rückemann, K.J., "Dynamic Stability Testing of Aircraft - Needs versus Capabilities". Progress in Aerospace Sciences 1975, Vol 16, No 4, pp 431-447.
23. Orlik-Rückemann, K.J., "Techniques for Dynamic Stability Testing in Wind Tunnels", AGARD-CP-235, May 1978, Paper 1.

24. Orlik-Rückemann, K.J., "Review of Techniques for Determination of Dynamic Stability Parameters in Wind Tunnels", AGARD-LS-114, March 1981, Lecture 3.
25. Hanff, E.S., "Direct Forced Oscillation Techniques for the Determination of Stability Derivatives in Wind Tunnels", AGARD-LS-114, 1981, Lecture 4.
26. Jansson, T. and Torngren, L., "New Dynamic Testing Techniques and Related Results at FFA", AGARD-CP-386, 1985, Paper 20.
27. O'Leary, C.O. "Wind Tunnel Measurement of Aerodynamic Derivatives Using Flexible-Sting Rigs", AGARD-LS-114, 1981, Lecture 5.
28. Hanff, E.S., "Applications of Half-Model Technique in Dynamic Stability Testing", AGARD-LS-114, 1981, Lecture 9.
29. Tobak, M. and Schiff, L.B., "Aerodynamic Mathematical Modeling - Basic Concepts", AGARD-LS-114, 1981, Lecture 1.
30. Malcolm, G.N., "Rotary and Magnus Balances", AGARD-LS-114, 1981, Lecture 6.
31. O'Leary, C.O. and Rowthorn, E.N., "New Rotary Rig at RAE and Experiments on HIRM". AGARD-CP-386, 1985, Paper 19.
32. Tristrant, D. and Renier, O. "Récents développements des techniques de simulation dynamique appliquées à l'identification des paramètres de stabilité", AGARD-CP-386, 1985, Paper 22.
33. Chambers, J.R., Grafton, S.B., and Lutze, F.H., "Curved-Flow, Rolling-Flow, and Oscillatory Pure-Yawing Wind Tunnel Test Methods for Determination of Dynamic Stability Derivatives", AGARD-LS-114, 1981, Lecture 7.
34. Hanff, E.S. "Determination of Non-Linear Loads on Oscillating Models in Wind Tunnels", ICIASF '83 Record, pp 145-151, Sept. 1983.
35. Hanff, E.S., "Instrumentation and Other Issues in Non-Linear Dynamic Testing in Wind Tunnels", ICIASF '85 Record, pp 200-208, Aug. 1985.
36. Hanff, E.S., "Dynamic Nonlinear Airloads - Representation and Measurement", AGARD-CP-386, 1985, Paper 27.
37. Hanff, E.S., "Non-Linear Representation of Aerodynamics of Wing Rock of Slender Delta Wings", AIAA-85-1931, Snowmass, Co. August 1985.
38. Nguyen, L.T., Yip, L. and Chambers, J.R., "Self-Induced Wing Rock of Slender Delta Wings", AIAA Paper 81-1883, August 1981.
39. Ericsson, L.E. and Reding J.P., "Review of Support Interference in Dynamic Tests", AIAA Journal, Vol 21, No 12, December 1983, pp 1652-1666.
40. Useilton, B.L. and Haberman, D.R., "Summary of Sting Interference Effects for Cone, Missile and Aircraft Configurations as Determined by Dynamic and Static Measurements", AIAA-82-1366, August 1982.
41. Graham, G.M. and Strickland, J.H., "An Experimental Investigation of an Airfoil Pitching at Moderate to High Rates to Large Angles of Attack", AIAA-86-0008, January 1986.
42. Jumper, E.J., Shreck, S.J. and Dimmick, R.L., "Lift-Curve Characteristics for an Airfoil Pitching at Constant Rate", AIAA-86-0117, January 1986.
43. Robinson, M.C. and Lutges, M.W., "Vortices Produced by Air Pulse Injection from the Surface of an Oscillating Airfoil", AIAA-86-0118, January 1986.
44. Brandon, J.M. and Nguyen, L.T., "Experimental Study of Effects of Forebody Geometry on High Angles of Attack Static and Dynamic Stability", AIAA-86-0331, January 1986.
45. Gera, J., "Dynamics and Controls Flight Testing of the X-29A Airplane", AIAA-86-0167, January 1986.
46. Beyers, M.E., "SDM Pitch - and Yaw - Axis Stability Derivatives", AIAA-85-1827, August 1985.

6. BIBLIOGRAPHY

1. Orlik-Rückemann, K.J. (Ed.) "Dynamic Stability Parameters", AGARD FDP Symposium, Athens (Greece), AGARD-CP-235, May 1978.
2. Orlik-Rückemann, K.J. (Ed.) "Dynamic Stability Parameters", AGARD FDP Lecture Series, NASA Ames (USA) and von Karman Institute (Belgium), AGARD-LS-114, March 1981.
3. Orlik-Rückemann K.J. (Ed.), "Unsteady Aerodynamics - Fundamentals and Applications to Aircraft Dynamics", AGARD FDP Symposium, Göttingen (Germany), AGARD-CP-386, May 1985.

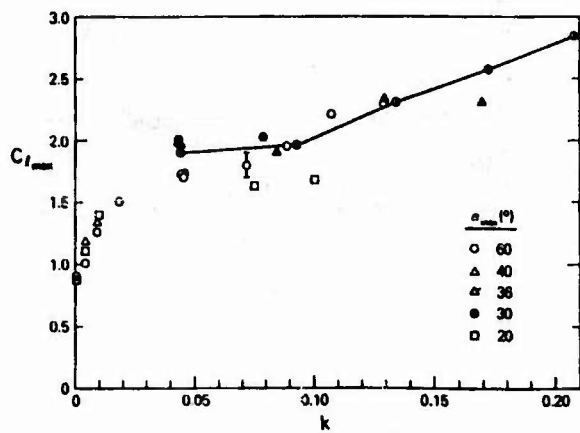
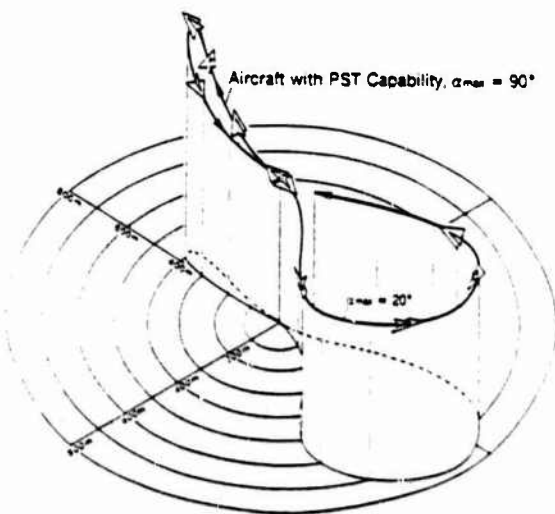
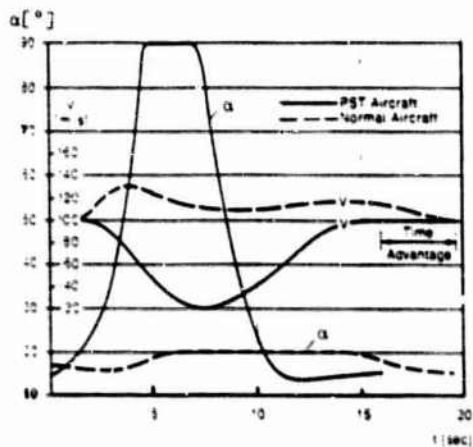


Fig. 1. Maximum lift coefficient vs pitch rate for NACA 0012 (open symbols) and NACA 64 A012 (13) (half solid symbols) (Ref. 2)



(a) Trajectory comparison



(b) Time histories

Fig. 3. Supermaneuverability. Minimum time maneuvers (Ref. 4)

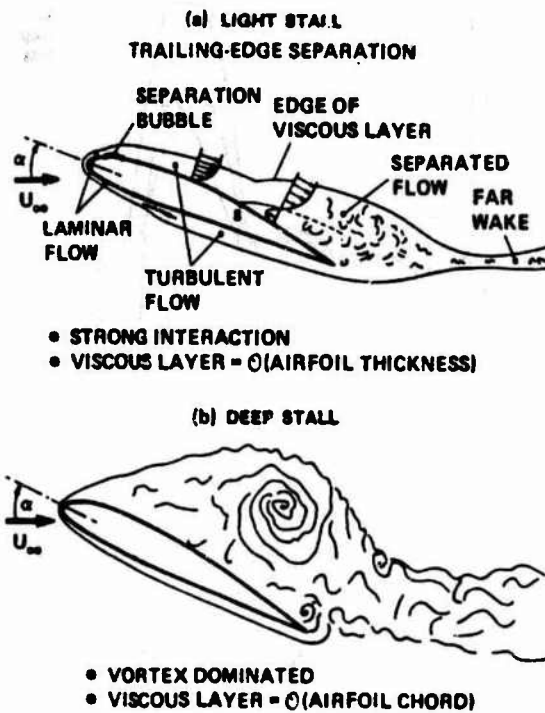


Fig. 2. Sketches of flow fields during dynamic stall (Ref.3)

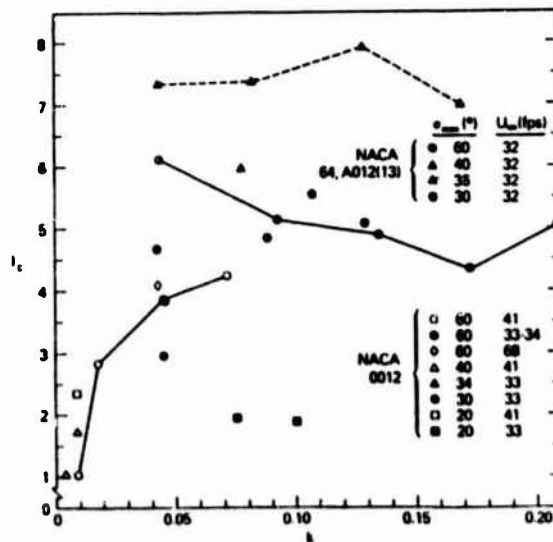


Fig. 4. Impulse function vs pitch rate (Ref. 2)

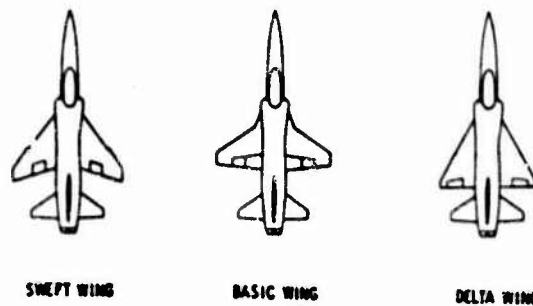


Fig. 5. Wing models tested with model based on F-5 configuration (Ref. 8)

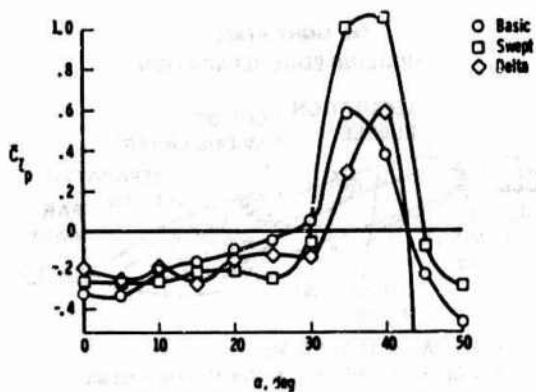


Fig. 6. Low-speed damping in roll for models of Fig 5 (Ref. 8)

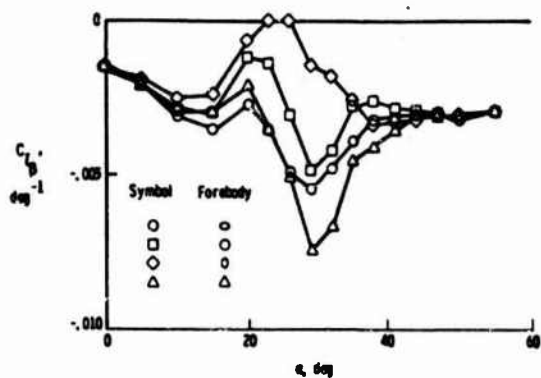


Fig. 7. Effect of forebody cross-section on static lateral stability. Generic fighter model (Ref. 8)

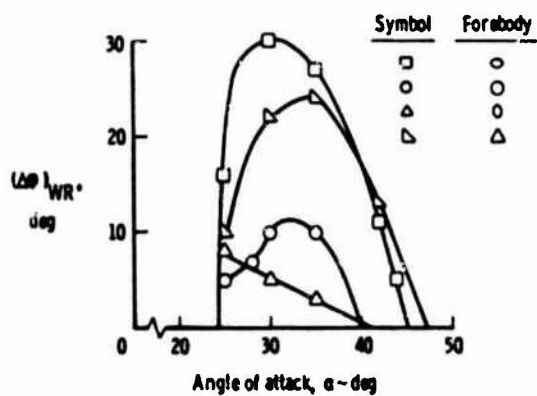


Fig. 8. Effect of forebody cross-section on wing rock amplitude. Generic fighter model (Ref. 8)

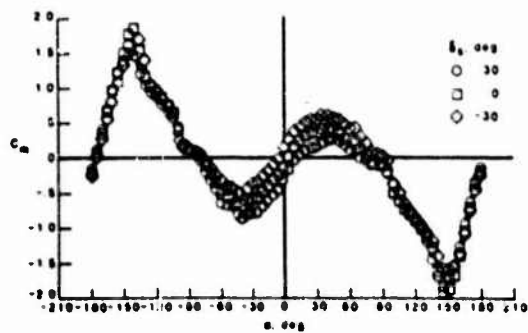


Fig. 9. Pitching moment coefficient for X-29 A model (Ref. 8)

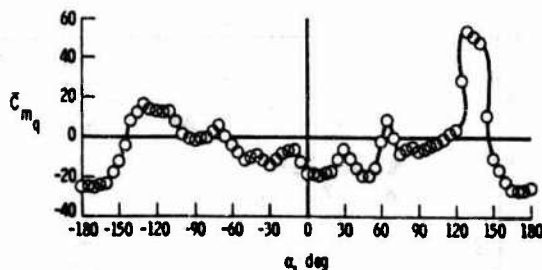


Fig. 10. Damping in pitch parameter for X-29 A model (Ref. 8)

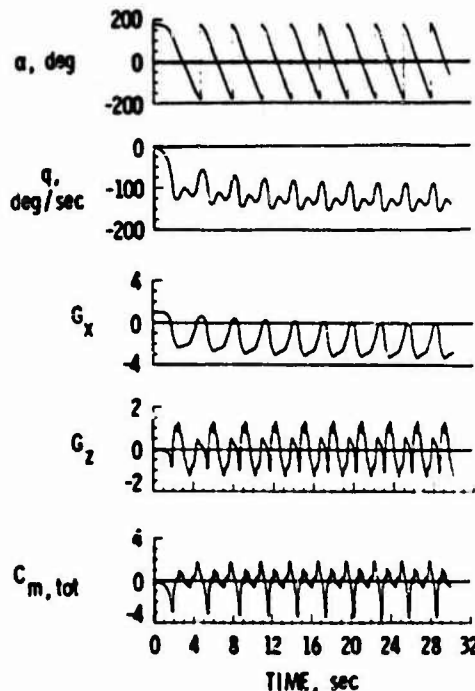


Fig. 11. Time histories of a computed tumbling motion, X-29 A configuration (Ref. 8)

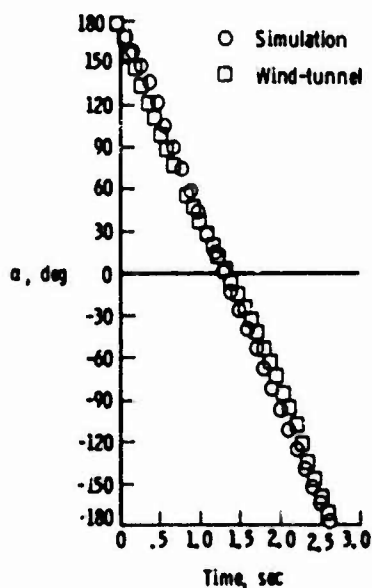


Fig. 12. One cycle of X-29 A tumbling - experiment vs computation (Ref. 8)

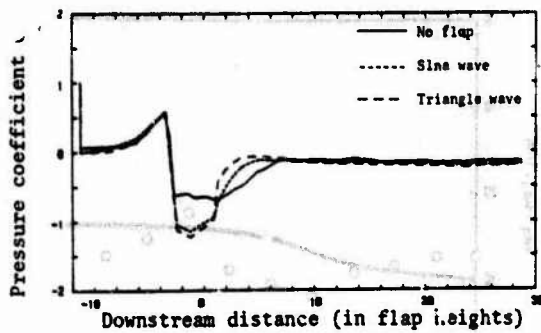


Fig. 13. Effect of oscillating flap on flow separation resulting from an upstream wedge, $X'/H=-3$, (Ref. 15)

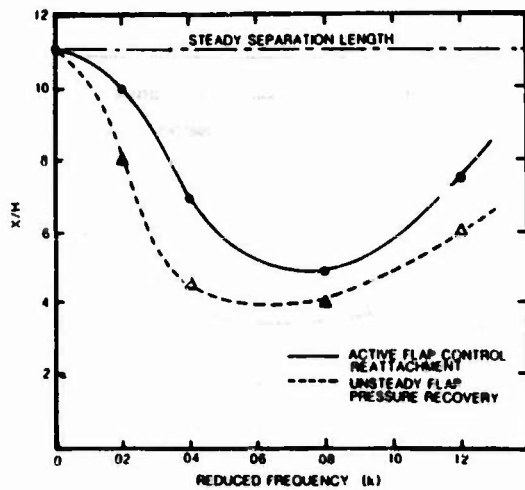


Fig. 14. Effect of reduced frequency on flow attachment length (Ref. 15)

- STABLE
- ▨ CANARD/WING INDUCED OSCILLATIONS
- ▧ WING INDUCED OSCILLATIONS
- ▩ NONSYMMETRICAL OSCILLATIONS
- ▤ RANDOM, UNSTABLE MOTION

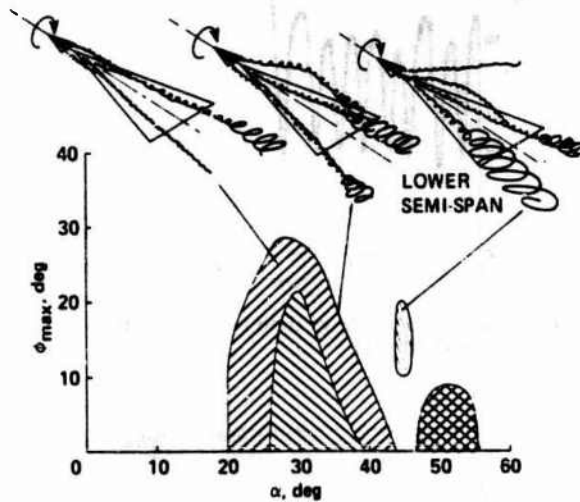


Fig. 15. Angle of attack range for self-induced roll oscillations for a 76° delta wing (Ref. 18)

Configuration	Speed Regime	C_{L_d}	C_{n_d}	C_{l_d}	C_{o_d}	C_{L_p}	C_{n_p}	C_{y_p}	C_{r_p}	C_{L_r}
Body	Subsonic	o	o	o	o					
	Transonic	o	o	o	o					
	Supersonic	o	o	o	o					
Wing	Subsonic	o	o	o	o	o	o	o	o	o
	Transonic	o	o	o	o	o	o	o	o	o
	Supersonic	o	o	o	o	o	o	o	o	o
Horizontal Tail	Subsonic	o	o	o	o	o				
	Transonic	o	o	o	o	o				
	Supersonic	o	o	o	o	o				
Vertical Tail- Ventrol Fin	Subsonic					o	o	o	o	o
	Transonic					o	o	o	o	o
	Supersonic					o	o	o	o	o
Wing-Body	Subsonic	o	o	o	o	o	o	o	o	o
	Transonic	o	o	o	o	o	o	o	o	o
	Supersonic	o	o	o	o	o	o	o	o	o
Wing-Body- Horizontal Tail	Subsonic	o	o	o	o	o	o	o	o	o
	Transonic	o	o	o	o	o	o	o	o	o
	Supersonic	o	o	o	o	o	o	o	o	o
Wing-Body- Vertical Tail- Ventrol-Fin	Subsonic	o	o	o	o	o	o	o	o	o
	Transonic	o	o	o	o	o	o	o	o	o
	Supersonic	o	o	o	o	o	o	o	o	o
Wing-Body- Horizontal Tail- Vertical Tail- Ventrol Fin	Subsonic	o	o	o	o	o	o	o	o	o
	Transonic	o	o	o	o	o	o	o	o	o
	Supersonic	o	o	o	o	o	o	o	o	o

o output available
 / output only for configurations with straight-tapered wings

Fig. 17. Configurations and speed regimes for which Digital Datcom can be used for prediction of dynamic direct and cross derivatives in the attached flow region (Ref. 19)

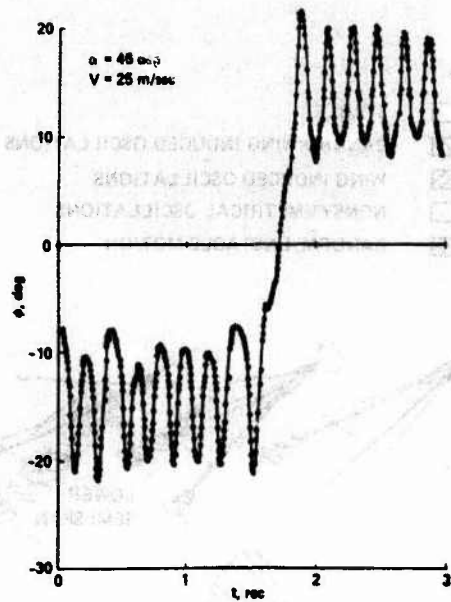
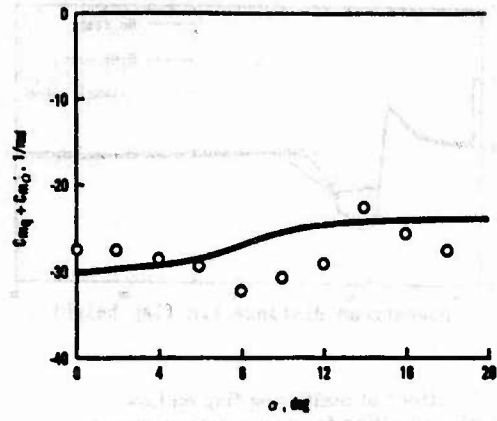
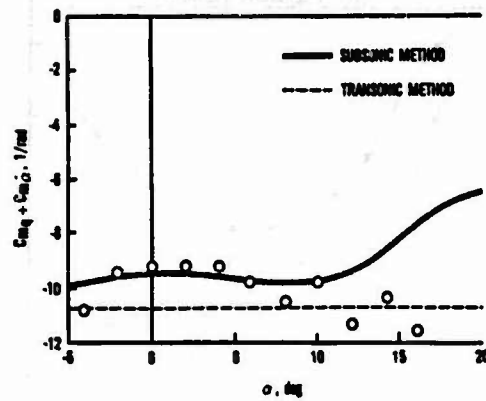


Fig. 16. Rolling angle vs time for asymmetric oscillation (Ref. 18)



(a) F-111, $M = 0.4$



(b) Standard Dynamics Model, $M = 0.8$

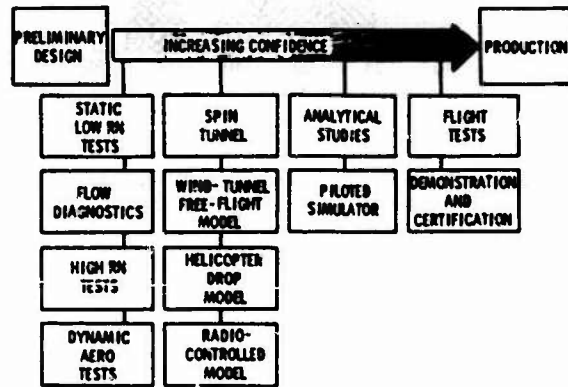


Fig. 19. Methodology for prediction and analysis of high α -characteristics (Ref. 20)

Fig. 18. Comparison of Digital Datcom predictions with experiment (Ref. 19)

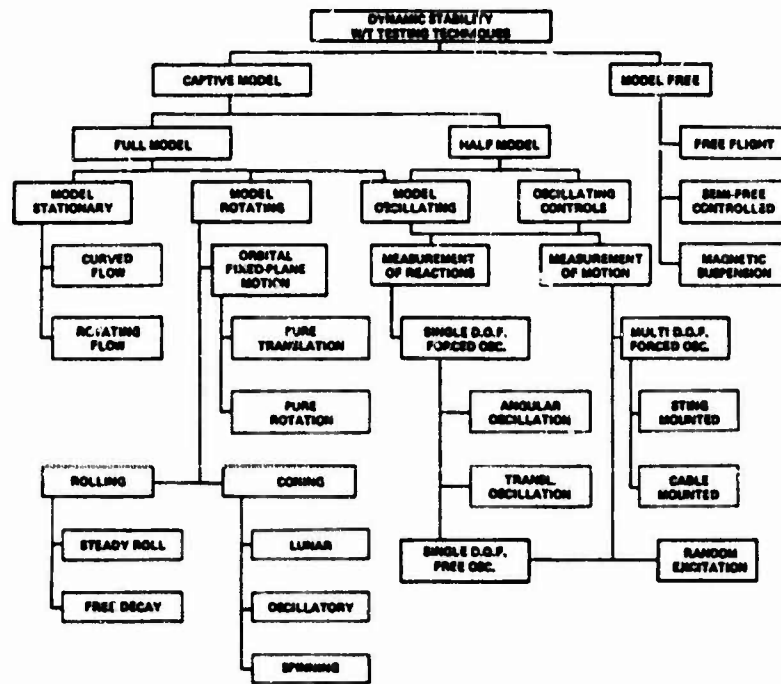


Fig. 20. Wind tunnel techniques for dynamic stability testing

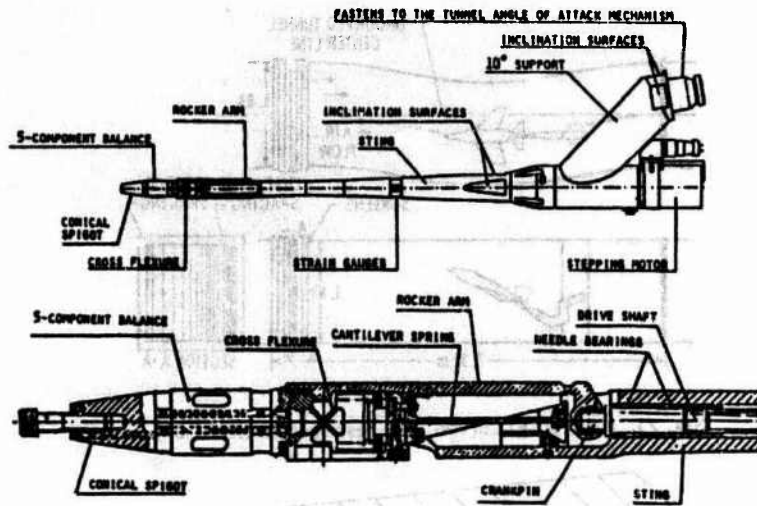
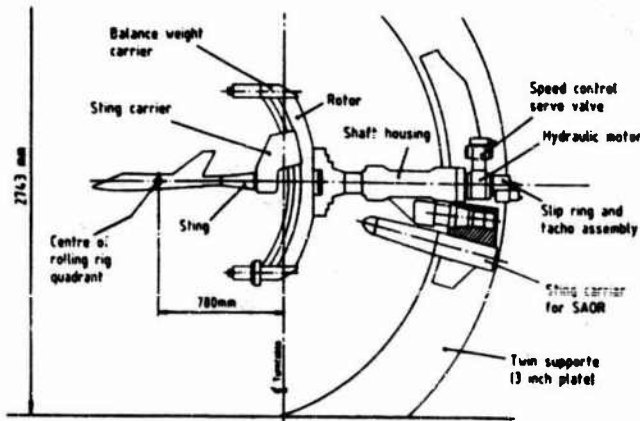


Fig. 21. FFA pitch/yaw forced oscillation apparatus (Ref. 26)



(a) Rotary balance mounted in RAE 4 m x 2.7 m wind tunnel

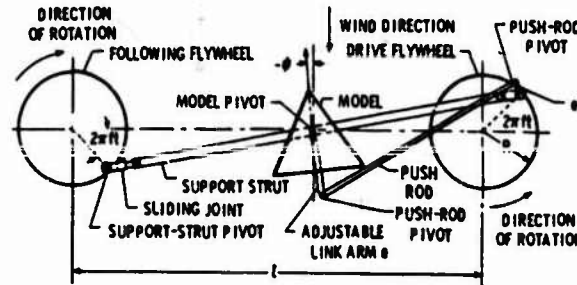
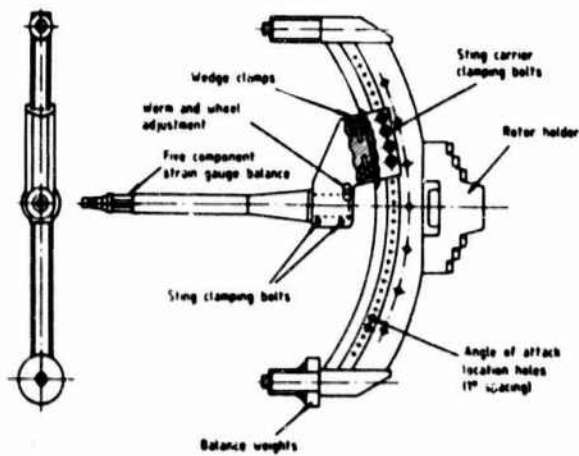


Fig. 23. NACA/VPI apparatus for snaking motion (Ref. 33)



(b) Details of rotor and sting

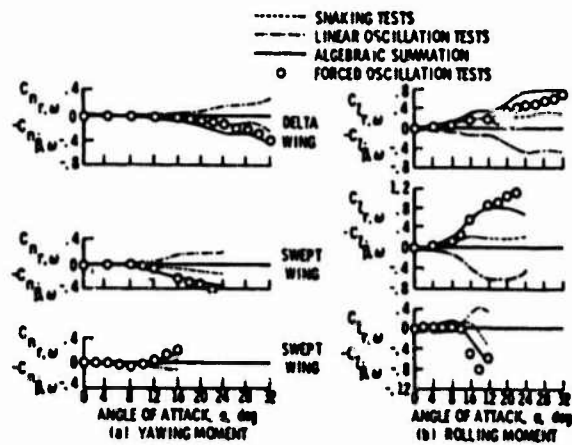


Fig. 24. Comparison of combined snaking and linear test results with forced oscillation results (Ref. 33)

Fig. 22. RAE - Bedford rotary balance (Ref. 31)

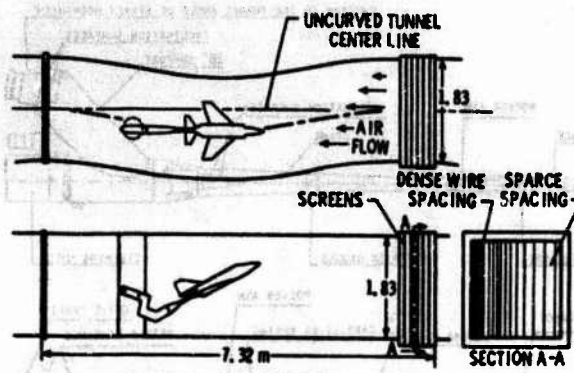


Fig. 25. NACA/VPI curved flow test section (Ref. 33)

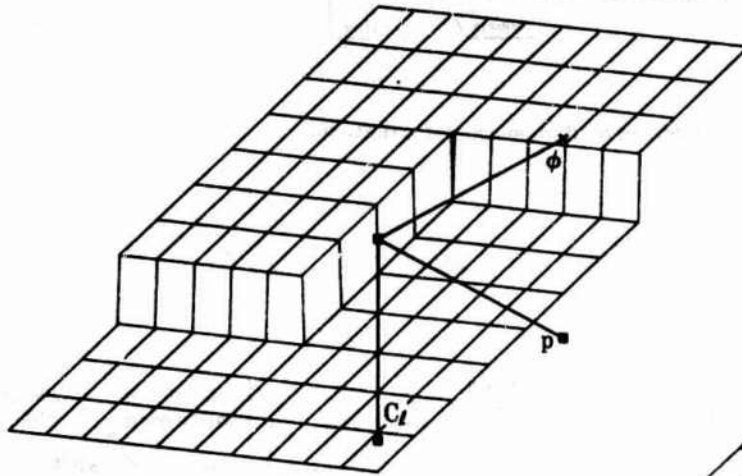


Fig. 26. Schematic reaction surface - threshold values independent of rate (static hysteresis), minor loops permitted (Ref. 36)

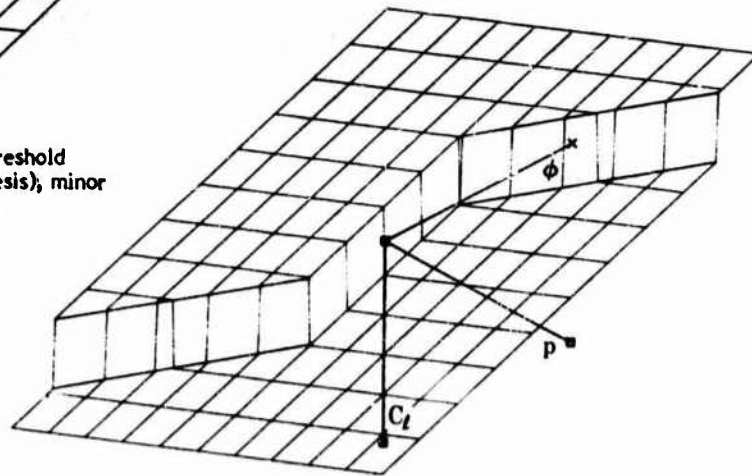


Fig. 27. Schematic reaction surface - threshold values linearly dependent on rate (Ref. 36)

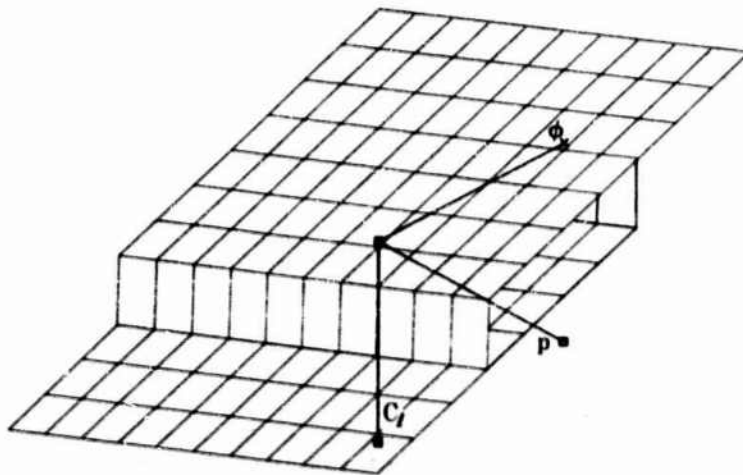


Fig. 28. Schematic reaction surface - threshold values independent of rate, minor loops not permitted (Ref. 36)

Aerodynamic Aspects of Aircraft Dynamics at High Angles of Attack

K. J. Orlik-Rückemann

National Research Council of Canada, Ottawa, Ontario, Canada

Introduction

TO achieve tactical superiority in the air, a fighter aircraft must be capable of high-performance maneuvers. To perform such maneuvers, the aircraft must be able to carry out controlled flight at high angles of attack. To safely predict and analyze such flight conditions, our understanding of the aerodynamics of aircraft at high angles of attack (high α) may require further improvements.

In the context of this review, the aerodynamic phenomena at high α will be discussed mainly from the point of view of their impact on stability parameters of an aircraft. Adequate knowledge of these parameters is required for the prediction of an aircraft's behavior before departure, for the description of its departure/spin-resistance characteristics, and for the difficult analysis of the flight range between the departure and the fully developed spin, if such an analysis is required. Stability parameters are needed also for the assessment of the tracking capabilities of an aircraft, for the efficient design of the control system, and for the evaluation of the range of maneuvers that can safely be induced by the pilot. Such maneuvers at high angles of attack are not only relevant in situations involving air combat and missile avoidance actions, but may also be necessary during certain phases of the landing approach.

Flow Phenomena in Steady and Oscillatory Flight at High Angles of Attack

The aerodynamics of an aircraft performing a *steady* flight at high angles of attack has been studied for several years and a considerable amount of information is now available in this area.^{1,2} It is well known that such an aircraft is exposed to a variety of flow phenomena that usually are nonexistent or have much less significance at lower angles of attack. These phenomena encompass all kinds of transitional, separated, and vortical flows over the body, the wings, and the control surfaces of the aircraft. Of particular interest herein are those flow phenomena that significantly vary with the angle of attack and that, at high enough values of that parameter, can

cause asymmetric effects even if the aircraft itself continues to head symmetrically into the wind (i.e., has zero sideslip). Two of the most important phenomena of that kind are 1) the formation and asymmetric shedding of forebody vortices and 2) the formation and asymmetric bursting of wing leading-edge vortices. It is also known that the behavior of the forebody vortices can be affected by blowing^{3,4} or by introduction of a mechanical disturbance near the nose of the forebody.

If an *oscillatory* motion is superimposed on the primary steady flight of the aircraft, the aforementioned phenomena become much more involved due to the introduction into an already complex picture of an additional variable, namely, the element of time. Let us consider, for instance, an oscillation in pitch. During such an oscillation the forebody vortices will change their lateral and vertical positions as functions of the angle of attack, which itself is a function of time. Similarly, leading-edge vortices will periodically vary the longitudinal location at which they burst. The various components of the aircraft, such as the fin(s) and the horizontal stabilizer, will move in and out of the local flow regions in which they are embedded. To make matters even more complex, all of these motions will take place not in a manner simultaneous with the motion of the aircraft, but with a certain delay, mainly due to the convective time lag. This delay is a function of the distance of the station under consideration (say, at the fin) from the station at which a particular flow phenomenon originates (in the case of the forebody vortices, at the vicinity of the nose).

The response of the forebody vortices to the oscillatory pitching motion of a symmetrically mounted cone-wing configuration was investigated at the National Aeronautical Establishment (NAE) by flow visualization motion pictures made in a water tunnel. The periodic lateral motion of the vortices as well as the time delay between the motion of the vortices and that of the model could be clearly seen. It is obvious that such a lateral motion of the vortices must cause lateral aerodynamic reactions in response to the pitching motion and that the observed time delay requires a vectorial

Dr. Kazimierz J. Orlik-Rückemann, a Principal Research Officer at the National Research Council of Canada, was born in Warsaw, Poland, and obtained his M.Sc., Tekn. Lic. and Tekn. D. degrees in Aeronautical Engineering at the Royal Institute of Technology (K.T.H.) in Stockholm, Sweden. In 1955, after being associated for some years with various aspects of aerodynamic research at the Division of Aeronautics at the K.T.H. and the Aeronautical Research Institute of Sweden (F.F.A.), he moved to the National Aeronautical Establishment (NAE) of the National Research Council in Ottawa, Canada, where he was appointed Head of the High Speed Aerodynamics Laboratory in 1958. In 1963 he became the Head of the newly formed Unsteady Aerodynamics Laboratory which was set up for work on unsteady flow phenomena and dynamic stability problems at high speeds. In 1963-64 he served as Chairman of the Supersonic Tunnel Association, and since 1974 he has been a member of the AGARD Fluid Dynamics Panel where he also served as Chairman in 1980 and 1981. He was for many years an Associate Editor of the *CASI Transactions*. He is a Fellow of the CASI and a Fellow of the AIAA. His present interests encompass high-angle-of-attack aerodynamics, flight mechanics, dynamic experiments in wind tunnels, and problems related to space transportation systems.

Presented as Paper 82-1363 at the AIAA 9th Atmospheric Flight Mechanics Conference, San Diego, Calif., Aug. 9-11, 1982; submitted Sept. 1, 1982; revision received Feb. 18, 1983. Copyright © 1982 by the National Research Council of Canada. Published by the American Institute of Aeronautics and Astronautics with permission.

Reprinted with permission from *Journal of Aircraft* Vol. 20 No. 9, pp. 737-752, September 1983.

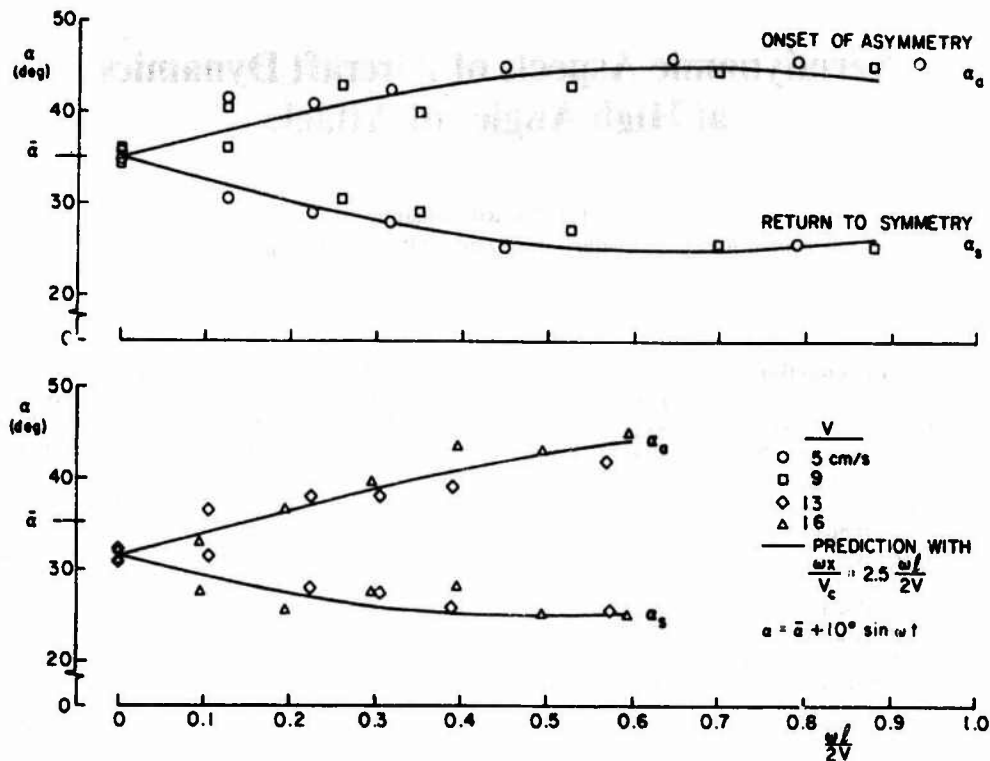


Fig. 1 Phase lag on model oscillating in pitch in water tunnel (NAE).

Table 1 Dynamic moment derivatives

Pure rotation			Translational acceleration			Oscillation around fixed axis		
$C_{lp} = \frac{\partial C_l}{\partial pb}$	$C_{mp} = \frac{\partial C_m}{\partial pb}$	$C_{np} = \frac{\partial C_n}{\partial pb}$	$C_{lb} = \frac{\partial C_l}{\partial \dot{b}}$	$C_{mb} = \frac{\partial C_m}{\partial \dot{b}}$	$C_{nb} = \frac{\partial C_n}{\partial \dot{b}}$	Damping derivatives	Cross derivatives	Cross-coupling derivatives
$C_{lq} = \frac{\partial C_l}{\partial qc}$	$C_{mq} = \frac{\partial C_m}{\partial qc}$	$C_{nq} = \frac{\partial C_n}{\partial qc}$	$C_{l\beta} = \frac{\partial C_l}{\partial \beta b}$	$C_{m\beta} = \frac{\partial C_m}{\partial \beta b}$	$C_{n\beta} = \frac{\partial C_n}{\partial \beta b}$	$C_{lp} + C_{l\beta} \sin \alpha$	$C_{lp} - C_{l\beta} \cos \alpha$	$C_{lq} + C_{l\beta}$
$C_{lr} = \frac{\partial C_l}{\partial rb}$	$C_{mr} = \frac{\partial C_m}{\partial rb}$	$C_{nr} = \frac{\partial C_n}{\partial rb}$				$C_{mq} + C_{m\beta}$	$C_{mp} + C_{n\beta} \sin \alpha$	$C_{mr} - C_{m\beta} \cos \alpha$
						$C_{nr} - C_{n\beta} \cos \alpha$		$C_{mp} + C_{m\beta} \sin \alpha$
								$C_{nq} + C_{n\beta}$

representation of those reactions, i.e., one in which both the components in phase with the motion of the model and the components in quadrature with that motion (or in phase with the angular rate) have to be considered. When presented in the derivative form, such components are usually referred to as static and dynamic derivatives, respectively, of the aerodynamic reactions with respect to pitching. By repeating the flow visualization motion pictures for several values of water speed V , and oscillation frequency ω , it was possible to obtain the diagram in Fig. 1, showing the angle of attack for the onset of asymmetry, α_a , when α was increasing, and the angle of attack for the return to symmetrical flow conditions, α_s , when α was decreasing during the oscillation. Simple expressions were derived for α_a and α_s in which the phase lag was proportional to the reduced frequency of oscillation, and it is shown here that it was possible to obtain a good correlation between these expressions and the experimental points when the phase lag was assumed to be

$$\omega x / V_c = 2.5 (\omega l / 2V)$$

where V_c is the convective velocity and x/l is the dimensionless longitudinal coordinate.

The NAE film also demonstrated how the direction of the vortex asymmetry on a symmetrically mounted model could be controlled by normal blowing or by introducing a mechanical disturbance on the forebody.

Another movie film, made in the Northrop water tunnel, showed the relation between the oscillation in roll of a highly swept delta wing and the differential oscillatory displacement of the longitudinal location on the wing at which the vortices emanating from the wing leading edge break down. It is known that vortex-burst location is sensitive to both the angle of attack and the angle of sideslip, and the effective values of these angles on each half of the wing vary periodically as the wing oscillates in roll. Although the time scale of the Northrop experiment was such that phase lags could not easily be observed, it is a safe assumption that such lags must have been present during the experiment, with the resulting static and dynamic aerodynamic reactions due to oscillation in roll.

It should be noted that the oscillatory flow phenomena, that involve shedding of the forebody vortices and their asymmetrical motion, will occur on all oscillating, pointed, slender bodies that fly at a high angle of attack and, therefore, have impact on the dynamics of not only high-performance aircraft but also of missiles. Although this paper deals mostly with problems related to aircraft, much of the material can also be applied to missiles and, indeed, one or two examples of such applications will be included.

Effects on Dynamic Stability Parameters

The aforementioned high- α flow phenomena have large effects on all of the aerodynamic characteristics of the aircraft including, of course, the static and dynamic stability parameters. For the dynamic stability considerations that are the subject of this review, the most important such effects are: 1) large nonlinear variations of stability parameters with angle of attack, angle of sideslip, and rate of coning, as well as with amplitude and frequency of oscillation; 2) significant aerodynamic cross-coupling between longitudinal and lateral degrees of freedom; 3) time-dependent and hysteresis effects; and 4) strong configuration dependence.

Before discussing these effects in some detail, let us first briefly consider the various categories of dynamic stability derivatives. For simplicity, the discussion will be restricted to dynamic moment derivatives, which, in general, are much more important than the corresponding dynamic force derivatives. The two main categories of the dynamic moment derivatives (Table 1) are those due to pure rotation ($\dot{\alpha}, \dot{\beta}, \dot{q}, \dot{r}$) and those due to the time rate of change of the two aerodynamic angles ($\dot{\alpha}, \dot{\beta}$). The latter is equivalent, in the first approximation, to the translational acceleration in the same plane of motion. In oscillatory experiments around a fixed axis, these two effects are present at the same time and, therefore, the results of such experiments are obtained as the sum of a pertinent rotary derivative and a pertinent acceleration derivative. Such sums are called *composite* derivatives. Depending on the degrees of freedom involved, we can further distinguish between the *damping* derivatives and the *cross* and *cross-coupling* derivatives, as indicated in the table.

Nonlinearities with Angle of Attack

Large variations with the angle of attack of the various complex flow features discussed in the previous section frequently cause significant nonlinearities in the dynamic stability parameters. Some examples of these nonlinearities are presented in Fig. 2, which shows two damping derivatives and one dynamic cross derivative obtained at NAE for a wing-body configuration at a Mach number of 0.7 (Ref. 5). These results amply illustrate both the magnitude and the suddenness of the variations in dynamic derivatives with the angle of attack. It can be appreciated that, if the angle of attack about which the oscillation takes place happens to be in the region where a sudden change in a derivative occurs, large effects of the amplitude of oscillation may be expected. In cases like this the derivative concept can only give an equivalent linearized description of the dependence of the aerodynamic reaction on the variable of motion and a better mathematical formulation may be needed.

Significant nonlinear effects were also obtained at NASA Langley^{6,7} for fighter aircraft at low subsonic speeds. The damping-in-yaw derivative (Fig. 3) exhibits a very sudden and very large (ten times the low- α value and the sign reversed) unstable peak at angles of attack about 60 deg, while the two dynamic cross derivatives (Fig. 4) exhibit an equally large and sudden variation with α , but occurring at different values of that variable. It is interesting to note from these references that the angle of attack at which these peaks occur is largely independent of both the wing sweep angle and the presence of vertical tails, suggesting that the primary mechanism for these effects is associated with some flow phenomena located

upstream of the wing and tails, a likely candidate being forebody vortices.

An example of the variation of a derivative with both the angle of attack and the oscillation amplitude is shown in Fig. 5, where the damping-in-roll derivative of a fighter configuration, obtained at NASA Langley⁶ at low subsonic speeds, is plotted vs angle of attack. The large unstable peak that occurs at $\alpha = 35$ deg when the amplitude of oscillation is ± 5 deg decreases at larger amplitudes and completely disappears at an amplitude of ± 20 deg.

Nonlinearities with Rate of Roll (Spin)

Considerable nonlinearities with spin rate, together with important effects of both angle of attack and Reynolds

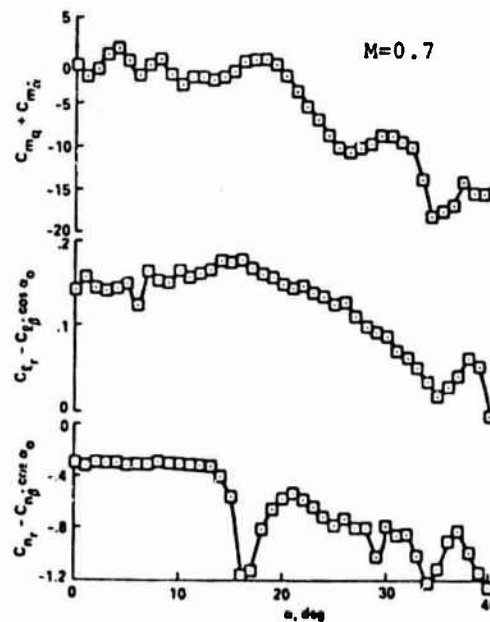


Fig. 2 Nonlinearities in damping and cross derivatives, $\Delta\theta = \Delta\psi = \pm 1$ deg (NAE).

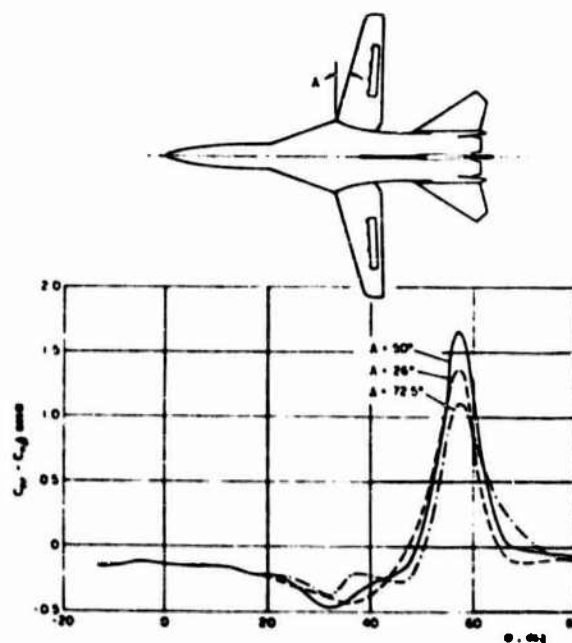


Fig. 3 Damping in yaw for a fighter configuration, $M < 0.1$, $\Delta\psi = \pm 5$ deg (NASA LRC).

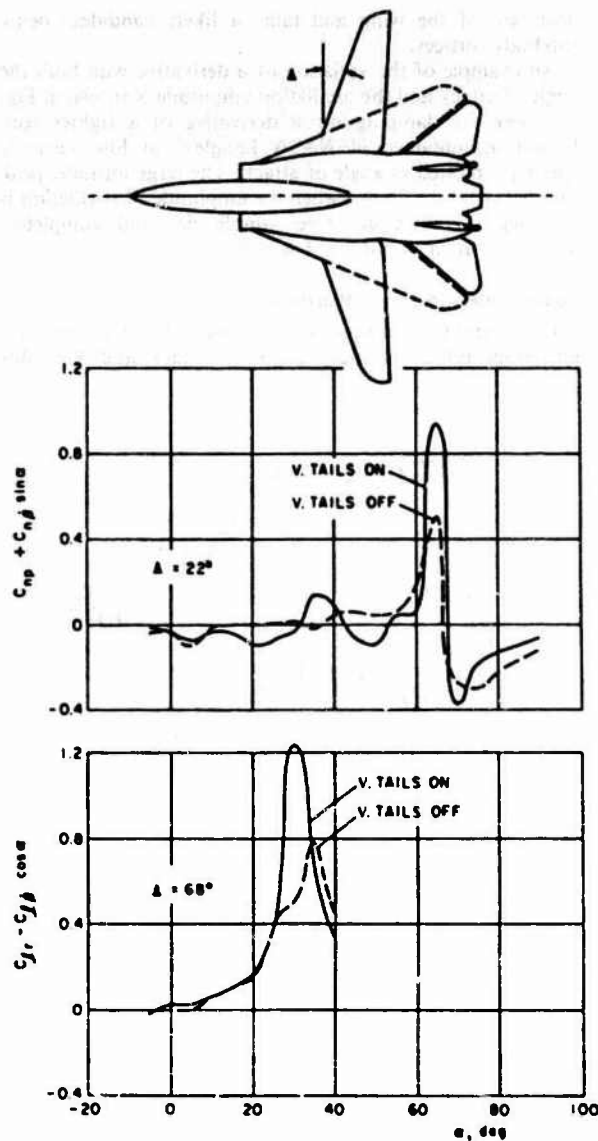


Fig. 4 Cross derivatives for a fighter configuration, $M < 0.1$, $\Delta\phi = \Delta\psi = \pm 5$ deg (NASA LRC).

number, are shown in Fig. 6, where the nose side-force coefficient for a model with a square forebody cross section but with rounded corners is shown as a function of the spin rate at $\alpha = 75$ deg and for various Reynolds numbers. These experiments, performed at NASA Ames Research Center,⁸ show a strong nonlinear prospin contribution at all but the two lowest Reynolds numbers investigated. No such prospin contributions were detected at $\alpha = 45$ deg.

Another example⁹ of large nonlinearities with spin rate is shown in Fig. 7. Pitching, rolling, and yawing moments for a series of general aviation models at $\alpha = 60$ deg are shown vs reduced spin parameter. The nonlinearity is pronounced and the sense of the rolling and yawing moments can change with rotation rate from autorotative to damping. The pitching moment increases most significantly over the static value, primarily due to the effect of the horizontal tail.

Occurrence of Wing Rock

An important manifestation of the effect of nonlinearities is the well-known phenomenon of wing rock. This phenomenon, primarily associated with the loss of damping in roll at higher angles of attack (Fig. 8), requires the presence of one or more nonlinear terms in the equation(s) of motion to

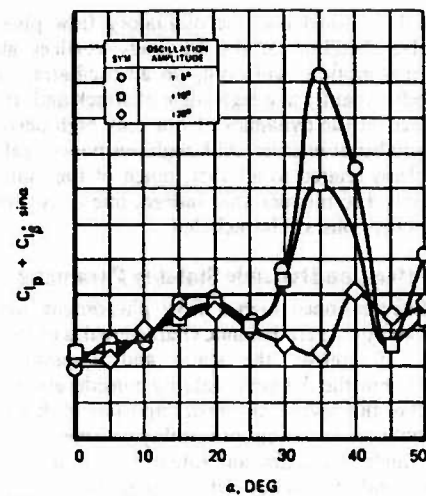


Fig. 5 Effect of oscillation amplitude on damping in roll (NASA LRC).

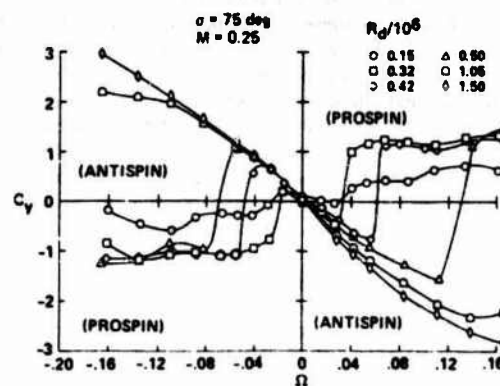


Fig. 6 Nose side-force coefficient vs reduced spin rate. Square cross section with rounded corners (NASA ARC).

render possible the characteristic limit-cycle type of oscillation in roll. It can be assumed that the aerodynamics of the problem, in principle, is related to the motion (or burst) of the forebody vortices or the leading-edge vortices, or else to the periodic variations from the attached to separated flow on some portion of the wing as the wing oscillates in roll. At transonic speeds an additional aerodynamic cause can be the periodic motion of the local shock waves. It is not yet well understood how these aerodynamic causes can be expressed mathematically in the equations of motion, but certain nonlinear terms have been experimentally determined and their effect on the resulting limit-cycle motion confirmed. Of course, different nonlinearities can be expected to exist for different configurations and different flight conditions. Three such scenarios, all involving wing rock at subsonic speeds, will be briefly described below.

Variation of Damping in Roll with Angle of Sideslip

The variation of the rolling moment with the reduced roll rate for various angles of attack and sideslip was recently studied at NASA Langley.¹⁰ The data were obtained for an 80-deg delta wing at low subsonic speeds using a rotary balance (with the rotation taking place about the wind axis). Some of the results are shown in the upper part of Fig. 9. The slope of the curves represents the damping in roll and is negative for positive (stable) damping and vice versa. At $\alpha = 10$ deg the damping is positive for all β investigated. At $\alpha = 30$ deg the damping is negative at small β but positive at higher β . A set of curves (bottom left of Fig. 9) constructed by combining the above results with the results of some forced-oscillation experiments shows the variation of the damping in

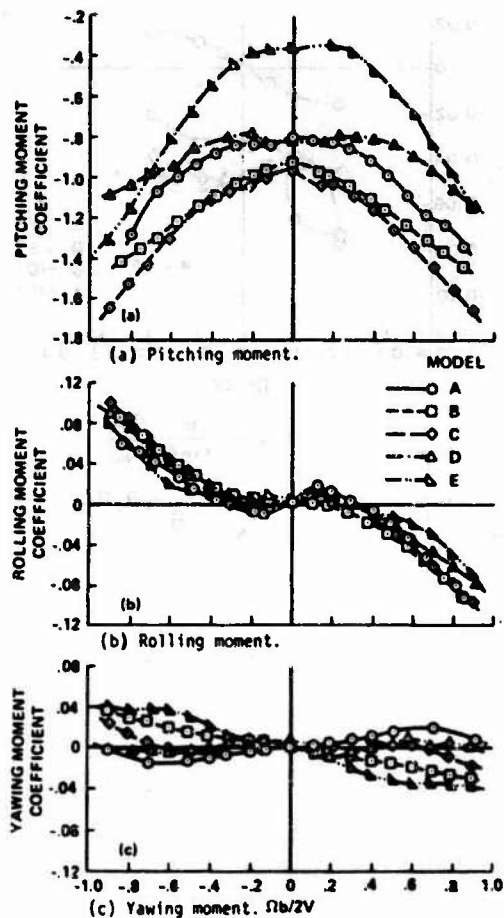


Fig. 7 Moment coefficients vs reduced spin rate. General aviation configuration, $\alpha = 60$ deg (NASA LRC).

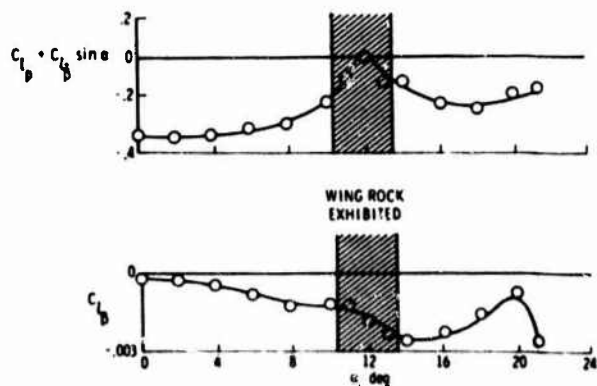


Fig. 8 Rolling moment derivatives for a fighter configuration (NASA LRC).

roll with the magnitude of sideslip for different angles of attack. The damping in roll changes from unstable to stable in the range of 5 to 7 deg of sideslip. Concurrent flow visualization studies (not shown) have indicated that this effect is associated with the upward displacement of the leeward vortex from the surface of the upgoing part of the wing, while the windward vortex remains close to the upper surface of the wing. A nonlinear simulation using these data yielded a wing-rock motion in close agreement with the results of a free-to-roll experiment, as can be seen on the bottom right of Fig. 9, where the comparison is shown in terms of the limit-cycle amplitude, $(\Delta\phi)_{NR}$, and the period, P_{NR} , of the wing rock observed at various angles of attack. Also shown

are the results of an approximate analytical solution based on a simplified linear variation of the damping in roll with the magnitude of sideslip.

Cubic Variation of Lateral Derivatives with Roll Rate and Sideslip

The representation of the observed nonlinearities by the addition of a cubic term to certain static and dynamic stability derivatives was investigated at RAE.¹¹ It was shown that by including such a cubic term in the damping-in-roll derivative a fairly good agreement could be obtained between the flight and computed time responses for the roll rate and the angle of sideslip of a Gnat aircraft in a wing-rock situation (Fig. 10, top). It was also indicated that an inclusion of a similar cubic term in the cross derivative of the yawing moment due to the roll rate could probably have a beneficial effect on the prediction accuracy. In a separate study, cubic terms were introduced in the static yawing and rolling moment derivatives due to sideslip and it was shown that, although limit cycles could not normally be expected to occur through nonlinearities of a single-valued stiffness term in a second-order differential equation, such a limit cycle could and indeed did occur in a multimode system where the two stiffness terms were affecting both the frequency and the distribution of damping between the two modes involved (yawing and rolling). For a usual combination of the linear terms of the two derivatives ($l_{r,r} > 0, n_{r,r} > 0$) it was found (Fig. 10, bottom) that with a positive (stiffening) $n_{r,r}$ the limit cycle was predicted to occur for a large range of values of $l_{r,r}$, while with a negative (softening) $n_{r,r}$ the limit cycle was computed only for $l_{r,r} > 190$. Two different prediction methods (analog and approximate) were used in this study with good agreement. Since this type of nonlinearity in the moment derivatives due to sideslip can lead to divergence as well as to limit cycle, it was recommended that it be considered in the design of augmentation systems.

Aerodynamic Hysteresis in Steady-State Rolling Moment

Several reports^{12,14} indicate the existence of aerodynamic hysteresis in the variation of the rolling moment coefficient with the angle of sideslip (or angle of roll) at higher angles of attack. Such hysteresis can be accounted for mathematically¹⁵ by introducing into the aerodynamic formulation for the rolling moment a function $h(t)$ that can have two possible values in a given range of the angle of roll (Fig. 11, center). As shown in Ref. 15, for a fixed amplitude of oscillation the effective damping in roll can be expected to vary *inversely* with reduced frequency if the aerodynamic hysteresis is present, rather than *quadratically* as is normally the case without hysteresis. It was further shown in Ref. 15 that some early damping-in-roll results from NASA Langley¹⁶ obtained for a twin-jet fighter aircraft at low subsonic speeds (Fig. 11, left) can be accurately correlated (with the exception of one point) by the expression for the effective damping in roll that takes into account the presence of hysteresis (Fig. 11, right). A formulation is suggested in Ref. 15 for the rolling moment in an arbitrary rolling maneuver (Fig. 11, bottom), which contains the double-valued function $h(t)$ and in which the effective damping-in-roll coefficient must be determined from roll oscillation around a fixed roll angle with the oscillation amplitude small enough to ensure that the deflection always remains on one branch of the hysteresis loop.

The aforementioned examples illustrate three possible scenarios for the occurrence of the wing rock, each on a different configuration. No doubt other such scenarios exist. When preparing the equations of motion for predicting the dynamic behavior of a new, unknown configuration, the mathematical model (at least initially) should be made sufficiently general to encompass all such scenarios.

Aerodynamic Cross-Coupling

The high- α flow phenomena discussed previously illustrate cases where 1) lateral aerodynamic reactions, such as those

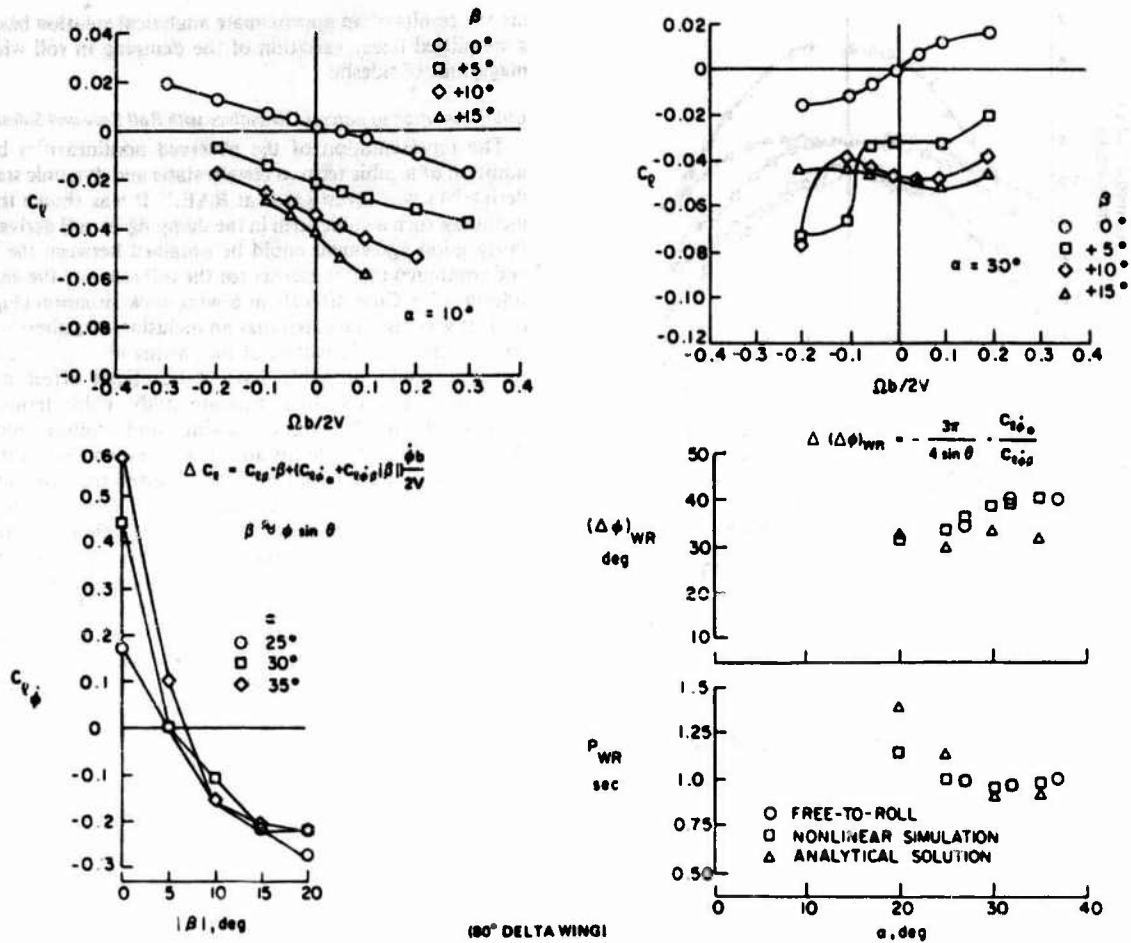


Fig. 9 Wing rock: variation of damping in roll with angle of sideslip (NASA LRC).

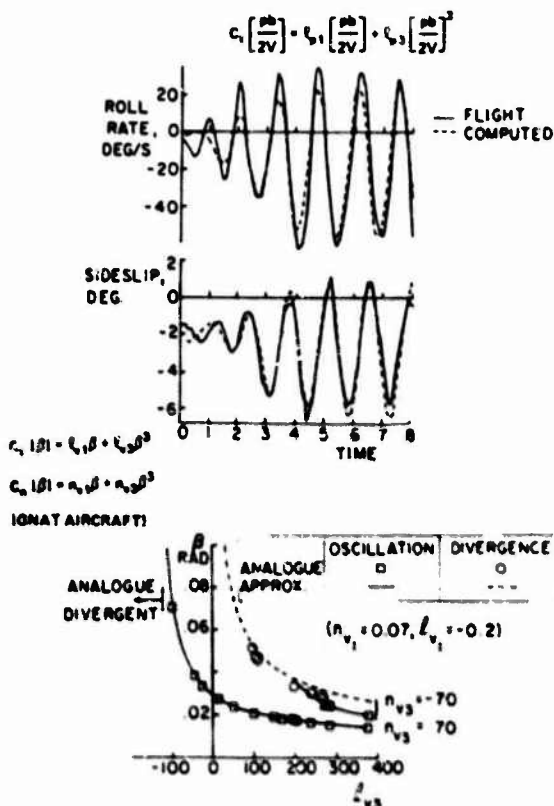


Fig. 10 Wing rock: cubic variation of lateral derivatives with roll rate and sideslip (P.A.E.).

caused by the lateral motion of the forebody vortices, may occur on an aircraft as the result of some longitudinal motion, such as pitching or vertical translation, and where 2) longitudinal aerodynamic reactions, such as those caused by the longitudinal motion of the vortex burst locations, may occur on an aircraft as a result of some lateral motion, such as rolling, yawing, or lateral translation. Because of this relation between the longitudinal and lateral degrees of freedom, the above aerodynamic reactions can be said to represent the aerodynamic cross-coupling between the longitudinal and the lateral degrees of freedom. As already mentioned, the cross-coupling reactions are, in general, shifted in time in relation to their causative motions and, therefore, will have components which are both in phase and in quadrature with these motions. When related to the causative displacements and their time rates of change, these components of the cross-coupling reactions become static and dynamic cross-coupling derivatives, respectively. (The term cross derivatives should, however, still be used to denote the traditional derivatives that relate two lateral degrees of freedom, such as roll and yaw.) It should be noted that the introduction of cross-coupling derivatives requires simultaneous consideration of all the equations of motion of an aircraft, rather than of separate groups of equations for the longitudinal and for the lateral motions, as often done in the past.

The concept of aerodynamic cross-coupling, especially in relation to the dynamic derivatives, was introduced only relatively recently.¹⁷ New experimental capabilities had to be developed to permit the measurement of the pertinent derivatives. Thus far, only relatively few measurements of this kind have been performed. Some examples of the dynamic cross-coupling derivatives obtained at NAE on a simple wing-body-fin configuration⁵ are given in Fig. 12.

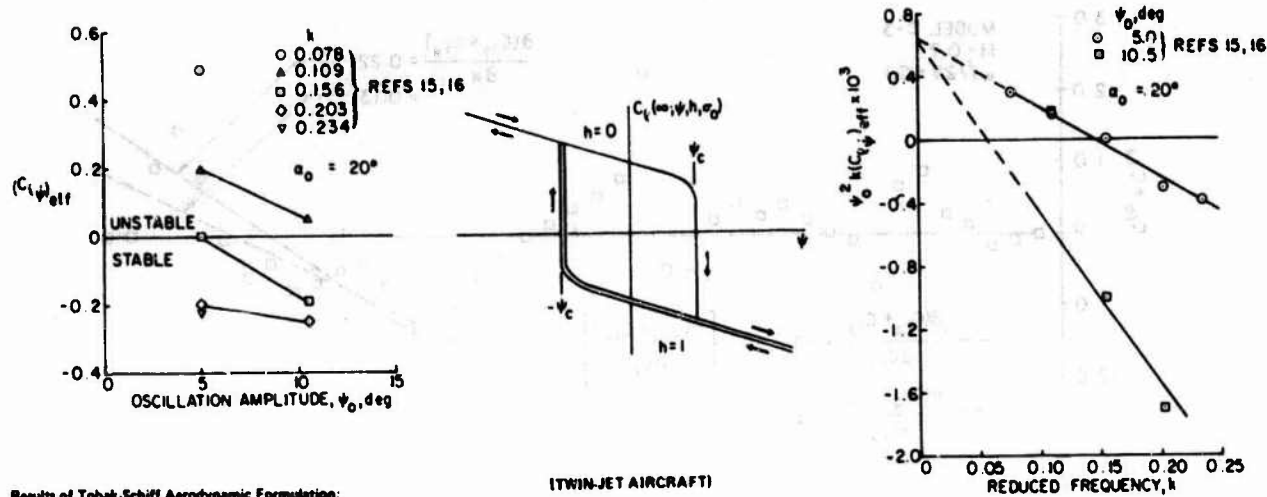


Fig. 11 Wing rock: aerodynamic hysteresis in steady-state rolling moment (NASA ARC; data measured at NASA I.R.C.).

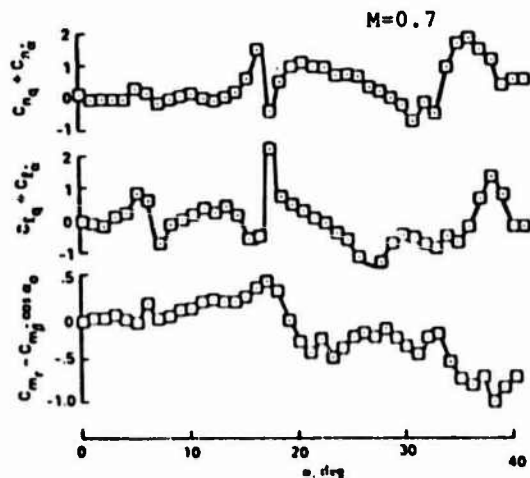


Fig. 12 Dynamic cross-coupling derivatives; wing-body-fin configuration; $\Delta\theta = \Delta\psi = \pm 1$ deg (NAE).

From top to bottom, the dynamic yawing and rolling moment derivatives due to oscillation in pitch are shown, followed by the dynamic pitching moment derivative due to oscillation in yaw. In all cases, the derivatives are relatively small for low angles of attack, but attain large values and display sudden variations at angles of attack between 15 and 20 deg, and become quite irregular at higher angles of attack especially in the region between 32 and 38 deg. Both the levels attained and the suddenness of variations is larger for the derivatives of the lateral moments due to oscillation in pitch than for the pitching moment derivative due to oscillation in yaw. It should be noted that these cross-coupling derivatives may be of the same order, and sometimes even larger, than the corresponding traditional damping derivatives (except for the damping-in-pitch derivatives at high angles of attack), such as previously shown in Fig. 2. The same conclusion can also be reached when comparing, instead of the derivatives, the corresponding terms in the pertinent equations of motion.⁶ Dynamic cross-coupling derivatives (at a Mach number of 0.6) were also measured at AEDC,¹⁸ and the maximum values obtained were approximately one half of the maximum values

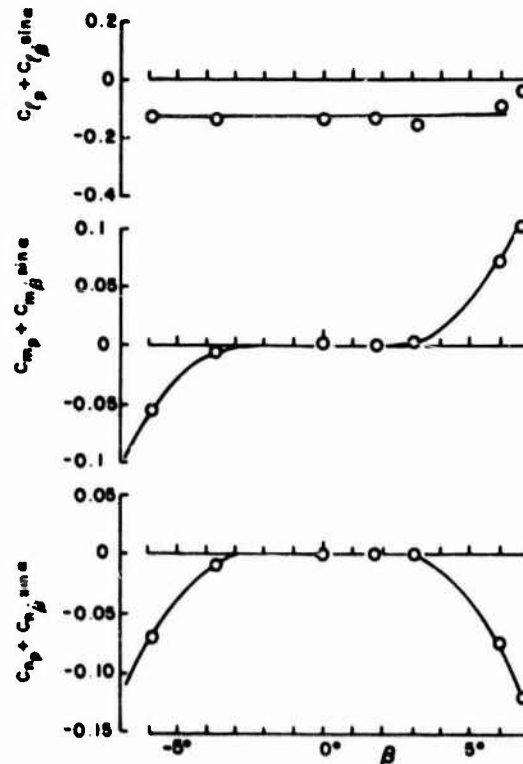


Fig. 13 Dynamic rolling moment derivatives vs angle of sideslip. $M=0.6$; $\alpha=17.5$ deg; $\Delta\theta = \pm 2$ deg (NAE).

obtained at AEDC, which, considering the fact that the AEDC experiments were performed on a different configuration and in the angle-of-attack range of only up to 25 deg (rather than up to 40 deg at NAE), constitutes a good collaboration of the initial NAE results.

As can be expected from basic aerodynamic considerations, the direct and the cross derivatives should be symmetrical with respect to zero angle of sideslip, whereas the cross-coupling derivatives should change sign with the direction of sideslip. This is demonstrated in Fig. 13, where the three dynamic

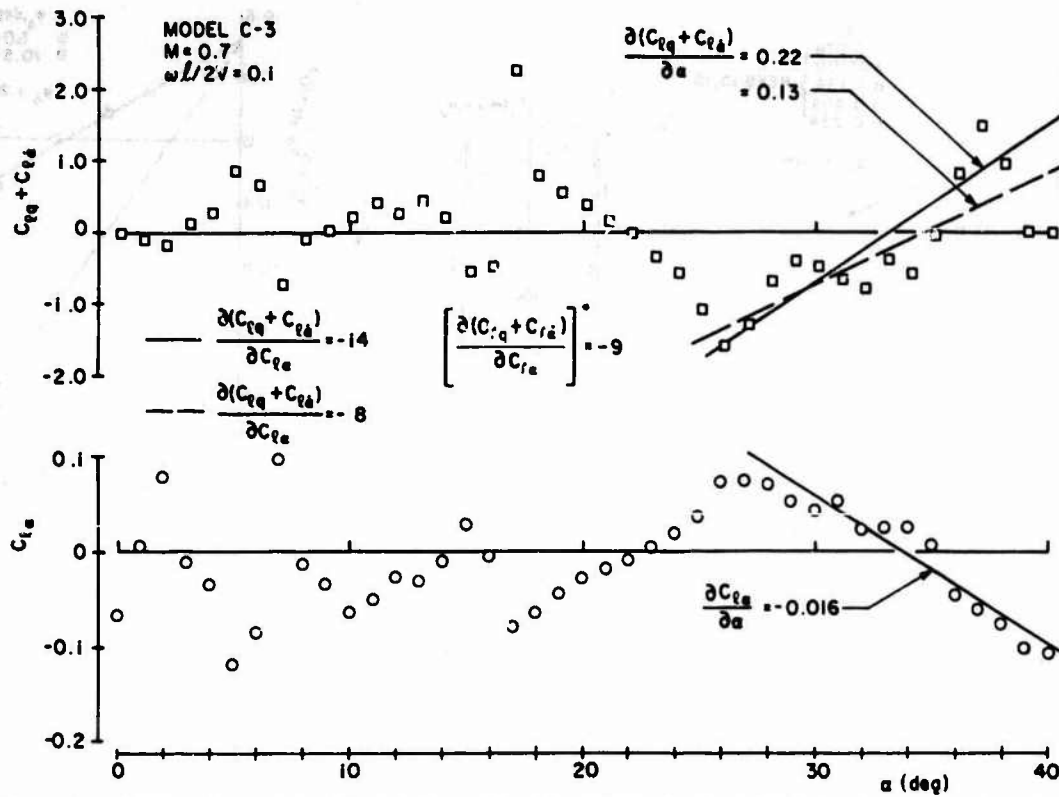


Fig. 14 Comparison of ratios of dynamic to static derivatives obtained in wind tunnel and calculated (*) using phase lag determined in water tunnel (NAE).

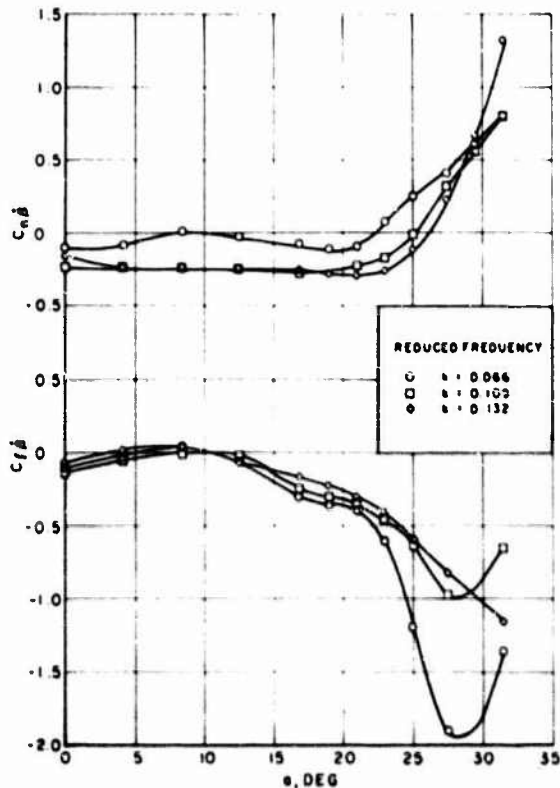


Fig. 15 β -derivatives for a schematic delta-wing-body-tail configuration, $M < 0.1$ (NASA LRC).

moment derivatives due to oscillation in roll are plotted as functions of the angle of sideslip.¹⁹ The antisymmetric variation of the cross-coupling derivative with the angle of sideslip is clearly visible. Another example of such a variation is given in Fig. 9 of Ref. 5.

For very simple configurations (such as the cone-wing-fin model used in the NAE movie), it may be possible to relate the dynamic derivatives to the corresponding static derivatives if the phase lag associated with the main flow-separation or vortex-shedding phenomenon is known. In Fig. 14 the ratio of dynamic-to-static rolling moment derivatives due to pitching obtained from such phase lag consideration (with the phase lag determined in the water tunnel, as shown in Fig. 1) is compared with the ratio of slopes of the two derivatives obtained on a similar (but not the same) configuration in a wind tunnel at a Mach number of 0.7. The ratios are of the same order of magnitude and the approximate mirrorlike symmetry of the dynamic and static curves is immediately apparent. The reader must be cautioned, however, that even if the phase lags could be easily measured or calculated (which, as a rule, they cannot), such a procedure would not necessarily be applicable to more realistic configurations, on which there would be a multitude of separated or vortical flow phenomena, each one with its own individual phase lag and each causing reactions acting on different parts of the configuration.

Time-Dependent Effects

In addition to quasisteady effects, such as represented by derivatives of various aerodynamic reactions due to angular velocities, we have to consider the existence of purely unsteady effects, such as those represented by derivatives due to the time rate of change of angular deflections, $\dot{\alpha}$ or $\dot{\beta}$. These derivatives have been known for many years, since they constitute part of the dynamic results obtained with standard wind-tunnel techniques of oscillation around a fixed axis.

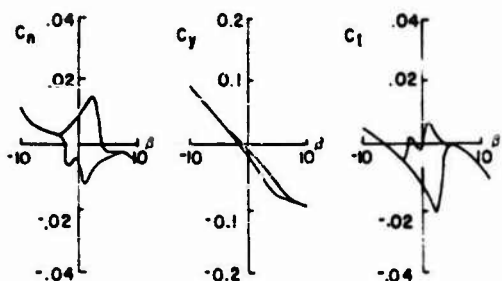
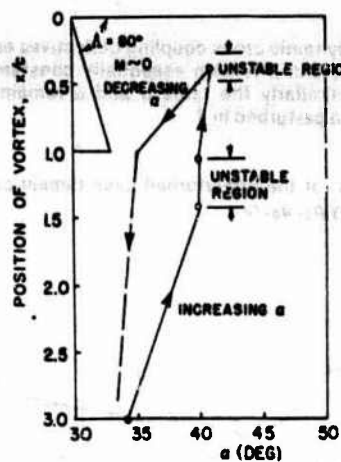


Fig. 16 Aerodynamic hysteresis a) with angle of attack, b) with sideslip.

which always give composite derivative expressions such as $(C_{mq} + C_{ma})$. Up to now, however, it was standard practice to ignore the $\dot{\alpha}$ and $\dot{\beta}$ effects (or to introduce a simple correction for them) and to use the composite derivatives in place of the purely rotary ones. At low angles of attack the error introduced by such a procedure was often small and the simplification large enough to be justifiable.

At higher angles of attack, however, the $\dot{\alpha}$ and $\dot{\beta}$ effects unfortunately become quite substantial and can no longer be ignored or corrected for in a simple fashion. This is illustrated in Fig. 15, based on Ref. 20, in which the yawing and rolling moment derivatives due to the time rate of change of the angle of sideslip are shown for a schematic delta-wing-body-tail configuration. These results were obtained from a translational oscillation experiment at very low speeds. The small values of the C_{nd} and C_{ld} derivatives at low angles of attack and their sudden increase at $\alpha \geq 22$ deg are clearly demonstrated.

Derivatives due to the time rate of change of angular deflections are aerodynamically equivalent (in the first approximation) to derivatives due to translational acceleration in the same plane of motion. This fact renders them of high interest for aircraft designs using direct-lift or direct side-force controls and also makes it possible to determine them experimentally using a translational oscillatory motion in the vertical or lateral direction. Because of this relation, $\dot{\alpha}$ and $\dot{\beta}$ derivatives are often referred to as translational acceleration derivatives.

Hysteresis Effects

As already discussed in connection with the wing-rock phenomenon, high angle-of-attack flow phenomena such as asymmetric vortex shedding, vortex breakdown (burst), or periodic separation and reattachment of the flow are frequently responsible for aerodynamic hysteresis effects. Such hysteresis is characterized by a double-valued behavior of the steady-state aerodynamic response to variations in one of the motion variables such as angle of attack, angle of

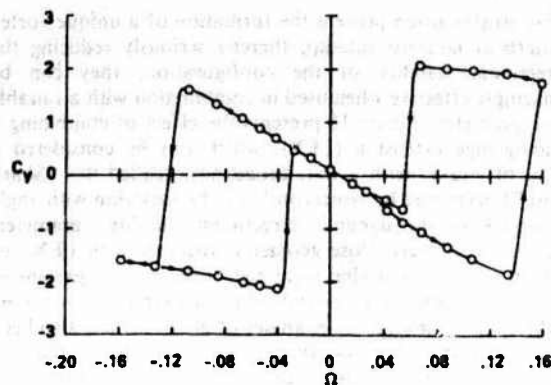


Fig. 17 Aerodynamic hysteresis with spin rate. Same experiment as in Fig. 6 but $\alpha = 90$ deg, $Re_d = 0.6 \cdot 10^6$ (NASA ARC).

sideslip, or spin rate. Figure 16 shows an α -hysteresis in the variation of location of the vortex burst on a delta wing,²¹ and an example of the already described β -hysteresis in the variation of lateral aerodynamic coefficients for an aircraft configuration.¹⁴ Figure 17 shows an example of an Ω -hysteresis in the side-force coefficient for the previously mentioned square forebody with rounded corners⁸ rotating at $\alpha = 90$ deg (flat spin). (This hysteresis effect was not observed at $\alpha = 75$ deg and below, and even at $\alpha = 90$ deg it occurred only in a relatively narrow range of Reynolds number.) Another illustration of hysteresis effects is the delayed lateral motion of the forebody vortices in response to pitching oscillation, as shown in the aforementioned NAE water tunnel movie film.

In the presence of hysteresis the dynamic derivatives measured in large-amplitude oscillation experiments may have two distinct components, namely, one associated with the small-amplitude oscillation (i.e., small enough to remain on one branch of a hysteresis loop), and a second one representing the effect of the hysteresis. This was shown in Ref. 15 for the case of the damping-in-roll derivative. The large-amplitude oscillatory results, such as the magnitude of peaks shown in Fig. 4 (see Ref. 7), often display an inverse variation with frequency, which is characteristic of the presence of hysteresis. In such cases it must be remembered that the effective value of the derivative will depend on whether the oscillation amplitude falls inside or outside of the range that encompasses the hysteresis loop.

Configuration Dependence

The intricate vortex pattern that exists around an aircraft configuration at high angles of attack is very sensitive to even small changes in aircraft geometry. So is the behavior of this vortex pattern on an oscillating configuration. The forebody vortices are greatly dependent on the planform and the cross-sectional geometry of the aircraft nose as well as on the presence of various forms of protuberances on the forebody (including nose boom) that may affect the stability of an existing vortex pattern, give rise to new vortices and create conditions for strong vortex interactions. The wing leading-edge vortices, in addition to being a strong function of the leading-edge sweep, are also known to be greatly affected by various leading-edge modifications, such as apex drooping, discontinuities or contouring, and by various modifications of the wing itself, such as addition of wing leeside fences and deflections of leading- or trailing-edge flaps. All of these variations of the geometry of the wing affect not only the position and the strength of the wing vortices but also the all-important location at which these vortices break down.

The most common modification of the aircraft geometry intended to eliminate or delay the onset of asymmetric effects is the use of forebody strakes. Although, when used alone,

these strakes often prevent the formation of a unique vortex pattern at nonzero sideslip, thereby seriously reducing the directional stability of the configuration, they can be amazingly effective when used in combination with a suitable nose geometry. Figure 18 presents the effect of combining a leading-edge extension (LEX), which can be considered a form of strake, with a flat, broad nose (called the "Shark Nose") developed by Northrop,¹⁴ on the variation with angle of attack of the dynamic directional stability parameter, C_{NDYN} . The Shark Nose geometry, together with LEX, attenuates the unfavorable local reduction in that parameter and at the same time extends this favorable influence on stability to somewhat lower angles of attack. It has also been demonstrated in Ref. 14, (but is not shown here), that the presence of Shark Nose greatly enhances the directional stability at small nonzero angles of sideslip ($|\beta| < 5$ deg).

The effect of strakes (or leading-edge extensions) on various dynamic stability derivatives is illustrated in Fig. 19. In all cases shown, the addition of strakes reduces the magnitude of derivatives, practically eliminates nonlinearities with angle of attack in the range investigated (except for pitch damping derivative), and makes the derivatives almost independent of reduced frequency.²² The dynamic yawing derivatives due to rolling become essentially zero. The

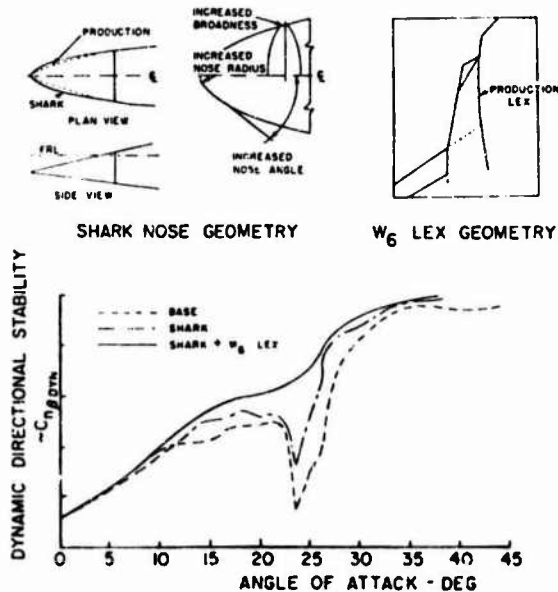


Fig. 18 Effect of forebody geometry and leading-edge extensions (Northrop).

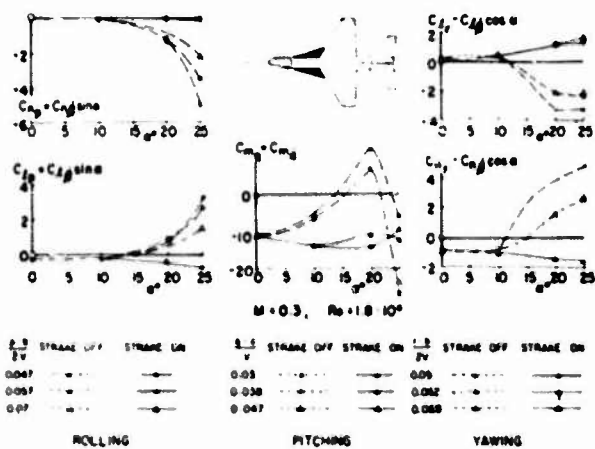


Fig. 19 Effect of strakes (MBB/ONERA).

Note 1: With all aerodynamic cross coupling derivatives equal to zero, the rates p , r , and $\dot{\beta}$ remain essentially constant when perturbed in α ; similarly the rate q and $\dot{\alpha}$ remain essentially constant when perturbed in β .

Note 2: Angular rates for the unperturbed case remain constant and are denoted by p_0 , q_0 , r_0 .

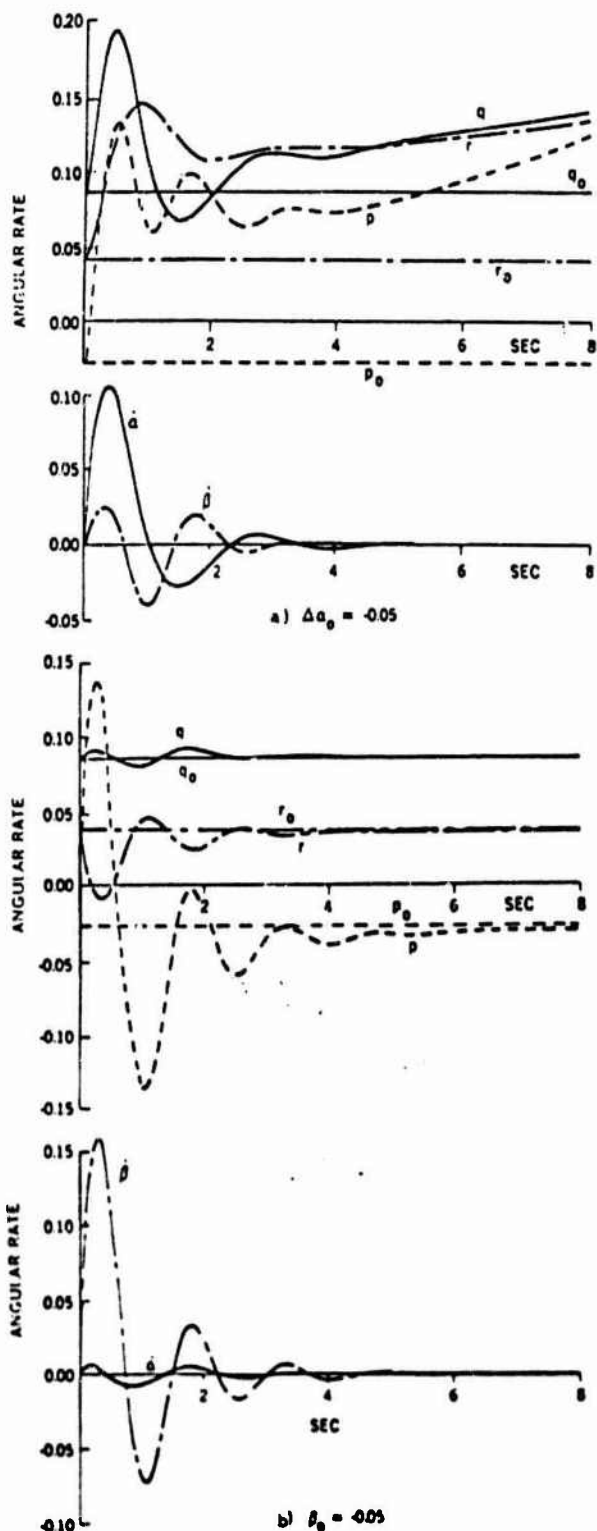


Fig. 20 Effect of cross-coupling derivatives due to pitching and yawing on the angular rates for 2g turning flight (NAE).

negative damping in roll (for $\alpha > 13$ deg), in pitch (for $12 < \alpha < 23$ deg), and in yaw (for $\alpha > 11$ deg) completely disappears. It should be noted, however, that the range of angle of attack investigated extends only to $\alpha = 25$ deg, without reaching the range where the most significant nonlinearities may be expected.

As is well known, however, strakes do have certain disadvantages. Their successful development for a particular application may require much trial and error. They often adversely affect the directional stability. If mounted near the tip of the nose radome, they may disturb the radar operations. The strake vortices may adversely interact with aircraft components farther downstream, such as air intakes or control surfaces. Therefore, alternative approaches, such as the use of forebody blowing, forebody deflection, or a mechanical disturbance on the forebody, continue to be of high interest.

Although most of the important flow phenomena occur on the leeward side of an aircraft, configuration changes on the windward side may also have a noticeable effect on the stability characteristics of the aircraft. For instance, an unsymmetrical store release can be expected to create aerodynamic cross-coupling effects, without even the necessity of flying at high angles of attack. The possible importance of such asymmetries is not very well known at the present time.

Sensitivity of High- α Aircraft Motion to Dynamic Stability Parameters

The need to introduce the dynamic cross-coupling and acceleration derivatives into the mathematical model, applicable to flight at high angles of attack, increases, in principle, the number of dynamic derivatives that may have to be included by a factor of two. This total number, however, can be significantly reduced if a judicious selection and assessment of the importance of some of these derivatives can be made. This is usually done by carrying out, on a computer, so-called "sensitivity studies," during which the sensitivity of the predicted aircraft behavior to the inclusion in the

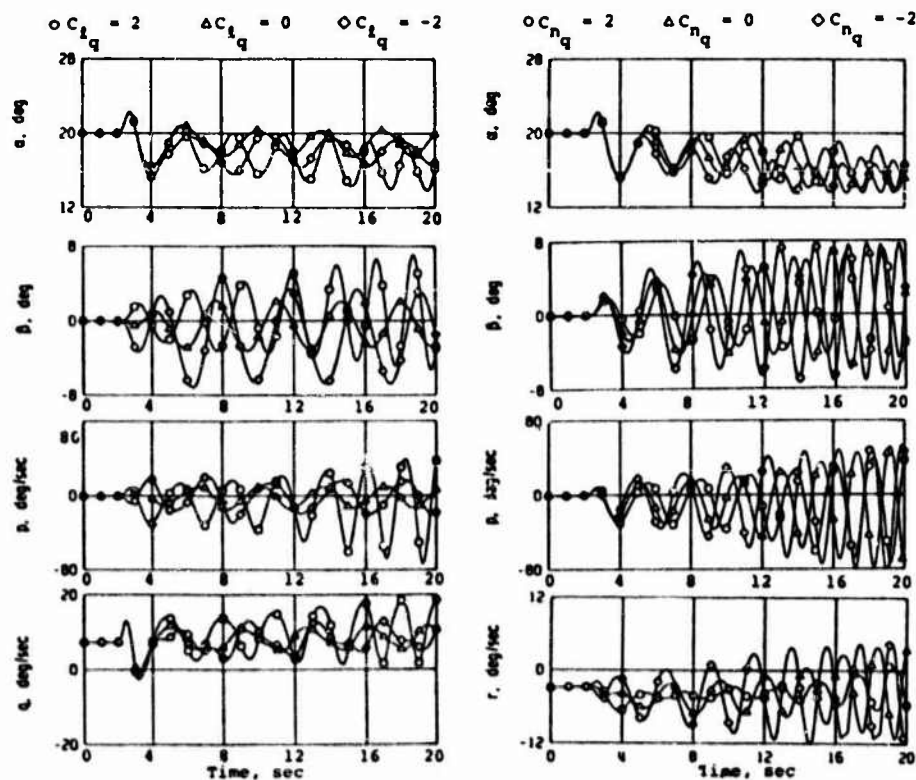
equations of motion of the cross-coupling and acceleration derivatives and of the taking into account the various nonlinear effects is examined. Some studies of this type have been performed in recent years and these were reviewed in Ref. 23, from which some examples will be included here.

Sensitivity studies are usually carried out by 1) programming, on a computer, a complete set of equations of motion pertinent to a particular configuration and particular flight condition, 2) inserting a set of stability parameters, including, if required, some nonlinear effects, 3) varying those parameters in a predetermined manner, and 4) observing the responses of the variables of motion to some form of disturbance applied to the set of equations. The stability parameters are usually varied individually, but may also be studied in combinations. The difference between responses obtained for two different values of a parameter or for two different combinations determines the sensitivity of the aircraft behavior to the variation of that particular stability parameter or that particular combination of parameters.

As already discussed, both the cross-coupling and the acceleration derivatives, and, in fact, most of the other derivatives as well, display significant nonlinear effects at higher angles of attack. Since an analytical description of the variation of a derivative with angle of attack may be rather complex, it is often more practical to limit the range of angle of attack, for which the analytical description is made, to the immediate vicinity of the equilibrium angle of attack and to assume that the derivative varies linearly with α in that narrow range of angle of attack. Such a locally linearized derivative can then be written as $a + b(\alpha - \alpha_T)$, when α_T is the trim (or equilibrium) angle of attack.

Dynamic derivatives that are subject to sensitivity study are often varied in a relatively wide range, such as from zero to perhaps twice the nominal value including, in some cases, also a change of sign. It is important that during such a variation the remaining derivatives be kept at their nominal values rather than zero, otherwise gross misrepresentation and, in some cases, even an erroneous elimination of the effect of a given derivative may result. Sometimes there may be some

Fig. 21 Effect of C_{lq} and C_{nq} derivatives, fighter/bomber in 3g turning flight, β derivatives zero, elevator doublet (AEDC).



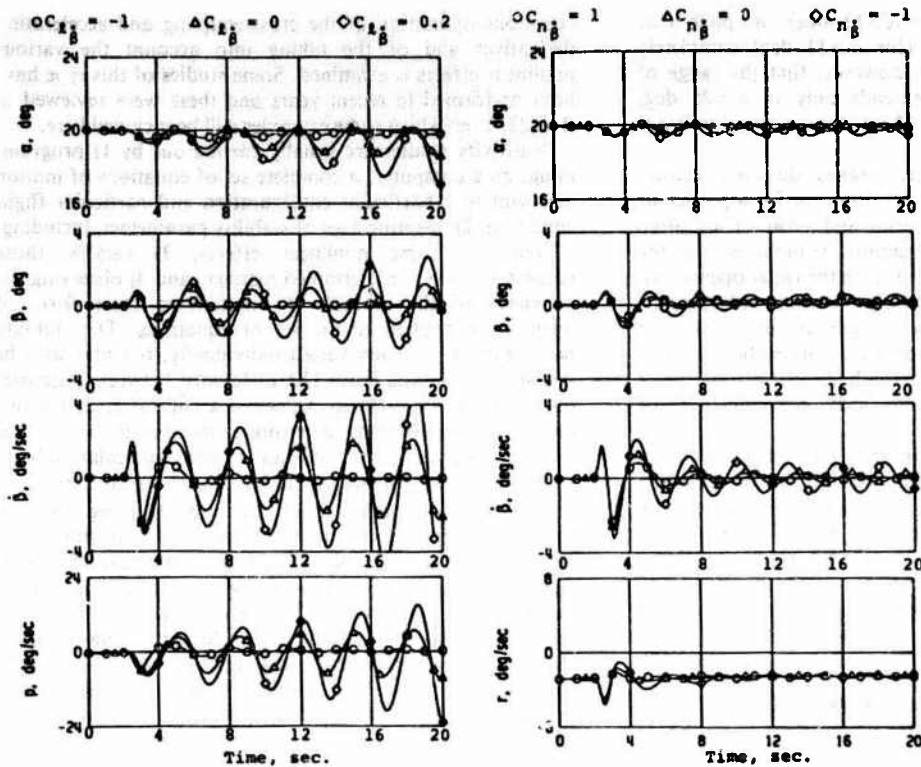


Fig. 22 Effect of $C_{l\dot{\beta}}$ and $C_{n\dot{\beta}}$ derivatives, fighter/bomber in 3g turning flight, rudder doublet (AEDC).

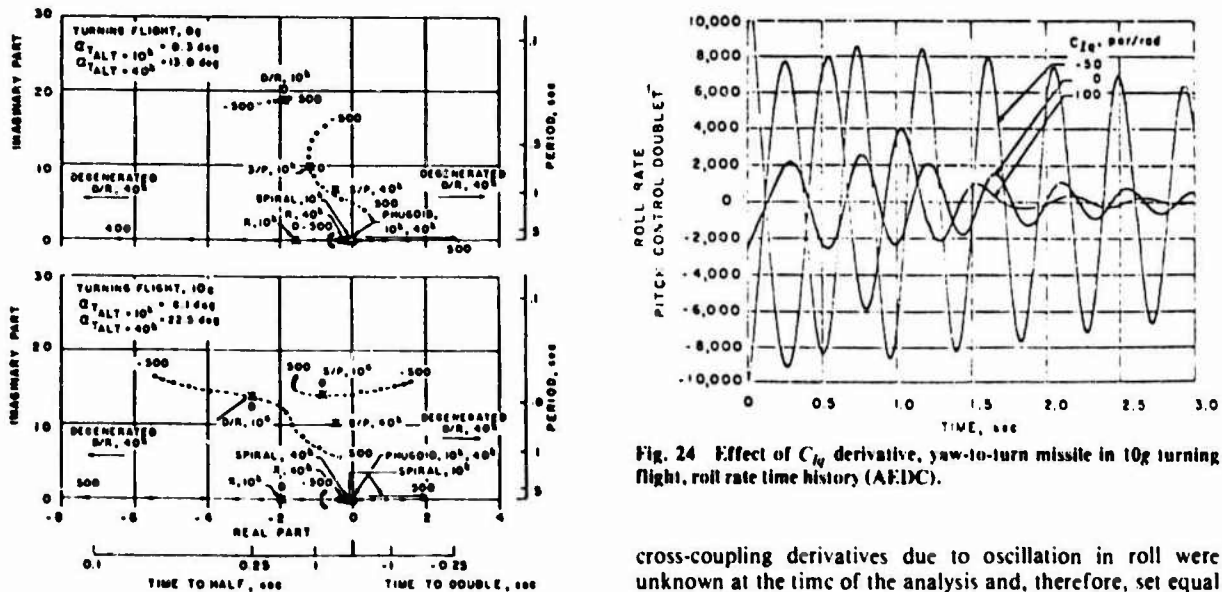


Fig. 23 Effect of C_{lq} derivative, yaw-to-turn missile in 10g turning flight, root locus (AEDC).

Fig. 24 Effect of C_{lq} derivative, yaw-to-turn missile in 10g turning flight, roll rate time history (AEDC).

interest in investigating the effect of a whole group of derivatives such as cross-coupling derivatives, by including or excluding the entire group all at once. In cases involving composite derivatives it is often of interest to divide the total value between the two component parts in different proportions and to insert the resulting two derivatives at their proper place in the equations of motion, as purely rotary and purely time-rate-of-change or acceleration effects.

The significance of cross-coupling moment derivatives was studied in Ref. 24 and is illustrated in Fig. 20. The measured values of composite derivatives were equally distributed between their rotary and acceleration parts. The nonlinear effects were taken into account by local linearization. The

cross-coupling derivatives due to oscillation in roll were unknown at the time of the analysis and, therefore, set equal to zero. The various angular rates ($p, q, r, \dot{\alpha}$, and $\dot{\beta}$) are shown as functions of time after an initial disturbance in the angle of attack (Fig. 20a) and the angle of sideslip (Fig. 20b). The constant angular rates for the unperturbed case (p_0, q_0, r_0) are also shown. Had the cross-coupling derivatives not been included, the rates p, r , and $\dot{\beta}$ in Fig. 20a and the rates q and $\dot{\alpha}$ in Fig. 20b should have remained essentially constant. It can be seen that the departures of p, r , and $\dot{\beta}$ in Fig. 20a from their constant values is much larger than the corresponding departures of q and $\dot{\alpha}$ in Fig. 20b, indicating a much larger effect of the cross-coupling derivatives of the rolling and yawing moments due to pitching than of the cross-coupling derivative of the pitching moment due to yawing. Figure 20 pertains to a 2g turning flight at $\alpha = 33$ deg.

Studies of the sensitivity of the aircraft behavior to variation of an individual cross-coupling or acceleration derivative were carried out both in Refs. 24 and 25. Although

the two studies were performed using two significantly different approaches, the results were quite similar. Some examples of the results obtained in Ref. 25 for a fighter/bomber configuration in a 3g turning flight are shown in Figs. 21 and 22. In the study, the variations in each successive derivative were performed with all the other derivatives fixed at their nominal values. The cross-coupling derivatives were again based on the results of Ref. 5, but were treated as purely rotary derivatives in the equations of motion. The acceleration derivatives were based on data in Ref. 26. The nominal values used represented extreme values that had actually been measured in the wind tunnel experiments. The initial disturbance was introduced as an elevator or a rudder doublet.

Large effects of variations of both C_{lq} and C_{nq} can be seen in β , p , and r motions (Fig. 21). These motions display almost a mirror image for the positive and negative values of the pertinent derivatives. The inclusion of C_{lq} derivatives causes instability in the β and p motions. However, it should be noted that this effect is strongly dependent on the values of the remaining dynamic rolling moment derivatives, such as C_{lp} and C_{lr} , which, in this particular example, were very small or zero, respectively.

The motion sensitivity to variations of $C_{l\dot{\beta}}$ derivative (Fig. 22) is quite significant. In particular, it should be noted that for $C_{l\dot{\beta}}$ values of 0.2 and greater, the α , β , $\dot{\beta}$, and p motions show strong oscillatory divergence. Conversely, the negative value of -1 of $C_{l\dot{\beta}}$ derivative has a strong damping effect on all of these motions. By comparison, the motion sensitivity to variations in $C_{n\dot{\beta}}$ is less significant.

Additional results, not shown here, indicate that most of the above-mentioned effects are quite dependent on the remaining stability characteristics of the aircraft. The smaller the static margin and the lower the aerodynamic damping, such as represented by C_{lp} , C_{lr} , C_{nr} , or C_{nr} derivatives, the more sensitive the aircraft motion to the variations in cross-coupling derivatives and vice versa. The sensitivity of the flight behavior during a turning maneuver is, in general, larger than in a straight flight.

Although this paper is mainly concerned with stability and motion of aircraft, a brief mention has to be included about the corresponding studies related to the motion of missiles. A comprehensive investigation of missile motion sensitivity to dynamic stability derivatives has recently been completed.²⁷ In that investigation the importance of dynamic stability derivatives for the simulation of motion of both bank-to-turn and yaw-to-turn missile configurations was examined, using a six-degree-of-freedom linearized stability program.

Among the most pronounced effects due to the variation of a dynamic cross-coupling derivative was that due to the variation of C_{lq} at high Mach number, high load factor, and relatively low altitude. Sample results showing the influence of that derivative on the simulated motion of the yaw-to-turn missile are shown in Figs. 23 and 24. It can be seen that the short period (S/P), dutch roll (D/R), and roll (R) modes are quite sensitive to the variation of C_{lq} over the range ± 500 (per radian) and that the dutch roll sensitivity increases with an increasing load factor (Fig. 23). Even a variation of C_{lq} within a much more narrow range (0 to -50) results in a large effect on the roll rate time history (four times higher roll rates at $C_{lq} = -50$ than at $C_{lq} = 0$), as shown in Fig. 24.

On the basis of sensitivity studies, such as those described above, and on the basis of some additional studies included in Ref. 23, it has been shown that the inclusion in the equations of motion of the cross-coupling derivative C_{lq} (and to a lesser extent C_{nq}) and of the acceleration derivatives $C_{l\dot{\beta}}$, $C_{m\dot{\beta}}$, and possibly $C_{n\dot{\beta}}$ may be important for the correct prediction of the behavior of aircraft and missiles at high angles of attack (Table 2). It was shown in these studies that the aforementioned derivatives in some cases could have an effect on the predicted motion that was as large as that of some of the well-known damping and cross derivatives. It was also shown that

it is important to be able to separate the purely rotary and the acceleration derivatives and use them in their proper places in the equations. Furthermore, it was found that the cross-coupling derivative C_{mp} is relatively important for missiles but less so for aircraft, and that the cross-coupling derivative C_{nr} appears to be insignificant in both of these cases.

Since the above studies were limited in scope with regard to both geometry of configurations and type of maneuvers, some of the derivatives found insignificant in these studies may become important in other situations. For a new aircraft or missile that has to perform a variety of maneuvers, the recommended set should encompass all the derivatives found important, even if only once, in previously examined situations. In addition, for a satisfactory prediction of aircraft behavior in a spin, the aerodynamic coefficients and possibly also the static and dynamic derivatives may be required as functions of spin rate.

Mathematical Modeling

The mathematical modeling used in most countries at the present time to describe the aircraft flight history applies strictly to flight at small to moderate angles of attack, where nonlinearities are small, time-dependent effects insignificant and aerodynamic cross-coupling nonexistent. In view of the complexity of the aerodynamic phenomena reviewed here and their effects on the forces and moments that govern the behavior of flight vehicles at high angles of attack, a much more sophisticated modeling is obviously required.

Substantial progress has recently been made in this area. A generalized formulation which includes the nonlinear pitch-yaw-roll coupling and nonlinear coning rate is now available.²⁸ Time-history and hysteresis effects have recently also been included in that formulation.^{15,29,30} Among things still to be done is an adequate modeling of the suddenness with which the aerodynamic reactions may vary with the angle of attack or sideslip. As already mentioned, in the presence of such sudden and large nonlinearities, the derivative concept and the principle of linear superposition may no longer be adequate and a better mathematical formulation may be needed. One theory that offers considerable promise for adequate representation of sudden variations, hysteresis effects, and limit-cycle motions is the bifurcation theory, such as discussed in Ref. 31. It appears that this theory can also represent spinning as a genuine property of the appropriate set of differential equations.

Any advanced mathematical model must, of course, be suitably verified. The verification should be conducted by determining a complete set of stability parameters for a particular configuration, by predicting a series of maneuvers, and by comparing them with the actual flight histories. One of the principal difficulties in conducting such a verification at the present time is the lack of complete static and dynamic aerodynamic data for the required test cases.

Table 2 Relative significance of dynamic moment derivatives at high α (preliminary assessment)

Type of derivative(s)	Derivative(s)	Significant	
		Aircraft	Missiles
Direct	C_{mq} , C_{nr} , C_{lp}	Yes	Yes
Cross	C_{np} , C_{lr}	Yes	Yes
Cross-coupling	C_{lq} , C_{nq}	Yes	Yes
Cross-coupling	C_{mp}	No	Yes
Cross-coupling	C_{nr}	No	No
Acceleration	$C_{m\dot{\beta}}$, $C_{l\dot{\beta}}$, $C_{n\dot{\beta}}$	Yes	?
Acceleration	$C_{n\dot{\beta}}$, $C_{m\dot{\beta}}$, $C_{l\dot{\beta}}$?	?

Splitting of composite derivatives into component parts and using the different parts in their proper place in the equations of motion is in many cases important.

Aerodynamic coefficients and derivatives as functions of coning rate may be required for spin prediction.

Table 3 Dynamic stability testing capabilities at National Aeronautical Establishment

Apparatus	Primary motion	Static derivatives	Dynamic derivatives
Pitch/yaw	Pitching oscillation	$C_{l\alpha}, C_{m\alpha}, C_{n\alpha}$	$C_{lq} + C_{l\dot{\alpha}}$ $C_{mq} + C_{m\dot{\alpha}}$ $C_{nq} + C_{n\dot{\alpha}}$
Pitch/yaw	Yawing oscillation	$C_{l\beta}, C_{m\beta}, C_{n\beta}$	$C_{lr} - C_{l\beta} \cos \alpha$ $C_{mr} - C_{m\beta} \cos \alpha$ $C_{nr} - C_{n\beta} \cos \alpha$
Roll	Rolling oscillation	$C_{l\beta} \sin \alpha$ $C_{m\beta} \sin \alpha$ $C_{n\beta} \sin \alpha$ $C_{Y\beta} \sin \alpha$ $C_{N\beta} \sin \alpha$	$C_{lp} + C_{l\beta} \sin \alpha$ $C_{mp} + C_{m\beta} \sin \alpha$ $C_{np} + C_{n\beta} \sin \alpha$ $C_{Yp} + C_{Y\beta} \sin \alpha$ $C_{Np} + C_{N\beta} \sin \alpha$
α/β	Plunging oscillation	$C_{l\alpha}, C_{m\alpha}, C_{n\alpha}$	$C_{l\dot{\alpha}}, C_{m\dot{\alpha}}, C_{n\dot{\alpha}}$
α/β	Lateral oscillation	$C_{l\beta}, C_{m\beta}, C_{n\beta}$	$C_{l\dot{\beta}}, C_{m\dot{\beta}}, C_{n\dot{\beta}}$
Pitch (half-model)	Pitching oscillation	$C_{m\alpha}$	$C_{mq} + C_{m\dot{\alpha}}$
Plunge (half-model)	Plunging oscillation	$C_{m\alpha}$	$C_{m\dot{\alpha}}$

New Dynamic Stability Test Techniques

The determination of a complete set of static and dynamic stability data for a test case of a high-angle-of-attack flight requires the availability of test techniques with the following, greatly expanded capabilities:

- 1) To test at high angles of attack, and to carry the associated high loads
- 2) To test at small to moderate angles of sideslip
- 3) To measure dynamic cross-coupling derivatives
- 4) To measure effects due to $\dot{\alpha}$ and $\dot{\beta}$
- 5) To measure effects due to coning and continuous rolling
- 6) To test at large amplitude of oscillation, particularly in the case of oscillation in roll.

A fairly complete review of existing testing techniques for determination of dynamic stability parameters in a wind tunnel was given by the present author in Ref. 32. This review included the significant developments that have taken place in the last few years at several research establishments in various countries of the world, and notably those at NASA Ames, NASA Langley, AEDC, RAE Bedford, BAC Warton, DFVLR, ONERA, and NAE. Since the development of experimental techniques plays such an important role in our progress toward obtaining better prediction capabilities of the aircraft behavior in high-angle-of-attack flight, this topic clearly deserves to be mentioned in the present paper. As an example, a brief account will be rendered of the techniques presently available at the NAE in Ottawa, which may be considered as fairly representative of the new experimental trends in this field.

In Table 3 a list is given of the presently available three full-model and two half-model apparatuses that can be used to study the primary oscillations in five degrees of freedom, providing means to determine all the moment derivatives and some of the force derivatives associated with these motions. Both static and dynamic derivatives are included and the list encompasses the direct, cross, and cross-coupling derivatives, as discussed previously. It should be noted that in all cases the derivatives are obtained from a direct measurement, which is based only on an assumed relation between the aerodynamic reaction measured and the causative primary motion. Often this relation is linear, but can be replaced by a nonlinear or higher-order formulation if the need arises. Since the motion

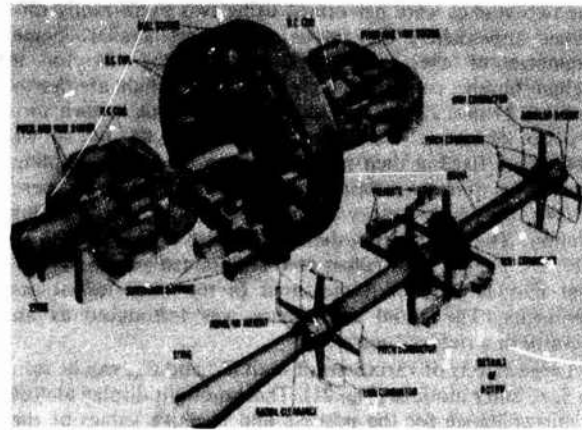


Fig. 25 3-DOF dynamic calibrator (NAE).

is essentially in one degree of freedom, the measurement is independent of the remaining parts of the equations of motion and, therefore, the results may be expected to be valid for any formulation of these equations as long as the principle of superposition is still applicable.

In most of the full-model apparatuses the model is mounted on a balance that in turn is attached to an elastic support system capable of deflecting in the appropriate degree of freedom. The primary motion is imparted by an electromagnetic drive system which oscillates the model with a constant amplitude at the resonance frequency in the primary degree of freedom. Each balance has a multicomponent capability (but always without axial force) and is made in one piece, a most desirable feature for dynamic testing. Each drive mechanism utilizes a high-current coil (or coils) moving in a strong magnetic field that is generated by compact rare-earth permanent magnets. As a result, the apparatuses are relatively slender and permit testing of realistic models of current aircraft configurations. Other apparatuses, employing a mechanical drive system, are used for experiments performed in the presence of large aerodynamic restoring moments. More details about the NAE apparatuses and test techniques can be found in Refs. 32 and 33.

The high complexity of the aforementioned techniques and the lack of any previous data on some of the recently identified dynamic derivatives made it necessary to develop a system that would independently verify the validity of the experimental technique and data reduction methods employed. The same system was also conceived as a diagnostic tool to identify, on a regular basis, equipment faults or software errors. A pictorial view of such a system developed at NAE and called a dynamic calibrator is shown in Fig. 25. The aircraft model is replaced on the dynamic stability apparatus by a special calibrating frame (or "rotor"), which is then oscillated in the primary degree of freedom by the drive mechanism of the apparatus. The inertia characteristics of the rotor duplicate, at least approximately, the inertia characteristics of the model, resulting in a similar dynamic response of the rotor and of the model in all three degrees of freedom. The three oscillatory aerodynamic moments, that act on the oscillating model during a wind tunnel test, are simulated by accurately known, electromagnetically induced, alternating loads, whose phase and amplitude can be adjusted at will. A comparison between the known applied loads and the outputs of the dynamic stability apparatus, obtained by processing the balance data and other relevant information by means of the same procedure as in the wind tunnel experiments, provides an overall calibration of the technique and of all the mechanical and electronic systems involved. Other dynamic calibrators, simpler but based on similar principles, have been developed for the half-model dynamic apparatuses.

When conducting dynamic experiments in a wind tunnel, careful attention must be given at all times to minimizing and/or correcting for the inevitable static and dynamic sting interference effects. These problems were extensively discussed in Refs. 34 and 35. Also of great concern is the possible seriousness of Reynolds number effects. At high angles of attack the aerodynamic characteristics are often dominated by separated flow effects and it is known³⁶ that the boundary-layer transition process may also depend on the vehicle motion. Hence the possibilities for simulating flight Reynolds numbers by means of boundary-layer tripping devices in subscale dynamic experiments (as often proven successful in static experiments) are more limited. No universally accepted simulation methods seem to exist at the present time. Very few, if any, reliable comparisons of dynamic derivatives obtained at high angles of attack in flight and in wind tunnel are available, and those that do exist may easily be affected not only by the difference in the Reynolds numbers, but also by support interference problems in wind tunnel testing on the one hand and the need for a preconceived mathematical model and a practical (not too large) number of the unknown parameters (to be solved for) in flight testing on the other. It is, therefore, rather difficult to draw any definite conclusions as to the seriousness of the problem. There are some indications, however, that in many cases the dynamic behavior of the aircraft, as observed in flight tests, drop model tests and spin tunnel experiments, shows a fair overall agreement, despite the large differences in test Reynolds numbers.^{14,37} Any such observations are likely to be strongly dependent on the configuration being tested.

Concluding Remarks

In this paper a review was presented of some of the aerodynamic phenomena associated with the dynamic behavior of an aircraft flying at high angles of attack and of the various effects that these phenomena have on the dynamic stability parameters of aircraft or missiles at those flight conditions. Although only very limited quantitative information on these effects is available at the present time, an attempt was made to offer a tentative assessment of the relative significance of the various effects and parameters. The deficiencies of the commonly used mathematical models of the aerodynamics of high-angle-of-attack maneuvers were pointed out and the need was postulated for the development and verification of more sophisticated models that would probably have to include significant nonlinearities, hysteresis, some aerodynamic cross-coupling, and some time-dependent effects. Finally, developments in the wind tunnel techniques needed to provide the aerodynamic inputs required for such more advanced mathematical modeling were discussed and illustrated by examples of some of the novel techniques that have been developed at the author's laboratory.

References

- ¹ "High Angle of Attack Aerodynamics," AGARD FDP Symposium, Sandefjord, Norway, Oct. 1978, AGARD-CP-247, 1979.
- ² Tobak, M. and Peake, D.J., "Topology of Three-Dimensional Separated Flows," *Annual Review of Fluid Mechanics*, Vol. 14, 1982, pp. 61-85.
- ³ Skow, A.M., Moore, W.A., and Lorincz, D.J., "Control of Forebody Vortex Orientation to Enhance Departure Recovery of Fighter Aircraft," *Journal of Aircraft*, Vol. 19, Oct. 1982, pp. 812-819.
- ⁴ Peake, D.J. and Owen, F.K., "Control of Forebody Three-Dimensional Flow Separations," Paper 15, AGARD-CP-262, 1979.
- ⁵ Orlik-Rückemann, K.J., "Aerodynamic Coupling Between Lateral and Longitudinal Degrees of Freedom," *AIAA Journal*, Vol. 15, Dec. 1977, pp. 1792-1799.
- ⁶ Chambers, J.R., Gilbert, W.P., and Nguyen, L.T., "Results of Piloted Simulator Studies of Fighter Aircraft at High Angles of Attack," Paper 33, AGARD-CP-235, 1978.
- ⁷ Grafton, S.B. and Anglin, E.L., "Dynamic Stability Derivatives at Angles of Attack from -5° to 90° for a Variable-Sweep Fighter Configuration with Twin Vertical Tails," NASA TN D-6909, 1972.
- ⁸ Malcolm, G.N., "New Rotation-Balance Apparatuses for Measuring Airplane Spin Aerodynamics in the Wind Tunnel," *Journal of Aircraft*, Vol. 16, April 1979, pp. 264-268.
- ⁹ Birhle, W. Jr. and Bowman, J.S. Jr., "Influence of Wing, Fuselage and Tail Design on Rotational Flow Aerodynamics Beyond Maximum Lift," *Journal of Aircraft*, Vol. 18, Nov. 1981, pp. 920-925.
- ¹⁰ Nguyen, L.T., Yip, L., and Chambers, J.R., "Self-Induced Wing Rock of Slender Delta Wings," AIAA Paper 81-1883, Aug. 1981.
- ¹¹ Ross, A.J., "Lateral Stability at High Angles of Attack, Particularly Wing Rock," Paper 10, AGARD-CP-260, 1978.
- ¹² Ottensmeyer, J., "High Angle of Attack Aerodynamic Data for a 0.10 Scale A-7 Model Evaluated in the 7 by 10-Foot Transonic Wind Tunnel for Investigating the Stall Departure Phenomena, Phase 1," NSRDC TM-16-76-16, Oct. 1975.
- ¹³ Herman, J.G. and Washington, E.S., "Wind Tunnel Investigation of the Aerodynamic Hysteresis Phenomenon on the F-4 Aircraft and its Effects on Aircraft Motion," AEDC-80-10, Sept. 1980.
- ¹⁴ Skow, A.M. and Titiriga, A. Jr., "A Survey of Analytical and Experimental Techniques to Predict Aircraft Dynamic Characteristics at High Angles of Attack," Paper 19, AGARD-CP-235, 1978.
- ¹⁵ Schiff, L.B. and Tobak, M., "Some Applications of Aerodynamic Formulations to Problems in Aircraft Dynamics," Lecture 16, AGARD-LS-114, 1981.
- ¹⁶ Grafton, S.B. and Libbey, C.E., "Dynamic Stability Derivatives of a Twin-Jet Fighter Model at Angles of Attack from -10° to 110° ," NASA TN D-6091, Jan. 1971.
- ¹⁷ Orlik-Rückemann, K.J., "Dynamic Stability Testing of Aircraft—Needs Versus Capabilities," *Proceedings of International Congress on Instrumentation in Aerospace Simulation Facilities*, 1973, pp. 8-23.
- ¹⁸ Coulter, S.M. and Marquart, E.J., "Cross and Cross-Coupling Derivative Measurements on the Standard Dynamics Model at AEDC," AIAA Paper 82-0596, 1982.
- ¹⁹ Hanff, E.S., Orlik-Rückemann, K.J., Kapoor, K.B., Moulton, B.E., and LaBerge, J.G., "New Oscillatory Roll Apparatus and Results on Direct, Cross and Cross-Coupling Subsonic Moment Derivatives for an Aircraft-Like Model," NRC, NAE LTR-UA-50, 1979.
- ²⁰ Lichtenstein, J.H. and Williams, J.L., "Effect of Frequency of Sideslipping Motion on the Lateral Stability Derivatives of a Typical Delta-Wing Airplane," NACA RM L57F07, 1957.
- ²¹ Lawson, M.V., "Some Experiments with Vortex Breakdown," *Journal of the Royal Aeronautical Society*, Vol. 68, May 1964, pp. 343-346.
- ²² Staudacher, W., Laschka, B., Schütze, B., Poisson-Quinton, P., and Canu, M., "Some Factors Affecting the Dynamic Stability Derivatives of a Fighter-Type Model," Paper 11, AGARD-CP-235, 1978.
- ²³ Orlik-Rückemann, K.J., "Sensitivity of Aircraft Motion to Cross-Coupling and Acceleration Derivatives," Lecture 15, AGARD-LS-114, 1981.
- ²⁴ Curry, W.H. and Orlik-Rückemann, K.J., "Sensitivity of Aircraft Motion to Aerodynamic Cross-Coupling at High Angles of Attack," Paper 34, AGARD-CP-235, 1978.
- ²⁵ Langham, T.F., "Aircraft Motion Sensitivity to Dynamic Stability Derivatives," AEDC-TR-79-11, 1980.
- ²⁶ Coe, P.L. Jr., Graham, B.H., and Chambers, J.R., "Summary of Information on Low-Speed Lateral-Direction Derivatives Due to Rate of Change of Sideslip, $\dot{\beta}$," NASA TN D-7972, 1975.
- ²⁷ Langham, T.F., "Missile Motion Sensitivity to Dynamic Stability Derivatives," AIAA Paper 81-0400, 1981.
- ²⁸ Tobak, M. and Schiff, L.B., "On the Formulation of the Aerodynamic Characteristics in Aircraft Dynamics," NASA TR R-456, 1976.
- ²⁹ Tobak, M. and Schiff, L.B., "The Role of Time-History Effects in the Formulation of the Aerodynamics of Aircraft Dynamics," Paper 26, AGARD-CP-235, 1978.
- ³⁰ Tobak, M. and Schiff, L.B., "Aerodynamic Mathematical Modelling—Basic Concepts," Lecture 1, AGARD-LS-114, 1981.
- ³¹ Guicheteau, P., "Application de la théorie des bifurcations à l'étude des pertes de contrôle sur avion de combat," Paper 17, AGARD-CP-319, 1981.
- ³² Orlik-Rückemann, K.J., "Review of Techniques for Determination of Dynamic Stability Derivatives in Wind Tunnels," Lecture 3, AGARD-LS-114, 1981.

³³Hanff, E.S., "Direct Forced-Oscillation Techniques for the Determination of Stability Derivatives in Wind Tunnels," Lecture 4, AGARD-LS-114, 1981.

³⁴Ericsson, L.E., "Support Interference," Lecture 8, AGARD-LS-114, 1981.

³⁵Beyers, M.E., "Measurement of Direct Moment Derivatives in the Presence of Sting Plunging," NAE-AN-1, 1983.

³⁶Ericsson, L.E. and Reding, J.P., "Scaling Problems in Dynamic Tests of Aircraft-Like Configurations," Paper 25, AGARD-CP-227, Sept. 1977.

³⁷Chambers, J.R., DiCarlo, D.J., and Johnson, J.L. Jr., "Applications of Dynamic Stability Parameters to Problems in Aircraft Dynamics," Paper 17, AGARD-LS-114, 1981.

Bibliography

¹"Unsteady Aerodynamics," AGARD FDP Symposium, Ottawa, Canada, AGARD-CP-227, Sept. 1977.

²"Dynamic Stability Parameters," AGARD FDP Symposium, Athens, Greece, AGARD-CP-235, May 1978.

³"High Angle of Attack Aerodynamics," AGARD FDP Symposium, Sandefjord, Norway, AGARD-CP-247, Oct. 1978.

⁴"Dynamic Stability Parameters," AGARD FDP Lecture Series, NASA ARC, USA and VKI, Belgium, AGARD-LS-114, March 1981.

⁵"High Angle of Attack Aerodynamics," AGARD FDP Lecture Series, NASA LRC, USA, VKI, Belgium, and DFVLR, Gottingen, Germany, AGARD-LS-121, March 1982.

⁶Tischler, M.B. and Barlow, J.B., "Dynamic Analysis of the Flat Spin Mode of a General Aviation Aircraft," *Journal of Aircraft*, Vol. 19, March 1982, pp. 198-205.

⁷Carroll, J.V. and Mehra, R.K., "Bifurcation Analysis of Nonlinear Aircraft Dynamics," *Journal of Guidance, Control and Dynamics*, Vol. 5, Sept.-Oct. 1982, pp. 529-536.

⁸Bihle, W. Jr. and Barnhart, B., "Spin Prediction Techniques," *Journal of Aircraft*, Vol. 20, Feb. 1983, pp. 97-101.

⁹Hui, W.H. and Toback, M., "Bifurcation Analysis of Nonlinear Stability of Aircraft at High Angles of Attack," AIAA Paper 82-0244, 1982.

TECHNIQUES FOR PERFORMANCE OPTIMISATION IN CRUISE AND MANOEUVRABILITY
 Generally the minimum weight aircraft can be selected as the best design. The minimum weight aircraft can be selected as the best design. The minimum weight aircraft can be selected as the best design.

Pierre PERRIER
 Chef du Département d'Aérodynamique Théorique
 Division des Etudes Avancées
 AVIONS MARCEL DASSAULT-BREGUET AVIATION
 78, Quai Carnot - 92214 SAINT CLOUD

0. GENERAL REMARKS

The design of a combat aircraft cannot be left to a pure trial and error design when a definite performance target is precisely defined. It is obvious that there is a large variation in the possible aerodynamic aircraft shapes having the internal volume required for fuel, engine, equipment and weapon system accommodation. Among all possible shapes, the "best" aircraft will have definite advantages over a poor design in terms of performance for a given cost or in terms of cost for given performance. Imagine that the best (in that meaning) aerodynamic definition is to be left to experienced designers in the design office, that is no longer efficient when efficient theoretical-experimental processes of optimisation are available in the aerospace industry.

We successively present what is the state of Art of the reflexion and application of optimisation i.e. the optimisation targets and the optimisation tools and survey some actual results and perspectives in the combat aircraft design.

1. THE OPTIMISATION TARGETS

1.1 - Problem statement for aircraft and special adaptation to fighters

It is well known that the heavier than air vehicles are subjected to hard requirements on weight reduction and that experience of design may always put a figure larger than 5 to the weight amplification factor that relates the increase of a final design weight to an initial variation of mass of a component for the same performance level of the initial and final aircraft. That sensitivity factor is crucial in the design of any new aircraft. If that figure increases to a value as high as 10, that means that the corresponding requirement will be excessively difficult to fulfill but if it decreases to a value as low as 2 it means that the design is probably too conservative. Typically the latter figure can be related to a rough vehicle (basic trainer or utility aircraft) and the former to a limit of aircraft technology (vertical take-off and landing with difficulties to fulfill performance requirements).

If the performance requirements allow only that the useful payload P is a part of the total take-off weight it generally implies that an extra weight has to be considered as a payload increase and in that case W/P gives the weight amplification factor, the figure being lower if there is an extra dependent requirement (fuel, load). Current practice gives the name of "snowball effect" to the consequences of errors in weight estimation in the preliminary design phases of a new aircraft.

That figure gives an idea of the gain obtained by an efficient optimisation process.

For a given aerodynamic shape, it is possible to design a family of aircraft that have homogeneous qualities or constraints and that can be expressed as a parameter approximation of main variables. Generally one chooses a geometric similitary factor for volume V (fuel and usable volume requirement), for lifting surfaces A and/or vertical lift capabilities (CTOL or VTOL), expressed as a reference area parameter and an acceleration capability due to the engine, expressed as a thrust T or thrust to weight parameter. The family of studied projects allows the possibility of drawing domains of acceptable aircraft in the fulfillment of performance requirement. A n parameter diagram gives the weight of an aircraft for a given useful volume, lifting capabilities (surface area), acceleration capabilities (thrust of the engines) (figure 1)

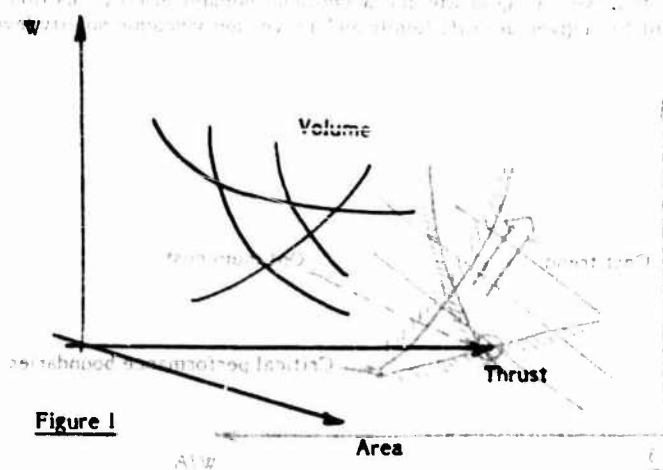


Figure 1

Generally the minimum weight can be obtained with the minimum volume, and the different performance requirements can be expressed in non dimensional requirements T/W , W/A and can be selected as requirements for capabilities in take-off and landing, subsonic acceleration, supersonic acceleration, fuel requirements for main missiles, manoeuvring capabilities sustained or maximum. It is often possible to reduce to a bidimensional, easily tractable, diagram of selection of main parameters T/W , W/A with forbidden domains for each requirement (figure 2)

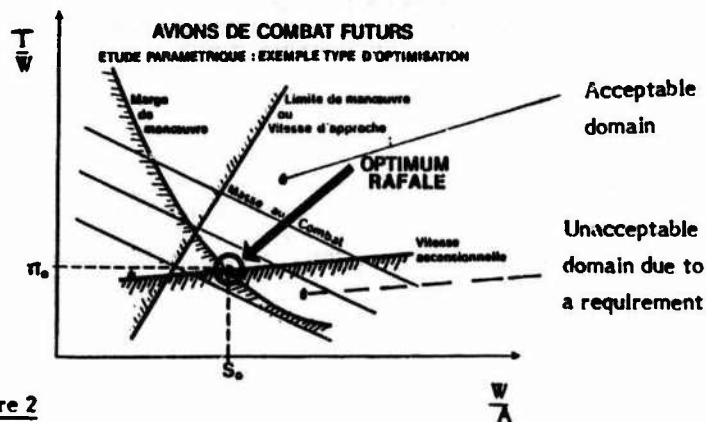


Figure 2

The main interest of such a presentation is the selection of the most stringent requirements and the aerodynamic characteristics of utmost importance. The size of an acceptable aircraft domain can be zero or very small for certain aircraft aerodynamic shapes. At that stage, the alternative is the following :

- the requirements are to be changed due to their inadequacy to the "State of Art",
- or the aerodynamic choices that have been maintained homogeneously in the family of aircraft on the basis of that diagram is no longer acceptable. The aircraft manufacturer has to survey all the "innovative" designs that he can collect in order to check if any is not the only answer to the problem.

Many times in the past, the customer (Air Force) had to decide if the innovative design was acceptable or "risky" before reducing the requirements to a level that can be attained by refinement of current design or acceptable technology steps. For example the approach speed constraints on a carrier for naval fighters has been solved many times in the past by blowing flaps, but Super-Etendard high lift optimised devices had superseded ancient blownflaps technology with a pure mechanical system at lower cost and same performance as blownflaps prototype.

Being conscious of that preliminary loop of optimisation that select potential aerodynamic configurations and their critical performance level and continuous iteration between the designer and the customer for selecting realistic objectives we can survey the criteria and constraints of any aircraft shapes optimisation.

1.2 - Criteria for optimisation

The direct criteria for customer of a combat aircraft is how to maintain an air superiority in a warfield inside an budgetary envelope. On one hand the competition at the top of air superiority can be expressed after long studies in true flights or combat simulations as requirements on mission, performance and weapon system, all things that are connected to menace estimation ; on the other hand the budget envelope gives an acceptable size for the combat vehicle if the number of vehicles in the battle is given at its lower acceptable figure.

So the cost function of the optimisation is generally also the true cost or any related quantities as the total weight of the combat aircraft. We can reformulate the general optimisation diagram of the projected aircraft in two steps.

In the first step, we can graduate the acceptable domain in cost function (for example weight) and select the optimum point for a given aircraft family and a given aerodynamic quality level (figure 3)

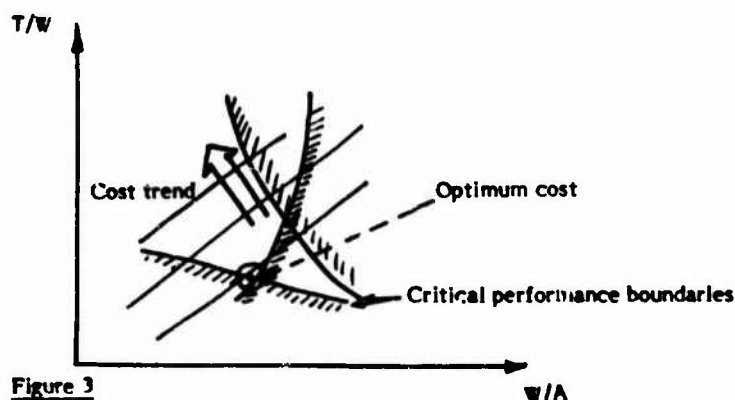
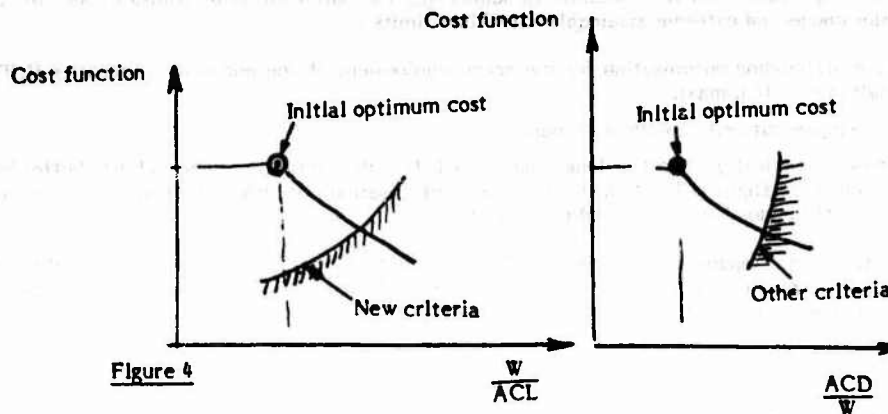


Figure 3

In the second step, we can select optimum points and express the cost function as a variable with the level of excellence of any aerodynamic characteristics. We can also notice that the aircraft with minimum weight has a minimum volume so is constrained severely as we shall discuss later. We can plot the minimum weight as a function of the aerodynamic efficiency (figure 4) for the critical performance boundaries corresponding to optimum.



In the new diagrams, the acceptable W/A varies because it is in fact W/ACL and CL (lift for a given performance) is improved, or T/W varies because the drag to balance decreases (for a given performance C_z). It is clear that, for the two limits that interest at the critical point can be shown in T/W , W/A diagram. If aerodynamic efficiency improves. The limit of improvement is given by the optimisation process and also the appearance of new boundaries that was not critical in the original design. The ideal situation, where all the characteristics are critically optimum, is not usual but the improvement of the most critical ones (the boundaries near critical boundaries) is necessary if we keep in mind that during the long life of the actual aircraft (longevity more than 20 years for Mirage 3 derivatives) the criteria can vary a lot.

We have to add to the obvious optimisation in cost (Minimum of structural weight, of engine size, ...) the necessary optimisation in survivability by reducing the visibility (Radar or infrared cross section) the intolerance to damage (redundant manoeuvre flaps, damage tolerant aerodynamics ...) and limitation to external load or weapons installations.

1.3 - Constraints for optimisation:

In the same way, as the combat aircraft design had actually been oriented forward, the optimisation of its general characteristics, in the same way the geometrical constraints had been systematically expressed on all the characteristics phasis of the flight.

The first constraints are connected to operational requirements for visibility. For the pilot, it corresponds to an envelope of head position, that gives a sufficient visibility in all directions, being evident that the front view is the more stringent on the shape of the nose and canopy and rear view on the restraint area distribution after maximum height of the cabin. For the radar, an antenna overall dimension is required with a preference for axisymmetric well oriented radome; for counter measure equipments, the capability to cover all directions with a reduced number of antennas puts in critical positions on the aircraft (wing tip or fins ...). The gun trajectory line is also a type of visibility requirement.

The constraints given by landing ground clearance or weapons ground-aircraft clearance are particularly important for the general fuselage camber and diedral or height of wing attachment and for carriage location.

All that constraint requirements have to be correctly weighted against their cost in drag or performance for optimum and/or realistic selection of shape (figure 5)



Figure 5



We have also to add the requirements for structural stiffness or resistance (static or unsteady flutter limitations).

1.4 - Local and domain optimisation

One main characteristic of combat aircraft versus commercial or transport aircraft is the emphasis put on the flight envelope extension. It is possible to summarize the optimisation of transport aircraft as a 3 points optimisation plus connected extreme attainable safe flight limits :

- take off/landing optimisation for the norm requirement of one-engine-out operation (L/D) with given stall margin (CL max),
- one engine out ceiling with stall margin,
- cruise optimisation (short or long range) $M \times L/D$ with margin on compressibility buffet boundary. The envelope of flight is limited, but the main optimisation concern is L/D in cruise (consumption) and take-off (payload and fuel weight limitation).

Exactly on the opposite side, the trend for combat aircraft is to enlarge the flight envelope, well beyond a margin on sustained flight envelope, so the optimisation of main performance points does not preclude any extreme points on maximum flight envelope (figure 6)

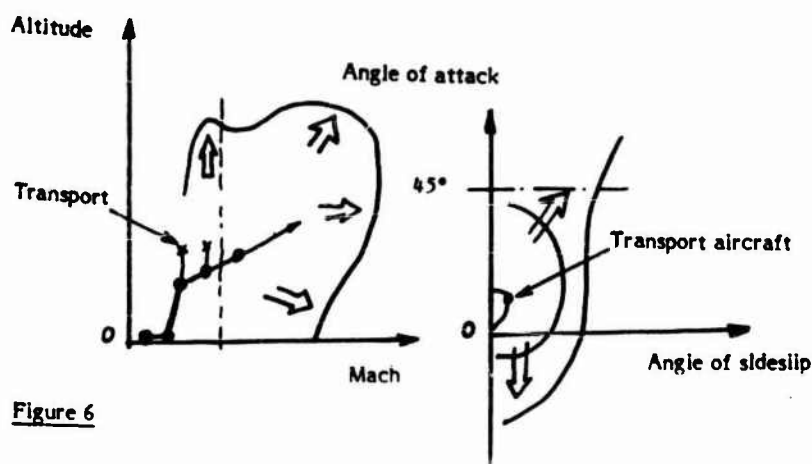


Figure 6

2. THE OPTIMISATION TOOLS

The tools in use in aerospace industry for optimisation of aerodynamic shapes are specific to optimisation problems (mathematics, numerical analysis) but also to industry constrained geometry and aerodynamics (non linear flows problems).

2.1 - Constrained geometry

The geometry data base in common use in aerospace industry is made of patch i.e. the surface of the aircraft is subdivided in small quadrangular or triangular patches, each one has its own analytical definition of the surface. The typical number of patches ranges vary from 2 000 to 20 000. The choice of that type of definition has been gradually generalized for taking in account local modifications of shapes during the development phasis of the geometric shape of the aircraft (same choice in automotive industry and now in any CAO general purpose program). If the idea of dividing the surface of the aircraft in small parts easier to handle is only a rational or cartesian necessity, the requirement of easy expression for constrained geometry is not always perceived at its true importance. However all the constraints in § 1.3 would be difficult to fulfill if no explicit way of satisfy them was at the disposal of the aerodynamic designer. So expressing that shape at a point or a normal vector, or a local curvature given is to be expressed explicitly and the family of geometric shapes that has a given constraint, must be swept as an internal loop necessary for the cost function evaluation with some aerodynamic based criteria. We can sum up the particular set of geometric subroutines that can be operated by the optimizer :

- Be piecewise continuous at the level required by fluid mechanics (continuity in curvature for transonic analysis)
- Be patch-like distributed
- Be able to express any constraint on point, tangency and/or curvature at any given set of points
- Be continuous for a variation of any constraint and/or limit of patches
- Be as near as a given error of any continuous shape (ability to approximate at a given precision any curve or surface with a small number of patches).

The AMD-BA system for constraint geometric optimisation is based on point, tangent vector and tangent ellipsoid fixation at the vertex of quadrangular-triangular patches and a unique definition of internal surface with smoothness subset of polynomials amongst the canonic system of polynomial approximation for given vertex and boundary lines. We had the possibility of any deformation of the space (point, tangent and curvature) that allows the simple camber or torsion effect very useful for plate or stick-like objects as wing and fuselage.

The connexion between different points has to be expressed also in the same way so that the family of surfaces can include for example the variable camber obtained by deflection of a flap sliding on a rounded leading edge without gap (figure 7)

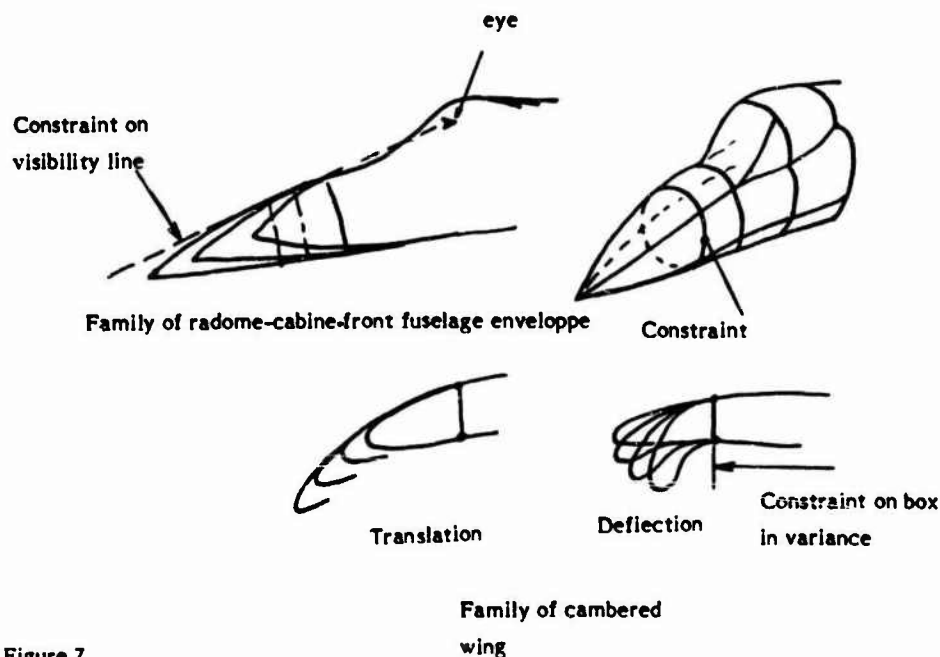


Figure 7

2.2 - General manual - automatic optimisation procedure

The author's experience confirms that the business of defining beforehand, what is good and what is feasible or admissible, is difficult. We know that a good engineer, familiar with any approach to problem solving is an intuitive optimizer. He knows how to adjust 2 to 3 parameters to reach within 5 % a physically meaningful objective model with the following restrictions :

- he must have worked for a long time with the system,
- the new optimisation does not introduce any new phenomena or non linearities that he does not have the habit to handle,
- the problem, sufficiently elliptic and linear for interpolation and even extrapolation, can succeed in an intuitive Newton-like procedure.

In fact the good engineer is very efficient for extracting subcriteria from an imprecise criterion, and selecting approximate pseudo-optimal solutions. The inclusion of such criteria in a more general criterion is a very difficult task from the mathematical point of view (pseudo-optimum problems), as the systematic constraint selection.

2.3 - Mathematical tools

For elliptic problems a detailed analysis of the mathematical tools is given in the book of PIRONNEAU (ref. 1). We can generalize the results to hyperbolic flows, but the existence of theoretically well defined method is dubious and it is better to understand well that the optimal design is for a long time reserved to purely elliptic cases, where it could be very efficient if the mathematical complexity not preclude the systematic programming effort for specific applications. We can separate the optimal shape research in direct optimal design as described by PIRONNEAU and the french school of numerical analysis and explicit iterative research of minimisation of a cost function without any information on the direction of the descent

We can sum-up the different methodologies as follows :

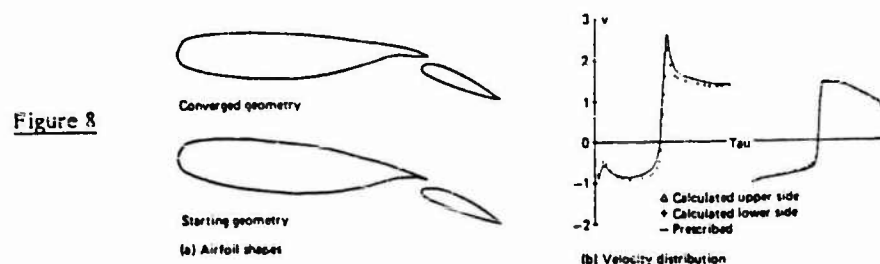
Optimum design

- The criterion can be differentiated relatively to a variation of the boundary, giving the possibility of using Newton's method, or the steepest descent or the conjugate gradient method. The last method is the most efficient only if the constraints have no direct influence on the solution (the subset of constraints points is very small compare to the free boundaries).
- The criterion can be expressed as an optimal control of distributed systems (cf LIONS 1971 ref. 2) if the problem can be expressed in a variational formulation and consequently the gradient of the solution can be, in the same way, expressed with the adjoint of the original problem, that gives a formulation for the natural cost function of the aerodynamic problem. Generally speaking, such a method is well adapted to Finite Element approach and has the advantage of giving the exact optimal shape if it exists.

Optimum approximation

- Assuming that we have a family of geometric shape functions of n parameters, the research of an optimum approximation is a current optimisation procedure with these n parameters. A set of $2n$ tests for initial cost function estimation gives with some accuracy the shape of the cost function and the problem is to try to find the lowest value of the cost function by test and error and reajustement of the shape of the cost function with all the intermediate results.
- In the case of explicit constraints, that cannot be included inside the geometric family, it is necessary to add to that procedure a selection of surfaces of constraints or to penalize the cost function with the errors on constraints requirements. Such a procedure is computation time or programmer time consuming. That explains the importance of ability to generate a geometric family of surfaces directly including all constraints with the minimum of parameters.

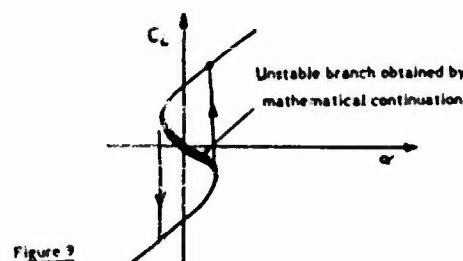
The main difference between procedure a and c is the ability for expressing the local gradient of the cost function for a variation of the boundary. That expression is usually easy with linear approach and is of common use in incompressible optimal shape design. Probably the best approach is the integral method and the classical method for incompressible definition is well detailed in LARRUYERE (réf. 3) which uses a Newton method for fast convergence to the prescribed C_p pressure coefficient shape ajustement (figure 8)



The main interest of direct optimisation of physical meaningful parameters is the knowledge given to the true sensibility of each geometrical parameters by the cost function derivatives estimated from the shape of the cost function. Such derivatives give a direct idea to the designer of the final aircraft shape for a given cost function. If there are charges of constraints such sensibility can give the way for better optimisation. We give, on the figure 9, a typical data collection of sensitivity and descent problems that is the indicator of an optimisation process in the case of a complex non differentiable cost function. Such c or d methodologies are alone for giving direct optimisation of truly interesting cost function like the aerodynamic drag or transonic flow optimisation.

2.4 - Highly non-linear optimisation

Everybody knows that there cannot be uniqueness of solution of potential or viscous flows in transonic regime or in highly viscous flows. One of the way of "innovative" aerodynamic design is to charge the flow in a discontinuous way as a function of the geometric parameters. Such a discontinuity can arise either of the discontinuity in the position or the number of the shock waves, or of the discontinuity in the position, or the number of the vortex cores fed by the separation on the aircraft at high angle of attack. One of the main reason for such a discontinuity as to be search in the very complex evolution of shock-wave or separation lines with the angle of attack or the Mach number. If we follow the position of such a discontinuity, it can happen that some evolution are instable (a new displacement is not stable for a small perturbation in another or in the same area of the aircraft). For the transonic case, it is possible for example to follow by computation the instable branch of C_z vs α and curve of transonic discontinuity of some wing sections (figure 9)



If we are able to make a complete survey of all the different types of flow pattern in transonic and, more interestingly, in separated vortical flows and to associate a cost function with that different flows, then the innovative design at high angle of attack could be optimized. We can give for example the following logic tree (fig. 10-A):

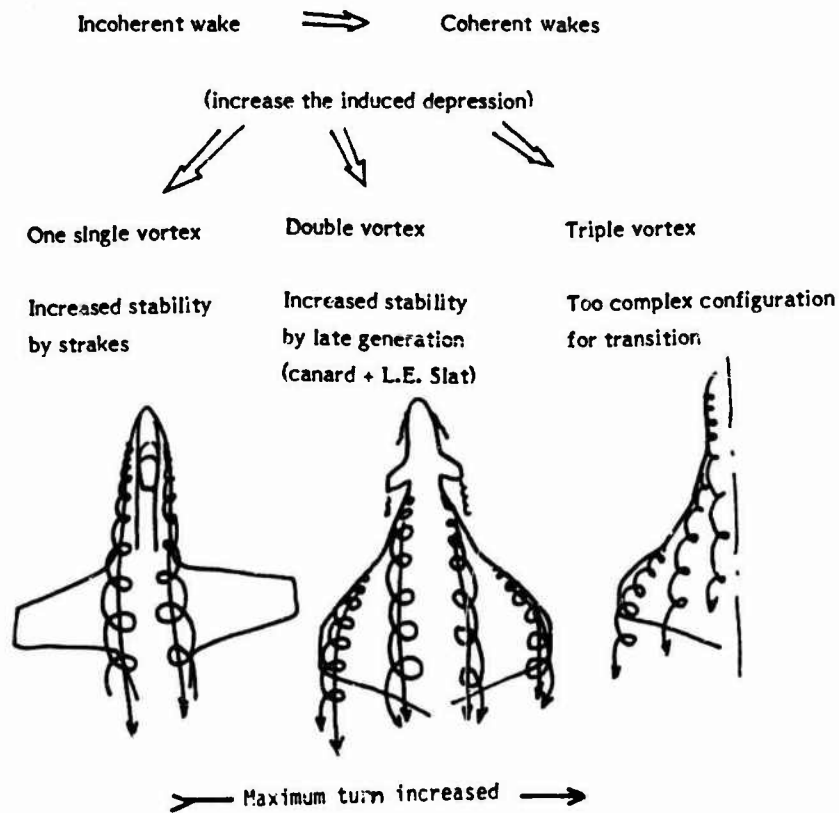


Figure 10-A

We can hope to optimise numerically leading edge shapes for optimal lift at given high angle of attack by a correct selection of the good hole in the descent process (fig. 10-B).

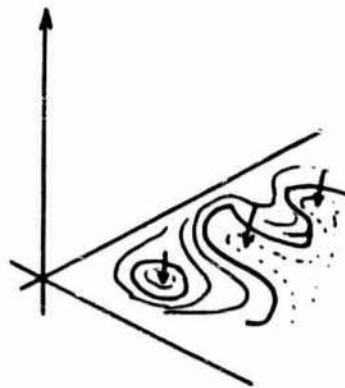


Figure 10-B

3. SOME APPLICATIONS IN COMBAT AIRCRAFT DESIGN

3.1 - General procedures

The process of optimisation of complete aerodynamic shape is now starting in some major design department. It is limited only by computational capabilities and cost and indeed by the numerical modelisation of complex flowfields.

When the optimised cost function is complex (non linear, i.e. drag, or relative to deformable geometry, like flaps) and/or the equation to be modelised is highly non linear (transonic or separated vortical flows) the procedure is necessary of the c type described previously in 2.4. The gradient of the descent is not tractable and the cost function is defined by successive tests and interpolations of 2 or more times the number of parameters. The minimum number of definition of a complex surface is of the order of 10 to 20 and the iteration process requires generally 20 to 40 tests. The bottom of the valley or hole of optimum shape is obtained by classical optimisation algorithm which fits a continuous approximate polynomial within the calculated points. The AMD-RA program developed by Philippe PERRIER (réf. 4) is highly efficient due to the use of low order polynomial approach (quadratic) with an exclusion of irrelevant points by limitation to the best neighbourhood of the solution. Such a procedure is useful for highly non linear problems that implies narrow valleys of optimum relation between parameters expressing continuity requirements on all the shape. Another way is to use "natural" parameterisation i.e. selection of a base of surface equations that are continuous on all the surface. The minimum requirement is then to have an orthogonal succession of shapes for avoiding high frequency harmonics. Some authors have used TCHEBYTCHEFF series (because Fourier series are generally of poor efficiency and the expression of constraints is costly or cumbersome). On the other hand, some of them have used a basis given by existing current design shapes for which they try to select weighting parameters.

Such a procedure can be generalised to optimisation of wind-tunnel results for a set of different shapes but that way of iteration is ineffective because the experimental errors generally exclude precise selection of optimum shapes. Generally the optimisation in wind-tunnel is limited to human direct selection and had to be reserved to selection of slowly varying characteristics or complex flows optimisation with a few number of geometric parameters (flap deflection, sweep or dihedral effects, position of canard ...). The main interest of numerical optimisation, and its complementary position versus experimental one, is precisely the high accuracy of optimisation process. It becomes possible with it to made comparison of equally optimised shapes, that otherwise could be difficult because of the confusing mixture of influence of out of optimum and general trend due to wanted parameter variations. For example, it is well known that the direct wave drag comparison in transonic of two different designs of combat aircraft is impossible, if the optimisation processes have not been previously applied to the first drawing.

3.2 - Some 2D/3D examples

The main activity of optimisation in the transport aircraft design was oriented to the selection of wing sections and such an exercise has given the opportunity of comparing the different optimisation procedure on simple cases. We give on the following figure 11 the result of ANGRAND (réf. 5) for optimum wing section with the pressure distribution presented. Such a F.E.M. optimum design computation can give, with grid refinements, an extremely precise design but with limited applications. One example of effective use of such a procedure can be the design of a nozzle with an optimum flow-field (cf. PIRONNEAU - réf. 1)



Figure 11

Same types of result have been obtained on an integral (sources and sinks) solution of Laplace equation : find the multi-element airfoil having given pressure distribution. LARRUYERF gives some results of such procedure with Newton iteration on a differentiable cost function, without constraints on closure or thickness.

The complexity of non differentiable equation can be seen on the example of research of the optimum shape of a combat aircraft wing section at high sweep angle (55°) in transonic regime ($M=1.2$) with variable leading edge devices. The cost function is the wave drag. We give one over 20 iteration procedure.

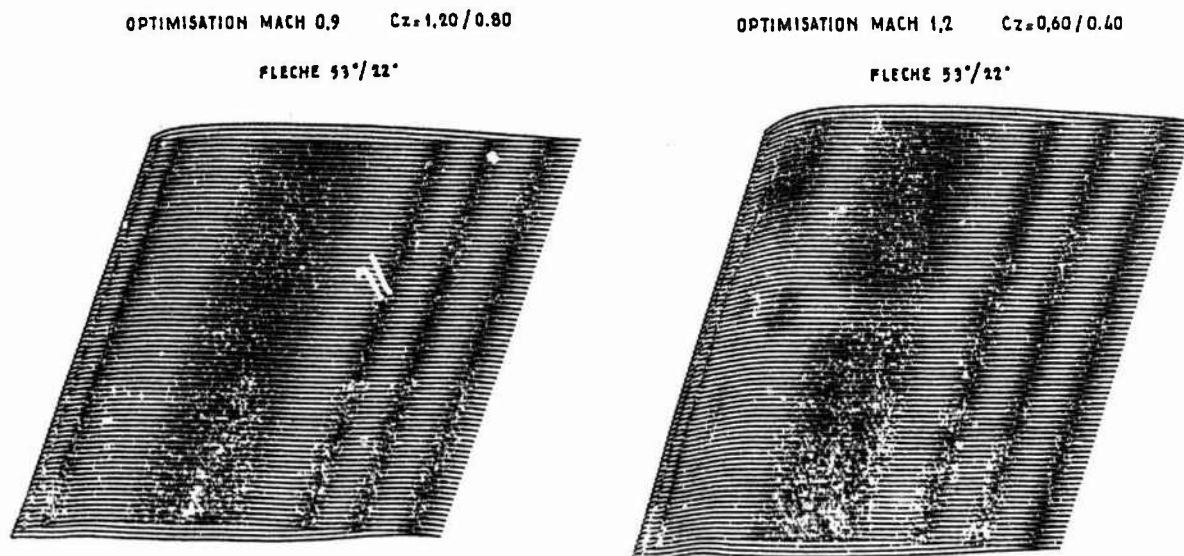


Figure 12

During the iteration process the flowfield pattern is characterized by a one shock - two shocks oscillation, the optimizer has to select the best compromise (figure 13)

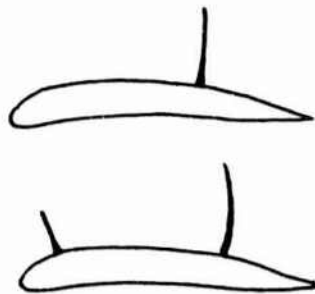


Figure 13

That 3D problem can only be tractable with a small number of parameter due to its complexity. It corresponds to a wing with high sweep angle, two section plus camber definition. The complete aircraft, wing with fuselage, cannot be optimised actually but the wind-tunnel test shows a good agreement on optimal shock-wave position and resultant wave drag decrease. Such a procedure gives the opportunity to optimise a part of the aircraft in the flowfield of complete aircraft with the limitation of no iteration on the complete flowfield.

Such a procedure can be used for a direct optimisation of wave drag in transonic. It is well known that the area rule concept can give a first-order accurate evaluation of transonic (or supersonic with supersonic area-ruling) but it is not sufficient for evaluation of optimum fuselage shape for a given wing. Cost of computation of 2nd order fuselage wave drag plus 1st order wing wave drag is acceptable and gives a much better answer in accuracy. With such a computation, an optimisation process with constraints on the rear fuselage due to engine housing requirements, critical main airframe location with volume for main undercarriage wheels can be imposed and gives realistic optimal fuselage.

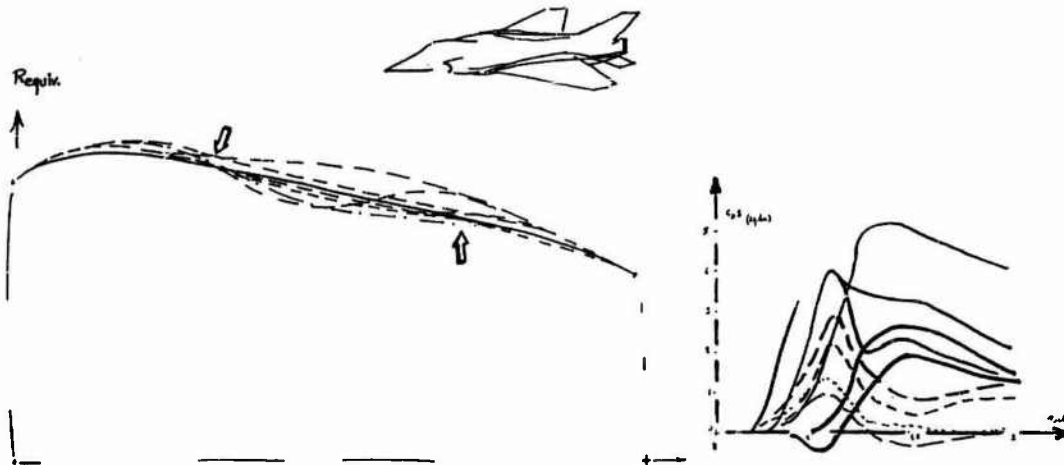


Figure 14

The optimisation of wing and canard can be also obtained by selecting the "optimum aerodynamic zero-camber". For a given Mach number, C_L and center of gravity there is an optimal 3D camber that minimizes wave drag for that point (M , C_L , C_m), but the camber of the fuselage is generally sufficient for giving (at $C_L = 0$ and $C_m = 0$ by control deflection and angle of incidence selection) an induced flowfield requiring camber of the wing for minimum wave drag. From that point it is possible to define a merit factor for the gain in wave drag in a certain Mach number and C_L range for a given center of gravity position.

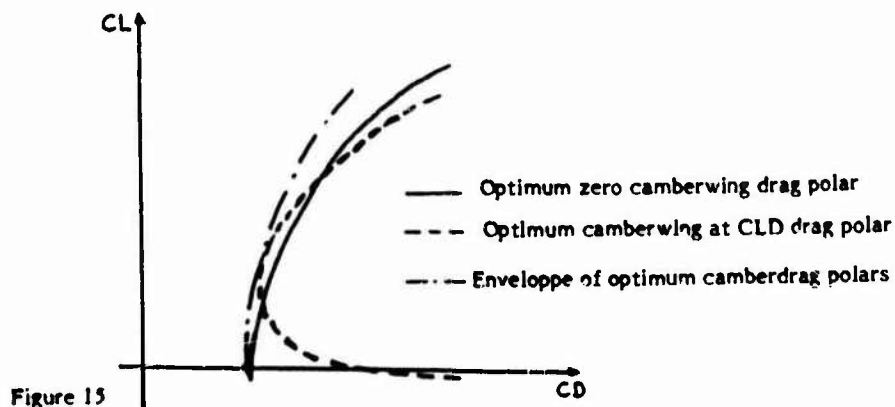


Figure 15

It is only by an optimisation procedure that the calculation of the basic and cambered wing can be selected for a given optimum target in performance (acceleration or steady trim).

When there is competing choices for optimisation the cost function can be a weighted optimisation in 2 or 3 points. This procedure is necessary for avoiding "peak-optimisation". An example is obvious in the design of airfoils where there will be kink in slope at stagnation point and shock or separation points without specification of continuity (figure 16).

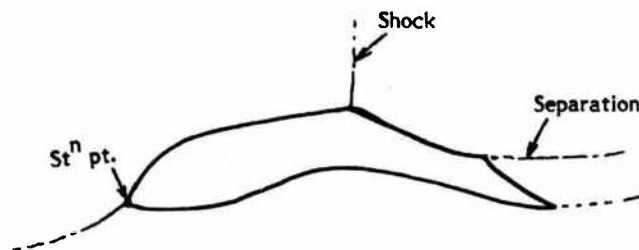


Figure 16

In fact the engineer is requiring smoothness of characteristics around optimum design so that optimal design of figure 16 is without any useful interest except for reference solutions.

The main limitation given by the time of computation can be seen on the figure 17 result. It corresponds to the optimisation of the lateral surface of front fuselage of a Mirage 2000 with the cost function being the Mach distortion at the air intake. The constraints are imposed at the junction of radar axisymmetric shape and on the main frame of canopy attachment. A gain of 30 % of distortion can be obtained with a very small fuselage shape modification. Such a computation can be completed in few minutes of IBM 3081 but corresponds to 15 optimization parameters. If we apply such a procedure for partial optimization on many points of the fuselage for drag, or flowfield distortion optimisation for different angle of attack and Mach number the total amount of computer time may be large.

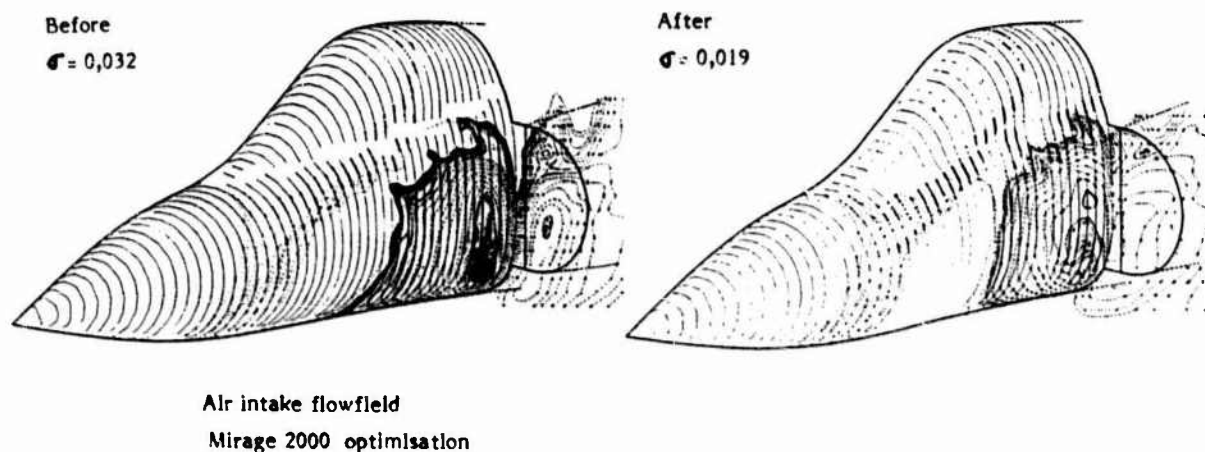


Figure 17

Very high optimization of wing in drag can be very costly in transonic with basic computation time of the order of the hour. However our experience in AMD-BA is that it is valuable as soon as the computer can give the result at a reasonable cost (typically 10 hours of the larger available computer). The aircraft optimized is better by 5 to 20 % (depending on optimized characteristics) than unoptimized aircraft and it gives a new standard for quality of combat aircraft, as the optimization of commercial transonic wings was last years, particularly for non-obvious optimisation as RCS-aerodynamic compromises.

3.3 - Concluding remarks

The optimization of combat aircraft has not attained a phase of systematic use.

It gives opportunity for giving more importance to the definition of true objectives and their relative weighting importance.

It gives the first direct comparison between intuitive results of valuable quality given by a long experience and direct rational results where the hypothesis and constraints are explicitly expressed. Any rational approach gives a long-term improvement in technics. It seems that the process of optimisation, open with the actual computational tools, can pay-off for many simple case (wing section, wing camber, fuselage wave optimisation ...) and many new complex case (deformable optimum shapes, coupled stiffness - aerodynamic requirements ...).

The discussion on the first purely computational aerodynamic shapes improves very efficiently the evaluation of the function to minimize (drag, wave drag, separated area ...) and of the constraints to keep freezed (fuel volume or straight hinge lines ...) and gives the opportunity to the manager as to the engineer to access to a new quality of design.

REFERENCES

1. O. PIRONNEAU : Optimal shape design for elliptic systems. (1984) Springer Verlag
2. J.L. LIONS : Optimal control of systems governed by partial differential equations. Springer Verlag New York (1971)
3. T. LABRUYERE, W. LOEUVÉ and J. SLOOF : An approximated method for the calculation of the pressure distribution and wing-body combination at subcritical speeds. AGARD CP No 71 - Paper 11 (1970)
4. Ph. PERRIER : Méthode de minimisation de fonction sans calcul de gradient (1977) - Note interne DEA n° 7079
5. F. ANGRAND : Numerical methods for optimal shape design in aerodynamics. Thesis (in French), University of Paris (1980)
6. F. ANGRAND, R. GLOWINSKI, J. PERIAUX, P. PERRIER, O. PIRONNEAU and G. POIRIER : Optimal design for compressible flows. Proc. Finite Elements Fluids. Banff (1980)
7. J. CEA : A numerical method for the computation of an optimal domain. Lecture notes in computer sciences, Vol. 41. Springer Verlag, New York (1976)
8. J. CEA and E.V. HAUG : Optimization of distributed parameter structures. Alphen aan der Rijn, Amsterdam (1982)
9. A. NASTASE : New concepts for design of fully-optimized configurations for future supersonic aircraft. ICAS 80
10. G.N.VANDERPLAATS : An efficient algorithm for numerical airfoil optimization. 17th ASM - New Orleans (1979)
11. S. BRENT and A. HOLT : Optimization techniques in aircraft configuration design. Sudaar (1970)
12. H.P. HANEY and E.G. WAGGONER : Computational transonic wing optimization and wing tunnel test of a semi-span wing model. Huntsville (1978)
13. R. HICKS : Wing design by numerical optimization. Seattle, Washington (1977)

FUNDAMENTALS OF FIGHTER AIRCRAFT DESIGN : ENGINE INTAKE AND AFTERBODY

by
 J. Leynaert
 Office National d'Etudes et de Recherches Aéronautiques
 29, Avenue de la Division Leclerc
 Châtillon
 92320
 France

SUMMARY

Basic conditions, study parameters and various solutions of fighter intake and afterbody (except VTOL) are reviewed.

Airframe integration and intake adaptation to the flight Mach number are discussed.

Special topics of intake flow are analysed : buzz phenomenon, internal bleed flow, high incidence, low speed, mean flow and distortion index, unsteady distortion.

Afterbody discussion covers variable geometry, thrust vectoring, and reverse.

Wind tunnel test technics are also commented on.

Air intake and afterbody will be successively considered.

CONTENTS

I. AIR INTAKE

I.1. BASIC INTAKE FLOW CHARACTERISTICS

- I.1.1. Intake flow description
- I.1.2. Intake "characteristics" ; Mass flow relation
- I.1.3. Thrust and drag components - Intake optimisation
- I.1.4. Various types of intakes, and typical pressure recovery
- I.1.5. Buzz phenomenon
- I.1.6. Engine face flow as a function of the flight conditions

I.2. FLIGHT MACH NUMBER ADAPTATION AND INTAKE DESIGN

- I.2.1. "Pitot" intake
- I.2.2. External supersonic compression intake
 - Design conditions and variables geometry
 - Internal shock foot bleed and mass flow control

I.3. AIR INTAKE/AIRFRAME INTEGRATION

- I.3.1. Intake positioning and airframe adaptation
- I.3.2. Fuselage boundary layer diverter

I.4. INTAKE ADAPTATION TO LOCAL FLOW, AND HIGH INCIDENCE DESIGN

- I.4.1. Intake adaptation to cross flow
- I.4.2. High incidence design
 - Sharp lip problem
 - High angle of attack special devices (variable geometry)

I.5. LOW SPEED INTAKE PERFORMANCES AND ADAPTATION

- I.5.1. A general relation
- I.5.2. Subsonic pressure recovery loss of a thin cylindrical intake
- I.5.3. Real intake equivalence
- I.5.4. Lip thickness and auxiliary intake design

I.6. AIR INTAKE RADAR CROSS SECTION (R.C.S.)

I.7. THEORETICAL CALCULATION METHODS

I.8. WIND TUNNEL AIR INTAKE TEST TECHNIC

I.9. NON-UNIFORM ENGINE FACE FLOW QUALIFICATION

- I.9.1. Pressure recovery definition
- I.9.2. Engine face flow distortion
 - Engine sensitivity to flow distortion - Distortion index basis
 - Distortion index definitions
 - Unsteady distortion
 - Test equipment and acquisition system
 - ONERA real time conditional acquisition system
 - Distortion index analog computer
 - RMS analysis

II. AFTERBODY

II.1. AFTERBODY BASIC DATA

II.2. CLASSIC AFTERBODY DESIGNS

- II.2.1. Long variable flap ejector
- II.2.2. Fixed shroud, trailing edge flap ejector
- II.2.3. Two-flap ejector nozzle

II.3. TWO-ENGINE AFTERBODY DESIGN

- II.3.1. Twin engines integration
- II.3.2. Nozzle spacing of a two-engine afterbody

II.4. PLUG NOZZLE

II.5. THRUST VECTORING

- II.5.1. Vectoring axisymmetric nozzle
- II.5.2. Vectoring 2-D nozzle with reverse

II.6. THEORETICAL METHODS

II.7. AFTERBODY WIND TUNNEL TEST TECHNIC

- II.7.1. Afterbody model support
- II.7.2. Internal balance
- II.7.3. External balance
- II.7.4. Afterbody test bookkeeping and performance evaluation

III. REFERENCES

I. AIR INTAKEI.1. BASIC INTAKE FLOW CHARACTERISTICS
-----I.1.1. Intake flow description (fig. 1)- Intake "adaptation"

A supersonic intake defined with a forward external supersonic compression profile is called "adapted" when the oblique shock attached to the spike or to the leading edge of the profile is inclined exactly on the lip of the cowl.

In this case, the upstream flow reaches the entire intake leading edge contour without deviation.

The upstream Mach number, M_0 , is the adaptation Mach number.

At a lower Mach number, the oblique shock is less inclined and the stream line which defines the mass flow captured by the intake is deviated between the oblique shock and the cowl lip. Less mass flow is captured. The intake is "underadapted".

- Intake flow "critical" regime

At the end of the external supersonic compression, the intake flow becomes subsonic through a normal shock, and is slowed down to the engine face Mach number M_2 in the intake subsonic "diffusor". M_2 is monitored by the reduced engine RPM.

When the normal shock is exactly at the entry of the intake, the flow regime is called "critical".

At higher values of M_2 , the normal shock moves down the diffusor. The captured mass flow is unchanged, but the shock is stronger. The regime is "supercritical".

These designations (critical, subcritical, supercritical) can also be applied under subsonic flight conditions. When the flow has just become choked at the entry of the intake (exactly sonic at the entry), the maximum mass flow is reached : the flow regime is critical. At higher values of M_2 , an internal supersonic expansion occurs, which is ended by a normal shock : the regime is supercritical. At reduced values of M_2 , the mass flow is reduced and the regime is subcritical.

I.1.2. Intake "characteristic" ; Mass flow relation (fig. 2)

In order to qualify the intake flow condition, two parameters are used :

- The mass flow ratio, m_R

m_R is the ratio of the area A_0 of the captured upstream flow, to the intake reference area A_E (defined by the upstream projection of the entire intake leading edge contour) :

$$m_R = \frac{A_0}{A_E}$$

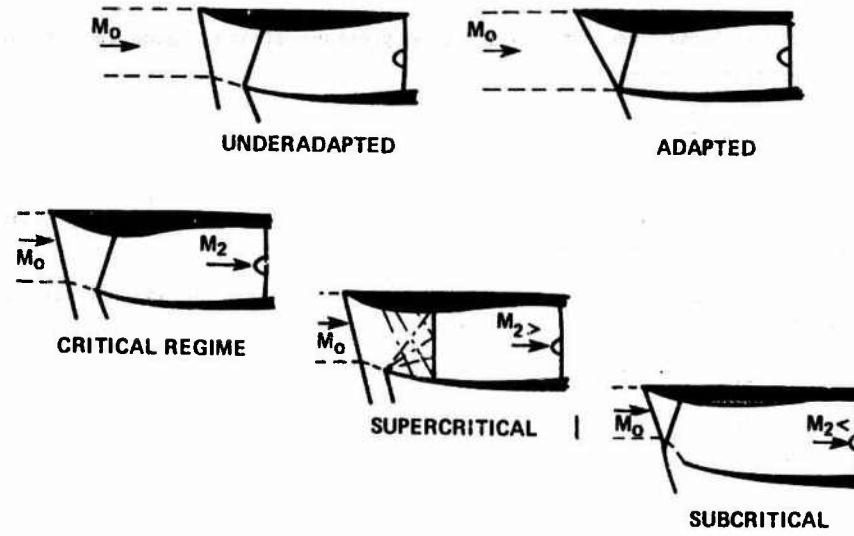


Fig. 1 - Intake flow description.¹

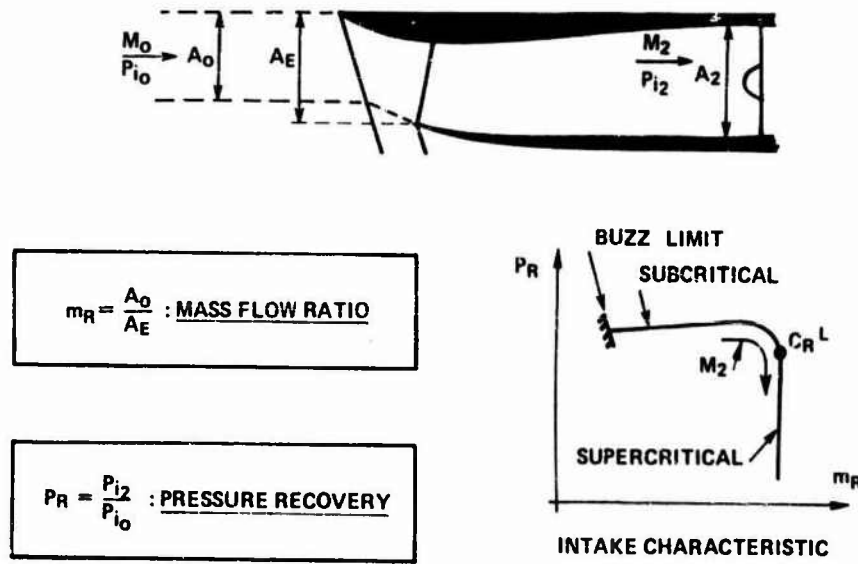


Fig. 2 - Intake characteristic

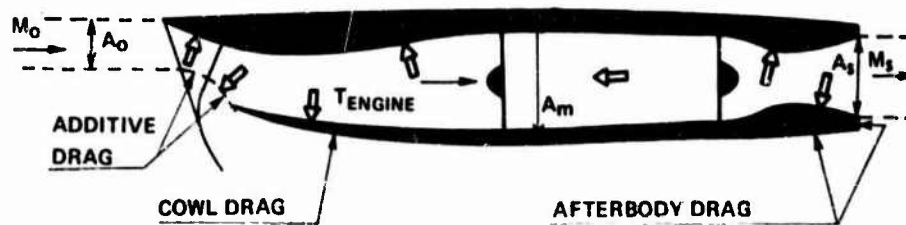


Fig. 3 - Thrust and drag components.

- The pressure recovery, P_R

P_R is the ratio of the local isentropic stagnation pressure of the engine face flow, p_{12} , to the upstream isentropic stagnation pressure, p_{10} :

$$P_R = \frac{p_{12}}{p_{10}}$$

The intake "characteristic" is the curve of P_R as a function of m_R . This curve can be graduated by M_2 . The vertical part represents the supercritical regime.

Reduction of the mass flow in subcritical regime is often limited by an unstable flow phenomenon called "buzz". This phenomenon is described in § I.1.5.

The following basic assumptions are used to study the intake flow :

- Aircraft is a galilean referential,
- Permanent flow,
- Perfect gas,
- No heat exchange (adiabatic flow).

As a consequence, the mean value of the stagnation temperature of the flow is constant :

$$T_1 = \text{Cst.} = T_{10}$$

Let A_c be the critical (sonic) area of the local flow, and $\Sigma = \Sigma(M) = \frac{A}{A_c}$ the corresponding Mach number function.

The mass flow can be expressed by :

$$q_m = \left(\frac{1+\gamma}{2}\right)^{-\frac{\gamma+1}{2(\gamma-1)}} \frac{\sqrt{\gamma}}{nR} \frac{p_1 A_c}{\sqrt{T_1}}$$

(air : $\gamma = 1.4$ - $nR = 287.04$ (international unit, SI)).

The mass flow conservation law with $T_1 = \text{Cst.}$ is then expressed by :

$$p_1 A_c = \text{Cst.}$$

or by the following relation between the main parameters of the intake flow :

$$m_R = \frac{A_2}{A_E} \frac{\Sigma_0}{\Sigma_2} P_R$$

I.1.3. Thrust and drag components - Intake optimisation (fig. 3)

Definitions

- Engine thrust, T_{ENG}

The thrust of the engine, as defined by the engine company (engine data book) is the result of internal forces represented by white arrows (fig. 3). These forces are supposed to be opposed to p_0 (external ambient pressure), as usual.

- Additive drag, D_{AD}

If the flow is deviated ahead of the intake cowl lip by the intake profile (underadaptation), or by subcritical functioning, the engine thrust includes some forces applied to the deviated streamlines, but not applied to the intake.

These forces (expressed in $p - p_0$), to be subtracted from the engine thrust, represent the additive drag of the intake.

- Cowl drag, D_{CO}

External drag of the intake cowl.

- Intake drag, D_{INT}

The intake drag is the sum of the additive drag and the cowl drag.

- Afterbody drag, D_{A-B}

Drag of the rear part of the nacelle (including the base drag).

- Nacelle drag, $D_{NACELLE}$

The nacelle drag is the sum of the intake drag and afterbody drag.

- Nacelle net thrust (Nacelle thrust), $T_{NET NACELLE}$

Difference between the engine thrust and the nacelle drag.

Analytical expressions

The various terms can be expressed as follows, at zero degree of angle of attack :

$$T_{ENG} = p_s (1 + \gamma_s M_s^2) A_s - p_o (p_o (1 + \gamma M_o^2) A_o - p_o (A_s - A_o))$$

$$D_{AD} = \int_{A_o}^{A_E} (p - p_o) dA$$

$$D_{CO} = \int_{A_E}^{A_{max}} (p - p_o) dA + D_{friction}$$

$$D_{A-B} = \int_{A_{max}}^{A_s} (p - p_o) dA + D_{friction}$$

$$D_{INT} = D_{AD} + D_{CO}$$

$$D_{NACELLE} = D_{INT} + D_{A-B}$$

$$T_{NET NACELLE} = T_{ENG} - D_{NACELLE}$$

Spillage drag (subcritical regime), D_{SPILL}

Intake drag increment due to subcritical regime is called the spillage drag :

$$D_{SPILL} = (D_{AD} + D_{CO}) - (D_{AD} + D_{CO})_{CRITICAL}$$

Pressure recovery effect and intake optimisation

Considering the engine itself, the engine reduced RPM (or engine rotation Mach number) and the engine face Mach number M_2 are determined by the exit sonic throat area of the engine and by the fuel-to-air ratio.

For a given engine nozzle geometry and a given fuel-to-air ratio, any change of the intake configuration and pressure recovery P_R only alters the general level of the engine internal pressures, proportionally to P_R .

Moreover, for adapted intakes, intake dimensions and mass flow are proportional to P_R , as given by the mass flow relation :

$$A_E = A_o = A_2 \frac{\Sigma_o}{\Sigma_2} P_R \quad (m_R = 1)$$

Then, the nacelle thrust can be expressed by :

$$\begin{aligned} \frac{T_{NET NACELLE}}{p_o A_s} &= \left(\frac{p_s}{p_{i_2}} \frac{p_{i_o}}{p_o} (1 + \gamma_s M_s^2) - (1 + \gamma M_o^2) \frac{\Sigma_o A_2}{\Sigma_2 A_s} \right) P_R - \\ &- \left(1 - \frac{\Sigma_o A_2}{\Sigma_2 A_s} P_R \right) - \frac{D_{NACELLE}}{p_o A_s} \end{aligned}$$

where the coefficients of P_R , $| |$ and $\frac{\Sigma_o A_2}{\Sigma_2 A_s}$, are independent of P_R .

In fact, if the nozzle geometry is also readjusted, a higher value of P_R makes it possible to increase the nozzle expansion ratio and to adapt the nozzle with a higher value of M_s and A_s . In this case, the thrust increase with P_R is amplified.

We can take as a reference the ideal thrust of a nacelle with the same nozzle geometry, but with an ideal isentropic intake ($P_R = 1$) and an ideal zero-drag nacelle ($D_{NACELLE} = 0$):

$$\frac{T_{IDEAL}}{P_0 A_s} = \left[\right] - \left(1 - \frac{\sum_2 \frac{A_2}{A_s}}{\sum_0 \frac{A_2}{A_s}} \right)$$

The loss of thrust as refers to the ideal nacelle is :

$$\frac{|\Delta T|}{P_0 A_s} = \left(\left[\right] + \frac{\sum_0 \frac{A_2}{A_s}}{\sum_2 \frac{A_2}{A_s}} \right) (1 - P_R) + \frac{D_{NACELLE}}{P_0 A_s}$$

This expression shows that the loss of thrust is a direct function of the loss of pressure recovery, and is directly affected by the nacelle drag.

The loss is even more severe if the nozzle geometry was adjusted.

Consequently, the aim of the intake optimisation will be to achieve the highest pressure recovery and the minimum intake drag (cruise adaptation with zero additive drag, and minimum cowl drag).

The specific fuel consumption is also improved by increasing P_R , since the fuel flow is proportional to the intake mass flow which is proportional to P_R , and the net thrust can be increased more than proportionally to P_R , by readjusting the nozzle.

I.1.4. Various types of intakes, and typical pressure recovery (fig. 4)

Pressure recovery of various types of intakes are compared on fig. 4. "Pitot" intake, or "normal shock" intake, has the poorest pressure recovery at high Mach number. External supersonic compression intakes, either two-dimensional with a supersonic compression ramp focusing the compression waves on the lip of the cowl, or axisymmetric with a conical or a two-cone spike, have a better pressure recovery.

This pressure recovery is improved even more when the interaction between the normal shock at the entry of the diffuser and the ramp (or the cone) boundary layer at the foot of the shock is controlled by boundary layer bleed.

External supersonic compression intakes are used when a high cruise Mach number is required.

On actual fighter aircraft, there is a tendency to adopt Pitot intakes, because they are simpler and they usually accept large subcritical regime without buzz. Moreover, they offer a better manoeuvring margin in angle of attack and yaw, which can be more attractive than high Mach number capability.

I.1.5. Buzz phenomenon (fig. 5)

Intake buzz is a pulsatory flow which usually occurs with an external supersonic compression intake when the mass flow is reduced in subcritical regime.

In this case, the normal shock emerging from the entry and the oblique shock of the external supersonic compression merges in a unique shock at a focus point F ahead of the cowl lip.

Then, downstream of F, a shear line separates two flows: the high stagnation pressure flow which has been compressed by the supersonic compression profile, and the lower stagnation pressure flow which has crossed the stronger outer shock.

If, for a given value of M_2 , this shear line enters the diffuser, there occurs a separation or a large expansion of the flow which enters the diffuser along the internal profile of the cowl due to the lower stagnation pressure of this flow facing the high internal pressure level of the main flow.

What appears is a sudden, strong reduction of the captured mass flow due to the blockage effect of the separated or expanded flow.

On the graph of the internal pressure (represented by P_{12}) as a function of the entry mass flow ratio m_1 , this first phase of the intake buzz is represented by the upper part of the curve (fig. 5).

Now, if the intake diffuser is considered as a tank, this tank being no longer fed will empty, and its internal pressure will decrease.

When the internal pressure becomes lower than the stagnation pressure of the flow along the cowl (P_{12} limit of choking), the separation of this flow disappears, and its blockage effect, too.

Moreover, as the internal pressure P_{12} has become very low, the intake flow turns to supercritical.

This phase is represented by the lower part of the curve.

The exit mass flow being proportional to P_{12} (for the given constant value of M_2), this exit mass flow is low whereas the entry mass flow is maximum: the diffuser will progressively fill up, and pressure will increase. The normal shock moves toward the entry.

This phase corresponds to the vertical part of the curve.

Finally, when the normal shock tends to a position of equilibrium for the mass flow, the shear line

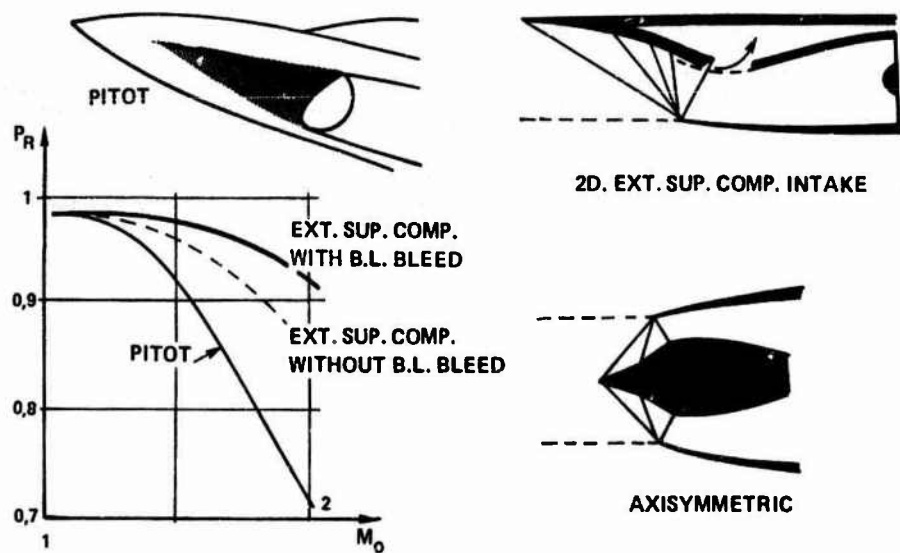


Fig. 4 - Various types of air intake, and pressure recovery.

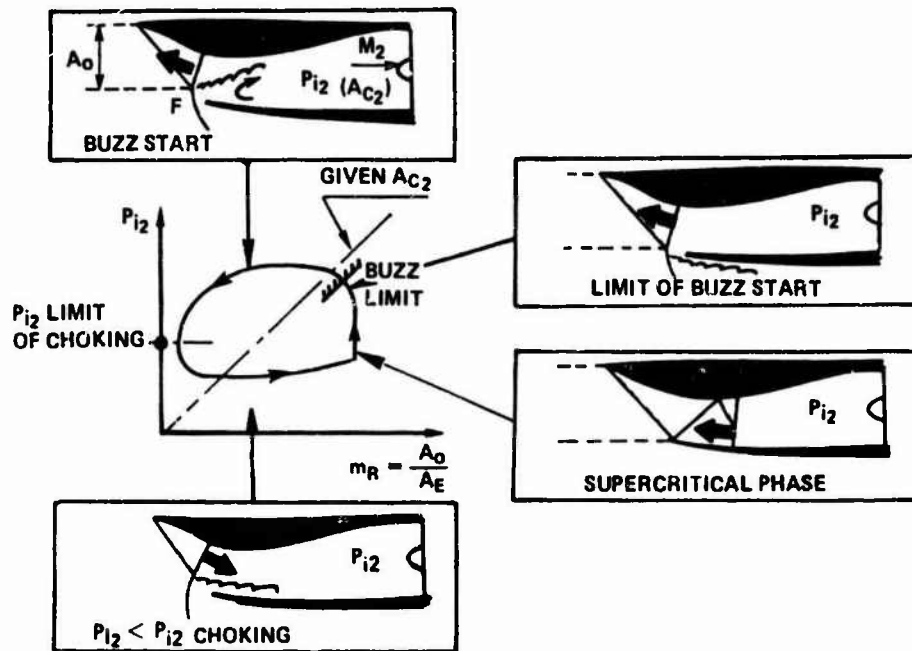


Fig. 5 - Buzz cycle.

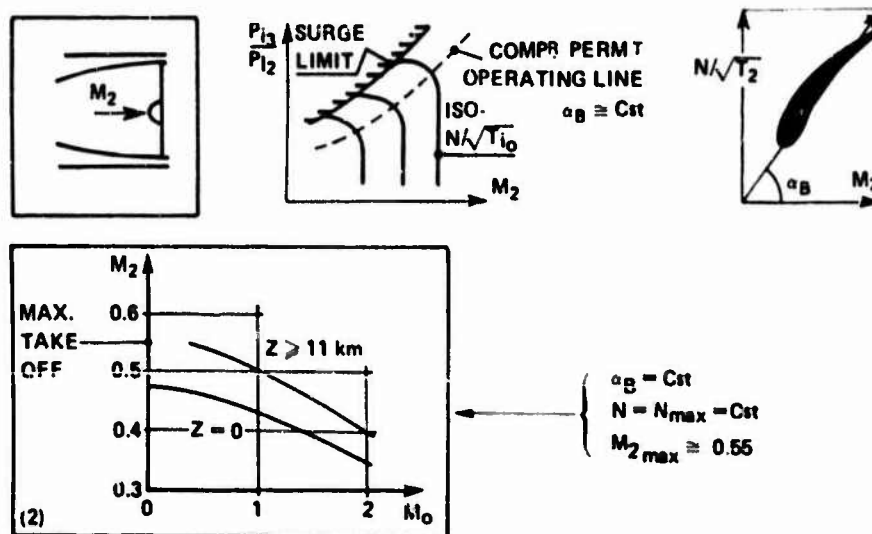


Fig. 6 - Engine face Mach number.

again enters the intake, and a new buzz cycle starts.

It is easy to understand that this buzz phenomenon can also occur each time a fillet of low stagnation pressure stream enters an inlet, even in subsonic flight. For instance, the vortex wake of a canard surface, or the thickened boundary layer of a fuselage at yaw can trigger buzz.

The buzz frequency is of the order of 10 Hertz (airplane scale), and, during a buzz sequence, the pilot is shaken up, and very often the engine surges or lights off. If the airplane has two intakes side by side, large interaction effects cause the second engine to surge.

So, it is very important to avoid the occurrence of buzz. Pitot intakes are favourable to this end. Various solutions of buzz avoidance systems with external supersonic compression intakes will be discussed later.

I.1.6. Engine face flow as a function of the flight conditions (fig. 6)

In order to have an idea of the engine face M_2 Mach number values and, therefore, of the intake flow adjustment for different flight conditions, it can be stated that, roughly speaking, the engine control (nozzle throat control...) is such that the compressor (except in transient) operates on its maximum efficiency line, which corresponds to a nearly constant angle of attack of the rotating blades (optimum angle of attack). Then the axial component M_2 of the flow Mach number relatively to the blade, is proportional to the tangential component, which is equal to $N/\sqrt{\gamma RT_2}$. So, M_2 is in relation with N and T_{10} :

$$\frac{T_2}{T_{12}} = \left(1 + \frac{\gamma-1}{2} M_2^2\right)^{-1} \quad \text{and} \quad T_{12} = T_{10},$$

and it can be seen that the maximum value of M_2 is obtained at the maximum RPM (N_{\max}) and at the lowest value of T_{10} (high altitude and low flight Mach number).

A maximum value of M_2 is usually of the order of 0.55.

Let this value be achieved at $Z > 11$ km ($T_0 = 217$ K) and $M_0 = 0.5$; let intake conditions be considered at N_{\max} . N_{\max} is supposed to be constant which is also usual. M_2 variation as a function of T_{10} is then determined by the preceding relations. The result is presented on fig. 6, as a function of the flight Mach number at various altitudes.

These basic engine data (which normally are detailed in engine data books) will be used to study the intake adjustment in the entire flight envelope.

I.2. FLIGHT MACH NUMBER ADAPTATION AND INTAKE DESIGN

I.2.1. "Pitot" intake (fig. 7)

Pressure recovery of "Pitot" or "normal shock" intake is given on fig. 4. It is the product of the normal shock pressure recovery and the subsonic diffuser mean pressure recovery.

The mass flow ratio m_R of such an intake as a function of the flight Mach number and altitude is presented on fig. 7. The calculation is obtained by the mass flow relation (I.1.2), and the following data:

- Pressure recovery is the critical or subcritical one given on fig. 4.
- Engine face Mach number M_2 is the one given on fig. 6.
- Intake dimensions (front reference area A_E) are defined in order to be adapted ($m_R = 1$) at $M_0 = 1.5$, $Z > 11$ km.

Under these conditions, it can be seen that the intake will operate subcritically ($m_R < 1$) in a large part of the flight domain, and namely in supersonic flight at low altitude, which represents a very important domain for a fighter aircraft.

We shall see later (§ I.4.2) that subcritical regime can be useful for improving the manoeuvrability margin of the aircraft, but, of course, the net thrust is reduced by the additive drag.

If the intake had been adapted to a lower altitude, with a smaller entry area A_E , the same calculation would have indicated a higher mass flow ratio than 1 in supersonic at high altitude. As, in fact, in supersonic flow, the maximum mass flow ratio is limited to 1, this means that the assumption of a critical pressure recovery is not verifiable. In this case, the intake would operate in supercritical regime, with a loss of pressure recovery and thrust.

Supercritical flow is also more sensitive to angle of attack and yaw, concerning the flow distortion at the engine face.

So the solution opted for is usually a larger intake, operating mainly in subcritical regime.

In supersonic flow, and under adaptation conditions ($m_R = 1$), the thinner the lip of the cowl, the lower the cowl drag (wave drag of the rounded lip).

However, in subcritical regime, a rounded lip limits the increase of the drag induced by the reduction of the captured flow (spillage drag), as shown on fig. 8 [Hawkins J.E., 1974]: the suction effect on the lip contour partially compensates for the additive drag.

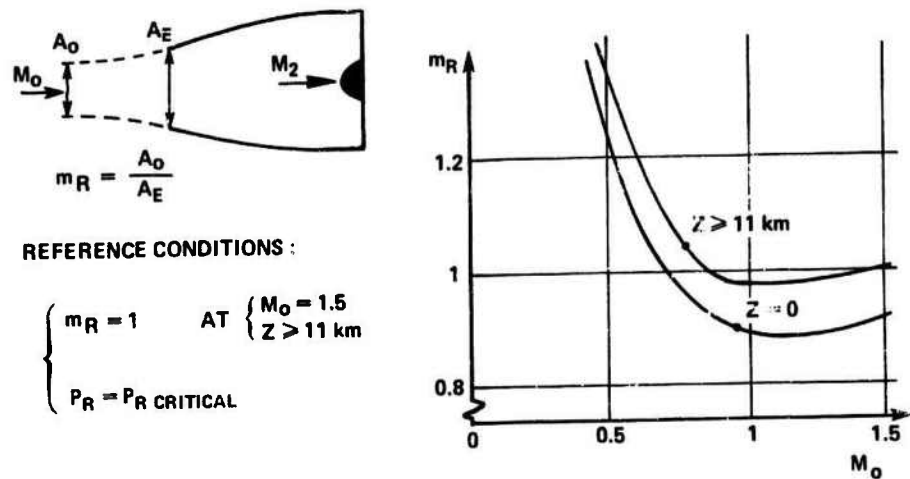


Fig. 7 - Pitot intake mass flow ratio.

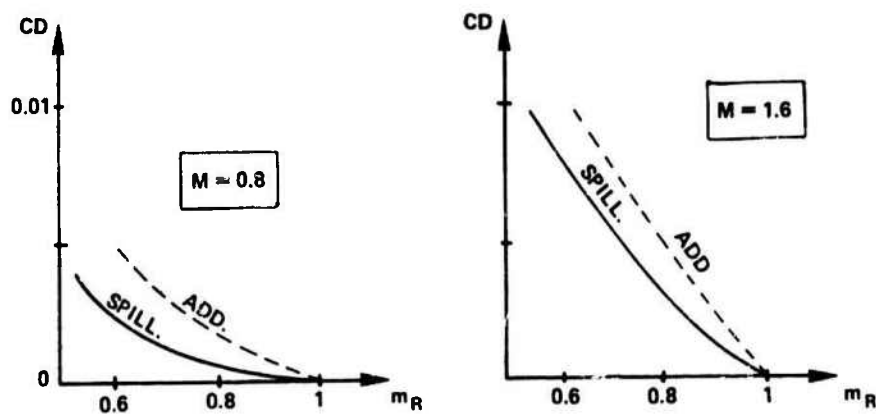


Fig. 8 - Additive drag and spillage drag of rounded lip pitot intake [Hawkins].

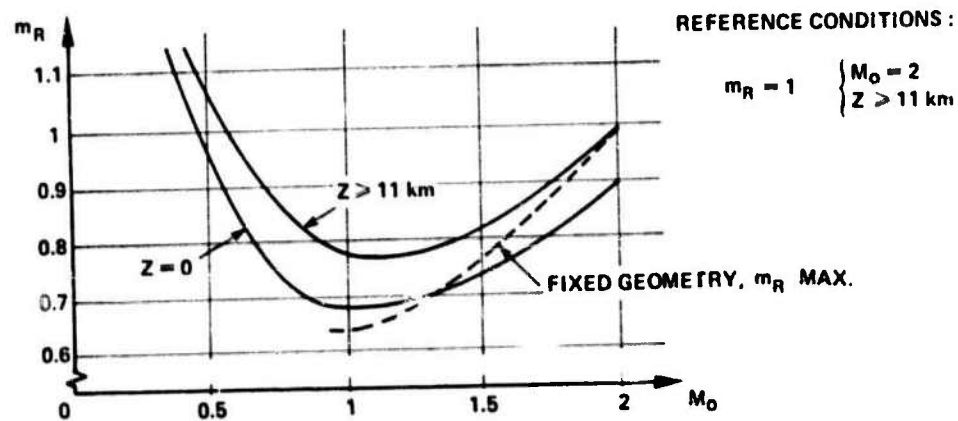


Fig. 9 - External supersonic compression intake mass flow ratio.

A rounded lip also reduces the sensitivity to angle of attack and yaw.

Finally, slightly rounded lips are usually adopted, with a lip radius of a few percent of the entry diameter.

1.2.2. External supersonic compression intake

Design conditions and variable geometry

The same calculation process than for "Pitot" intakes can be followed for an external supersonic compression intake.

A typical result of the mass flow ratio as a function of the Mach number M_0 is presented on fig. 9, relating to an external supersonic compression intake adapted to $M_0 = 2$, $Z > 11$ km.

On the same figure the maximum mass flow ratio of a fixed geometry intake is sketched. This limitation is due to the flow deviation at reduced Mach number imposed by the supersonic compression profile ahead of the entry.

Examination of the curves shows that, without variable geometry, the intake would operate subcritically (and, usually, would run into buzz) at high Mach number and low altitude. Also it would operate supercritically in transonic flight, due to the limitation of the mass flow at the entry under these flight conditions.

Variable geometry is used to solve these problems, by increasing the forward flow deviation at high Mach number and low altitude, in order to avoid the subcritical regime and buzz, and also by decreasing this flow deviation at reduced Mach number, to avoid the entry choking and the supercritical regime.

Some examples of variable geometry external supersonic compression intakes are given on figs. 10 and 11.

A Mirage's half axisymmetric intake has a half cone or a double cone spike moving over a curved ramp. The curved ramp helps to avoid internal throat blockage at low flight Mach numbers, when the spike is retracted inside the low diverging (and low drag) intake cowl.

An F111's quarter axisymmetric intake includes a spike which is moved forward at low Mach numbers, and two series of flaps which are retracted. Such a solution allows the adjusting of the intake in the various flight conditions, with a smooth deviation of the exceeding flow and, therefore, a small additive drag.

Two-dimensional intakes very often incorporate a fixed front wedge followed by a movable ramp.

An F14's ramp includes two movable parts to optimize the flow deviation for each flight condition.

The forward part of an F15's intake is entirely rotating. A first wedge is followed by a movable ramp to adjust the supersonic compression. At reduced Mach numbers, a small rotation of the intake enables the flow deviation to be shared between the upper part of the first wedge and the lower part of the intake, with a very low additive drag. Of course, the rotation of the intake is also used to improve the intake capability under high angle of attack flight conditions.

When choosing a solution, it is clear that the intake's adaptation capability must be balanced against simplification, minimum weight, and general aerodynamic and structural airframe integration. The best compromise depends on the overall aircraft program.

Internal shock foot bleed and mass flow control

On external supersonic compression intakes, namely two-dimensional types, large pressure recovery improvement is obtained by a boundary layer bleed at the foot of the entry shock, as indicated on fig. 4. This is to avoid a large flow disturbance due to the shock-boundary layer interaction.

Sometimes, the boundary layer or the compression profile is controlled by suction through a porous ramp, (fig. 12), but, in this case, the pressure loss of the bleed flow is high, as is the resulting drag term.

Another efficient solution is to bleed the boundary layer by means of a large internal gap, like on the Concorde, or the Tornado (fig. 13).

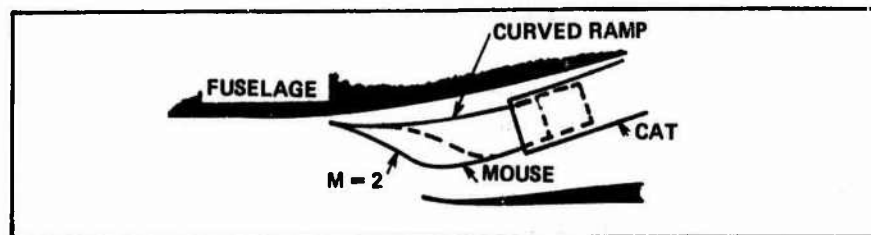
At design conditions (fig. 13a), the front shock (F) is not straight, but curved towards the bleed gap. An internal supersonic expansion takes place over the gap, which is ended by a terminal shock (T) of a small extension. At the foot of this shock T, just ahead of the diffuser flap leading edge, the boundary layer flow is deviated towards the bleed gap.

One of the advantages of this kind of solution is that if the engine Mach number is reduced, the intake does not immediately become subcritical, and the occurrence of buzz is delayed.

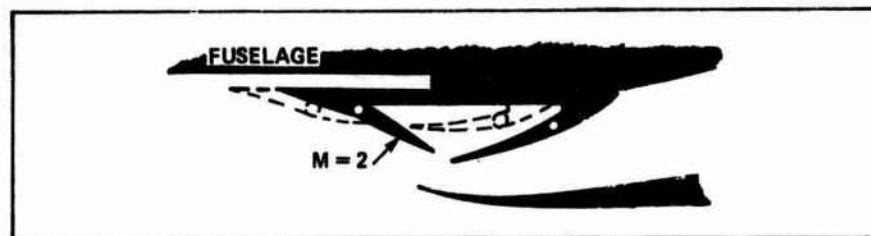
Let A_{c_b} be the bleed flow sonic exit area. The bleed mass flow is proportional to the product of $p_b \times A_{c_b}$.

By reducing M_2 (fig. 13b), what is observed at first is that the mass flow which is refused by the engine is forced back into the bleed cavity.

For a constant value of A_{c_b} , the cavity pressure p_b is increased proportionally to the bleed mass

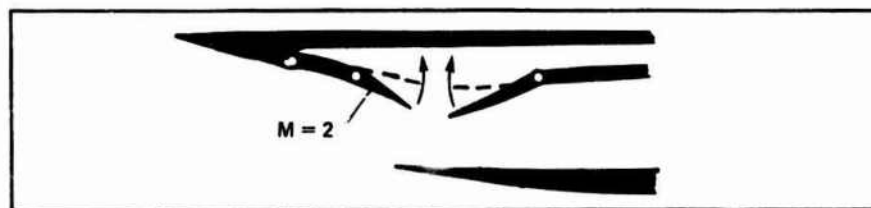


1/2 AXISYMMETRIC (MIRAGE)

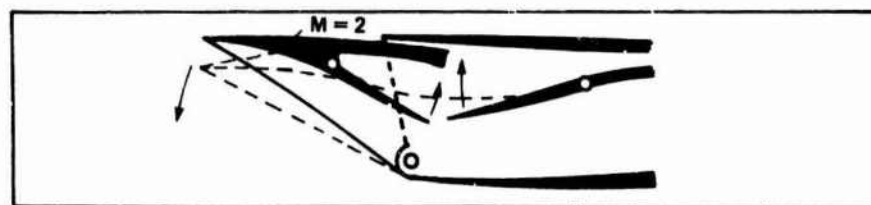


1/4 AXISYMMETRIC (F111)

Fig. 10 - Variable geometry examples. Axisymmetric type.



FIXED FIRST WEDGE



ROTATING FORWARD INTAKE

Fig. 11 - Variable geometry examples. Two-dimensional type.

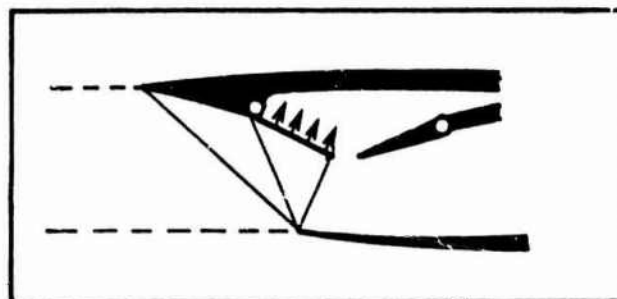


Fig. 12 - Porous ramp boundary-layer bleed.

flow, and the internal supersonic expansion, which is controlled by p_b , is reduced to a small transonic zone. At the same time, the entry shock becomes straighter. The cavity pressure can be increased in this way from $p_b/p_{10} = 0.45$ to $p_b/p_{10} = 0.52$. A higher increase would finally result in the subcritical shock detachment.

However, if, at the same time that the engine flow is reduced, the bleed exit area A_{cb} is increased, the pressure in the cavity returns to its starting value, and the same flow structure is reestablished with a supersonic expansion over the gap (fig. 13c).

So, in order to delay the occurrence of buzz when the engine Mach number M_2 is reduced, it is advantageous to increase A_{cb} when p_b tends to rise, that is to say, when more mass flow is deviated into the bleed cavity.

The opening of A_{cb} can be automatically achieved if the bleed flow serves as the secondary flow of the engine converging-diverging exhaust nozzle, as represented on fig. 14. As a matter of fact, in this case, when the engine RPM is reduced (M_2 reduction), more mass flow is forced into the bleed cavity, but, at the same time, the stagnation pressure of the engine jet is decreased. Thus, the blockage effect of the jet on the secondary flow (which determines A_{cb}) is reduced.

The By-pass mass flow is of course limited, and, in the case of large engine throttle and mass flow reduction, complementary means are necessary to avoid subcritical regime and intake buzz.

Lowering the ramp (δ angle increase) is usually used, as is sometimes the opening of a dump door (θ angle) (fig. 15).

Control of these parameters can be based on the value of p_b/p_{10} . Critical regime corresponds to given values of " $p_{b\max}/p_{10}$ " (which can be refined as a function of flight Mach number M_0 , angle of attack α and angle of sideslip β).

When p_b becomes higher than $p_{b\max}$, δ is increased up to δ_{\max} (given as a function of M_0), and the dump door begins to open.

Direct control of δ and θ as a function of M_0 , α , β , and of the engine reduced RPM, N/\sqrt{T} , can also be provided. However, such a direct control requires more margin, due to the differences between individual engines (engines aging...).

I.3. AIR INTAKE/AIRFRAME INTEGRATION

I.3.1. Intake positioning and airframe adaptation (fig. 16)

Fig. 16 presents some examples of flow fields in front of the intake for different fuselage shapes and different intake positions.

Two-dimensional intakes in supersonic flow can be pretty easily adapted to local angle of attack, by adjusting the compression ramp angle. It is more difficult to cope with transverse flow (sideslip flow angle) which can be induced by aircraft yaw, but also by aircraft angle of attack. Some examples of sideslip angle maps, induced only by aircraft incidence, are presented on fig. 16 ($M_0 = 2.2$, $\alpha = 15^\circ$, $\beta = 0^\circ$).

It can be seen on the figure that the fuselage shape may have a big influence on flow uniformity in front of the intake.

A "Rafale" forebody is an example of a sophisticated shape designed to keep the flow as parallel as possible to the fuselage surface, whatever the flight conditions may be.

The same result has been sought by wing shielded intakes.

An under fuselage position -like on F16- seems a very advantageous one. However, in the case of a two-engine aircraft, such a position presents some difficulties in avoiding interferences between the two inlets, for instance in the case of an engine failure.

I.3.2. Fuselage boundary layer diverter

In order to achieve the best pressure recovery and also to avoid internal flow distortion, it is important to prevent the fuselage boundary layer from entering the intake.

Some examples of diverter configurations are presented on figs. 17 and 18. The Mirage's boundary layer diverter consists of a space between the intake and the fuselage at the position of the intake cowl leading edge. This position allows a deviation of the cone boundary layer to occur towards the diverter, which, at the same time, reduces the cone boundary layer interaction with the entry shock.

On the "Rafale", fuselage boundary layer is diverted from the intake by a splitter plate.

The F111's intake flow is protected against the fuselage boundary layer by a sideplate, and the intake itself is protected against the sideplate boundary layer by a secondary boundary layer diverter.

The F17's intake is also protected against the corner flow at the junction between the fuselage and the wing strake by some leakage windows open through the strake.

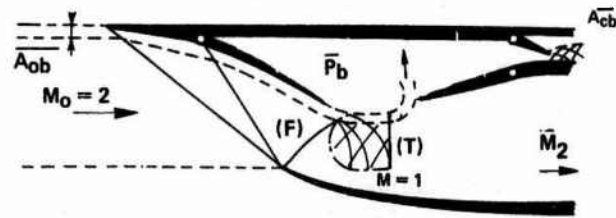
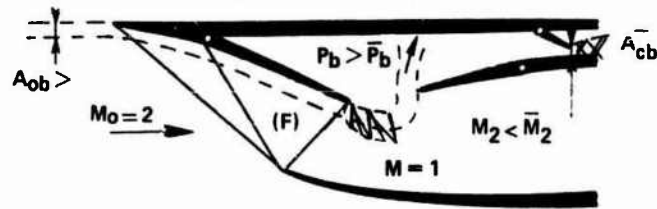
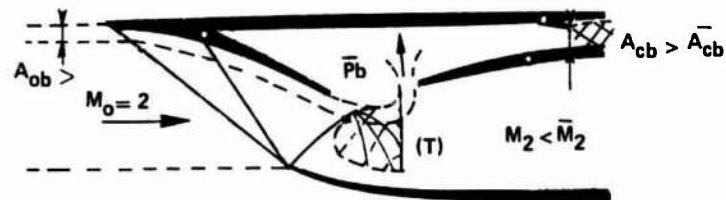
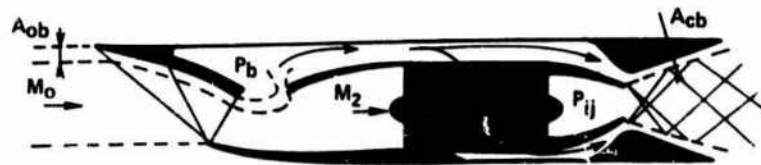
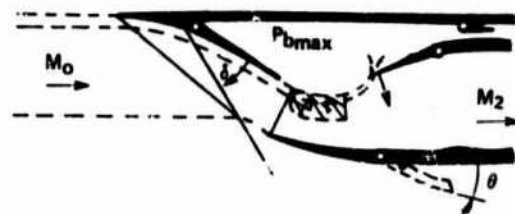
13a. DESIGN CONDITIONS $P_b/P_{i0} \cong 0.45$ 13b. $N\sqrt{T_i}$ REDUCTION, $M_2 < \bar{M}_2$. $(P_b/P_{i0})_{\max} \cong 0.52$ 13c. $N\sqrt{T_i}$ REDUCTION AND A_{cb} INCREASE. $P_b/P_{i0} = 0.45$

Fig. 13 - Internal shock foot bleed by large internal gap (Concorde, Tornado,...).

Fig. 14 - Example of A_{cb} self-control (Concorde).Fig. 15 - Additional mass flow reduction without front shock detachment (intake buzz). δt and θt controlled by $P_{b\max}$.

I.4. INTAKE ADAPTATION TO LOCAL FLOW, AND HIGH INCIDENCE DESIGN

I.4.1. Intake adaptation to cross flow

A sidewall out-off of a 2-D intake is a well known means of improving the yaw-capability of the intake.

As shown on fig. 19, with a straight sidewall, a leading edge vortex takes place along the sidewall at cross flow, since the Mach number normal to the leading edge is subsonic. The wake of this vortex interacts with the entry shock and can produce a large distortion of the internal flow.

A cut back sidewall allows the inner flow (behind the wedge shock) to spill outside in the opposite direction to the cross flow. This effect delays the formation of the inner vortex, and the occurrence of the internal distortion.

At zero yaw, of course, the spillage induced by the cut causes an additive drag, but this drag is usually very small and when compared to the improvement in yaw capability, appears very acceptable indeed.

When the sidewall of a 2-D intake is extended ahead of the cowl lip (for instance in order to separate two side by side intakes), the leading edge of the sidewall is supersonic (for the normal Mach number), and the cross flow simply induces an expansion fan giving higher inner Mach numbers along the sidewall, as presented on fig. 20. As a consequence, the wedge shock is locally more inclined, and impinges under the cowl lip, which gives rise to a strong shock/boundary layer interaction on the sidewall under the cowl lip.

A cut in the cowl lip near the side wall lets the interacted flow spill outside the cowl and restores regular stream flow (fig. 20).

In this case also, there is an equilibrium between additive drag due to spillage at zero yaw, and improvement of the flow at yaw.

As a matter of fact, it is always possible (or desirable) to effect a spillage so as to deviate some spoiled stream flow outside the intake.

I.4.2. High incidence design

Sharp lip problem

When the flow just ahead of the lip of the cowl is at incidence, which is often the case in subsonic high angle of attack flight conditions, an internal leading edge separation can occur. Then the wake of this separated zone is equivalent to a boundary layer of low pressure recovery along the internal cowl wall and the losses can be amplified by the compression in the diffuser.

To limit this subsequent effect, vortex generators can be fitted onto the cowl surface above the diffuser pressure gradient (fig. 21).

An other possibility is to bleed the boundary layer at the same position, which was the solution applied to the Concorde air intake.

When entry flow disturbance cannot be avoided, a long diffuser helps to attenuate the turbulence level and the distortion at the engine face station, as outline on fig. 21.

Another way to improve the lip flow at high incidence is to operate subcritically. The flow deviation caused by the subcritical regime is in the opposite direction to the incidence near the lip and internal separation is thus avoided (fig. 22).

Such a subcritical regime can be assured by engine control, some engine throttle being determined by the aircraft angle of attack.

Subcritical regime can also be imposed by a slightly overdimensioned Pitot intake. In this case however, compromise with additive drag is again encountered.

A rounded lip obviously also delays the internal separation at the lip at incidence, but at the expense of the lip drag in supersonic, as previously discussed.

High angle of attack special devices (variable geometry)

The orientation of the entire forward part of the intake in front of the upstream flow at incidence, with the same kind of solution as on the F15, could be of course very efficient, but would be very heavy.

It is simpler to try to solve the high angle of attack problem by using the same devices as those used to improve the intake flow at take off and low speed. As a matter of fact, the flow situation near the cowl lip is the same in both cases : at low speed, the suction of the mass flow by the engine also induces high angle of incidence and internal separation at the leading edge of the cowl. The difference however, is that at low speed, the internal pressure of the diffuser is lower than the external one, contrary to the higher Mach number situation. In this last case, it is necessary to be even more cautious in designing the shape of the auxiliary device in order to assure an efficient recompression of the flow.

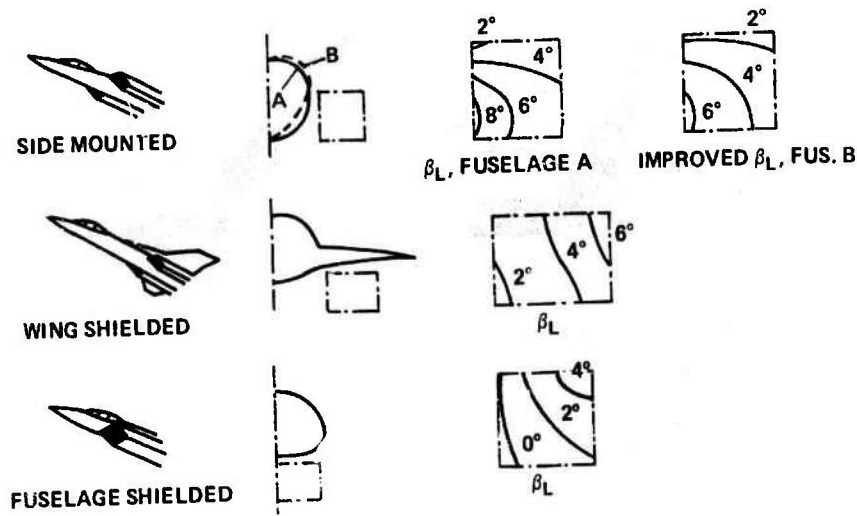


Fig. 16 - Air intake/airframe integration. [Richey, Surber, Laughrey]. Angle of sideslip map at $\alpha = 15^\circ$, $\beta = 0^\circ$, $M_0 = 2.2$.

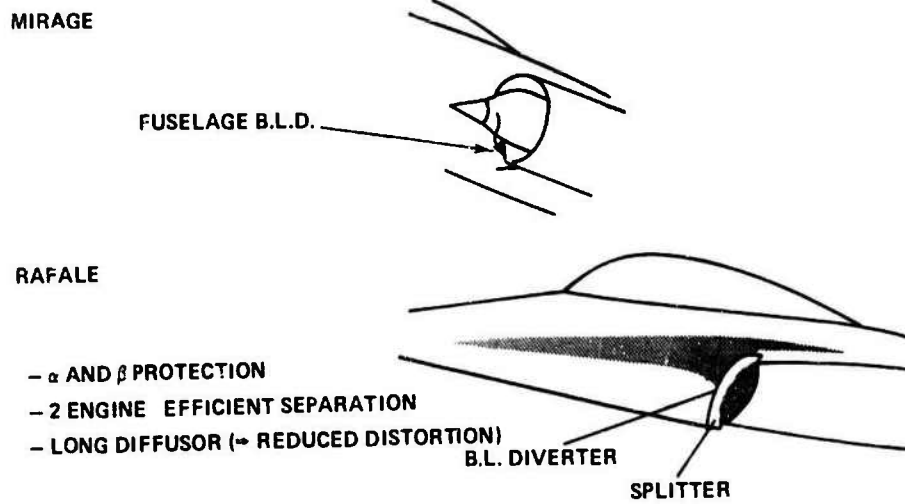


Fig. 17 - Fuselage boundary layer diverter. Mirage. Rafale.

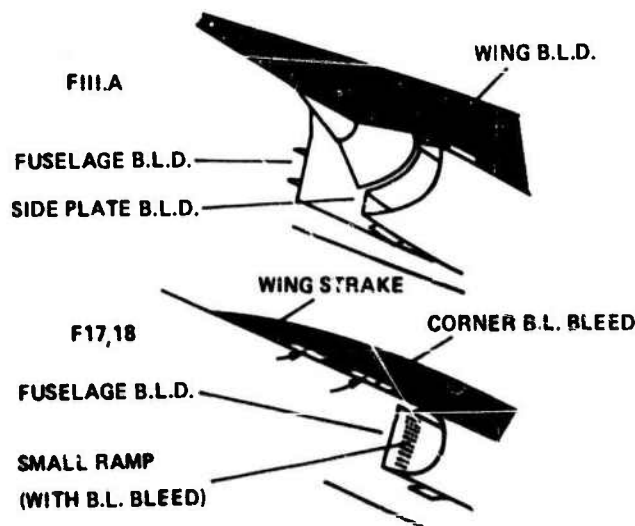


Fig. 18 - Fuselage and wing boundary layer diverter. F111A. F17, F18.

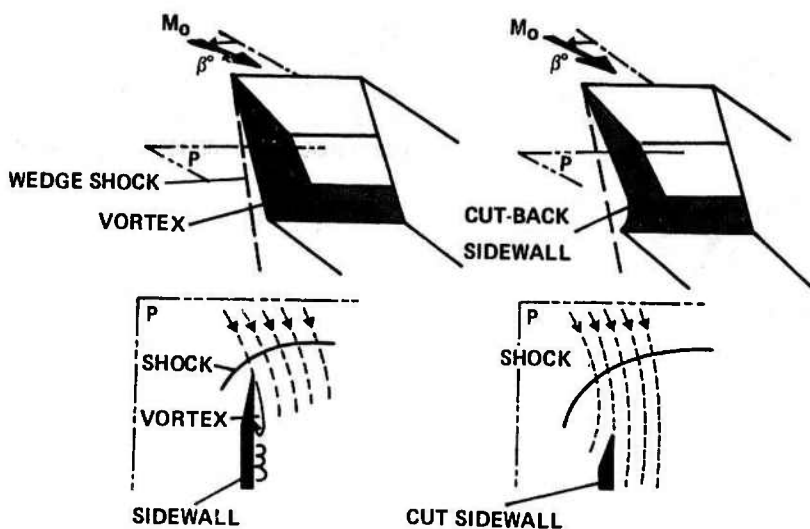


Fig. 19 - Local adaptation to cross flow (at yaw...). Sidewall cut-off. [Leynaert, Brown, Collard, 74].

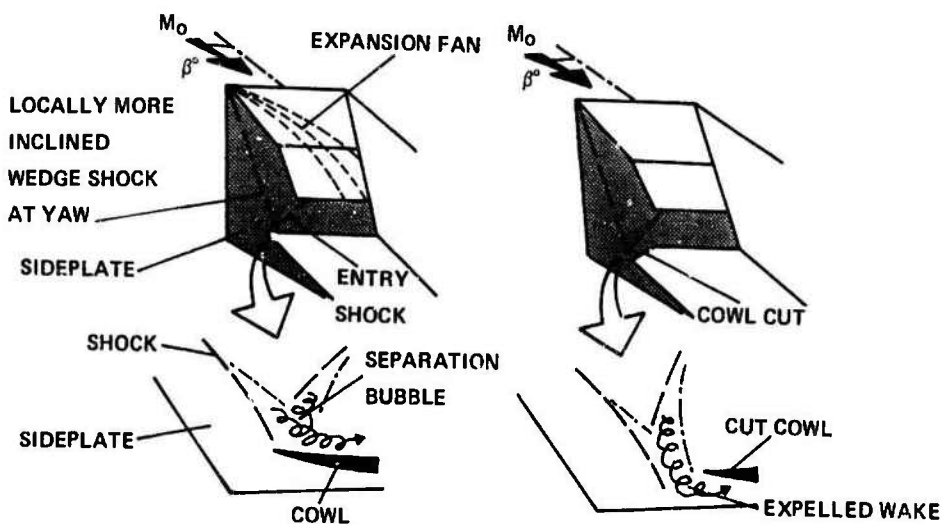


Fig. 20 - Local cowl cut near a sideplate [Leynaert, Brown, Collard, 74].

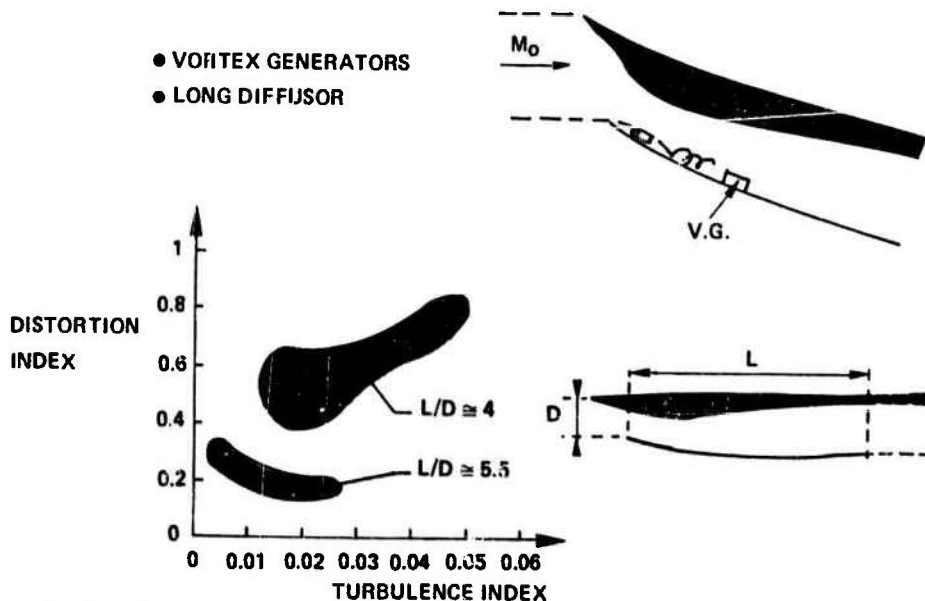


Fig. 21 - Sharp lip angle of attack sensitivity improvement. Vortex generators. Long diffuser. [Surber, Stone - 71] [AGARD LS 53 - 72]

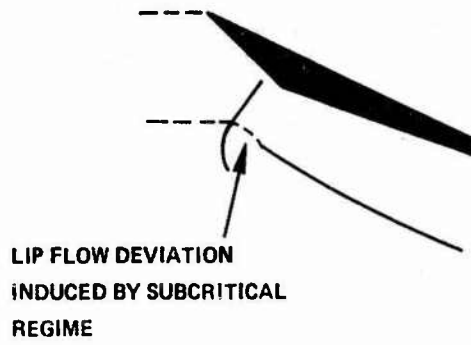


Fig. 22 - Angle of attack sensitivity improvement by subcritical regime.

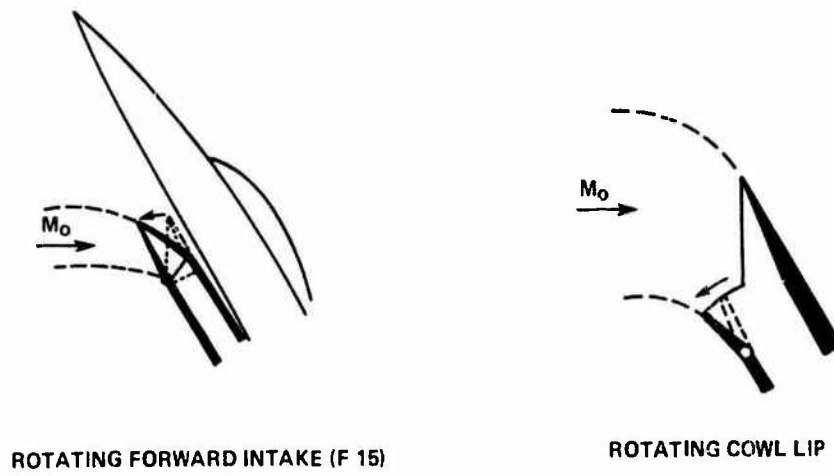


Fig. 23 - High angle of attack special devices.

HIGH INCIDENCE DEVICES

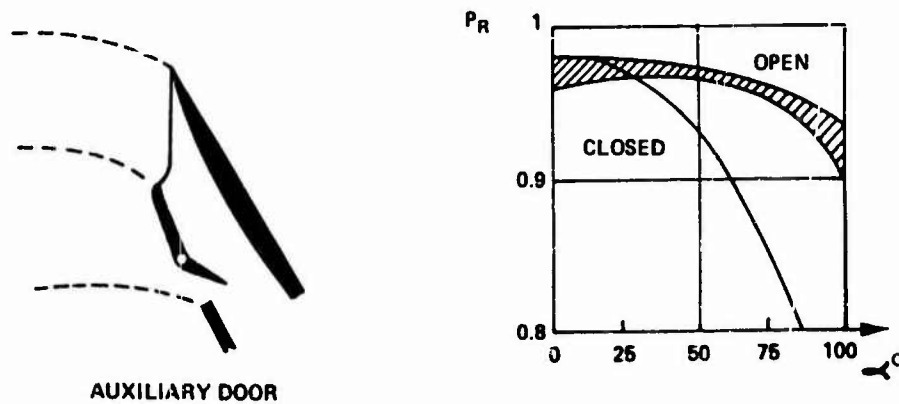


Fig. 24 - Auxiliary door at high angle of attack [Lottor, Malefakis, 78].

Such an auxiliary device can be a rotating lip, as sketched on fig. 23, or an auxiliary door, as sketched on fig. 24. The pressure recovery results reported on the graph show that thanks to the opening of an auxiliary intake, high values of P_R can be preserved up to an angle of attack of at least 75° at $M_0 = 0.5$.

I.5. LOW SPEED INTAKE PERFORMANCES AND ADAPTATION

I.5.1. A general relation

The pressure recovery loss of a sharp leading edge intake at take off or at low speed can be approximated by an elementary theory which is recalled hereafter.

The following definitions will be used (fig. 25) :

Intake net thrust, T_{NET}

This is the result of the internal and external forces applied to the intake, respectively from the leading edge (A_E) to the engine face area (A_2) and from the leading edge to the maximum external area of the cowl (A_m). The ambient pressure p_0 is supposed to be applied to the fictitious cut limiting the intake part (area $A_m - A_2$), or, which is equivalent, the pressures are considered in $p - p_0$.

Let $\int_{A_2}^{A_m}$ be the integral on the contour (A_2), (A_E), (A_m), then :

$$T_{NET} = - \int_{A_2}^{A_m} (p - p_0) dA - D_{friction, ext. + int.}$$

Intake drag

As already defined, this is the sum of the additive drag and the cowl drag.

$$D_{INTAKE} = \int_{A_0}^{A_m} (p - p_0) dA + D_f ext.$$

Isentropic ideal thrust

For the same values of A_2 and M_2 , this is the intake net thrust when the internal flow is isentropic ($P_R = 1$) and the intake drag is null.

It can also be said that the external flow is isentropic, too. A necessary condition for real flow to satisfy this assumption is that the upstream Mach number M_0 be subsonic. In this case, making the further assumption that the afterbody shape of the nacelle downstream of A_m can be replaced by a cylindrical tube without any significant modifications of the upstream pressure field, the property of the subsonic potential flow (which is that the drag is null) can be applied to the stream tube from A_{0is} to A_m :

$$\int_{A_{0is}}^{A_m} (p - p_0) dA = 0$$

(A_{0is} : captured stream tube upstream area when $P_R = 1$).

The assumptions of $P_R = 1$ and intake drag = 0 allows us to write :

$$T_{ideal} = - \int_{A_2}^{A_m} (p - p_0) dA = \int_{A_0}^{A_2} (p - p_0) dA, \quad \text{or :}$$

$$T_{ideal} = p_{2is} (1 + \gamma M_2^2) A_2 - p_0 (1 + \gamma M_0^2) A_{0is} - p_0 (A_2 - A_{0is})$$

or, with $\frac{p}{p_1} = \omega(M)$, $\frac{A}{A_0} = \Sigma(M)$,

$$\frac{T_{ideal}}{p_0 A_2} = \frac{\omega_2}{\omega_0} (1 + \gamma M_2^2) - \gamma M_0^2 \frac{\Sigma_0}{\Sigma_2} - 1, \quad \text{or}$$

$$\boxed{\frac{T_{ideal}}{p_0 A_2} = f(M_0, M_2)}$$

... the ideal thrust of an intake is the thrust of the stream tube (A_{0is} , A_2). It is entirely defined by M_0 , M_2 , and is independent of the shape of the intake.

General relation

For given values of A_2 , M_2 , M_0 , the net thrust of a real intake is obtained by :

$$T_{net} = p_2 (1 + \gamma M_2^2) A_2 - p_0 (1 + \gamma M_0^2) A_0 - p_0 (A_2 - A_0) - D_{intake}$$

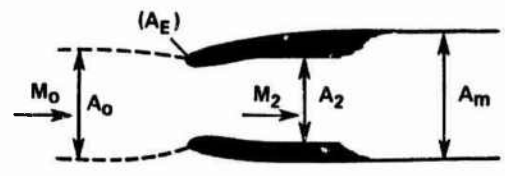


Fig. 25 - isentropic thrust condition .

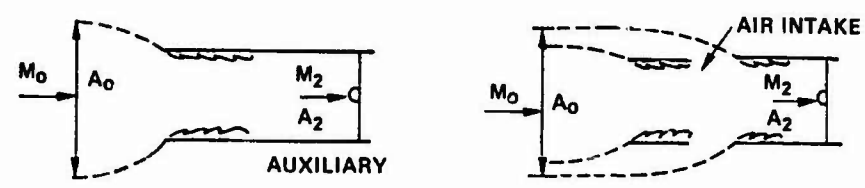


Fig. 26 - P_R losses of a thin cylindrical intake.

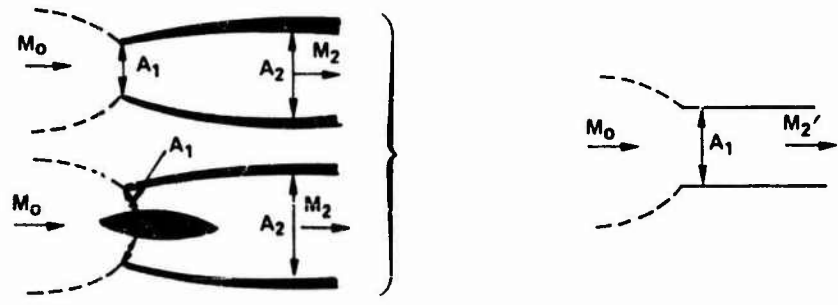


Fig. 27 - Real intake equivalence.

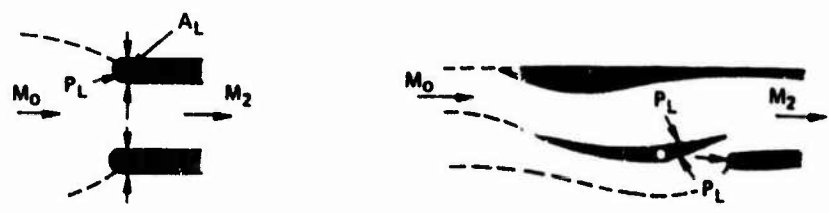


Fig. 28 - Lip thickness and auxiliary intake design.

then, with $P_R = \frac{P_{i2}}{P_{i0}}$, $A_0 = P_R A_{0is}$,

we obtain the general relation :

$$\frac{T_{NET}}{P_0 A_2} = P_R \frac{T_{ideal}}{P_0 A_2} - (1 - P_R) - \frac{D_{INTAKE}}{P_0 A_2}$$

1.5.2. Subsonic pressure recovery loss of a thin cylindrical intake (fig. 26)

In subsonic flow, when the mass flow ratio of such an air intake becomes higher than 1 ($M_2 > M_0$), the main viscous effects take place in the separated zone inside the intake entry from the sharp leading edge.

By neglecting the wall friction, the external flow can be considered as entirely isentropic and, therefore, the intake drag is null. The net thrust of the cylindrical intake is obviously null also and the following relation gives directly the pressure recovery :

$$P_R = \frac{1}{1 + \frac{T_{ideal}}{P_0 A_2}}, \quad \text{with } \frac{T_{ideal}}{P_0 A_2} = f(M_0, M_2)$$

It is interesting to note that the pressure recovery loss of a cylindrical inlet with an auxiliary opening, as represented on fig. 26, is identical to the one without an auxiliary opening. This result shows that it is not sufficient to open an auxiliary passage to improve the pressure recovery of a sharp lip intake at take off or at low speed. Comments are given on § 1.5.4.

1.5.3. Real intake equivalence

The pressure recovery loss of a real intake at take off and low speed is mainly determined by the local flow turning around the sharp leading edge of the cowl. Thus, it is possible to replace the intake by a cylindrical one having about the same local flow in order to calculate an approximate value of the pressure recovery. This is accomplished if the cylindrical intake has the same local entry area as the real one, and the same mass flow ratio, as sketched on fig. 27.

1.5.4. Lip thickness and auxiliary intake design

In order to achieve a pressure recovery equal to 1 at take off and low speed, it is necessary for the intake to give the ideal thrust. As the flow is supposed to be isentropic, it is easy to roughly calculate (by a two-dimensional approximation) the thrust of the diffusor, and to obtain by the difference, the thrust of the leading edge.

As this leading edge thrust usually corresponds to leading edge pressures lower than p_0 , it is called the leading edge suction. If p_1 is the mean value of the leading edge pressure, the suction force is the product of $-(p_1 - p_0)$ and the front area of the lip, A_1 (fig. 28).

Knowledge of p_1 - that is to say, of the mean leading edge overspeed - as a function of A_1 allows us to discuss the risk of a subsequent flow separation and to orientate the preliminary design of the lip thickness.

Inversely, knowing the lip suction as limited by a separation criterion allows us to calculate the pressure recovery by using the general relation.

If the leading edge is sharp, without any lip suction, the general relation gives the value of the forces which must be applied on the surfaces of an auxiliary passage to obtain the ideal thrust. The result of this calculation can also be used as a first guideline when defining the passage geometry.

1.6. AIR INTAKE RADAR CROSS SECTION (R.C.S.) (fig. 29)

Air intake R.C.S. is a new problem which can only be mentioned here because all the studies devoted to this subject are classified. Nevertheless, it's a very important problem if one considers that the R.C.S. of the aircraft intakes can easily represent up to 50% of the entire R.C.S. of the aircraft.

Upper surface intakes have been suggested as a mean of escaping radar detection, but they don't completely solve the problem, due to the existence of the high altitude airborne alert systems. Moreover, upper surface flow conditions are not the best ones for an intake when considering a large domain of flight manoeuvres.

1.7. THEORETICAL CALCULATION METHODS

General non-viscous or viscous theoretical calculation methods are used for designing the air intakes.

An example of application of the finite volume method is reported on fig. 30. This method seems well adapted to intake flow calculation.

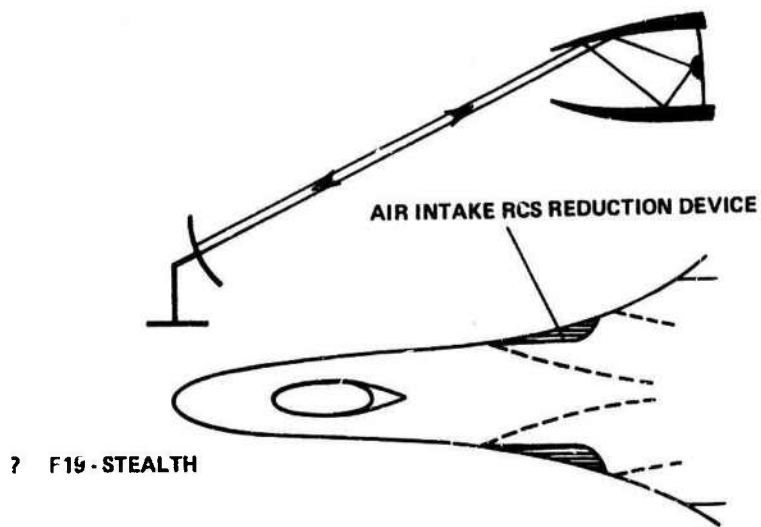


Fig. 29 - Air intake Radar Cross-Section (R.C.S.).

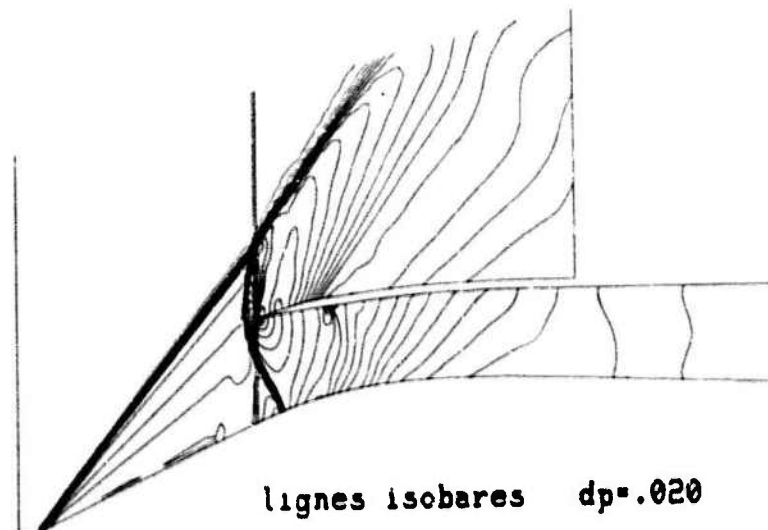
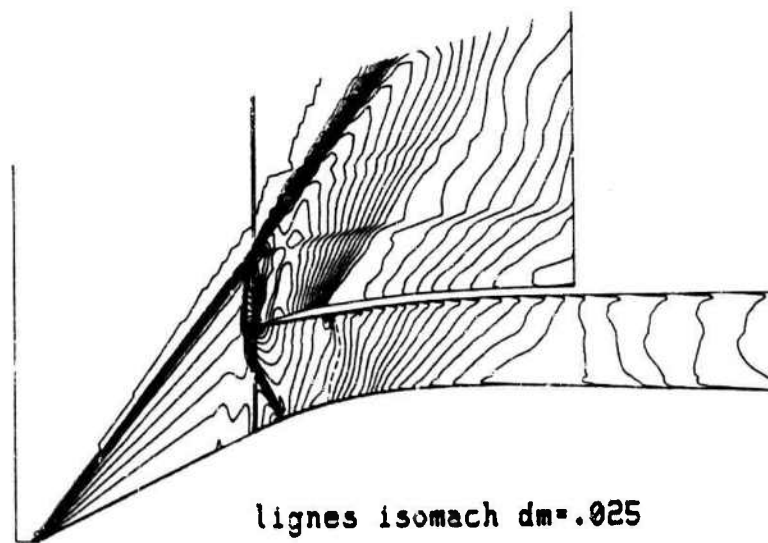


Fig. 30 - Finite volume theoretical method application [Borrel, Montagné, 85].

However, only the main features of the intake definition and of the intake airframe integration can be designed on the basis of theoretical calculations. Detailed adjustments like boundary layer control or local shape modifications, and precise evaluations of pressure recovery, internal flow distortion or inlet drag are based on wind tunnel model tests.

I.8. WIND TUNNEL AIR INTAKE TEST TECHNIC

As boundary layer phenomena are mainly involved in air intake performance, it is important to simulate the flight Reynolds number in the air intake wind tunnel tests.

This is usually achieved by large scale models limited to the forward part of the airplane, as sketched on fig. 31.

Pressure recovery and engine face flow distortion are measured by total pressure probes equipping the engine face station.

The intake flow exhaust system includes mass flow measurement and control devices.

Partial drag measurement of the forward part of the aircraft and the intakes is very useful for comparing small geometry difference effects, like rounded lips, local leading edge cuts, or boundary layer control devices.

An example of such a drag measurement system is sketched on fig. 31.

The forward part of the model is sustained by a balance, and calibrated seals are installed at the external cut of the fuselage and intake skin, and at the internal cut of the intake duct.

In order to obtain the drag of the forward fuselage and intake, it is necessary to subtract from the balance force measurement, the internal drag of the captured stream flow from A_0 to A_2 . This term is obtained by knowing the intake mass flow and the exhaust flow momentum which is derived from the flow survey at the engine face station.

Complete model drag measurements are necessary in order to evaluate the complete aircraft drag, or to compare the drag of various configurations very different in nature.

The wind tunnel test arrangement is presented on fig. 32 ("second step").

The model is supported by an internal balance. In order to know exactly the internal drag which is to be subtracted from the balance force, it is useful to have the internal duct terminated by a throat, as indicated on the figure.

A precise knowledge of the throat flow momentum can be obtained if the mass flow is calibrated by a preliminary test, as presented on fig. 32 ("first step"). For this test, the balance is not used, but the model exit throat is equipped with a mass flow meter installed behind it.

I.9. NON-UNIFORM ENGINE FACE FLOW QUALIFICATION

I.9.1. Pressure recovery definition

As the real engine face flow is never uniform, an equivalent uniform flow has to be defined, the stagnation pressure of which will be used to represent the pressure recovery of the intake (fig. 33).

A uniform flow being defined by 4 parameters, 4 relations have to be established.

Three of them are unanimously adopted : the conservation of :

- the area,
- the mass flow,
- the total enthalpy.

Marking by upper dashes the quantities related to the equivalent uniform flow (or "mean flow"), we have :

$$\overline{A}_2 = A_2$$

$$\frac{\overline{p}_{12} \overline{A}_2}{\sqrt{\overline{T}_{12}}} = [] \cdot \int_{(A_2)} dq_m \quad dq_m : \text{local mass flow. } [] : \text{Cst. (I.1.2).}$$

$$C_p \overline{T}_{12} = \int_{(A_2)} \frac{H_{12} dq_m}{q_m}$$

The fourth assumption is more controversial.

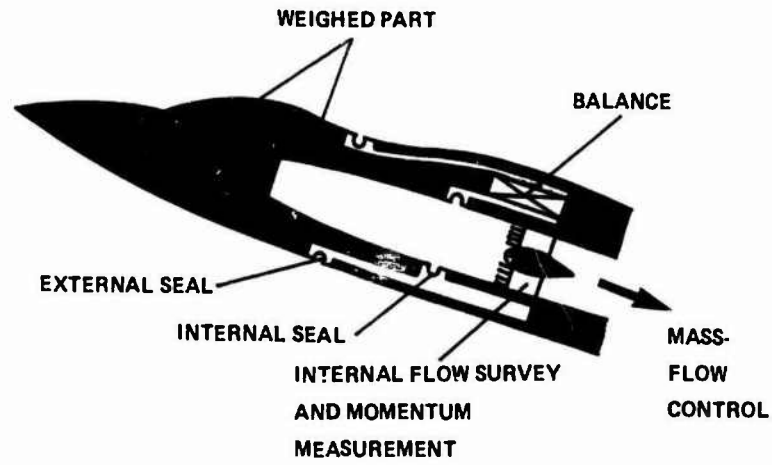


Fig. 31 - Internal flow survey and partial drag measurement.

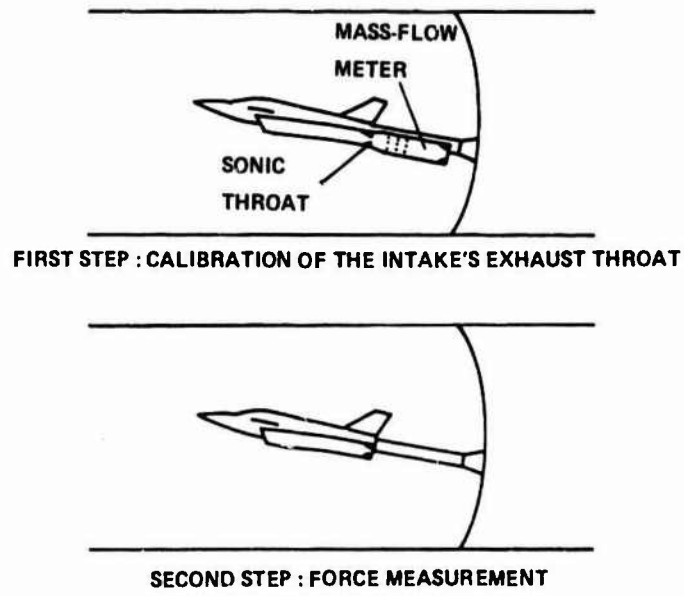


Fig. 32 - Complete model drag measurement.

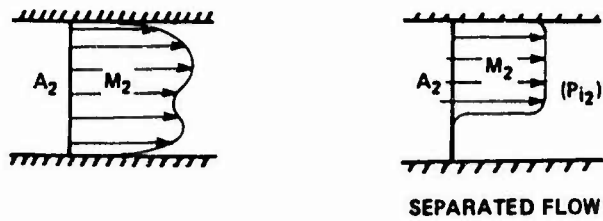


Fig. 33 - Engine mean flow conditions.

A "functional" definition has been proposed [AGARD AR 182] :
 If an ideal compressor is supposed to supply some work to each stream tube of the real flow in order to raise the pressures to a given common level p_{i3} at the compressor exit, the mean flow is defined by the condition that, applying the same compressor total work to it, the same exit pressure p_{i3} is obtained.

The ideal compressor being supposed to be adiabatic and isentropic, the compressor work w is :

$$w = \int_{(A_2)} (H_{i3} - H_{i2}) dq_m$$

$$\text{with } H_{i3} = C_p T_{i3} = C_p T_{i2} \left(\frac{p_{i3}}{p_{i2}}\right)^{\frac{\gamma-1}{\gamma}}$$

Then,

$$\left[C_p T_{i2} \left(\frac{p_{i3}}{p_{i2}}\right)^{\frac{\gamma-1}{\gamma}} - H_{i2} \right] q_m = \int_{(A_2)} \left[C_p T_{i2} \left(\frac{p_{i3}}{p_{i2}}\right)^{\frac{\gamma-1}{\gamma}} - H_{i2} \right] dq_m$$

or

$$\left(\frac{p_{i3}}{p_{i2}}\right)^{\frac{\gamma-1}{\gamma}} = \int_{(A_2)} \frac{T_{i2}}{T_{i2}} \frac{1-\gamma}{\gamma} \frac{dq_m}{q_m}$$

This result expresses the mean stagnation pressure $\overline{p_{i2}}$ as the integration of the local values of p_{i2} balanced in a certain way by the local mass flow dq_m .

A simpler fourth assumption is also proposed in order to directly balance the local values of p_{i2} by the mass flow dq_m .

These definitions have, in fact, the drawback of not penalising the intake when a part of the intake flow is separated, as sketched on fig. 33. As $dq_m = 0$ for the separated part of the flow, the equivalent mean flow would have the same pressure recovery as the outer flow.

If an engine is fed with such a separated flow, the loss of thrust would be entirely attributed to the real compressor (which is not ideal) but not to the intake. Such a definition can of course be very interesting for the intake designer, but not for the engine manufacturer.

Another class of definitions is based on the assumption of the momentum conservation, which corresponds to a uniform flow supposed to be obtained by a natural mixing process in a constant area duct without wall friction.

In this case, the fourth relation is :

$$\overline{p_2} (1 + \gamma M_2^2) A_2 = \int_{(A_2)} p_2 (1 + \gamma M_2^2) dA_2$$

However, as the engine Mach numbers are relatively small, some simplifications are also used :

- By ignoring the terms in γM_2^2 respectively to 1, we obtain :

$$\overline{p_2} A_2 = \int_{(A_2)} p_2 dA_2$$

Another advantage of this very simple definition is that only the measuring of the mass flow and the static pressure are necessary to obtain the mean pressure recovery. Thus, this definition is used when the engine face station is not equipped with total pressure probes.

- By ignoring the terms in $\frac{\gamma M_2^2}{2}$ respectively to 1 (as is usual in incompressible flow), we obtain :

$$\overline{p_{i2}} A_2 = \int_{(A_2)} p_{i2} dA$$

These last three definitions usually give almost the same result. The last one is the most often adopted.

Experience shows that, when the flow is not too disturbed, this definition permits a pretty good evaluation of the engine thrust and so it can be recommended.

1.9.2. Engine face flow distortion

Engine sensitivity to flow distortion - Distortion index basis (fig. 34)

In order to obtain a physical meaning of the flow distortion effect on the engine, it is possible (as was already done in § 1.1.6) to consider the flow behaviour relative to the rotating blades of the compressor.

The two components of this flow are the rotation Mach number $N/\sqrt{\gamma RT_2}$, and the engine face Mach number M_2 . When the flow is uniform, the compressor works on its normal operating line and the flow angle of attack relative to the blades, α_b , is the design angle of attack of the blade profile. In non-uniform flow, if the stagnation pressure p_{12} is lower than its mean value in any part of the engine face area, and taking into account that the static pressure p_2 is practically uniform, the local Mach number is lower than the mean one. As a consequence, α_b is increased locally. If α_b becomes too high, a separation takes place on the upper surface of the blade, and compressor surge can occur.

On the compressor characteristic curves (fig. 34), M_2 being locally reduced, for a given value of $N/\sqrt{T_{12}}$, the operating point moves locally towards the surge limit.

Of course, if the low- p_{12} area is of a small extension, the global effect can be very limited.

Then, the surge limit is in fact only encountered when the low stagnation pressure region covers a pretty large sector of the engine face area, for instance 60° .

This general flow condition is the basis of the various distortion indexes which are used by the different engine manufacturers.

Distortion index definitions

Some examples of a flow distortion index are indicated hereafter.

DC60. (Rolls-Royce) (fig. 35)

It's a direct transcription of a 60° sector of low stagnation pressure :

$$DC60 = \frac{(p_{12} \min 60^\circ) - \bar{p}_{12}}{\bar{q}_2}$$

where $(p_{12} \min 60^\circ)$ is the minimum value of the mean value of p_{12} on any sector of 60° of the engine face station,

\bar{p}_{12} is the mean value of p_{12} over the entire section,

\bar{q}_2 is the mean dynamic pressure.

At high RPM, a high level of distortion corresponds to about $DC60 < -0.3$.

K_θ . (Pratt and Whitney) (fig. 35)

If, on each radius R_j of the engine face station divided into rings of equal area, p_{12} is plotted as a function of the radius angle θ , a Fourier analysis of the curve gives p_{12} in the following form :

$$p_{12}(\theta)_j = A_0 + \sum_1^{\infty} A_n \cos(n\theta + \phi)$$

A_1 qualifies a unique large section of low p_{12} , A_2 qualifies a 2-sectors type of low p_{12} , and so on. As the largest sectors are the most efficient, A_n is balanced by $1/n^2$, and the highest value of the successive terms A_n/n^2 (limited to $n = 4$) is selected to qualify the ring distortion coefficient A_j :

$$A_j = \left[\frac{A_n(j)}{n^2} \right]_{n=1 \text{ to } 4} \text{ max.}$$

As the rotation speed is proportional to the radius, A_j terms are balanced by W_j/R_j (usually $W_j = 1$), whence :

$$K_\theta = \frac{\sum_1^J A_j \frac{W_j}{R_j}}{\bar{q}_2 \sum_1^J \frac{W_j}{R_j}}$$

K_θ can be complemented by the radial distortion index K_{RA} :

$$K_{RA} = \frac{\sum_1^J (\bar{p}_{12} - \bar{p}_{1j}) \frac{1}{R_j}}{\bar{q}_2 \sum_1^J \frac{1}{R_j}} \text{ where } \bar{p}_{12} - \bar{p}_{1j} = 0 \text{ if } \bar{p}_{1j} > \bar{p}_{12}$$

Then a complete distortion index K_A is defined by :

$$K_A = K_\theta + K_{RA}$$

At high RPM, a high level of distortion corresponds to about $K_\theta > 0.3$, and $K_A > 0.6$.

IDC (General Electric)

In the same manner as DC60, IDC is based on the lowest values of p_1 at the engine face station :

On each ring j of equal area,

$$IDC_j = \frac{\bar{p}_{1j} - (p_{1 \min})_j}{\bar{p}_{12}} \times S_A$$

IDC is completed by a radial distortion index :

$$IDR_j = \frac{\bar{p}_{12} - \bar{p}_{1j}}{\bar{p}_{12}} \times S_R$$

S_A and S_R are some coefficients to be specified for each engine.

They may be equal to 1. Maximum values of IDC_j and IDR_j are selected.

A complete distortion index is defined by :

$$ID = (IDC)_{\max} + (IDR)_{\max}$$

Various distortion index consequences

A comfortable result for the various engine companies in using a specific distortion index is that the sensitivity of competitive engines to the flow distortion is difficult to compare since the result depends on the flow distortion profile which is considered...

Unsteady distortion

If the flow is unstable, the angle of attack α_b of the rotating blade varies in function with the time t as shown in the example on the upper left hand sketch of fig. 36. At a given time, the resulting instantaneous flow stream relative to the blade is as sketched on the right-hand drawing of fig. 36.

It is obvious that to induce a significant separation of the upper surface blade flow, it is necessary for the length l of the region of high incidence flow to be a pretty long part of the blade chord c . Thus, an order of magnitude is given by the condition $l \gg c$.

Let T be the period of the flow fluctuation, and V_b the mean value of the flow speed relative to the blade.

l is equal to $V_b \frac{T}{2}$, whence, the condition : $V_b \frac{T}{2} > c$, or, by projection on the compressor axis (lower sketch of fig. 36), $V_2 \frac{T}{2} > c_\phi$, c_ϕ being the thickness of the rotating stage. Thus, the maximum frequency to be considered is :

$$f_{\max} = \frac{V_2}{2c_\phi}$$

As an example, for typical values like $M_2 = 0.5$, $V_2 = 170$ m/s, $c_\phi = 0.1$ m, $f_{\max} = 850$ Hertz.

This result is coherent with $f_{\max} = 1000$ Hertz which is occasionally indicated for fighter engines.

At a scale of $\frac{1}{5}$, wind tunnel tests of the air intake will require a band pass of 5000 Hertz.

Test equipment and acquisition system

A standard equipment for measuring the distortion is defined, and it seems convenient, at least for military aircraft air intake studies : 8 rakes of 5 probes each, on rings of equal area, are installed at the compressor face station (fig. 37). The probes are Pitot tubes equipped with steady and unsteady pressure transducers. Band pass is 1000 Hertz at scale 1. The duration of acquisition for each measurement point is 30 to 60 seconds, which represents roughly the time for the aircraft to operate under the most severe of the distorted flow conditions in its flight schedule.

In wind tunnel tests, it is important to obtain steady and unsteady distortion index measurements practically in real time in order to compare various configurations and to pilot the test program. However, the number of the high rate samples of the 40 unsteady channels is such that the acquisition and calculation processes are only possible on huge computers which usually are not available in wind tunnel test centers. Simplified systems are then used, some examples of which are given hereafter.

ONERA real time conditional acquisition system (fig. 38)

The core of the system is the "quick acquisition system" activated by the "distortion index analog computer". The analog computer delivers a signal proportional to the value of a given distortion index, like K_ϕ . This signal is used to start the quick acquisition of a given number of pressure distributions (pressure maps) as soon as its value exceeds a given threshold. This threshold is progressively increased as a function of the RMS value of the signal from the beginning of the process.

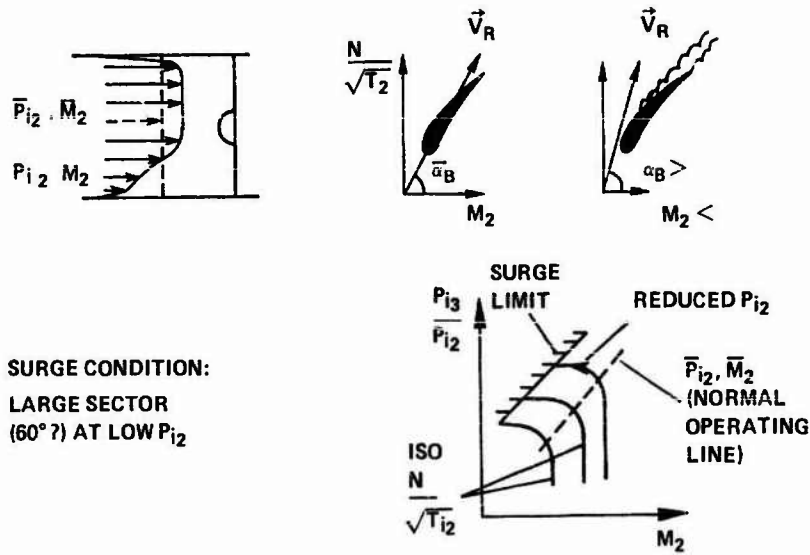


Fig. 34 - Engine flow distortion sensitivity.

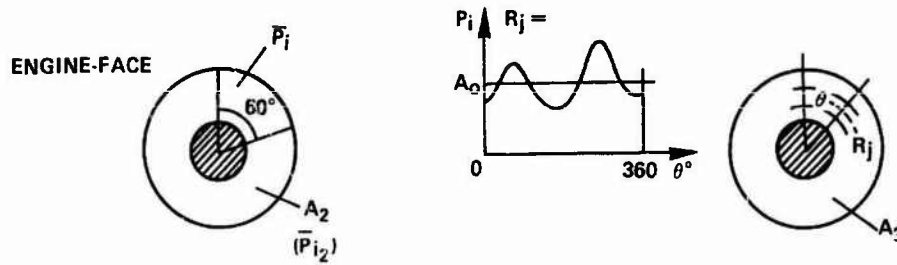


Fig. 35 - Engine face flow distortion index.

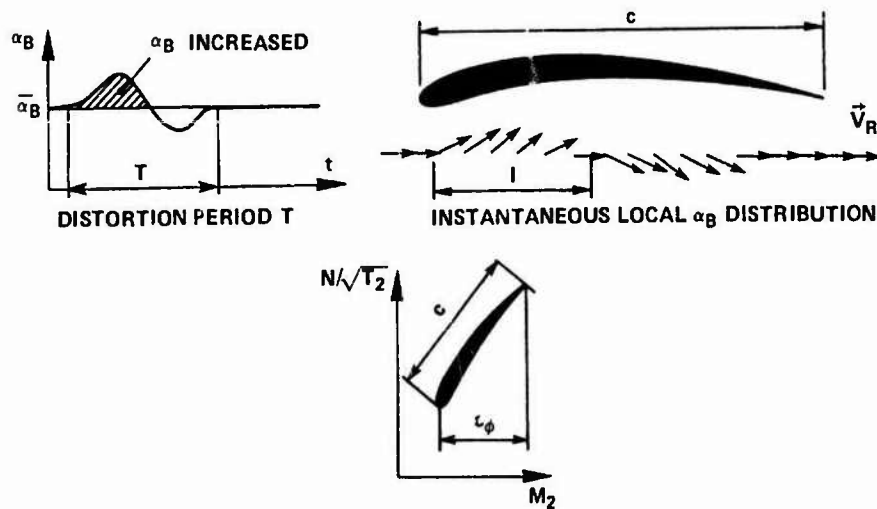


Fig. 36 - Rotating blade relative flow unsteady condition.

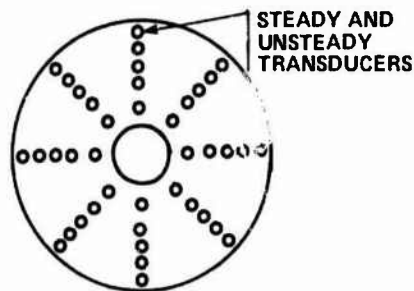


Fig. 37 - Distortion index measurement. Standard equipment.

The quick acquisition is limited to 256 maps of 64 pressures acquired at a maximum rate of 16000 Hertz, and can only be repeated at intervals of 0.5 sec. During this time interval, acquisition is inhibited and storage is transferred to the wind tunnel computer for the calculation of the various distortion indexes, and eventually for the plotting of the pressure maps.

The acquisition system is then reactivated until the threshold is no longer overpassed during a given length of time.

The result is a complete flow analysis, in certain time intervals selected on the basis of a privileged distortion index.

At the same time, a continuous digital record of the 64 channels at a rate of 16000 Hertz is provided by a P.C.M. (Pulse Code Modulator) recorder, but the reading and the data reduction of this record are only possible in deferred time, in order to complete the unsteady distortion analysis, if necessary.

Distortion index analog computer

Distortion index analog computers can be built to obtain in real time the unsteady distortion characteristic of the flow. They are widely used, but, of course, the results are unfortunately restricted to the programmed distortion index.

RMS analysis

Very simpler are the unsteady flow analyses based only on the measurements of the mean and RMS values of the pressure probes. A turbulence scheme is then adopted to convert the results into unsteady pressure maps, and to calculate the distortion indexes. Assumptions on the turbulence vortex radius are proposed by [Melick, 78]. A simpler and random process is proposed by [Borg, 81]. These theories allow the prediction of the distortion within an error margin of about 20%, which often can be considered as acceptable, as regards the unsteady distortion.

II. AFTERBODY

II.1. AFTERBODY BASIC DATA (fig. 39)

. The main parameters defining the afterbody design conditions are :

- the given shape of the upstream part of the afterbody, which is characterized here by a diameter of ϕ_m
- the throat diameter of the nozzle, ϕ_T
- the pressure ratio of the nozzle jet, $\tau = p_{1j} / p_o$.

. ϕ_j , the adapted nozzle exit diameter (jet expanded to the ambient pressure p_o) is directly derived from τ and ϕ_T by the nozzle expansion ratio ϕ_j / ϕ_T which is a function of τ .

. q_b and $p_{1b \text{ max}}$, the mass flow and the maximum available pressure of a secondary flow (cooling flow, intake bleed flow...) are also significant parameters.

Typical values of the afterbody parameters as a function of the flight Mach number M_o are drawn on fig. 39. They are related to the two design flight conditions : cruise flight and maximum reheat.

At cruise flight, the nozzle throat ϕ_T is restricted and the jet is slightly expanded. The nozzle exit ϕ_j is much smaller than the upstream afterbody dimension ϕ_m .

At maximum RPM and reheat, ϕ_T is largely open, and the jet expansion ratio is much bigger. It increases with M_o , and the nozzle exit ϕ_j becomes equivalent to ϕ_m at about a flight Mach number M_o equal to 2.

II.2. CLASSIC AFTERBODY DESIGNS

II.2.1. Long variable flap ejector (fig. 40)

A direct but weight-ridden solution of afterbody adaptation is to adjust the external profile by a series of long variable flaps, and the internal convergent-divergent nozzle by two series of flaps.

Secondary air, q_b , can be injected either into the base of the afterbody, or the throat of the nozzle, depending on the amount of the secondary mass flow and on the maximum pressure $p_{1b \text{ max}}$ available.

Afterbody design study usually proceeds by using ϕ_E (nozzle exhaust diameter) as the optimisation parameter.

At supersonic Mach numbers, by increasing ϕ_E , the internal thrust overtakes a maximum when the jet is exactly adapted (exit pressure $p_E = p_o$), but the external drag continuously reduces, so the optimum value of ϕ_E corresponds to a slightly overexpanded nozzle (fig. 40).

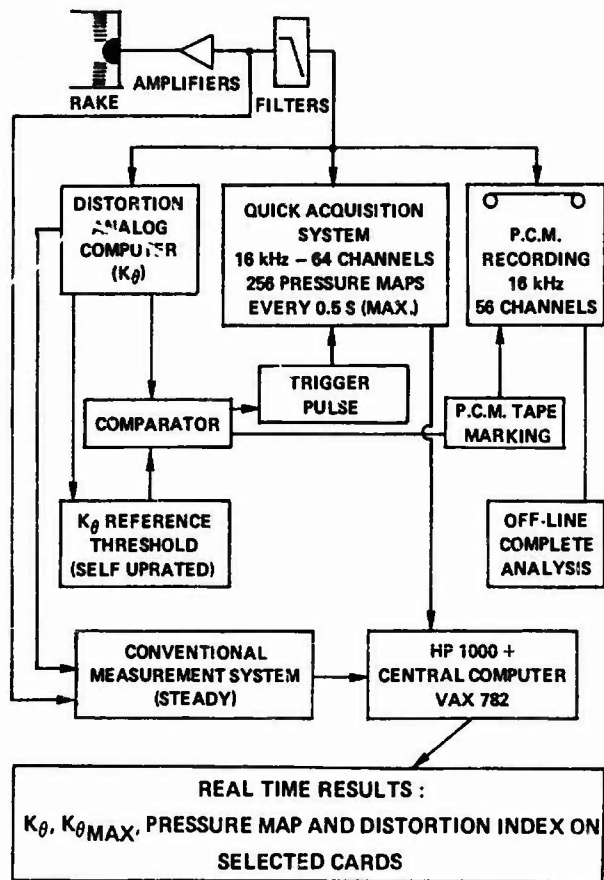


Fig. 38 - Unsteady flow distortion index measurement. ONERA hybrid system with conditional real time acquisition.

AFTERBODY BASIC DATA

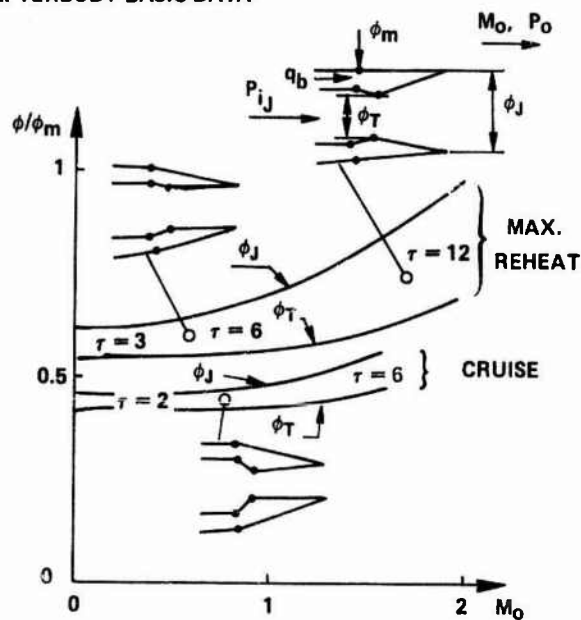


Fig. 39 - Afterbody basic data : $\phi_m, \phi_T, \tau = P_{ij}/P_o (\approx \phi_J), q_b, P_{ib_{max}}/P_o$.

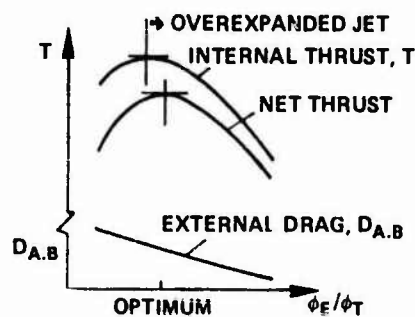
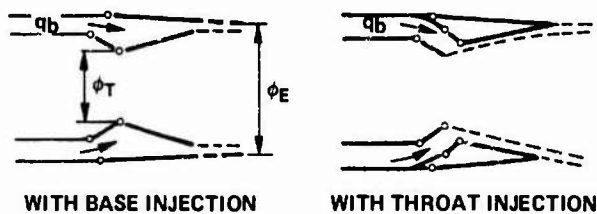


Fig. 40 - Long (heavy) variable flap ejector. Supersonic adaptation.

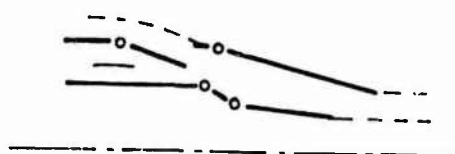


Fig. 41 - Subsonic auxiliary door.

Concerning the secondary flow, the maximum thrust is obtained by using the maximum pressure $p_{i,b \text{ max}}$ available. If this pressure is pretty high, as it is for the bleed flow of an intake throat, it is more efficient to admit the secondary flow to the nozzle throat due to the possibility of a supersonic expansion of this flow in the diverging nozzle.

If the secondary mass flow is very small, or of a low maximum pressure, it is simpler as well as acceptable to blow it towards the afterbody base.

At subsonic cruise Mach number and reduced RPM, it would be necessary to close up the nozzle exit to avoid an internal overexpansion. However, in this case, external overspeed and separation would occur on the afterbody boattail. In order to avoid this occurrence, it is possible to combine a moderate closure of the external flaps with the opening of auxiliary doors (fig. 41). In this case, the door flow fills up the space between the external flaps and the internal flaps adapted to the jet expansion.

II.2.2. Fixed shroud, trailing edge flap ejector (fig. 42)

A less weight-ridden but also less performing solution of afterbody design is the one sketched on fig. 42.

A fixed shroud is equipped with a series of trailing edge flaps which permits the simultaneously varying of the boattail shape and the nozzle exit area. Auxiliary doors are open at subsonic flight conditions. The door flow is then full and fills the space between the adapted jet and the nozzle flaps.

In fact, in the same flight conditions, it is also possible to admit more secondary flow rather than door flow at the throat of the diverging nozzle. The result presented on fig. 43 shows that the larger the length L of the nozzle, the higher the optimum value of the secondary mass flow. In the particular conditions of the study, an auxiliary door opening would only improve the thrust at values of $\frac{L}{\phi}$ larger than 1. Such large values of $\frac{L}{\phi}$ are only encountered when the design flight Mach number is pretty high, of the order of M_0 equal to 2.

Actual solutions of fixed shroud, trailing edge flap ejector with reverse capability, as respectively applied to prototype and on-line "Concordes" are presented on fig. 44.

The prototype afterbody includes a fixed shroud and trailing edge flaps, auxiliary doors, nozzle throat flaps, and internal reverse bucklets, the closure of which opens a passage to reverse cascades.

The final design for on-line aircraft is simpler. It includes a "TV" (television) nozzle exit shape which is more convenient for the case of two side-by-side engines. The variation of the nozzle exit area, the opening of an auxiliary passage, and the reverse operation are ensured by only adjusting the closing up of the rear bucklets. With such a solution, flexibility and aerodynamic performance are of course more limited, but the weight is greatly reduced.

II.2.3. Two-flap ejector nozzle (fig. 45)

The two series of flap ejector nozzle which is sketched on fig. 45 represents a still more simplified solution of afterbody adaptation. It is used on a lot of combat aircraft, for instance on the "Mirage" family.

Only the throat area and the external boattail are adjustable with such a system.

As shown on fig. 45, the distance L between the throat and the trailing edge of the external flaps is a very sensitive parameter for designing the length of the external flaps in supersonic flight conditions. If this distance is too short, the internal jet expands up to the external flow, which corresponds to an overexpanded jet and to a low base pressure p_b penalizing the thrust. The optimum distance is the one for which the jet is correctly expanded and reattached at the extremity of the flaps.

The subsonic adaptation is different. In subsonic flow, it is expedient to close the external flaps to profit from the subsonic recompression of the external flow on the flaps. However, this recompression is limited to maximum flap angle values as a function of the Mach number. A pretty general law for these values is given on fig. 46.

On the other hand, this maximum closure of the flaps is often not sufficient to achieve an adapted expansion of the internal jet. In such a case, if reattachment occurs, the jet is overexpanded, the base pressure is low, and the thrust is penalized, so it is more advantageous to limit the closure of the flaps, at the expense of the external drag and to leave the internal jet detached. The limit is given on fig. 47, which summarizes the results of a lot of tests within a large domain of flow conditions. The distance H between the jet boundary and the flap is obtained by a calculation of the jet expansion in an ambient pressure p_0 by the method of characteristics. The drop in the base pressure p_b begins for distance H smaller than 0.4 the length of the jet boundary.

This limit can be improved by secondary air flow injection, as indicated on fig. 48.

II.3. TWO-ENGINE AFTERBODY DESIGN

II.3.1. Twin engines integration (fig. 49)

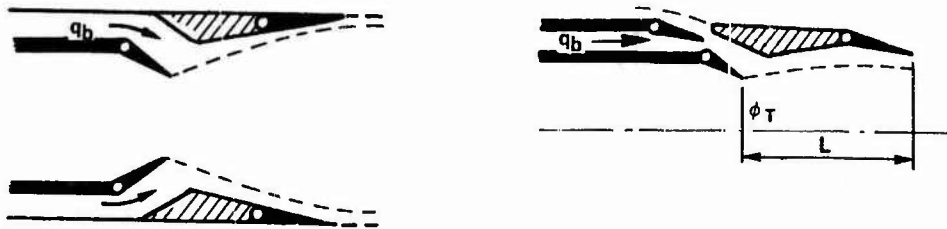


Fig. 42 - Fixed shroud ejector with trailing edge flaps and auxiliary door.

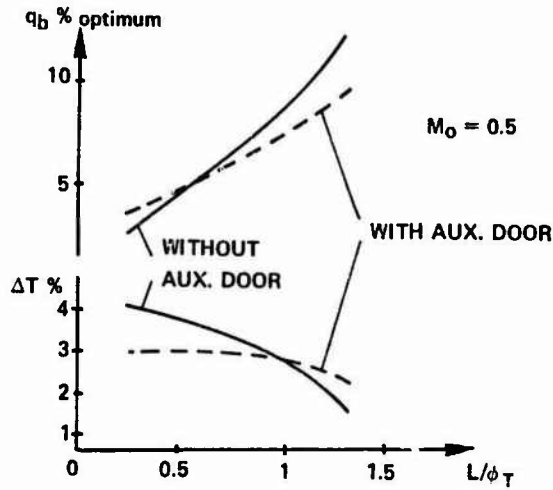


Fig. 43 - Secondary flow q_b and auxiliary door effectiveness [Hardy, 83].

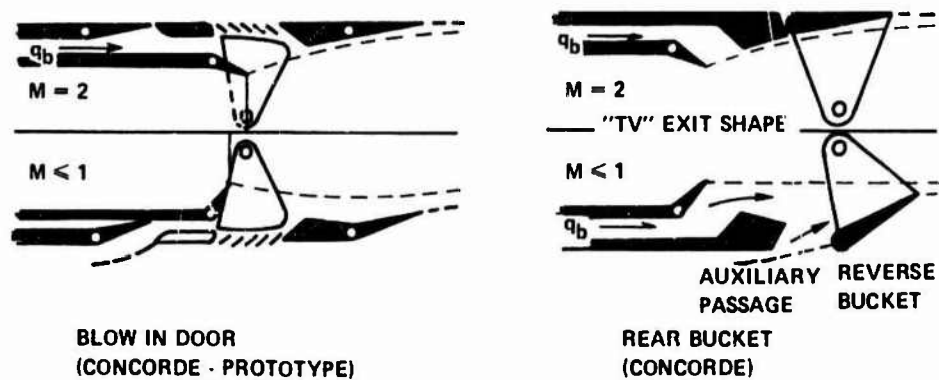


Fig. 44 - Fixed shroud ejector with reverse. Actual design

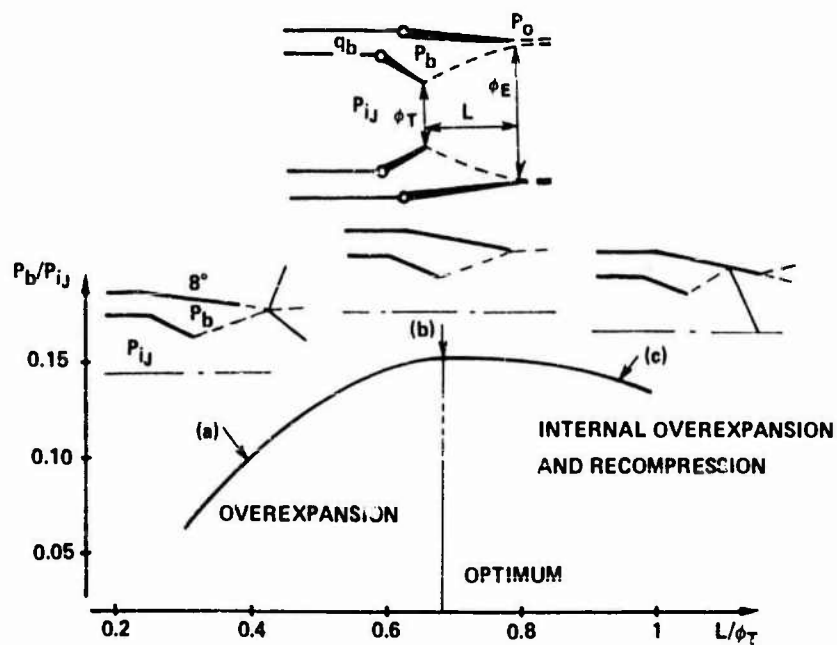


Fig. 45 - Two flap (light) ejector nozzle. Supersonic flap length adjustment [de Richemont, Delery, 84].

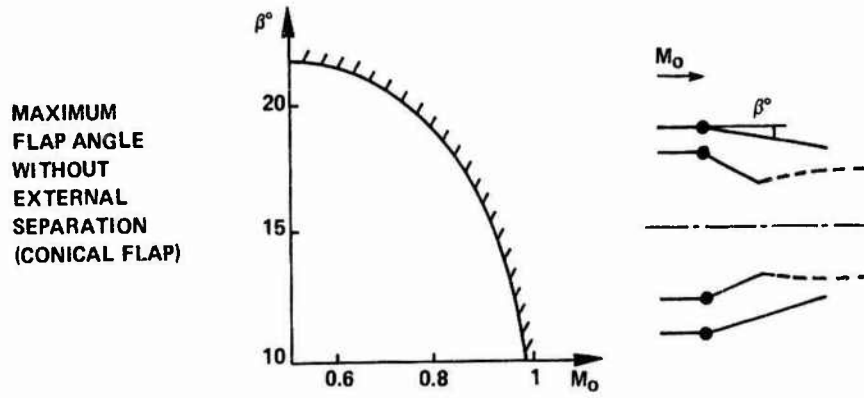


Fig. 46 – Two flap ejector nozzle. Subsonic external drag. [Carrière, Sirieix, Hardy, 68].

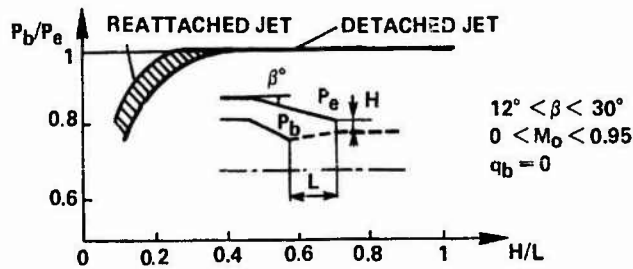


Fig. 47 – Two flaps ejector. Subsonic internal performance. Jet reattachment limit [Carrière, Sirieix, Hardy, 68].

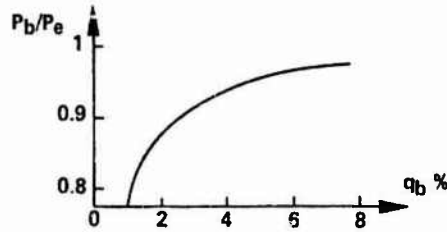
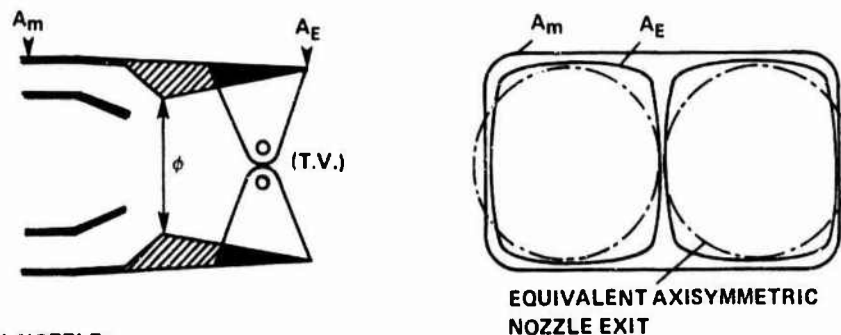


Fig. 48 – Two flap ejector. Subsonic internal performance. Secondary flow effect.



T.V. NOZZLE :
 EXTERNAL DRAG GAIN (% OF THRUST) : 0.6
 INTERNAL THRUST LOSS : - 0.15
 NET THRUST GAIN (%) : 0.45

Fig. 49 – Twin engine aircraft nozzle installation. 3D (TV) nozzle [Hardy, 71].

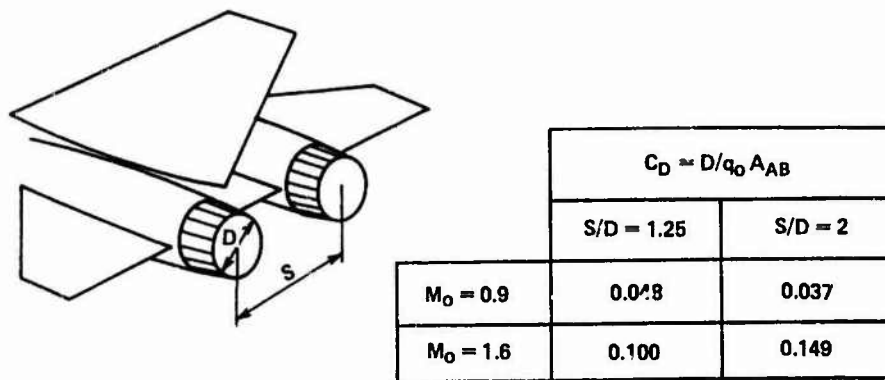


Fig. 50 - Two engines afterbody design. Spacing effect [Richey, Surber, Laughrey, 74].

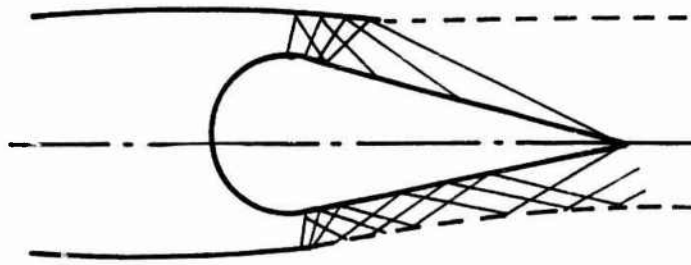
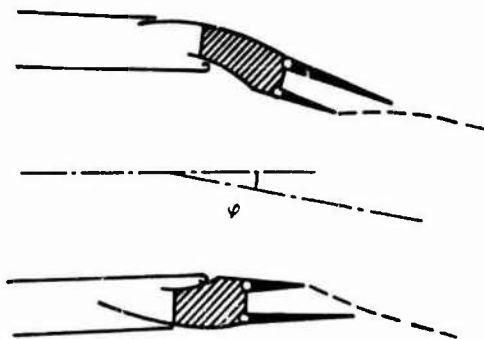


Fig. 51 - Plug nozzle.



	THRUST LOSS	ψ/ψ_{GEOM}
$\varphi < 15^\circ$	0.3 %	1
$\varphi = 20^\circ$	0.6 %	1.1

Fig. 52 - Vectoring axisymmetric nozzle [Drevillon, Fer, 83].

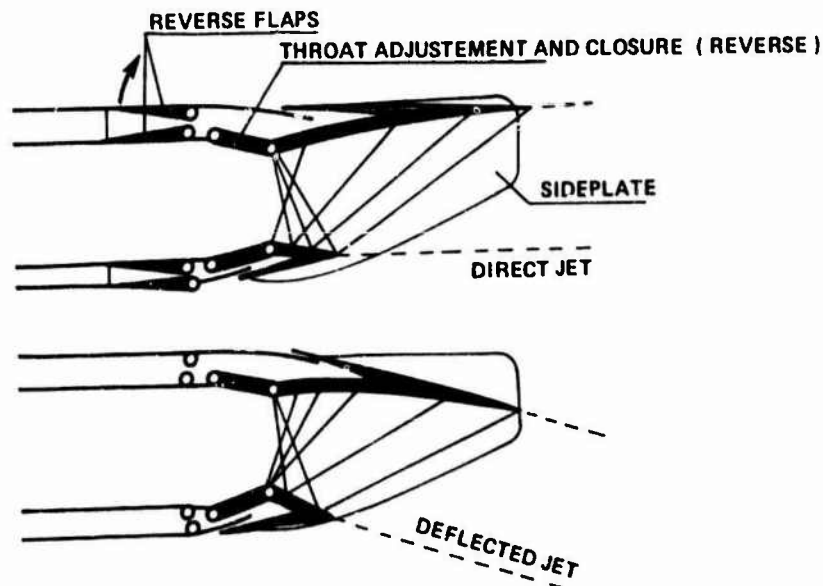


Fig. 53 - Vectoring 2D nozzle with reverse.

A first example of an integration study of a two-engine configuration is the one of the twin engines of the "Concorde".

In this case, the best integration was obtained by a 3-D "TV" (television) shape of the nozzle, as shown on fig. 49.

In comparison with a twin axisymmetric side-by-side exhaust system, the result of the study at flight Mach number $M_0 = 2$ shows that the 3-D shape of the nozzle causes a loss of internal thrust of 0.15%, but the external drag of the afterbody is reduced (0.6% gain of thrust) so the net thrust is improved by 0.45%.

II.3.2. Nozzle spacing of a two-engine afterbody (fig. 50)

A second example of an optimisation study of a two-engine fighter configuration is the design of the spacing between the exhaust nozzles.

In such a case, a large spacing is advantageous in subsonic speed due to the recompression of the flow on the boattail between the nozzles, but it is disadvantageous in supersonic speed, due to the supersonic overexpansion on the same boattail.

This is clearly indicated by the drag terms given on fig. 50 at $M_0 = 0.9$ and $M_0 = 1.6$, and is a pretty common example of the conflict between the subsonic and the supersonic performances.

II.4. PLUG NOZZLE (fig. 51)

Axisymmetric plug nozzles, as represented on fig. 51, are very attractive from the aerodynamic point of view, due to the smooth recompression of the flow around the emerging spike at subsonic speed. They have been intensively studied in the past, but without practical development. The reasons for this are certain technical difficulties arising from strength and cooling problems on the plug, and also performance losses when designing an actual solution with variable throat area and secondary flow.

II.5. THRUST VECTORING

VTOL aircrafts are not considered within the framework of this paper.

For more conventional aircraft however, new thrust vectoring systems are being developed which represent an important field of research for the next generation of fighters. The aim is to improve aircraft manoeuvrability. The use of forward "canard" control surfaces on the present fighters also affords the opportunity to balance the rear lift of a vectored nozzle.

Two types of solutions are presented hereafter as examples.

II.5.1. Vectoring axisymmetric nozzle (fig. 52)

An axisymmetric vectoring nozzle proposed by the SNECMA is presented on fig. 52. It's a classical "two series of flaps" ejector nozzle, which entirely pivots ahead of the nozzle throat. The advantage of such a solution is that the thrust can be oriented in any direction.

The thrust performance and the deviation effectiveness are indicated on the figure. A surprising result is that at high angle of rotation, the jet is more deviated than the nozzle axis. This effect is imputed to the detailed flow field ahead of the nozzle throat.

II.5.2. Vectoring 2-D nozzle with reverse (figs. 53, 54)

Another class of solutions is the vectoring 2-D nozzle realized by 2-D flap arrangements. These solutions can be more efficient due to the more favourable external flow field interferences, but there are also more weight-ridden than the axisymmetric ones.

Many detailed arrangements have been proposed. One of them is presented on fig. 53.

The throat area is made adjustable by a first pair of flaps.

The nozzle expansion ratio and the flow deviation are insured by a second pair of profiled flaps.

Among the advantages of this solution, it is possible to totally close the nozzle throat by the throat flaps, and to ensure an efficient reverse flow by simultaneously opening reverse flaps.

The benefit of very favourable external flow field interferences is substantiated on fig. 54. In subsonic flow, a large induced lift is added to the lift alone of the deviated jet.

II.6. THEORETICAL METHODS

A typical afterbody theoretical flow field calculation is presented on fig. 55 as an example.

The internal transonic flow field up to the nozzle throat is calculated by a finite difference method using hodographic parameters which are well adapted to the straight parts/sharp edges internal duct shape.

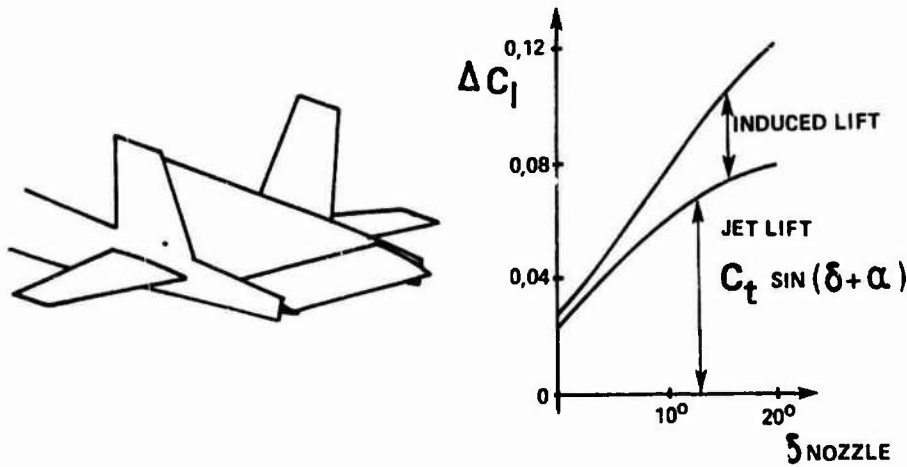


Fig. 54 - Vectored 2D nozzle. Jet induced lift [Berrier, Re, 78].

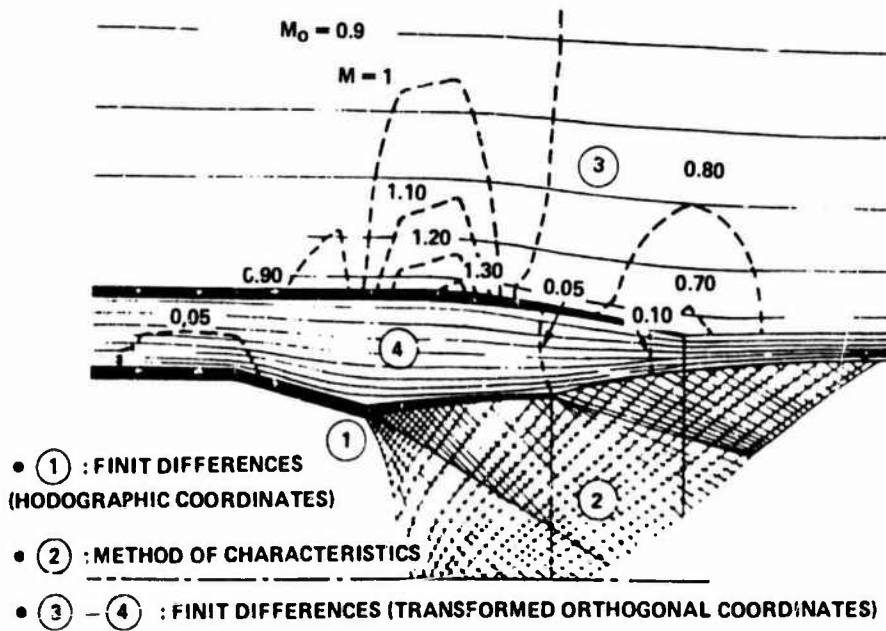


Fig. 55 - Afterbody study. Theoretical methods [Hardy, Dutouquet, 81].

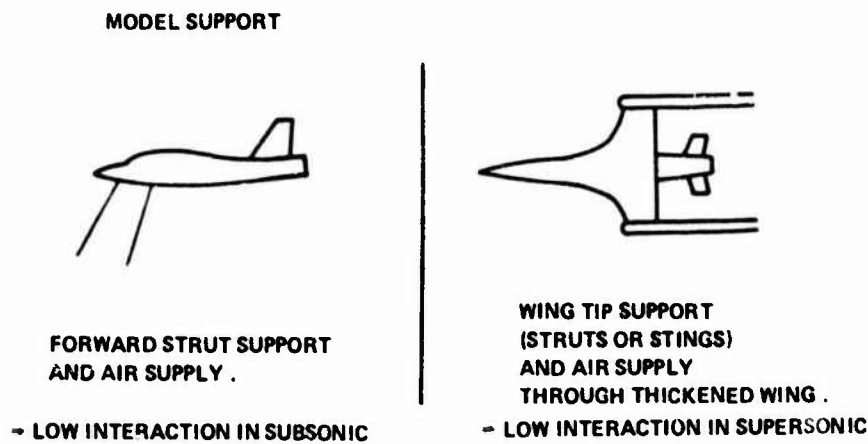


Fig. 56 - Afterbody wind tunnel test mounting.

The supersonic nozzle flow and the jet expansion are calculated by the method of characteristics which gives a precise description of the jet and a fine evaluation of the internal thrust.

The secondary flow and the external flow are calculated by a finite difference method in a suitable coordinate system.

Coupling processes are insured between the various calculations, including boundary layer calculations and viscous shear line displacement effect.

II.7. AFTERBODY WIND TUNNEL TEST TECHNIC

II.7.1. Afterbody model support (fig. 56)

The most difficult problem is to design a model support which doesn't disturb the flow field in the vicinity of the afterbody.

The difficulty of designing such a support is amplified by the thickness of the support which must supply the compressed air to the exhaust nozzle and which must also resist the aerodynamic loads.

Two types of supports are used, which are sketched on fig. 56.

The "forward" strut presents the advantage of not modifying the area rule of the rear part of the model. It seems that this kind of support is the less unfavourable in subsonic flow.

The "wing tip" support can be designed in such a way that the waves attached to the support no longer reach the afterbody above a given supersonic Mach number. Although the wing shape has to be modified to admit the passage of the compressed air, the supersonic perturbation of such an arrangement can be quite reduced, and less penalizing than the forward strut rig.

II.7.2. Internal balance (fig. 57)

The net thrust measurement of the afterbody can be obtained by an internal balance arrangement, as sketched on fig. 57.

External and internal seals are necessary to separate the weighted part from the forward part of the model. The momentum of the internal flow at the separation section which is an important term of the weighting system must be calibrated. In some cases, the flow enters the weighted part perpendicularly to the longitudinal axis in order to minimize the flow momentum effect.

The measured thrust of the afterbody is compared on the same rig to the drag of the afterbody of the complete aircraft model as it is wind tunnel tested on a sting support, in order to obtain the net thrust of the aircraft.

Of course, some corrections must still be applied, such as the hot gas effect corrections which can be studied on a static test bench.

A more precise evaluation of the afterbody effect on the aircraft performance would also have to take into account the lift and the moment of the afterbody forces by using a three component balance.

As a matter of fact, such an internal balance is not easy to realize and calibrate and so it is sometimes more practicable to use an external balance arrangement at the wall of the wind tunnel as described hereafter.

II.7.3. External balance (fig. 58)

Another possibility for measuring the afterbody performance is to put the complete rig (support strut and aircraft model) on a wall balance of the wind tunnel, the balance being equipped with a calibrated uncoupling system of compressed air supply, as sketched on fig. 58.

It is then easier to measure the three components (or the six components, if necessary).

Again, the comparison of the real afterbody (with the real jet) to the reference afterbody of the complete aircraft model must be made on the same support.

Some details on the performance evaluation process are presented in the next section.

II.7.4. Afterbody test bookkeeping and performance evaluation (fig. 59)

For a more detailed evaluation of the performance of the afterbody, it is necessary to know the reference thrust of the nozzle equipping the model of the real afterbody, T_{ref} . This thrust can be defined by a test of the nozzle on a static test bench.

Thus, knowing the forces applied to the reference afterbody model configuration (D_{ref}) and to the real afterbody (D_T), as described on fig. 59, the exhaust system installation drag can be defined and obtained by the following equation :

$$D_{installation} = D_T - (D_{ref} - T_{ref}).$$

D_{inst} represents the sum of the internal thrust loss and the external afterbody drag (compared to the reference afterbody).

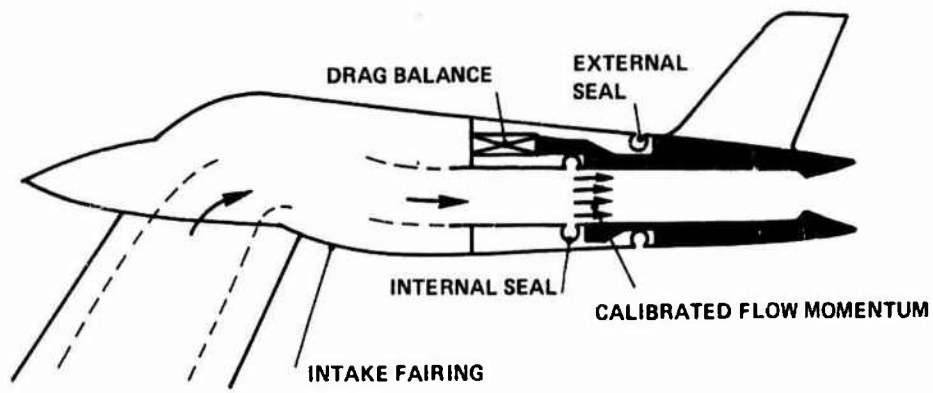


Fig. 57 — Afterbody wind tunnel test. Internal balance arrangement.

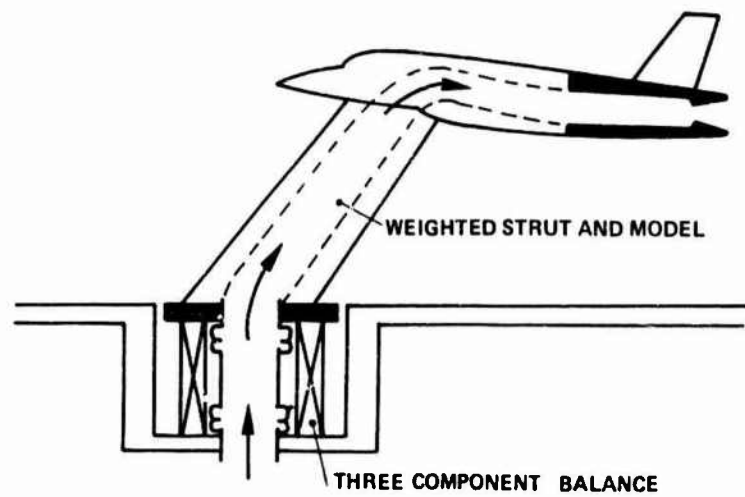


Fig. 58 — Afterbody wind tunnel test. Wall balance arrangement.

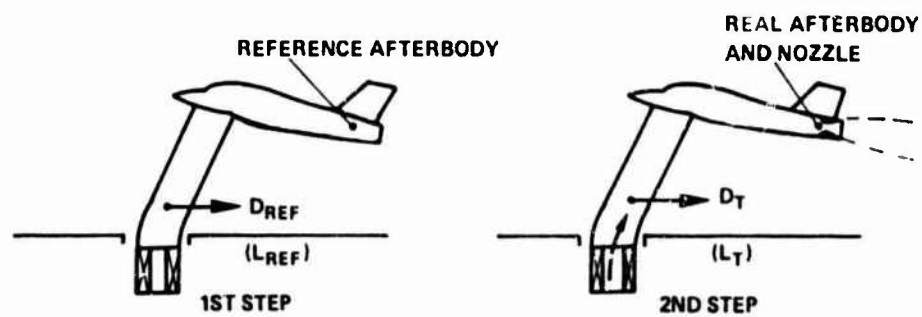


Fig. 59 — Nozzles afterbody installation test sequences.

If there is a lift effect, ΔL being the difference between the lift forces measured with the real afterbody and with the reference afterbody, it can be established [Leynaert, 74] that this lift improvement is equivalent to a drag reduction given by :

$$\Delta D = -\Delta L \frac{dC_D}{dC_L},$$

where $\frac{dC_D}{dC_L}$ is the inverse of the local slope of the polar curve of the complete aircraft.

By converting in the same way, the difference of the moments of the afterbody forces by an equivalent equilibrium drag, the net installation drag of the exhaust system can finally be obtained.

III. REFERENCES

- General references

- P. Carrière, J. Leynaert : Prises d'air - Tuyères. Cours de l'Ecole Nationale Supérieure de l'Aéronautique et de l'Espace, Av. Edouard Belin, Toulouse, France.
- J. Seddon and E.L. Goldsmith : Intake aerodynamics. Collins, 8, Grafton Street, London (1985).

- General AGARD publications relating to air intake and afterbody study

- Supersonic inlets (I. FARO). AGARDograph 102 (1965).
- Aerodynamics of powerplant installation. AGARDograph 103 (1965).
- Advanced components for turbojet engines - AGARD CP 34 (1968).
- Aerodynamic interference - AGARD CP 71 (1970).
- Inlets and nozzles for aerospace engines - AGARD CP 91 (1971).
- Airframe/engine integration - AGARD LS 53 (1972).
- Supersonic ejectors - AGARDograph 163 (1972).
- Aircraft performances - prediction and method of optimization - AGARD LS 56 (1973).
- Aerodynamic drag - AGARD CP 124 (1973).
- Prediction methods for aircraft aerodynamic characteristics - AGARD LS 67 (1974).
- Airframe/propulsion interference - AGARD CP 150 (1974).
- Performance prediction methods - AGARD CP 242 (1977).
- Variable geometry and multicycle engines - AGARD CP 205 (1976).
- Aerodynamics of powerplant installation - AGARD CP 301 (1971).
- Technology for sustained supersonic cruise and manoeuvre - AGARD CP 358 (NATO confidential) (1983).

- Cited individual references

- AGARD AR 182 (1983) - Méthode d'établissement des caractéristiques moyennes dans les écoulements internes hétérogènes.
- Berrier B.L., Re R.J. (1978) - A review of thrust vectoring schemes for fighter applications. AIAA paper n° 1023.
- Borg R. (1981) - A synthesis method for estimating maximum instantaneous inlet distortion based on measured inlet steady state and RMS pressures. AGARD CP 301.
- Borrel M., Montagné J.L. (1985) - Numerical study of a non-centered scheme with applications to aerodynamics. 7th AIAA Computational Fluid Dynamic Conference, July 85 - ONERA TP 1985-75.
- Carrière P., Sirieix M., Hardy J.M. (1968) - Problèmes d'adaptation de tuyères. AGARD CP 34, part 2.
- Drévilion M. Fer R. (1983) - Vectored thrust afterbody nozzles for future combat aircraft. 6th ISABE.
- Hall G.N. (1974) - A criterion for prediction of airframe integration effects on inlet stability with applications to advanced fighter aircraft. AGARD CP 150.
- Hardy J.M., Dutouquet L. (1981) - Etudes d'écoulements multiflux par juxtaposition de processus numériques différents. L'Aéronautique et l'Astronautique n° 90, 1981-5.

- Hardy J.M. (1983) - Exhaust system for combat aircraft optimized for supersonic cruise. AGARD CP 358.
- Hawkins J.E. (1974) - YF 16 inlet design and performance. AIAA paper 74-1062.
- Leynaert J. (1965) - Fonctionnement du piège à couche-limite interne d'une prise d'air à compression supersonique externe - AGARDograph 103.
- Leynaert J. (1974) - Problèmes d'interaction entre la prise d'air et l'avion - AGARD CP 150.
- Leynaert J., Brown T.W., Collard D. (1974) - A study of the Concorde air intake at yaw. ICAS paper 74-50. ("Une étude des prises d'air de Concorde en dérapage". L'Aéronautique N° 58, 1976-3).
- Lotter K.W., Malefakis J. (1978) - Intake design and intake/airframe integration for a post-stall fighter aircraft concept. AGARD CP 247.
- Melick H.C.L., Ybarra A.H. (1978) - Estimating maximum instantaneous distortion from inlet total pressure RMS measurements - AIAA paper 78-970 (2).
- De Richemont G., Détery J. (1974) - Effet des conditions extérieures sur le fonctionnement d'une tuyère supersonique double flux - AGARD CP 150.
- Richey G.K., Surber L.E., Laughrey J.A. (1974) - Airframe/propulsion system flow field interference, and the effect on air intake and exhaust nozzle performance. AGARD CP 150.
- SAE (1978) - ARP (Aerospace Recommended Practice) n° 1420.
- Surber L.E., Stava D.J. (1971) - Supersonic inlet performance and distortion during manoeuvring flight. AGARD CP 91.

**COMMENTS ON PROPULSION/AIRFRAME INTEGRATION
FOR IMPROVING COMBAT AIRCRAFT OPERATIONAL CAPABILITIES(*)**

by

Ph.Poisson-Quinton
Senior Advisor
ONERA
B.P.72, 92322 Châtillon, France

Amongst the main requirements for the next generation of Combat Aircraft, three of them involve the development of advanced engine intakes and nozzles fully integrated to the airframe, with the purpose of:

- a) a low detectability: reduction of Radar and Infrared Signatures for a better survivability,
 - b) a combat "supermanoeuvrability", requesting excursions at very large angles of attack, beyond maximum lift, combined with large sideslip,
 - c) a short-airfield capability, both for take-off and landing.
- f) The "stealth" concept involves a range of technologies to be incorporated at the preliminary design stage. It is well known that the way of detecting -and engaging- hostile Aircraft is by radar surveillance (ground based or carried in AWACS type Aircraft), followed by autotracking and radar or infrared missile launching, for example.

The two solutions for a low observable configuration (Fig. 1) are:

- a reduction of the radar cross-section, thanks to :
 - . a suitable airframe shaping (smooth curves, good blending of discontinuities like wing/tail/fuselage junctions, suppression of sharp corners, better external stores integration);
 - . the use of radar-absorbant material coated on the airframe skin, or advanced composite structure design;
 - . an engine intake location less "visible", above wing/fuselage, for example.
- a reduction of the infrared signature, thanks to a deflectable propulsive nozzle, which reduces the infrared emission from the hot turbine or afterburner flow.

FIG. 1

**A NEW CHALLENGE for AIRFRAME/ENGINE INTEGRATION :
SURVIVABILITY = STEALTH CONCEPT**



- * REDUCTION of the RADAR CROSS-SECTION (R.C.S.)
- + Better weapons/stores integration under wing/fuselage .
- + Foreign objects ingestion suppression .
- Lower inlet efficiency of supersonic speed
- Sensitivity to sideslip ?

- * REDUCTION of the INFRA-RED SIGNATURE (I.R.S.)
- + Thrust vectoring { STOL capability
Super manoeuvrability
- + Thrust reversing (STOL landing)

(*) Prepared unclassified remarks to complement the survey paper on "Fundamentals of Fighter Aircraft Design: ENGINE INTAKE AND AFTERBODIES", by J. LEYNAERT (ONERA), at the AGARD/FDP-VKI Special Course, Feb. 1986.

II) Concerning the TOP-INLET concept to reduce the radar signature, some published wind-tunnel results [ref. 1, 2], show that the Pitot intake efficiency remains quite good, even at large angle of attack, if a vortex sweeping phenomena is developed from a slender front wing (strake with large L.E. sweep), as illustrated on Figure 2 by NASA and Northrop tests at low speed. However an unsymmetrical vortex bursting with side-slip is quite dangerous when a combination of large incidence and yaw angles occurs. The same conclusions were found by FFA/Sweden [2] on a Fighter model tested with a top-inlet at subsonic/transonic/supersonic speeds, again with a pitot-type intake (Fig. 3); it is interesting to note that vortex generators are efficient to reduce a large boundary-layer separation in front of the inlet at supersonic regime.

Positive aspects of this top-wing mounting are to avoid some problems related with a conventional ventral intake location: easier integration of the external-ventral stores, and no more ingestion of foreign objects (or hot gas) when rolling on the ground.

FIG. 2
TOP INLET/ SLENDER WING
 for a "STEALTH" FIGHTER
 Forebody/wing shielding of the inlet (RCS)

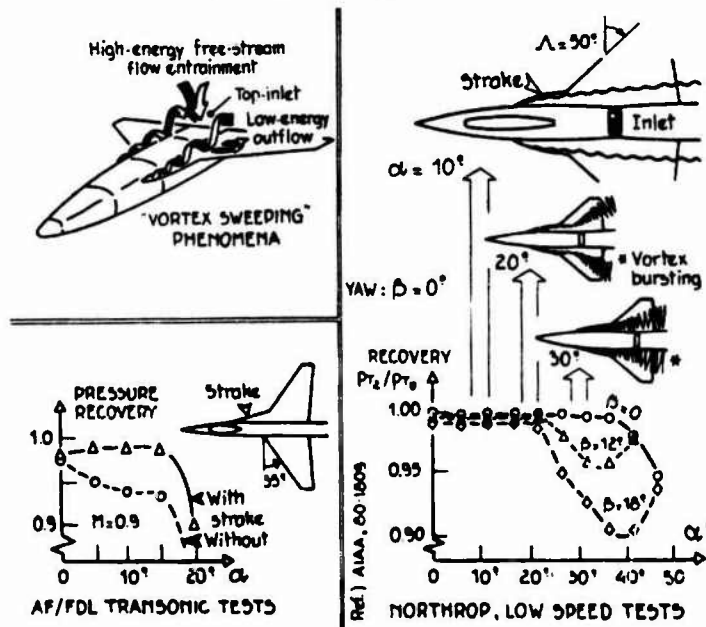
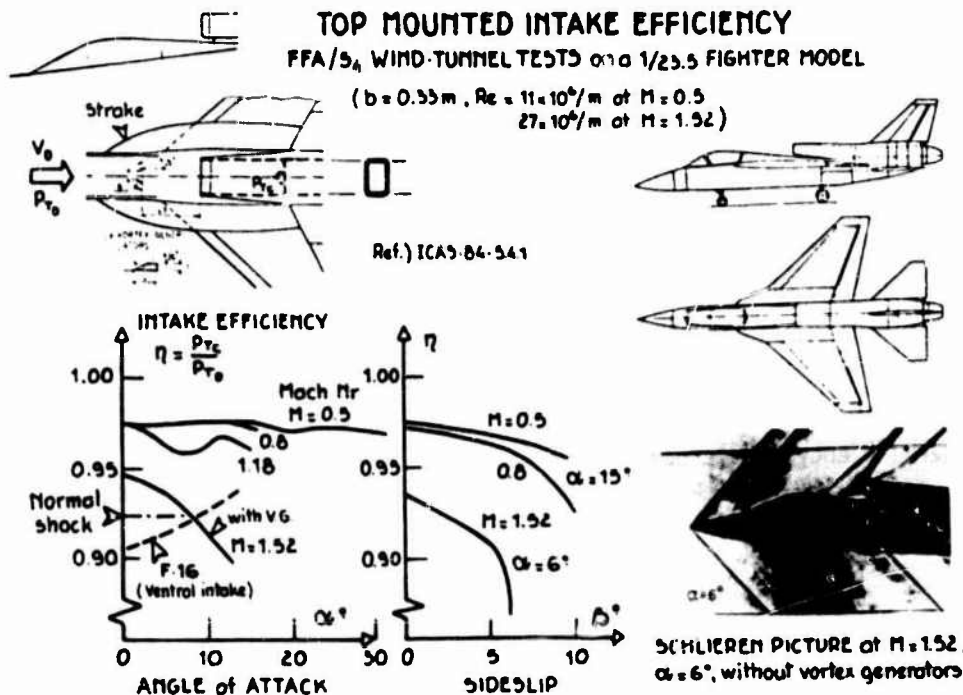


FIG. 3



III) On the Aircraft propulsion side, a lot of fundamental and applied Research were [3], and are still devoted to the use of the jet-engine for inducing aerodynamic lift.

III.1) Figure 4 summarizes two well-known approaches:

- a) A small amount of compressed air bleed, taken on the turbojet HP compressor^(*), can be used for:
 - boundary-layer control, by blowing on leading-edge or on trailing-edge flap;
 - spanwise blowing, for enhancing a powerful vortex lift on a slender wing;
 - or for direct reaction controls around the three axis of an Aircraft during Hovering/ Transition regimes (VTOL), or during post-stall manoeuvre (future fighters).
- b) Another approach is to use the full exhaust flow of the turbojet, and to deflect it at the rear part of the wing to induce some aerodynamic lift by "jet flap effect", which is added to the vertical thrust component of the jet.

This thrust vectoring optimization is illustrated on Figure 5, where the induced lift is much larger when the deflected nozzle is located at the wing trailing-edge of a fighter configuration.

FIG. 4

HOW TO USE A JET-ENGINE TO INDUCE AERODYNAMIC LIFT ...

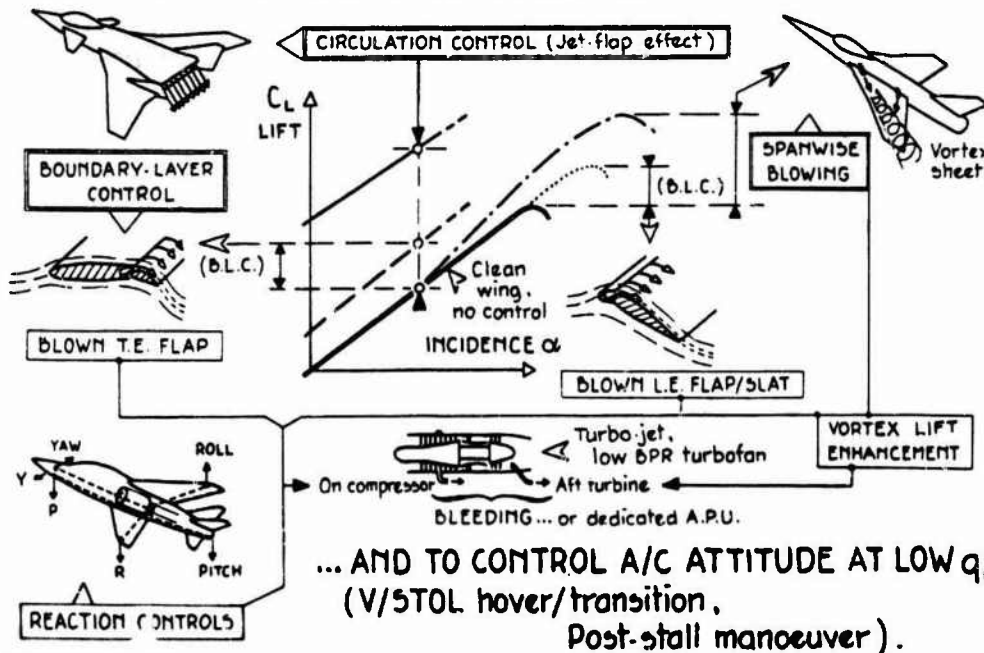
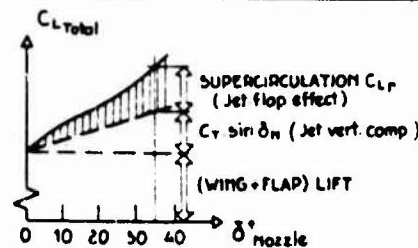
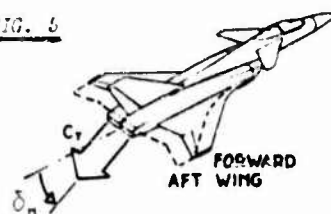


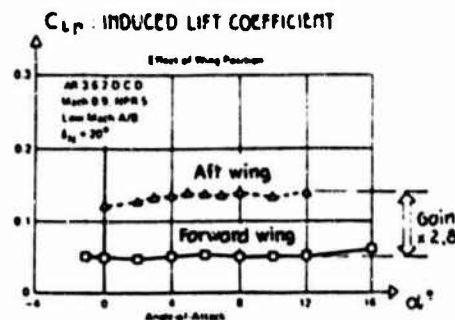
FIG. 5



THRUST VECTORING OPTIMIZATION:

The propulsive deflected jet must be located near the wing trailing-edge to take advantage of the jet-flap effect.

Ref.) Mc Donnell/Douglas



(*) The thrust penalty due to this bleed on a conventional jet-engine is quite severe: about 10% thrust losses for a 5% compressed air bleed, a specific engine cycle design for an economic permanent bleed would be very rewarding for future V/STOL or supermanoeuvrable A/C projects.

III.2) A practical combat configuration was tested by NASA/Ames at large scale (Fig. 6), with two actual jet engines exhausting on the upper surface of the flaps and used for thrust vectoring. A spanwise blowing at the wing mid-chord was also generated from a side-fuselage port capturing directly a small amount of the aft-turbine hot flow: the induced vortex lift at large angles of attack is clearly visible on the curves, and the maximum lift obtained at high thrust regime is very impressive; lastly, the large nose-down pitching moment is self trimmed with this actual unstable configuration.

Manoeuver improvement during high speed combat (Mach 0.6) thanks to thrust vectoring is illustrated on Figure 7 for a similar fighter configuration, tested on a small wind-tunnel model [1].

FIG. 6

"FULL-SCALE" TESTING of THRUST VECTORING and SPANWISE BLOWING CONCEPTS

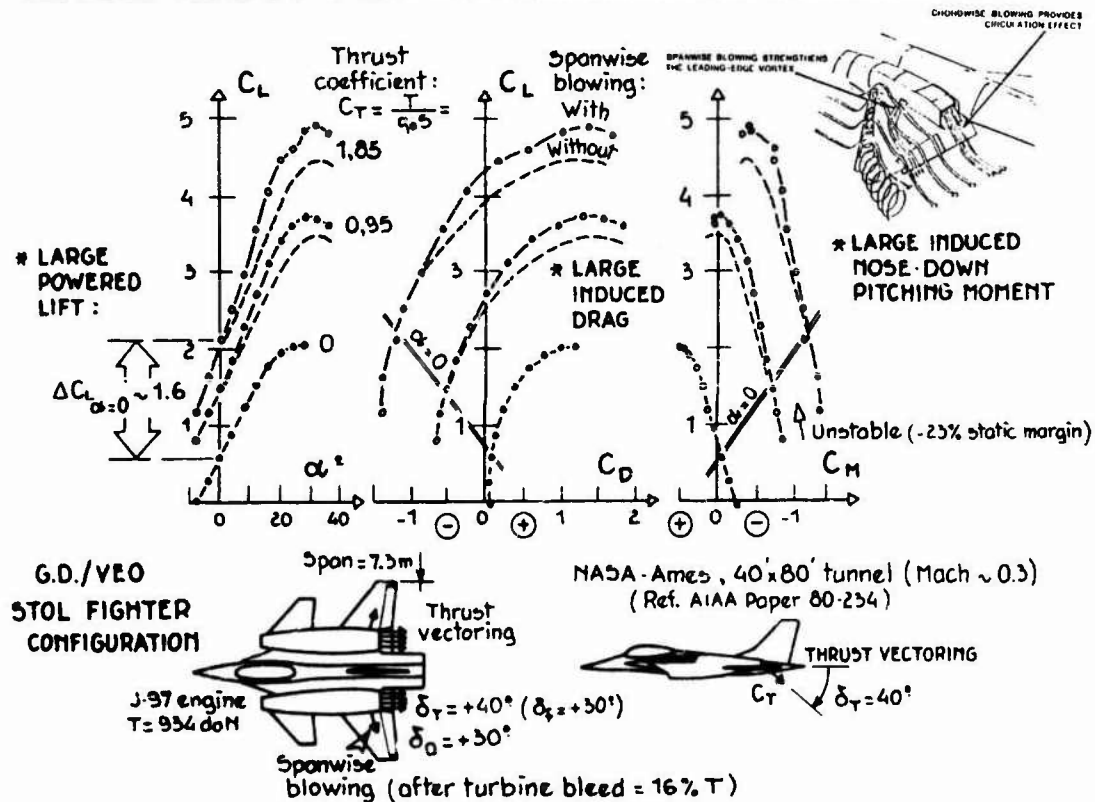
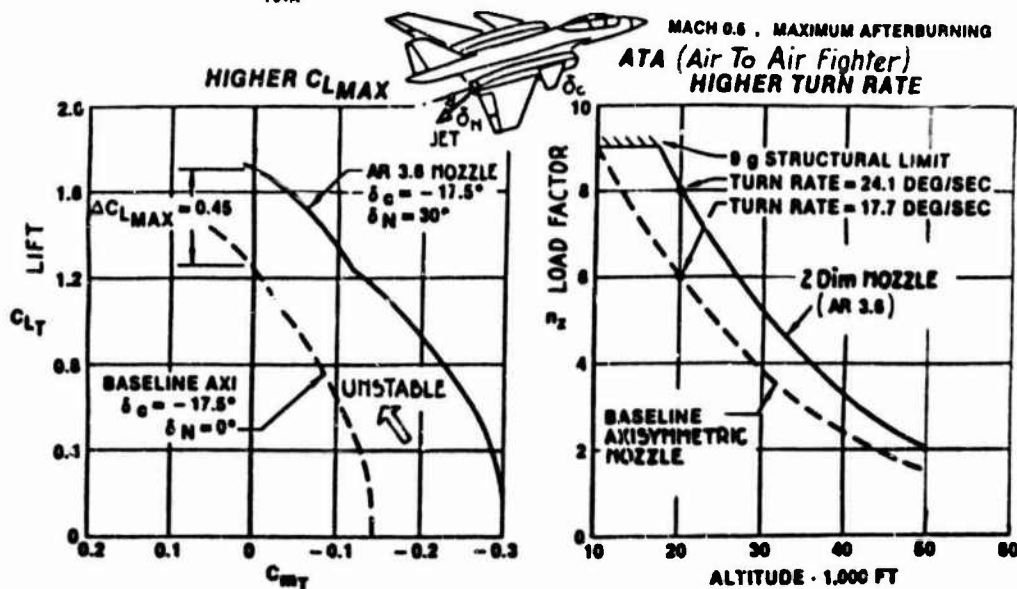


FIG. 7

IMPROVEMENT IN $C_{L_{MAX}}$ AND TURN RATE WITH THRUST VECTORING (Ref. USAF/FDL)



III.3) Various configurations of two dimensional nozzles have been proposed and tested by several US laboratories (Fig. 8), which are able to ensure:

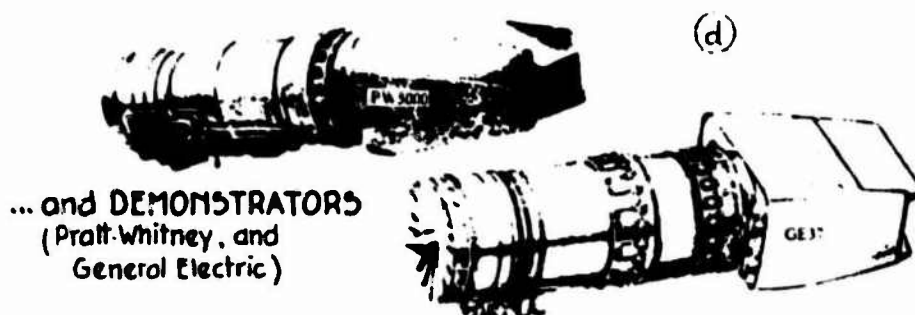
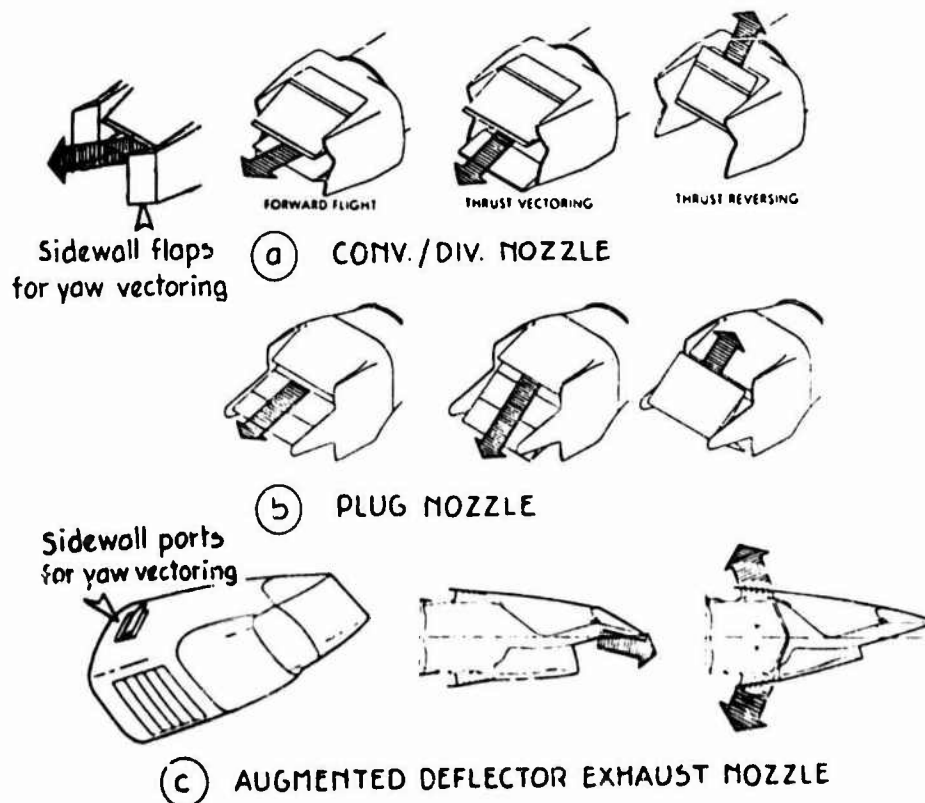
- the cruise propulsion, including at supersonic regime (with a convergent-divergent nozzle),
- the lift enhancement thanks to thrust vectoring,
- a braking effect through thrust reversing, usable for landing roll reduction and quick deceleration in flight manoeuvre,
- and even some yaw vectoring capability, when using sidewall flaps or ports.

Moreover, in the framework of the Joint Advanced Fighter Engine Program [4], launched by USAF for the Advanced Tactical Fighter (ATF), the two Technology Demonstrators, designed by General Electric and Pratt and Whitney (low BPR augmented turbofans, 30000 lb thrust class) will have 2 dimensional vectoring and reversing nozzles (Fig. 8d); such nozzles will "give pilots manoeuvring advantages in air combat and shorten landing rolls, reduce base drag, and help minimize the ATF's infrared and radar signatures. Extra weight seems the greatest disadvantage" [4].

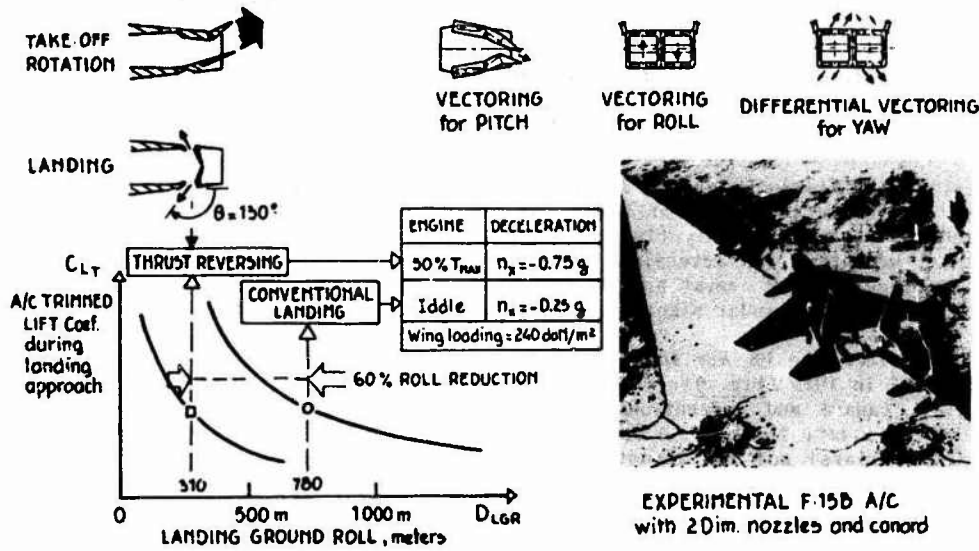
In the meantime, the US Air Force will evaluate in flight the 2D nozzle Technologies on a modified F-15 in 1988 (Fig. 9): a new digital fly-by-wire flight control system will coordinate 2D-nozzles, canard and conventional existing control surfaces from standard flight-control inputs by the pilot; thanks to a large thrust reversing, a 60" landing roll seems possible (use of damaged runways) and the thrust vectoring will be used for take-off rotation, low speed approach and supermanoeuvrability in combat.

FIG. 8

2 Dim. NOZZLE CONCEPTS for THRUST VECTORING ...



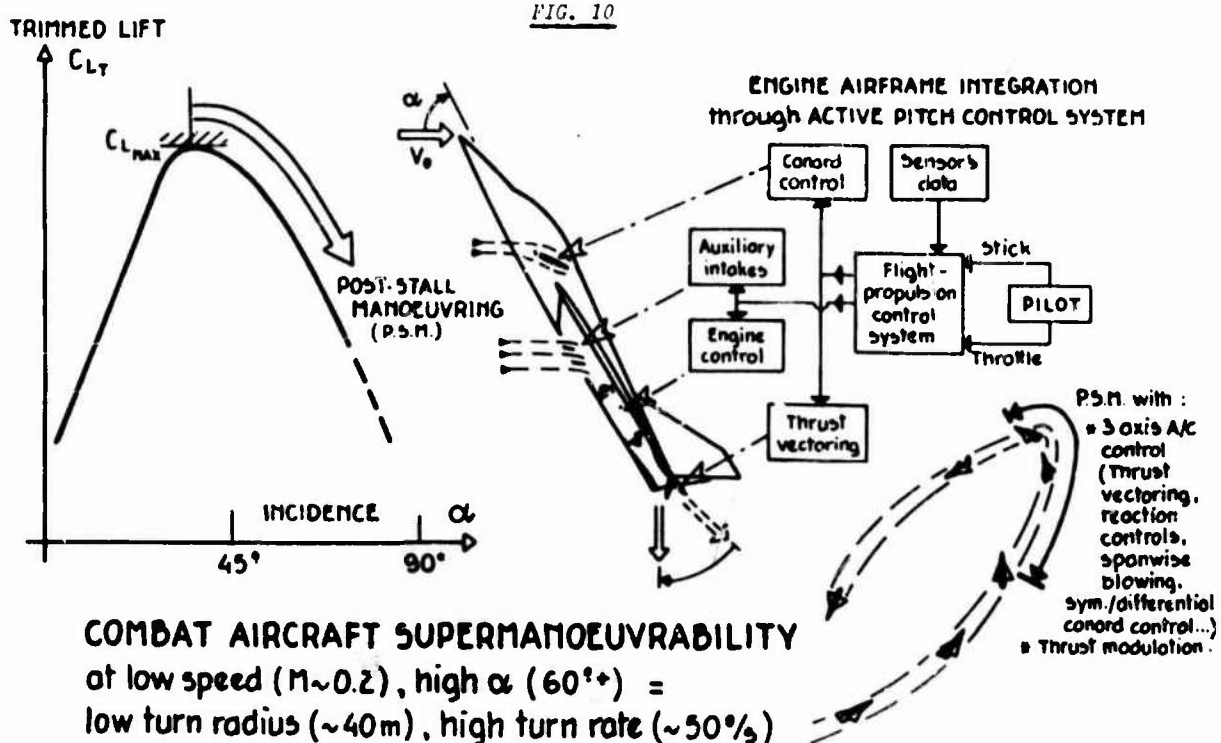
THRUST VECTORING with afterburning + SUPERMANOEVRABILITY for COMBAT



SHORT FIELD CAPABILITY through 2 Dim nozzles vectoring/reversing.

FIG. 9

IV) Combat Aircraft Supermanoevrability is defined as the capability to manoeuvre and control the Aircraft at angle of attack beyond the maximum lift, as shown on Figure 10: the main objective of this post-stall excursion is to allow instantaneous manoeuvre at low speed: small radius of turn at high turn rate can provide a unique tactical advantage in air combat. To perform such post-stall manoeuvre, it is necessary to generate large control forces (independent of the poor aerodynamic control forces available at those low dynamic pressures, and with a strong flow separation regime): the solution is to use the powerful engine thrust vectoring integrated inside the active flight control system (Fig. 10); this active control includes orders to canard surfaces, auxiliary intakes, engine RPM, and possibly to reaction controls or unsymmetrical spanwise blowing (for roll?), valuable air-data informations (speed, Aircraft attitude, etc.) must be provided to the computer, but it is not so easy at such flight regime...



- V) To conclude these remarks on the leading role of the engine for Aircraft manoeuvrability improvement, it must be recalled that a well-known operational VTOL Aircraft, the Harrier/AV-8, with its Pegasus engine equipped with four vectoring nozzles, is already able to use them not only for instantaneous high turn rate, but also for rapid deceleration in combat (or during steep approach before vertical landing).

The next step, studied by Rolls-Royce [5], would be to develop an engine configuration with "plenum chamber burners" inside the "cold" rotating nozzles (Fig. 11) for supersonic flight capability, combined with an axisymmetric vectoring "hot" nozzle for pitch and yaw control (+ reaction controls for roll?).

Such supersonic combat configuration would be able to perform a highly loaded STOL take-off followed by a vertical landing when unloaded (STOVL concept).

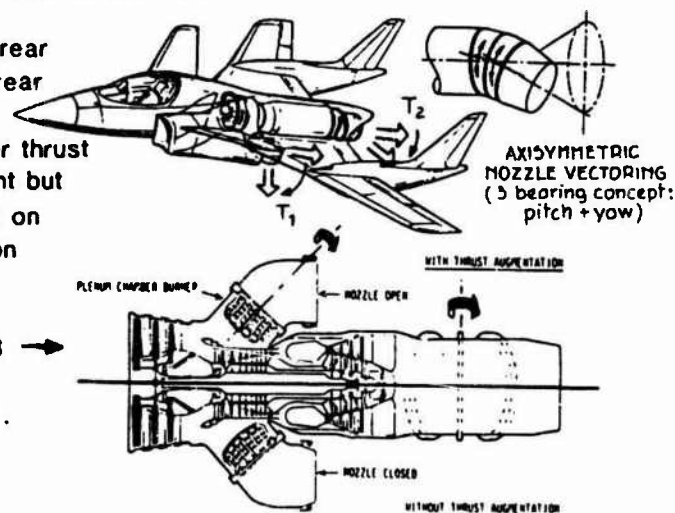
FIG. 11

A STOL AIRCRAFT CONFIGURATION WITH A PEGASUS ENGINE CONCEPT

- Independent vectoring of side and rear nozzles with all axis vectoring on rear
- Shorter moment arm requires larger thrust vector angle for same pitch moment but provides ability to balance aircraft on propulsive lift for V/STOL operation

 Engine configuration with PCB →

Ref.) Rolls-Royce, AGARD/FMP, 1986.



References

- 1 - Airframe-Propulsion Integration for Fighter Aircraft, by G.K. RICHEY, L.E. SURBER and B.L. BERRIER (USAF/FDL), AIAA Paper 83-0084, Jan. 1983.
- 2 - Efficiency of a Top-Mounted Inlet System at Transonic Supersonic Speeds, by K. WIDING (FFA), ICAS Paper 84-5.4.1.
- 3 - Survey of French Research on the Control of Boundary-Layer and Circulation, by Ph. POISSON-QUINTON and L. LEPAGE (ONERA), in Boundary-Layer and Flow Control, edited by G.V. Lachmann, Pergamon Press, 1961.
(see also "Use of the Jet-Engine Thrust for STOL Aircraft Induced Lift, by Ph. POISSON-QUINTON, in AGARDograph Nr. 40, 1960).
- 4 - The Next Hot Fighter Engine, by J.S. PETTY et al. (USAF ASD), in Aerospace America, June 1980.
- 5 - Propulsion System Technologies for Thrust Vectoring, by P. RUMSD and R.F. TAPE (Rolls-Royce, UK), AGARD FMP Symposium on Improvement of Combat Performance for Existing and Future Aircraft, Treviso, April 1980.

AIRFRAME/STORE COMPATIBILITY

C L Bore

Head of Research
British Aerospace, Kingston
Surrey, UK

SUMMARY

By considering the various parameters that dominate the value of a fighter air-force, we can isolate those terms which respond to influences of store installation and store release features. It is shown that stores affect the transport capacity of the air-force through the lift/drag ratio, the availability factor through the agility term, and the target-killing factor through the delivery accuracy term.

Next we examine the physical effects of store installations, identifying ways to minimise the undesirable effects. Thus drag prediction and drag reduction are considered in some depth. The effects of drag on the agility of the aircraft are examined and stability and flutter effects are reviewed. Store release considerations are reviewed. Finally, some recent approaches to store/airframe integration are considered.

INTRODUCTION

Our task here is to consider the whole topic of airframe/store compatibility, in the context of the fundamentals of fighter aircraft design. Now this context tends to concentrate our attention more on the basic fighter design aspects of airframe/store compatibility rather than going into details of store technologies in general. It also suggests that we should consider the fundamental reasoning behind various choices we have to make. We will concentrate on understanding the basic interactions of stores with fighter design, together with some indications of magnitudes of the numbers involved. Fuller follow-ups of these lectures can be made by reading selected references, such as references 1 and 2.

The first section is an analysis of the main parameters which dominate the value of a fighter air-force. The other sections are all concerned with the effects of store/airframe interactions. Thus the sections are as follows:

SECTION HEADINGS

- The "leverage" of store/airframe effects on air-force value
- Drag and other installed forces
- Agility, as affected by drag
- Stability and flutter
- Store release
- Airframe/store integration

1) THE "LEVERAGE" OF STORE/AIRFRAME EFFECTS ON AIR-FORCE VALUE

From my experience in fighter aircraft design, I felt that aircraft designed before (say) 1976 tended to be something like figure 1. The airframe itself was designed carefully to be smooth for low drag, but the stores tended to have excrescences more appropriate to a heavy truck. If one complained that the store designer was squandering the drag which had been won by means of painstaking attention to detail on the aircraft, one was liable to be met by remarks to the effect that stores had to be very cheap (because they had to be thrown away in large numbers) and in any case they were not meant to be carried on the way back. The point that draggy stores require bigger and more expensive aircraft seemed not to be appreciated. Furthermore, there were many pylon and store-carrier features that were to be carried most of the time, and these also had too many high-drag features.

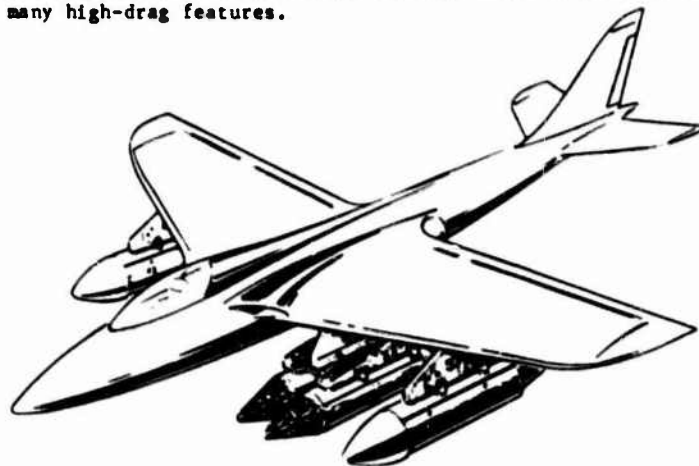


FIGURE 1 WHY SHOULD AERODYNAMIC CLEANLINESS STOP AT THE PYLON?

Clearly, if financial controllers were to be persuaded of the benefits of making improvements to the aerodynamics of stores and their installations, it would be necessary to argue in their language: money. I made my first attempt to assess the value of aircraft design improvements in chapter 1 of the AGARD Working Group's report (reference 1), and a better attempt in reference 3. The latter is the basis for the analysis which follows.

Assessing the Value of an Airforce

Value is related to the amount that one would be prepared to pay for the usefulness supplied, in the circumstances of use. Thus the value may vary greatly with the circumstances. If you have just fallen out of an aircraft, you would place a high value on a parachute, but if you are drowning you would not.

We cannot be sure in advance about the range of scenarios in which our aircraft will be used eventually. For example, the Harrier was designed to destroy tanks in central European air/ground battles, but it was actually used 13,000 km from home for ship-based air/air combat (and extremely successfully!). So in practice, our evaluations should be done for a mixture of possible scenarios. Simply to illustrate this lecture, we will assume Close Air Support (CAS) operations in a short, sharp war - at the end of which the losing side's aircraft are out of action. In this circumstance, replacement manufacture will not contribute.

Factors of effectiveness value

The effectiveness, and therefore the value of an airforce is proportional to the number of targets it can knock out before the airforce is put out of action. Clearly this is proportional to a number of factors, such as the rate at which the aircraft can transport warload (W), the overall availability of the aircraft with their bases in wartime (A), and the target-killing effectiveness (K). Let us examine these propositions more closely. We have :

Value \propto Effectiveness

Effectiveness \propto Warload transport rate (unimpeded)

\propto Availability in wartime (including bases)

\propto Kill effectiveness

whence $V = WACK$

where C is the constant of proportionality.

We can see that if any one of these factors becomes zero, the overall value becomes zero.

Warload Transport rate (w)

W = mass of ordnance transportable when unimpeded, relative to datum aircraft

= (load of ordnance per sortie) x (number of sorties per day)

= m . N

Here the sortie rate (N) depends on :-

* turn-round time	(r)	} $N = \frac{1}{r + \frac{2d}{M}}$
* block speed	(M)	
* distance from base to target area	(d)	

Therefore $W = \left(\frac{m}{r + \frac{2d}{M}} \right)_R = \left(\frac{Mm}{2d + rM} \right)_R \dots (2)$

Where the suffix R indicate that the parameter is to be made "relative" by dividing by the comparable parameter for the datum aircraft.

It can be seen that a small aircraft capable of operating from nearby bases may transport as much as a large aircraft that has to use far-back bases.

Availability in Wartime (A)

Availability = average fraction of aircraft time usable during war

This depends on four factors

- * fraction of total time usable (t) {
 - night-time capability
 - bad weather capability
 - availability of targets within range

- * fraction of aircraft usable (a) {
 - survivability, agility
 - repairability
 - maintainability

- * fraction of bases usable (b) {
 - runway length requirement
 - ground hardness requirement
 - base detectability/survivability

- * availability of stores (s) {
 - logistics
 - interchangeability

Thus $A = (t a b s)_R \dots \dots \dots (3)$

Thus the Availability term depends on many "ilities".

Target Killing Effectiveness (K)

K = specific rate of knocking out targets (per unit of ordnance released) relative to datum aircraft and stores.

This depends on various aspects, but not generally in simple proportional laws :-

- * power of weaponry
- * active guidance of weaponry
- * aiming accuracy of aircraft {
 - aircraft controllability
 - sighting system
 - pilot's workload and fatigue
- * accuracy of stores trajectory {
 - ejector/carrier dynamics
 - aerodynamic release disturbance

The Constant of Proportionality (C)

If we arrange that all the factors of value are made non-dimensional by making them ratios, relative to the factors appropriate to the known datum aircraft, then the constant C amounts to the value of an airforce comprising a given number of the datum aircraft. That value is not set by engineers or accountants : it is a political judgement. We can assume that the government, in its collective wisdom, has decided that the value of the datum airforce is not less than its lifetime cost. Then it follows that the constant C is not less than the lifetime cost of the datum airforce. For most comparisons, the value of C is not needed accurately, but it seems that typically it is around 5 times the cost of buying the aircraft (figure 2).

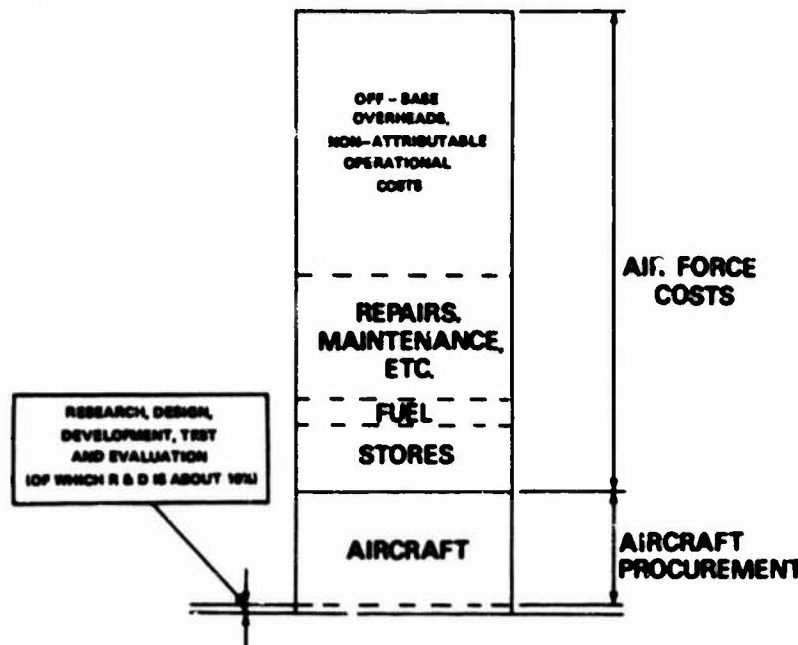


FIGURE 2 APPROXIMATE LIFE-CYCLE COSTS OF C.A.S AIRFORCE

Nowadays, for an airforce 120 C.A.S. aircraft, the value of C must be in the vicinity of \$10 billion. So if we are able to increase any of the factors discussed by a mere 1%, the value of that improvement is about \$100 m. I trust you will agree that even such a minor improvement is quite worthwhile.

Overall Value (V)

Substituting from (2) and (3) into (1) we get :-

$$V = C \left(\frac{Mm}{2d+rm} \right) (t a b s)_R K_R \quad (4)$$

Effects of Stores

Now we can examine the terms in equation (4) to determine which of them may be affected by store/airframe interactions. Obviously the datum constant C is unaffected by our proposed new design. In the transport rate factor (equation 2) the block speed (or block Mach number) M may be affected by store drag. The ordnance mass per sortie (m) also may be affected, for if the drag can be reduced substantially, ordnance may be exchanged for fuel. In the denominator, the average distance (d) from forward base to target is determined by the basing versatility (e.g. whether the aircraft is V/STOL, STOL or CTOL) but not directly by the store installation. The turn-round time (r) depends clearly on the accessibility and serviceability of the store installation.

In the availability term (which embraces many "ilities") there are four factors. The usable time factor (t) may be increased sometimes if reduced drag increases range enough to bring targets within range. The "aircraft usable" term (a) can be affected quite markedly, for reduced drag may increase both the penetration speed and agility - both of which may reduce the attrition rate. The stores installation may affect the radar and infra-red signature, repairability and maintainability aspects. The last two terms (b,s) will not concern us very much, except to remark that there are strong arguments in favour of NATO-wide interchangeability of stores to make overall logistics more economical and also there are good reasons to tighten up on dimensional tolerances.

The target knock-out term (K) obviously can be sensitive to the store installation, but assessments may not be easy. If the stability and controllability of the aircraft are improved, clearly the pilot will be able to do a better job of aiming. Even more important, if store trajectories are made more repeatable and accurate, fewer sorties will be needed. This latter topic will concern us in some depth.

There are, incidentally, other possible effects of release disturbances. For example, there have been cases where a release disturbance to a guided missile has disrupted "lock-on", and there have been many cases where jettisoned stores have flown about so wildly that they have struck the aircraft and caused damage or even destruction of the aircraft.

To summarise, the terms of equation (4) which will concern us further are:

- * M block speed
- * m mass of ordnance per sortie
- * t target availability : effect of range
- * a aircraft availability : survivability - penetration, agility
- * K target knock out { : effects of stability and controllability
 : store trajectory

For the remaining relevant terms we will simply note that due care must be taken to ensure that the store installations will afford rapid turn-round, maintenance and repair, and that radar and infra-red signatures must be within the bounds decreed. Store interchangeability also needs attention, internationally.

The most important conclusion from this section is that the "leverage" or sensitivity of improvements can be regarded as proportional to the factors of equation (4). If we take the value of C as (say) \$10 billion then a 1% improvement to the overall value V could be regarded as worth about \$100 million. It follows that it is quite important to improve our designs.

2) DRAG AND OTHER INSTALLED FORCES

The significance of Drag reductions

When we first study aircraft design, we soon learn the importance of the (lift/drag) ratio in relation to the range of the aircraft. In fact, it can be shown that for an aircraft cruising at constant lift coefficient at any altitude, the generalised range equation applies (reference 5);

$$R = a_0 \frac{(M^2/D) \ln(W_1/W_2)}{(1+\epsilon) (S/\sqrt{\theta})} \quad \text{--- (5)}$$

(usually small)

Where a_0 is the speed of sound at sea level, M is the cruise Mach number, and $(S/\sqrt{\theta})$ is the jet engine's specific fuel consumption generalised by the relative temperature of the atmosphere, which is constant during cruise climb.

The weight ratio term reflects the consumption of fuel over the stage of route concerned. Now it can be shown (reference 6) that this logarithmic term can be replaced closely by (F/W_m) , where F is the fuel consumed and W_m is the geometric or logarithmic mean of all-up weight over the stage concerned. Then the generalised range equation can be rewritten:-

$$\therefore R = \frac{a_0}{(S/\sqrt{\theta})} (M^2/D) \frac{F}{W_m} \quad \text{--- (6)}$$

The significance of this form becomes evident when we note that the first term is determined by the choice of engine, the second term expresses the aerodynamic efficiency, and the third term embraces the fuel usage in terms of the mean stage weight.

Clearly, if we double the drag of our aircraft while leaving the third term fixed, the range will be halved. In practice, on many aircraft a doubled drag would lead to reduced cruise Mach number, so the range would be reduced on that account also. Incidentally the doubled cruising thrust would greatly reduce the thrust reserve available for acceleration and manoeuvring, so the agility will be severely impaired.

Now let us examine what course we could adopt if the basic drag of our aircraft were unavoidably doubled by the store array (noting that typical store arrays are often much worse than this!). From equation 6, we would have to double the fuel mass ratio (F/W_m) to restore the range. First see what happens if we simply double the internal fuel capacity, without altering the exterior size or shape of the aircraft. The weight of fuel tanks would be doubled (or possibly more, if tanks had to be crammed into small corners). The mean stage weight W_m would increase - perhaps by some 12%. So next we have to increase the internal fuel capacity by a further factor of 1.12, just to keep up with the increased mass of the aircraft (at constant dimensions). Thus we soon find we have to increase the fuel capacity of the basic aircraft by a factor above 2.24. If there is not enough internal volume to cram inside an extra 125% of the basic tankage, we have to enlarge the aircraft overall, and this increases the drag as well as the mass. Perhaps an alternative would be to install the extra fuel in external fuel tanks, but this increases the drag greatly. Next we find that the cruise Mach number and the agility are severely impaired, so we have to choose a more powerful engine. Usually a bigger engine has higher specific fuel consumption, particularly at lower throttle settings, so now the first term of equation 6 has been worsened. So if we accept the typical drag penalty for the store load, the size of the aircraft has to be increased. Since aircraft purchase cost is driven mainly by engine power and aircraft mass, we find that the purchase cost of the airforce has increased substantially, and the fuel cost has increased greatly.

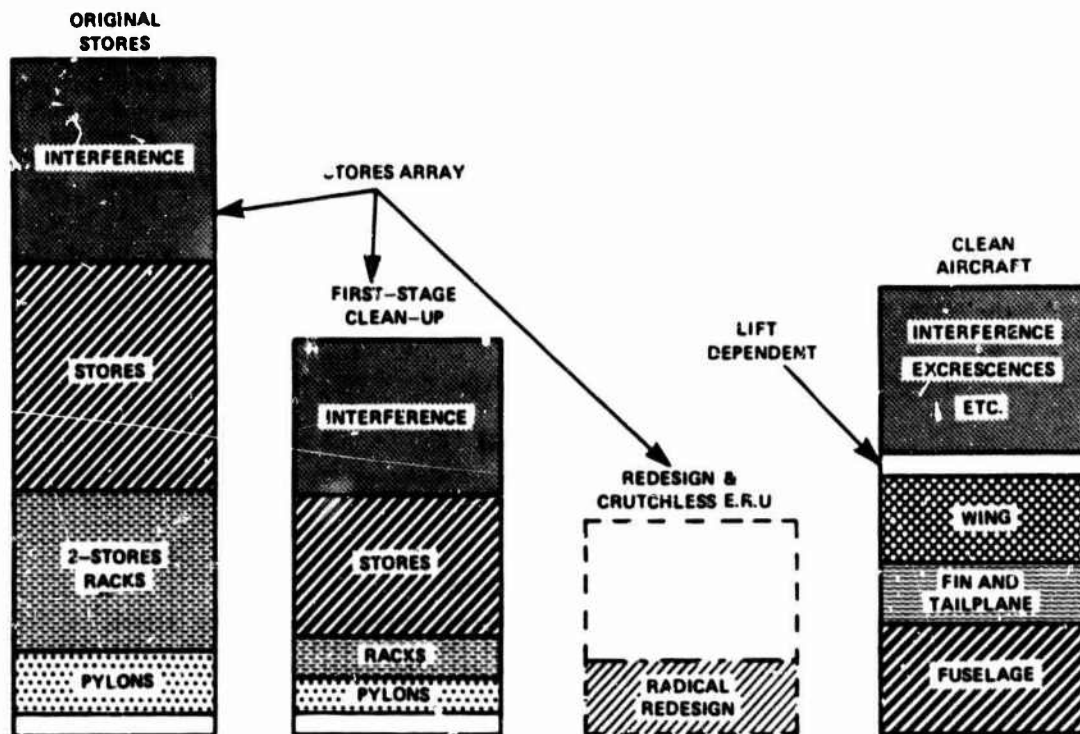


FIGURE 3 DRAG OF STORE ARRAY, AND CLEAN AIRCRAFT

Now let us turn our attention to the problem of reducing store drag. First consider the magnitude of the numbers involved, using the example quoted in reference 3 (6 years ago). Figure 3 shows on the left the total drag caused by an array of stores hung on 2-store racks, on four pylons. The drag of this store array was well above the drag of the clean aircraft. The "first-stage clean-up" involved fairing of all excrescences on the 2-store racks and the stores. Crutching arms were retained for all stores, but these were aerodynamically faired. If crutching arms were removed by redesigning all the Ejector Release Units (ERUs), and the 2-store racks were re designed, the total store drag could be reduced to the dotted outline. By this stage, the reduction of drag overall is equal to the entire drag of the clean aircraft.

That example was based on quite old techniques. By taking a much more radical approach, involving stagger or tandem carriage, and tangential carriage, we could now expect to reduce the total drag of the store array to about one-tenth of its classical counterpart, as indicated by the shaded area of the dotted rectangle. Thus by using all the store array techniques now available, we could save more than the entire drag of the clean aircraft. Even now, there are many new ideas to be followed up.

Thus if current knowledge were put to use fully, we could be happy that research into reduction of store-array drag had led to really major improvements in the value of NATO airforces. Unhappily, it usually needs some investment in new equipment (such as redesigned store carriers, and cleaner stores) before these value improvements can be reaped, and some countries have government departments which can count the cost of investments but which are often incapable of recognising the value of the improvements that ensue. In the case of store drag, I estimate the ratio of improved value to investment is over 50: In other words, the payback will be 50-fold or more. Some other nations are not so backward in recognising worthwhile investment. France - for example is already using improved 2-store carriers.

Drag Prediction and Reduction

These topics are both important and specialised. For further reading, the reviews by Barry Haines should be sought (references 7,8,4). However I have less time, so I will have to be less comprehensive. I will outline the main points relying heavily on Barry Haines' papers.

The conclusions of reference 8 make a useful starting point for this section:

- 1) With existing external store arrangements, the drag increments can be very large, e.g. larger than the drag of the clean aircraft without stores.
- 2) Research has however already shown how major improvements could be achieved, many of the suggestions even being feasible on existing aircraft.
- 3) New multiple carriers and underfuselage arrays of stores should aim to exploit the concepts of tandem carriage and store stagger and should avoid very close lateral spacing of stores.
- 4) There should be further exploitation of the favourable interference possibilities from wing tip carriage of slender missiles.
- 5) On new projects, wing/underwing pylons should be designed together with the aim of alleviating adverse interference at low C_L and achieving some favourable interference on the flow breakdown at high C_L at moderate and high subsonic speeds.
- 6) For new aircraft, the complete configuration should be designed as an entity with due regard to its longitudinal distribution of cross-sectional area and with the stores mounted either in conformal packages or from conformal pallets.

Reviewing the principles recommended in these conclusions, it is clear that methods for predicting store-array drag have to take into account multiple carriage, whether tandem or staggered - with effects of lateral spacing. The interferences between stores and pylons, and the underwing surface, and the overall cross-sectional area distribution all need to be predictable. The effects of carrying stores in close arrays tangential to the surface, or on pallets, need to be quantifiable. Finally the drag effects of wingtip carriage of slender stores need to be calculable.

That list of interactions seems formidable, but useful predictions can now be made for all of them. The approach adopted in the UK since 1977 (successively by Pugh, Sadler of Ross and RAE) has been semi-empirical, using extensive sets of research experiments to understand the aerodynamics but fitting empirical curves to the correlated results.

Previously a "drag index" approach had been in use, in which

$$\Delta\left(\frac{D}{q}\right) = K_I \left(\frac{D}{q}\right)_{\text{isolated}} \quad \text{--- (7)}$$

where K_I varies with Mach number and depends on the type of store array, and $\left(\frac{D}{q}\right)_{\text{isolated}}$ is the drag of the store, carrier and pylon tested remote from an aircraft. Since we are concerned with an array of stores, this relation became

$$\Delta\left(\frac{D}{q}\right) = K_I K_A \left(\frac{D}{q}\right)_{\text{isolated}} \quad \text{--- (8)}$$

where K_A is an assembly factor to account for interferences between the various stores in the array. However, Dyer and Gallagher (in the USA) had soon found out that multiplying the interference factors together did not work: additive factors were better. The RAE team found that it was better to split each

of the terms of equation (8) into low-speed and Mach-dependent parts, to be factored separately. Thus, for example, when calculating the drag of an assembly of staggered side-by-side stores, the equation is of the form:

$$K_A = \frac{K_{Ai} \left(\frac{D}{d}\right)_i + K_{AW} \left(\frac{D}{d}\right)_w}{\left(\frac{D}{d}\right)_i + \left(\frac{D}{d}\right)_w} \quad \dots \quad (9)$$

where: $\left(\frac{D}{d}\right)_i$ is the low-speed or "incompressible-flow" drag of a single store.

$\left(\frac{D}{d}\right)_w$ is the increment with Mach number in the isolated store drag,

K_{Ai} is the low-speed assembly factor

K_{AW} is an assembly factor on the Mach-dependent drag.

In general, K_{Ai} is not equal to K_{AW} , and both terms can depend on lateral spacing, stagger and shape of the stores. Methods for predicting $\left(\frac{D}{d}\right)_i$ and $\left(\frac{D}{d}\right)_w$ are improving, but for best results wind-tunnel tests should be done on models large enough to represent the detailed excrescences of the full-scale store, at a reasonable Reynolds number.

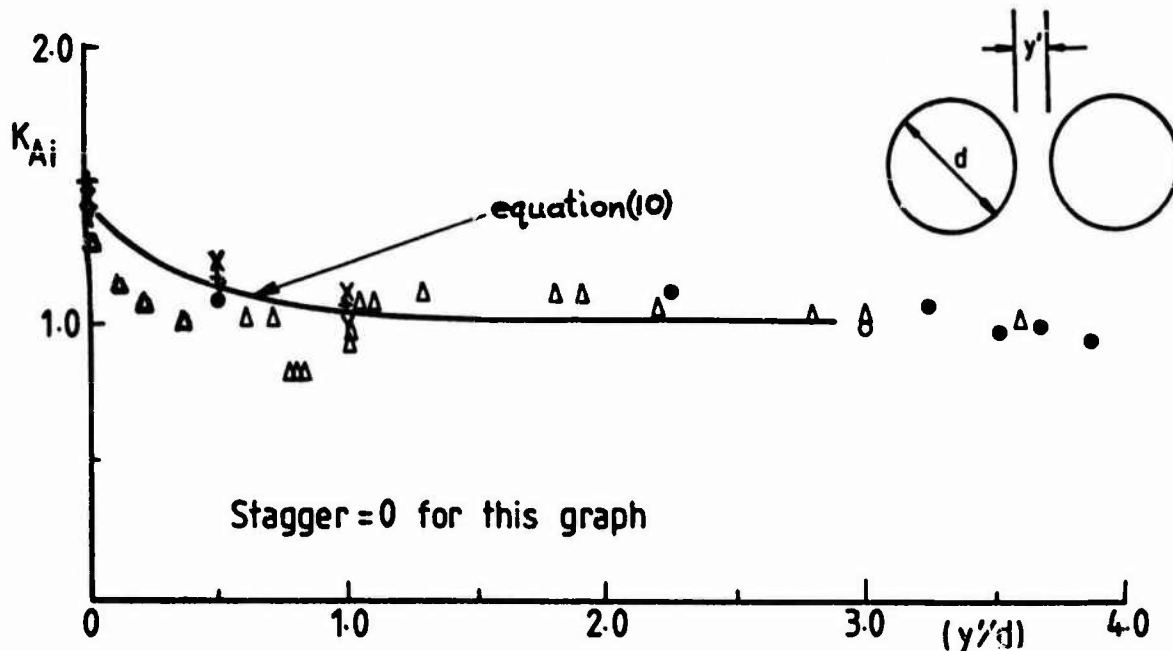
Figure 4,5 show illustration of how K_{Ai} and K_{AW} are estimated in the RAE method.

Figure 4 shows the variation of K_{Ai} with lateral spacing (y/d) for two side-by-side stores with no longitudinal stagger (y' being the smallest gap between the stores, and d being the store diameter). The equation:

$$K_{Ai} = 1 + \frac{0.42}{\exp(y/0.4d)} \left[\frac{\text{store length} - \text{stagger}}{\text{store length}} \right] \quad \dots \quad (10)$$

provides a reasonable representation of experiment for various different stores and test Mach numbers low enough to be regarded as "incompressible". The allowance for stagger is a simplification which is not very accurate, but it gives a quick simple estimate which will often be good enough for the low-speed component of the assembly drag.

symbols Measured values



K_{Ai} = low speed assembly factor

FIGURE 4 ASSEMBLY FACTOR FOR PAIRS OF SIDE-BY-SIDE STORES AT LOW MACH NUMBER

Figure 5 shows the variation of K_{AW} (i.e. the wave drag part) with store stagger. The variation with lateral spacing is judged to be trivial at $M=1.0$, and not much at other M . The parameter N is regarded as the "effective number" of side-by-side stores. Because adjacent stores can shield any given store from the effects of stores further away in a row, the intention was to take N as 2 when there are 2 or more stores and no stagger, and not more than 3 when there are 3 or more stores with stagger. However, it is not quite so simple, and the rules may become more general as data is accumulated.

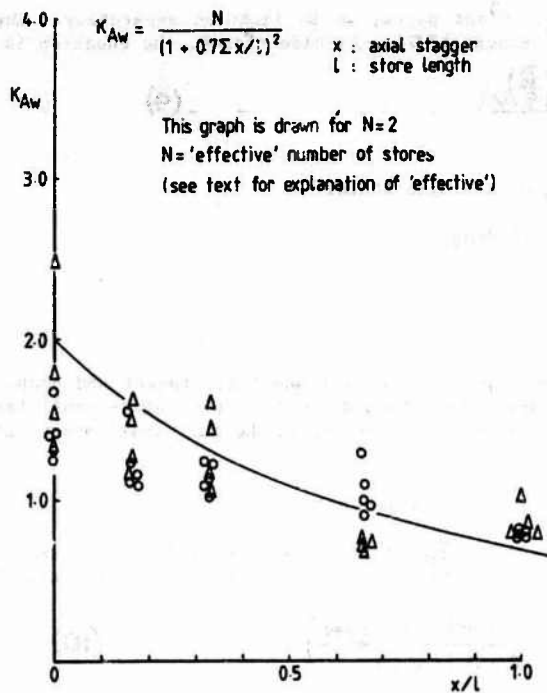


FIGURE 5. EFFECT OF AXIAL STAGGER ON HIGH SPEED ASSEMBLY FACTOR

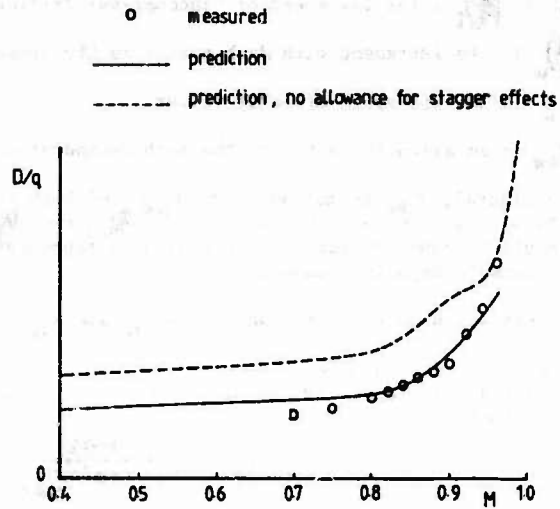
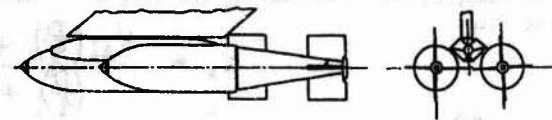


FIGURE 6. 2 BOMBS ON A STAGGERED TWIN CARRIER

Figure 6 shows a comparison between predicted and measured values of drag for an assembly of two Mk10 bombs in a staggered arrangement on a standard carrier. The difference between the two curves shows the effect of stagger.

The RAE method also includes allowance for tandem-carriage effects. The forward store leaves a wake with reduced dynamic pressure, and a dead-air region close behind its base, these effects being bigger for a bluff-nosed store. Also there is effectively a reduced Mach number for the flow over the down-stream store. Figure 7 shows a comparison between prediction and measurement for two stores on a tandem beam. Note the magnitude of the tandem carriage effects.

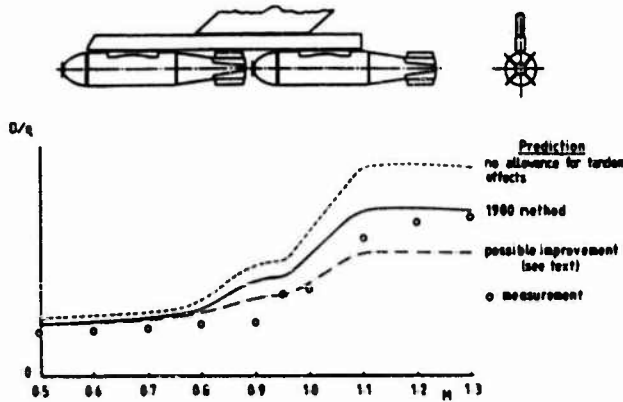


FIGURE 7. TANDEM MOUNTING OF 2 BOMBS

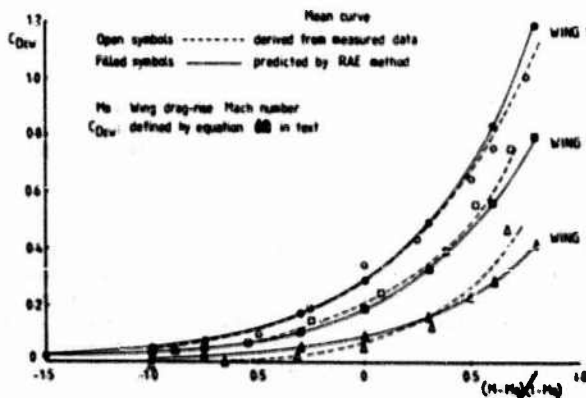


FIGURE 8. CORRELATION OF EXCESS WAVE DRAG WITH WING MD PYLON - MOUNTED UNDERWING INSTALLATIONS

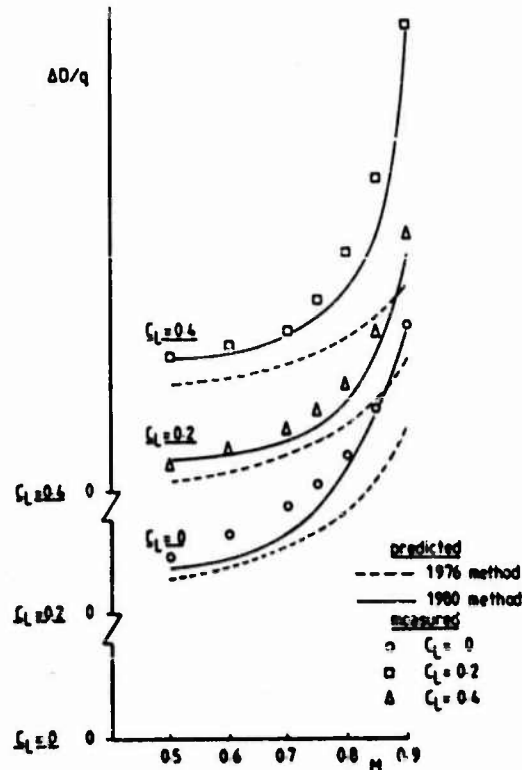


FIGURE 9. INSTALLED DRAG OF STANDARD CBTs FULLY LOADED WITH MK.10 BOMBS ON BUCCANEER

The installation factors, K_I , for arrays of underfuselage stores are generally not higher than 1.3, and can be below 1.0 for small stores semi-submerged into the fuselage. For pylon-mounted underwing stores, however, estimation of K_I is much more significant and difficult. Values of K_I at high subsonic speeds for underwing stores can be high, and very dependent on the wing design. After considerable research, simple multiplicative installation factors have been abandoned in favour of an equation of the form:

$$\left(\frac{D}{q}\right)_I = K_{Ii} \left(\frac{D}{q}\right)_{Ai} + \left(\frac{D}{q}\right)_{AW} + F_A C_{DEW} \quad (11)$$

where K_{Ii} = low speed installation factor,
 $\left(\frac{D}{q}\right)_{Ai}$ and $\left(\frac{D}{q}\right)_{AW}$ are respectively the low-speed and Mach dependent drags of the store assembly isolated from the aircraft,

F_A = frontal area of store assembly,

C_{DEW} = "excess" interference drag derived as a function of wing (thickness/chord) and clean wing drag-rise Mach number (M_D) through a relationship of the form:-

$$C_{DEW} = f\left(\frac{t}{c}\right) \exp\left(1.76 \frac{M - M_D}{1 - M_D}\right) \quad (12)$$

Wherever possible, one should use measured values for $\left(\frac{D}{q}\right)_{Ai}$ and $\left(\frac{D}{q}\right)_{AW}$.

Figure 8 shows the variation of excess drag with excess Mach number for three different combat wing designs. The full-line curves are predicted from equation (12), while the dotted curves are from experiment. Clearly the agreement is good. Note that reduced wing thickness benefits the drag rise in two ways: M_D is increased, and C_{DEW} for given $(M - M_D)$ reduces.

A leading conclusion from research on underwing stores is that the wing lower surface and pylons should be designed to reduce the peak suction near the wing/pylon junctions. Thus there is more to this than merely reducing (thickness/chord) of the wing. Presumably, in time the prediction methods will introduce some features of the lower-surface pressure distribution.

Figure 9 shows the method as applied to the installed drag of a standard triple carrier fully loaded with Mk.10 bombs. Clearly the accuracy has been improved substantially, and a wide range of effects can now be predicted, at useful accuracy. Guided by these predictions, one can devise improved arrays, and then tunnel test for best accuracy.

Installed Forces and Moments

There are three main reasons for wanting to know the aerodynamic forces on "installed" stores. Firstly and obviously the total installed forces in flight must not be allowed to exceed the strength of the structure (including the ERU and the store casing). Here, the total installed force is the sum of the aerodynamic force plus the inertia force.

Secondly, the installed forces just before release are a valuable pointer to the impulses that will act upon the store just after release. Indeed, some release trajectory methods (e.g. E.J. Dalley's CLOSER) rely on the pre-release forces for the major aerodynamic impulse effect. In any case, any unduly large installed force or moment may be a crucial warning that there will be an important initial impulse after release.

Thirdly, in our present context, we may choose to interpret the term "installed" to mean "held in place". Many of the methods that can be used to calculate the forces for a store held in place on the ERU can equally be used to calculate the forces on a store momentarily "in place" on its trajectory. For conciseness we will adopt this interpretation, where convenient.

Distinction between drag and streamwise force

Before going on to discuss the various methods for predicting installed forces, please excuse a brief diversion to discuss the fundamental distinction between drag caused by a store, and the streamwise force acting on it. Basically, drag arises only when some turbulence or residual heat or downwash or sidewash is left behind in the wake of the aircraft as a whole. We usually think of the mechanisms for producing drag as boundary-layer-wakes, separated-flow wakes, shockwaves (leaving very fine-grain turbulence, as heat) or vortices.

Now when we put a store under an aircraft, it will of course produce a wake of its own, but it may also cause an extra drag-producing wake on (say), the pylon/wing junction. So the drag may arise elsewhere than from the wake of the store itself. This is evidently the case with supersonic wave drag, for supersonic interferences generally shed their wakes over a wide frontage, and some of these interferences may reduce total drag.

Another fundamental point arises from buoyancy forces. Any body placed in a pressure gradient experiences a force opposite to the pressure gradient, but buoyancy forces (even in the streamwise direction) must not be confused with drag forces. Indeed, it is quite common to find that when one aerodynamic body is placed close to another, one will experience a forwards-acting force while the other experiences a rearwards-acting force (the pair of these forces together more or less balancing out). Sometimes (to keep aerodynamicists alive to fundamentals?) the drag mechanism will be operating mostly on the component which experiences the forward-acting force. In such a case, the drag may usefully be regarded as arising because the forward-acting force is, in practice, less than it should be ideally.

The main conclusion to be noted here is that drag is essentially the result of turbulence-producing mechanisms, whereas forces can arise from buoyancy effects, as well as from drags. Consequently we should always beware of the distinction between streamwise force and drag, especially when we measure installed forces by force transducers.

Predicting Forces and Moments

In general, there are two major parts to any force-prediction computation. Firstly, there is the task of computing the flow-field around the aircraft to a sufficient distance below it, where disturbances to a store trajectory are judged to be minor. Secondly there is the problem of calculating the forces and moments that will act on a particular store placed at any attitude and position in that flowfield. We will see that there are various ways of combining these two parts of the overall calculation. Euler methods, now coming into use, essentially combine both parts.

Flow-field calculations

1. The Nielsen method(9) has been developed widely to become more convenient and cost-effective, both in the USA (Northrop, 10) and in the UK(11), where the RAE team have named their developments RAENEAR. This method includes modelling of the stores, and the store force estimate, in the overall computation.

The original NEAR method required elaborate modelling of the aircraft/store configuration, which took many man-weeks of data preparation. The developments have greatly reduced the data input; RAENEAR now taking about 2 man-days. This has sacrificed some accuracy. Many trajectory calculations have been satisfactory, but some flow-field calculations have been disappointing, - notably for aircraft with large air intakes. Results have been mostly satisfactory up to about Mach 0.9.

Until recently, loads for stores in place on the aircraft have been inaccurate, but Isaacs (11) has recently described a set of improvements to deal with this. The main modifications were to cover the following topics: improved modelling of store, wing and pylon thickness effects (notably treatment of the wing root), pylon/store interference, allowance for store/fuselage interferences, and more accurate methods for calculating the loading on stores in uniform or non-uniform flow. Despite its limitations in some respects (which are still being improved) RAENEAR is likely to continue in use because it is economical and quick, and gives useful guidance for design purposes.

2. PANAIR panel codes (12, 13, 14, 15) have been developed and used extensively in the USA. Both subsonic and supersonic versions are available. To quote (15), "Panair provides the user with considerable freedom and flexibility in modelling complex configurations. For regions where linear theory is valid, it provides good correlation with test data". Results for supersonic speeds have been in reasonable agreement with experiment except where real shock waves arise. This is because linear theory assumes that flow disturbances propagate above Mach lines (i.e. an assumption of sonic propagation relative to the free stream flow) whereas in reality real shocks are substantially steeper (propagating at supersonic speeds relative to the local flow). A modification has been introduced to deal with this, and it has been concluded that PANAIR will be capable of giving good supersonic predictions, as well as good subsonic predictions.

3) SPARV (the Source Panel and Ring Vortex method - reference 16) has been developed in the UK as a subcritical panel method for aircraft configuration calculations. It is well adapted to lifting configurations, and can deal with vortex wake and lift-dependent drag (to first order) and is adaptable to calculate constraint effects due to ground proximity or wind-tunnel walls. First order viscous effects also can be included. Being widely available in the UK and user-friendly, it has been used successfully as the flow-field part of installed-load computations. Further developments are in progress.

4) TSP (transonic small perturbation method, based on the RAE TSP code) has been used successfully at BAE Brough (17).

5) The Hunt-Semple Mk. II panel method, from BAE Warton (18) is an early panel method which has been used successfully for store load work, as well as for general aerodynamics.

6) Mutual Interference

We have discussed "the aircraft flowfield" as though that is definite, but in practice an array of stores may exert a lot of interference upon the aircraft. For example, suppose we are considering a large store on an inboard pylon. If we are going to use the flow angles and pressures along the store position in order to calculate the forces on the store by some secondary method, it seems unreasonable to exclude any distortions of the flowfield caused by the store itself. Now one way to calculate "the flowfield" at the end of a pylon would be to compute the flow for the fuselage, wing and pylon without the store in position. Then the singularities computed for fuselage, wing and pylon will all pertain to having no store in position. If a store were regarded as in position (a "ghost store"), the singularities at fuselage, wing and pylon will all be appropriate to this case. To enable assessments to be made of this store interference, UK panel methods have introduced "ghost store" facilities. All singularities can then be calculated as though the store is in place. Then the store singularities are set to zero, and the flow field to be imposed on the store is calculated. This approach is particularly relevant to the NUFA method for calculating store forces in non-uniform flow. However, the experimental evidence to justify this argument is, at present, "underwhelming".

Store Force Calculations

Panel methods such as PANAIR and SPARV are time-consuming and costly, so aircraft designers are unwilling to repeat them hundreds of times over, to deal with the wide variety of stores and store positions, and particularly to deal with all the positions and attitudes that stores will pass through on release trajectories. Consequently secondary force calculation methods have been devised, whereby the forces and moments on stores in various positions will be deduced from a very limited number of flow-field computations. The two principal methods are IFM (in USA) and NUFA (in the UK).

1) IFM (The Influence Function Method) has been developed in the USA. The combination of PANAIR and IFM has been dubbed as COST (Cost-effective Option for Store Trajectories). The basic assumptions underlying IFM can be found in many US references (e.g. reference 19). The method assumes that one can divide the length of the store into a number (N) of elements, and that then the normal force and pitching moment on the store in a non-uniform flow-field can be represented as a function of the incidence distribution along the store by equations of the following form:-

$$C_N - C_{N0} = \sum_{i=1}^N A_i (\alpha_i - \alpha_0) \quad \text{--- (13)}$$

$$C_M - C_{M0} = \sum_{i=1}^N B_i (\alpha_i - \alpha_0) \quad \text{--- (14)}$$

A_i and B_i are the influence coefficients, α_i is the incidence at the local element, α_0 is the isolated-store angle of zero lift, and C_{M0} is the zero-lift pitching moment of the isolated store. Similar equations apply for the side force and yawing moment.

In the original formulation of the method, there were three main steps:-

- Calibrate the store in a known non-uniform flow field to determine the influence coefficients.
- Obtain force and moment data for one particular store in a longitudinal traverse in the flow-field of the aircraft concerned, then using the influence coefficients derive the flow angularity for that traverse.
- Using this derived flow data, the loads for other calibrated stores mounted on that traverse can be deduced.

For subsonic speeds, the stores were calibrated by traversing them longitudinally past an ogive-cylinder. For supersonic speeds, the calibration was usually a traverse below a plate giving a 4 degree oblique shock wave.

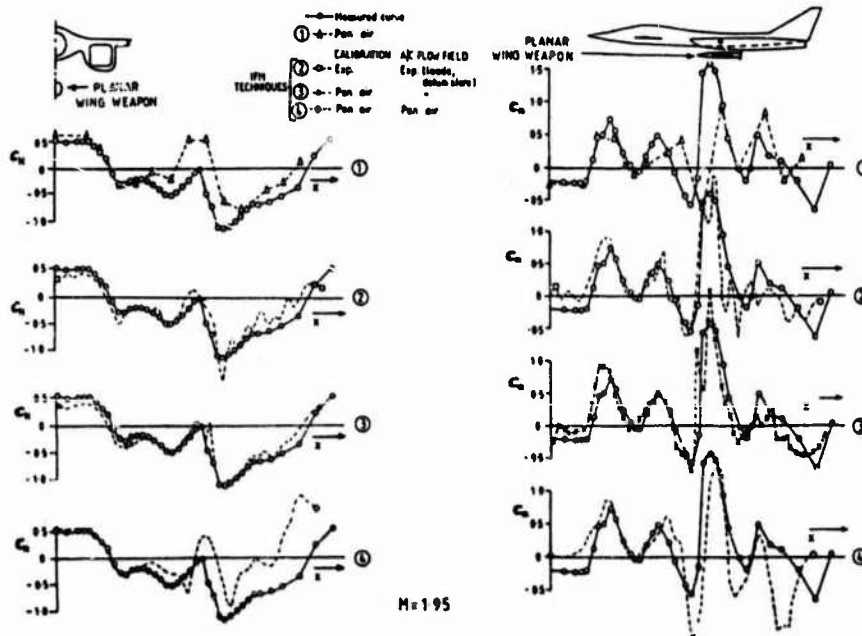


FIGURE 10 PREDICTIONS OF STORE LOADS BY PAN AIR AND IFM TECHNIQUES

Figure 10 shows typical results from various stages of application of IFM, taken from reference 15 and 19. It can be seen that the two predictions where the loads are derived from experimental traverses agree well with the measurements, so the IFM techniques can be used (in this case) to obtain the influence coefficients. When PANAIR was used to give the flow-field (case 4) there were bigger discrepancies. This was due to inaccurate representation of the position and strength of the air intake shock wave, in the calculation, so far as the front part of the store was concerned. However, correction of the shockwave would still leave a discrepancy at the rear end of the model. US reports suggest that IFM may be more accurate for deriving store loads in a given flow-field than PANAIR, for the limitations of PANAIR'S linear theory are avoided in the IFM loads calculation. Thus they conclude that COST may be more accurate as well as cheaper and quicker than using PANAIR for both parts of the calculation.

A recent paper (20) brought this outline up to date. Just as flow angularities can be used to deduce forces, so can force traverses be used to deduce flow angularities. For results obtained no closer than one diameter to another store, the deduced flow angularities agree with measurements.

The assumption of linear connection between angle and force leads to little error on most of the traverses encountered in their tests so far, but could lead to errors when angles exceed (say) 25 degrees. Furthermore, neglect of buoyancy effects may be significant for stores mounted closer than (say) half a diameter apart.

2) NUFA (Non Uniform Flow Aerodynamics) was developed at British Aerospace Bristol (21) from ABACUS, - a well-tried method for predicting missile loads in a uniform free stream. Since NUFA exploits the extensive body of knowledge that went into ABACUS, it will be worthwhile to examine first the scope and restriction of that data.

The missile covered in ABACUS (22) had a reasonably general form, with up to two sets of wings - either monoplane or cruciform (but not with sweptforward leading edges), with the bodies regarded as a nose, a central part of two cylindrical portions joined by a frustrum, and an afterbody which could be either a flare or a conical boat-tail. The flow parameters covered are quite wide: up to 90 degrees of incidence, speeds up to Mach 5.0 and roll angle 0 to 360 degrees. The aerodynamics effects taken into account include vortices shed from the forebody at high incidence, vortex interferences from body and wing vortices, non-linear lift (by the DATCOM method), and some wake interference reducing the lift of the downstream "wings" (or tail, as we may think of it). Body-induced upwash effects are included.

Knowing the crossflow force on every part of the missile as a (non-linear) function of the incidence, a relatively evident generalisation to respond to a non-uniform distribution of incidence leads to NUFA (though the extension to supersonic conditions is not yet complete). For body forces, additional crossflow buoyancy forces are added.

The overall loading on a body is obtained by summing the individual contributions of a number of small axial segments. 40 segments are generally adequate, but a maximum of 100 can be specified. The crossflow loading is calculated using H.J.Allen's concept of adding the viscous crossflow separation force to the potential flow crossflow lift. The segment forces in the Z and Y directions are expressed by :-

$$C_{NZi} = A_i \left(\frac{V_x}{V_\infty}\right)_i + B_i \left(\frac{V_x}{V_\infty}\right)_i^2 \dots \dots \dots (15)$$

$$C_{NYi} = A_i \left(\frac{V_y}{V_\infty}\right)_i + B_i \left(\frac{V_y}{V_\infty}\right)_i^2 \dots \dots \dots (16)$$

Where A is the linear coefficient and is usually obtained by slender-body theory, and B is the non-linear coefficient (crossflow drag). The buoyancy loadings are evaluated by equations of the form :-

$$C_{NZBi} = C \left(\frac{V_x}{V_\infty}\right)_i \frac{d}{dx} \left(\frac{V_x}{V_\infty}\right)_i \dots \dots \dots (17)$$

The NUFA calculations can be applied to flow field data from experiment or from flow field computations - such as SPARV. the NUFA program uses 204 K of memory, and a trajectory of 1.0 second takes typically 3.5 seconds on an IBM 3083.

Figure 11 shows an example of trajectory that would present a stiff test to most prediction methods. The SPARV/NUFA combination predicts the change of pitch motion at 0.3 seconds adequately, whereas SPARV for both parts of the computation fails, because its force/incidence relationship for the store is linear. Thus the non-linear incidence/force relationships of NUFA can be very important for practical trajectories.

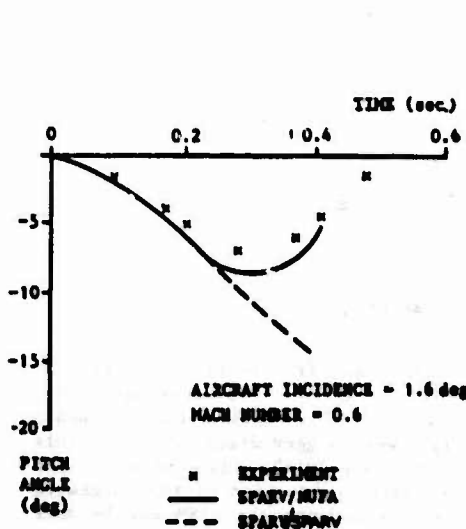


FIGURE 11 PREDICTION OF BOMB RELEASE PITCHING MOTION

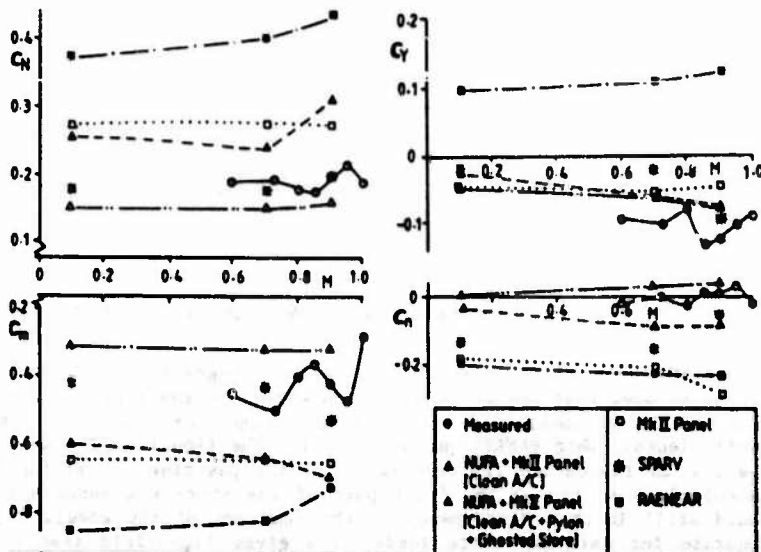


FIGURE 12 PREDICTIONS OF LOADS ON UNDERFUSELAGE STORE BY UK TECHNIQUES

Comparison of UK Methods

Figure 12 presents a comparison (by P. Kearney) of predictions by various UK methods, and measured data for loads on a store mounted on a shoulder station below a fuselage. It includes the Mk. II panel method (for flowfield) with NUFA, using alternatively the flowfield for the clean aircraft, and for the aircraft plus ghost store. Unfortunately for the argument for ghost-store flow fields, the predictions seem over-corrected (if that is the right term) by the ghost store stratagem. However, the accuracy of the experiments was judged as no better than ± 0.5 in C_n and ± 0.10 in C_m . However, SPARV again seems quite good.

Euler Methods

Euler computations are already coming into play for store/airframe interactions - including trajectories (23,24,25). It seems likely that they will come into use increasingly in the next 5 to 15 years, but probably they will stay in the hands of CFD specialists for the earlier part of that time. It is worth noting that although they can deal with compressible flows and shockwaves, they will not cope with major viscous effects, such as boundary layer separations. For these, the next step to Navier-Stokes codes will be needed.

3) AGILITY, AS AFFECTED BY STORES

The effects of stores on aircraft "agility" (in a broad sense) obviously vary greatly with the role of the aircraft (which determines the stores carried) and also with the particular missions flown. In order to assess the penalties caused by excessive store drags, and conversely by the benefits to be won by designing lower-drag store installations, it is necessary to calculate performance capabilities for a range of aircraft and sorties, with two standards of store drag.

An excellent survey of this kind was made by Dr J Barche (26). For present purposes, much of the detail can be omitted, for we are concerned with understanding the basic effects on fighter design. Similarly, typical results will be shown only for one aircraft role: the Close Air Support (CAS) role. This section of the lecture will be based firmly on ref. (26). However, it is worth noting that these hypothetical calculations are already 10 years old: it is already possible to envisage much bigger drag reductions than were assumed then.

Close Air Support example.

The main task for CAS aircraft is air support for ground forces and the examples of CAS types cited by Barche were: SU-7/17 Fitter, Jaguar, Alpha-jet, G-91, A-10, Harrier and Viggen. He considered that store penalties were similar for the Air Interdiction and Counter Air roles, which added the following aircraft examples: Mig-23 Flogger, Tornado, F-4, Buccaneer, F111.

The installed drag of typical stores (1970s vintage) are shown in figures 13 and 14. The example calculated was for a CAS aircraft of 20 000 lb MTOW and a cruise T/W of 0.4 to 0.5. A typical store load was taken as :-

- e 300g fuel tank, under the fuselage
- e 3 x 530 lb bombs on each minor wing station
- e air/ground missile on each outer wing station

The drag increments, above the drag of the clean aircraft, in the various stages of the mission are shown in fig 15. This shows that the relative drag increase:

- e exceeds 100% during acceleration and climb
- e is roughly 100% in the cruise and loiter phase at high Mach numbers
- e about 150% during high-speed descent, cruise and attack with the ventral fuel tank already dropped
- e still around 50% with all droppable stores dropped, but with pylons and triple carriers still attached

Performance characteristics

The influence of stores drag and mass together on performance is manifest on the Specific Excess Power, sustained load factor, and specific range. Maximum speed versus altitude, longitudinal acceleration, climb rate and turn rate are directly connected with these parameters.

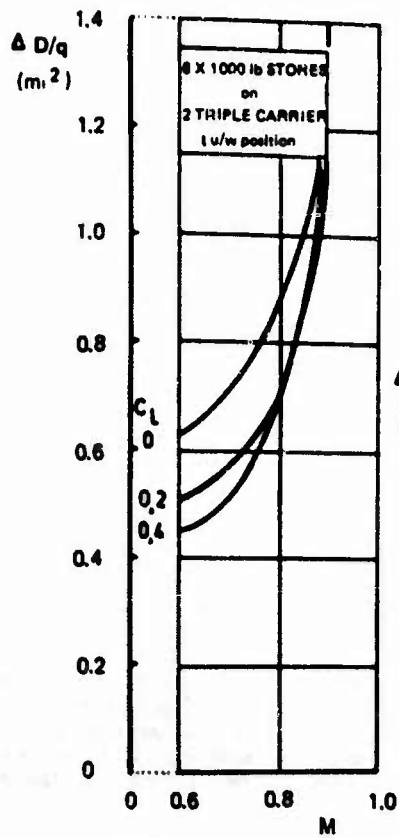
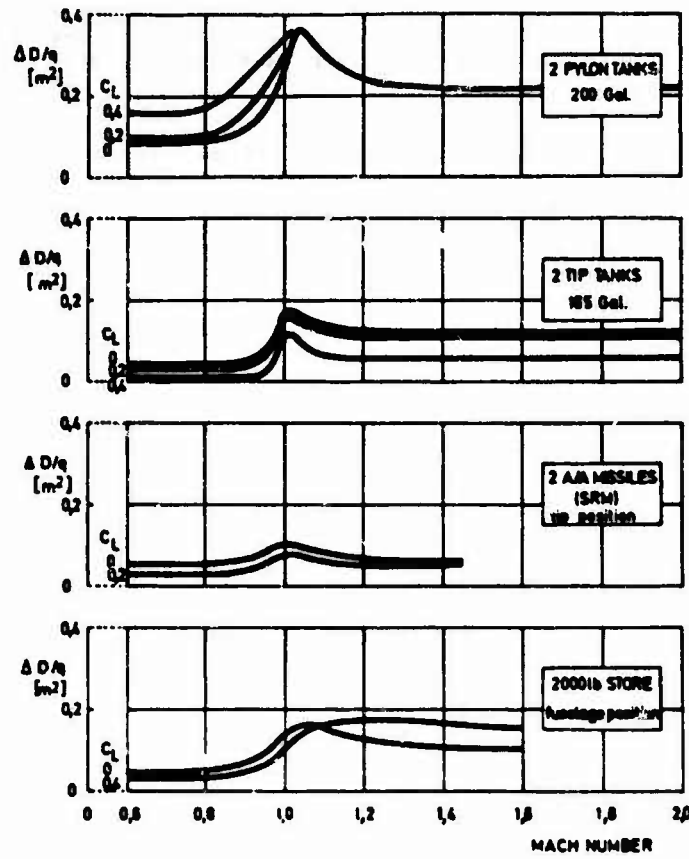
Specific Excess Power is shown in figure 16, both for the clean aircraft and the fully loaded aircraft. The difference between the full lines and the dotted lines indicates the loss of envelope due to stores. The flight envelope ($P_s=0$) is drastically reduced, both in maximum altitude and maximum speed. The envelope corresponding to 50% of the maximum clean-aircraft P_s almost vanishes with full stores. The loaded manoeuvrability is very poor, so if attacked, all stores have to be dropped and the mission aborted.

Load factors are shown in fig 17. The losses of capacity are just as dramatic as for SEP.

Specific Range is shown in fig 18. At higher altitudes the range losses are almost 50% (partly due to store weight, as well as drag). At sea level, the range losses are in the 30% - 40% range (mostly due to drag).

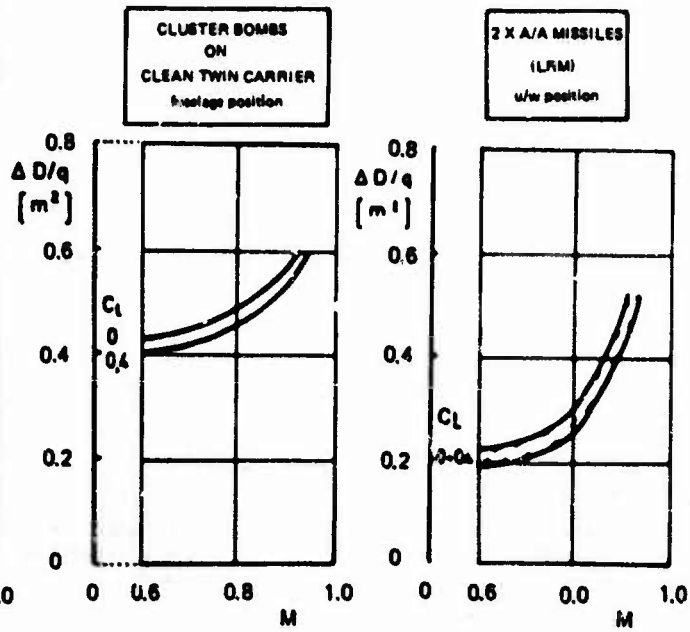
**INSTALLED DRAG
of typical stores ①**

FIGURE 13



**INSTALLED DRAG
of typical stores ②**

FIGURE 14



Sensitivity to Improvements

Barche's paper (26) gives interesting sensitivity analyses for all of the combat types considered (Air Defence, CAS, Air Interdiction, Counter Air, and Tactical Air Reconnaissance). He expressed his sensitivity results by means of the equation:-

$$F + f_M + \frac{\Delta M}{M} + f_W \frac{\Delta W}{W} + f_T \frac{\Delta T}{T} + f_n \frac{\Delta n_2}{n_2} = f_0 \frac{\Delta C_{D0}}{C_{D0}} \quad \dots (10)$$

The various terms in this equation are given in his table below, where $C_0 = C_{D0}$, $C_1 = \frac{D_n}{W}$. To understand this it is instructive to write out and simplify the equations for the various performance parameters.

PERFORMANCE PARAMETER	F	f _M	f _W	f _T	f _n	f ₀
max. Mach number thrust	0	2(1-2C ₀)	2(C ₀ -1)	1	2(C ₀ -1)	C ₀
specific range	Δr/r	4C ₀ -3	-2(C ₀ -1)	0	-2(C ₀ -1)	-C ₀
SEP	ΔP ₀ /P ₀	4C ₀ C ₁ -2C ₁ -1	1-2C ₁ (C ₀ -1)	-(1+C ₁)	-2C ₁ (C ₀ -1)	-C ₀ C ₁
load factor	0	(1-2C ₀ /C ₀ -1)	1	0.5/(C ₀ -1)	1	0.5C ₀ /(C ₀ -1)
turn rate	Δw/w	1	0	0	1	0

Example: Specific range

Table shows: $\Delta r/r + (4C_0 - 3)\Delta M/M - 2(C_0 - 1)\Delta W/W + 0\Delta T/T - 2(C_0 - 1)\Delta n_2/n_2 = -C_0\Delta C_{D0}/C_{D0}$
 If $\Delta M = \Delta T = \Delta n_2 = 0$, then: $\Delta r/r - 2(C_0 - 1)\Delta W/W = -C_0\Delta C_{D0}/C_{D0}$

Conformal Carriage

Barche's whole message (ten years ago) was that it was very important to reduce the drag penalties of stores, but his expectations for possible store-drag reductions have already been surpassed in many respects. His examination of the benefits of conformal carriage were closer to a foretaste of the improvements we should aim to incorporate into new designs, though even these benefits are not the best that can be done. With this preamble, we will look at the benefits of conformal carriage relative to conventional multiple ejector-rack carriage on F-4 aircraft (pioneered by J H Nichols, reference 7).

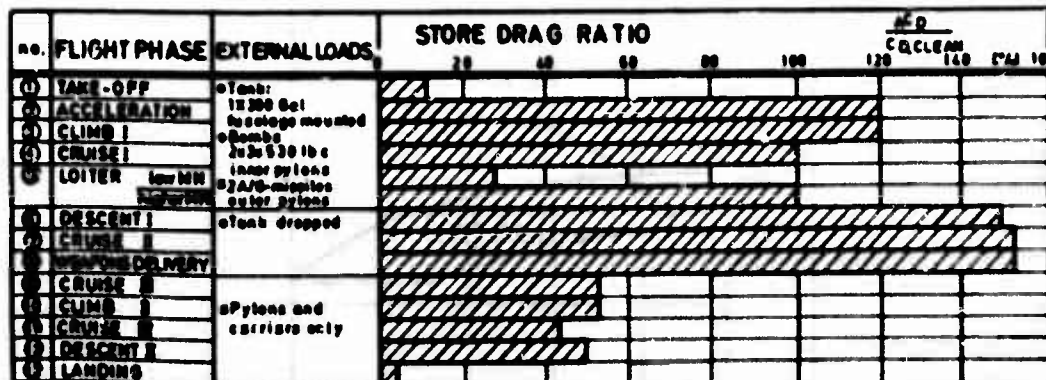
Figure 19 shows in the bar-chart form the specific range of an F-4 aircraft with empty TER/MER/TER racks, and with the racks loaded with "low drag" Mk 82 bombs. The empty racks alone reduced the range 11% in cruise and 18% at low altitude. Adding the bombs, the range degradation relative to clean aircraft came to 20% in cruise and 31% at low altitude.

Alternatively the F-4 when fitted with an unloaded conformal adaptor actually had 4% more range in low level flight. When loaded with 12 bombs, the range penalty was only 7% (instead of 20%) for cruise and 8% (instead of 31%) for low altitude flight.

The effects on the flight envelope are quite radical, as shown in fig 20. Note that with conventional carriage, the F-4 had no supersonic capability, but with the conformal loading, the majority of the clean-aircraft supersonic flight envelope was available. Doubtless, if this had been designed into the aircraft in the first place, instead of as a retrofit, the benefits would have been better still.

**STORE DRAG INCREMENT
CAS-aircraft**

FIGURE 15



SPECIFIC EXCESS POWER
CAS AIRCRAFT

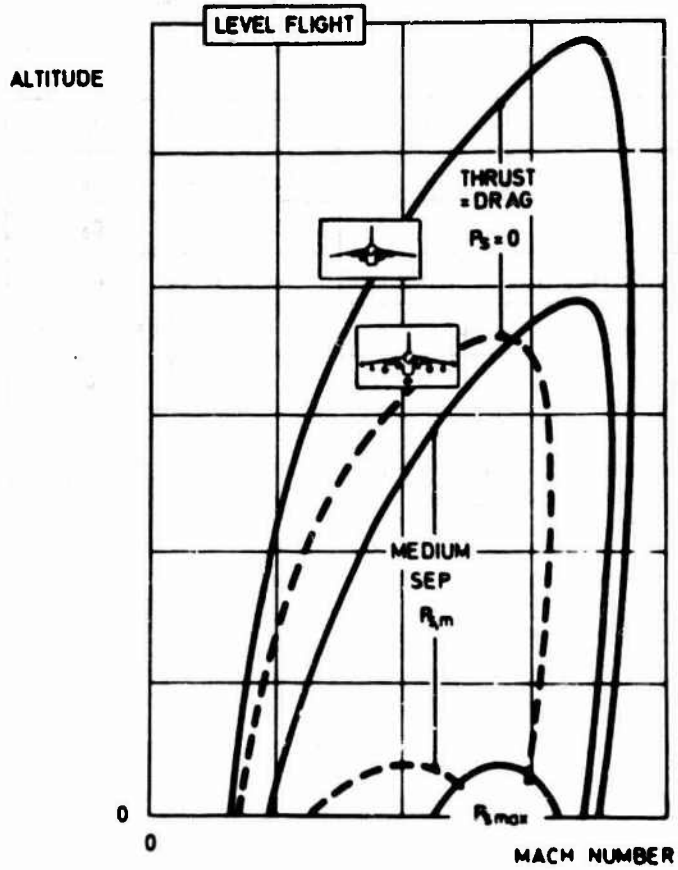


FIGURE 16

LOAD FACTOR n_z

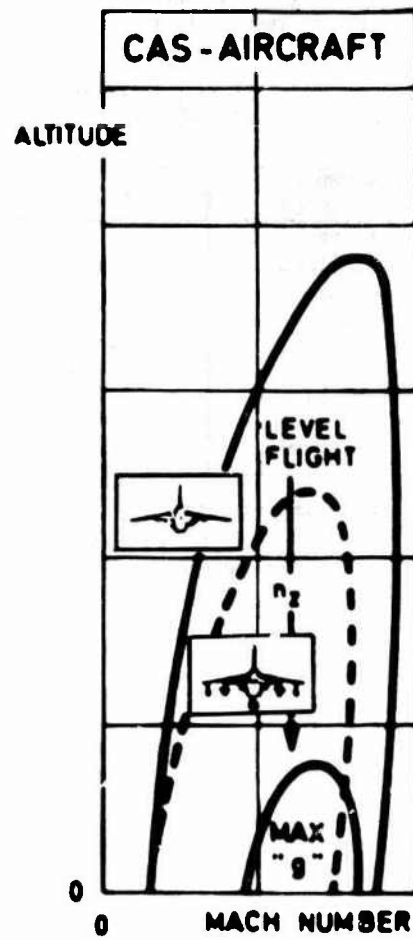
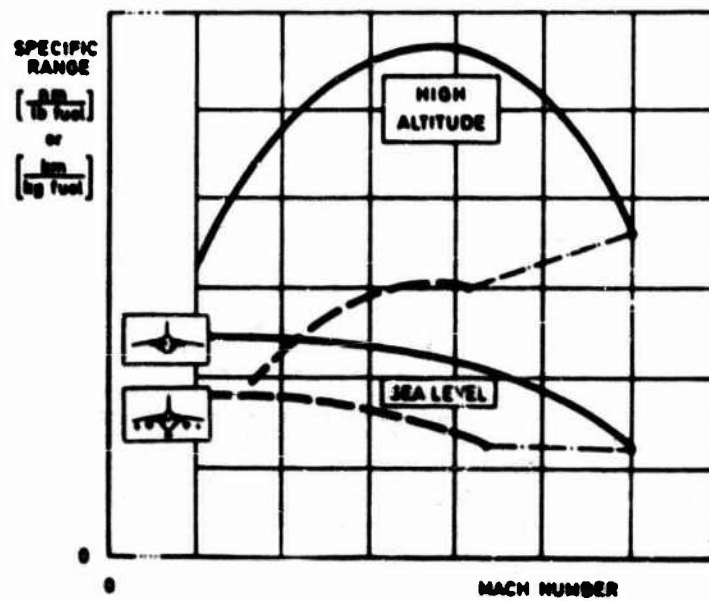


FIGURE 17

SPECIFIC RANGE
CAS-aircraft

FIGURE 18



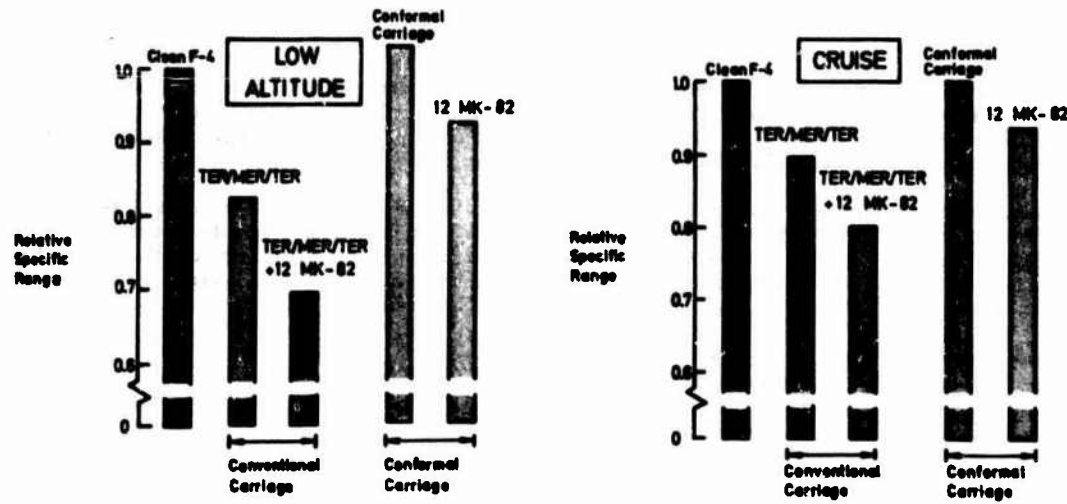


FIGURE 19

SPECIFIC RANGE
Conventional / Conformal Carriage

FLIGHT ENVELOPE
clean a/c - conventional - conformal carriage

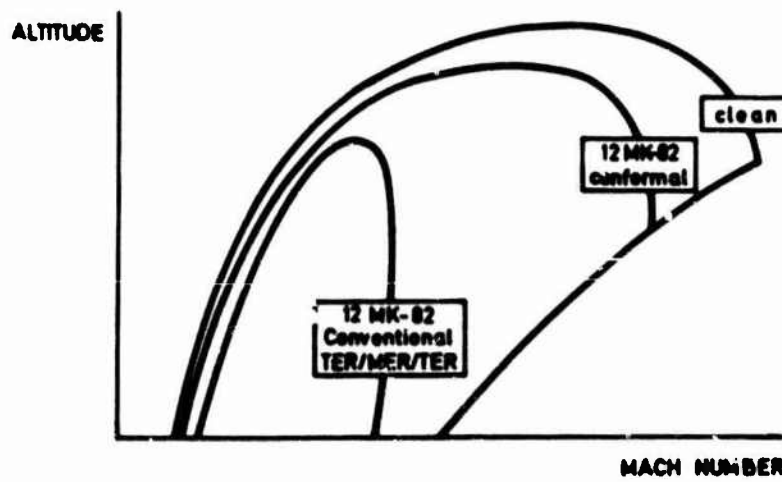


FIGURE 20

4) STABILITY AND FLUTTERStability

Systematic relationships between store arrays and stability are few, but the conclusions of a survey by Coursimault (27) can be summarised.

Lateral Stability

Pylon-mounted external under the fuselage can decrease the directional stability and also lead to excessive sideslips in abrupt rolls - see fig 21. Conformal carriage of stores under F-4 led to greater directional stability stores than an F-4 with conventional multiple-rack loading. Wing-pylon stores also can have a detrimental effect on lateral stability, but this can be kept within bounds.

Not enough generalised work has been done to permit firm rules, but it can be speculated that part of the lateral effects are due to "forward fin" aerodynamics, but for fuselage-mounted stores there is also always a likelihood of any thick boundary-layer wake affecting the behaviour of the tail fin of the aircraft. This produces both a reduction of fin effectiveness, and a tendency towards limited snaking, as the fin oscillates back and forth through the thickness of the wake.

From such arguments one could postulate two rules:

- 1) Minimise the forward - fin behaviour of the stores, and
- 3) Minimise the drag of the store installations.

Longitudinal Stability

Generally, aircraft carrying external wing stores experience reduced pitching stability, as illustrated by fig 22. Taissere (28) concluded from tailplane-off/tailplane-on tests that most of the stability loss arose from extra downwash acting on the tailplane.

Stores alone (not fixed to a pylon) cause change in the aircraft neutral point, but no tailplane downwash contribution. Pylons experience increasing outwards lift as the wing incidence increases, and this leaves a trailing vortex wake which gives increasing downwash inboard of the pylon. The tailplane reacts to this with increasing download. Presumably aircraft without a conventional inboard tailplane would not experience this stability degradation. When stores are added to the end of the pylons, the outwards lifting force on the pylon/store combination is increased. This increases the strength of the trailing vortices, and would normally increase the unstable contribution on the tailplane.

These contributions depend, of course, on the relative heights of stores and tailplane, and so vary with aircraft incidence. They also vary with the amount of lift acting outwards on the pylon/store combination, so if the pylon is angled and cambered to have low lift, the tailplane-reacted instability is reduced. It has also been found that it is beneficial to reduce the sideways facing area of the pylon, particularly under the wing leading edge, where the outwards flow is greatest. Tails on the stores may reduce the instability contribution, but this is mostly due to reduced downwash effects on the aircraft tailplane.

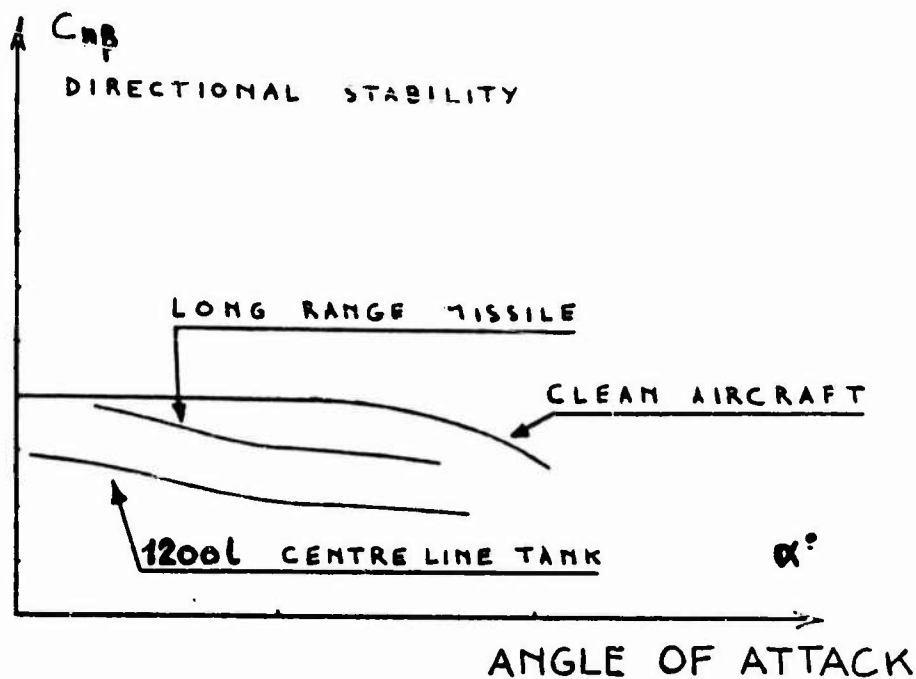


FIGURE 21 INFLUENCE OF FUSELAGE STORES ON DIRECTIONAL STABILITY

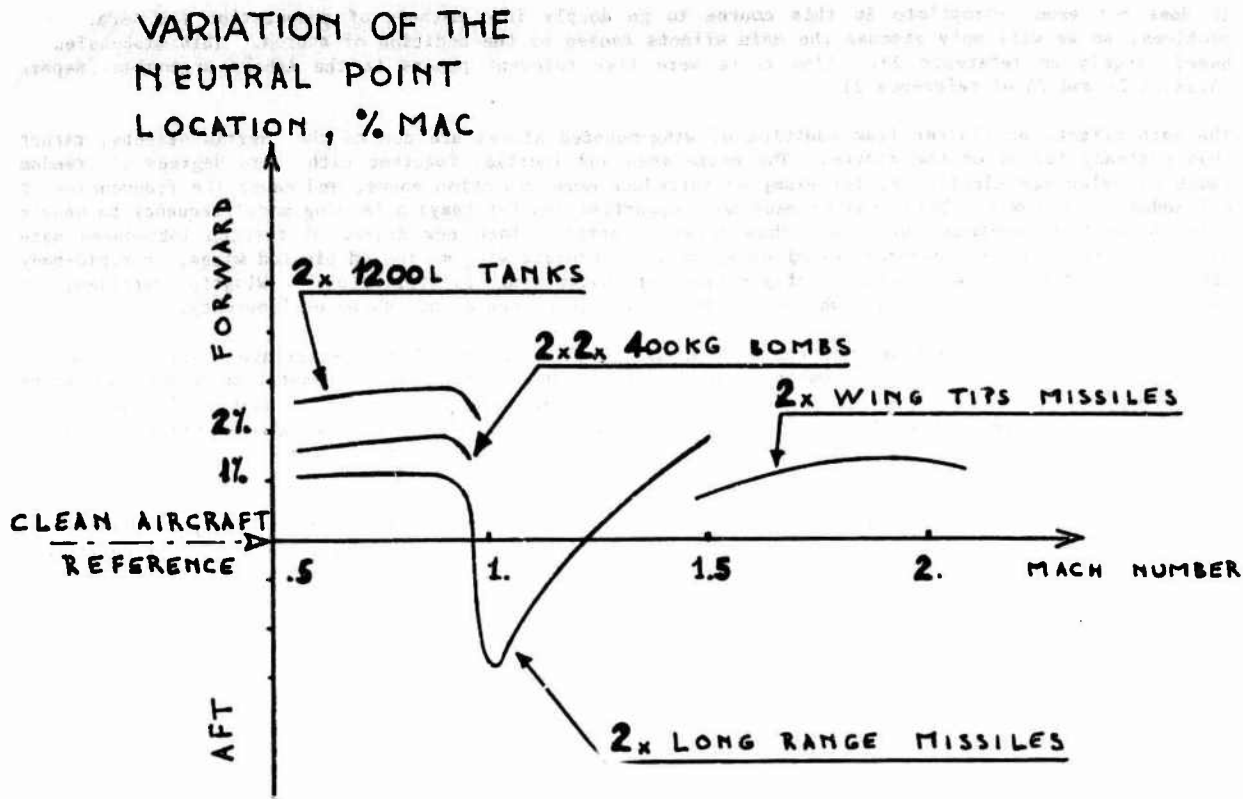


FIGURE 22 INFLUENCE OF WING STORES ON NEUTRAL POINT LOCATION

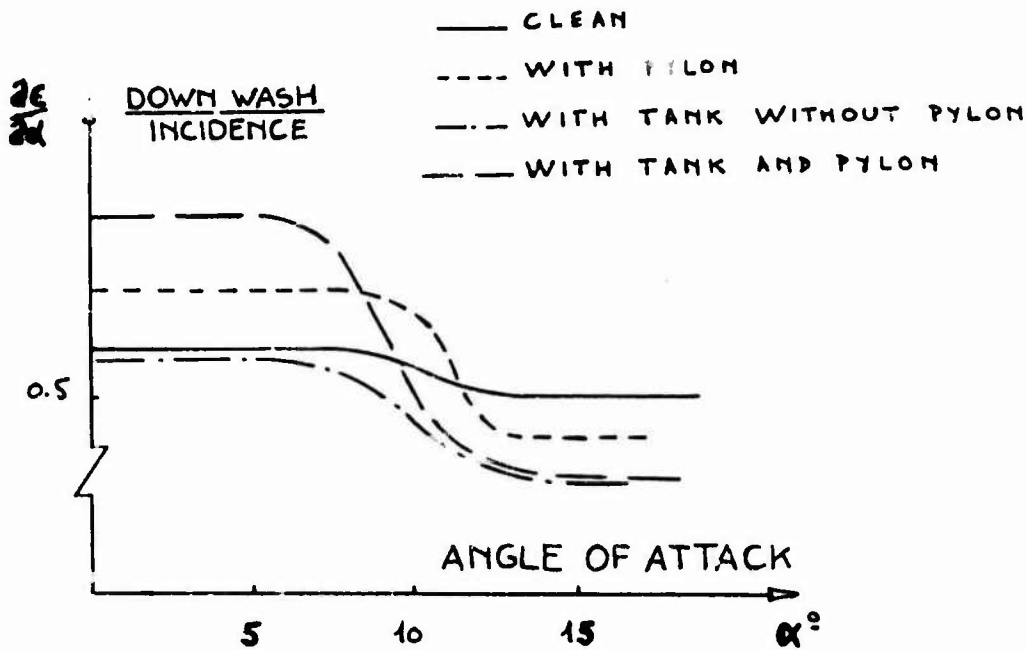


FIGURE 23 INFLUENCE OF PYLONS AND STORES ON DOWNWASH AT TAIL STATION

Flutter, and other unsteady interactions

It does not seem appropriate in this course to go deeply into methods of computation for aeroelastic problems, so we will only discuss the main effects caused by the addition of stores. This discussion is based largely on reference 29. Also there were five relevant papers in the Athens symposium (papers 15,18,23,24 and 25 of reference 2)

The main effects on flutter from addition of wing-mounted stores are due to the inertia effects, rather than unsteady forces on the stores. The extra mass and inertia, together with extra degrees of freedom (such as pylon yaw elasticity, for example) introduce more vibration modes, and cause the frequencies of all modes to be lower. This creates many more opportunities for (say) a bending mode frequency to nearly coincide with a torsional mode, and thus permit flutter. Each new degree of freedom introduces more opportunities for mode frequency coincidence, such as fore-aft wing motion on pivoted wings, or rigid-body pitching on forward-swept wing configuration or pylon/wing flexibilities. Wingtip carriage, in particular, may lead to need for substantial ballasting to change a mode shape or frequency.

The great number of store types, in combination with a variety of store-carriage station, leads to an enormous number of possible combinations to check out. Since each computation itself is quite elaborate, the aeroelastics specialists are always seeking ways to reduce the number of cases to be computed. It has been shown (ref. 30) that clean-wing modes alone are not enough to give good flutter predictions: a combination of wing-flap modes, wing/discrete load modes and wing/pylon modes gives far better representation.

In some cases, the flutter speed is sensitive to store C.G., to pylon yaw stiffness, or pylon frequency. It is not always simply a matter of increasing the stiffnesses, for the tuning required aims to prevent coincidence of (say) torsion and bending mode frequencies. For example, a low flutter speed may occur when the frequency for a bending mode (wing or pylon bending) is in the vicinity of a wing mode having considerable torsional motion induced by inertia loads on the store. Other modes, such as pylon yaw, may be involved.

Unsteady aerodynamic pressures, which comprises in-phase and out-of-phase components of the pressures, are obtained by specialised codes such as NLR or NASTRAN doublet-lattice codes. Although both subsonic and supersonic codes can be obtained, relatively little work has been published on transonic codes. For unsteady pressures, any effects likely to arise from separated boundary layers (during buffet, for example) are unexplored.

Since the main basis for prediction, prevention and control of flutter is generally regarded as a corroborated mathematical - analytical model, and some elements of the aerodynamic modelling are not yet demonstrated to be adequate, there is usually a call for aeroelastic model testing to back up the computations. Dynamic similitude is necessary to scale the modelling.

Buffet effects

Not all oscillating loads are due to aeroelastic phenomena, for an important class of loading actions arises from fluctuating boundary layer separations, which may occur over large or small areas of surface. Sometimes a local buffeting action may impose structurally significant loads on an aircraft component: for example perhaps 70% of the static strength at 50 times per second. It does not take long to build up fatigue damage on (for example) an aileron operating rod or hinge, if such strong local buffeting occurs. This could occur perhaps, if a fuel tank or store group leads to a shock induced separation under the aileron or flap. At present, such loadings cannot be predicted reliably: it is better to conduct wind tunnel tests using oil-flow flow visualization, and measure local pressure fluctuations in any structurally significant areas. Sometimes, such effects are missed during the design stage, and eventually the measurements are found necessary during flight development (a more expensive stage).

STORE RELEASE

In general, there are two categories of store release to contend with: firstly releases of stores which merely have to leave the aircraft without damaging it, and secondly releases of weapons, which then have to knock out a target. In both cases, it is essential to ensure no damage to the aircraft. In the second case there is the additional requirement that the store should not suffer undue disturbance on release. The big difference is the size of release disturbance which can be tolerated.

Now the total disturbance to a store on release includes all the aerodynamic disturbances acting upon it during its trajectory (especially the part nearest the aircraft). We have already considered the problems of calculating these disturbances in the section headed "DRAG AND OTHER INSTALLED FORCES". The forces imposed by the ejector release unit also have to be taken into account carefully. On British ERU's there are two ejector rams to each store, and it is possible to alter the ratio of the two forces, so that the mechanical impulse applied may be nose-down, through level to nose-up. Typically, an end-of-stroke velocity is intended to be about 3 m/s. A cordite cartridge produces high-pressure gas which flows through an orifice ("throttle") to each ejector ram, and different sizes of throttle can be fitted. Unfortunately, the total impulse generated is not generally within close tolerances, and worse, sometimes a coarse particle of debris from the cartridge may block or partially block one of the throttles. Then the impulse applied to the store is greatly different from what was "expected". Any reasonably probable malfunction of this sort has to be allowed for.

The energy applied to the store is not dictated by the ERU alone. An ejector ram is usually a device producing a certain amount of work output. If the aerodynamic force on the store when installed is (for example) such as to hold the store up, then some of the work done by the ram is expended on moving the store against the aerodynamic forces, so the end-of-stroke velocity of the store is reduced. Other important factors are the effective mass and stiffness of the wing, pylon and remaining stores at the station concerned. If these are low, the ram may be expending more work on pushing the wing up, than on pushing the store down. Cases have been cited (31) where the net impulse on the 4th store from a 4-store rack was only about one-tenth as much as the impulse on the first to go.

It follows that for wing-mounted stores, quite elaborate calculations may be needed to work out the required ERU throttle settings. Experimental ERU firings are needed to verify the main assumptions of such releases, wherein a simulated (or real) wing/pylon/ERU/ set up is fired above a pit in which the store is caught. These are known as "pit drops".

If stores are mounted under a fuselage, many of the above mass and stiffness problems largely vanish.

If a store is particularly unstable, it may be regarded as necessary to mount the store on a trapeze arm which swings down through a substantial angle before the hinge disengages. In other cases, special forms of launcher may form a major part of a project study.

Experimental Prediction Methods

Since the number of possible combinations of stores, stations, adjacent stores and release conditions is enormous, any store release development and proving programme that depended solely on flight trials would be extremely expensive. Because of this, a great deal of effort has gone into developing reliable calculations (see DRAG AND OTHER INSTALLED FORCES) and wind-tunnel based experimental methods which reduce the flight test programme. Applying this philosophy, the wind-tunnel programme for the A-7D store release certification saved over \$16,000,000 at 1970 prices (ref 32).

It would be out of place to review experimental store release techniques in any depth here. For an excellent review, see Mathews (31). All we do is to outline the nature of the wind-tunnel techniques now in use, to bring out their strengths and weaknesses. Basically there are two classes of tunnel-based techniques: (1) free drop and (2) captive trajectory.

Free-drop Techniques

Naturally, the earliest experimental techniques involved dropping model stores in wind tunnels. As usual, we have to choose which similarity rules are to be respected for the models. For trajectory tracing there are three ways of choosing similitude: Froude scaling (which simulates all dimensions properly, provided that Mach number does not matter significantly), and the so-called "light model" and "heavy model" techniques which both specify equal Mach numbers for model and flight.

For any free-drop technique, it is well-known that the ratios of aerodynamic to gravitational forces must be the same both for the model tests and flight.

$$\frac{\left(\frac{F}{mg}\right)_M}{\left(\frac{F}{mg}\right)_F} = \frac{\left(\frac{\gamma}{2} p M^2 C_F S_s\right)_M}{\left(\frac{\gamma}{2} p M^2 C_F S_s\right)_F} \bigg/ \frac{\left(\frac{\gamma}{2} p M^2 C_F S_s\right)_M}{\left(\frac{\gamma}{2} p M^2 C_F S_s\right)_F} = 1 \quad - (19)$$

where σ is store density, p is ambient pressure, M is test Mach number, V_s is store volume.

Froude Scaling

For this form of scaling, the gravity accelerations for model and flight are accepted as equal, as are the force coefficients. Putting the model scale as k_n , so that area S scales with k_n^2 and the volume B scales with k_n^3 , equation 19 reduces to:-

$$\left(\frac{\rho M^2}{\sigma}\right)_M n = \left(\frac{\rho M^2}{\sigma}\right)_F \quad \text{--- (20)}$$

writing $U = aM$ where a is the speed of sound, and \sqrt{T} we get:-

$$\left(\frac{\rho U^2}{\sigma T}\right)_M n = \left(\frac{\rho U^2}{\sigma T}\right)_F \quad \text{--- (21)}$$

The speed scale then becomes $n^{1/2}$ and the scale for densities becomes

$$\frac{\sigma_M}{\sigma_F} = \left(\frac{\rho_T}{\rho_T}\right)_F \quad \text{--- (22)}$$

This form of scaling is ideal for tests where the Mach number of the free-stream flow is of little consequence, and in particular it is used for simulations of snow and ice build-up, sand ingestion and low-speed trajectory work. However, for transonic and supersonic tests it is often essential to test the model at flight Mach number. Then with Mach number set, some part of the model simulation may be wrong. There is scope to choose which part of the simulation may be disregarded.

Heavy Model Scaling

For heavy model scaling, the main choices are $M_M = M_F$, and $g_M = g_F$

$$\therefore \frac{\sigma_M}{\sigma_F} = n \frac{\rho_M}{\rho_F} \quad \text{--- (23)}$$

(for test nominal Mach number)

Because all accelerations are related to the gravitational acceleration, which leads to a low vertical velocity at the lowest edge of the aircraft model flowfield, it follows that all model store velocities relative to the local airflow are too low. Therefore true relative Mach numbers are not properly simulated, despite the intention. It is therefore erroneous, no matter how important the establishments which use it.

Another difficulty arises for small models, for the very high density required for the model stores may not be practical.

Light Model Scaling

The aim of light-model scaling is to get all relative velocities scaled correctly. Firstly the free-stream Mach number for the model is set to the flight Mach number. In order to achieve the proper relative velocities between the local airflow and the model store, the model store has to reach full-scale values of perturbation velocity. Thus the aerodynamically caused accelerations have to be scaled to n times the flight accelerations.

Ideally, the gravitational acceleration acting on the store must be scaled by the same factor as the aerodynamic accelerations; that is by n . Then all relative Mach numbers would be correct. Then we can set $M_M = M_F$ in equation (19), and the geometrical scaling gives:

$$\left(\frac{S}{V_s}\right)_M n = \left(\frac{S}{V_s}\right)_F \quad \text{--- (24)}$$

so equation (19) reduces to

$$\left(\frac{\rho}{\sigma g}\right)_M n = \left(\frac{\rho}{\sigma g}\right)_F \quad \text{--- (25)}$$

Now in accordance with the argument above, we take $g_M = n g_F$ then:-

$$\left(\frac{\rho}{\sigma}\right)_M = \left(\frac{\rho}{\sigma}\right)_F \quad \text{--- (26)}$$

In practice, it is not easy to simulate a multiplied gravity acceleration on the store. A strong magnetic field could be considered, but has not been engineered. The nearest practical approach is to accelerate the aircraft model upwards at an acceleration of $(n-1)$ times gravity, as in the Accelerated Model Rig (AMR) technique (33,34). This will be outlined briefly. Otherwise, the deficiency in the gravitational acceleration is accepted with or without some corrections.

Deficiencies of light model jettisons

The errors due to providing a gravitational acceleration on the model store of 1.0 g instead of n g are obviously greater if the model scale is smaller. In France, the solution has been often to test a large-scale model at Modane, and hope that the errors are not important. If we take a simple minded view, for the moment, we can argue that the model store drops too little distance under gravity in simple light-model tests. If we are concerned merely with the store falling away without hitting the aircraft, it could be argued: "if the store clears the aircraft in a light-model test, it would clear by a greater margin with properly simulated gravity". Such an argument lay behind much early store clearance testing.

A simple minded trajectory "correction" can be calculated by calculating an additional drop for the store, according to this equation:

$$\Delta h = \frac{1}{2}(h-1)t^2 \quad \text{--- (27)}$$

where t is the elapsed time since release. This "corrects" the trajectory further downwards, but because the model store has remained too close to the aircraft for too long, it will have been subject to inappropriate aerodynamic disturbances for too long.

Accelerated Model Rig (AMR) Techniques

The aim of the modelling is to achieve a model trajectory which is the same shape as the flight trajectory, and of model scale. Light model scaling arranges that the aerodynamic accelerations are properly scaled. The motion of the store through the aircraft flowfield in the direction of gravity needs more thought. The basic aim is to arrange that the model store passes through the model flowfield at the scaled rates. Since the movement of the store relative to the ground remains at 1.0 g, we have to move the aircraft and its flowfield (relative to the ground) in order to make the path of the store relative to the aircraft correct. Suppose the model is full scale. With the AMR techniques (33,34) the aerodynamic accelerations have to be 1/30 times those of flight. The proper relative acceleration in the gravity direction is made up of 1.0g on the store and 29g on the aircraft and its flowfield. This corrects for all first order effects, but leaves a small angular rate discrepancy, which is corrected for by imparting the appropriate increment of pitching rate to the model store at release. Then the entire dynamic scaling is very close.

The technique has been validated at BAe (Brough) on Buccaneer, Harrier, Hawk and Tornado, including a particularly sensitive test case where an awkwardly shaped empty dispenser struck the flight aircraft.

An important advantage of this technique is that very awkward-shaped stores can be dealt with, and severely tumbling trajectories, without any need for separate tests or calculations to find the aerodynamics of the store at all speeds and altitudes. There are no support interferences on the stores, and multiple releases could be tested. Overwing releases also can be simulated. A disadvantage is the need to make the special moulds for the carefully ballasted stores. The techniques required have been perfected at BAe Brough, but for any new facility to acquire them would be a significant task.

Two-Sting rigs

Two-sting rigs were pioneered in the USA (35) but they have been emulated in the UK (36), France and Canada, at least. The model store is supported from a controllable sting, so that it can be positioned anywhere around likely trajectories, and measure the aerodynamic forces at each position. In principle, once the forces are known at one point in a trajectory, the next point in the trajectory can be calculated. So one way of using the rig is to read the forces into a computer and compute the next point of the trajectory on-line. It should be noted that the model store is effectively stationary in the flowfield at each point of its trajectory, so the forces measured are not the same as would be experienced by a store with the properly scaled crossflow and rotational velocities. The usual way of allowing for these effects is to incorporate estimated corrections for the calculated motions. This mode of operation is known as the Captive Trajectory System (CTS).

Another way of using the rig is to measure forces at a number of points on a three-dimensional grid which encloses the likely trajectories, and then to calculate the various points on a trajectory by interpolation for the forces, plus the motion corrections. This way of operating is the grid Survey mode.

Yet another way is to do a grid survey of local flow directions and total pressures, so that the trajectories could be calculated using a secondary force calculation procedure (e.g IFM or NUFA).

Recent experience (e.g 36) suggests that two-sting rigs are being used increasingly in the grid-survey mode, with fewer on-line captive trajectories. This is because the latter require substantially more time in the wind-tunnel, and therefore more cost. These rigs are proving their usefulness every day. They are especially useful for missile launches, and for understanding interference aerodynamics close to the aircraft.

6) AIRFRAME/STORE INTEGRATION

At every stage of fighter design, the same conclusions arise. It is worth a great deal to reduce store drag and the aerodynamic release disturbances. Although much can be done to improve on existing aircraft/store configurations, a great deal more could be done by designing new aircraft and new stores from the start so that the combination will be exceptionally efficient. We have already seen that conformal (or tangential) carriage of stores has a number of major advantages, and more recent thoughts naturally turn to semi-submerged carriage, or to store carriers designed to fit like blisters smoothly to the surface. Such arrangements are classed as "integrated".

The best-known example of the latter type of integration is the F-15 "Fastpack" (37), which incorporates smoothly blended quick-release units which accommodate various interchangeable role packs, such as fuel, ERU's with stores and so on. Figures 24, 25 and 26 show an early version of the F-15 Fastpack system, while fig 27 shows the large drag saving possible.

Work is continuing on various schemes of this sort, and on other schemes of semi-submergence and blister packs. It is not so easy to apply such schemes under wings, because of the small chordwise lengths available. However, the advantages are potentially so valuable that very substantial work is merited. These advantages include role-change and turn-round time, and stealth: matters which must not be under-rated.

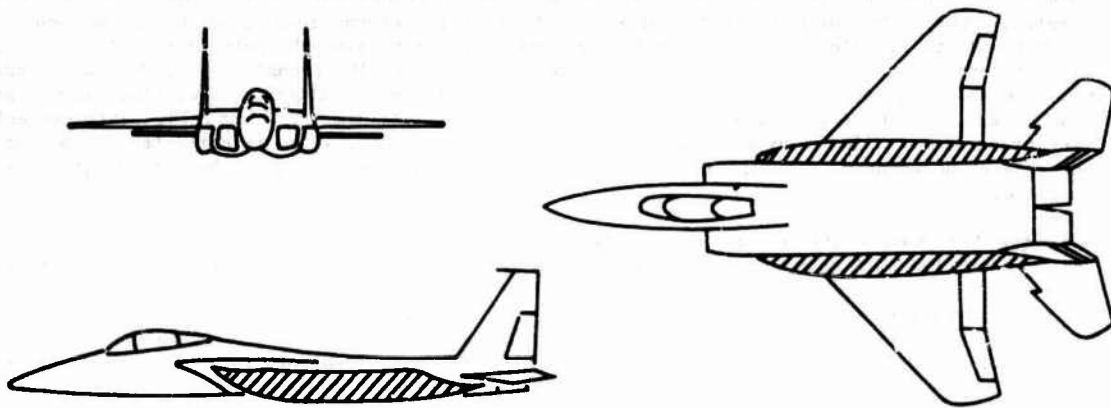
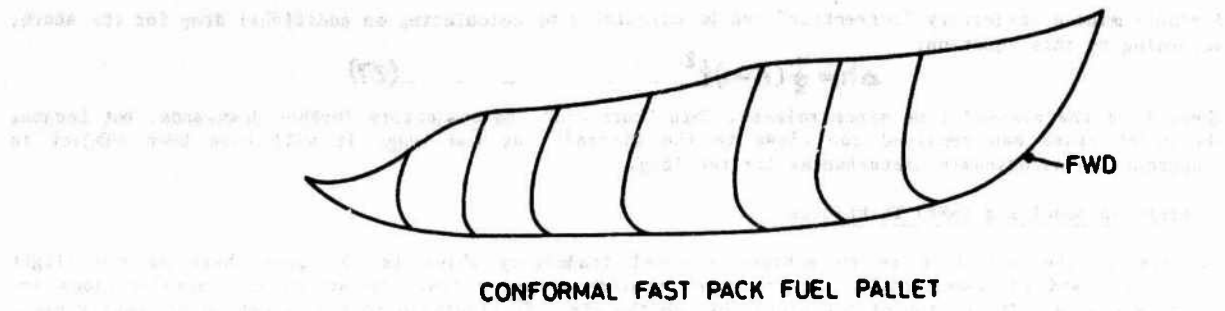


FIGURE 24 F-15 FAST PACK INSTALLATION

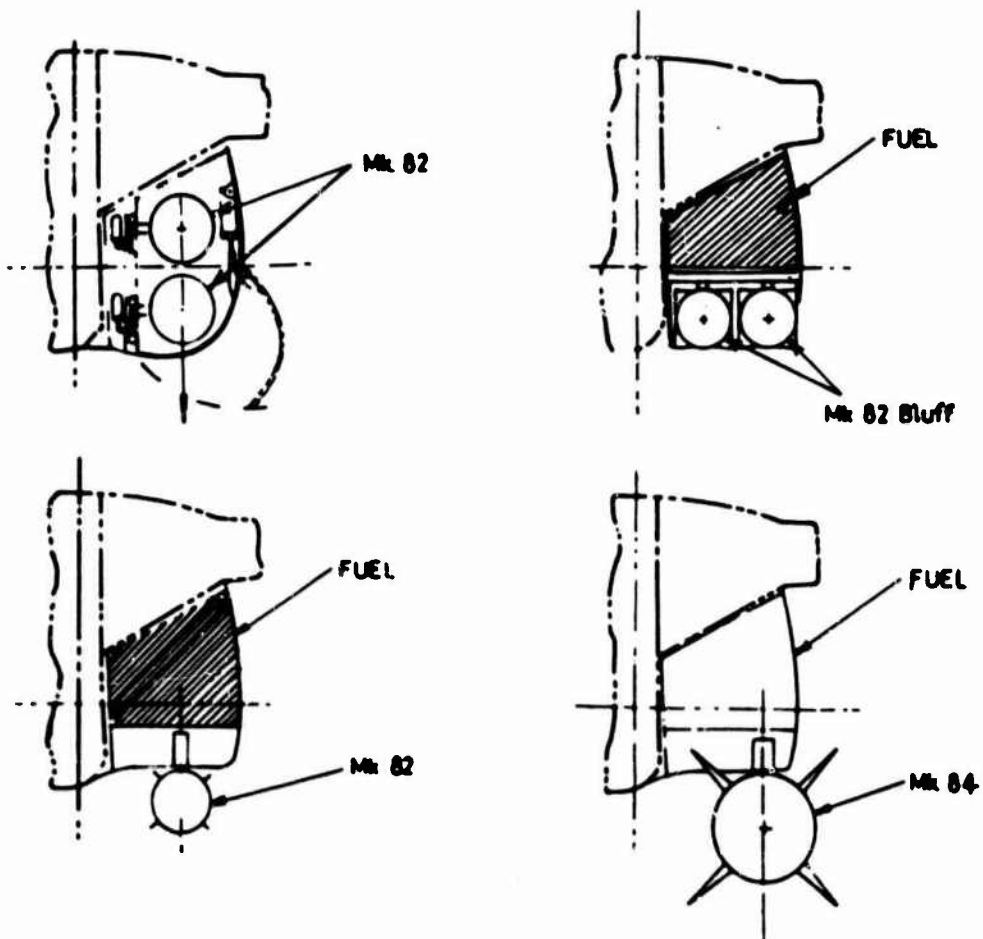


FIGURE 25 FAST PACK STORE LOADINGS

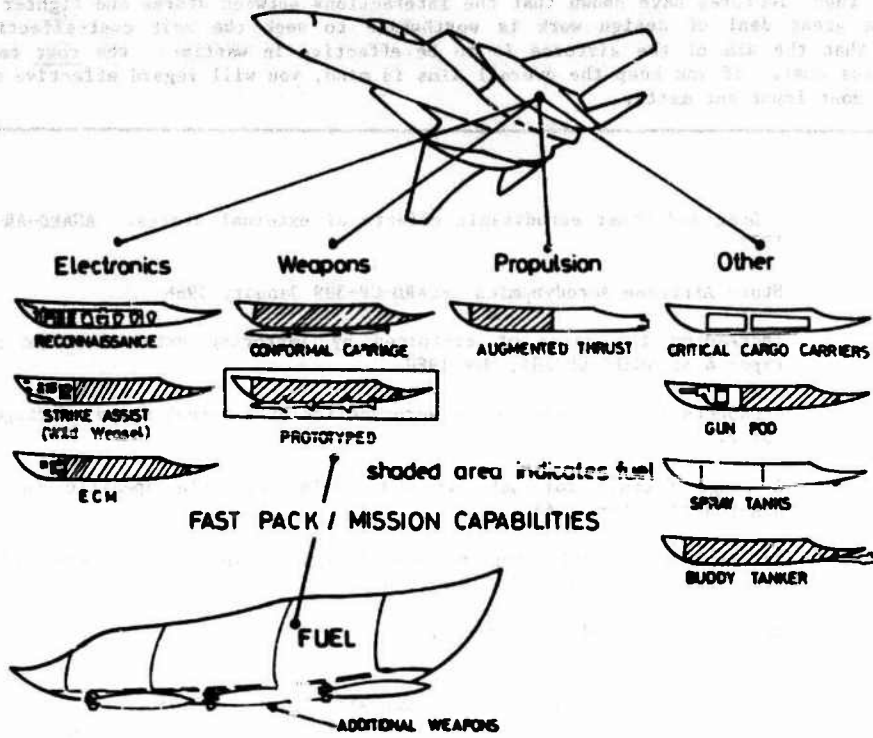


FIGURE 26 F-15 CONFORMAL WEAPONS / FUEL PALLET

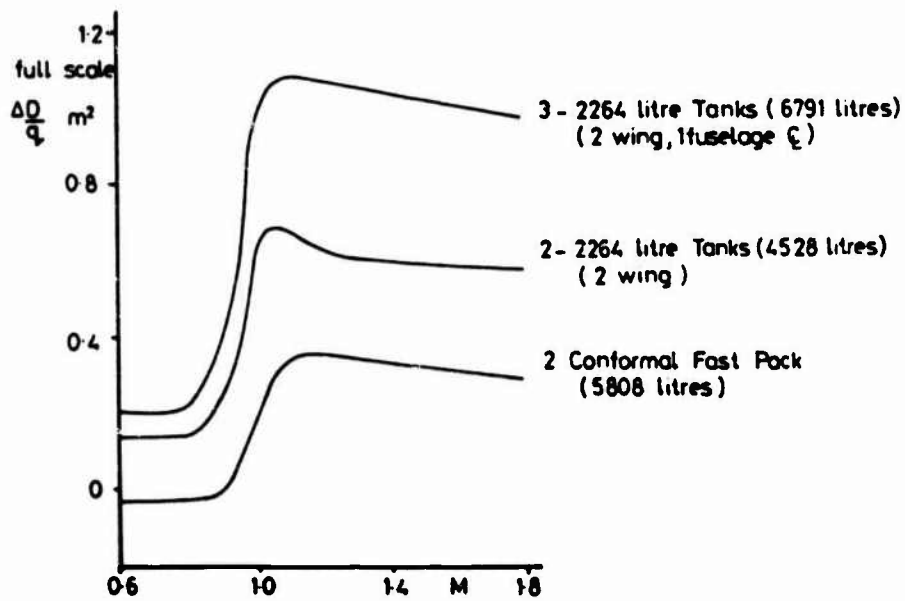


FIGURE 27 CONFORMAL VS. CONVENTIONAL FUEL TANK INSTALLATIONS, F-15

CONCLUSIONS

It is hoped that these lectures have shown that the interactions between stores and fighter design are so important that a great deal of design work is worthwhile to seek the most cost-effective solutions. Always remember that the aim of the airforce is to be effective in wartime: the cost tends to be the peacetime readiness cost. If you keep the overall aims in mind, you will regard effective store/airframe integration as a most important matter.

REFERENCES

1. C L Bora(Ed) Drag and other aerodynamic effects of external stores. AGARD-AR-107. November 1977
2. ——— Store Airframe Aerodynamics AGARD-CP-389 January 1986
3. C L Bore Increasing the value of airforces by improving external store configuration. Paper 4 of AGARD-CP-285, May 1980
4. A B Haines
J B Berry Prospects for progress in the aerodynamics of external store carriage. Paper 1 of raf 2.
5. C L Bore A range formula for jet aircraft having variable specific fuel consumption. HSA-PON-1276 June 1968
6. C L Bore An improved formula for payload carrying capacity in terms of fuel weight fraction. BAe-KRS-N-319. July 1985
7. A B Haines
J H Nichols Drag, chapter 2 of reference 1.
8. A B Haines Prospects for exploiting favourable and minimising adverse aerodynamic interference in external store installations. Paper 1 in AGARD-CP-285, 1980
9. Dillenius, MFE
Goodwin, FK
Nielsen, JN Prediction of 6 degree-of-freedom store separation trajectories at speeds up to the critical speed; Vol I: Theoretical methods and comparisons with experiment; Vol II: Users manual for the computer programs. AFFDL-TR-72-83, 1972
10. Nadir, S;
Wedan, BW The Northrop/Near subsonic store separation prediction method. Paper 21, 6th J.T.C.G Aircraft/stores Compatibility Symposium, 1982
11. D Isaacs Improvement in store carriage load prediction at subsonic speeds using a development of the NEAR trajectory calculation method. Paper 5 of reference 2.
12. Moran, S
Tinoco, EN
Johnson, FT User's manual - subsonic/supersonic advanced panel pilot code, NASA-CR-152047, 1978.
13. Magnus, AE;
Epton, MA PANAIR - a computer program for predicting subsonic or supersonic linear potential flows about arbitrary configuration using a higher order panel method; Vol 1, theory document, NASA-CR-3251, 1980.
14. Sidwall, KW;
Baruah, PK
Bussolletti, JE PANAIR - a computer program for predicting subsonic or supersonic linear potential flows about arbitrary configurations using a higher order panel method, Vols II and III, User's manual. NASA-CR-3552, 1980
15. Cenko, A Panel applications to complex configurations. Jour. Aircraft, vol 20, No 10, 1983.
16. J A H Petrie Description of the subcritical panel method SPARV including first order viscous effects and wake relaxation. BAe (Drough) Note YAD-3457, 1982
17. P M Sinclair Unpublished communication, BAe Brough.
18. B Hunt The prediction of external store characteristics by means of the panel method, BAC Report Ae-372, 1977.
19. Cenko, W
Waskiewicz, J Recent improvements in prediction techniques for supersonic weapon separation AIAA-84-0310, 1984
20. Cenko, A
Pessitara, F
Meyer, R IFM - a new approach to predicting store loads in proximity to fighter aircraft and their influence on the subsequent trajectories. Paper 12 of reference 2.
21. S A Bizon
M J Kearney NUFA - a technique to predict the aerodynamic characteristics of store configurations in a non-uniform flowfield. Paper 14 of ref 2.
22. P G Herring A computer program which evaluates the longitudinal aerodynamic characteristics of typical weapon configurations. AGARD-CP-336, (1982)
23. R Deslandes Zonal decomposition: an advanced concept for Euler codes in order to predict carriage loads of non-trivial external store configurations. Paper 2 of reference 2.

24. Lijewski, LE
Thompson, JF
Whitfield, D L
Computational fluid dynamics for weapon carriage and separation. Paper 3 of reference 2.
25. Dougherty, FC
Steger, JL
Applications of Chimera grid schemes to store separation. Paper 13 of reference 2
26. J Barche
Performance and manoeuvrability. Chapter 7 of ref 1.
27. A Coursimault
Flying qualities. Chapter 3 of reference 1.
28. R Taiseire
Analyse d'influence de charges externes fixées sous la voilure sur la stabilité longitudinale d'un flèche. AGARD-CP-71, 1970.
29. H W Forsching
et al
Structural Integrity chapter of ref 1
30. Sensburg, O
Lotze, A
Haidle, G
Wing with stores flutter on variable sweep wing aircraft, paper 6, AGARD-CP-162. 1975
31. C B Mathews
Store separation. Chapter 5 of ref 1.
32. Commander of
NASC
A-7D cost reduction. Letter from Commander of Naval Air Systems Command to HQ Aeronautical Systems Division, 30 March 1970
33. R E Burns
The accelerated light model technique of store separation as developed and used at British Aerospace, Brough. AGARD-CP-348, Feb.84.2.
34. M Elliott
The accelerated light model technique of store separation as developed and used at British Aerospace, Brough. Paper 8 of ref 2.
35. T W Binion, jr
Special wind tunnel test techniques used at the AEDC, paper 3, AGARD-CP-187, 1975.
36. M E Wood
Operational experience of the ARA two-sting rig and associated hardware, software and flight comparison experiments. Paper 7, reference 2.
37. ———
F-15 Weapon/fuel carriage improvements with fast pack conformal pallets. McDonnell Douglas Report MDC-A-3507, 1975.

AEROELASTICITY AND OPTIMIZATION IN FIGHTER AIRCRAFT DESIGN

H. Gödel and H. Hörnlein

Messerschmitt-Bölkow-Blohm GmbH.
Helicopter and Military Aircraft Group
P.O. Box 801160, 8000 Munich 80
W.-Germany

SUMMARY

Constraint functions and their differentiations are given in this paper for the most interesting physical disciplines of structural optimization and well-known optimization techniques are mentioned. Because of the growing significances of iterative methods a large space has been conceded to the iterative solution of linear equation systems and its use in various algorithms. It is shown that big computer time saving effects would be achieved if the special characteristics of the physical formulation could be exploited mathematically.

INTRODUCTION

The design of a recent highly manoeuvrable fighter aircraft is at the present time strongly influenced by advanced technologies whose applications are more and more growing in the future. This fact has been recognized not only in the statics domain where composite materials have gained already high significance but also in the aeroelastics and flight mechanics where control surface effectivenesses, CCV configurations and active control capabilities play an important role. Already in the preliminary design phase the design engineer has to regard all these recent requirements doing his complex investigations. Hence integrating effects are obtained during an optimization process. The main task of optimization is to minimize the objective function - in general the weight of the structure - whilst taking into account all the requirements derived from technologies mentioned above. Several disciplines are treated in this paper

- Formulation of the general optimization problem
- Description of an iterative solution of linear equation systems
- Derivation of constraints and sensitivity analyses
- Mathematical programming techniques

An important point of view in structural optimization is the performance of recent vector computers, available at the present time. Vector computers enable us to investigate large structures not only in the statics domain but also in the aeroelastics and structural dynamics region. Provided that the mathematical routines needed for analyses and optimization are embedded in the general data flow during design phase of an aircraft shorter time of development, increasing quality of the product and trend information for further development can be expected.

THE OPTIMIZATION PROBLEM IN AIRCRAFT DESIGN

Structural optimization of an aircraft is mainly influenced by the techniques which are used in the statics, dynamics, aeroelastics and aerodynamics domain. The specialist who is engaged in the interdisciplinary optimization process is highly dependent on these techniques. He is supposed to involve all these contributions in a joint analyses system which takes a lot of organization because of the different formulations, mesh grid for example. In addition, the mathematical process for optimization is a further important component. The mathematical formulation of the optimization task is at the beginning, given in a rather compact form

$$\begin{array}{lll}
 \text{minimize } f(x) & & \text{(objective function)} \\
 \text{subject to } g_j(x) \geq 0 \quad j \in J & & \text{(constraint functions)} \\
 x \in R^m & & \text{(design space)}
 \end{array} \quad (1)$$

The changeable structure which is taken as a base for optimization will be described by the design variable vector x . All other parameters of the structure remain unchanged during the optimization process. As objective function not only the weight of the structure is used but also deformations, root moments or aerodynamical efficiencies are usually taken as objective function. Using the weight we have a linear function of the sizing variable x . Two classifications can be made for the optimization process.

Classification by the type of chosen design space

- | | | |
|-------------------------|---------------------------|-------------------------------|
| • sizing variables | actual design of members | } challenge
for the future |
| • geometrical variables | shape design of structure | |
| • topological variables | arrangements of members | |

Classification by the kind of considered constraints

- | | |
|------------------------------|--------------------------------------|
| • statics | stress, displacement, buckling |
| • dynamics | frequency, acceleration |
| • aeroelastics, aerodynamics | efficiency, flutter divergence speed |

Constraint functions are highly non-linear functions of the design variable, except for side constraints which have a simple form. In most of the optimization procedures the constraints will be considered simultaneously during the optimization process, but some systems use an interactive proceeding. The mathematical assumptions for optimization are of that kind that the constraints and the objective function should show a convex progress, see Fig. 1 where a general proceeding is shown. However, by means of a simple two bar structure it can be shown that this supposition is violated, see Fig. 2.

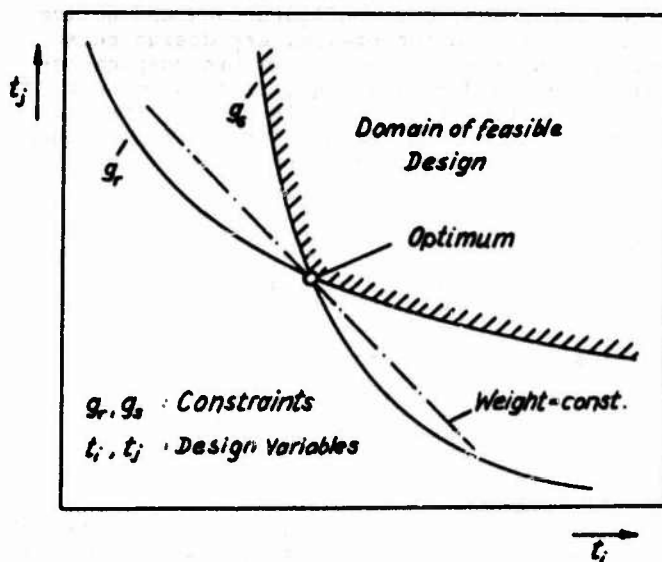


FIG. 1 GENERAL PROGRESS OF CONSTRAINTS

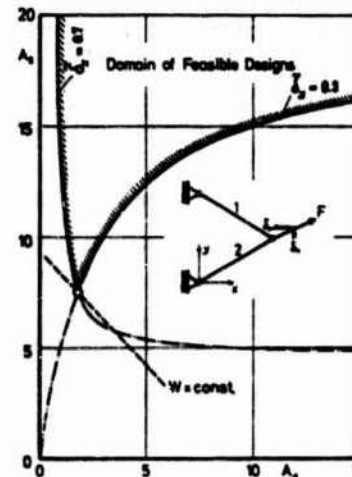


FIG. 2 DEFLECTION CONSTRAINTS ON A SIMPLE TWO BAR STRUCTURE

Furthermore the constraints should be manifold differentiable functions. That means, all of the implemented formulae of the analyses have to be known in the sensitivity analyses procedures. So-called black box solutions can not be used efficiently in the sensitivity calcs. In both statics and dynamics domain the physical behaviour of the problems can be formulated by linear equation systems or linear differential equation systems. In the steady aerodynamics domain a linear formulation is used in general. By means of an aerodynamical influence coefficient matrix C an aerodynamical distribution ΔC_p is given in equation (2) due to an angle of attack distribution α

$$\Delta C_p = C(g) \cdot \alpha(u) \quad (2)$$

where C is a real unsymmetrical matrix. This matrix depends mainly on the geometry of the aerodynamic system, whereas α is a function of the elastic deformations too. Formulation (2) has been commonly used and successful runs have been made for simple structures with corresponding procedures. On the contrary, however, recent aerodynamic codes show a non-linear behaviour which cannot be used immediately in the optimization process, because of the fine mesh grid, see Fig. 3 taking also into account interferences of different surfaces and so on. Mesh grid in aerodynamics as well as that of the statics should have a reasonable frame for optimization by means of a crude grid.

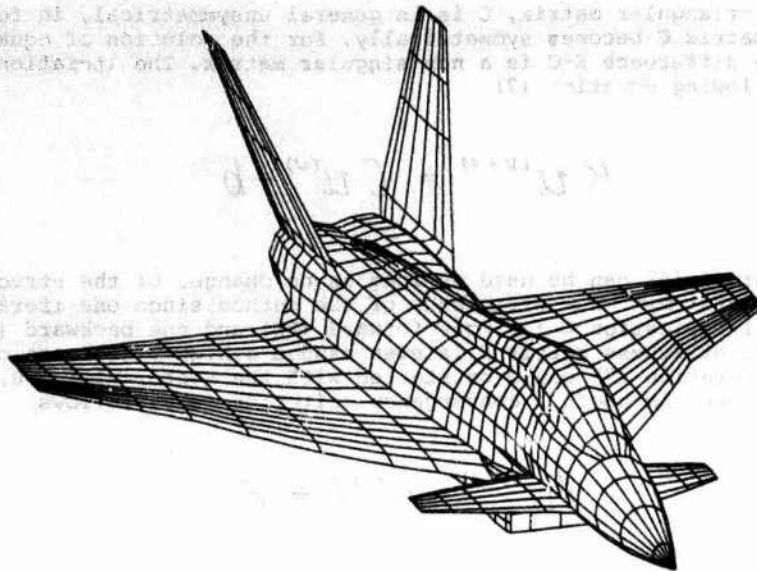


FIG. 3 RECENT AERODYNAMICS MESH GRID

A reasonable formulation of the aerodynamics for use in structural optimization could be as follows

$$\Delta c_p = \Delta c_p(g, u) + C^*(g, u) \cdot \Delta \alpha(\Delta u) \quad (3)$$

For a given deformation distribution u of the structure and on the base of its aerodynamic geometry the $\Delta c_p(g, u)$ -distribution could be calculated using recent aerodynamic codes. The matrix $C^*(g, u)$ should represent a constant aerodynamic influence coefficient matrix valid only in the environment of the deformed structure, that is, only small values $\Delta \alpha(\Delta u)$ would be allowed. By reasons of the insufficiencies in our tools, especially that mentioned above, analysis should be done as good as possible. Formulation (3) has never been considered for optimization in the past.

During an optimization process there are some restrictions in view of manufacturing aircraft structures. Minimum gauges have to be regarded. If composite materials are used not every fibre angle of the layers of the elements can be realized since allowable stresses for unorthodox combinations are not available. Skin thickness distributions could be prescribed which demands a special proceeding in the optimization process (variable linking).

Because of the fact that optimization proceeds in a more approximatively manner an increasing use of iterative methods could be recognized. Before describing the analyses and sensitivity analyses procedures a detailed description of a mathematical routine will be given which is used in some significant programs.

ITERATIVE SOLUTION OF LINEAR EQUATION SYSTEMS

Two main reasons for the use of iterative solutions are obvious. On the one hand a certain number of aeroelastical problems lead to an iterative solution of a linear equation system because of the complex coherencies. Direct solutions would be unefficient or even impossible in many cases. On the other hand there are conditions performing structural optimization for which the iterative process converges very quickly. The more progress we have in optimization the smaller changes on the structures occur and the faster converges the problem. By reasons of the significancy of iterative methods the description of the method in mind will be presented in a rather detailed manner. Equation (4) gives the general form of the task

$$Ku = Cu + b; K, C \in R^{n \times n}; u, b \in R^n \quad (4)$$

In most cases K represents a stiffness matrix which can be decomposed by CHOLESKY as follows

$$K = LL^T; L = \begin{pmatrix} L_{11} & & & \\ & \ddots & & \\ & & L_{nn} & \\ & & & 0 \end{pmatrix} \quad (5); (6)$$

L is a lower triangular matrix, C is in general unsymmetrical, in formulations without aerodynamics matrix C becomes symmetrically. For the solution of equation (4) it is necessary that the difference K-C is a non-singular matrix. The iteration process is running by the following equation (7)

$$Ku^{(v+1)} = Cu^{(v)} + b \quad (7)$$

CHOLESKY factorization (5) can be used as long as no changes of the structure occur. This fact is very important for the efficiency of the method since one iteration step requires only one multiplication $C \cdot u$, one forward (FW) and one backward (BW) substitution. In addition, if the stiffness matrix K is even banded a higher decrease of computer time is achieved. The iteration (7) could be started with the vector $u^{(0)} = 0$, unless a better approximation is known. An useful convergence criterion is as follows

$$\|u^{(v+1)} - u^{(v)}\| \leq \epsilon \quad (8)$$

where ϵ represents an appropriated value to the solution u . The iteration process (7) has been tested at MBB for a wide range of examples and provided that the process has shown a converging behaviour good results were obtained. During a cooperation between MBB and the University of Munich, Prof. W.R. RICHERT gave his opinion to the iteration and has made some proofs to it /1, 2/. A converging condition is given below. Convergence is provided for that case for which condition (9) is fulfilled.

$$\alpha\beta < 1 ; \alpha := \max \alpha_i ; \beta := \max \beta_i ; i = 1, \dots, n \quad (9)$$

For the calculation of α_i and β_i the equations below have to be performed by means of the elements of the matrices L and C.

$$\alpha_1 := \frac{1}{|l_{n1}|} \sum_{j=1}^n |c_{1j}| ; \alpha_i := \frac{1}{|l_{ii}|} \left[\sum_{k=1}^{i-1} |l_{ik}| \alpha_k + \sum_{j=1}^n |c_{ij}| \right] ; \bigwedge_{i=2, \dots, n} \quad (10); (11)$$

$$\beta_n := \frac{1}{|l_{nn}|} ; \beta_i := \frac{1}{|l_{ij}|} \left[\sum_{k=i+1}^n |l_{ki}| \beta_k + 1 \right] ; \bigwedge_{i=n-1, \dots, 1} \quad (12); (13)$$

Using the calculated values α and β an estimation of the error can be made at any iteration step v .

$$\|u^{(v+1)} - u\|_{\infty} \leq \frac{\alpha\beta}{1 - \alpha\beta} \|u^{(v+1)} - u^{(v)}\|_{\infty} \quad (14)$$

Convergence conditions as well as error estimations mentioned above are of that kind that the real relations mostly are of better behaviour as it is shown by these pessimistic criteria. A better estimation can be made by using the characterization of the dominant eigenvalue which is associated to the linear equation system. Considering u as the exact solution approximations at the iteration steps v and $v+1$ could be defined

$$u^{(v)} := u - \Delta u^{(v)} ; u^{(v+1)} := u - \Delta u^{(v+1)} \quad (15); (16)$$

Equations (15) and (16) used in (7) leads to

$$K \Delta u^{(v+1)} = C \Delta u^{(v)} \text{ or } \Delta u^{(v+1)} = K^{-1} C \Delta u^{(v)} \quad (17)$$

Equation (17) shows the well-known v. MISES iteration for eigenvalue problems. This iteration results after a certain number of steps in an approximation of the dominant eigenvalue λ_d .

$$\bigwedge_{i=1, \dots, n} : \frac{|\Delta u_i^{(v+1)}|}{|\Delta u_i^{(v)}|} \xrightarrow{v \rightarrow \infty} \lambda_d ; \quad |\lambda_d| < 1 \quad (18); (19)$$

The values $|\Delta u_i^{(v)}|, |\Delta u_i^{(v+1)}|, \dots$ decrease by a geometrical progression and vanish for $v \rightarrow \infty$, provided that a dominant value $|\lambda_d| < 1$ was achieved. Convergency condition (19) has been published in many reports. Nevertheless, in the following it is shown that linear equation systems can also be solved if $\lambda_d < -1$.

Convergency Improvements by an Eigenvalue Transformation

The eigenvalue problem associated to the iteration process (7) can be written as follows

$$(C - \lambda K)y = 0 \quad (20)$$

We have found that better convergency could be obtained by the use of a relaxation procedure which is given, equation (21) and (22)

$$KZ^{(v+1)} = Cu^{(v)} + b ; \quad u^{(v+1)} = pu^{(v)} + qz^{(v+1)} \quad (21); (22)$$

It was found that the values $p = 1 - \omega$ and $q = \omega$ lead to an eigenvalue transformation as follows

$$\lambda_t = \lambda_d \omega - \omega + 1 \quad (23)$$

This transformation is applied to equation (7) and the new iteration is achieved.

$$Ku^{(v+1)} = \omega Cu^{(v)} + (1 - \omega)Ku^{(v)} + \omega b \quad (24)$$

It is obvious that for the value $\omega = 1$ the original iteration process (7) is obtained. In case of convergency, that is $u^{(v+1)} = u^{(v)} = u$ equation (24) changes to

$$Ku = \omega Cu + (1 - \omega)Ku + \omega b \quad \text{or} \quad 0 = \omega(Cu + b - Ku) = \omega \cdot 0 \quad (25)$$

Hence, solution u is independent on the value ω . The main task is now to find an optimal ω -value, to find the smallest dominant eigenvalue, of course. The eigenvalue transformation (23) is valid for all eigenvalues of the problem in mind. Because of the unsymmetry of matrix C real and complex eigenvalues may occur. Provided that only real eigenvalues become dominant in the considered domain versus ω , Fig. 4 shows the linear behaviour of the transformed eigenvalues. In the past, all of the investigated real aero-elastic structures have shown this behaviour. In addition if only problems of the statics have to be solved matrix C becomes symmetrically and all eigenvalues appear as real eigenvalues.

During the iteration process the Δu -vectors of equation (17) are not known but after a certain number of iteration steps an approximation λ_d of the corresponding eigenvalue λ_d is achieved. By means of a small correction term we can write for any component k :

$$\Delta u_k^{(v+1)} = \Delta u_k^{(v)} \lambda_d (1 + \epsilon_k^{(v)}) \quad (26)$$

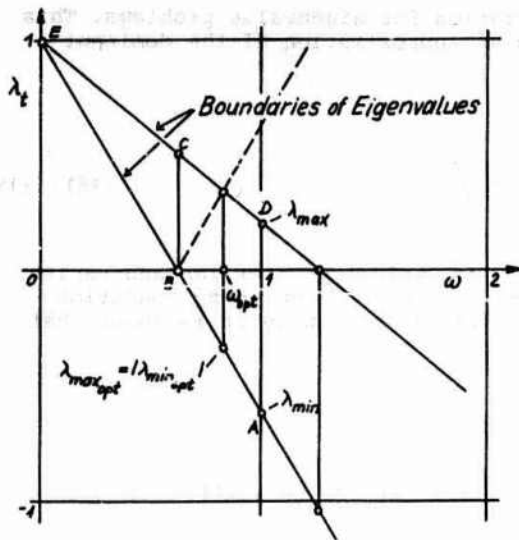


FIG. 4 BOUNDARIES OF REAL DOMINANT EIGENVALUES VERSUS ω

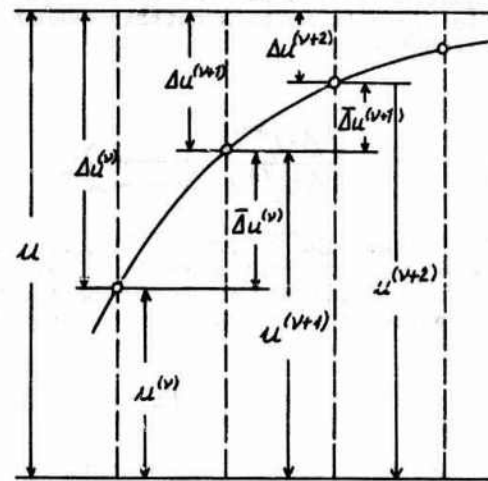


FIG. 5 PROGRESS OF DOMINANT EIGENVALUE ITERATION PROCESS

This behaviour is depicted in figure 5 for some iteration steps. From this figure we can deduce

$$\bar{\Delta}u_x^{(v)} = u_x^{(v+1)} - u_x^{(v)} = \Delta u_x^{(v)} - \Delta u_x^{(v+1)} = \Delta u_x^{(v)} [1 - \lambda_d (1 + \epsilon_x^{(v)})] \quad (27)$$

$$\bar{\Delta}u_x^{(v+1)} = u_x^{(v+2)} - u_x^{(v+1)} = \Delta u_x^{(v+1)} - \Delta u_x^{(v+2)} = \Delta u_x^{(v)} \lambda_d (1 + \epsilon_x^{(v)}) [1 - \lambda_d (1 + \epsilon_x^{(v+1)})] \quad (28)$$

$$\frac{\bar{\Delta}u_x^{(v+1)}}{\bar{\Delta}u_x^{(v)}} = \lambda_d (1 + \epsilon_x^{(v)}) \cdot \frac{1 - \lambda_d (1 + \epsilon_x^{(v+1)})}{1 - \lambda_d (1 + \epsilon_x^{(v)})} \xrightarrow{v \rightarrow \infty} \lambda_d \quad (29)$$

Equation (29) converges to the dominant eigenvalue λ_d if ϵ decreases. A geometrical progression of the decreasing error components $\bar{\Delta}u_x$ is obvious. An useful formulation is given as follows

$$\lambda_d \approx \lambda_{\text{approx.}} = \frac{\|\Delta u^{(v+1)}\|}{\|\Delta u^{(v)}\|} \quad (30)$$

In certain cases it may happen that the convergency of the solution u is much faster than that of the v . MISES-Iteration. In these cases eigenvalues are rather small so that transformations are not necessary for time saving. In Fig. 4 the iteration provides at $\omega = 1$ the eigenvalue λ_{\min} , point A, since $|\lambda_{\min}| > |\lambda_{\max}|$. The iteration at point B converges to the dominant eigenvalue, point C. By means of the points E and C λ_{\max} can be computed, point D. The optimum condition $|\lambda_{\min, \text{opt}}| = |\lambda_{\max, \text{opt}}|$ leads to the optimally ω -value and to the smallest convergency rate.

$$\omega_{\text{opt}} = \frac{2}{2 - \lambda_{\min} - \lambda_{\max}}; \quad \lambda_s = \lambda_{\max, \text{opt}} = \frac{\lambda_{\max} - \lambda_{\min}}{2 - \lambda_{\min} - \lambda_{\max}}; \quad S \approx \frac{-d}{\lg |\lambda_s|} \quad (31); (32); (33)$$

Considering a case where $|\lambda_{\min}| = |\lambda_{\max}|$ no convergency improvements can be achieved. An estimation of the number of necessary iteration steps s is given by equation (33) where d is the number of valid digits of accuracy. Supposing that the matrix C contains a variable ratio q/q_r - dynamic pressure for example - it is obvious that the eigenvalue depend linearly

on this ratio. Under the assumption that $\lambda_{max} > 0$ has been calculated for $q/q_r = 1$ an upper boundary for the ratio in question is achieved by equation (35).

$$C^* = \frac{q}{q_r} C ; \left(\frac{q}{q_r}\right)_{max} < \frac{1}{\lambda_{max}} \quad (34); (35)$$

In Fig. 6 results are depicted for iterations performed for a real aeroelastic structure at certain ω -values. At $\omega = 1$ a minimum eigenvalue has been detected which is less than -1 . No convergency for solution u was obtained but the v. MISES iteration converged very fast, see line #1.

Line #2 and #3 show the progress of eigenvalues for $\omega = 0.7$ and 0.5 . The iteration at the optimum ω shows an alternating behaviour which could be caused by the multiple dominant eigenvalues.

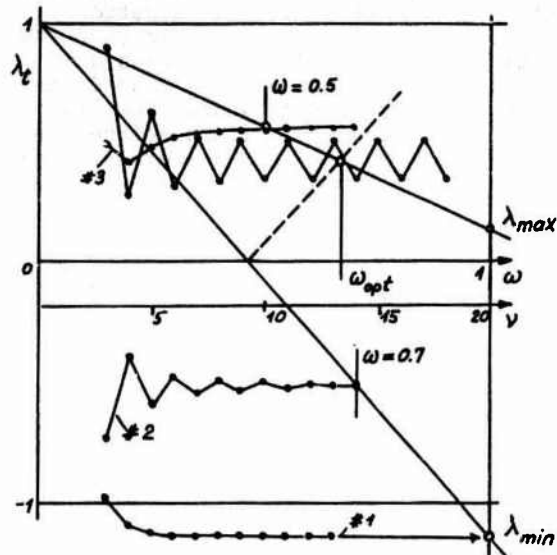


FIG. 6 DOMINANT EIGENVALUE BEHAVIOUR CALCULATED FOR A REAL AERO-ELASTIC STRUCTURE

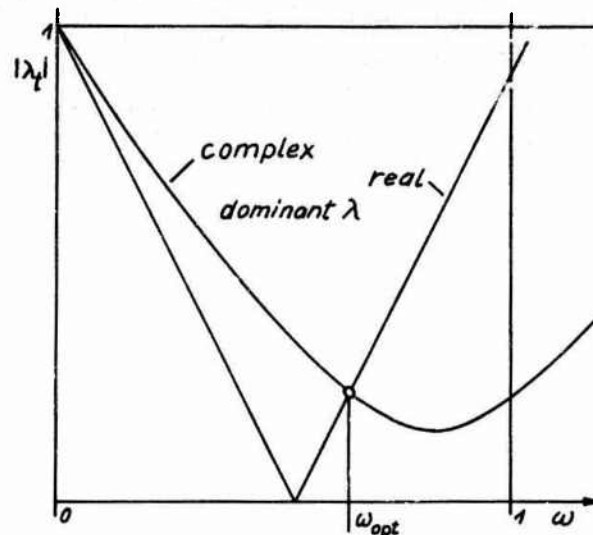


FIG. 7 REAL AND COMPLEX DOMINANT EIGENVALUE PROGRESS

If both complex and real eigenvalues become dominant during the iteration process the behaviour versus ω could be studied only for the absolute value of the eigenvalue. Since the imaginary parts remain unknown the formulae derived for real eigenvalues are not valid. For a given accuracy d obtained after s iteration steps an estimation of an average convergency rate could be achieved by

$$|\lambda_t| \approx 10^{-\frac{d}{s}} \quad (36)$$

The calculation of ω_{opt} seems to be an iterative search process.

Application to statics and dynamics problems

Recent solutions of the statical problems are based on the finite element formulation which enables us to assemble the total stiffness matrix K as a sum of a big number of element stiffness matrices. During an optimization process it may happen that small changes of the structure lead to a linear formulation of the new stiffness matrix \bar{K} , with K^* as a constant matrix and α as a variable value, $\alpha > 0$.

$$\bar{K}u = (K + \alpha K^*)u = b \text{ or } Ku = -\alpha K^*u + b ; \left(\frac{\alpha}{\alpha_r}\right)_{max} < \frac{1}{\lambda_{max}} \quad (37); (38)$$

Provided that $0 < \lambda_{max} < 1$ for a given value $\alpha = \alpha_r$ at $\omega = 1$ was achieved, a maximum ratio α/α_r is given in equation (38); if $\lambda_{max} \leq 0$ no upper boundary occurs. This behaviour is obtained having a positiv definit matrix K^* .

In the past vibration calculation of big structures were mostly performed in a condensed form on the base of assumed modes whereby the results of this approach have been

highly influenced by the choice of these modes. Before eigenvalue extraction could be done a big amount of computer time has been spent on the calculation of the condensed matrices. Recent computers - especially vector computers - allow now a higher degree of freedom number. Both stiffness and mass matrix could be assembled in the structures grid model and vibration calculation could use these matrices. Because of the frequent changes of the structure during the optimization process an eigenvalue extraction procedure could be useful which uses results of an earlier step. Such a procedure could be a modification of the perturbation method by H. WITTMAYER /3/. This routine contains a solution procedure for a linear equation system which is used during vector iteration. Because of the symmetry of stiffness matrix as well as mass matrix only real eigenvalues are considered. By reasons of the small changes in the stiffness and mass matrices the iterative solution, equation (24), used in the perturbation method would show a distinguished efficiency.

ANALYSES PROCEDURES AS BASE OF OPTIMIZATION

During the optimization process of an aircraft very different analysis programs are used. A certain number of physical disciplines contribute simultaneously to a better sizing of an aircraft. The general base for an aircraft design is a finite element formulation, but other bases are used too, /4/. The combination of the different mesh grid systems of statics, aerodynamics and structural dynamics are performed using transformation matrices. These matrices describe the relation between the forces and/or moments of the one system (a) to those of the other system (s), equation (39). If we define the deformation relation for both systems by equation (40), the virtual work in both systems is equal, equation (41), independent on the behaviour of transformation matrix T.

$$p_s = T_{sa} p_a ; u_a = T_{sa}^T u_s ; u_s^T p_s = u_a^T p_a \quad (39); (40); (41)$$

In view of the validity of these transformations the design engineer has to be very carefully using these matrices. The general statics equation based on a finite element model with loads R(x) independent of the deformation u(x) is given by equation (42)

$$K(x) \cdot u(x) = R(x) ; K = L L^T \quad (42); (43)$$

where : $x \in \mathbb{R}^m$ design variable; $u \in \mathbb{R}^n$; $R \in \mathbb{R}^n$; m is number of design variables; n is number of degrees of freedom (DOF). The matrix $K \in \mathbb{R}^{n \times n}$ is in general a banded positiv definit matrix which can be decomposed by the CHOLESKY factorization, equation (43), where L is a lower triangular matrix. This factorization is done only once for each optimization step and the solution vector is obtained by one FW/BW substitution per load case. In the statics domain with fixed loads two types of constraints are considered, stiffness constraints and strength constraints. Stiffness constraints can be treated by affin linear relationship (44), whereby displacements, twist and camber could be handled. Normalizing the general restriction (45), the equivalent formulation of the imposed constraints can be written by (46), \sim stands for allowable,

$$p(x) = \alpha + a^T u(x) ; 0 \leq p(x) \leq \tilde{p} ; 1 \geq g(x) := 1 - \frac{p(x)}{\tilde{p}} \geq 0 \quad (44); (45); (46)$$

or in general form

$$g(x) = g(p(u(x))) \quad (47)$$

Stress constraints depend on the type of the finite elements. These constraints depend on the displacement vector u and explicite on the design variable x. The non-linear elements beam, plate and shell describe the general case. In the following we consider per element x_c only one constraint g_c without loss in generality. Using the formulation $FM = (N, M, Q)$, where N represents the internal normal forces, M moments and Q shear forces, we obtain for element c:

$$FM_c(x) = FM(x, u) := F_c(x_c) \cdot u_c ; g_c(x) = g_c(x, FM_c) := S_c(x_c) \cdot FM_c \quad (48); (49)$$

$F_c(x)$ describes the non-linear finite element behaviour of the element geometry and design variable x . Superposition of FM_c leads to the stress vectors, equation (49). Using a differentiable hypothesis (v. MISES, TSAI-WU, HILL and others) for the calculation of the equivalent stress $\bar{\sigma}_c$ the vector σ_c can be reduced to a scalar value, (50), and after normalizing the restriction (51), we achieve the constraint function (52)

$$\bar{\sigma}_c = \bar{\sigma}_c(\sigma_c); 0 \leq \bar{\sigma}_c(x) \leq \bar{\sigma}_c^{\max}; 1 \geq g_c(x) := 1 - \frac{\bar{\sigma}_c(x)}{\bar{\sigma}_c^{\max}} \geq 0 \quad (50); (51); (52)$$

Composition of all these mentioned relations leads to equation (53).

$$g_c(x) = g_c(\bar{\sigma}_c(\sigma_c(x, FM_c(x, u(x))))); g_c(x) = g_c(\bar{\sigma}_c(u(x))) \quad (53); (54)$$

For linear elements, bar, membrane, shear for example equation (53) becomes more simple, (54). Strain constraints could be treated in an analogous manner.

In view of efficiencies of the steady aeroelasticity equation (42) must be extended by a deformation dependent term. Equation (55) will be solved by the iterative method equation (24), mentioned above.

$$K(x) \cdot u(x) = Q \cdot u(x) + R(x), Q \in R^{n \times n}; \eta(x) = 1 + b^T u(x) \quad (55); (56)$$

The efficiencies (rudder moment, lift ...) are defined by the affin linear relationship (56). Vector b contains the behaviour of the geometry and the aerodynamics for the rigid structure. Normalizing the restriction (57), which contains the desired efficiency η_d leads to the equivalent constraint definitions

$$0 \leq \eta_d \leq \eta(x); g(x) := \frac{\eta(x)}{\eta_d} - 1 \geq 0; g(x) = g(\eta(u(x))) \quad (57); (58); (59)$$

Calculating natural frequencies ω and the associated normal modes v equation (60) has to be solved by an eigenvalue extraction method.

$$(K(x) - \lambda(x) \cdot M(x)) v(x) = 0; \omega = \omega(\lambda) := \sqrt{\lambda} \quad (60); (61)$$

K is stiffness matrix, M mass matrix, $\lambda \geq 0$, only distinct eigenvalues should occur. Two cases are considered, isolation of frequencies, see Fig. 8, and lower restriction of frequencies, see Fig. 9. Vibration mode shape constraints are not considered in this paper.

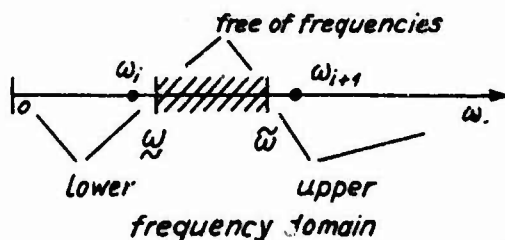


FIG. 8 FREQUENCY ISOLATION

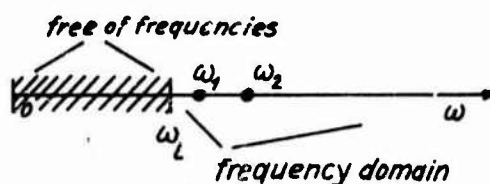


FIG. 9 LOWER BOUND OF FREQUENCY

In the first case two restrictions has to be treated hereof and normalizing is done.

$$0 \leq \omega_k(x) \leq \omega, k=1, \dots, i; 0 \leq \omega \leq \omega_k(x), k=i+1, \dots, n \quad (62); (63)$$

$$g_{\omega}(x) := 1 - \frac{\omega_k(x)}{\omega} \geq 0, \quad k=1, \dots, l; \quad g_{\omega}(x) := \frac{\omega_k(x)}{\omega} - 1 \geq 0, \quad k=i+1, \dots, n \quad (64); (65)$$

For a given ω_1 we have to decide which one of the two restrictions should be taken. This may have an important influence on the optimization process as well as on the final design. Treating the second case only one restriction is considered, equation (66) and normalizing of it leads to equation (67).

$$0 \leq \omega_1 \leq \omega_i(x); \quad g_{\omega_1}(x) := \frac{\omega_i(x)}{\omega_1} - 1 \geq 0; \quad i=1, \dots, n \quad (66); (67)$$

The basic equation system for solving the flutter problem is given below.

$$\left[\frac{v_f^2(x) p^2(x)}{k^2} M(x) + K(x) - \frac{\rho v_f^2(x)}{2} A(k, M_a) \right] q(x) = 0 \quad (68)$$

This formulation is based on normal modes of the structure and hereby M represents the generalized mass matrix, K stiffness matrix and A unsteady aerodynamic matrix, q generalized coordinates, v_f stands for flutter speed and p is the eigenvalue of the problem. Matrix A is a function of the reduced frequency k and Mach number M_a , where $k = b\omega/v$ is built by the reference length b and by the frequency ω of oscillation. Equation (68) is an implicate function for the flutter speed v_f . Restriction and constraint function are given by (69) and (70).

$$0 \leq \tilde{v}_f \leq v_f(x); \quad g(x) := \frac{v_f(x)}{\tilde{v}_f} - 1 \geq 0 \quad (69); (70)$$

It is obvious that over the full mission domain of an aircraft more than one critical flutter case may occur which all have to be considered during the optimization process. For divergence investigations equation (68) becomes more simply for a non-oscillatory motion, $p = 0$.

$$\left[K(x) - \frac{\rho v_d^2(x)}{2} A(k=0, M_a) \right] q(x) = 0 \quad \text{or} \quad (K(x) - \lambda(x)A) q(x) = 0 \quad (71)$$

The smallest real eigenvalue $\lambda = \rho v_d^2/2$ of equation (71) gives the divergence speed v_d . The restriction and the constraint function are similar to these of the flutter formulation.

$$0 \leq \tilde{v}_d \leq v_d(x); \quad g(x) := \frac{v_d(x)}{\tilde{v}_d} - 1 \geq 0 \quad (72); (73)$$

All of the main analysis procedures are now treated and the corresponding constraint functions are defined, which are the base of the sensitivity analysis tools described in the following.

CALCULATION OF THE GRADIENTS OF CONSTRAINTS

Sensitivity analysis plays the dominant role during the optimization process. In the past, sensitivity analysis has been done sometimes using the numerical differentiation method, but this proceeding is restricted to a rather small number of design variables. Provided that m represents the number of design variables the expense on computer time increases proportionally to m^4 whereas for the analytical approach it is proportional to m^3 . At the present time 500 and more design variables are desired. Analytical sensitivity analysis is expensive in any case.

Notation: By means of the CHAUCHY symbol D the so-called Jacobian is formulated for a vector function g

$$g = \begin{Bmatrix} g_1 \\ \vdots \\ g_j \\ \vdots \\ g_m \end{Bmatrix}; \quad D_x g = \left(\frac{\partial g_j}{\partial x_i} \right)_{\substack{j=1, \dots, m \\ i=1, \dots, n}} \quad (74); (75)$$

Sensitivity analysis will be done here in the stress domain for the most complicated case of non-linear elements. Formal derivation is made using equation (53). Differentiation of this equation with respect to the design variable x , using chaine rule and regarding the explicite dependency on the design variable x provides

$$D_x g_c = \frac{D g_c}{d\sigma_c} \cdot D\sigma_c \cdot \left[\frac{\partial \sigma_c}{\partial x} + D\sigma_c \left\{ \frac{\partial FM_c}{\partial x} + DFM_c \cdot D_x u_c \right\} \right] \quad (76)$$

Distributive multiplication gives

$$D_x g_c = a_c^T + b_c^T + c_c^T \cdot D_x u_c \quad (77)$$

where: $a_c^T := \frac{D g_c}{d\sigma_c} \cdot D\sigma_c \cdot \frac{\partial \sigma_c}{\partial x} \quad , \quad \in \mathbb{R}^{1 \times m} \quad (78)$

$$b_c^T := \frac{D g_c}{d\sigma_c} \cdot D\sigma_c \cdot D\sigma_c \cdot \frac{\partial FM_c}{\partial x} \quad , \quad \in \mathbb{R}^{1 \times m} \quad (79)$$

$$c_c^T := \frac{D g_c}{d\sigma_c} \cdot D\sigma_c \cdot D\sigma_c \cdot DFM_c \quad , \quad \in \mathbb{R}^{1 \times d_c} \quad (80)$$

d_c DOF of element c

The vectors a , b and c , simple to calculate, depend on the design variable x only. In addition, vectors a and b are sparse populated, only the c -th component is nonzero. Because of the value d_c vector c is rather small. The term $c_c^T \cdot D_x u_c$ is the most time consuming part in numerical calculation. Formal partial differentiation of equation (55) with respect to variable x_i provides:

$$K \left\{ \frac{\partial u}{\partial x_i} \right\} = Q \left\{ \frac{\partial u}{\partial x_i} \right\} + \left[-\frac{\partial K}{\partial x_i} u + \frac{\partial R}{\partial x_i} \right] , \quad i = 1, \dots \quad (81)$$

With the abreviations $v_i := \left\{ \frac{\partial u}{\partial x_i} \right\} \quad ; \quad p_i := \left[-\frac{\partial K}{\partial x_i} u + \frac{\partial R}{\partial x_i} \right] \quad (82); (83)$

we obtain a linear equation system which can be solved iteratively like equation (55) and solution for all design variables provides equation (85).

$$K v_i = Q v_i + p_i \quad ; \quad D_x u = V = (K - Q)^{-1} P \quad (84); (85)$$

where $V = (v_i) \quad ; \quad P = (p_i)$ built by columns (86); (87)

Considering all constraints of the actual type we can summarize

$$A = (a_c^T) \quad ; \quad B = (b_c^T) \quad ; \quad C = (c_c^T) \quad \text{built by rows} \quad (88); (89); (90)$$

and equation (76) changes in a general form

$$D_x g = A + B + \underbrace{C (K - Q)^{-1} P}_V \quad (91)$$

Two different approaches are considered in the following description. Using design space method columns of matrix V are calculated (pseudo displacements) based on the iterative solution like (55). Premultiplication of V with matrix C is needed finally. For the state space method we define

$$W^T = C (K - Q)^{-1} \quad (\text{rowwise solution, virtual displacements}) \quad (92)$$

and solution will be done for the equivalent equation system in the same manner.

$$KW = Q^T W + C^T \quad (93)$$

Postmultiplication of W^T with the matrix P is needed also. Caused by the finite element formulation matrices P and C are sparse populated. Provided that we have only loads independent of the deformations matrix Q becomes zero and no iterative solution is necessary. The numerical amount for the state space method is linear dependent on the number of constraints, whereas for the design space method there is a linear dependency on the number of design variables. The remaining stiffness and strength constraints for linear elements can be solved analogously, note that $A = B = 0$. From the numerical point of view it should be mentioned that for mixed constraints (statics and aeroelasticity constraints) the state space method shows a general superiority.

Many mathematical programming systems lead to subproblems of the following type.

$$\text{minimize } \varphi(x) ; \varphi(x) := f(x) + G(g(x)) \quad (94)$$

Formal differentiation provides equation (95). The row vector β^T of equation (96) is easily available after analysis has been done for the structure

$$D_x \varphi = D_x f + D_g G \cdot D_x g ; \beta^T = D_g G \quad (95); (96)$$

Equations (91) and (96) used in (95) we obtain

$$D_x \varphi = D_x f + \beta^T A + \beta^T B + \eta^T (K - Q)^T P ; \eta^T = \beta^T C \quad (97); (98)$$

where η^T is called an adjoint variable. Finally we have to solve equation (99) using state space formulation

$$W^T = \eta^T (K - Q)^T \text{ or } KW = Q^T W + \eta \quad (99)$$

From equation (99) it can be seen that the iterative solution for only one vector is necessary. In view of operation counting the significant speed up factor m (number of actual constraints) is obtained.

Sensitivity analysis for natural frequency constraints is done by differentiation of equation (60) and the general constraint function (100) with respect to x_i , resp. x

$$g(x) = g(\omega(\lambda(x))) ; D_x g = D_\omega g \cdot D_\lambda \omega \cdot D_x \lambda \quad (100); (101)$$

$$\left[\frac{\partial K}{\partial x_i} - \frac{\partial \lambda}{\partial x_i} M - \lambda \frac{\partial M}{\partial x_i} \right] v + [K - \lambda M] \frac{\partial v}{\partial x_i} = 0, \quad i = 1, \dots \quad (102)$$

The most interesting term of equation (101) is the last one. Premultiplication of (102) with a normalized vector v^T , where $v^T M v = 1$, provides equation (103) since the second part of (102) vanishes.

$$\frac{\partial \lambda}{\partial x_i} = v^T \frac{\partial K}{\partial x_i} v - \lambda v^T \frac{\partial M}{\partial x_i} \quad (103)$$

Sensitivity analysis done for divergence constraints is similar to the natural frequency process. The general form of the constraint function (104) and the differentiation of it with respect to x lead to

$$g(x) = g(v_d(\lambda(x))) ; D_x g = D_{v_d} g \cdot D_\lambda v_d \cdot D_x \lambda \quad (104); (105)$$

Furthermore differentiation of (71) with respect to x_i provides:

$$\left[\frac{\partial K}{\partial x_i} - \frac{\partial \lambda}{\partial x_i} A \right] q + (K - \lambda A) \frac{\partial q}{\partial x_i} = 0, \quad i = 1, \dots \quad (106)$$

Premultiplication with the left hand eigenvector q^* (caused by the unsymmetrical matrix A) gives equation (107) since the product of the second term of (106) vanishes.

$$\frac{\partial \lambda}{\partial x_i} = \frac{q^{*T} \frac{\partial K}{\partial x_i} q}{q^{*T} A q} \quad (107)$$

Differentiation for all of the design variables provides the most interesting term $D_x \lambda$ of equation (105).

For sensitivity analysis of the flutter speed constraint equation (70) is extended to

$$g(x) = g(v_f(m(x))) \quad (108)$$

where $m(x)$ represents the linear dependency of the element mass on the design variable x . Differentiation of (108) with respect to x gives

$$D_x g = D_{v_f} g \cdot D_{m_f} v_f \cdot D_x m \quad (109)$$

The derivation of the term $D_{m_f} v_f$ has been published by RUDISILL and BHATIA /5/. These so-called flutter velocity derivatives have been successfully used in the optimization procedure FASTOP /6/. The terms $D_{v_f} g$ and $D_x m$ are of simple type.

OPTIMIZATION PROCEDURES

In the last years various optimization procedures have been established for solving the non-linear programming problem, equation (1). The solution of these problems is usually attempted by two different iterative approaches. On the one hand procedures have been developed on the basis of "optimality criteria", (OC) /7, 8, 9/. For this kind of optimization physical facts of the constraints have to be included. The mathematical formulation is given by equation (110).

$$x_i^{(\nu+1)} := \psi(x_i^{(\nu)}) ; \nu \in N ; x \in R^m ; i = 1, \dots, m \quad (110)$$

where ψ is an appropriate recurrence relation. On the other hand methods called "mathematical programming" (MP) are used to find an optimal design of a structure. In these routines a search direction vector $s^{(\nu)}$ is calculated and in combination with a step size value $\alpha^{(\nu)}$ a better design could be found, equation (111).

$$x^{(\nu+1)} := x^{(\nu)} + \alpha^{(\nu)} \cdot s^{(\nu)} ; \nu \in N ; \alpha \in R ; x, s \in R^m \quad (111)$$

All MP-methods are based on solving the local KUHN-TUCKER conditions. These methods are usually divided in three categories, transformation methods, primal and dual methods. Among optimization experts transformation methods are known as

- Barrier functions
- Penalty functions
- Methods of multipliers (augmented Lagrangian)

whereas the primal methods are divided into the indirect methods

- Sequential linear programming (SLP)
- Sequential quadratic programming (SQP)

and direct methods

- Gradient projection methods
- Generalized reduced gradients (GRG)
- Method of feasible directions (MFD)

The dual techniques are methods which try to solve the so-called dual problem.

Whilst primal methods treat the constraint problem the transformation methods deal with a sequence of unconstrained problems. Penalty and barrier function methods show an ill-conditioned behaviour the more progress in optimization we have. Methods of multipliers do not show those insufficiencies.

Seven years ago MBB has started optimization with the known procedure FASTOP. This routine is characterized by an iterative proceeding. Stress and flutter constraints could be treated with FASTOP. Whilst stresses are treated by means of a fully stressed ratio-procedure flutter constraints would be handled using a redesign formula for satisfying an optimality criterion. In this routine it is attempted to obtain unique flutter velocity derivatives $\partial v/\partial m_i = \text{const.}$ for the so-called critical elements. Full description of the capabilities of FASTOP and test results are given for a calculated simple wing structure in /10/. Modifications in FASTOP have been made for the handling of deflection constraints too. For deflection constraint handling a deflection gradient method has been developed and calculations of well known examples have been performed. Comparisons of these calculations were published in /11/.

Nevertheless, two years ago MBB has started the development of an own optimization program system, called LAGRANGE, where all of the significant constraints mentioned above are treated simultaneously. Mainly mathematical programming is used for optimization. In this program system barrier function method, augmented Lagrangian and sequential linear programming is realized already.

CONCLUSION

For structural design of modern airplanes the use of an recent optimization program system is mandatory to fulfil the requirements of the whole mission domain of an aircraft. Constraint formulation and sensitivity analysis for it plays an important role. The use of modern iterative solution procedures provides high quality of the analysis calcs, computer time saving effects and shorter development phases of an aircraft. In the future recent vector computers will support optimization in a quite specially manner.

REFERENCES

- /1/ RICHERT, W. R. Über die numerisch-mathematischen Eigenschaften eines Verfahrens für Aeroelastik-Gleichungssysteme
Internal MBB-Report 1985
- /2/ RICHERT, W. R. Über konvergenzbeschleunigende Verfahren für Aeroelastik-Gleichungssysteme auf Großrechnern
Internal MBB-Report 1985
- /3/ WITTMAYER, H. Berechnung einzelner Eigenwerte eines algebraischen linearen Eigenwertproblems durch Störiteration
ZAMM, Band 35, Heft 12, Dezember 1955
- /4/ TRIPLETT, W. E. Aeroelastic Tailoring Studies in Fighter Aircraft Design
AIAA-Paper 79-0725
- /5/ RUDISILL, C. S. Optimization of Complex Structures to satisfy flutter requirements
BHATIA, K. G.
- /6/ WILKINSON, K. An Automated Procedure for Flutter and Strength Analysis and Optimization of Aerospace Vehicles
MARKOWITZ, J. et.al. Vol. 1 - Theory and Application, AFFDL-TR-75-137

- /7/ RAZANI, R. The behaviour of the fully-stressed design of structures and its relationship to minimum weight design
AIAA J., 3, December, 2262-2268 (1965)
- /8/ POPE, G. The design of optimum structures of specified basis configuration
Inf. J. Mech., Sci., 10, 251-265 (1968)
- /9/ WILKINSON, K. Practical design of minimum-weight aircraft structures for strength and flutter requirements
LERNER, E.
TAYLOR, R. F.
J. Aircraft, Vol. 13, No. 8 (1976)
- /10/ GÖDEL, H. Application of a structural optimization procedure for advanced wings
SCHNEIDER, G.
AGARD-Report No. 691, January 1981
- /11/ GÖDEL, H. Preliminary design of aircraft using structural optimization methods
SCHNEIDER, G.
HÖRNLEIN, H.
AGARD-Report No. 354, April 1983

MATERIALS FOR FIGHTER AIRCRAFT

by

R.J.Sellars
British Aerospace plc
Preston, Lancs PR4 1AX, UK

1. INTRODUCTION

Of the many important decisions to be made during the initial conception and design of advanced fighter aircraft, one of the most critical is that made by the materials engineer. Together with the designer, he will recommend the type of material to be incorporated in the aircraft's structure. Such recommendations, while respecting the criteria of minimum mass and minimum cost, must also ensure that the structure will possess a long life and be simple to service and maintain.

This is indeed a challenge!

This paper discusses some of the new materials and production processes that are available for use on advanced fighter aircraft. Comparisons are made between the advanced light alloys that are now becoming available (i.e. aluminium-lithium), and the latest intermediate modulus fibres for use in carbon fibre components.

2. NOTATION

b	panel width
E	Young's modulus
E_T	tangent modulus for metal panels, Young's modulus for CFC panels
f_{ty}	tensile yield stress
f_{tu}	ultimate tensile stress
K	buckling coefficient
M	Mach number
P	spanwise compressive load per unit chord
s	specific gravity
t	panel thickness
C_v	coefficient of variation
T_0	ambient temperature
TRAM	ram temperature
T_{REC}	Recovery temperature
σ_b	buckling stress
σ_{OPT}	optimum compressive stress

3. OPERATING ENVIRONMENT

Before any discussion on the comparison of the mechanical properties of the various candidate materials can begin, it is essential to define the operating environment of the aircraft.

The most significant aspect which distinguishes the design of the structure (and also choice of materials) of supersonic aircraft from those of lower performance aircraft, is the high temperature environment caused by kinetic heating in sustained supersonic flight.

Moisture, in combination with high temperature also has a detrimental effect on the mechanical properties of materials - especially on composite materials.

3.1 TEMPERATURE

Two temperatures are important to the structural designer, and both are a function of Mach number.

Ram (or stagnation) temperature = TRAM = $T_0 (1 + 0.2M^2)^{\circ} K$

$$\text{Recovery temperature} = T_{REC} = T_o (1 + 0.18M^2) \text{ } ^\circ\text{K}$$

Leading edges of all components experience ram temperature. For fighter type aircraft such as the Tornado and the experimental aircraft EAP, the high localised ram temperatures do not present any great problems as the leading edges are made from metal to meet rain erosion and birdstrike requirements. However, ram temperatures are usually too high for current epoxy-based CFC.

Problems may arise with future aircraft structures of hybrid construction because of thermal stresses which may be induced due to different expansion coefficients of the metal leading edge and (say) a CFC main wing torsion box.

Being away from the leading edges, the majority of the external structure experiences recovery temperature. As the major portion of the external skin is at recovery temperature, this is the most important one to be considered by the materials/structures engineer.

As stated above, because temperature reduces the material mechanical properties (and hence increases weight), the materials/structural engineer should always be prepared to challenge, if necessary, the overall aircraft design assumptions.

For example, assuming the aircraft is designed to $V_d = 800$ knots, and a design Mach Number $M = 2.2$. - see FIGURE 1, at the critical intersection point and assuming ISA conditions, the recovery temperature of the structure is 136°C . However, if one is prepared to "cut the corner" of the envelope (as shown in FIGURE 1), the maximum recovery temperature can be reduced to 120°C . Thus, by reducing the performance of the aircraft by a negligible amount at the critical point, the design temperature of the structure is reduced from 136°C to 120°C which in turn increase the compression properties of CFC by 11%.

3.2 MOISTURE

With current epoxies, the resin-dominated CFC strength properties (shear and compression) suffer a reduction with moisture absorption and increasing temperature. These reductions in properties are discussed more fully in Section 5. Currently, there is no product available which will give CFC complete protection from water ingress, so until superior resins are available the reduction in mechanical properties of epoxies must be accepted.

It may be thought that owing to the heat generated during supersonic flight the moisture absorbed by CFC would be dissipated by evaporation. However, as tactical military aircraft fly for only about 300 hours per year (and only a proportion of this is at high speed), compared with approximately 8500 hours per year on the ground, moisture reduction due to kinetic heating will not occur to any great extent.

The general design level on recent CFC designs in the U.K. has assumed a moisture uptake of 1% by weight.

Research and in-service measurements in the U.K. and the U.S.A. show that the external skins of typical CFC structures using current material will absorb around 1% by weight in moisture during the life of the aircraft. However, because of the increasing use of CFC in internal structure, together with a fuller understanding of the mechanism of absorption, this convenient assumption is being reviewed.

Be that as it may, considering a typical CFC material, 1% moisture at 120°C will reduce the compressive strength by 30% (but the tensile strength by only 5%) when compared with room temperature, dry properties.

With metallic structures, moisture problems are generally avoided by close quality control and internationally accepted protection procedures.

Metal structures of aircraft capable of sustained supersonic flight do require careful protection from corrosion, but the technology is available, in particular from Concorde experience..

4. METALLIC MATERIALS

The majority of the current generation of supersonic aircraft, including those which were designed for sustained supersonic cruise are constructed from conventional copper or zinc based aluminium alloy. Titanium (which has excellent high temperature properties), is used locally in the regions of the power plant or at points of high load concentration.

This limited use of titanium is due to the high initial cost of the material, together with the very high fabrication and forming costs when conventional manufacturing techniques are employed. One military aircraft however which has a high titanium content (considering it was designed in 1970) is the Panavia Tornado, which has the wing carry-through box and the main pivot lugs manufactured from this material. The percentage structural material distribution of the Tornado (which is representative of a modern, supersonic variable geometry, tactical aircraft) is given in TABLE 1, where it will be noted that 17.5% of the structural mass is titanium.

Future supersonic military aircraft will have a completely different material distribution to that of the Tornado, and will feature wings, fins, foreplane (or taileron) and major portions of the fuselage made from CFC. TABLE 1 also gives the material distribution of the EAP demonstrator aircraft currently under construction in the U.K. and scheduled to fly in 1986, together with the distribution for the European Combat Aircraft currently being developed by an international consortium of AIT, BAe, CASA and MBB.

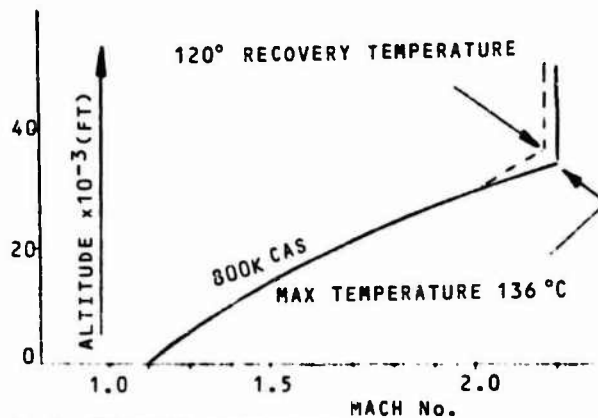


FIG 1 RECOVERY TEMPERATURE BOUNDARIES

MATERIAL	AIRCRAFT		
	TORNADO	EAP	EFA
ALUMINIUM ALLOY	71.0	58.8	47.0
STEEL	6.4	3.9	3.5
TITANIUM ALLOY	17.5	10.5	5.6
C.F.C.	0	19.7	36.8
MISCELLANEOUS	5.1	7.1	7.1

* INCLUDES GLASS REINFORCED PLASTIC
TABLE 1 DISTRIBUTION OF STRUCTURAL MATERIAL

4.1 ALUMINIUM ALLOY

Table 1 shows that aluminium alloy has a very important part to play in the structure of advanced military aircraft, though it is certain that any new aircraft will use different types of aluminium alloy to those currently used in the structure. These new alloys are the aluminium-lithium type, as well as the developed zinc based 7150 alloy and the powder metallurgy 7090 and 7091 type alloys.

4.1.1 CONVENTIONAL ALUMINIUM ALLOY

The majority of the world's fighter aircraft are currently constructed from a combination of widely known and understood copper-based aluminium alloys 2014 and 2024, together with the zinc based 7010 and 7075 alloys. It is considered that the use of copper-based alloys on future fighter type aircraft will be minimal. However, development of zinc based alloys will continue, and the recent introduction of 7150 by ALCOA, which offers high strength and increased toughness compared with 7010, should ensure that it is used on future aircraft, especially if the high strength aluminium-lithium alloy (Al-Li type B) continues to have development problems.

A further improvement in the properties of aluminium alloys can be obtained by using the powder metallurgy process. This relatively new process gives the material a much finer grain structure which enhances its fatigue performance as well as increasing the basic mechanical properties. The ALCOA Company in the USA are currently working on developments of the 7090 type aluminium alloy which have an ultimate tensile strength

of the order of 620 N/mm^2 , and may within the next decade be increased to 800 N/mm^2 . TABLE 2 compares the basic mechanical properties of the powder metallurgy alloys with both aluminium-zinc and aluminium-lithium alloys (see also para. 4.1.2).

4.1.2 ALUMINIUM-LITHIUM ALLOY

Although it is considered to be a new alloy, the aircraft industry has already had manufacturing and service experience, albeit not entirely satisfactory with aluminium-lithium alloy. In the 1950's and 1960's the BAe TSR 2 and the North American Vigilante used X2020 aluminium-lithium alloy, despite its extremely short critical crack length. In addition it is known that the Russian TU 144 supersonic transport used a type of aluminium-lithium alloy, as well as some of the latest Soviet fighters.

Why is there this renewed interest in aluminium-lithium alloys, and are they so superior to the currently used copper and zinc based alloys?

A cursory glance at the mechanical properties show that they are very similar to those of 2014 and 7010 material. The most important difference between the current conventional alloys and aluminium-lithium is its reduced density, being approximately 90% of the former material. This then is the material's great attraction, since it is generally possible to achieve a lower mass by using a material with a smaller density rather than one with higher ultimate strengths.

An additional attraction of aluminium-lithium is that the Young's Modulus "E" has also increased by approximately 10% when, again, compared with conventional alloys. This will also reduce mass, especially for structures designed by panel buckling or instability.

If then this is such an attractive material why is it not being used in current airframes? Unfortunately, there have been manufacturing development problems (still not completely resolved) with the new aluminium-lithium alloys.

The U.K. approach in developing aluminium-lithium alloy has been to identify three targets; being the replacement of low, medium and high strength aluminium alloy. The major work has been carried out by British Alcan International Limited, using a chemical composition initially developed by the Royal Aircraft Establishment at Farnborough - the new alloys having an increased lithium content of the order of 2 to 3% compared with 1% of the old X2020 material. In addition to the United Kingdom, Alcoa in the United States and in France are also actively developing the alloy. The medium strength alloy known as Al-Li type 'A' is almost at the production stage, the evaluation process to assess formability, fabrication and determination of material allowables is complete, and early development material has been used in the construction of the trailing edge flaps of the EAP.

The high strength alloy (Al-Li type 'B') is still in the development stage, with production material planned to be available later in 1986. It is envisaged that this material will be used for the major fuselage wing carry-through frames on the European Fighter Aircraft (EFA).

For the purpose of comparison with other materials, the reduction in mechanical properties of aluminium-lithium at temperature will be assumed to be the same as 2014 for type 'A', and 7075 for type 'B'. These reduction factors are given in FIGURE 2.

The mechanical properties of aluminium-lithium are given in TABLE 2.

4.2 MAGNESIUM ALLOY

Because of their lack of resistance to corrosion, magnesium alloys will continue to be used only in areas which are readily accessible for inspection. To improve their performance however, efforts are being made by the manufacturers to improve their corrosion resistance, together with means of improving the protection by insulating coatings.

The magnesium alloys, notably A357, and the newer K01 material are normally used for complex castings such as canopy surrounds, windscreen arches etc. The major attraction of magnesium castings are the relatively low cost (when compared with a fabricated alternative design) and its low mass. The density of magnesium alloy is approximately 67% of aluminium.

	N/ m ² (MPa)		SPECIFIC GRAVITY	N/mm ² (MPa)		
	ULTIMATE STRESS	MODULUS		SPECIFIC STRENGTH	SPECIFIC MODULUS	
ALUMINIUM - 2 INC ALLOY (CONVENTIONAL MANUFACTURING PROCESS)	7075	500	72,000	2.80	179	25,710
	7010	515	72,000	2.80	183	25,710
	7150	605	72,000	2.80	216	25,710
ALUMINIUM ALLOY (POWDER METALLURGY MATERIAL 'X' MANUFACTURING PROCESS)	7090	620	72,000	2.80	221	25,710
		800	72,000	2.80	285	25,710
ALUMINIUM-LITHIUM ALLOY	TYPE 'A'	450	78,000	2.52	178	30,950
	TYPE 'B'	520	78,000	2.52	206	30,950

TABLE 2 COMPARISON OF BASIC PROPERTIES OF ALUMINIUM ALLOYS AT ROOM TEMPERATURE

4.3 TITANIUM

No new titanium material specifications are envisaged during the next decade, but because of new manufacturing processes currently being developed, the use of titanium on the next generation of supersonic aircraft may increase. One cannot of course be certain of this statement, as the use of titanium is also dependent upon the overall configuration of the aircraft and the structural loading index P/b .

TABLE 3 gives a comparison of the wing loading index of three aircraft developed (in conjunction with our European Partners) at the Warton Division of British Aerospace. The importance of this parameter is illustrated later in the paper (see Section 6.2).

The Tornado has a high loading index compared with the later EAP and EFA, this high loading being due to overall aircraft configuration; Tornado having a small highly loaded wing carry-through box whereas the EAP and EFA have low aspect ratio wings.

The Tornado carry-through box is titanium, the lower skin of the box being electron-beam welded to the ribs and shear webs.

The new manufacturing processes mentioned above are Superplastic Forming (SPF) and Diffusion Bonding (DB).

The Superplastic Forming process involves the application of gas pressure at approximately 900° C to form sheet into a tool die representative of the component shape to be manufactured. The process is a controlled operation where the material is subjected to a pressure-time cycle, carefully selected to produce the correct strain rate variation throughout the forming operation.

Diffusion bonding can take place at the same level of temperature when pressures are high enough to produce continuous and homogeneous bonds between the sheets of material being joined together.

Positioning 'stop-off' compound strategically between the sheets enables the diffusion bonded areas to be differentiated from those areas which are to be blown apart during subsequent superplastic forming operations.

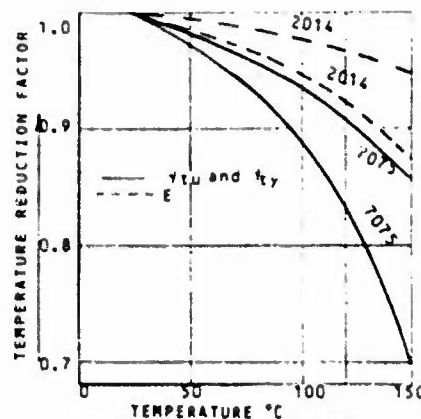


FIG 2 ALUMINIUM ALLOY-TEMPERATURE REDUCTION FACTORS

AIRCRAFT	WING LOADING INDEX	
	P/b	N/mm ²
TORNADO		30
JAGUAR		23
E. A. P.		12

TABLE 3 WING LOADING INDICES

The majority of the work at British Aerospace has concentrated on the 6Al 4V Titanium alloy, this material being in the annealed condition, thus allowing complex thin sheet structures to be produced by the process without any subsequent heat treatment being required.

Employment of the SPF/DB process to titanium in aircraft designs leads to large cost and weight savings being achieved. The cost saving proves to be very substantial as a result of the minimised labour involvement during the fabrication process.

Savings up to 50% of the cost of conventional manufacture have been demonstrated in design studies carried out to date.

Weight savings are not as great although they can be quite significant, especially when full advantage can be taken of the high specific strength of titanium, and where the conventional alternative designs would involve a large number of mechanical attachments, with their associated structural weight penalties especially from bearing requirements.

Design and development programmes to demonstrate the potential advantages of the SPF/DB process are currently being carried out at British Aerospace.

These programmes (which are partially funded by the U.K. Ministry of Defence) deal with manufacturing development, basic technology (including design allowables) and structural demonstrators.

Results obtained from the basic technology programme indicate that the mechanical properties (including fatigue performance) of SPF/DB titanium are only marginally reduced when compared with the "as-received" material. The extent of the reduction being dependent upon the method of manufacture - i.e. hot open die or the muffle box process.

One of the structural demonstrators included in the U.K. MoD programme which is of direct relevance to future military aircraft is a full scale foreplane initially designed for the BAe P.110 project. This component is currently being manufactured and will be statically tested during 1986. FIGURE 3 shows the details of the construction while TABLE 4 gives the cost saving and also the weight penalty when compared with a CFC foreplane (and of course its titanium spigot). Despite the slight weight penalty, a SPF/DB titanium foreplane offers a competitive solution for the future canard configurations, because of the large saving in cost.

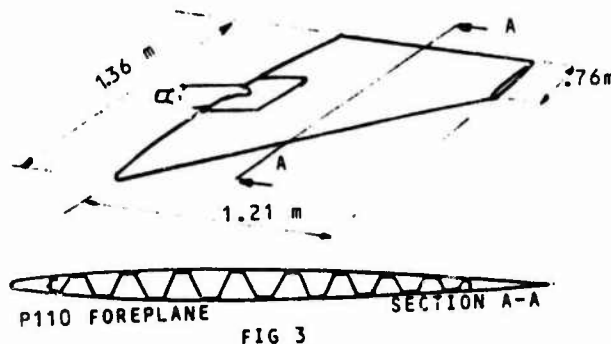


FIG 3

MATERIAL	RELATIVE COST *	MASS OF FOREPLANE (INCLUDING SPIGOT)
SPF/DB TITANIUM ALLOY	0.70	72 kg
C.F.C.	1.00	68.5 kg

*RELATIVE COST BASED ON PRODUCTION RUN OF 300 AIRCRAFT

TABLE 4 P110 FOREPLANE COMPARISON OF MASS AND COST

4.4 STEEL

Steel has a negligible loss in mechanical properties at 120° C and consequently has been used for some supersonic aircraft. For example, the Bristol 188 research aircraft and also the North American B70 had predominantly steel airframes. One other aircraft which must be mentioned is the General Dynamics F111 which has a steel carry-through box. However, because of the high density, together with the cost of fabrication, it is most unlikely that steel will feature predominantly in the structure of the next generation of supersonic aircraft, but will of course, be continued to be used at points of high load concentration. The mechanical properties of currently used steel material are given in TABLE 6.

4.5 METAL MATRIX COMPOSITES

Metal matrix composites may be divided into four main types categorised by the metal form of re-inforcement employed:-

Whisker	- 0,2 μ m diameter
Particulate	- 1,0 μ m to 100 μ m plus diameter
Short fibre	- 10 μ m to 60 μ m diameter
Long continuous fibre	- 60 μ m diameter

The nature of the re-inforcing materials is usually ceramic, examples being Silicon Carbide (SiC) Alumina (Al_2O_3), Boron Carbide (B4C).

For Aerospace applications, each of these types of metal matrix composites is being considered in conjunction with aluminium alloys. Only the long continuous fibre is currently being considered for titanium alloys.

The main benefits of re-inforcing alloys is to improve specific strength and stiffness.

The manufacturing method employed to make materials greatly affects the final, usable form. For example, whiskers and particulates usually employ casting or powder technologies which lead to semi-finished or finished articles (castings, forgings, sheet, extrusions etc). Short and long fibres usually lead to materials having a laminate arrangement of the re-inforcing materials, e.g. diffusion bonded sheet laminates and laminate casting.

Evaluations to date have been concerned with materials of each type obtained mainly from the USA. Research quantities of some types of metal matrix composites are becoming available in the U.K., and these too are being assessed.

The evaluations have resulted in attention being paid towards:-

- (a) U.K. material development and evaluation of particulate re-inforced aluminium alloys, adopting the powder technology route of manufacture. One example is:-

SiC flake-like particles in 2014 alloy.

Such materials are currently being assessed by BAe and new, lower density variants, are being considered.

- (b) Evaluation of continuous fibre re-inforced titanium when fabricated within a diffusion bonded structure. Thus:-

SiC continuous fibre in Ti/6Al/4V alloy.

TABLE 5 provides a comparison of typical mechanical properties for these materials and base alloys.

The effect of adding SiC particulates to 6061 aluminium alloy is shown in FIGURE 4, where it can be seen that the ultimate tensile stress can be increased from 310 N/mm² to 490 N/mm² and the modulus from 72000 N/mm² to 110000 N/mm² by the addition of 30% SiC particulates (by volume). Unfortunately, the elongation also reduces from approximately 12% for the basic material to 4% when the particulates are added.

The main advantages associated with metal matrix composites are increased strength, stiffness and, in some cases, improved fatigue properties and reduced density. The main disadvantages are low ductility, sometimes pronounced anisotropy and high material and manufacturing costs.

Despite this disadvantage of reduced elongation, metal matrix composites are an exciting development, and if it were possible to add SiC particulates to Aluminium-Lithium Type B alloy (see para. 4.1.2) then this would really be a material for use in the year 2000!!

A comparison is made in TABLE 5 between the re-inforced titanium and 2010 aluminium alloys and the basic unreinforced material.

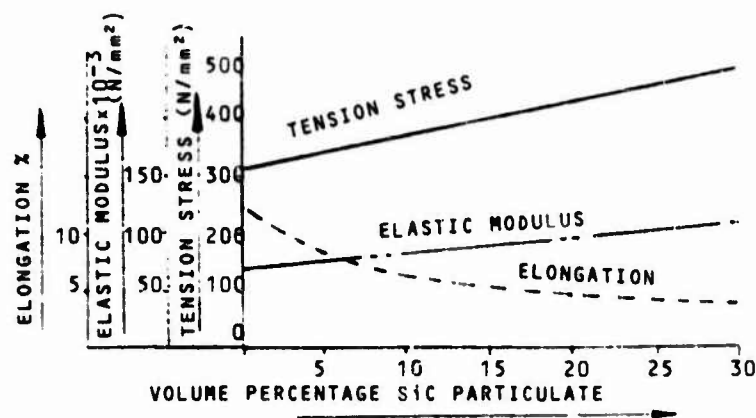


FIGURE 4
EFFECT OF ADDING
SiC PARTICULATE
6061 AL. ALLOY

MATERIAL	N/mm ²		SPECIFIC GRAVITY	N/mm ²	
	ULTIMATE TENSION STRESS	MODULUS		SPECIFIC TENSION STRENGTH	SPECIFIC MODULUS
TITANIUM 6 AL 4V. TA 10	920	113,000	4,512	203	25,000
SiC CONTINUOUS FIBRE REINFORCED 6AL 4V TITANIUM (40% VOLUME)	904	195,000	4.05	223	48,150
ALUMINIUM ALLOY PLATE 2014	460	69,000	2.80	164	24,640
SiC PARTICULATE REINFORCED 2014 ALUMINIUM ALLOY (30% VOLUME)	640	11,400	2.90	221	39,310

TABLE 5 COMPARISON OF THE PROPERTIES OF METAL MATRIX COMPOSITES WITH CURRENT ALLOYS AT ROOM TEMPERATURE

MATERIAL		N/mm ²		SPECIFIC GRAVITY	N/mm ²	
		ULTIMATE TENSION STRESS	MODULUS		SPECIFIC TENSION STRENGTH	SPECIFIC MODULUS
CARBON FIBRE	XAS	3,550	235,000	1.810	1,960	129,800
STEEL	S99	1,230	200,000	7.833	157	25,530
ALUMINIUM ALLOY	7075	500	72,000	2.796	179	25,750
TITANIUM ALLOY	TA-10	920	113,000	4.512	203	25,000

TABLE 6 COMPARISON OF BASIC PROPERTIES OF CURRENTLY USED MATERIALS AT ROOM TEMPERATURE

5. CARBON FIBRE COMPOSITES

Carbon fibre composite (CFC) is probably the most important new material to be introduced into the aircraft structure in the last two or three decades. Not only does CFRC possess excellent specific strength and modulus, but it offers an unusual opportunity to design the structure and the material simultaneously. The structural and materials engineer now have the ability to meet the ever growing demands made by the aerodynamicist in designing advanced military aircraft.

But what are the truths about carbon fibre? Is it as good a material as the popular press would have us believe? Is it a new wonder material which is stronger than steel and lighter than aluminium? Well, as with the majority of things in life, this statement is "partly true and partly false".

Firstly, a "new material"? Carbon fibre was developed at the Royal Aircraft Establishment at Farnborough and announced mid 1966; that is 20 years ago, so it can no longer be described as a new material. Secondly, is it stronger than steel? If a comparison of the basic properties is made between the currently available XAS carbon fibre manufactured by Courtaulds in the U.K., and metallic materials used in the aircraft structure, it can be seen from TABLE 6 and also in diagrammatic form in FIGURE 5 that carbon fibre is indeed much stronger than steel and lighter than aluminium. Unfortunately, owing to the various environmental and design constraints the extremely high strength and stiffness values of carbon fibre reduce considerably when manufactured into a practical aircraft structure. As discussed at previous symposia, (Refs 1 and 2), reduction factors are necessary to establish the design allowable strengths and moduli.

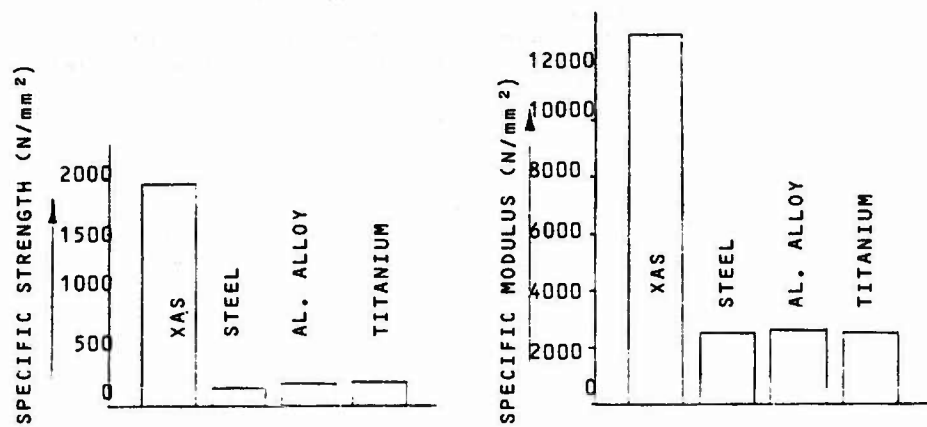


FIG 5 COMPARISON OF BASIC PROPERTIES OF CURRENTLY USED MATERIALS AT ROOM TEMPERATURE

5.1 REDUCTION FACTORS

The reduction factors briefly described below are given for the XAS fibre/914 resin material supplied in the form of uni-directional tape. Uni-directional tape being preferred to woven cloth (see also para. 5.4) for major structural Class 1 components because of its superior strength properties, being more adaptable to automatic lay-up and also allowing the engineer to design a more efficient laminate, (e.g. a 50% x 0°, 30% x ± 45° and 20% x 90° laminate would be impossible to produce using woven cloth).

5.1.1 PRE-IMPREGNATION

The strength of the carbon-fibre when embodied in a matrix of resin to form pre-impregnated uni-directional tape reduces the tensile strength to approximately 60% of its original value.

5.1.2 LAY-UP

As most structures must resist several cases of combined loading, multi-orientation lay-ups are necessary. The usual choice is to have lay-ups with fibres aligned at 0°, 90° and ± 45° relative to some datum direction, but variations may be required for particular applications such as aerodynamic tailoring. A typical laminate of 50% x 0°, 40% x ±45, and 10% x 90°, will have a strength of approximately 59% of its uni-directional equivalent.

5.1.2 ENVIRONMENTAL DEGRADATION

Current CFC materials absorb moisture during their service lives, typically to an average value of about 1% by weight in aircraft applications. This moisture, together with the effect of high temperature, will reduce the mechanical properties. For example, when wet at 120°C the resin-dependent shear and compression properties can fall by about 30% relative to room temperature/low moisture conditions. In addition, repeated excursions to such high temperatures reduce the resistance of epoxies to moisture absorption.

5.1.3 VARIABILITY

The coefficient of variation (Cv) of strength of CFC components is higher than equivalent metal assemblies. Analysis of tests of CFC specimens has shown that typical mean test values should be reduced by approximately 20% to obtain minimum design values. CFC moduli variation also currently exceeds that for metal, but not to such a marked extent. Greater use of automated tape-laying machines will reduce the variability, and the latest test results show that the Cv for CFC is approaching that obtained from metal assemblies.

Until recently it had been the practice in the U.K. to establish the design allowables based on the 'A' level of confidence (as defined in ref. 3), this decision has now been modified to accept a 'B' level of confidence for all structural assemblies apart from very localised single load paths.

The definition of 'A' and 'B' values is defined as follows:-

'A' Value

At least 99% of the population of values is expected to equal or exceed the 'A' basis mechanical property allowable, with a confidence of 95%.

'B' Value

At least 90% of the population of values is expected to equal or exceed the 'B' basis mechanical property allowable, with a confidence of 95%.

The effect of using the 'B' rather than 'A' values is summarised in TABLE 7.

CONDITION	ROOM TEMPERATURE / AS RECEIVED		120°C/1% MOISTURE	
	A	B	A	B
TENSION	840	915	770	840
COMPRESSION	650	745	420	480

MATERIAL XAS/914 LAY-UP 60°x0°, 30° x ± 45°, 10°x90°

TABLE 7 COMPARISON OF 'A' AND 'B' DESIGN VALUES

5.1.6 NOTCH SENSITIVITY

Owing to the elastic behaviour to failure of fibre-dominated CFC properties, the stress concentrations due to notches are not relieved by plasticity as they are with metal construction. FIGURE 6 shows the stress-strain curve of a typical CFC laminate compared with the curve for a currently used copper-based aluminium alloy L65 (2014).

Because of this lack of plasticity, stress concentrations cannot be ignored in the static design of CFC, and the strength can be reduced by up to 67% - the actual value being dependent upon the lay-up as well as the severity of the notch.

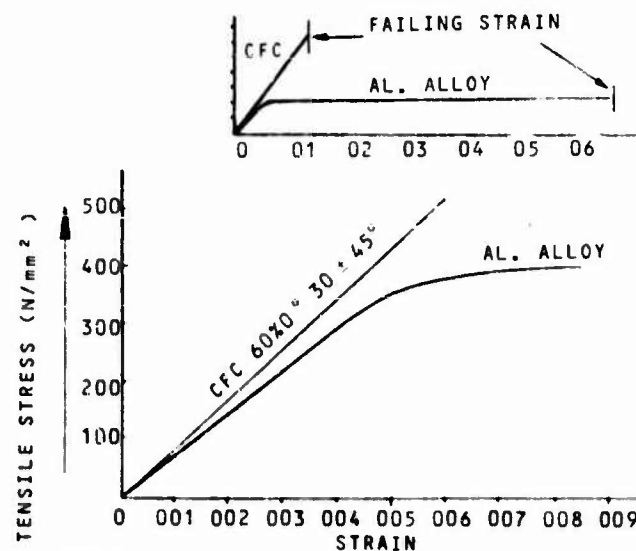


FIG 6

5.2 YOUNG'S MODULUS

The moduli also suffers from the various reduction effects described above. The reduction factors to be applied to moduli are however smaller than the strength reduction factors and are summarised in FIGURE 7.

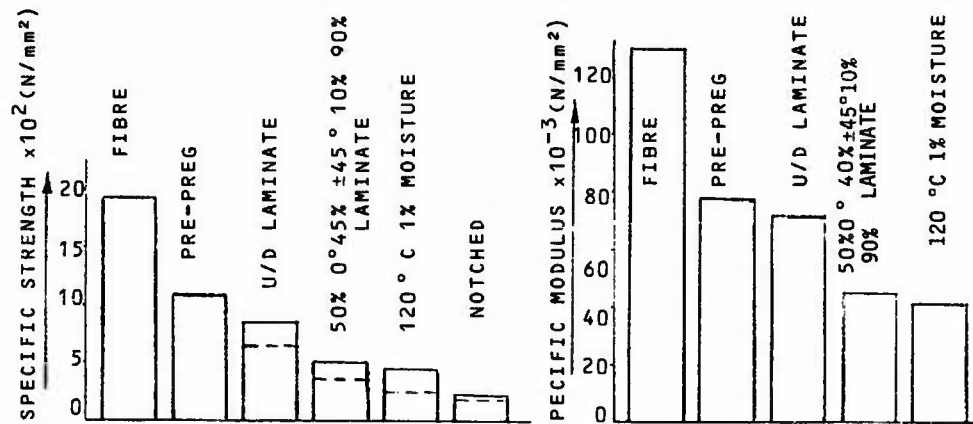


FIG 7 EFFECT OF REDUCTION FACTORS ON THE SPECIFIC STRENGTH AND MODULUS - XAS/914 MATERIAL

5.3 C.F.C. ALLOWABLE STRESSES AND MODULI

The cumulative effects of the reduction factors described in 5.1 on the strength and modulus of CFC are shown in FIGURE 7. It will be noted that the strength of carbon fibre as originally manufactured is 3550 N/mm², but the allowable stress used for design after all of the various reduction factors have been considered reduces to 465 N/mm² in tension, and 290 N/mm² in compression.

The tensile modulus of CFC is also reduced from 235000 N/mm² for pure carbon fibre to an allowable design modulus value of 77400 N/mm².

5.4 WOVEN CLOTH

CFC, and also glass and Kevlar can be obtained in woven cloth form rather than as uni-directional tape described above. Various forms of cloth having different weave patterns are available for use, the most popular type being the 'Plain Weave' - this cloth having approximately equal strengths in both the weft and warp direction.

Laminates made from cloth suffer a reduction in strength of approximately 15% when compared with laminates manufactured from uni-directional tape, this reduction in strength being due to the kinked warp fibre passing over or under the weft.

Despite this reduction in strength, cloth has many attractions compared with UD tape, the most important being the ability to 'drape over' complex double curvature surfaces, and is normally used for the manufacture of secondary components such as fairings etc.

Cloth is usually supplied to the aircraft manufacturer pre-impregnated with resin, and suffers similar types of reductions in strength due to variability, environmental degradation, etc. as described in section 5.1.

5.5 IMPROVEMENTS IN CFC MATERIALS

Of most interest to the materials engineer is the improvement in properties which can be expected for the next generation of fighter aircraft.

5.5.1 HIGH STRAIN FIBRE

The failing strain of fibre currently used on military aircraft is of the order of 1.5%. The ultimate tensile modulus is 230000 N/mm². Rapid improvements by the fibre manufacturers have been made recently, with predicted failure strains of the order of 2% and the tensile failure stresses increased to approximately 5500 N/mm². Unfortunately, the tensile modulus has not been increased, and remains at approximately 230,000 N/mm².

5.5.2 HIGH MODULUS FIBRE

High modulus fibres are currently available having tensile moduli varying between 345,000 N/mm² and 450,000 N/mm². These fibres however suffer in having low failure strains of 0.76% and 0.48%. Because of these low failing strains, the high modulus fibre will probably not find widescale use on future fighter aircraft.

5.5.3 INTERMEDIATE MODULUS FIBRE (I.M. FIBRE)

Recent developments in the U.S.A., Japan, and the U.K. have shown that the modulus of elasticity of carbon fibre can be increased without any serious reduction in the overall failing strain of the fibre.

Typical properties for intermediate - modulus fibre

Failing strain = 1.7

Tensile failing stress = 5000 N/mm²

Modulus of elasticity = 290000 N/mm²

As large regions of modern low aspect ratio delta wings are designed by a combination of stiffness and panel buckling, (both being dependent upon Young's Modulus) the intermediate modulus fibres will be used on the next generation of aircraft.

One disadvantage of the I.M. fibre is its relatively small diameter when compared with the older fibres (Diameter of I.M. fibre is approximately 4.5×10^{-6} m compared with 7.2×10^{-6} m for XAS fibre). As a consequence of this reduction in the diameter, the notched compression strength of I.M. fibres has been disappointing, being only slightly better than the old XAS fibre. Obviously the manufacturer who can produce a fibre with a diameter of 7×10^{-6} m together with the properties listed above will have a winner!!

5.6 RESINS

At the Warton Division of British Aerospace the resin used on CFC Jaguar wing and Tornado taileron demonstrator projects and also (in conjunction with AERITALIA in TURIN) on the EAP demonstrator is BSL 914 - an epoxy resin manufactured by Ciba-Geigy (UK) Limited. This is an excellent material to use in manufacture, but does (in common with all epoxies) have reduced mechanical properties when subjected to a combination of moisture and high temperatures (of the order of 120°C.) Thus if improvements are to be made in future aircraft structures, an alternative resin to the current available epoxies must be made available.

At least five different types of resin systems are being developed for use on the next generation of fighter aircraft.

- . Toughened Epoxy Systems
- . Bismaleimide Systems
- . Epoxy-Bismaleimide Systems
- . Polyimide Systems
- . Thermoplastics

5.6.1 TOUGHENED EPOXY

For the past three years the resin manufacturers have been working towards producing a tougher epoxy system which will give a better balance between the hot wet notched compression and compression after impact properties. This has been achieved by modifications to the epoxy system, by changes to the chemical formulates and by the addition of toughening agents. A typical example of this type of resin system is the Ciba Ceigy 6376. The operating temperature for the resin is still approximately 120°C, but test results have shown increases in laminate performance when combined with the intermediate modulus fibres in a fully or 90% saturated condition.

5.6.2 BISMALEIMIDE (BMI)

The bismaleimide systems offer higher operating temperatures (of the order of 220°C) than epoxy resin but suffer the disadvantage of being more brittle and more difficult to process. Several current aircraft use bismaleimide resins including the AV8 B in areas subject to high temperatures in the region of the engine nozzles.

5.6.3 EPOXY-BISMALEIMIDE

As the name implies, this is an epoxy based system with the addition of bismaleimide. Operating temperatures and overall laminate performance is very similar to the toughened epoxy resin. NARMCO 5245 is a typical example of this type of resin system.

5.6.4 POLYIMIDES

These resins are cured by a condensation reaction system and offer higher operating temperatures of the order of 275°C. Currently, these resins are more expensive than the modified epoxies and are more difficult to process, requiring higher cure temperatures and pressures. Post processing is required to achieve full cross-linking and glass transition temperature. These systems tend to be more brittle than either the epoxy or BMI resins.

Despite this somewhat dismal picture, polyimide resins have been used on demonstrator aircraft in the USA.

5.6.5 THERMOPLASTICS

Recently developed thermoplastic systems offer a high Tg (>140°C) good impact performance, adequate moisture resistance and most importantly compatibility with high strain fibres. Against these design advantages problems have been encountered during the manufacture of laminates. The lack of tack in particular causes handling problems, and processing conditions of 380°C demand press-type forming operations. However, re-processing due to the thermoplasticity is possible together with re-cyclability of scrap for injection mouldings. A typical thermoplastic currently under development in the U.K. is PEEK (Polyether-Ether-Ether-Ketone) manufactured by ICI, and it is hoped that components made with PEEK will fly on the EAP later this year.

6. COMPARISON OF MATERIALS

The basic mechanical properties of metallic and non-metallic materials, together with their buckling characteristics and fatigue strength will all be compared at a temperature of 120°C and, in the case of CFC, at the design moisture level of 1% by weight.

6.1 TENSION AND COMPRESSION PROPERTIES

Using the temperature reduction factors for aluminium and titanium given in Fig. 2 and, in the case of CFC, with the combined reduction factors described in Section 5.1, a comparison of current materials can be made. The comparison of the specific strength and modulus properties is given in FIGURE 8 where it will be observed that CFC is still the most efficient material.

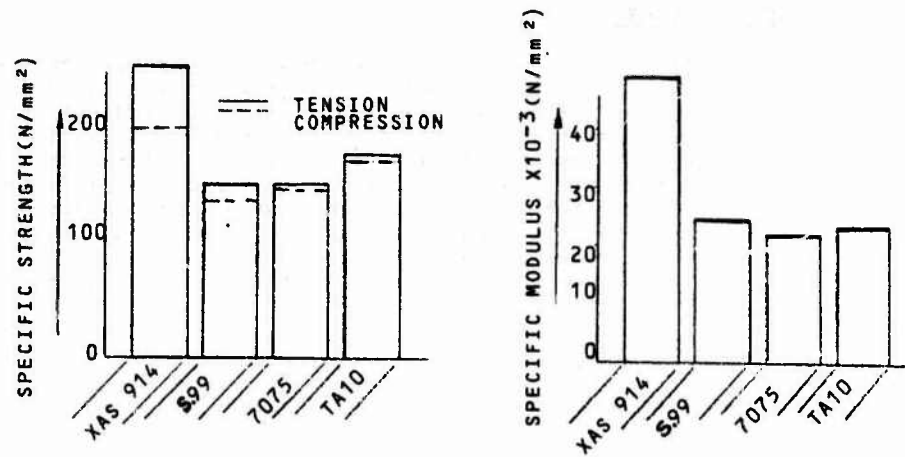


FIG 8 COMPARISON OF COMMON AIRFRAME MATERIALS

6.2 BUCKLING

Thickness/chord ratios of 4% and less are proposed for the next generation of high performance aircraft. For wings of such small depth and consequently high compression loading skin buckling is a major design constraint. It is therefore desirable to compare the buckling efficiencies of the alternative materials.

Considering the simple example of a long panel in uni-axial compression.

Referring to FIGURE 9 the panel buckling simple stress is $\sigma_b = KE_t \left(\frac{t}{b}\right)^2$

The direct compressive stress is $\frac{P}{t}$. If the panel just buckles under the applied stress

$$\sigma_{OPT} = \sigma_b = \frac{P}{t} \text{ and therefore}$$

$$\sigma_{OPT} = \frac{(K E_T)^{1/3}}{S} (P)^{2/3}$$

FIGURE 9 shows the buckling merit index $\frac{\sigma_{OPT}}{S}$ for

CFC in comparison with metallic materials by considering long panels, representing a multi-spar design, with simply supported edges, giving $K = 3.62$ for metal panels. There is an upper cut off for each material at the compressive one percent proof stress for metallic materials, and the notched, degraded design ultimate compression for CFC. Also plotted on FIGURE 9 are the wing loading indices for the Tornado, Jaguar and EAP.

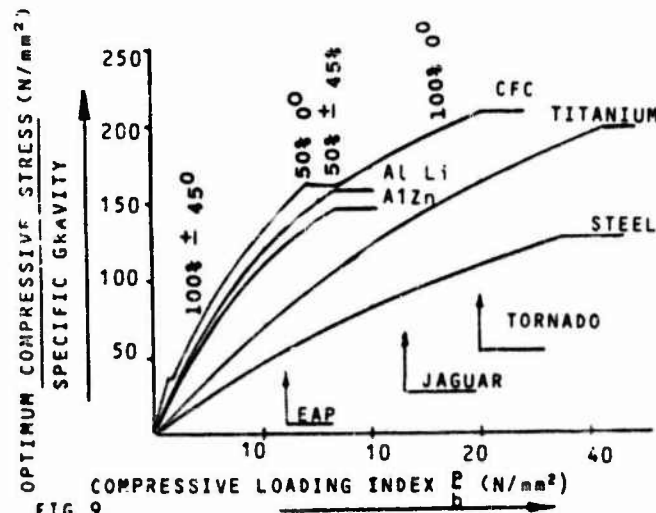


FIG 9

6.3 FATIGUE

Metallic materials for aircraft use are notch sensitive in fatigue, but almost notch insensitive under static loading. In contrast, CFC is very notch sensitive under static loading and relatively notch in-sensitive in fatigue. Consequently, fatigue may not be a problem for CFC structures designed to static ultimate.

Considering a representative combat aircraft spectrum and a service life of 4000 hours, the allowable ultimate stresses for wing lower tension skins, assuming good detail design are given for both aluminium alloy and titanium in TABLE 2.

These values are below the respective static allowable stresses. Aluminium or titanium compression skins are not fatigue critical. Considering typical CFC notched, degraded lay-ups, designed to ultimate static loads, shows that fatigue will not be critical for either tension or compression.

The information on the fatigue characteristics of CFC has been obtained from two United Kingdom Ministry of Defence programmes [FADD (fatigue and Damage Tolerance Design Data) and VALID (Variability and Life Data)] performed by the Warton Division of British Aerospace. See also ref 4. FIGURE 10 compares the fatigue performance of CFC (XAS/914) with aluminium alloy.

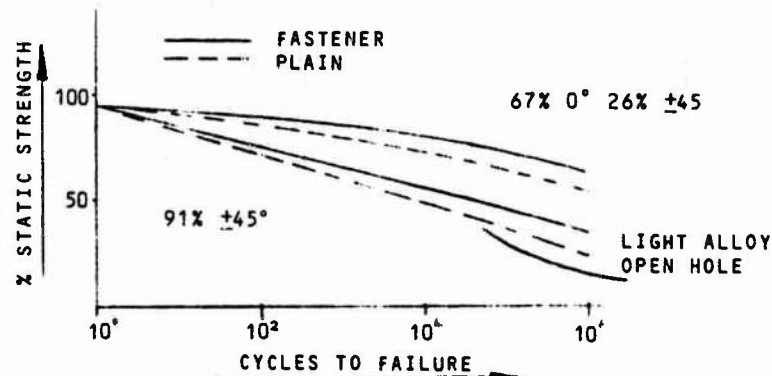


FIG. 10 FATIGUE PERFORMANCE OF CFC COMPARED WITH LIGHT ALLOY

MATERIAL	ALLOWABLE FATIGUE STRESS N/mm ²	SPECIFIC GRAVITY	SPECIFIC FATIGUE STRESS N/mm ²
CFC XAS/914 (50.40.10)	406	1.61	252
STEEL	1125	7.833	143
ALUMINIUM ALLOY (2014)	340	2.796	121
TITANIUM ALLOY (6AL.4V)	740	4.512	164

TABLE 8 COMPARISON OF FATIGUE DESIGN STRESSES

6.4 ALLOWABLE DESIGN SPECIFIC STRENGTHS

It was shown in section 6.3 that the allowable design tension stresses for metallic materials have to be reduced in order to achieve the required fatigue life. Figure 11 shows the final design specific tension and compression stresses for current airframe materials.

6.5.1 MODULUS - Figure 8

CFC has the highest specific modulus of all the materials under consideration. Steel, titanium and aluminium alloy having achieved approximately 60% of CFC.

6.5.2 TENSION - Figure 11

CFC has the highest specific tension strength and is not affected by fatigue consideration. The metallic materials are all critical in fatigue.

6.5.3 COMPRESSION - FIGURE 11

Despite the reduction factors (section 5.1) applied to the compression strength, CFC has still the highest specific strength. Titanium however is only marginally inferior to the older XAS fibre.

6.5.4 BUCKLING - FIGURE 9

At the lower values of the loading index, CFC is marginally more efficient than aluminium-lithium and conventional aluminium alloy. At the higher values of the loading index, titanium is clearly the most efficient material.

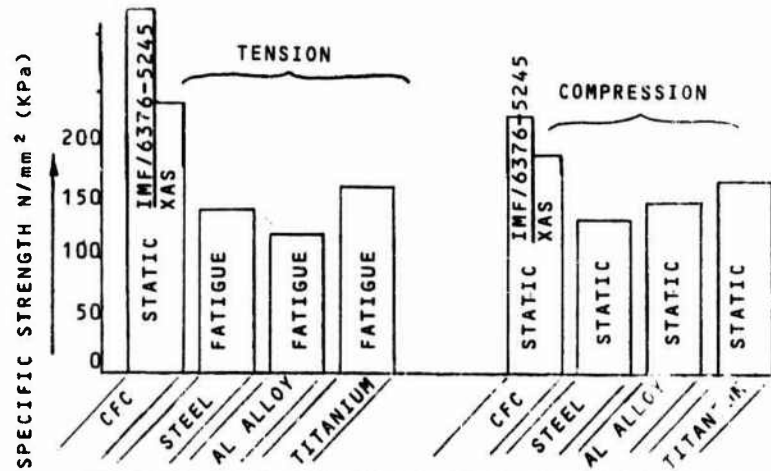


FIG 11 ULTIMATE DESIGN SPECIFIC STRENGTH FOR COMBAT AIRCRAFT STRUCTURAL MATERIALS

7. COMPARISON OF FUTURE MATERIALS

It is an almost impossible task to predict which materials will be used on future fighter aircraft designed, say, in the late 1990's and the year 2000. As was shown in TABLE 3 and FIGURE 9, the aircraft's overall configuration determines the structural loading index; the design Mach Number determines the recovery temperature. Thus, unfortunately, we are in the hands of the aerodynamicists and configuration engineers before we can, with confidence, determine the material usage on future aircraft.

However, despite having to rely on the aerodynamicist, the future appears to be an exciting one for the materials engineers. The competition now developing between the carbon manufacturers and the suppliers of metallic materials augurs well for reducing structural mass on newer aircraft.

TABLE 9 and FIGURE 12 show the materials that may be available in the mid 1990's, compared with the latest materials which are available today. Obviously any such look ahead requires an extrapolation of the strength properties of existing materials. On the basis of this extrapolation, CFC will apparently continue to have the highest specific strength and stiffness. However, should future fighters have a higher design Mach number than they now have (giving a recovery temperature of (say) 150/160° C), then reinforced titanium alloy may become the more attractive material.

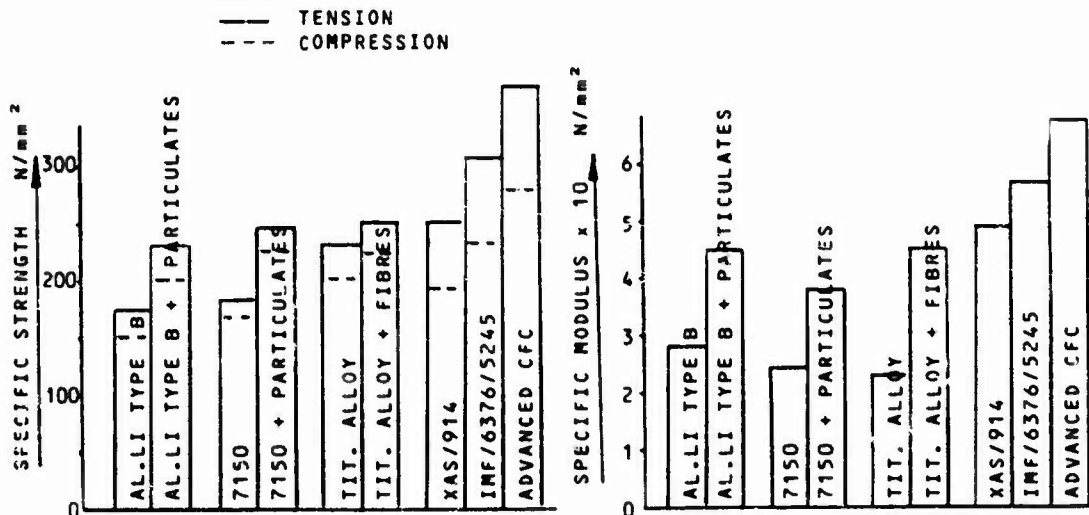


FIGURE 12 COMPARISON OF FUTURE MATERIALS

MATERIAL	N/mm ²			SPECIFIC GRAVITY	N/mm ²		
	f _{tu}	f _{ty}	E		SPECIFIC TENSION STRESS	SPECIFIC COMPRESSION STRESS	SPECIFIC MODULUS
ALUMINIUM-LITHIUM TYPE 'B'	440	380	72000	2.52	174	151	28600
ALUMINIUM-LITHIUM 'B' PLUS PARTICULATE ▷	610	530	118000	2.61	234	203	45210
ALUMINIUM ALLOY 7150	510	480	66600	2.80	182	171	23790
ALUMINIUM ALLOY 7150 PLUS PARTICULATE ▷	710	660	110000	2.90	245	228	37900
TITANIUM ALLOY 1M1 550	1050	920	105000	4.51	232	204	23280
TITANIUM ALLOY 1M1 550 PLUS CONTINUOUS FIBRE ▷	1030	900	182000	4.05	254	222	44940
CFC XAS/914 ▷	406	312	79000	1.61	252	193	49000
CFC IMF/6375-5245 ▷	490	370	91000	1.60	306	231	56800
FUTURE CFC MATERIAL ▷	570	430	105000	1.55	368	277	67700

TABLE 9 POSSIBLE FUTURE MATERIALS COMPARED WITH CURRENTLY AVAILABLE MATERIALS
TEMPERATURE 120°C.

- ▷ PROJECTED ALLOWABLES
- ▷▷ TYPICAL LAMINATES
- ▷▷ TENSION MODULUS

8. CONCLUSION

- 8.1 Aluminium-Lithium and the advanced aluminium-zinc alloys will displace the currently used aluminium-zinc and - copper alloys within the next few years.
- 8.2 Metal Matrix Composites (especially with the addition of particulates) are exciting materials for the future.
- 8.3 CFC will be used in ever increasing quantities on the aircraft's structure.
- 8.4 Intermediate Modulus Fibres and improved Resins will be introduced on the next generation of fighter aircraft.
- 8.5 The "Leap-frogging" type of competition now developing between the suppliers of carbon fibre and the manufacturers of metallic materials will ensure that better and more efficient materials are available in the future. Such competition should be encouraged.

9. REFERENCES

1. SHARPLES T. APPLICATION OF CARBON-FIBRE COMPOSITES TO MILITARY AIRCRAFT STRUCTURES
THE AERONAUTICAL JOURNAL VOL 84 No. 834 JULY 1980.
2. SELLARS R.J. & TERRY G. - SOPHISTICATED AIRCRAFT STRUCTURES DEVELOPMENTS - COMBAT AIRCRAFT
THE AERONAUTICAL JOURNAL VOL 85 No. 847 SEPTEMBER 1981.
3. U.S.A. MILITARY SPECIFICATION
4. SELLARS R.J. & SWADLOW S.J. - MATERIALS AND STRUCTURES FOR ADVANCED SUPERSONIC AIRCRAFT - AGARD SYMPOSIUM - BRUSSELS - OCTOBER 1983

ACKNOWLEDGEMENTS

Some of the work described above has been carried out with the support of The Procurement Executive of the U.K. Ministry of Defence.

Thanks are due to British Aerospace P.L.C. for permission to publish this paper.

The views expressed are those of the author.

THE ROLE OF EXPERIMENTAL INVESTIGATION AND COMPUTATIONAL FLUID DYNAMICS
DURING FIGHTER AIRCRAFT DESIGN

by
P.W. Sacher, LKE122
Messerschmitt-Bölkow-Blohm GmbH
Helicopter and Military Aircraft Division
P.O. Box 80 11 60, D-8000 München 80, FRG

- 11.1 Introduction:
Two ways to simulate compressible flowfields, advantages versus disadvantages of numerical and experimental investigations
- 11.2 General Trends in Time/Speed and Costs in Experiment and Computation
- 11.3 State of the Art in Numerical Aerodynamics
 - 11.3.1 Model for numerical simulation
 - 11.3.2 Applications, typical results
 - 11.3.3 Code validation
- 11.4 Results from Windtunnel/Critical Review
 - 11.4.1 Effects of Reynoldsnumber
 - 11.4.2 Effects of Windtunnel
 - 11.4.3 The Role of CFD during Windtunnel Testing
 - 11.4.4 The Role of Windtunnels during Configuration Development
- 11.5 Conclusion:
The computer is not going to replace the windtunnel; the role of computers is a complementary one to save time and costs and to improve the quality of the final product.
- 11.6 References
- 11.7 Attachment

11.1 Introduction

During the design Phase I and II according to L. M. Nicolai /1/, the simulation of the complete 3D complex flowfield around the A/C configuration is absolutely necessary. In principle two ways exist for this important analysis:

- the Experiment in Wind Tunnels using models of reduced size
- the Computation solving Potential, Euler or Navier-Stokes Equations using high speed computers with large storage devices.

Fig. 1 shows typical results obtained by experiment and calculation using the same fighter model. Both approaches have their merits and both suffer from a number of handicaps (Fig. 2). It is the purpose of the present lecture to point out the special benefit and the shortcomings of both most important tools for the engineering work.

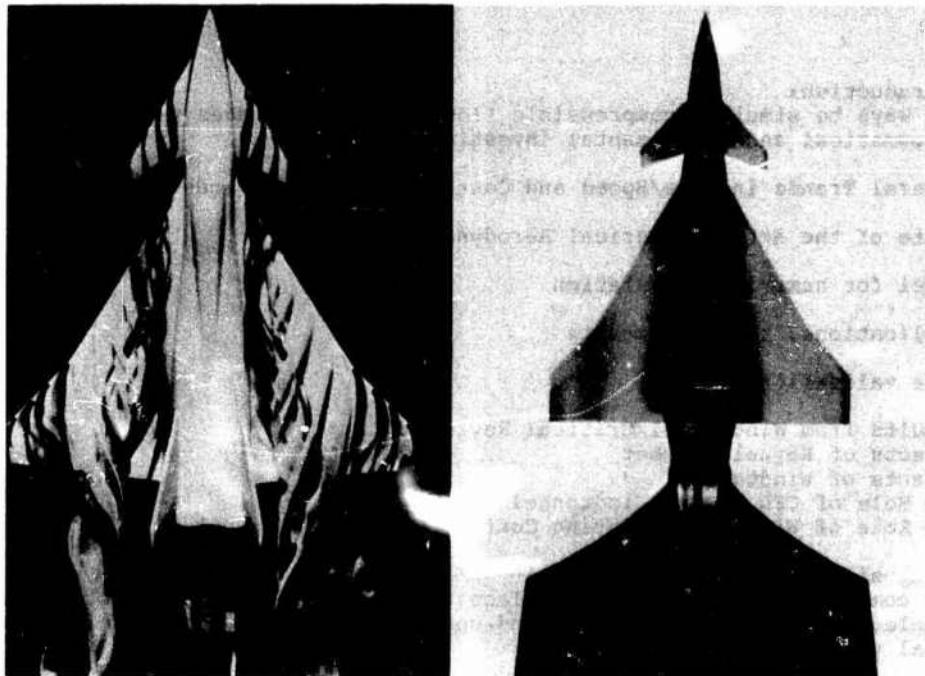


Fig. 1 Results from Experiment (MBB-Watertunnel, left) and Computational Fluid Dynamics (MBB-EUFLEX /21/)

EXPERIMENTAL APPROACH "WINDTUNNEL"	NUMERICAL APPROACH "SUPERCOMPUTER"
<ul style="list-style-type: none"> - scaled geometry - model flexibility limited - not always defined - Re-number too low - long term (time consuming) - cost increasing + accuracy of measuring technique known ? sometimes hidden ? questionable (experimental "skill") + real flow (flow quality?) 	<ul style="list-style-type: none"> + real geometry + no limits for variation of parameters + known boundary conditions + real Re-number + short response + cost decreasing with time - errors not known - systematical errors (equation) + good reproducibility /objectivity - flow representation by model approximation - computer speed and memory limited

Fig. 2 Compilation of advantages (+) and disadvantages (-) of experimental and numerical Flow Field Simulation

From time to time it is tried to determine the point of progress in the field of computational fluid dynamics by critically analyzing computed results through comparison with experimental results. Due to the development of more and more powerful computers one truly can get the impression of huge steps in progress in the field of computational theory, whereas experimental test facilities experience a slow but more steadily extension. However, in the near future experimental research will do also a substantial step forward by applying cryogenic technology.

Though progress during the past 20 years in numerical flow simulation around aircraft can clearly be recognized, comparisons of theory with experiment always favored experimental results /2/, /3/, /4/. Tests done with identical models in different wind tunnels at seemingly "identical" test conditions however show some irregularities of measured data. As an example the projects of GARTEUR Action Group 01 and 02 are referenced /5/, /6/. In one case seven physical models from one section definition were built and measured in seven wind tunnels at transonic speed, (pressure distribution). In the second case an identical 3D wing model was investigated in four different facilities. A third example, a test on a 2D-airfoil in three wind tunnels at overlapping Reynoldnumbers (between 0.3 to 40 millions) will be referenced later in much more detail /7/, /8/.

11.2 General Trends in Time/Speed and Cost in Experiment and Computation

As previously mentioned data of A/C development demonstrate a clear trend. Fig. 3 shows the growing number of necessary wind tunnel hours for aircraft development during the past. Considering the relationship between hours and cost you can extrapolate, that the next generation of aircraft will require 10 years permanent measuring time at costs of 100 million \$.

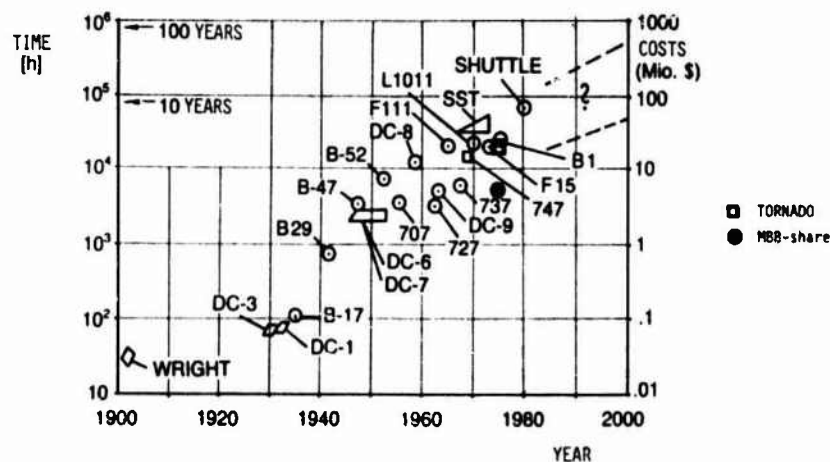


Fig. 3 The use of Wind Tunnels for A/C Development /2/

On the other hand we must accept that cost for computing time (CPU) are reduced by one order of magnitude in one decade (Fig. 4). This can be explained by the development of larger and faster processors with smaller size (Large Scale Integration), by new computer architecture (sequential-, parallel-, vector-processing), but also by the development of new "fast solving" algorithms (e.g. Multigrid).

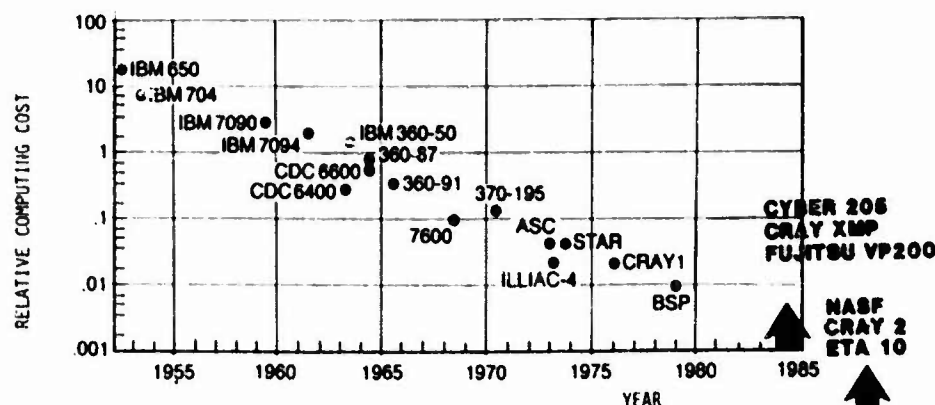


Fig. 4 Computing Costs due to Progress in Development of Computers and Numerical Methods /3/

11.3 State of the Art in Numerical Aerodynamics

11.3.1 Model for numerical simulation

The simulation of "Real Flow" has to take into account viscous effects. This can be done by definition of a (inner) region where viscous effects play a dominating role, the "Boundary Layer", and the (outer) flow region where viscous effects may be neglected (= Potential Flow). If there is a strong coupling between both regions, as in the case of viscous flow separation, this Potential Flow/Boundary Layer-Model fails and the full Navier-Stokes equations have to be applied (Fig. 7).

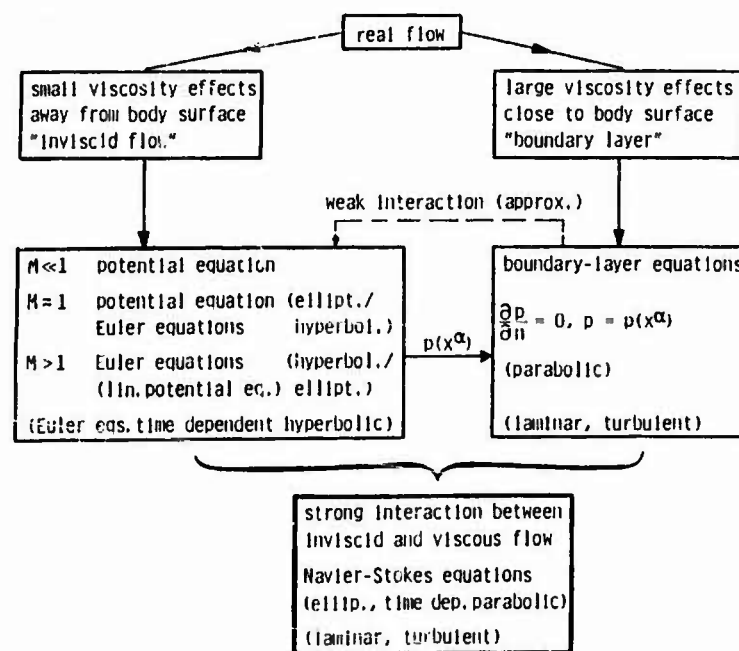


Fig. 7 Model for numerical simulation of viscous "Real" flow /9/.

In fact the development of computer codes has followed this outline starting in the early 60ties and has reached the highest level for inviscid flows, the solution of the Euler-equations, in 1980, see Fig. 8

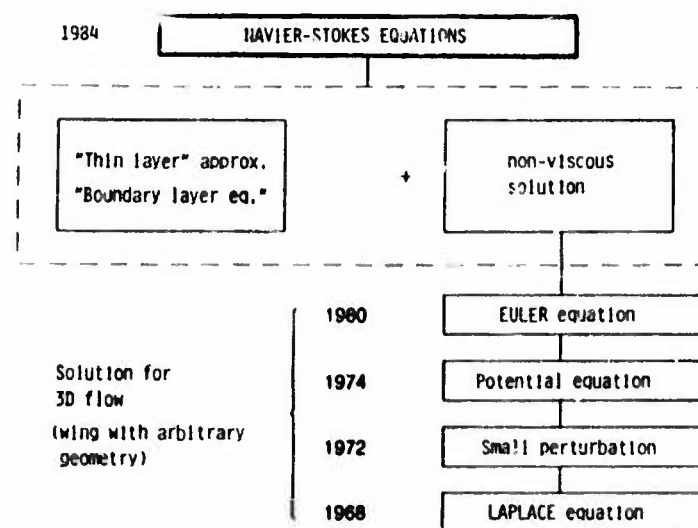


Fig. 8 Availability of 3D Computer Codes for engineering practical applications.

11.3.2 Applications, typical results

For each class of flow representation a typical application will be shown and numerical results in comparison with test data will be presented.

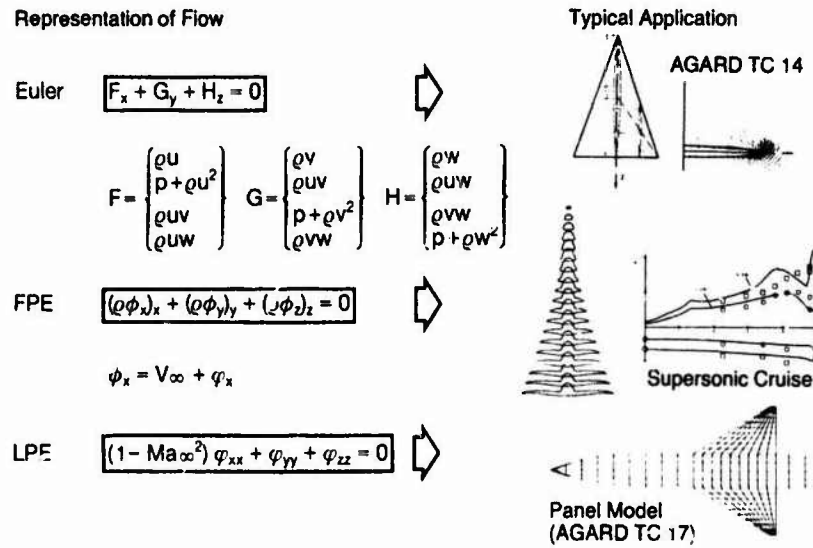


Fig. 9 Governing equations for numerical steady, inviscid, isoenergetic flow simulation

Fig. 9 shows schematically the main classes for inviscid flow representation starting from the Laplace-equation (LPE) to the Full Potential Flow (FPE) and the highest level of Euler-equations. From the view of engineering, practical application is still limited, and the highest level of geometric complexity is shown. So Panel methods solving LPE are applied for complex wing body combinations without restrictions, but they are only valid for attached flow and pure subsonic or supersonic speed. The FPE may be used for transonic flow, but there are still restrictions in geometric complexity. Simple wing-body configurations may be handled today. The application of 3D Euler-codes in industry is restricted at present time mainly due to storage-requirements to isolated wings but they work satisfactorily for all speeds, applications for more complex geometries have been already published by research institutes. Fig. 10 represents results obtained for a supersonic cruise airplane. Predicted pressure distributions and overall coefficients for lift, drag and pitching moment are in good agreement with experiment.

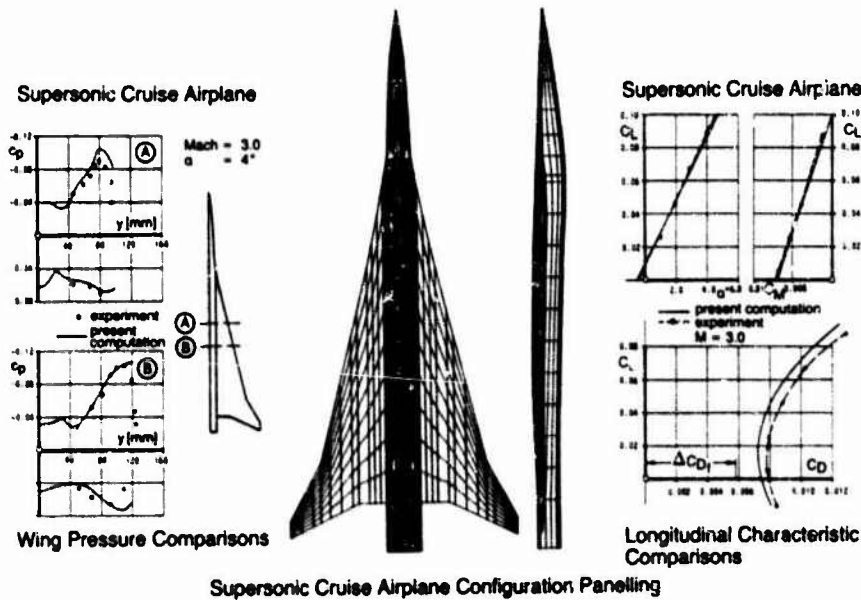


Fig. 10 Potential flow solution using Panel Methods for supersonic flow /10/.

A more sophisticated presentation of numerical results is given by Fig. 11 where isobar patterns are shown on a recent combat A/C.

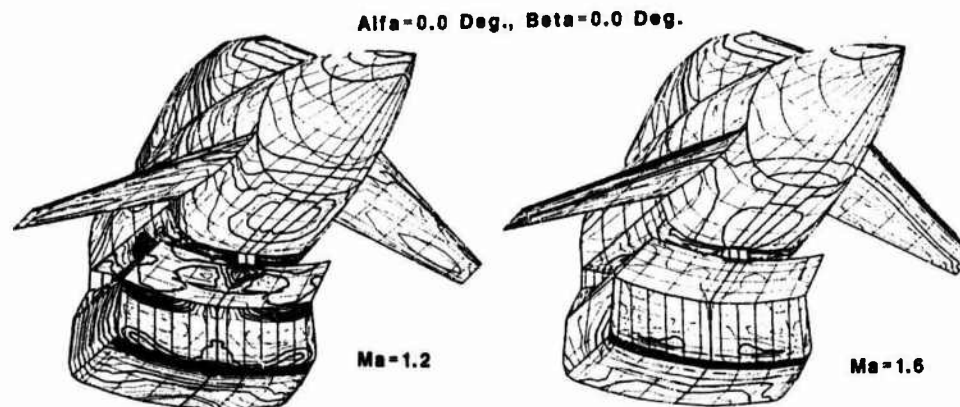


Fig. 11 Forebody-Canard-Intake representation of recent combat A/C, results obtained by Panel Method "HISSS"/10/

The second set of examples will refer to 3D Euler-solutions. In contrast to Potential flow this class of results covers (inviscid) flow separation at the leading edge (LE) of highly swept wings of low aspect ratio (AR). Fig. 12 shows such typical data obtained recently /11/ by applying the so-called Marching Technique in space. One can see clearly the LE-Vortex at two stations in spanwise direction.

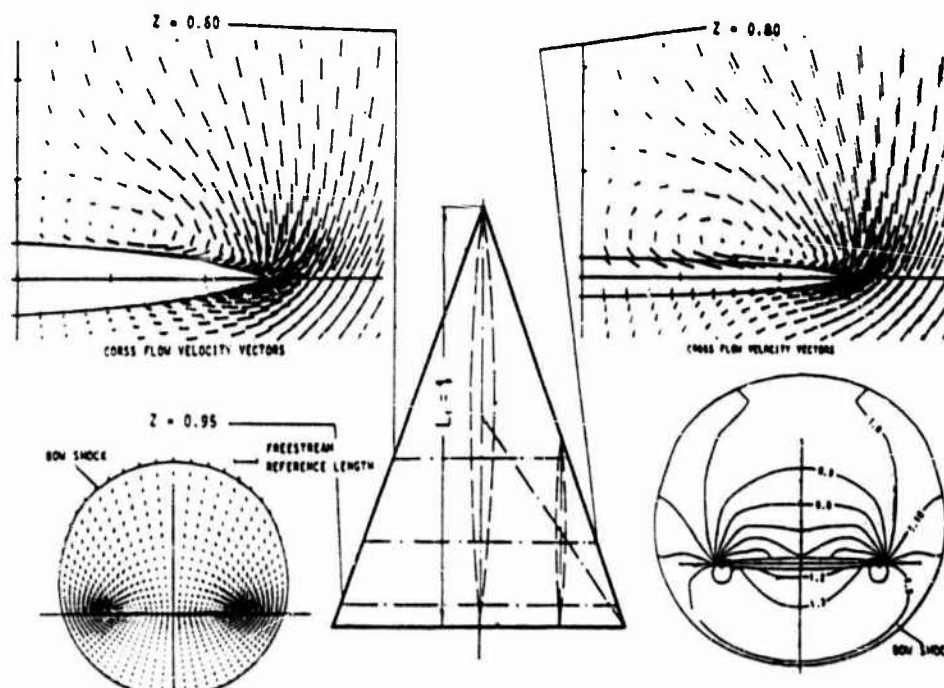


Fig. 12 3D Euler Space Marching Procedure applied to a Deltawing with sharp Leading Edge at $Ma = 2.0$ and $\alpha = 10^\circ$, /11/.

A more specific investigation of the flow field angularity at the forebody of a fighter A/C is performed to optimize the position and shape of the intake at supersonic speed according to Fig. 13. For these results, viscous flow correction has been applied to get the correct distance of the boundary-layer-diverter from the A/C body and to produce streamline patterns.

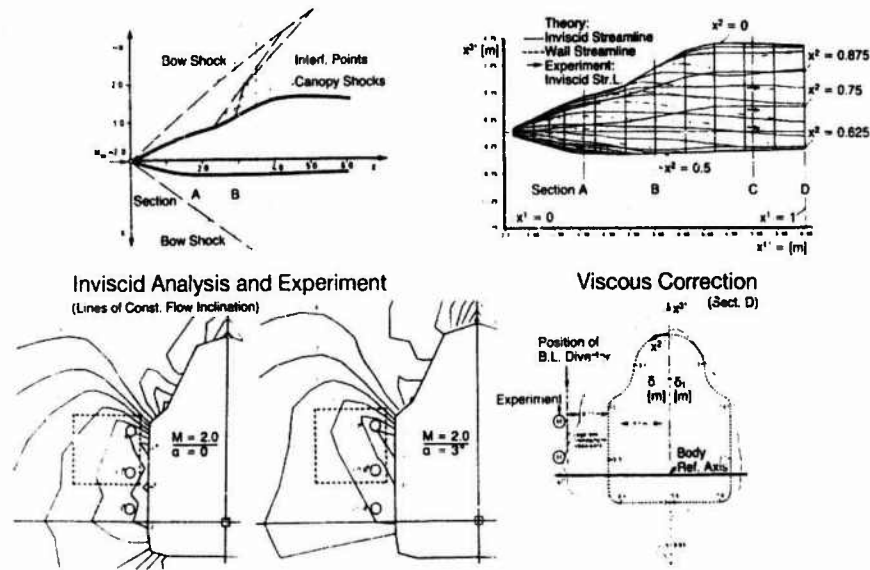


Fig. 13 Intake-Optimization during project development using Euler-Space-Marching Solution with viscous Boundary-Layer corrections /11/

The comparison of (Full) Potential Flow- and Euler-Solutions is a useful exercise which has to demonstrate agreement where attached flow exists and no strong shocks appear. Fig. 14 shows such a comparison.

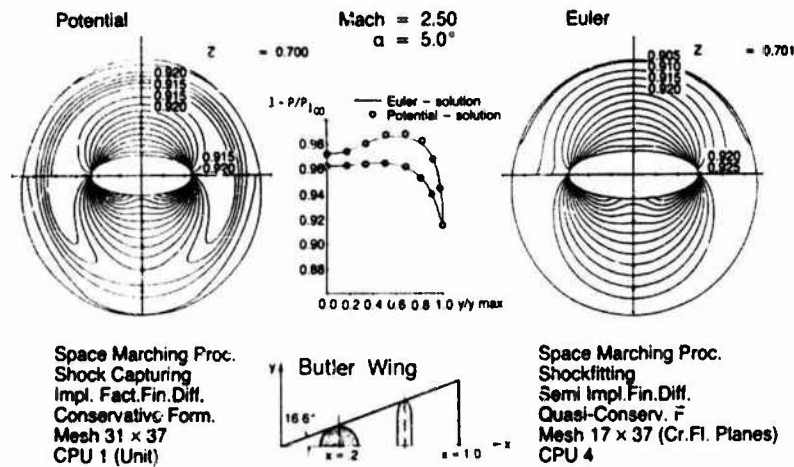


Fig. 14 Comparison of Full Potential-Flow and Euler Solution /11/

Another important area of flow field simulation is the A/C afterbody which contributes up to 50 % of total drag to the configuration. Fig. 15 shows schematically the complexity of the flow region at the boattail of a typical fighter A/C configuration.

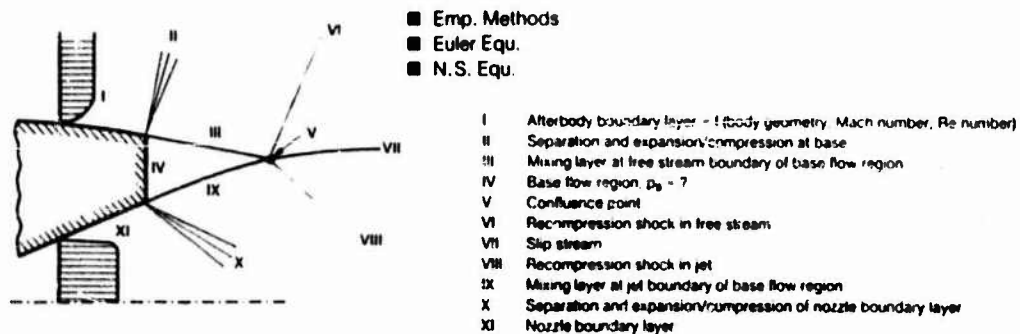


Fig. 15 Axisymmetric A/C Boattail including Jet-interference

In order to compile the present state of the art, AGARD FDP has formed Working Group 08 to specify Test Cases for Numerical Flow-Field-Analysis. Fig. 16 compiles typical results obtained for different classes of solutions.

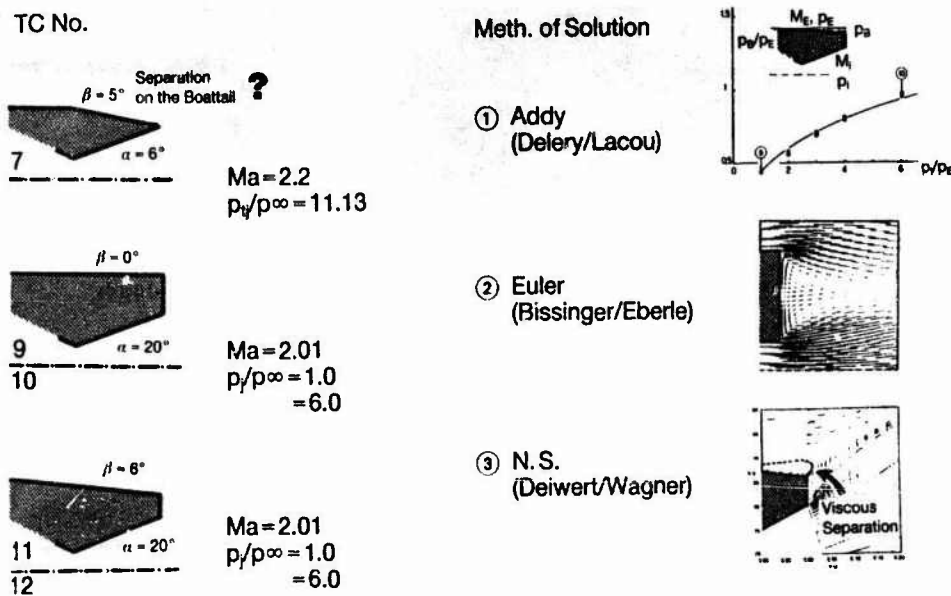


Fig. 16 AGARD FDP WG 08, Test Cases for Numerical Flow Calculation /12/

At least for the last set of test cases one can see that the flow is dominated by large regions of separated flow and the flow around the afterbody is characterized by thick Boundary Layer which interacts strongly with the separated flow regions. This leads us to examples for CFD solving the (viscous) Navier-Stokes-Equations. Even for this highly complicated numerical algorithms, progress has been tremendous during the past years. Due to economic reasons a first approach was the formulation of a zonal solution according to Fig. 17.

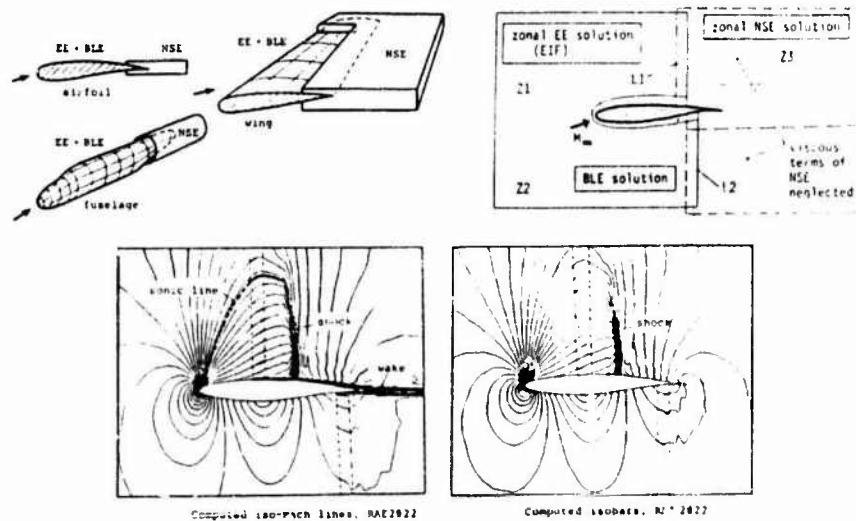


Fig. 17 Zonal solutions for viscous flow problems /13/

But even the full Navier Stokes Solution has been achieved recently as e.g. Fig. 18 shows. But the enormous amount of numerical data requires color-graphics to analyze the complex flow characteristics.

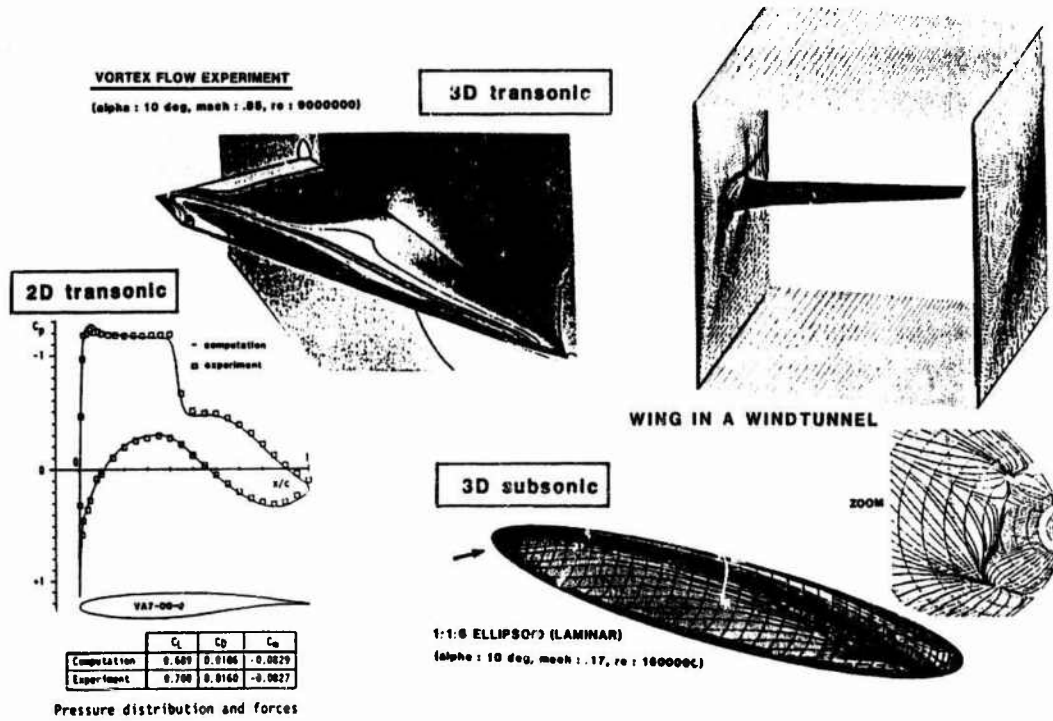


Fig. 18 Compilation of results obtained by the solutions of the Navier-Stokes-Equations, NSFLEX by M. A. Schmatz /14/.

- solves compressible Euler or Reynolds-averaged Navier-Stokes equations, respectively
- basis for zonal Euler-, boundary layer-, Navier-Stokes method
 - finite-volume method (2-D, 3-D)
 - third-order accuracy of upwind flux extrapolation (Godunov type)
 - implicit time relaxation of unfactored equations (point Gauss-Seidel)
 - shock capturing
 - Euler switch
 - laminar, turbulent (Baldwin-Lomax eddy viscosity model)
 - fully vectorized
 - $0.01 \leq M_\infty \leq 10$

Results: wall-shear stress, wall-heat flux, wall temperature, skin-friction lines, separation, aerodynamic loads, shocks, vortices

11.3.3 Code validation

As the previous chapter has shown, a huge amount of numerical data has been produced during computer code development and application. The question arises, whether it is justified to spend so much money in computertime. So in 1978 a first attempt was to specify 2D Test Cases and to invite experts of all countries to contribute their own results /15/. Fig. 19 demonstrates the variety of results obtained using different codes solving different equations.

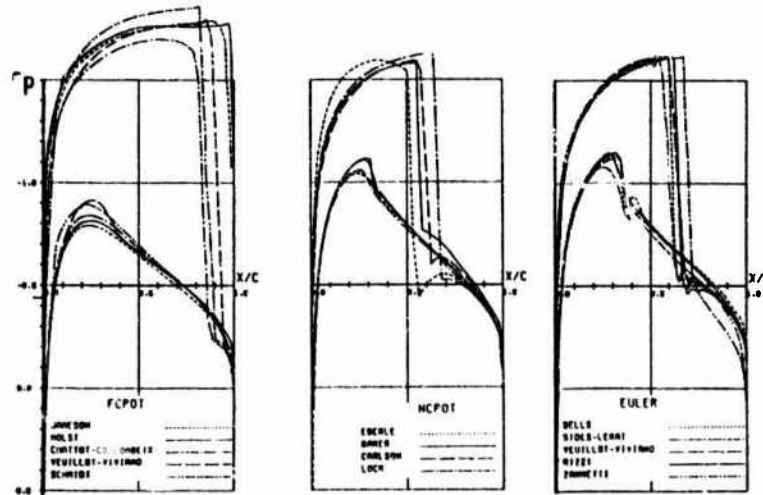


Fig. 19 Comparison of results of numerical methods (GAMM-Workshop) NACA 0012/
M = 0.8/ $\alpha = 1.25^\circ$

Integration of the pressure distributions to aerodynamic coefficients for lift and drag according to Fig. 20 leads to the conclusion, that an improved exercise has to be repeated. The computer codes have to be restricted to the same class of equation and furthermore detailed flow quantities like total pressure, local velocities and entropy have to be analyzed throughout the complete flowfield.

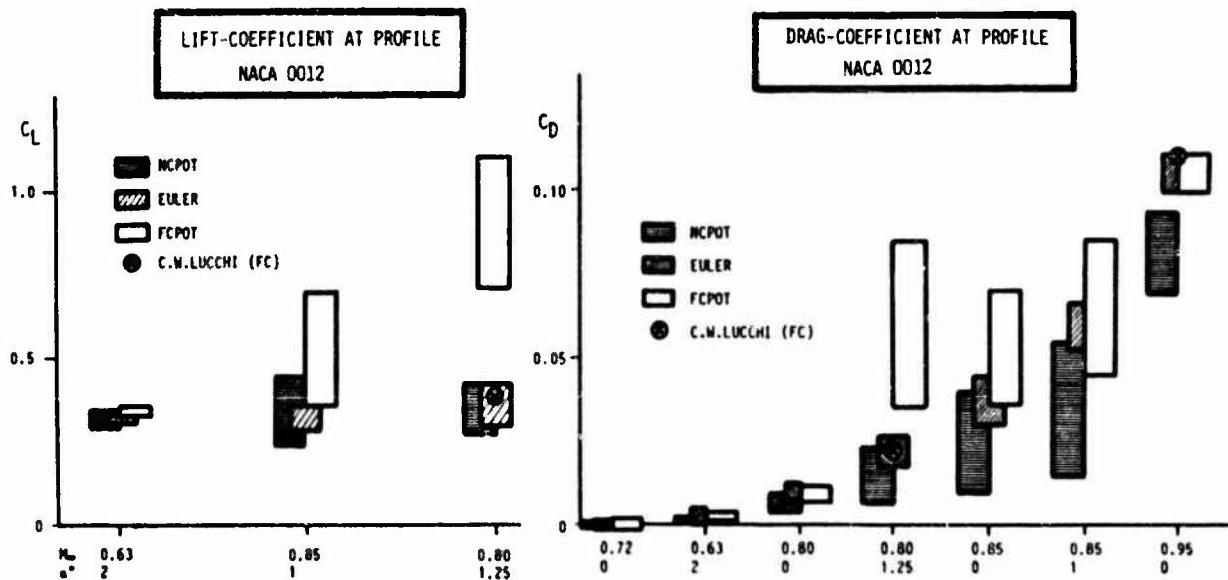


Fig. 20 Comparison of results of numerical methods (GAMM-Workshop) NACA 0012
NCPOT Non-Conservative Full Potential Flow
FCPOT Fully-Conservative Full Potential Flow

Fig. 21 presents the scope of work defined by AGARD WG 07 in 1982. Only Euler-Codes have been included in the report.

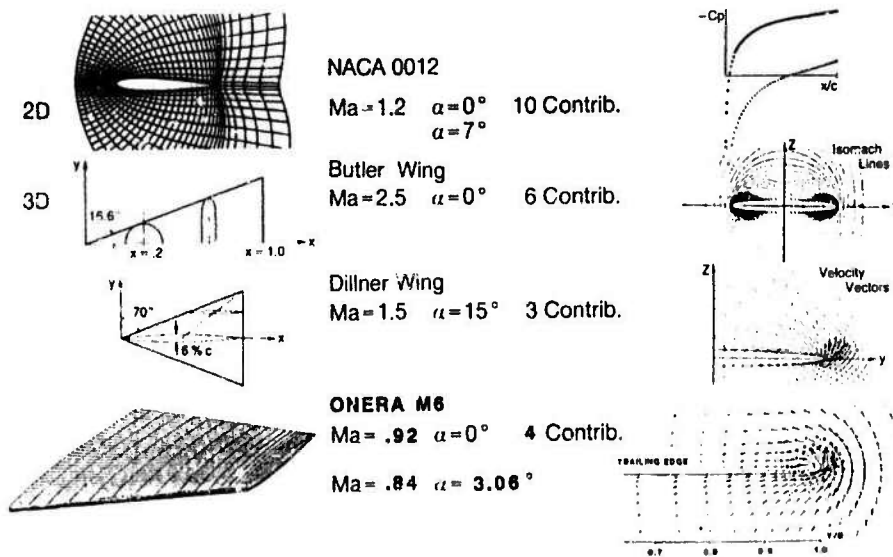


Fig. 21 AGARD WG 07: Test Cases for inviscid flow calculations /16/

As Fig. 22 shows, the results are still without acceptable agreement and differences still exist for the pressure distribution on the airfoil upper side.

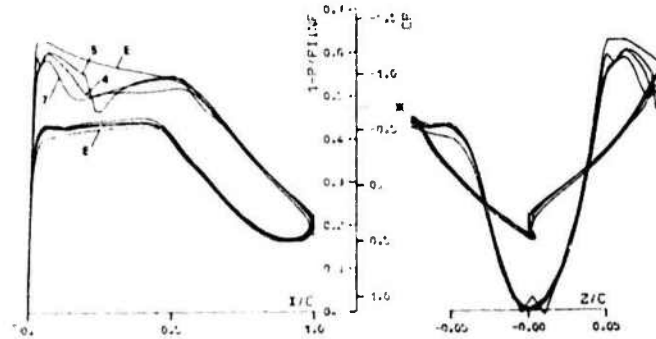


Fig. 22 AGARD WG 07, Test Case 07, NLR 7301, $Ma = 0.720957$, $\alpha = -0.194^\circ$ /16/. Pressure distribution versus x/c and z/c .

The results for integrated coefficients (lift, drag, pitching moment) show again significant scattering of data. But it seems at least for some of the contributed results that "convergence" at certain level could be achieved (Fig. 23).

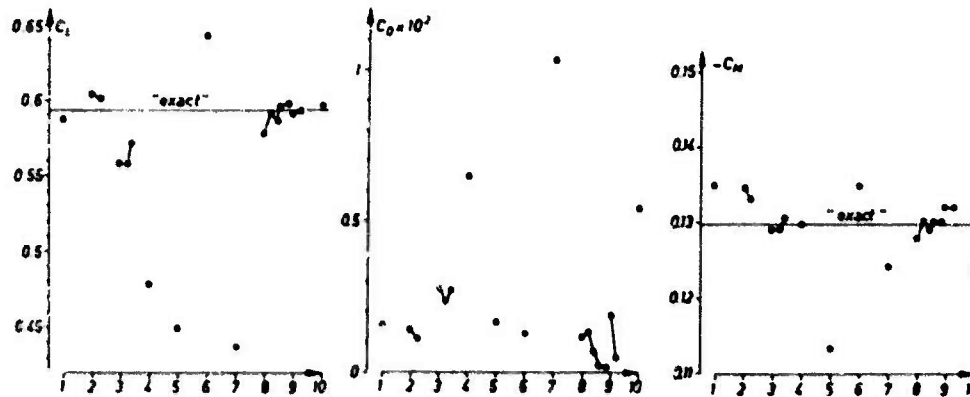


Fig. 23 AGARD WG 07, Test Case 07, NLR 7301, $Ma = 0.720957$, $\alpha = -0.194^\circ$ /16/. Integrated coefficients for lift, drag and pitching moment.

For 2D-Flow calculations a simple moderate swept wing was specified as a test case (ONERA M6). 4 different computer codes could be identified to provide solutions like Fig. 24 shows.

AGARD ADVISORY REPORT No.211

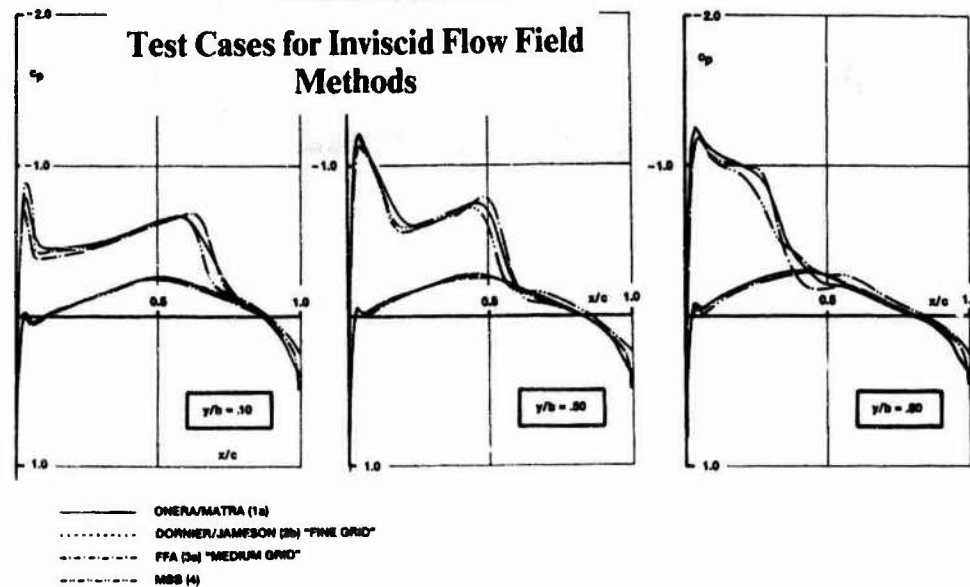


Fig. 24 AGARD WG 07, Test Case 11, ONERA M6, $Ma = 0.84$, $\alpha = 3.06^\circ$
Pressure Distribution (C_p) at spanwise sections

Surprisingly the agreement is much better than for 2D test cases, (with exception of the region where the shock occurs). Also in the tip region differences exist due to different representation of the tip geometry in the computer codes and consequently also due to flow separation around the tip (Fig. 25).

As a result of the different treatment of the tip region local aerodynamic load coefficients for lift, drag and pitching moment obtained by different codes disagree significantly

INFLUENCE OF MESH-GRID REFINEMENT ON SPANWISE LOAD-DISTRIBUTION

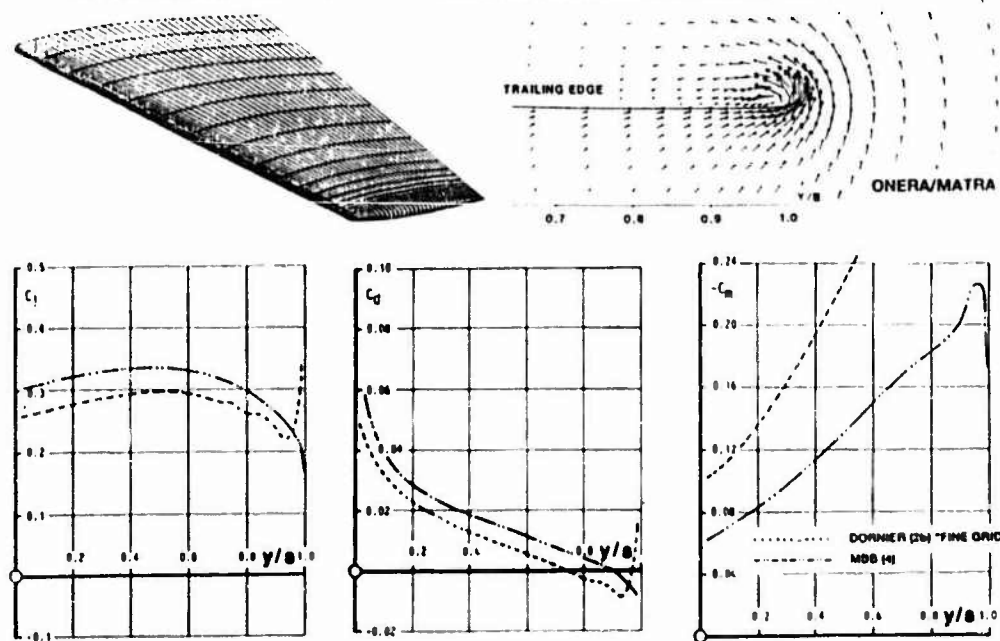


Fig. 25 AGARD WG 07, test case 11, ONERA, $Ma = 0.84$, $\alpha = 3.06^\circ$
Geometry for tip discretization on flow around side edge
Local load coefficients for lift, drag and pitching moment in spanwise direction.

To demonstrate the capabilities of Euler-Solutions and to predict also Leading-Edge-Flow-Separation, an additional configuration was defined: the so-called "Vortex Flow Experiment" according to Fig. 26. For this geometry 2 wind tunnel models have been built and tested throughout the whole speed range up to $Ma = 4$.

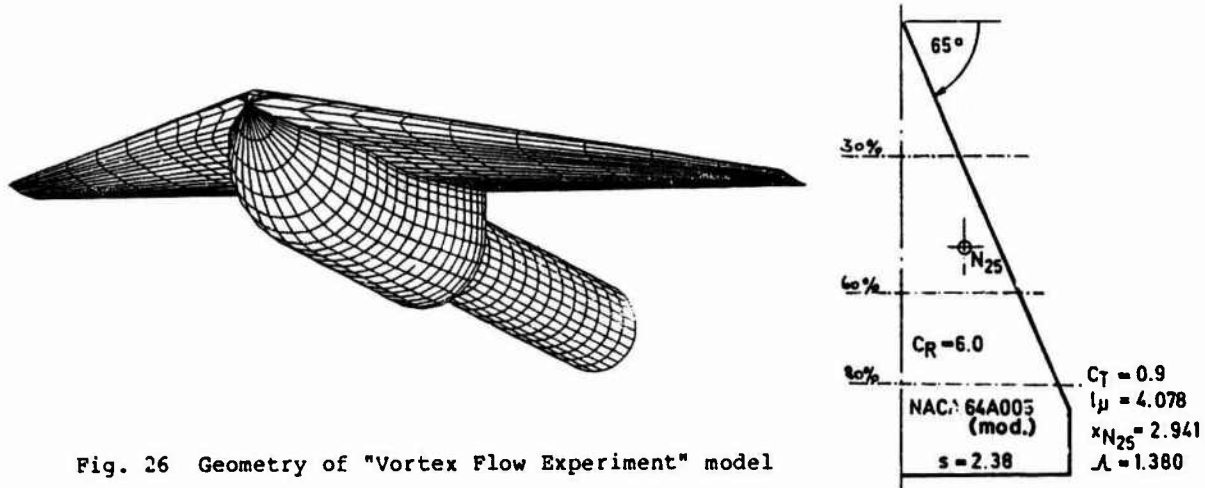


Fig. 26 Geometry of "Vortex Flow Experiment" model

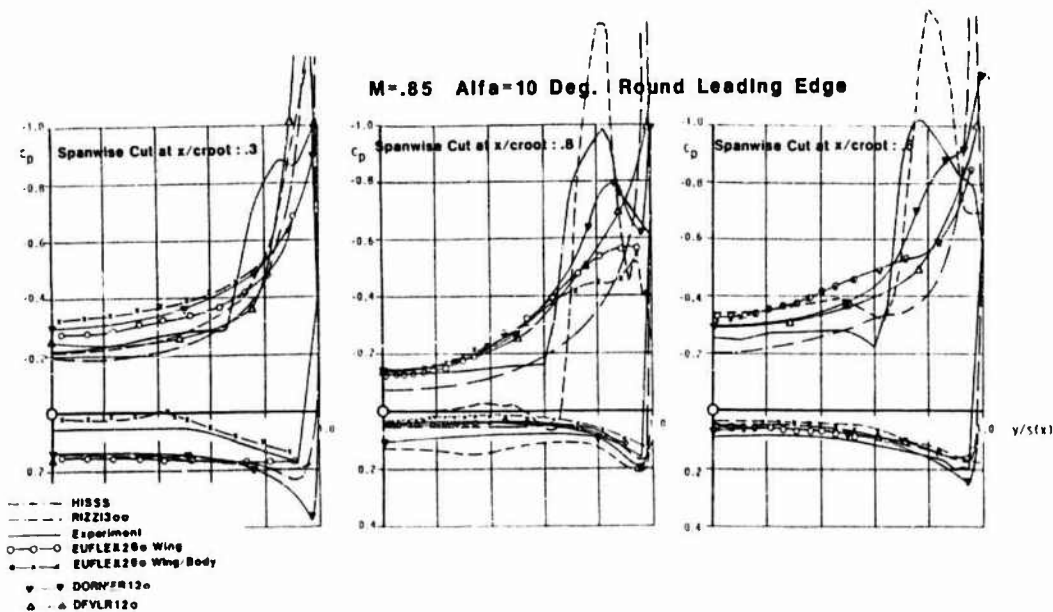


Fig. 27 Vortex Flow Experiment, compilation of numerical results

As could have been expected from previous results, the comparison of numerical data according to Fig. 27 shows again severe deviations from experiment as well as from each other.

Going to the highest level of numerical flow field simulation also Navier-Stokes solutions obtained recently do not agree satisfactorily with experimental data, see Fig. 28

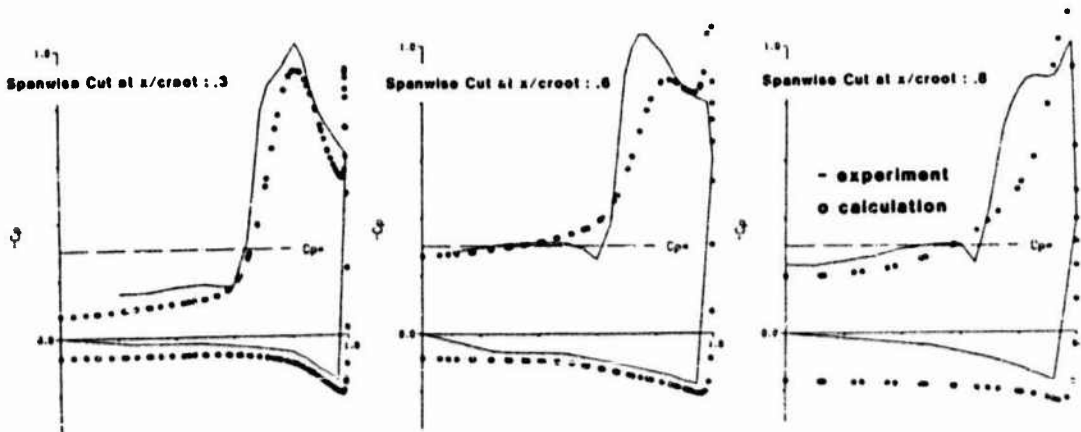


Fig. 28 Navier-Stokes-Solution for Vortex-Flow-Experiment-Wing, comparison with experimental data at $Ma = 0.85$, $\alpha = 10^\circ$, $Re = 9.10^6$ using 277400 mesh grid points /14/, /18/.

In conclusion to the compilation of data for code validation the question has to be answered to which extent the various disagreements have to be assigned to possible sources of errors in numerical flow field simulation. According to Fig. 29 at least 4 levels of explanations may occur in a computation. The most important class is the error of discretization. Usually different analytic modeling and different mesh grid size and type have been used in different computer codes. So further detailed studies have to be undertaken until the best numerical finite solution of a certain class of equations has been identified. But it will be demonstrated in the next chapter, also experimental results suffer from unexplained disagreements which have to be investigated.

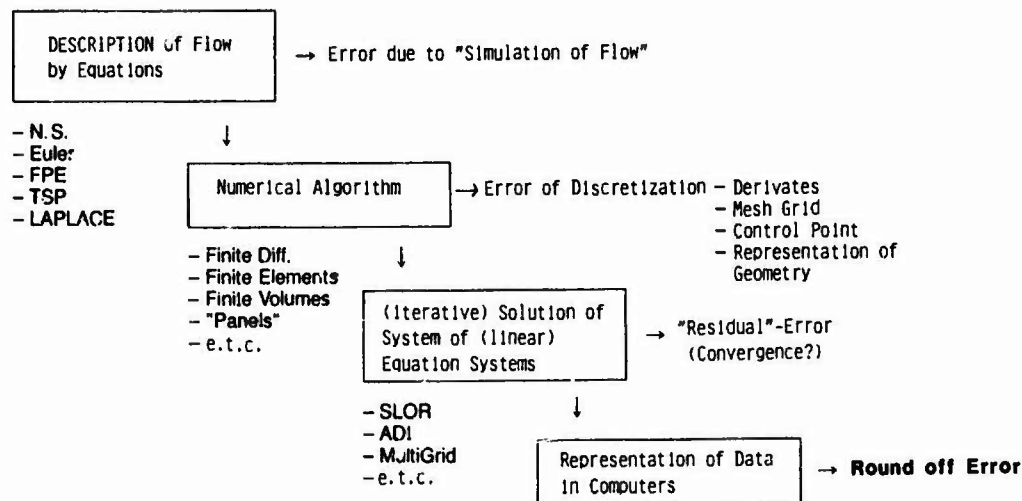


Fig. 29 Classification of sources of errors in numerical methods.

11.4 Results from Wind Tunnel/Critical Review

11.4.1 Effects of Reynoldsnumber

With few exceptions Wind Tunnel Testing has to be done using models having reduced geometric size. Because of viscous effects the influence of Reynoldsnumber must be considered. The most important effects can be studied at high angle of attack looking at C_L (max) and at high (transonic) speed where shocks occur. Fig. 30 shows a typical result for the pressure distribution variation of the parameters Angle of Attack and Machnumber for the pressure distribution measured on the upper side of a 2D Airfoil-Section.

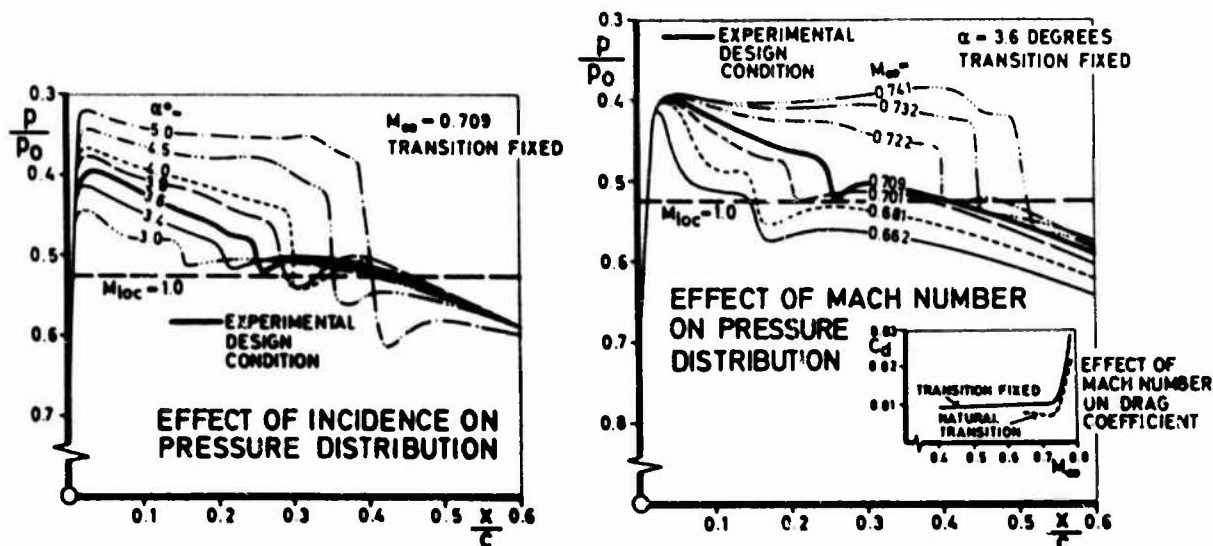


Fig. 30 Effect of Angle of Attack and Machnumber on Transonic Shock Location.

It can be seen quite clearly that a design condition exists where the shock disappears and transonic drag rise could be avoided. But obviously if there exists a strong sensitivity to Reynoldsnumber this "Design Point" is not easy to achieve because of the different test conditions in Wind Tunnel and Free Flight. This "Sensitivity Studies" have been undertaken in the past many times and Fig. 31 also shows again representative data. Two observations have to be reported:

- there is a significant disagreement of experimental data obtained in different Wind Tunnels using the same model
- Extrapolation of experimental data to full (free flight) Reynoldsnumber is problematic.

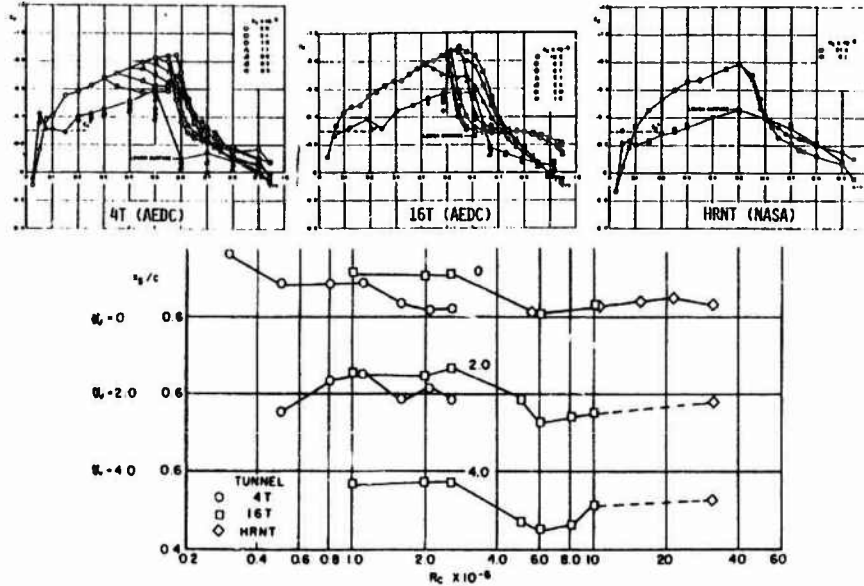


Fig. 31 Effect of Reynoldsnumber on transonic shock position
Experiments with at Profile C-141 in 3 Wind Tunnels /7/
 $0.3 \leq Re \leq 31.3 \cdot 10^6$ (nat. transition)
 $Ma = 0.8, \alpha = 2^\circ$

From these measurements can also be stated that there exists no general trend in shock location versus Reynoldsnumber. There are regions where the shock moves forward and others where the trend is opposite with rising Re-number. Fig. 32 shows data where the shock is moving forward and it will be shown later that computational results will predict generally the opposite trend.

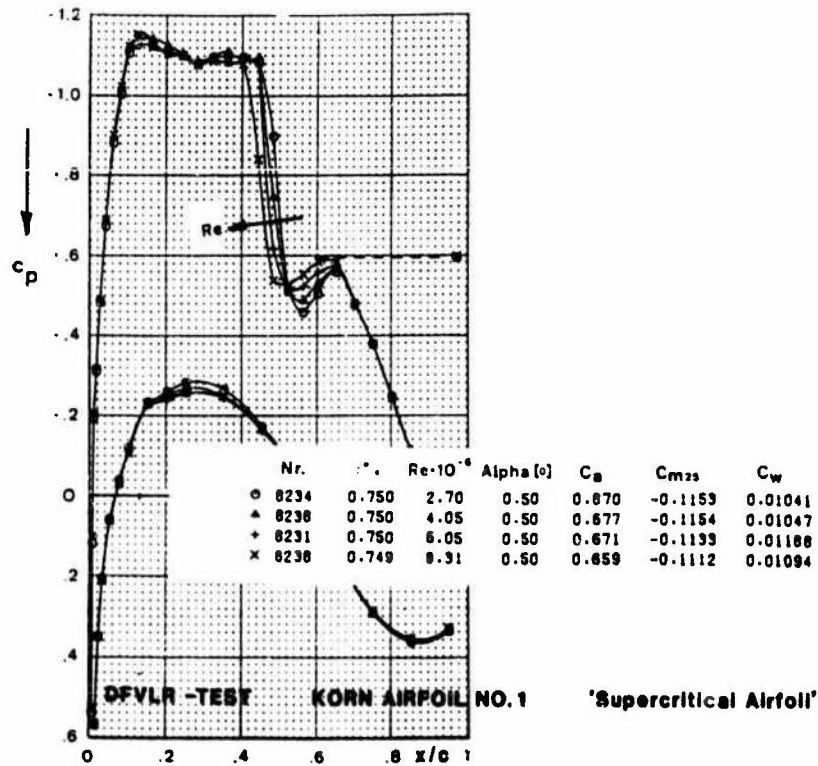


Fig. 32 Effect of Reynoldsnumber on transonic shock position /17/

11.4.2 Effect of Wind Tunnel

But first of all the reproducibility has to be achieved for Wind Tunnel testing using different facilities having in addition their own "home-made" procedures for transition and Wind-Tunnel-Wall-Corrections. In 1983 GARTEUR AG 02 /5/ reported results obtained in 7 European Wind-Tunnels on 7 models of different size at the same Reynolds-number near the design condition. Fig. 33 represents just one (representative) result for pressure distribution and lift coefficient. As can be seen the shock location varies within 10 % and consequently the situation for drag is even worse.

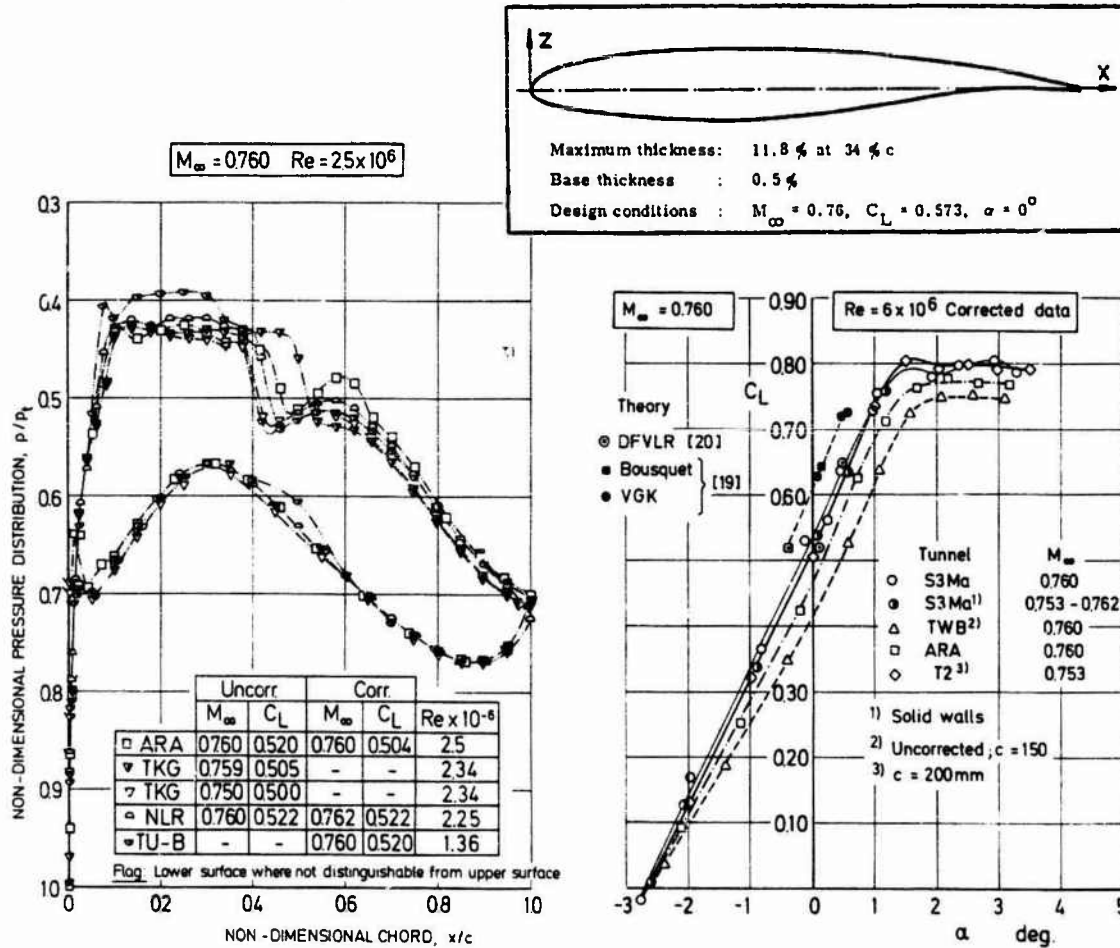


Fig. 33 "Effect of Wind Tunnel" on measured data /5/
 $M_a = 0.76$, $C_L = 0.51$, CAST 7 Profile Section

The same situation can be found for 3D-Model Wind Tunnel testing according to Fig. 34 and 35. This exercise has been published in 1983 also by GARTEUR AG 01. A 3D Wing-Body model has been built and measured in 3 European Wind Tunnels. But inspite of significant differences in pressure distributions at spanwise sections the overall coefficients agree remarkably well at design conditions.

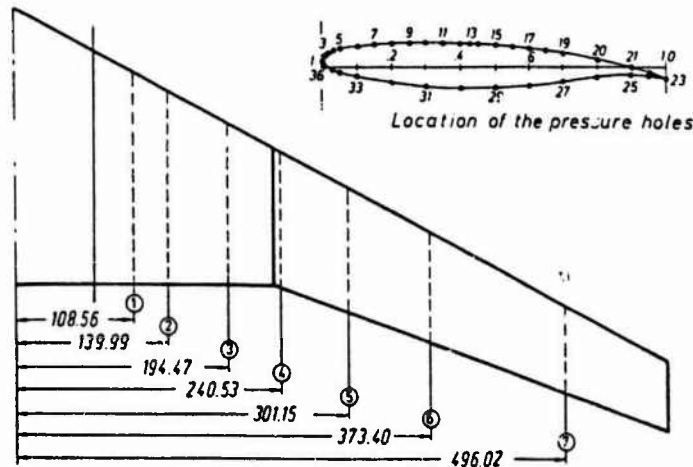


Fig. 34 GARTEUR AG 01, DFVLR-F4 Wing Body Configuration /6/

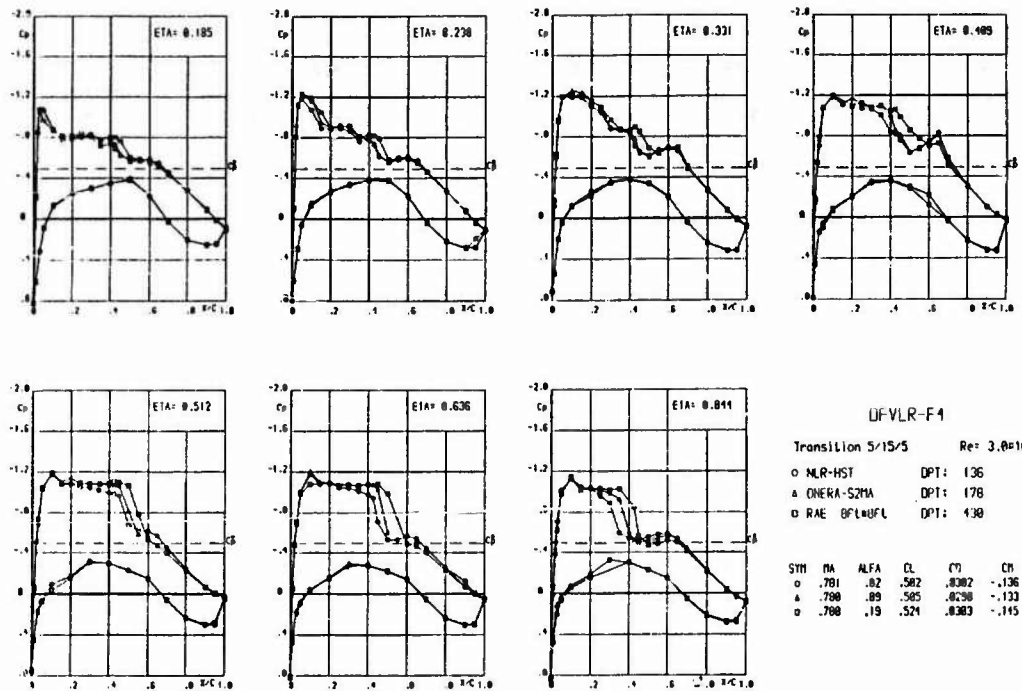


Fig. 35 Pressure distribution on DFVLR-F4 Wing Body Configuration obtained in 3 Wind Tunnels using the same model /6/.

The results shown above are representative for a typical "Attached Flow" design condition for civil A/C projects. If we consider fighter A/C configurations with low Aspect Ratio wings, having in addition Leading-Edge-Vortex-Separation, the results from different Wind Tunnels compare like Fig. 36. This model has also been used for the comparison of theoretical results in Fig. 27. It is not clear whether the discrepancies of experimental data can be attributed to different Reynoldsnumber or to different Wind-Tunnel-Wall-Effects.

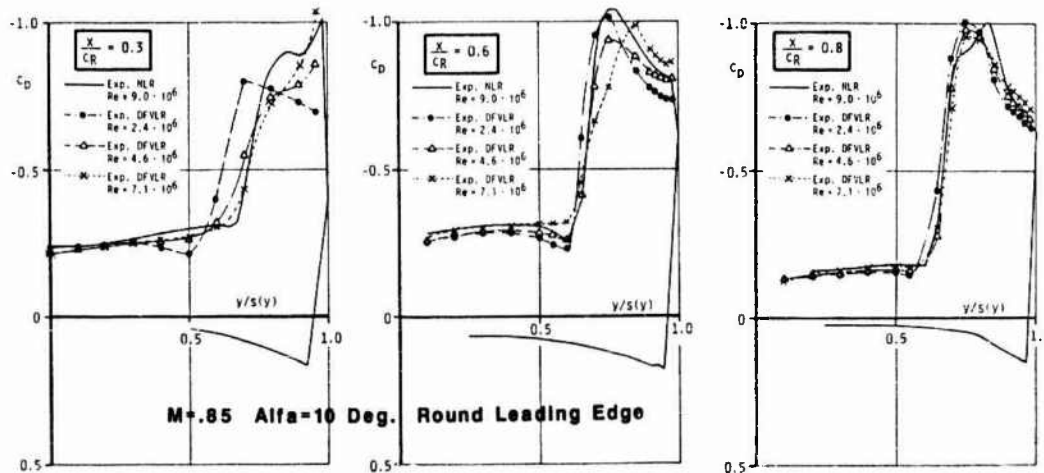


Fig. 36 Comparison of experimental pressure distributions at 3 spanwise sections obtained at NLR and DFVLR for the "Vortex Flow Experiment" /18/

11.4.3 The Role of CFD during Wind Tunnel Testing

If the situation is like shown before, the question arises: "Could CFD explain discrepancies observed as effects due to Reynoldsnumber or to Wind Tunnel characteristics?"

Considering theory one must concede that the aim of simulation of viscous flow is in sight, but current known performance of computer codes demonstrate reasonable gaps and inconvenience. First of all one has to meet arguments that the application of computerized procedures are, if available at all, by far too extensive for engineering use. That means in other words one has to prove that costs for calculation of the flow field does not extend to the order of expenses for experiments.

A first attempt to predict Reynoldsnumber effects on transonic shock location could be made by using Potential flow or EULER flow codes which have to be corrected by Boundary-Layer calculations. Fig. 37 shows results obtained by application of a viscous flow corrected full potential flow solver /19/.

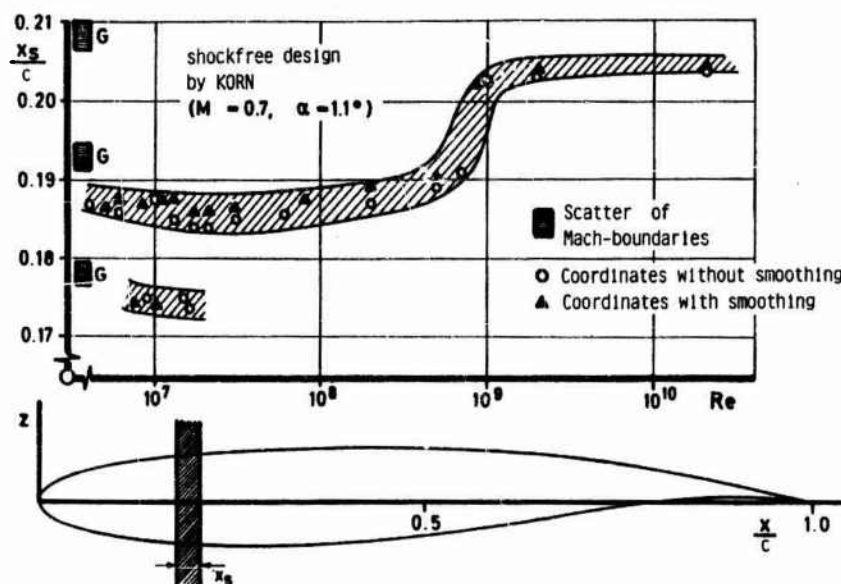


Fig. 37 Prediction of Reynoldsnumber-Effects by Full Potential Flow with Boundary-Layer-Correction /19/.

Obviously the results cannot reproduce the experimental shock drift of about 10 % section chord. Even worse, the predicted shift in shock position is correlated more or less to 1 % chord, which corresponds exactly to the mesh-grid-size used. So the "Shock-capturing" method works on the limit of geometrical discretization!

A more sophisticated attempt to predict transonic shock location has been undertaken more recently /14/, using a Navier-Stokes solver. Fig. 38 demonstrates good agreement with the experiment at least for one Reynoldsnumber on a RAE 2822 Profile and it shows the rearward trend of shock position with rising Reynoldsnumber. But the prediction explains only about 2 - 3 % chord as due to viscous effects.

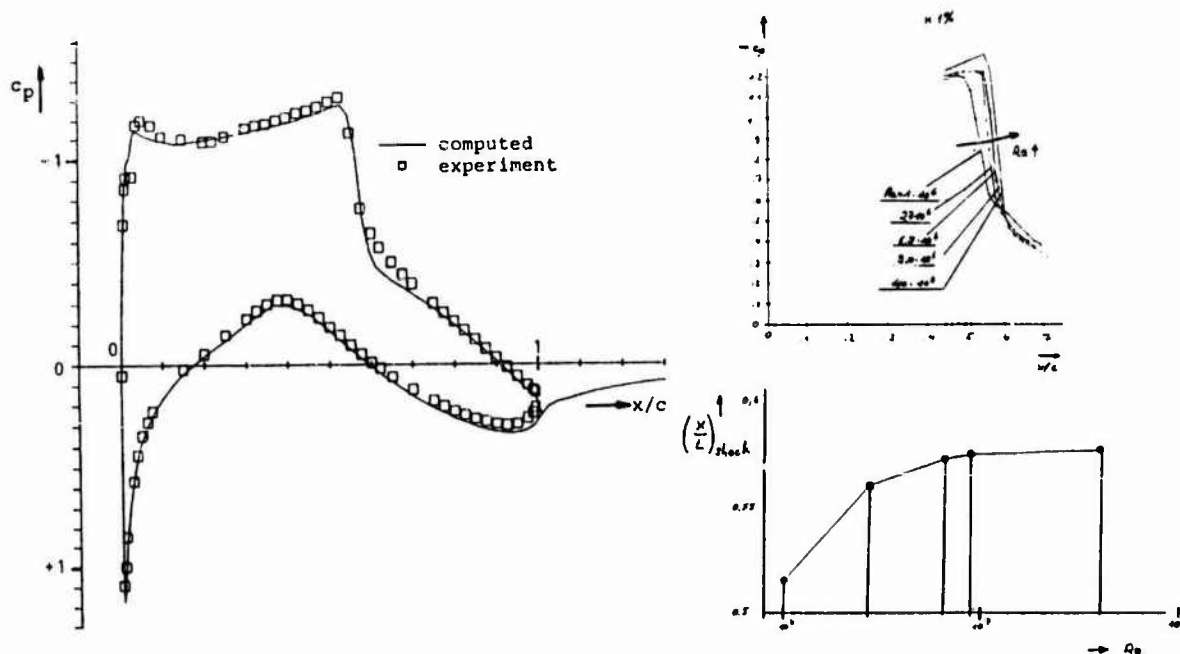


Fig. 38 Prediction of Reynoldsnumber-Effects by Navier-Stokes, solution NSFLEX at $Ma = 0.73$, $\alpha = 2.79^\circ$ for RAE 2822 /14/

If only 3 % of a shock drift of about 10 % could be attributed as effected by Reynoldsnumber, then the remaining difference must be explained by Wind Tunnel effects. First of all, the wall interference effect ("Blockage") has to be investigated. For nearly incompressible subsonic flow no wall effect exists according to Fig. 39.

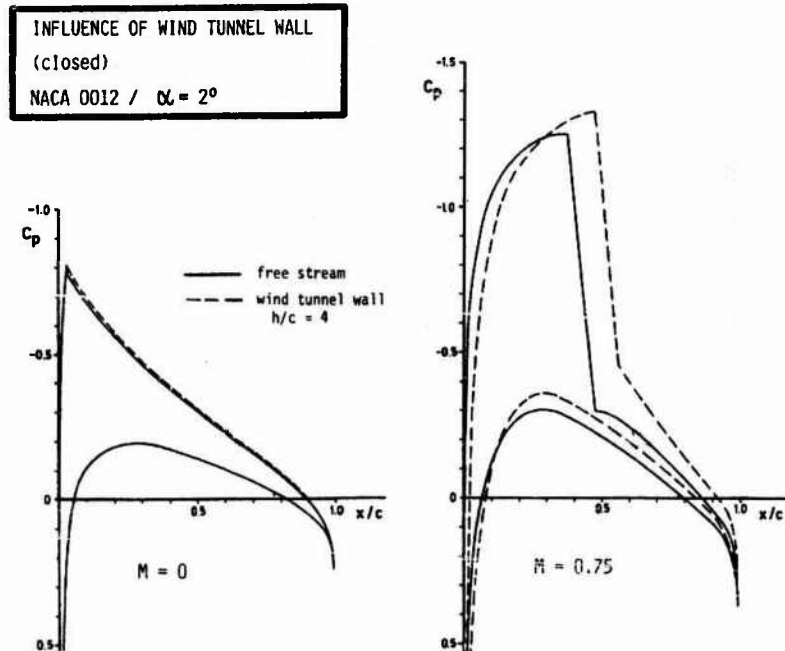


Fig. 39 Prediction of Wind Tunnel Wall effects using inviscid EULER flow code EUFLEX /20/

An inviscid EULER flow code has been used to predict blockage effects. The situation changes dramatically if we go to transonic Machnumber like Fig. 40 demonstrates. Only a distance of more than $H/C = 8$ could represent free stream conditions. For $H/C = 4$ we observe 25 % rearward shift of the transonic shock position.

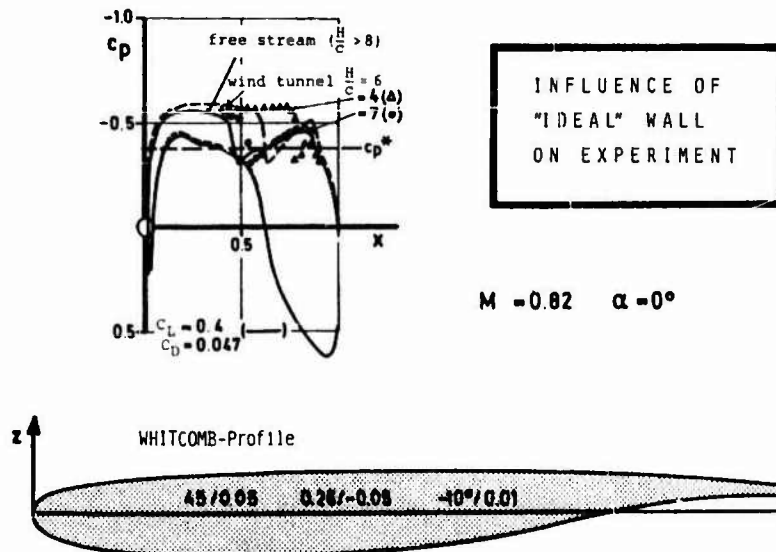


Fig. 40 Effect of Wind Tunnel Blockage on transonic shock position, prediction by EULER /20/.

But not only pure blockage interferes with the pressure distribution. If there exists any kind of pressure gradient at the Wind Tunnel wall in flow direction, an important effect on measured data could be observed according to Fig. 41.

In addition a constant pressure level applied at the wall could affect as well the shock location as Fig. 41 shows.

Extrapolation from Wind Tunnel to full scale flight requires answering the question:

"How much effect is related to Reynoldsnumber and to what degree Wind Tunnel wall inference plays a dominating role?"

The answer obviously depends also on the "Sensitivity" of shock position to small changes in Machnumber and AOA.

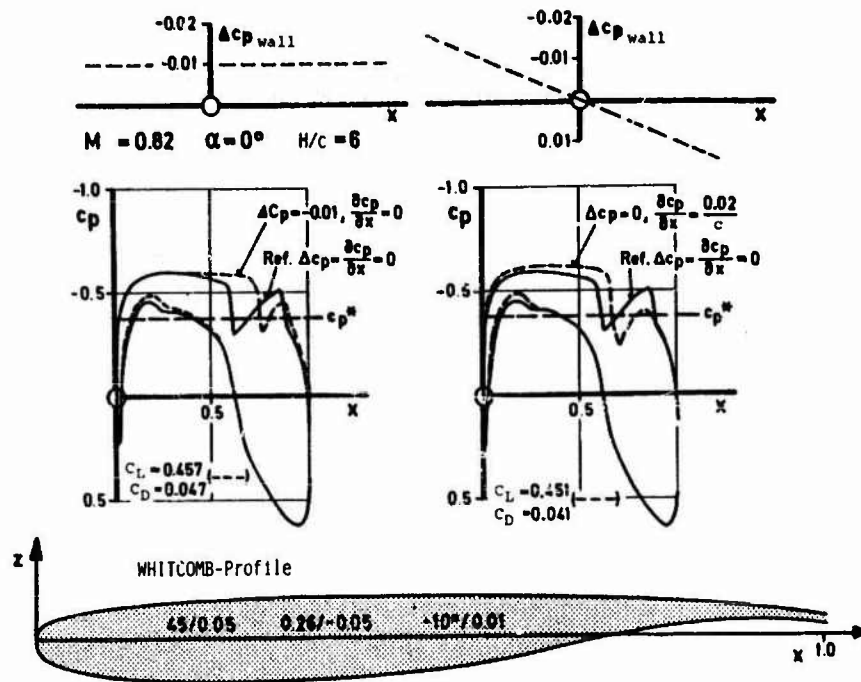


Fig. 41 Effect of pressure gradient at Wind Tunnel Wall on transonic shock location, prediction by EUPLEX /20/

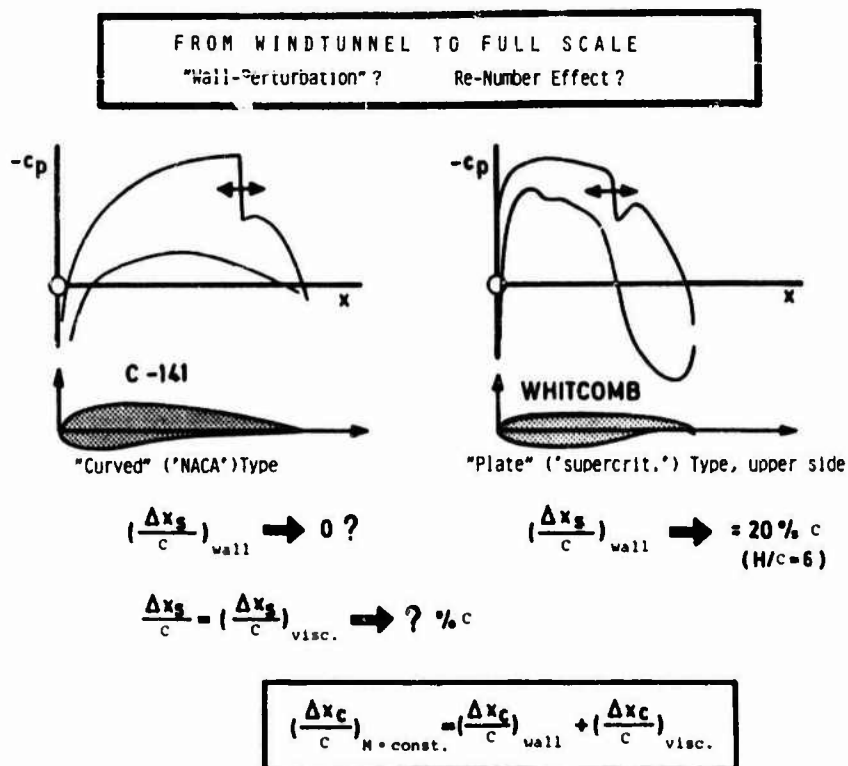


Fig. 42 Sensitivity of Shock Location for "Classes of Airfoils"

For more conventional "Classical NACA-Type" sections the shock always exists at transonic Machnumbers. For advanced "Supercritical" Airfoils the shock disappears at design condition - but this class of airfoils is by definition extremely sensitive to any changes of the flow conditions, therefore extrapolation to full size is risky and requires validated CFD codes of the highest level.

11.4.4 The Role of Wind Tunnels during Configuration Development

Although so many objections have been made in the previous sections the role of Wind Tunnel Experiments during research and configuration development remains still dominating.

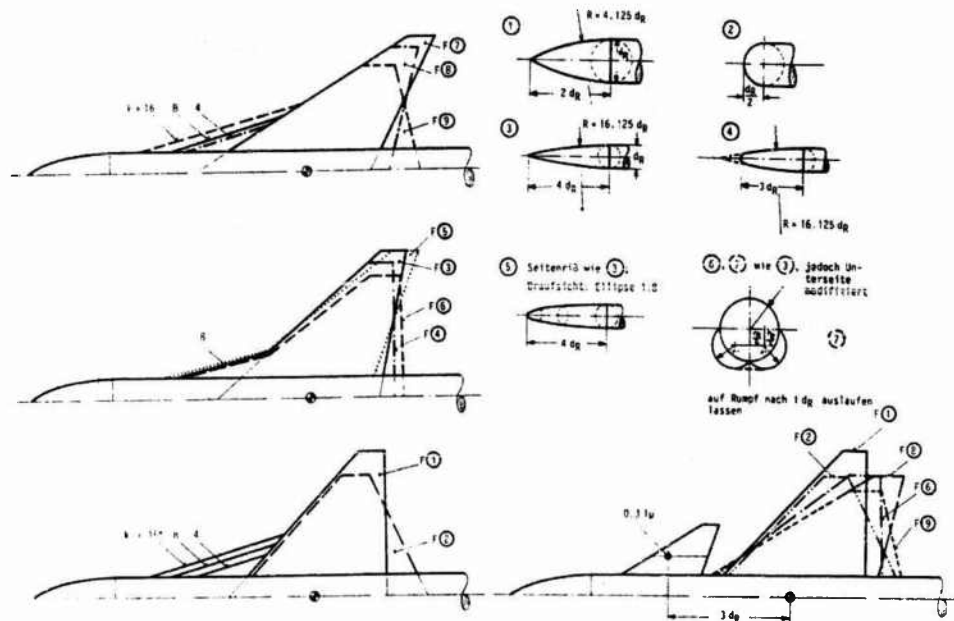


Fig. 43 Modular Wind-Tunnel-Model for Research

As Fig. 43 shows, a typical modular model for nonlinear flow conditions has been used to study leading-edge-flow-separation and vortex-vortex interaction. And a more realistic configuration for a new fighter A/C (see. Fig. 44) shows even more complexity. There is absolutely no flow code in sight which can give real flow simulation including all configurational details. The present paper does not cover engine integration and exhaust interference and the aerodynamics of controls, just to mention the most important missing ones.

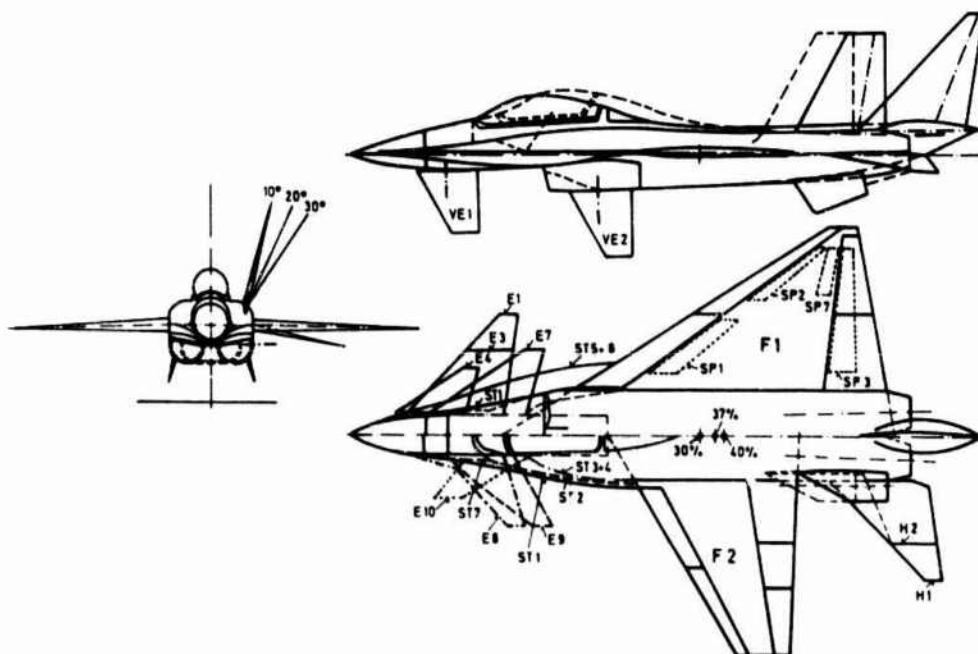


Fig. 44 Wind Tunnel modular model for Fighter A/C configuration development.

For fighter A/C the outcome of "Highlights" due to the application of "Strakes" (typical for the last generation of flying A/C) could be summarized as follows:

Summary of Advantages Due to Strakes

Subsonic/Transonic

- Increased maximum lift
 - Trimmed and untrimmed
- Lower level of induced drag at high AOA
- Higher useable lift limits
 - Buffet onset and penetration
 - Drag reduction
 - Rudder efficiency increased
- Improved dynamic behaviour

Supersonic

- Reduction in wave drag
 - Area ruling
 - Wing body blending
- Reduced trim drag
- Neutral point shift

This result could not have been achieved by numerical calculation but the number of variations of model components has been reduced drastically by the support of CFD to Wind-Tunnel work.

The next chart shows another example obtained during civil engineering. The design of supercritical airfoils has been achieved only by numerical computation - but the application for 3 D Transport-Type wings has to be validated by extremely careful performed Wind-Tunnel work.

Supercritical Design: High Lights

Comparison of the performances of two wings of identical planform ($AR = 4.5/\varphi$ 35° $\lambda = 0.33$) but with differences in wing sections (conventional NACA profile 64A (1.33)(6.5), supercritical profile MBB-A3 $t/L = 8.9\%$) gave high lights for the supercritical design due to:

- Better maneuver boundary buffet onset (10-20%, sub-, transonic)
- Higher maximum lift
- Drastically improved wing efficiency (gains in lift/drag ratio 20-80% for $M \leq M_{des}$ and $CL > 0.15$)
- Lag of drag creep
- Good off-design behaviour

The "Off-Design" performance of the newly developed airfoils has proved to be of even more importance - a feature which has been really hard to predict by CFD up till now.

11.5 Conclusion

The question, when the new coming branch of Numerical Aerodynamics will substitute, at least partly, the experiment is of course inadequate. The most important result at this time is the fact, that the computer should no longer be separated from experiment. Typical examples are the so-called adaptive sting for evaluating the trajectory of weapon release and the automatic control of flexible wind tunnel walls to minimize interference during tests.

But even for simpler tasks, like the measurement of pressures at transonic speed, a computerized procedure is necessary for highly sophisticated corrections covering not only blockage effects but also wind tunnel wall imperfections.

So far at present two main reasons exist for considering CFD as a valuable supplement to Wind-Tunnel-Tests:



REDUCTION OF DEVELOPMENT COST

- model manufacturing
(reduction of models and model components)
- wind tunnel time
(variation of parameters)
- flight test
(no. of flights, clearance for store installation)
- design cycle time
 - automatization
 - expert systems (AI)
 - data access and storage
 - transparency of information



INCREASE PRODUCT QUALITY

- conservation of compatibility
- increase of design broadness (no. of configurations)
- reduction of design risk
- access to new flight regimes ("emerging technology"?)
- quality assurance (Independency of personal skill)
 - transparency of design procedures
 - reproducibility of design process
 - standardization of procedures

NUMERICAL ANALYSIS - SUPPLEMENT TO WIND-TUNNEL TEST

Future investigations will require "TASK-SHARING" between theory and experiment to a large extent. Due to permanently growing cost for experimental work this means

(A) Computation as much as possible

- for explanation of disturbance effects
- to correct measured data
- to reduce the number of parameters for Wind Tunnel tests

(B) Measurement to minimum extent (as necessary)

- to reduce costs
- to evaluate "corner point values" for project development
- to back up new development in theory
- to improve physical understanding of complex fluid flow.

Engineering work in industry will be influenced more and more directly and indirectly by CFD in the near future. The result will be an increase of effectivity or in other words reduction of cost as Fig. 45 tries to simplify.

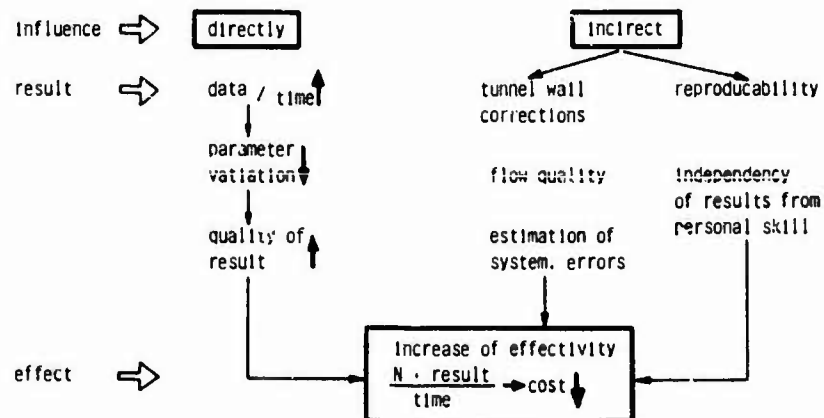


Fig. 45 Computer Assisted Development of A/C Configurations

Conclusion:

The computer is not going to replace the windtunnel; the role of computers is a complementary one to save time, cost and to improve the quality of the final product.

11.6 References

- /1/ NICOLAI L. M.
Fundamentals of Aircraft Design, Domicone Print Services, Ohio, (1975)
- /2/ CHAPMAN D. R./MARK H./BIRTLE M. W.
Computers vs. windtunnels for aerodynamic flow simulations A + A pp. 22-35 (1975)
- /3/ CHAPMAN D. R.
Computational aerodynamics development and outlook, AIAA J. Vol. 17/12
pp. 1293-1313 (1980)
- /4/ HEINZERLING W.
Bedeutung und Problematik von experimentellen und numerischen Simulationen komplexer Strömungsvorgänge mit großer Reynolds-Zahl für die Projektentwicklung von Flugzeugen, MBB/FE 120/S/PUB/33 - (DGLR 80-028) (1980)
- /5/ GARTEUR AD (AG-02)
Two-Dimensional Transonic Testing Methods, Final Report, NLR TR 83086L - GARTEUR/TP-11 (1981)
- /6/ REDEKER G./MÜLLER R.
A Comparison of experimental Results for the Transonic Flow around the DFVLR-F4 Wing Body Configuration, DFVLR-IB 129-83/21-GARTEUR/TP-018 (1985)
- /7/ LO C. F. CARLETON W. E.
Transonic scaling effect on a quasi, two-dimensional C-141 airfoil model, AEDC-TR-73-61 (1973)
- /8/ BLACKERBY W. T./CAHILL J. F.
High Reynolds number tests of a C-141A aircraft semispan model to investigate shock-induced separation, NASA CR-2604 (1978)
- /9/ HIRSCHHEL E. H.
Numerical Aerodynamics at MBB, MBB-LKE122-AERO-MT-726
- /10/ FORNASIER L.
HISSS - a Higher Order Subsonic/Supersonic Singularity Method for calculating linearized Potential Flow, AIAA-84-1646, (1984)
- /11/ WEILAND C.
A Comparison of Potential- and Euler-Methods for the calculation of 3-D Supersonic Flows post wings, Notes on Numerical Fluid Mechanics, Vol. 7, Vieweg (1983)
- /12/ AGARD WG 08
Report on the Working Group on Aerodynamics of Aircraft Afterbody, AGARD AR No. 226 (1986)
- /13/ SCHMATZ M. A./HIRSCHEL E. H.
Zonal Solutions for Airfoils using EULER, Boundary-Layer and Navier-Stokes Equations, AGARD CP 412 (1986)
- /14/ SCHMATZ M. A.
NSFLEX-A Computer Program for the solution of the compressible Navier-Stokes Equations, MBB-LKE122-AERO-MT-778 (1987)
- /15/ VIVIAND H./RIZZI A.
Numerical Methods for the calculation of inviscid transonic flows with shock waves, Notes on Numerical Fluid Mechanics, Vol. 3, VIEWEG, (1981)
- /16/ AGARD WG 07
Test Cases for inviscid Flow Field Methods. AGARD AR No. 211 (1985)
- /17/ HEINRICHS W.
Messungen am Profil KORN No. 1 im transsonischen Windkanal der DFVLR in Braunschweig, DVLR IB 129-81/20 (1981)
- /18/ ELSENAAR A./ERIKSSON G.
International Vortex Flow Experiment on Euler Code Validation, Proceedings Symposium 1.-3. Oct. 1986, PFA, Stockholm
- /19/ BAVITZ P. C.
An Analysis Method for two-dimensional transonic viscous flow, NASA TN-D-7718 (1975)
- /20/ EBERLE A., AULEHLA F.
Reynolds Number Effects on transonic Shock Location, AGARD CP 335(1982)
- /21/ EBERLE A.
Characteristic Flux Averaging Approach to the solution of Euler's Equations, VKI LS 1987-4, (1987)

11.7 Attachment

Will the Wind Tunnel replace the computer?

We all know of the importance of computers in today's aerospace engineering environment. The latest advances in cryogenically cooled semi-superconductor technology and microscopic germanium sub-water assembly has made desktop 100 MINS (Millions of Navier-Stokes solutions) machines commonplace in engineering use.

We are also aware, however, of the high cost of this aging technology. The most accurate aerodynamic prediction code available today, FLO-1234.5, is so complex and expensive that it has never been run. Many other codes, if run to completion, would require CPU time exceeding the average human lifespan. Most engineers attribute this situation to the time when the task of writing aerodynamic computer programs was automated and handed over to the computers. We now have codes too complex to be understood by any human being. The cost of computing has been rising exponentially over the years. Clearly, if these trends continue unabated computational solutions will soon be beyond anyone's means.

Fortunately, there is an exciting new technology on the horizon which may someday replace the computer for aerodynamic design and analysis. Two workers at UNCAF (United Nations Computational Aerodynamics Facility) have recently made a startling discovery. They found that by building a small wooden model of an airplane and then blowing air past it in an enclosed tunnel, reasonably accurate predictions may be made of what the flow codes would compute. They refer to the method they have discovered as a "wind tunnel". At present, "wind tunnel" modeling is still in an early and relatively crude stage, and cannot be expected to precisely reproduce numerical results. For example, the continuous surface of a wood or metal airplane model will never exactly duplicate the discrete nature of a computational grid. Also, some factors, such as artificial viscosity, are neglected completely in wind tunnel modeling. It may be especially hard to accurately predict linearized potential flow in the tunnel. Nevertheless, in many cases, the wind tunnel agrees surprisingly well with the computer.

Constructing a wind tunnel model is much quicker and less labor-intensive than running all but the simplest computer programs. Shops such as Minicraft or Static Engineering complete even a highly detailed titanium model in a mere matter of months. Thus, many design iterations and trade-off studies can be conducted in a fraction of the time required via the computer. Advances in wind tunnel technology and model fabrication are expected to proceed at a rapid pace. Many promising new techniques, such as the chiseling of facets in Plaster-of-Paris models to more-closely resemble computational panelings and grids, are already being suggested by researchers around the world. The future prospects of this amazing new wind tunnel technology are bounded only by the imagination.

But what, you may ask, will be the fate of the millions of computational aerodynamicists presently employed in the aerospace industry? Is the wind tunnel a threat to their job security? While it is true that some may lose their jobs, a brand-new demand will be created for those well-versed in state-of-the-art wind tunnel technology. Engineering graduate schools are already replacing course offerings in Finite Volume Methods and Grid Generation with curricula in Woodworking and Whittling. Clearly, the engineer will be freed from the tyranny and drudgery of computational methods, giving him more time to concentrate on creative tasks. It is doubtful, however, that the computer will ever be completely eliminated; the thought of an airplane designed solely from wind tunnel data without the aid of the computer seems too incredible to believe. While the wind tunnel may never fully replace the computer, it is almost certain to become the most useful engineering tool of the future.

**REQUIREMENTS AND RECOMMENDATIONS FOR THE
DEVELOPMENT OF THEORETICAL CODES
AND EXPERIMENTAL FACILITIES IN THE NEAR FUTURE**

by

B. Costes
Aerodynamic Department
ONERA
B.P. 72
92322 Châtillon, France

SUMMARY

In order to properly use all the available tools, the aircraft designer has to be acquainted with both their qualities and shortcomings. This guides the improvement studies in a context characterized by :

- the general development of the potential of methods and calculation means, wind tunnels and relevant instrumentation.
- the new requirements for aircraft performance and the ever growing industrial risks.

Successively, we will examine the incoming developments for various levels of calculation codes, used for an industrial design or for fundamental researches. In the same way, we will examine the improvements needed for wind tunnels and testing methods, depending on the character of the studies to be carried out.

Examples will allow us to define the present state-of-the-art and to examine improvements under study which may be exploitable in a not too distant future.

1 - INTRODUCTION -

The development of a new fighter involves formidable industrial and military risks. To obtain the best possible design, all the available tools at a given time have to be used as long as they prove profitable. The requirements for improvements of these tools are more demanding than ever in aerodynamics.

We will examine successively the requirements for improved theoretical codes, using the new computer capacities, and the requirements for improved experiments in wind-tunnels. In each case, the need for improvement is a consequence of the qualities and shortcomings of the present tools.

2 - THE DEVELOPMENT OF AERODYNAMICAL CODES -

Let us remember that some engineers began their careers using the slide-rule and that, now, these same people have access to computer networks including CRAY or CYBER supercomputers. The current attempts at Navier-Stokes calculations, on schematic configurations, are a foreshadowing of what will be operational in 5 or 15 years for fighter design.

Of course, the aerodynamical codes represent only a part of the codes needed. Aerodynamics is already strongly linked to flight mechanics and to structure calculations (for the study of the aeroelastic behaviour) and we can foresee new connections with other disciplines, for instance, for the prediction of radar signatures or the fatigue behaviour.

From the strict point of view of aerodynamics, many characteristics of a future aircraft have to be predicted : global performance in steady flight (subsonic, transonic, supersonic) but also the dynamic stability, the air-intake performances and, if possible, the complete nonlinear behaviour which can occur in flight. According to these various aims and the necessary accuracy, the codes may be very different in their capabilities of handling the aircraft geometry and the equations of fluid mechanics.

A fifteen year projection

Let us begin by considering the state of Computational Fluid Dynamics in 2000. In 1982, U.S. experts published a study [1] of a fifteen year projection about the influence of CFD on Experimental Aerospace Facilities. This document makes it clear that calculations and tunnel testing will remain complementary, their roles evolving however as the capabilities of the two technologies develop.

Considering in the next 15 years a probable improvement of 30 in computer cost effectiveness and of 30 in numerical algorithm efficiency, the study concluded that the Reynolds-averaged Navier-Stokes equations could be expected to be largely used for computing the flowfield around a complete aircraft ; however uncertainties arising from transition and turbulence modeling were viewed as the major limitations in the confidence of the results. It was clearly not anticipated that the problem of turbulence modeling would receive fully satisfactory answers before 2000, "the lack of adequate modeling may stand in the way of a complete flow field analysis", since complex flows have to be studied

(separated regions, vortex and viscous flows).

New Euler codes will be emerging for an efficient study of unsteady flows (dynamic airloads, flutter, buffet...). More rapid convergence of the algorithms will be obtained by suitable techniques such as multigrid techniques.

The document also made clear that various problems may not be solved if important steps are not taken, concerning for instance :

- actions in order to enhance confidence in CFD (many correlations with tunnel and flight experiments...)
- development of techniques for grid generation and, more generally, development of user orientated methods in such a way as to adequately address the engineering problems and suitable for the new computer architectures.
- methods of quickly recognizing unsatisfactory or potentially dangerous flow characteristics from the mass of computed data.

In addition various strengths and weaknesses of CFD are pointed out :

- to obtain integrated forces and moments in an accurate manner (drag, pitching moment) will remain difficult, or even unreliable (high lift conditions)
- to obtain the off design characteristics need a large number of computations (many values of Mach numbers and angles of attack to be checked).
- on the other hand, Navier-Stokes solvers may enable a classification of a small number of stall patterns and the development of simpler and cheaper models. They will provide a better understanding of the physical phenomena occurring in the flow
- interesting possibilities can be contemplated with the improvement of flow visualization techniques from CFD results and of "inverse" methods giving the shape corresponding to a prescribed result.

Today, these statements remain fundamentally valid.

User viewpoint

Reference [2] provides a number of important observations related to the challenges existing for the aerospace industry in learning how to exploit the opportunities being created by computational research carried out worldwide.

As seen in the figure (1), the initial algorithm will be written and malaxated before pay-off ; in search of the best possible tool at a given time, much time and money may be saved with proper management of the various development phases. A new breed of engineer is seen necessary to develop correctly the computational tools with a view to applications ; these CFD professionals stand between the professional programmers, the engineering managers and the design engineers. In other respects, a complete code development cycle requires from 4 to 12 years before having enough confidence to make decisions based on a code. In practice, P.E. Rubbert states that this confidence cannot be obtained without having, in support of the user, all the specialists (numerical and experimental people) involved in the aerodynamic problem to be computed.

Following Kutler [3], the software design goals can be enumerated : transportable, flexible, usable, affordable, maintainable, reliable, cost effective development. Miranda [4] tries to evaluate the effectiveness of software, depending on quality and acceptance factors, in order to manage the development of the CFD software (fig.2).

The overall characteristics and possibilities wanted for the codes are various, for instance :

- modular structure, not depending too much on the computer architecture, capabilities of connection with geometric data base, automated grid generation, video and graphic workstations, automatic optimization processes. In [6], the Fortran 77 is given as the basic language for the main programs, the need of visualization in real time of intermediate results or convergence rates is also pointed out, as also means to evaluate the efficiency of the code in effective industrial use (information to the programmer and operator on the critical path).
- user hand-books and adequate comments inside the code, example data.
- possibility of simulating by the calculation both flight and wind tunnel experiments (including specific effects of walls, supports and plumes).
- capacity for computing various configurations, including schematic configurations for fundamental validations of the physical and numerical aspects.
- increased capacity to create visualizations (streamline tracing, numerical schlieren, films, 3D visualizations...).
- an opening to other scientific disciplines, using similar partial differential equations.

Users have to be prepared to apply the new techniques which are continuously being proposed to them. Papera [1,2] emphasize the gap between CFD research and application by industry. Management has to take much more this fact into account : to fill this gap, some resources have to be set aside independently of a given project.

In parallel, it is assumed that fundamental studies (numerical and experimental) are going on in order to provide 1) the models (turbulence, ...) which give a good representation of physical phenomena and 2) the detailed flow field data for the validation of the codes.

Present calculations, some weaknesses

Some years ago, a realistic lift could be obtained for a profile provided that a significantly reduced angle of attack had been used in the calculation. The development of methods taking into account a weak coupling with the boundary layer, the transition prediction, and subsequently the strong coupling methods has finally made it possible to have correct results for the lift (probably more accurate than many present experiments in 2D wind tunnels).

Nevertheless, today we have to admit that even in such an elementary case as a 2D calculation of a profile, the drag prediction is not completely reliable: from the same code (full potential), the calculation of the drag by:

- pressure drag + friction drag
or - wake drag

can yield differences in drag up to 10% at the design point. These differences can have two sources: numerical inaccuracies due to locally insufficient mesh resolution (in particular, near geometrical singularities), inadequate turbulence modeling. It remains therefore difficult to state if one profile is better than another.

In 3D inviscid calculations (e.g. of transport aircraft in cruise conditions), generally, different research teams cannot provide the same results (problems of grid generation, convergence criteria, boundary conditions?)

If we examine in detail various results, we have to note some anomalies, such as mass flow changes in calculations of internal flows, unexpected entropy jumps and oscillations, unexpected dependence on the mesh generation... These anomalies present a challenge for further improvements of the methods. In some cases, there are considerable discussions between experts in order to determine whether or not problems are well-posed (from a mathematical point of view) and have a unique solution. Reference [6] details important difficulties encountered when trying to obtain a good mesh generation, a correct boundary condition handling and the simulation of viscous 3D effects.

The existing turbulence models give good results in some conventional cases but are unable to correctly predict the separation or the secondary flows in other cases (flows along a corner...). Introducing new parameters or hypotheses into the model for a given case, it is generally possible to improve some results but others can be worse [5]. The numerical simulation of turbulence makes it possible to check some models but the numerical viscosity, intrinsic in any calculation, must be carefully taken into account.

Accurate turbulence modeling is truly one of the main limitations of the future calculations of fighters by the Reynolds-averaged Navier-Stokes equations. More generally, it should be clear that the above weaknesses are temporary and that CFD in its present status is already a useful tool in decision making, combined with other complementary techniques like tunnel testing when it is necessary.

Many papers (for instance in the present course) present typical examples of complete aircraft calculations, now in a mature capability phase for flight conditions not too much complex (moderate viscous effects and minor separated regions). Therefore, only 2 examples of fundamental researches are presented briefly.

The first one is relating to 2D calculations with unsteady NS equations (finite volume, implicit method [7], laminar regime at a Reynolds number of 10 000). The fig.3 shows at zero angle of attack, Mach number 0.85, a vortex street behind a NACA 0012 profile. Such calculation needs typically one second for a time step (C mesh 278 x 48) using a CRAY 1 computer.

The second example is an axisymmetric application of a fundamental research on unsteady Euler equations, using a second order upwind scheme [8] and a zonal technique. An air intake, adapted to an inflow at Mach 2, is there computed for $M = 1.8$ (fig.4). The internal flow is subsonic and a strong expansion fan develops on the outer side of the leading edge. With such a scheme, both the shocks and the slip line are well captured on few meshes.

Various levels of codes

According to the different development stages of each project, several code levels or classes can be distinguished.

First, there are codes rather simple, from an aerodynamic viewpoint, within an optimization procedure (more or less automatic) allowing to clear the general characteristics of a future project in the preliminary design. In the granted calculation time (e.g. 10 minutes of the available computer), these codes must provide the most realistic results possible for comparisons between various shapes. Other requirements include robustness and easy use. The most critical points, where it will be necessary to optimize the configuration, will be made clear. For the validation of these codes - which generally means introducing empirical functions in order to have useful results - various sets of reliable experiments have been necessary including calculations and tunnel or flight results. With regard to figure (1), these codes are in their mature capability phase and the designers have the necessary experience to use them validly.

For the critical points, more ambitious aerodynamic computations are undertaken by specialists (in numerical methods and aerodynamics, generally with the help of the code development specialists).

A typical time for such computations: a few hours of the available computer. For some flight conditions the codes are in their "mature capability phase" according to [2]. Others are at the end of their

development phase : new requirements and unexpected strengths (and weaknesses) will appear yielding significant improvements in accuracy or efficiency ; the coupling with other tools (graphics, computer aided design...) and the continuous need of confidence can also lead to some modifications.

During the final verification of the project characteristics (including extensive wind-tunnel experiments), these codes are used more routinely for the analysis of off design flight conditions.

While industry prepares its projects, other teams do research work and develop new codes (or parts of codes) for a future use by industry or for the fundamental research of models. Such calculations can require hours and hours of the best computer available at the moment. Validation also necessitates comparisons with (fundamental) experiments and calculations using other methods.

Thus, the maturing of the codes, the increase of computer power and the development of an aircraft project each follow their own path with frequent difficulties of synchronization.

The need for confidence

This need is emphasized, for instance in [1, 2, 6], so that right decisions are made before a final verification (in wind tunnel and in flight) and so that the time and money of intermediate tests is saved. Another question could be the connection with certification regulations and flight testing (gain in time and safety). However, in the given bibliography, there are few indications allowing to say exactly how to improve this confidence in CFD results. Pragmatically, we see that the confidence has to be deserved but certain actions can help to reach this goal.

The Boeing Company [2] has created a CFD laboratory, in order to acquire new skills and multiply the applications. The approach of Breguet-Dassault [6] (as well as some US companies according to [9]), is to organize a design team working as an off-line project activity and seeking improvements that can be made available to a project in a timely fashion. Such design refinements are possibly incorporated by the project manager. This management makes it possible to multiply applications in realistic cases and to use emerging techniques.

In the research centers, theoretical people have some means at their disposal :

- to check the convergence of codes on academic test cases (uniform flow, other analytical flows),
- to compare results with other methods which are more expensive but probably more precise,
- to compare results with other research teams, national or international, in the framework of more or less informal workshops (AGARD, GARTEUR,...),
- to submit a prototype code to the industry for criticism.

In other respects, at ONERA (and elsewhere), beside the theoretical aerodynamic divisions, teams of the "applied aerodynamic division" are in charge to validate codes, including all the possible comparisons with wind-tunnel experiments, and in particular to define the utilization limits.

The testing (both numerical and in wind tunnel) of realistic but schematic shapes, as a joint study of the research centers and the industry, is one of the ways to obtain progressively confidence in the CFD calculations.

CFD in the future

Many aspects have been surveyed above. In order to foresee the future computations, we can examine the present trends of the advanced researches :

- zonal (or "multi domains") techniques. Such techniques [10] give a large flexibility in mesh generation for complex geometries, different mathematical models and numerical methods may be used in different regions in order to obtain the best efficiency,
- adaptation to the new super computer architecture : vectorization, parallel computing,
- introduction of artificial intelligence (expert systems in aerodynamics [11]). It is not possible to give yet an accurate time-table for that ambitious project. Grid generation has been identified as having the most promise :

- conceptual or topological discretization,
- definition and application of grid-generation procedure,
- grid quality analysis,
- grid-point location adjustments.

We can also contemplate expert systems in order to help the engineers and the researchers to handle and create large codes : it is not possible to place an expert programmer behind each researcher who has access to supercomputers, in order to avoid mistakes and to obtain a satisfying efficiency of the means.

In other respects, solutions will have to be found for the knowledge base-keeping and for the transference between various design domains, aeronautical (fighters, transport aircrafts, turbomachines, test facilities, general aviation, missiles...) or not.

It also remains possible that completely new approaches may be discovered, using massively parallel architectures and algorithms such as the one recently proposed in [12].

3 - EXPERIMENTAL FACILITIES : THE WIND TUNNELS IN THE NEAR FUTURE -

To achieve success for any given project, fighter design requires and will require many facilities, such as flight simulators, radar and armament benches or aeropropulsion facilities. It is clear that taking into account for instance the various aspects of the system/man interface, the artificial intelligence

incorporation, the flight mechanics at high angle of attack, the stealth aspects or the real conditions for the engine operation (inlet distortion, firing influence...) will require both together theoretical studies and various experiments in relevant facilities. Some of these facilities may be already existing ones and may have to be modified, others will have to be created.

Considering the wind tunnels only, we have to note that a tunnel life-span is 50 years or more, with possibly refurbishments, moving, reactivations... Most tunnels needed for the next 20 years are already available.

We will examine later for each type of tunnel (from small laboratories up to the largest industrial ones) the present requirements, corresponding to 1) the evolution of aeronautical experience (new flight domains becoming attainable), 2) the technological progress and, specially now, the computational strides. The description of some recent tunnels allows us to see how and why the facilities are presently evolving.

Reference [1], "a fifteen year projection", shows that in the year 2000, wind tunnels and CFD will still be complementary because CFD will not yet be able to reliably provide for all the characteristics of a project. The cost of wind tunnel experiments has not to be considered since the tunnels continue to provide a little more confidence for a project.

In fact, this document does not call for any requirement for new ("industrial") test facility (with the possible exception of test requirements of V/STOL aircraft); however a permanent upgrading is foreseen for the facilities and their equipments, with improved testing methods. In particular it is quoted in chapter V that, in the next 15 years, "improved flow diagnostic techniques will allow better physical understanding and will provide the basis for a more efficient and systematic approach"... For dynamic airloads (gust, buffet, flutter...) "new techniques will be developed in the way of parameter identification to better understand the onset of flutter"...

The more distant future for the tunnels cannot be accurately predicted since it will depend on requirements still to be defined, especially for the future fighters. It will depend on whether or not they are VTOL or STOL, stealth, completely variable camber wings, hypersonic... But in any case, we can be sure that, in one way or another, experiments in wind tunnels will remain necessary for quite sometime in order to answer the questions concerning concept reliability, code validation or flight test safety. At a much later date, it is possible that new tunnels will have to be redesigned for the teaching of aerodynamics and physics of the flow phenomena...

General requirements for Wind Tunnels

The AGARD Advisory Report 184 [13], published in 1982, is relating to Flow Quality (fig.5) and Data Accuracy Requirements (fig.6). It represents a formidable effort and remains a reference book for many people. Some of the quoted requirements appear as unattainable as they were in 1982 (i.e. angle of attack measurement in absolute accuracy level). Is it possible to take measurements accurate enough to prove that such requirements are obtained and how can one be sure that there is no deviation during a test? We know for instance that the cleanliness of the settling chamber screens and the operation of the porous wall setting mechanisms have significant effects on the flow angularity.

If it is not possible to have a zero error, we must try to evaluate and minimize this error, learn how to take it into account and, above all, work to eliminate erratic deviations. If a tunnel could provide an exact result to the customer, the measurements would probably look so strange that nobody would dare place any confidence in them without a complete validation program! Fortunately, for many studies (for example, with minor configuration changes), the flow uniformities are not important as long as they stay the same over extended periods of time and engineers have a large experience for the result interpretation.

To complement the calculations, there are various levels of tests that condition the tunnel characteristics and the equipment involved. In any case, the largest production of data has to be obtained in a given time, with important consequences on the data acquisition system, the needed flow quality, the test organization and the new tunnel fittings [14].

For the facilities used for preliminary designs, cost and duration of a test (from the definition of a new shape to the result) are very important and this leads to consequences for the model technology, the access to the test section, the required repeatability of measurements.

In the industrial facilities, yielding the final selection of a configuration, a large versatility is required:

- quick sweep of the test domain (Mach, stagnation pressure, attitude of the model),
- efficient instrumentation (see fig.(7), use of new scanners, ...),
- flexibility of the exploitation codes, for an on line observation of the tests.

More and more, specialized study devices are necessary for detailed researches on fighter elements: air intakes, afterbodies, CCV controls, store dropping systems... [28]. Some of these devices can be operated in the tunnels as well as beside (validation of the acquisition procedure, done "without wind"). A single Captive Trajectory System can be used either to predict store trajectories or to analyse the complex aerodynamic flows around models with various kinds of probes.

For the code validation, some tests are carried out in the industrial tunnels on models with schematic but typical shapes. The test conditions are generally constant but considerable investigation means are used for the flow analysis (laser velocimetry, multi-hot-wires...); a good reliability (and short time for the instrumentation installation) is necessary.

For more fundamental studies, in research facilities generally smaller than the previous ones, important investigation means are also becoming compulsory. For such facilities, problems of duration are less important but the requirements in data quality are even stricter (in order to accurately reach the Reynolds tensor coefficients, or the coherence in high frequency turbulence...).

Each facility must be fitted with a computer system well suited to the data acquisition, the test control and the survey of results. Like numerical studies, the detailed analysis of the data requires thoroughly developed graphic capabilities.

There is inevitably a compromise between the time needed to obtain results and their quality. For instance, it is hard to imagine measurements with laser velocimetry during preliminary tests.

As a conclusion, it may be stated that, at least in the short term, the facilities will continue to develop, taking into account the needs of the customers, the technological possibilities and the theoretical deficiencies at a given time. This development concerns the following points :

- exploration of new flight domains (Mach number around 1, very high angle of attack, flight in turbulence, ...),
- study of better identified problems, like buffeting, air-intake distortion, store interaction, gunnery and firing simulation, non-linear flight mechanics, noise...
- better simulation of flight : high Reynolds number (cryogeny...), flow quality (better honeycombs, better computed circuit...), minimizing wall and sting effects (adaptive walls, possibly magnetic suspension), consideration of model deformations (measurements, possibly scaled aeroelastic models), powered models...
- gains in time and safety for the flight test : better studies of flutter, store separations, anemometry...
- increased productivity through process automation, automatic verifications, electronically-scanned pressure sensors, more remotely controlled surfaces, faster CTS displacements... [15], organization of the tests [14].

Rather than trying to reach what looks impossible, the facilities will make use of various emerging CFD capabilities : we can foresee things like 1) correctly analyzing tests on "rigid" models which are in fact deformed by the air loads, 2) testing configurations voluntarily distorted to reproduce a physical phenomena in flight (enlarged leading edges [16], fig.(8), high lift studies like the ones done by Boeing [17]), 3) taking into account the sting and wall effects in a stricter manner...

For the illustration of these ideas, we shall examine two examples of recent tunnels. Many other papers are available, describing similar trends for various refurbishments [18] or new projects (ETW : [19]).

An example of a fundamental research tunnel, the F2 tunnel and laser velocimetry

The research tunnel F2 of ONERA, at the Le Fauga-Mauzac center [20], was designed for fundamental researches in aerodynamics on 3 Dimensional complex flows in subsonic range. It began functioning in July 83. Its main characteristics are :

- "human size" test section ($1,4 \times 1,8m^2$; length 5m) making the job easier ; the models are large enough to be well equipped, their cost and manufacturing time can remain reasonable and it is possible to use models previously made by industry for development in conventional industrial wind tunnels,
- the facility was designed "around" and "inside" a Laser Doppler Velocimeter 3 Dimensional device, the measuring point being able to be moved within nearly the entire test section volume. The test section walls are made of glass allowing all kinds of visualization (viscous coatings, smoke...), fig.(9).
- the exploration devices for the flow field are automatically controlled by the facility computer, for an intensive use of 5 hole probes or multi-hot-wires...
- the acquisition system can be connected by telephone to a customer display, for a quick transference of results, facilitating the dialogue between the customer agent(s) on the field and the other researchers at Chalais-Meudon, 600 kilometers away,
- in order to save money and simplify the use of the tunnel, it is unpressurized and the maximum speed is 100m/s. A team of only 3 people operates the facility.

F2 is one of the first tunnels to have a fully computed contraction profile (axisymmetric inviscid optimization, coupling with turbulent boundary layer, then 3D computation by a finite element method : fig.10). This study yields a very short contraction ($L/\sqrt{S} = 0,8$ for a contraction ratio of 12), without separation in the inlet part and with an excellent flow uniformity in the exit plane. With such a shape, it is easy to provide flow visualization by smoke emitted from the settling chamber.

For fundamental aerodynamic researches, the Laser Doppler Velocimetry is a tool specially interesting because :

- its use does not perturb the flow,
- the algebraic sign of the instantaneous speeds can be obtained rather easily (fringe movement by Bragg cells),
- the apparatus is less exposed to failure than several hot wires.

Typical results in various research tunnels are briefly presented in order to show what can be obtained with LDV and some interpretation problems.

The first example concerns an experimental analysis of vortex breakdown [21]. The 3D laser velocimeter (fig.11) provides rather easily the mean velocity components (fig.12) and fluctuating terms u' , v' (fig.13). On the other hand, if we examine the instantaneous component histogram for points near the breakdown (fig.14), we notice two distinct populations : the probe volume is at one time inside

a "recirculation bubble" and at another time outside. These large scale and low frequency fluctuations set the problem of the adequacy of the usual averaged models for representing the real phenomena.

The second example concerns an experimental analysis of a strong 3D shock-wave/turbulent boundary-layer interaction occurring in a 3D transonic channel [22]. A test section wall is equipped with a 30" sweep bump (fig.15) yielding a very complex flow with a main vortex going off the bump. The aim of this experiment is to help in the physical understanding of a complex field, including several separations, and to provide a well documented case to test NS computational methods and turbulence models. A typical result is shown (fig.16) but visualizations by viscous coatings display strong interactions on the other walls so that, in a short term, only qualitative and local calculations may be expected in this very complex configuration.

To reach such a quality of results is due to considerable efforts :

- choice of reliable devices,
- acquisition systems able to take measurements on a few ten thousands particles per second : accurate results are obtained generally with 2000 particles for each point,
- calibration procedure : measurement point coordinates, fringe direction, fringe spacing, in order to reach a typical accuracy of 1% for the speed,
- particle seeding systems.

But progress remains desirable : better seeding, more accurate determination of the speed direction, measurements nearer the model surface, approach to spatial correlations and conditional analysis...

An example of a large tunnel, the National Transonic Facility

At the NASA Langley Center, the NTF gives us a good example of what an industrial modern tunnel must be : adequate size, well equipped [28-1], possibility of various test conditions (allowing in the NTF case the simulation, in cryogenic conditions, of the largest Reynolds numbers of real flight, with the determination of the independent effects of Reynolds number, Mach number and aeroelasticity of the model).

Among the numerous reports concerning this tunnel, reference [23] recalls us at once all the instrumentation developments required for the tunnel (fig.17). Of course, using tunnels at cryogenic temperature increases dramatically the difficulties of the measurements [24]. However, few tunnels, if any, have today at their disposal the instrumentation techniques at the required operational level, regarding particularly :

- model attitude with an accuracy of .01°
- model deformation with an accuracy a few hundredths of degree
- flow visualization around the model
- continuous determination of transition location, during the evolution of test parameters.

Such techniques have only begun to be tested for use in industrial tunnels, [24] ; sophisticated devices such as polarizing reflectors (torsionmeter : fig.18 from [25]), infrared scanings with insulated models, holographic tomography are being used. It seems to me that many tunnel teams will have to acquire new proficiencies specially in optics and relevant data processing.

On the figure 19, giving a result of model deformation from a torsionmeter in the French S1 Modane transonic tunnel ($\phi = 8m$), we can see the magnitude order of the deformation of half a wing for a transport aircraft model and remind the accuracy needed for a good comparison with calculation ; with the same accuracy, models have to be designed and built with a distorted shape in order to represent during the test at the design point, the shape of the real aircraft in cruise conditions.

The same paper [23] highlights the unique role of the NTF for a genuine validation of the existing tunnels with respect to flight. In particular, one can foresee that present boundary-layer trip techniques to simulate high Reynolds numbers -which are more or less empirical- will be replaced by new ones which will be scientifically justified once and for all (?).

Among the planned basic fluid mechanics experiments, we notice the test on a flat plate at Reynolds number exceeding one billion and many experiments on schematic configurations at flight Reynolds number, specially for the fundamental study of fighter aircraft aerodynamics with separated flows. Even if the capabilities of large cryogenic wind-tunnels are unique for high Reynolds number simulation, the other tunnels will still have to perform a great number of similar experiments for the code validation or complex phenomena modeling in applied or fundamental aerodynamics. Indeed, the NTF cannot perform the whole research, there is need for less expensive experiments in "conventional" tunnels if these tunnels are sufficiently well equipped and if the models can be built easily and quickly.

Cryogenic tunnels

Using flows at very low temperature (~ 100 Kelvin) is a very attractive way of improving the wind-tunnel performances in Reynolds number. The NTF [23] and the ETW project [19] prove that engineers trust this technique for new large tunnels. The modification of existing tunnels (T2 at ONERA [28-3], KKK at DFVLR [28-4]) is generally difficult for safety reasons and the modification cost must be compared with the one for a completely new project which should generally allow to incorporate other useful improvements.

It is now clear that :

- cryogeny is the only solution to reach economically very high Reynolds numbers,
- the flexibility of the tunnel is one of the main problems : a cryogenic tunnel must be able to provide

low cost results in conventional conditions (in order to fit together with results from other tunnels and with all the acquired engineer's experience) and to be operated with easy, quick and independent variations of all the flow parameters. The control of the stagnation temperature and pressure and of Mach number will allow, in particular, series of test at constant Reynolds number or at constant dynamic pressure,

- for any new tunnel project, the cryogenic capability must be considered as an interesting and feasible option.

Adaptive walls

To use "streamlined" wall shapes is a way for avoiding wall interferences on the models. This effect can be obtained, more and less completely, either with solid compliant walls or with ventilated (perforated or slotted) walls equipped for a local control of the flow through the wall (fig.22).

In reference [24,28], recommendations were made to continue to study this technique, in order to define the best ways of upgrading the existing tunnels. In reference [27], Ganzer reviews the various tunnels equipped with adaptive walls and the obtained results, in particular when using two adaptive walls for 3D model tests. He concluded that "for a number of problems, experimental verifications are required before a comparative evaluation of the 3D adaptive wall techniques can be made. Such experiments are planned for the near future. The results can be expected to become available within this decade".

Nevertheless, for 2D flows, the adaptive wall technique is almost in industrial use, for instance in the ONERA T2 and NASA Langley 1ft wind tunnels (solid walls, cryogenic conditions). On the profile, the 3D effects due to the boundary layers on the lateral walls still remain a difficult problem which appears all the more manifest as the results are more precise in other respects.

The tunnels presently equipped are small (cross section $< .65m^2$). Most of them are only working on improvement studies of the technique in 3D. In the range of $0.8 \times 0.8m$ test sections for aeronautical purpose, we have :

- the new DFVLR rubber tube [27], (fig.23).
- in project, a new test section for the ONERA S3 Chalais-Meudon transonic tunnel.

NTF and RTW are not considered with adaptive walls in their basic configuration ; more generally not any large tunnel is planned to be retrofitted in the short term. Trying to see why, we have to admit that the choice of a new configuration is still difficult :

- flexible or ventilated walls ?
- 2, 4 (or 8) walls, how to make corners and to permit good visualizations through the walls ?
- how to take the necessary measurements on control surfaces near the walls : static pipes, LDV... ? Are they accurate enough, how long for an adaptation cycle ?
- does it remain possible to use the tunnel for polars in continuous mode (variable angle of attack or even variable Mach number at given angle of attack) ?

In other respects, all the process must be fully reliable : the industry cannot wait a week before to be sure of the true angles of attack.

As concluded by Ganzer for the test of 3D configurations, the present state of the art calls for further investigation. However, for new tunnels, the designers must make provisions for a possible retrofit of the various test section walls. In [28-round table], Ritter recommends in particular to contemplate the systems for flow measurements near the tunnel walls. In any case, the precise wall assessment will be required (full adaptation is a particular case of computed zero interference) and Binion and Kraft [28-11] pointed out that the Reynolds number effects on the wall boundary conditions have to be taken into account.

An unsettled future

The complete elimination of support interference effects, due to stings and struts can be obtained with the Magnetic Suspension concept. Such a concept has been studied since 1937 and it is not yet in current use. Successive studies [26] have been published for a tunnel 8ft x 8ft like NTF : the project (fig.20 and 21) appears to be "practical and feasible" but the last estimated cost is today still 21.4M\$. Moreover, it would still take a week for the cooldown and the filling of the magnet cryostat. The total weight of the core would be 81,000kg (including 36,000kg for the coils used to produce 4180N in thrust). Many studies remain necessary for finalizing such a project and, in my opinion, the concept application is not yet for the next future in industrial tunnels. After this step, it will be necessary to simulate the propulsion effects and to transmit a lot of data by telemetry. The other option is to take into account by CFD the drag effects for angles of attack up to 45° or more. Fortunately, absolute measurements of the drag do not seem to require the same degree of accuracy for a fighter as for a commercial transport aircraft.

The pressing need for more visualizations of the complex flows, both qualitative and quantitative, will yield the use of new methods, that are today badly defined. What is the future, in industrial tunnels, of such techniques as holography, thermography or new developments in laser velocimetry ? What "spinoff", for the fighter studies in wind tunnels, of the techniques developed for hypersonic flows, flames, rotary wings (fluorescence, Coherent Anti-Stokes Raman Scattering (?), holographic interferometry...) ? Who is ready to put a lot of money into the development of such techniques, attractive but with a high risk of failure from a cost/efficiency point of view ?

It is difficult to answer these questions reliably without complete feasibility studies. One can

consider as likely a significant use of thermography for the detection of transition and separation because the necessary improvements of sensor technology, image treatment and model insulation seem within our reach.

Another possibility of new technique emergence in optics is the availability of computed visualizations allowing direct and global comparisons with experiment.

4 - CONCLUDING REMARKS -

Inexorably, the means for theoretical prediction are growing ; the facilities and the ways of using them are changing so that they provide the complementary results needed by the designers. A special type of management is introduced in order to achieve a better development of new codes, including various actions for improving confidence in the results. It is perhaps the time to recall that, as ever, a major constituent of progress remains human. A befitting education giving knowledge and skill is necessary but inherent qualities such as a taste for work well done, the aptitude for innovation, clear judgement, good down to earth sense... will remain as always essential. Nevertheless joint studies seem to me to have become the rule and educational projects and company structures will have to give more consideration to this fact.

REFERENCES

- [1] Committee on Computational Aerodynamics Simulation Technology.
The Influence of Computation Fluid Dynamics on Experimental Aerospace Facilities. A fifteen year projection.
National Academy Press - 1982.
- [2] Paul E. Rubbert
The emergence of advanced computational methods in the aerodynamic design of a commercial transport aircraft.
International Symposium on CFD - Tokyo - Sept.85.
- [3] P. Kutler
A Perspective of Theoretical and Applied CFD.
AIAA paper 830037.
- [4] L.R. Miranda
A Perspective of Computational Aerodynamics from the viewpoint of Airplane Design Applications.
AIAA paper 820018.
- [5] J.C. Le Balleur, D. Blaise
Calcul des écoulements internes décolles et de l'interaction couche-limite onde de choc par couplage visqueux-non visqueux.
La Recherche Aérospatiale 1985-4 (french and english editions).
- [6] P. Perrier
CFD around complete aircraft configurations.
ICAS 82.6.1.1
- [7] H. Hollanders, W. Ravalason
Résolution des équations de Navier Stokes en fluide compressible par une méthode implicite.
La Recherche Aérospatiale 1986-1. TP ONERA 1985-148 (french and english editions).
- [8] M. Borrel, J.L. Montagné
Numerical study of a non-centered scheme with application to aerodynamics.
7th AIAA CFD conference - July 85.
TP ONERA 1985-75.
- [9] W.F. Samlhaus Jr
Computational Aerodynamics and Design.
Lecture Notes in Physics (Aachen 1982) Vol 170 Springer-Verlag.
- [10] L. Cambier, F. Dussan, J.P. Veillot
Multidomain method for the Euler equations : application to overlapping subdomains.
La Recherche Aérospatiale 1985-3 (english edition).
- [11] P. Kutler, U.B. Mahta
Computational Aerodynamics and Artificial Intelligence.
AIAA paper 84.1531.
- [12] U. Frisch, B. Hasslacher, Y. Pomeau
A lattice gas automaton for the Navier Stokes equations.
To be published.
- [13] Wind Tunnel Flow Quality and Data Accuracy Requirements.
AGARD-AR 154 - Nov.82.
- [14] J. Christophe
Productivity : the economic aspects of cryogenic wind tunnel design and use.
VKI special course - April 85.
TP ONERA 1985-28.

12-10

- [15] AEDC Test Highlights
Spring 85.
- [16] J. Coulomb, M. Ledoux, J. Lerat
Mesures en vol et en soufflerie sur le bord d'attaque d'une aile de Nord 2501.
AAAF : 14ème colloque d'Aérodynamique Appliquée - Toulouse, Nov.77.
- [17] Paul E. Rubbert
The impact of computational methods on aircraft design.
AIAA Gray channel volume 6, number 4.
- [18] L.H. Ohman and al
Recent improvements to the NAE 5ft x 5ft blowdown wind tunnel.
NAE Aeronautical Note 31 NRC NO 24882 - Aug.85.
- [19] J.P. Hartzuiker
The European transonic wind tunnel ETW : a cryogenic solution.
The Aeronautical Journal of the Royal Aeronautical Society - Nov.84.
- [20] Afchain et al
La soufflerie F2 du centre du Fauga-Mauzac.
20ème colloque AAAF - Toulouse Nov.83.
TP ONERA 1983-139.
- [21] A. Boutier, D. Pagan, D. Soulevant
Measurement accuracy with 3D Laser Velocimetry.
International Conference on Laser Anemometry, Manchester dec.85.
TP ONERA 1985-171.
- [22] R. Benay, T. Pot
Interaction onde de choc/couche limite turbulente en écoulement de canal tridimensionnel.
22ème colloque AAAF - Lille Nov.85.
TP ONERA 1985-151.
- [23] J. Campbell
The National Transonic Facility, a research perspective.
AIAA 84 2150.
- [24] Wind tunnel capability Related to Test-Sections, Cryogenics and Computer-Wind Tunnel
Integration.
AGARD-AR-174 - April 82.
- [25] M. Bazin
Instrumentation for cryogenic wind tunnel.
VKI Special course - April 85.
TP ONRA 1985-29.
- [26] R.W. Boom and al
Magnetic Suspension and Balance System Advanced Study.
NASA Contrator Report 3937 - Oct.85.
- [27] U. Ganzer
A review of adaptive wall wind tunnels.
Prog. Aerospace Sci. Vol.22 - Pergamon Press Ltd - 1985.
- [28] Wind Tunnels and Testing Techniques
AGARD-CP-348 - Sept.83.

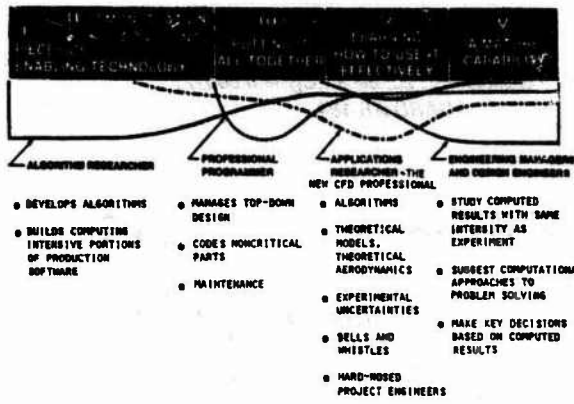


Fig. 1 - Some key player roles in the development of a computational capability.

EFFECTIVENESS = QUALITY x ACCEPTANCE

QUALITY FACTORS

- SOLUTION ACCURACY
- PHYSICS REALISM

ACCEPTANCE FACTORS

- APPLICABILITY
- USABILITY
 - SIMPLE
 - RELIABLE
 - FLEXIBLE
- AFFORDABILITY
 - MANPOWER
 - COMPUTER
- MAINTAINABILITY

MIRANDA L.R.

Fig. 2 - Software effectiveness (from Ref. 4).

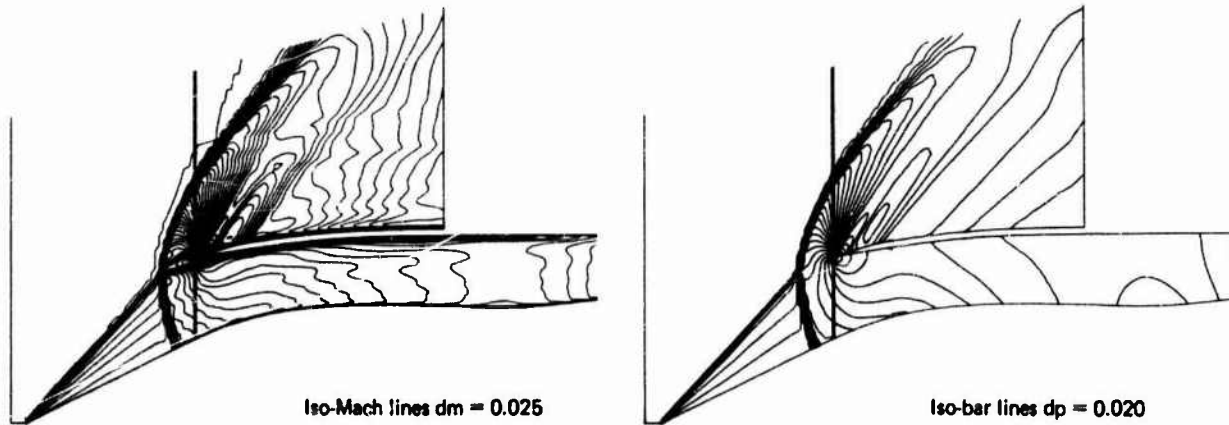


Fig. 3 - Axisymmetric air intake $M = 1.8$.

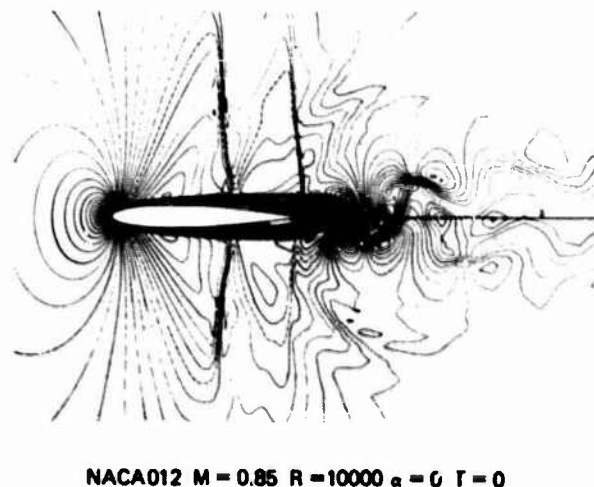


Fig. 4 - Unsteady viscous flow : iso-Mach lines $dm = 0.025$.

- FLOW ANGLE (W/U) $< 0.01^\circ$
- FLOW CURVATURE $< 0.03^\circ/\text{chord}$
- SPANWISE VARIATION IN FLOW ANGLE $< 0.1^\circ$
- MACH GRADIENT $< 0.0006 M$
- VORTICITY, NOISE, TEMPERATURE SPOTTINESS.....

Fig. 5 - Summary of flow-quality requirements (AGARD-AR-194).

- PRESSURES 0.001 P full scale
- STAGNATION TEMPERATURE 0.01 T₀
- MACH NUMBER 0.002
- ANGLE OF ATTACK 0.01°
- FORCES 0.0008 F balance capacity

Fig. 6 - Summary of data-accuracy requirements (repeatability, 2σ, basis: C_D = 0.0001): AGARD-AR-184.

Fig. 7 - Evolution of data production.

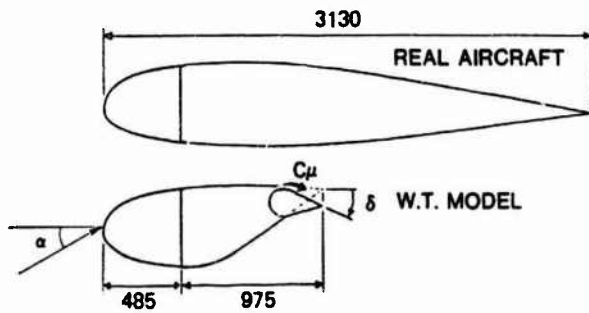
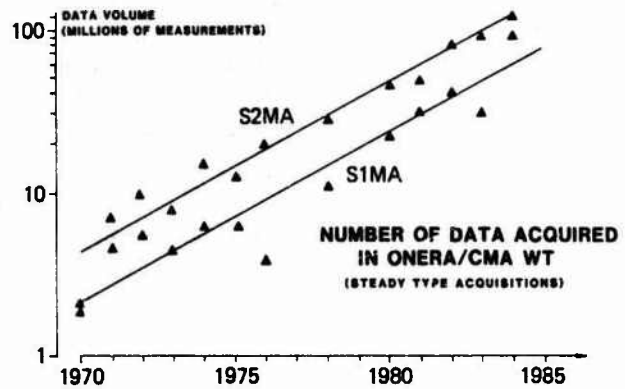
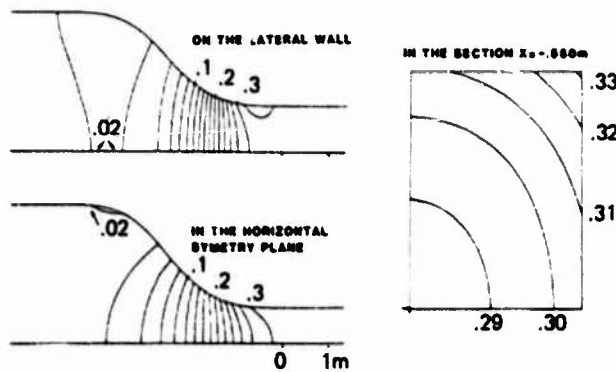
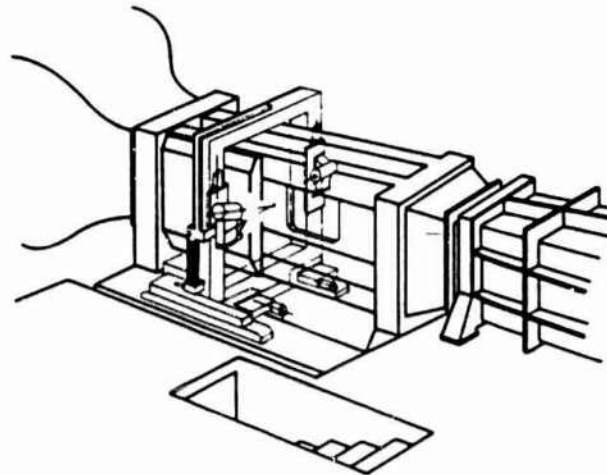


Fig. 8 - Enlarged leading-edge technique.

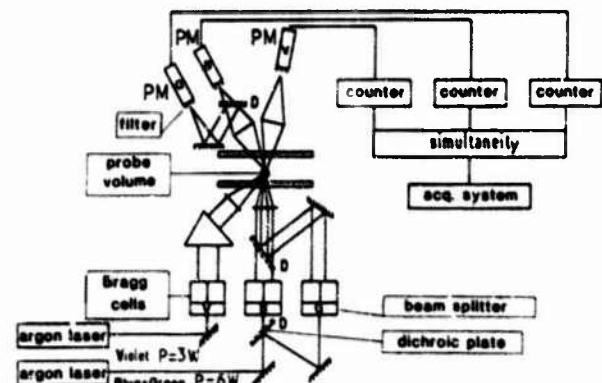
Fig. 9 - F2 : test section and LDV apparatus.



ONERA F2 WIND TUNNEL
COMPUTED ISO-MACH (M_∞ = 0.308)

Fig. 10 - Example of 3D calculation for a wind tunnel contraction.

Fig. 11 - 3D laser Doppler velocimeter.



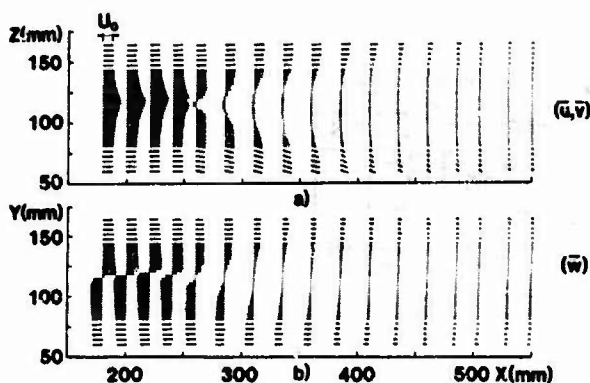


Fig. 12 - Vortex breakdown components of the mean velocity in the meridian plane. (a) (u,v) plot of the meridional component; (b) (w) plot of the tangential component.

Fig. 13 - Vortex breakdown: (a) lines of constant \bar{u}^2/U_0^2 ; (b) lines of constant $\bar{u}w/U_0^2$.

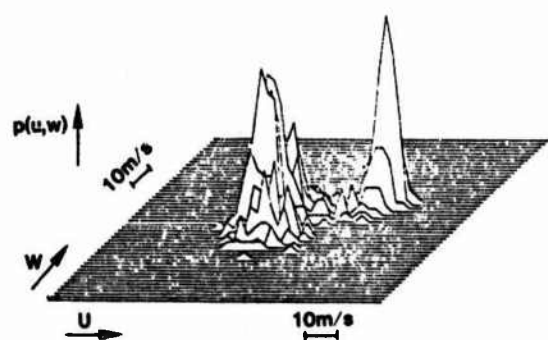


Fig. 14 - Vortex breakdown. Histogram of u and w components built from 1000 samples ($x = 260$ mm, $z = 115$ mm); (a) 3D visualization; (b) lines of constant population.

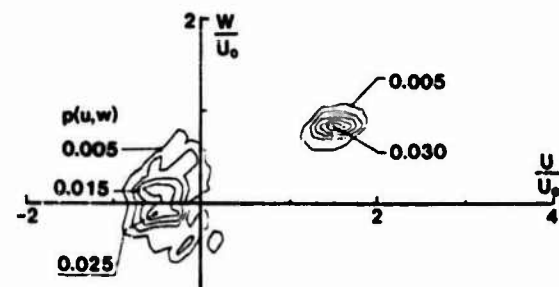
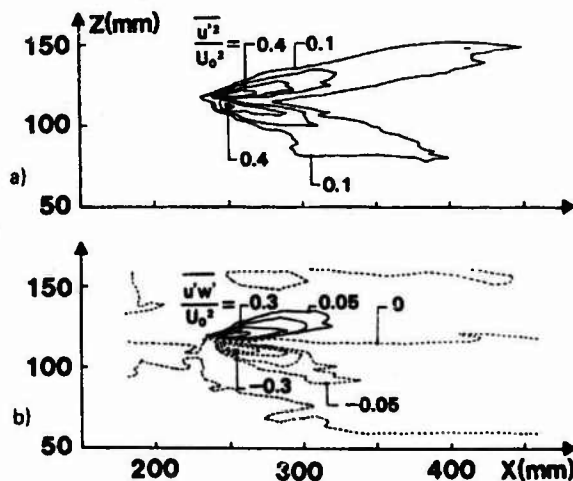


Fig. 15 - 3D transonic channel for the study of complex shock-wave/boundary-layer interaction.

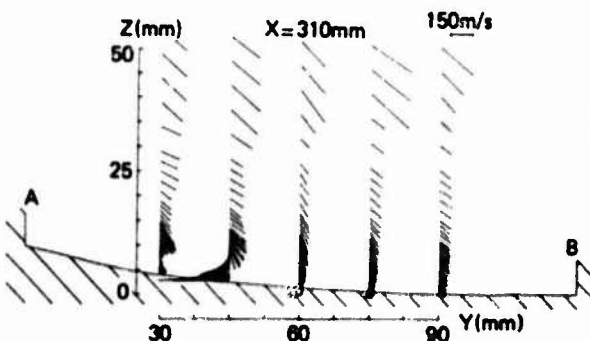


Fig. 17 - Measurement areas that required instrumentation developments for NTF. AIAA 84-2150.

DEFINITION OF EXPLORATION DOMAIN

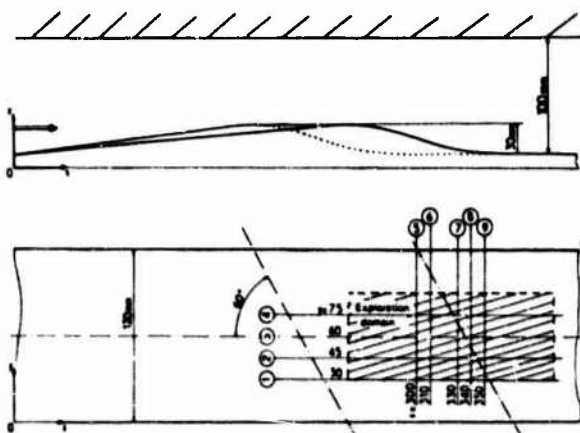


Fig. 16 - Shock-wave/boundary-layer interaction: speed components in the transverse plane 9.

- FORCE
- PRESSURE
- MODEL ATTITUDE
- MODEL DEFORMATION
- TEMPERATURE
- FLOW VISUALIZATION
- SKIN FRICTION
- FLOW TRANSITION
- LASER VELOCIMETRY

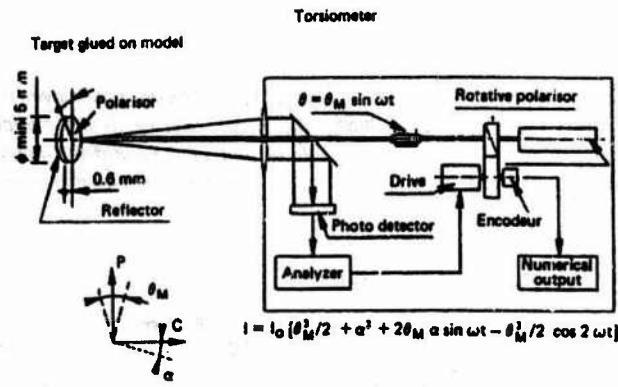


Fig. 18 - ONERA-BBT torsionmeter.

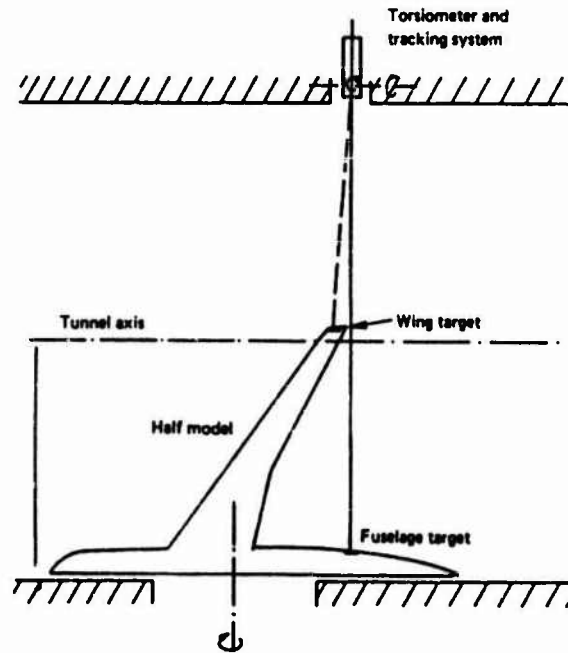
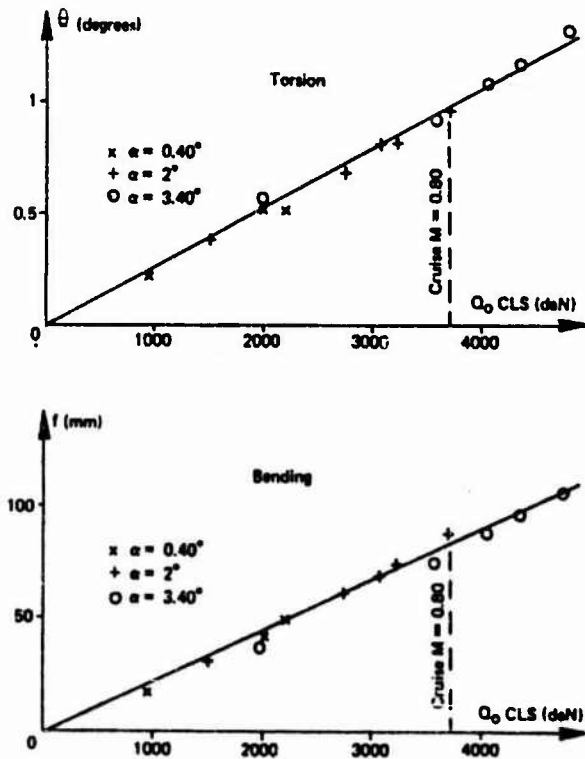


Fig. 19 - Measurement of wing deformation with the torsionmeter, in the S1MA.

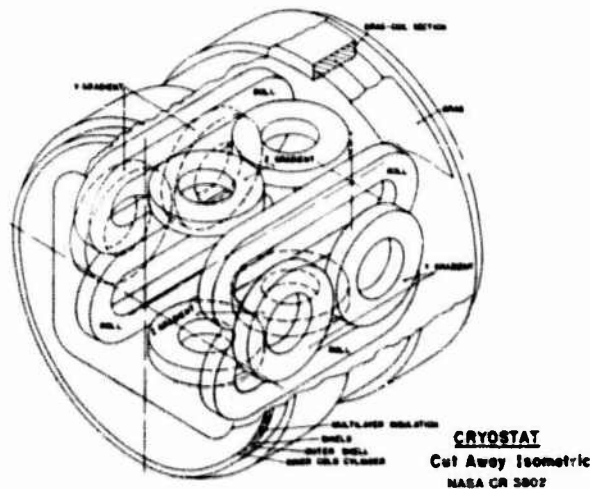


Fig. 20 - Magnetic suspension and balance system project : coils around the test section.

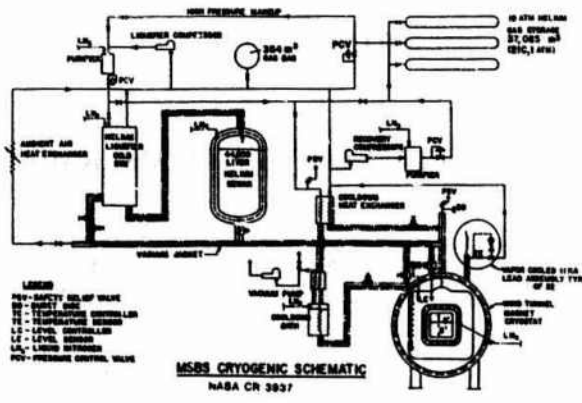


Fig. 21 - Magnetic suspension and balance system : cryogenic equipment.

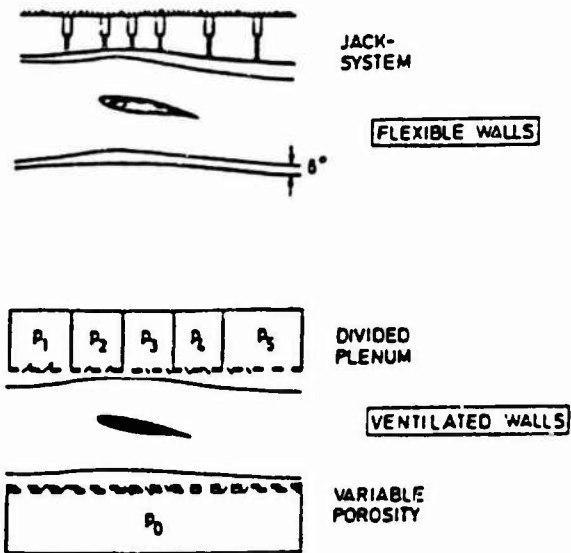


Fig. 22 - The different types of adaptive walls (from Ref. 27).

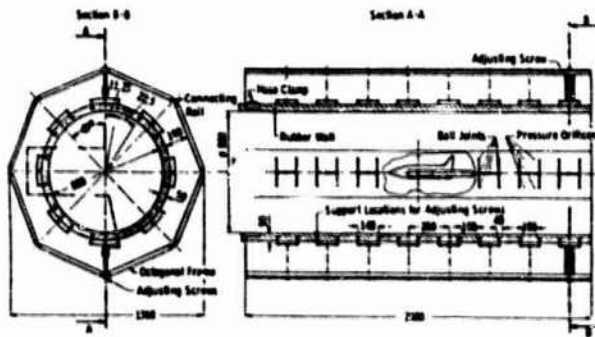


Fig. 23 - DFVLR test section with expandable (Rubber) wells (from Ref. 24).

REPORT DOCUMENTATION PAGE

1. Recipient's Reference	2. Originator's Reference	3. Further Reference	4. Security Classification of Document
	AGARD-R-740	ISBN 92-835-1560-9	UNCLASSIFIED
5. Originator	Advisory Group for Aerospace Research and Development North Atlantic Treaty Organization 7 rue Ancelle, 92200 Neuilly sur Seine, France		
6. Title	SPECIAL COURSE ON FUNDAMENTALS OF FIGHTER AIRCRAFT DESIGN		
7. Presented at	the von Kármán Institute, Rhode-St-Genèse, Belgium on 17-21 February 1986, and a Short Course at Athens, Greece on 24-25 February 1986 and at Ankara, Turkey on 27-28 February 1986.		
8. Author(s)/Editor(s)	Various	9. Date	October 1987
10. Author's/Editor's Address	Various	11. Pages	296
12. Distribution Statement	This document is distributed in accordance with AGARD policies and regulations, which are outlined on the Outside Back Covers of all AGARD publications.		
13. Keywords/Descriptors	<p>→ Fighter aircraft, Design, Aerodynamic characteristics,</p> <p>Materials, External stores, Engine inlets.</p>		
14. Abstract	<p>The Special Course on Fundamentals of Fighter Aircraft was sponsored by the AGARD Fluid Dynamics Panel and the von Kármán Institute and presented at the von Kármán Institute, Rhode-Saint-Genèse, Belgium, on 17-21 February 1986, at the Greek Air Force Academy, Athens, Greece, on 24-25 February 1986 and at the ARGE, Ankara, Turkey on 27-28 February 1986.</p> <p>→ The Course presented a comprehensive review of fundamental procedures used during a fighter pre-development phase concentrating on,</p> <ul style="list-style-type: none"> → basic mission requirements and aircraft sizing; + aerodynamic design including performance, stability and control; + materials, structural optimization and aeroelasticity; + aircraft dynamics; + engine intake and nozzle integration; and + airframe store-compatibility. <p>Experimental and theoretical work has been demonstrated to play complementary roles and recommendations for future development of engineering tools are given in conclusion.</p>		

<p>AGARD Report No.740 Advisory Group for Aerospace Research and Development, NATO SPECIAL COURSE ON FUNDAMENTALS OF FIGHTER AIRCRAFT DESIGN Published October 1987 296 pages</p> <p>The Special Course on Fundamentals of Fighter Aircraft was sponsored by the AGARD Fluid Dynamics Panel and the von Kármán Institute and presented at the von Kármán Institute, Rhode-Saint-Genèse, Belgium, on 17-21 February 1986, at the Greek Air Force Academy, Athens, Greece, on 24-25 February 1986 and at the ARGE, Ankara, Turkey on 27-28 February 1986.</p> <p>P.T.O.</p>	<p>AGARD-R-740</p> <p>Fighter aircraft Design Aerodynamic characteristics Materials External stores Engine inlets</p>	<p>AGARD Report No.740 Advisory Group for Aerospace Research and Development, NATO SPECIAL COURSE ON FUNDAMENTALS OF FIGHTER AIRCRAFT DESIGN Published October 1987 296 pages</p> <p>The Special Course on Fundamentals of Fighter Aircraft was sponsored by the AGARD Fluid Dynamics Panel and the von Kármán Institute and presented at the von Kármán Institute, Rhode-Saint-Genèse, Belgium, on 17-21 February 1986, at the Greek Air Force Academy, Athens, Greece, on 24-25 February 1986 and at the ARGE, Ankara, Turkey on 27-28 February 1986.</p> <p>P.T.O.</p>	<p>AGARD-R-740</p> <p>Fighter aircraft Design Aerodynamic characteristics Materials External stores Engine inlets</p>
<p>AGARD Report No.740 Advisory Group for Aerospace Research and Development, NATO SPECIAL COURSE ON FUNDAMENTALS OF FIGHTER AIRCRAFT DESIGN Published October 1987 296 pages</p> <p>The Special Course on Fundamentals of Fighter Aircraft was sponsored by the AGARD Fluid Dynamics Panel and the von Kármán Institute and presented at the von Kármán Institute, Rhode-Saint-Genèse, Belgium, on 17-21 February 1986, at the Greek Air Force Academy, Athens, Greece, on 24-25 February 1986 and at the ARGE, Ankara, Turkey on 27-28 February 1986.</p> <p>P.T.O.</p>	<p>AGARD-R-740</p> <p>Fighter aircraft Design Aerodynamic characteristics Materials External stores Engine inlets</p>	<p>AGARD Report No.740 Advisory Group for Aerospace Research and Development, NATO SPECIAL COURSE ON FUNDAMENTALS OF FIGHTER AIRCRAFT DESIGN Published October 1987 296 pages</p> <p>The Special Course on Fundamentals of Fighter Aircraft was sponsored by the AGARD Fluid Dynamics Panel and the von Kármán Institute and presented at the von Kármán Institute, Rhode-Saint-Genèse, Belgium, on 17-21 February 1986, at the Greek Air Force Academy, Athens, Greece, on 24-25 February 1986 and at the ARGE, Ankara, Turkey on 27-28 February 1986.</p> <p>P.T.O.</p>	<p>AGARD-R-740</p> <p>Fighter aircraft Design Aerodynamic characteristics Materials External stores Engine inlets</p>

<p>The Course presented a comprehensive review of fundamental procedures used during a fighter pre-development phase concentrating on</p> <ul style="list-style-type: none"> - basic mission requirements and aircraft sizing - aerodynamic design including performance, stability and control - materials, structural optimization and aeroelasticity - aircraft dynamics - engine intake and nozzle integration - airframe store-compatibility <p>Experimental and theoretical work has been demonstrated to play complementary roles and recommendations for future development of engineering tools are given in conclusion.</p> <p style="text-align: center;">ISBN 92-835-1560-9</p>	<p>The Course presented a comprehensive review of fundamental procedures used during a fighter pre-development phase concentrating on</p> <ul style="list-style-type: none"> - basic mission requirements and aircraft sizing - aerodynamic design including performance, stability and control - materials, structural optimization and aeroelasticity - aircraft dynamics - engine intake and nozzle integration - airframe store-compatibility <p>Experimental and theoretical work has been demonstrated to play complementary roles and recommendations for future development of engineering tools are given in conclusion.</p> <p style="text-align: center;">ISBN 92-835-1560-9</p>
<p>The Course presented a comprehensive review of fundamental procedures used during a fighter pre-development phase concentrating on</p> <ul style="list-style-type: none"> - basic mission requirements and aircraft sizing - aerodynamic design including performance, stability and control - materials, structural optimization and aeroelasticity - aircraft dynamics - engine intake and nozzle integration - airframe store-compatibility <p>Experimental and theoretical work has been demonstrated to play complementary roles and recommendations for future development of engineering tools are given in conclusion.</p> <p style="text-align: center;">ISBN 92-835-1560-9</p>	<p>The Course presented a comprehensive review of fundamental procedures used during a fighter pre-development phase concentrating on</p> <ul style="list-style-type: none"> - basic mission requirements and aircraft sizing - aerodynamic design including performance, stability and control - materials, structural optimization and aeroelasticity - aircraft dynamics - engine intake and nozzle integration - airframe store-compatibility <p>Experimental and theoretical work has been demonstrated to play complementary roles and recommendations for future development of engineering tools are given in conclusion.</p> <p style="text-align: center;">ISBN 92-835-1560-9</p>